Of Receptors and Responses: Characterizing GPCR Signalling Pathways and Interactome Networks to Inform their Pharmacological Profiles

Manel Zeghal

Thesis submitted to the University of Ottawa

In partial fulfillment of the requirements

For the PhD degree in Microbiology and Immunology

Department of Biochemistry, Microbiology and Immunology

Faculty of Medicine

University of Ottawa

December 2024

Abstract

G protein-coupled receptors (GPCRs) epitomize a preeminent class of drug targets, orchestrating a myriad of physiological processes. Notwithstanding their paramount biomedical importance, the advancement of GPCR-targeted drug discovery is impeded by the limitations of extant screening tools, which predominantly assess GPCR activation through agonist-induced G-protein and β-arrestin-2 activities. In this dissertation, we optimize and develop novel approaches to enhance the functional characterization of GPCRs and present non-canonical exemplars from the realm of GPCR-protein interactions.

We introduce Tango-Trio, a robust high-throughput cell-based platform that enables the parallel profiling of both basal and agonist-dependent activities of GPCRs. This platform captures the functional diversity of GPCRs, including β-arrestin-1/2 couplings, selectivities, and receptor internalization signatures. By constructing cumate-induced basal activation curves for approximately 200 receptors, including over 50 orphans, Tango-Trio provides a valuable tool for comprehensive GPCR screening and characterization.

Further, we develop the NbV5 tag system, an intracellular nanobody targeting the V5-tag, which enhances the study of protein-protein interactions (PPIs) in cellular assays. The smaller size of the V5-tag minimizes perturbations to protein stability and localization compared to larger functional moieties. This system is applicable in GPCR-based assays such as Bioluminescence Resonance Energy Transfer (BRET), NanoBiT, and Tango, and proves effective in live-cell imaging and microscopy, facilitating more accurate and versatile interrogation of GPCR signaling pathways.

Finally, we investigate the dynamic isoform-specific interactions between GPCRs and 14-3-3 proteins, a family of adaptor proteins that regulate various cellular processes, including signal transduction, cellular stress responses, apoptosis, and cell cycle progression. Utilizing stable reporter cell lines expressing all seven human 14-3-3 isoforms, we perform high-throughput agonist-based screening across approximately 100 non-orphan GPCR. Notably, we identify the neurokinin 3 receptor (NK3) receptor as a key candidate for in-depth study and demonstrate that different combinations of 14-3-3 isoform dimers modulate NK3 receptor activity, including surface expression and signaling pathways, thereby highlighting the intricate regulatory mechanisms of GPCR function.

Collectively, this work advances our understanding of GPCR signaling and PPIs in the proximal interactomes of GPCRs, offering new methodologies for drug discovery and providing insights into the sophisticated regulatory networks that underpin these receptors' myriad functions.

Table of Contents

List of Tables

List of Figures

List of Abbreviations

A2-AR adenosine receptor 2A

aGPCR adhesion GPCR

AGS activators of G-protein signaling

AKAP A kinase anchor protein

AT1R angiotensin II type 1 receptor

BCS bovine calf serum

BRET bioluminescence resonance energy transfer

cAMP cyclic adenosine monophosphate

CaSR calcium-sensing receptor

CDR complementarity-determining region

CNR1 cannabinoid receptor type 1

Cryo-EM cryo-electron microscopy

CXCR4 C-X-C chemokine receptor type 4

D2R/DRD2 D2 dopamine receptor

DAG diacylglycerol

DAMGO (D-Ala(2)-mephe(4)-gly-ol(5))enkephalin

DMEM Dulbecco's Modified Eagle's Medium

DOR delta/δ-opioid receptor

E0 baseline

EC50 potency

ECD extracellular domain

ECL extracellular loop

Emax efficacy

FBS fetal bovine serum

FEME Fast endophilin-mediated endocytosis

FRET fluorescence resonance energy transfer

G protein guanine nucleotide-binding protein

GAP GTPase-activating protein

GBA Gα-binding and activating

GDI guanine nucleotide dissociation inhibitor

GDP guanosine diphosphate

GFP green fluorescent protein

GIP GPCR-interacting protein

GPCR G protein-coupled receptor

GRK G protein receptor kinase

GTP guanosine triphosphate

Gαi/o/z inhibitory Gα protein family

Gαs excitatory Gα protein family

HBSS Hank's balanced salt solution

HEK human embryonic kidney

HTL HEK293T cells stably expressing TRE-Luc

HTLA HTL cells stably expressing β-arrestin-2-TEVp

HTTL HEK293T cells stably expressing TRE-Tight-Luc

HPA Human Protein Atlas

ICL intracellular loop

IP3 inositol triphosphate

IUPHAR International Union of Pharmacology

JAK Janus kinase

LgBit large fragment of Nanoluc

mGluR metabotropic glutamate receptor

MOR/μ-OR μ-opioid receptor

NanoBiT nanoluciferase binary technology

Nb nanobody

NK3/TACR3 neurokinin receptor 3/tachykinin receptor 3

NKB neurokinin B

oGPCR orphan GPCR

OR opioid receptor

PCA Protein-fragment Complementation Assay

PDZ postsynaptic density 95/disc large/zona occludens-1

PKA protein kinase A

PKC protein kinase C

PBS phosphate-buffered saline

PEI polyethylenimine

PI3P phosphatidylinositol 3-phosphate

PLCβ phospholipase Cβ

PLL poly-L-lysine

PMA phorbol 12-myristate 13-acetate

PPI protein-protein interaction

PTM post-translational modification

R* active state of the receptor

R inactive state of the receptor

RAMP receptor activity-modifying protein

RET Resonance energy transfer

RGS regulators of G protein signaling

RhoGEF Rho guanine nucleotide exchange factor

RLuc Renilla Luciferase

RLU relative luminescence unit

SAM Scanning Alanine Mutagenesis

SAP97 synapse-associated protein 97

SCAM Scanning Cysteine Accessibility Method

scFv single-chain variable fragments

SD standard deviation

sdAb single-domain antibody

SEM standard error of the mean

SmBit 11-amino acid Nanoluc fragment

SNX sorting nexin

SSTRs somatostatin receptors

ST kinases serine/threonine-specific protein kinases

SVM support vector machine

TANGO Tobacco Etch protease-dependent assay

TEVp tobacco etch virus protease

TEV219 TEVp carrying S219V-stop mutation

TM transmembrane

TRE tetracycline-response element

tTA tetracycline-controlled transactivator

vGPCR viral GPCR

WGD Whole-genome duplication

Y2H yeast two-hybrid

YFP yellow fluorescent protein

β2-AR β2-adrenergic receptor

Acknowledgements

"To My Guides" (inspired by the poem "To a Mouse" by Robert Burns)
On Completing My Thesis, with the Guidance of Many, August 2024

Wee, sleeket, cowran, timrous acknowledgment,
I owe a debt, nae small, but grand as any firmament,
To those who guided me wi' gentle hand,
An' set my course upon this academic land.

To Dr. Patrick Giguère, my gratitude runs deep,
He gave me space in his lab, where dreams and knowledge meet.
Wi' wisdom, patience, humor too, he led me with steadfast hand,
Thou shaped my work, and made it stand.

An' next, tae Dr. Geneviève Laroche, a mentor kind an' wise,
She stood beside me through it all, wi' skill an' keen advice.
She showed me how to work wi' care, to think, to trust, to grow,
A shining light, a model clear, of what it means to know.

My thanks tae those who judged my work, wi' insight and respect,
Dr. Mario Tiberi, Dr. Maxime Rousseaux, an' Dr. Marceline Côté, your wisdom I reflect.
Ye weighed my progress, gave me thought, your counsel sharp an' true,
In every line, in every word, your influence shines through.

An' to my friends within and outside the lab, who shared these days bright,
Your laughter, toil, an' company, made every burden light.

Last, tae my family dear, wi' love beyond compare,
For all the strength ye gave to me, for every tender care.
Ye stood wi' me through thick an' thin, an' lifted me when low,
Without your love, your steadfast grace, this work would never grow.

So here’s my thanks, in heartfelt verse, to all who helped me through,
May fortune smile upon your days, wi’ blessings rich an’ true,
To all who’ve shaped this precious time.
May fortune bless you, one and all,
Wi' joy and peace, both great and small.

Thesis format

According to the Department of Biochemistry, Microbiology and Immunology at the Faculty of Medicine of the University of Ottawa, this thesis is written as a general introduction, reviewing the literature surrounding the thesis topic, followed by a collection of manuscripts, and final chapter consisting of a general discussion and conclusion.

Chapter one, the general introduction, reviews the current body of knowledge surrounding the life cycle and interactomes of G-protein coupled receptors (GPCRs), as well as the methodologies used to pharmacologically characterize them. It further provides background knowledge and rationale for chapters two, three and four – the manuscripts describing the doctoral work.

Chapter two is entitled: “Profiling of constitutive and ligand-dependent GPCR activities by means of a polyvalent cell-based high-throughput platform”. This work was published in Nature Communications in 2023 and is included here exactly as published.

Chapter three is entitled: “Development of a V5-tag–directed nanobody and its implementation as an intracellular biosensor of GPCR signaling”. This work was published in the Journal of Biological Chemistry in 2023 and is included here exactly as published.

Chapter four is entitled: “The protean nature of 14-3-3 proteins in GPCR signaling: highlighting selectivity and dynamic interactions at the NK3 receptor interface”. This manuscript is ready for submission and peer-review to ACS Pharmacology & Translational Science.

Chapter five collectively summarizes the data presented in chapters two, three and four and interprets the findings. Furthermore, a discussion on potential future directions that can be undertaken with regards to each project is presented.

CHAPTER 1: Introduction

1. Significance of GPCRs in Physiology and Pathology

G protein-coupled receptors (GPCRs), constituting the largest family of cell surface receptors, are indispensable in orchestrating a vast array of physiological functions and are implicated in a multitude of diseases, thereby serving as invaluable targets for pharmacological intervention. These receptors mediate cellular responses to various external stimuli, including hormones, neurotransmitters, and environmental signals, thereby regulating critical biological senses such as smell and vision, as well as immune system function, synaptic transmission, and regulation of behaviour and mood, among other processes (Rajagopal and Ponnusamy, 2018). For instance, a broad spectrum of GPCRs are involved in cardiovascular function, maintaining vascular tone and cardiac output. Beyond the well-characterized adrenergic and angiotensin receptor systems, other receptors, including muscarinic M2 and relaxin family peptide members, also exert considerable functions in the heart (Foster et al., 2015).

In the occurrence of dysregulated GPCR signalling, the consequential aberrant cellular responses can precipitate the onset of diseases. Specifically within the cardiovascular system, such dysregulation can lead to a range of cardiac pathologies, such as hypertension, heart failure, and arrhythmias, with the standard treatment for said conditions being β-blockers and angiotensin II receptor antagonists (Kayki-Mutlu and Koch, 2023). The influence of GPCRs extends beyond cardiovascular diseases, encompassing metabolic, inflammatory, and central nervous system disorders. Moreover, orphan GPCRs (oGPCRs) have been established as factors involved in autoimmune diseases such as multiple sclerosis, rheumatoid arthritis, and systemic lupus erythematosus (Spiegel and Weinstein, 2004). In spite of their extensive functions, about one-third of non-olfactory GPCRs remain classified as orphans, thereby presenting opportunities for novel therapeutic targets, especially within metabolic tissues like pancreatic islets and adipose tissue (Zhao et al., 2021).

Dysregulation of GPCR signalling can arise through a variety of mechanisms, including receptor desensitization due to chronic stimulation, altered receptor expression, and genetic mutations.
Receptor desensitization is a well-documented phenomenon, particularly in the context of chronic opioid use, where it impacts both the efficacy of opioid analgesics and the progression of various diseases (Allouche et al., 2014). This desensitization is particularly pertinent as it leads to the

development of tolerance, necessitating higher doses to achieve the same analgesic effect. Notably, the desensitization of opioid receptors is not uniform across different tissues, attesting to the importance of differential site-specific GPCR signalling (Tobin et al., 2008). For instance, neurons in the Kolliker-Fuse area of the brain exhibit less desensitization of mu-opioid receptors compared to those in the locus coeruleus, correlating with the relative lack of tolerance to the respiratory depressant effects of opioids (Levitt and Williams, 2018). This differential desensitization is also influenced by protein kinase C and calcium/calmodulin-dependent protein kinase, highlighting the modulatory role of proximal signalling proteins with GPCRs (Mestek et al., 1995).

Additionally, numerous diseases arise from altered GPCR expression, whether over- or under-expression. Misfolding of GPCRs can result in conditions such as familial hypocalciuric hypercalcemia and reproductive disorders by causing intracellular retention and degradation of the receptors, thereby preventing them from reaching the cell surface and interacting with their ligands (Ulloa-Aguirre et al., 2021). Another example is pulmonary arterial hypertension, where altered GPCR expression in pulmonary artery smooth muscle cells contributes to increased vascular resistance and remodeling (Iyinikkel and Murray, 2018).

Mutations in GPCR genes and genetic variations have also been found to disrupt GPCR function in a wide range of human genetic diseases. The resulting inactive, overactive, or constitutively active receptors can alter key processes including ligand binding, G protein coupling, receptor desensitization, and receptor recycling. Notably, inactivating and activating mutations in 55 GPCR genes are known to cause 66 inherited monogenic diseases, while alterations in nine GPCR genes contribute to inherited digenic diseases such as hypogonadotropic hypogonadism involving the TACR3 receptor alongside a mutation in the NSMF gene (Schöneberg and Liebscher, 2021) (**Table 1.1**). Diseases caused by genetic disruptions of GPCR functions have the potential to be selectively targeted by drugs aimed at rescuing altered receptors. This has led to the development of therapeutics such as calcimimetics, calcilytics, drugs targeting melanocortin receptors in obesity, interventions for idiopathic hypogonadotropic hypogonadism, and novel drugs for congenital bleeding phenotypes associated with P2RY12 receptor mutations (Thompson et al., 2014).

Overall, the broad physiological relevance and therapeutic potential of GPCRs underscore their importance in both normal physiology and disease, making them a focal point for ongoing research and drug development.

GPCR Gene	Disease/Syndrome	Missense	Nonsense	In/del	Splice	Large
ADGRC1*°	Neural tube defect, spina bifida	28	1	3		
ADGRE2°	***Vibratory urticaria***	1				
ADGRG1°	Bilateral frontoparietal polymicrogyria	14	6	7	2	1
ADGRG2*°	Congenital bilateral aplasia of the vas deferens			3		
ADGRG6°	Arthrogryposis multiplex congenita, lethal congenital contracture syndrome-9	1	1	1		
ADGRV1°	Usher syndrome type IIC	69	21	41	7	4
AGTR1	Renal tubular dysgenesis	1	2	1		
AVPR2	X-linked NDI	135	23	75	3	27
AVPR2	***X-linked nephrogenic syndrome of inappropriate antidiuresis***	4				
CALCRL*	Autosomal recessive nonimmune hydrops fetalis with lymphatic dysplasia			1		
CASR	Hypocalciuric hypercalcemia, neonatal hyperparathyroidism	226	17	35	6	3
CASR	***Dominant and sporadic hypoparathyroidism***	62		1		
CHRM3*	Prune belly syndrome, familial congenital bladder malformation, impaired pupillary constriction, dry mouth			1		
CXCR4	WHIM syndrome	1	5	4		1
CXCR2	Autosomal recessive severe congenital neutropenia due to CXCR2 deficiency	3		1		
CYSLTR2	***Uveal melanoma, blue nevi***	2				
EDNRA*	Mandibulofacial dysostosis with alopecia	2				
EDNRB	Susceptibility to Hirschsprung disease 2, Waardenburg syndrome type 4A, ABCD syndrome	35	5	7	2	4
FPR1	Juvenile periodontitis	3				
FSHR	Hypergonadotropic ovarian dysgenesis	15				1
FSHR	***Ovarian hyperstimulation syndrome***	8				
FZD2	Autosomal dominant omodysplasia, Robinow syndrome	1	2			
FZD4*	Dominant familial exudative vitreoretinopathy	42	9	13		2
FZD5	Autosomal dominant coloboma			1		
FZD6	Recessive isolated congenital nail dysplasia	4	2			
GCGR	Mahvash disease	7	1	2		1
GHRHR	Growth hormone deficiency	21	2	6	10	1
GHSR	Growth hormone deficiency and short stature	7	1	1		
GNRHR	Hypogonadotropic hypogonadism	42	1	4	1	2
GPR88°	Childhood-onset chorea with psychomotor retardation		1			
GPR101°	***X-linked acrogigantism***	2				8

GPR143	Ocular albinism type I, congenital nystagmus, altered thickness of the iris	44	7	29	17	29
GPR179	Congenital stationary night blindness	5	1	5	1	1
GRM1*	Autosomal recessive spinocerebellar ataxia			3	1	
GRM1*	***Autosomal dominant spinocerebellar ataxia***	2				
GRM6#	Congenital stationary night blindness	17	5	6	1	
KISS1R	Hypogonadotropic hypogonadism	19	4	3	2	1
KISS1R	***Central precocious puberty***	1				
LHCGR	Leydig cell hypoplasia, pseudohermaphroditism, primary amenorrhea	18	6	5	2	5
LHCGR	***Male-limited precocious puberty, Leydig cell adenoma***	18				
LPAR6	Hypotrichosis, wooly hair	11	2	10		2
MC1R	Hypopigmentation	73	1	8		
MC2R	Glucocorticoid deficiency	34	3	8		
MC2R	***ACTH-independent Cushing syndrome***	1				
MC3R	Obesity	25				1
MC4R	Obesity	119	7	21		1
MTNR1B	Susceptibility to diabetes mellitus type 2	27				
OGR1 (GPR68)	Amelogenesis imperfecta	1		2		
OPN1SW#	Tritanopia	6				
OPN1MW	Deuteranomaly, cone dystrophy	5	1	1		6
OPN1LW*	Blue cone monochromacy	12	3	1		35
P2RY12	Bleeding disorder	9		2		
PROKR2	Kallmann syndrome	42	2	4		
PTH1R	Blomstrand chondrodysplasia, Eiken syndrome, primary failure of tooth eruption	6	8	9	9	
PTH1R	***Murk Jansen type of metaphyseal chondrodysplasia***	6				
RGR	Retinitis pigmentosa	4		1	2	
RHO	Congenital night blindness, autosomal dominant retinitis pigmentosa	141	9	20	6	3
RHO	***Autosomal dominant retinitis pigmentosa***	9				
S1PR2	Deafness	2				

SMO	***Basal cell carcinoma***	3				
SMO	Curry-Jones syndrome (Mosaizism)	1				
TACR3	Normosmic hypogonadotropic hypogonadism	19	6	2	2	
TBXA2R	Bleeding disorder	4		1		
TRHR	Hypothyroidism	1	2	1		
TSHR	Hypothyroidism	80	10	12	4	4
TSHR	***Congenital hyperthyroidism, hyperfunctioning thyroid adenoma, and carcinoma***	105		3		

Table 1.1 Monogenic diseases resulting from mutations in GPCRs (adapted from Schöneberg and Liebscher, 2021)

A compilation of currently recognized 66 monogenic inherited diseases in humans linked to GPCR mutations. This list includes the latest tally of causative mutations, encompassing missense, nonsense, splice-site, and large-deletion/rearrangement mutations, as documented in the Human Gene Mutation Database (HGMD). Diseases highlighted in bold are specifically caused by activating mutations.

2. Classification of GPCRs

This diversification of GPCRs is often attributed to several evolutionary mechanisms, including gene duplication events, which have expanded the repertoire of GPCRs and their associated ligands (Dehal and Boore, 2005). Whole-genome duplications (WGDs) during vertebrate evolution have notably contributed to the co-evolution of ligand-GPCR systems, particularly involving peptide hormones, neuropeptides, and their respective receptors (Vaudry, 2014). For example, genome duplications in vertebrates resulted in the divergence of CRH receptors into two forms, CRH1 and CRH2. Concurrently, this process led to the evolution of four paralogous ligand lineages: CRH, urotensin I/urocortin (Ucn), Ucn2, and Ucn3 (Lovejoy et al., 2014). Thus, the classification of GPCRs is deeply intertwined with their evolutionary history and can be classified based on sequence homology and structural characteristics, but with the inherent limitations of lack of comprehensiveness and applicability. Conversely, classification can also be based on functional pharmacological similarities, which has several benefits with regard to understanding receptor function, guiding drug discovery, and improving therapeutic interventions. However, these systems have limitations, particularly in dealing with oGPCRs, which lack known ligands or defined structures (Kingwell, 2017).

Thus, GPCRs in the human genome, encoded by over 800 genes, can be organized into different classes based on their pharmacological and/or phylogenetic properties, with the ABC and GRAFS systems being the most commonly used classification frameworks, as organized in **Figure 1.1**. The ABC system categorizes GPCRs into three main families: A (rhodopsin-like), B (secretin-like), and C (metabotropic glutamate/pheromone), focusing on their pharmacological properties and ligand-binding characteristics (Fredriksson and Schiöth, 2006). On the other hand, the GRAFS system, which stands for Glutamate, Rhodopsin, Adhesion, Frizzled/Taste2, and Secretin, is based on phylogenetic analyses and structural features, providing a more comprehensive evolutionary perspective. The GRAFS classification system identifies five main families, with the rhodopsin family being the largest and further divided into four main groups with 13 sub-branches. This system also highlights the evolutionary significance of gene duplication events and tetraploidizations in the diversification of GPCRs (Fredriksson et al., 2003). However, recent studies have emphasized the need for updating these classification systems to incorporate new

functional data and address inconsistencies, particularly in the subclassification of adhesion GPCRs (aGPCRs)(Scholz et al., 2019).

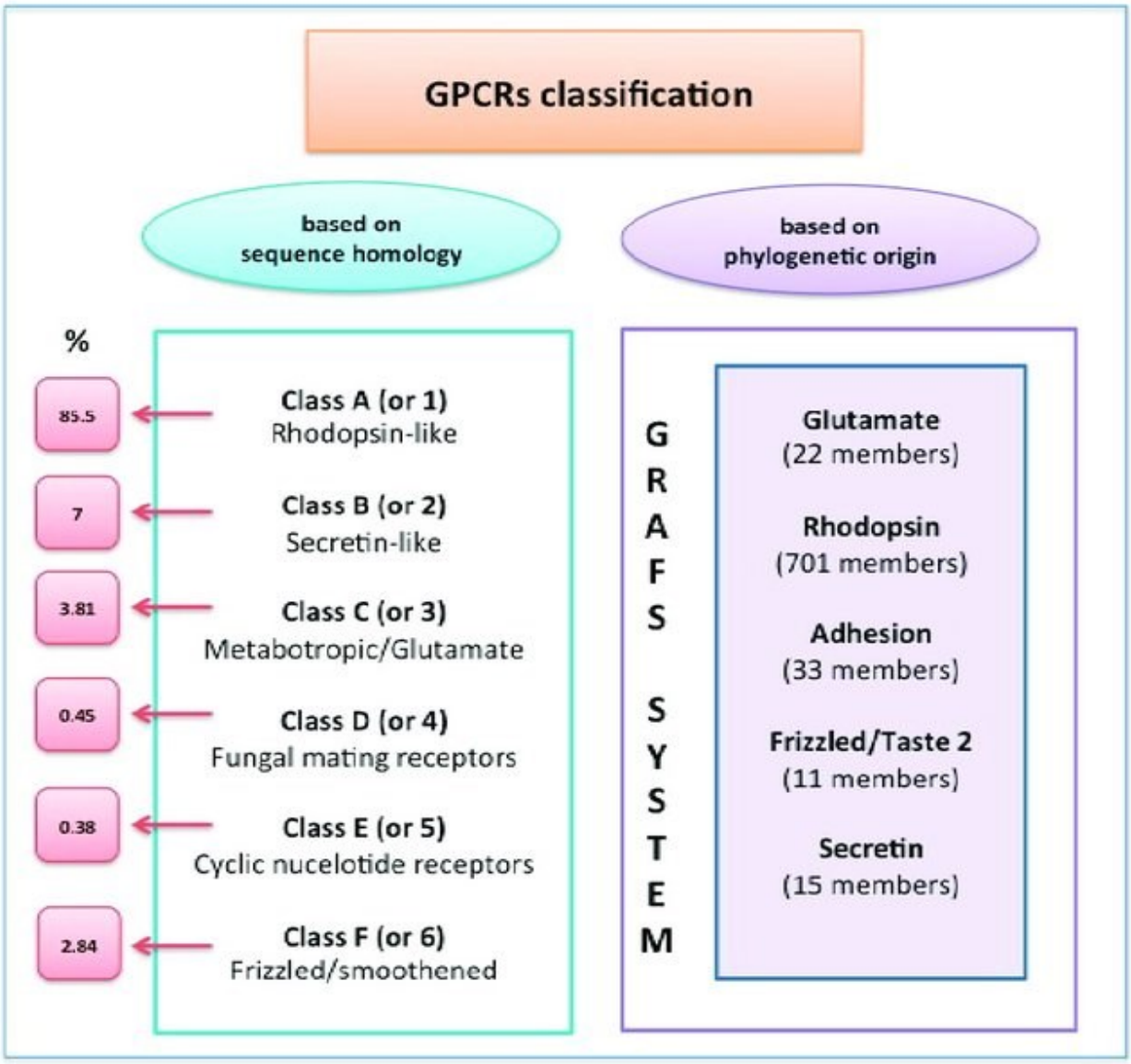

Figure 1.1 Classification of G-protein coupled receptors (taken from De Francesco et al, 2017).

The International Union of Pharmacology (IUPHAR) classification (left column) is applicable to both vertebrates and invertebrates, while the GRAPH system (right column), on the other hand, is tailored exclusively for vertebrates.

Several groups have previously discussed various methodologies and challenges in classifying these receptors. Seeing as they are challenging to crystallize, researchers are leveraging computational techniques like ab initio or homology modeling, as well as site-directed mutagenesis methods such as Scanning Alanine Mutagenesis (SAM) and Scanning Cysteine Accessibility Method (SCAM) to study ligand-protein interactions, structural requirements for binding, and receptor conformations upon binding different ligands. While crystal structures of GPCRs are becoming more common, mutagenesis methods like SAM and SCAM remain valuable due to their cost-effectiveness, speed, and ability to examine dynamic processes, allowing for the study of activation, helical movements, specific amino acid interactions, and changes in microenvironments over time in a larger cross-section of GPCR family members (Parrill and Bautista, 2010). Other methods that take into account crystallographic information include the CoINPocket method, which calculates the similarity of GPCRs based on binding site characteristics from available crystal structures, successfully identifying surrogate ligands for orphan receptors like GPR37L1(Kingwell, 2017). The integration of structure-activity data from databases like ChEMBL and WOMBAT has further refined the mapping of GPCR pharmacological space, providing a systematic way to relate GPCRs based on the chemical similarities of their ligands (Koutsoukas et al., 2013).

Machine learning models, such as support vector machines, random forests, and deep neural networks, as well as motif-based and alignment-free techniques, have been developed to enhance the classification accuracy of GPCRs, addressing challenges such as class imbalance and low sequence similarity among different GPCR families, and have shown promising results in classifying GPCRs and predicting their functions, thereby aiding in the discovery of novel GPCRs and their potential as drug targets (Davies et al., 2011). For instance, one group highlights the use of neural networks and support vector machines (SVMs) for classifying GPCRs, achieving high accuracy rates between 94% and 98% (Iqbal et al., 2016). Computational techniques have also been described to develop new GPCR prediction algorithms with high accuracy. For example, Gangal et al. presented a computational approach based on reduced protein functional alphabet representation, which relies on identifying conserved patterns or motifs in proteins (Gangal and Kumar, 2007). These numerous approaches are complemented by the use of databases like the MySQL database, GPCR-PEnDB, which aids in the classification and prediction of GPCRs by

providing a comprehensive dataset of confirmed GPCRs and non-GPCRs, aiding in distinguishing GPCRs from other transmembrane proteins, a task that remains challenging due to the functional and sequence diversity of this superfamily (Begum et al., 2020). Additionally, diagnostic resources like the PRINTS database, which houses GPCR-specific fingerprints, has provided more sensitive tools for identifying GPCR subtypes and understanding their structural and functional determinants (Attwood et al., 2002).

3. Mechanisms of GPCR Activation

GPCR signalling can be activated through different mechanisms, primarily categorized into constitutive and ligand-activated pathways, as represented in **Figure 1.2**. Advanced biophysical techniques, such as bioluminescence-resonance-energy-transfer (BRET)-based sensors, have been developed to quantify both ligand-induced and constitutive GPCR activity in living cells, providing insights into their signaling dynamics (Schihada et al., 2021). Constitutive activation refers to the receptor's ability to signal in the absence of a ligand, often due to intrinsic structural features or mutations that stabilize the active conformation (Tao, 2008). Constitutive activity is not merely an artifact of overexpression in recombinant systems but is also evident in native receptors, suggesting its physiological relevance and potential role in disease pathology (Seifert and Wieland, 2006). One notable example of constitutive activity in native tissue is the serotonin 6 receptor (5-HT6R). Research has demonstrated that 5-HT6R exhibits high levels of constitutive activity, which is essential for regulating cAMP signaling pathways that are integral in neuronal migration during corticogenesis (Jacobshagen et al., 2014).

Aside from intramolecular interactions, there are other external and cellular factors that could influence the constitutive activity of GPCRs. Environmental stimuli, such as fluid shear stress, hypotonic stress, or membrane fluidizing agents, also significantly increase the activity of specific GPCRs, such as the bradykinin B2 receptor in endothelial cells (Chachisvilis et al., 2006). Additionally, Receptor Activity-Modifying Proteins (RAMPs) are family of single-pass membrane proteins that can modulate the function of GPCRs (especially class B) by altering the conformation of the GPCR's transmembrane domain, which can affect the receptor's signaling capabilities. For example, RAMPs can influence the extracellular domain (ECD) of GPCRs, acting as allosteric regulators that modify receptor activity and ligand specificity (Routledge et al., 2017). This

modulation can lead to changes in the constitutive activity of GPCRs, as RAMPs may stabilize certain receptor conformations that favor or inhibit signaling.

On the other hand, ligand-activated GPCRs require the binding of an agonist to trigger conformational changes that facilitate G-protein coupling and subsequent signal transduction. This process involves a well-coordinated movement of transmembrane helices, particularly TM6, and is characterized by the disruption of stabilizing intramolecular interactions, often referred to as "molecular switches" (Zhou et al., 2019; Xie and Chowdhury, 2013). Ligand binding can bias the receptor's conformational ensemble towards active states, enhancing the cooperativity of the activation process and stabilizing functional isntermediates (Prosser et al., 2017). The activation mechanisms can vary across different GPCR classes, with class A receptors showing a common activation pathway involving specific residue pairs and motifs, while other classes exhibit distinct residue microswitch positions and contacts (Hauser et al., 2021).

3.1 Modalities of GPCR Activation

3.1.1 Constitutive Activation

A distinguishing feature of several GPCRs is their basal or constitutive activity, which refers to their inherent ability to activate intracellular signaling pathways in the absence of an agonist. This basal activity arises from the receptor's spontaneous isomerization from an inactive (R) state to an active (R*) state, a process that can be modulated by various factors such as receptor mutations, alternative splicing, and coupling to specific G-proteins (Seifert and Wenzel-Seifert, 2002a). For instance, the orphan GPCR GPR3 exhibits constitutive activity likely due to a lipid-like ligand bound within its hydrophobic groove, indicating a form of autoactivation (Russell et al., 2024). The β2-adrenergic receptor (β2-AR), also exhibits basal activity, that can be attenuated by inverse agonists, which stabilize the inactive conformation of the receptor (Lamichhane et al., 2015). This basal activity is not merely a biochemical anomaly but has physiological relevance, influencing the therapeutic properties of drugs targeting these receptors (Xiao et al., 2009). Constitutive activity has been documented in over 60 wild-type GPCRs and various disease-causing mutants, impacting both normal physiology and pathophysiology conditions (Seifert and Wenzel-Seifert, 2002b). For example, the mu opioid receptor (MOR) exhibits constitutive activity that can be modulated by chronic opioid exposure, with implications for opioid addiction and pain management (Bilsky et al., 2010). The molecular understanding of GPCR basal activity is

enhanced by structural studies, which reveal that the coupling between ligand binding and G protein or arrestin interaction is loose and involves multiple intermediate states (Weis and Kobilka, 2018). Single-molecule studies have shown that GPCRs like β2-AR can form transient homo-dimers, which are responsible for inducing basal signals, a process that can be specifically blocked by inverse agonists (Kasai et al., 2020). Furthermore, mutations that decrease basal activity often impair the receptor's ability to respond to agonists, suggesting a close interrelationship between basal and activated receptor conformations (Kleinau et al., 2008).

3.1.2 Ligand-Induced Activation

Various kinetic models have been proposed to explain GPCR activation; the simplest, the two-state model, posits that receptors exist in two primary states: inactive (R) and active (R*). While the concept of multiple active states has been introduced to account for biased-signaling phenomena, it must be emphasized that multiple active states are not sequential steps in the activation pathway but are instead thermodynamically parallel and in equilibrium with one another. Notably, the conformational changes from R to R* states are essential for the activation of intracellular G proteins and subsequent signal transduction (Zhang et al., 2016). The concept of a precoupled GPCR-G protein complex that remains inactive until ligand binding has also been proposed, with this interaction interfering with the intrinsic tight coupling between the cytoplasmic ends of TM3 and TM6, which is responsible for keeping class A GPCRs in an inactive state (Mafi et al., 2022).

The transition from R to R* involves significant structural rearrangements, particularly in the transmembrane helices and intracellular loops (Park et al., 2008). The canonical model posits that agonists induce GPCR activation by causing rearrangements in the transmembrane helices, which open an intracellular pocket for G-protein binding. This paradigm is supported by structural studies showing that agonist binding destabilizes hydrogen bonds in the intracellular regions of transmembrane helices 5-7, facilitating the formation of the G-protein binding cavity (Madsen et al., 2022). However, recent findings suggest alternative mechanisms, such as the direct rearrangement of intracellular loops by certain agonists, which can convert these agonists into inverse agonists upon specific mutations (Powers et al., 2023). Additionally, GPCR activation is an allosteric process that involves coupling agonist binding to G-protein recruitment, characterized by the outward movement of transmembrane helix 6 (TM6). This movement is part of a common

activation pathway involving key residue pairs and motifs like CWxP, DRY, Na+ pocket, NPxxY, and PIF, which link the ligand-binding pocket to the G-protein coupling region (Zhou et al., 2019). Furthermore, the activation process is marked by the formation of intermediary complexes, such as the R*·Gαβγ·GDP complex, which precedes GDP release and the formation of the nucleotide-free R*·G protein complex. This dynamic interface is imperative for the propagation of conformational changes from the receptor to the G protein (Scheerer et al., 2009). The activation of class A GPCRs, like the adenosine A2A receptor (A2-AR), has been studied to explore the conformational landscape and identify distinct functional states. Among these is a pseudo-active state that preferentially couples with β-arrestin rather than G-proteins, suggesting potential routes for biased signaling (D'Amore et al., 2023). As reported with the angiotensin II type 1 receptor (AT1 receptor), the activation mechanism of this receptor involves a synergistic transition with a key intermediate state possessing a cryptic binding site, which, when mutated, prevents downstream signaling, indicating an allosteric regulatory mechanism (Lu et al., 2021).

Experimental evidence suggests that different active conformations of GPCRs may be responsible for coupling to distinct signaling pathways, highlighting the complexity and multiplicity of GPCR activation states (Niv et al., 2006). The β2-adrenergic receptor–Gs complex has been a bona fide model for understanding active-state GPCRs, revealing that agonist binding alone is insufficient for full activation, and that additional restraints at the G protein-binding region are necessary (Taddese et al., 2013). To elaborate, GPCR activation is traditionally described by the ligand-first mechanism, where agonist binding shifts the receptor to its active conformation, enabling G-protein recruitment and activation. However, experimental and computational evidence shows that agonists alone often fail to stabilize the active conformation, with G-protein recruitment largely dependent on random collisions. This process is slow due to competition among various G-protein subtypes, yet cellular responses are typically rapid. Additionally, the ligand-first model cannot explain GPCRs' intrinsic basal activity, such as the constitutive activation seen in serotonin receptors (e.g., 5-HT2A, 5-HT2C), which is crucial for physiological functions. This has given rise to the alternative G-protein-first mechanism, where inactive GPCRs and G-proteins form a stable precoupled complex before ligand binding. This interaction disrupts the tight TM3-TM6 coupling in the receptor, creating a resting complex. Upon agonist binding, the complex transitions to a fully active state, facilitating GDP exchange and signaling (Mafi et al., 2022).

The kinetic, quaternary complex model further elucidates the binding dynamics of ligands, receptors, G proteins, and guanine nucleotides, providing a framework for understanding GPCR activation and downstream signaling based changes in ligand concentration, the ratio of G proteins to receptors, and the presence of GDP or GTP, among other factors (Stein and Ehlert, 2015). Moreover, the structural features differentiating active from inactive states often involve changes in the interaction patterns of conserved residues, such as the E/DRY motif, and increased solvent accessibility of specific cytosolic domains (Fanelli and De Benedetti, 2006). The activation mechanisms also vary among different GPCR classes (A, B1, C, and F), with each class exhibiting unique residue microswitch positions and contacts, despite sharing a common structural scaffold (Hauser et al., 2021).

While class A GPCRs have been studied more extensively, other GPCR classes, like the adhesion class (aGPCRs), also exhibit distinctive activation mechanisms. In aGPCRs, activation is triggered by the dissociation of the N-terminal fragment, which unveils a tethered agonist peptide. This peptide interacts with the seven-transmembrane domain, stabilizing conformational changes in transmembrane helices 6 and 7, thereby facilitating G-protein coupling (Barros-Álvarez et al., 2022).

3.2 GPCR-Ligand Interaction Dynamics

GPCRs respond to various ligands that can either activate or inhibit their function. Excitatory ligands, such as full agonists, bind to GPCRs and induce maximal intracellular responses, while partial agonists elicit submaximal responses (Kurose and Kim, 2022). Inhibitory ligands, including inverse agonists, bind to GPCRs and reduce their constitutive activity, as demonstrated by the structural analysis of the ghrelin receptor bound to the inverse agonist PF-05190457(Qin et al., 2022) (**Figure 1.2**). Neutral ligands, or antagonists, bind to GPCRs without activating them but can block the effects of agonists, with their activity influenced by the receptor's constitutive activity and intrinsic properties (Kurose and Kim, 2022) (**Figure 1.2)**. Based on the simplified two-state model, ligand efficacy depends on the extent to which it shifts the equilibrium of R and R*. Whereas inverse agonists stabilize R, full agonists preferentially bind and stabilize R*, while partial agonists, with affinity for both R and R*, induce only a moderate shift toward R* (Kobilka, 2006).

The concept of biased agonism, where ligands preferentially activate specific signaling pathways, is also an emerging and pivotal concept for developing drugs with fewer side effects. This bias

factor is correlated with allosteric communication, wherein conformational changes propagate from the ligand-binding site to the intracellular transducer-coupling sites, with the strength of said communication depending on the type of ligand, as well as the bound effector protein (Ma et al., 2021). Fluorescent ligands have been instrumental in studying these binding dynamics, offering insights into ligand-binding kinetics and allosterism (Stoddart et al., 2016). Moreover, computational methods, including multiscale QM/MM molecular modeling, have been utilized to identify key binding site residues and enabling the design of selective ligands (Nakliang et al., 2020).

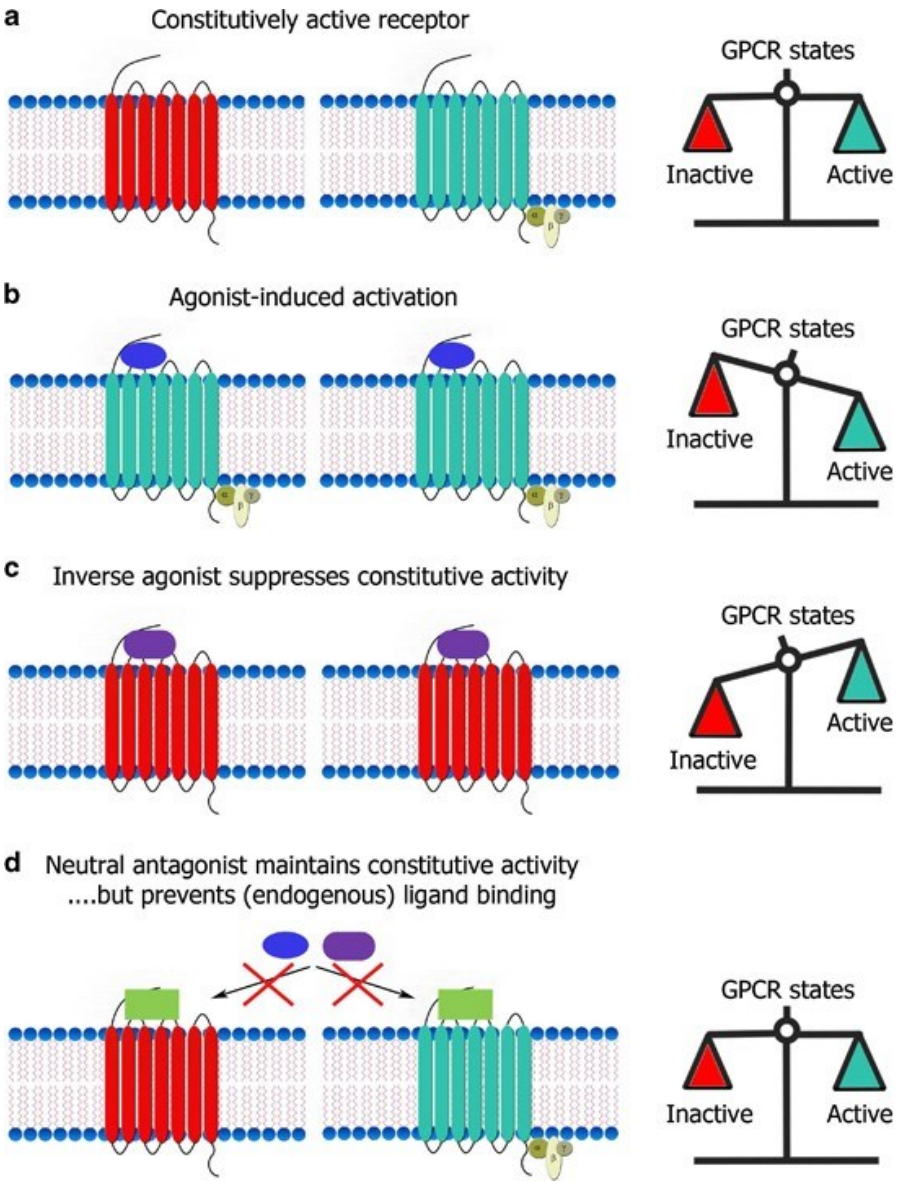

Figure 1.2 Modalities of GPCR activation (taken from Meye et al. 2014).

(a) Typically, GPCRs remain in their inactive conformations (red) when an (endogenous) ligand is absent, but some may spontaneously transition to an active conformation (blue). The degree to which this occurs represents the receptor population's constitutive activity, which is arbitrarily depicted as 50% (right) in this example for illustrative purposes. (b) When an agonist (blue ellipse) binds to GPCRs, it shifts the equilibrium towards a higher number of active receptors. In contrast, (c) inverse agonists (purple rounded rectangle) drive the balance toward more inactive receptors. This is accomplished through a dual mechanism: (1) suppression of the constitutive activity of GPCRs and (2) "antagonistic" inhibition of GPCR activation by (endogenous) agonists. (d) Neutral

antagonists (yellow squares), on the other hand, only block GPCR activation by (endogenous) agonists, without affecting constitutive GPCR activity. Importantly, neutral antagonists also prevent inverse agonists from inhibiting constitutive GPCR activation.

4. GPCR Intracellular Signaling Pathways

4.1 G-Protein-Dependent Pathways

G-protein-dependent signaling pathways are initiated when a ligand binds to a GPCR, triggering a conformational change that activates the associated heterotrimeric G-proteins by exchanging GDP for GTP on the Gα subunit. This activation causes the Gα subunit to dissociate from the Gβγ dimer, enabling both to interact with various downstream effectors. The development of non-invasive assays, such as conformational and activation-based cellular biosensors and dynamic mass redistribution, has advanced our ability to study these pathways in real-time without interfering with the biological processes, offering a more accurate depiction of GPCR signaling events (Wright et al., 2024; Seibel-Ehlert et al., 2021). For example, DMR relies on detection of refractive index alterations on biosensor-coated microplates that originate from stimulus-induced changes in the total biomass proximal to the sensor surface. Consequently, distinct optical signatures generated by DMR can be used to delineate the G-protein coupling profile of different GPCRs (Henstridge et al., 2010).

Elaborating upon the existing knowledgebase of G-protein dependent signaling, the Gα protein family is divided into four main classes: Gαs, Gαi/o, Gαq/11, and Gα12/13, each of which initiates distinct signaling cascades (Glukhova et al., 2018) (**Figure 1.3**). For instance, Gαs stimulates adenylyl cyclase to increase cyclic adenosine monophosphate (cAMP) levels, which then activate protein kinase A (PKA) and other effectors, influencing processes such as metabolism and gene transcription. Conversely, Gαi/o inhibits adenylyl cyclase, reducing cAMP levels and thus PKA activity, which can have opposing effects on cellular functions (Pizzoni et al., 2024). Gαq/11 activates phospholipase Cβ (PLCβ), leading to the production of inositol trisphosphate (IP3) and diacylglycerol (DAG), which mobilize intracellular calcium and activate protein kinase C (PKC), respectively, proving essential in processes like muscle contraction and cell proliferation (Xiang et al., 2022). On the other hand, Gα12/13 is involved in the activation of Rho guanine nucleotide exchange factors (RhoGEFs), which regulate the Rho family of GTPases, thereby impacting cytoskeletal dynamics and cell migration (Siehler, 2009).

The diversity of Gβ and Gγ subunits also shapes downstream signaling pathways; with five and twelve isoforms of Gβ and Gγ subunits, respectively, these aforementioned components can form various combinations, each conferring unique signaling properties. For instance, the Gβγ dimer is essential for the modulation of multiple downstream effectors, including ion channels, kinases,

and other signaling proteins (Smrcka, 2008). Particular pairings of Gβ and Gγ subunits can affect the kinetics and efficacy of GPCR responses at the plasma membrane and their selective translocation to cellular organelles, such as the Golgi apparatus, endosomes, and the nucleus, thereby influencing the spatial and temporal aspects of signal transduction (Masuho et al., 2021). For example, the specific combination of Gγ9, in complex with Gβ1, has been shown to translocate from the plasma membrane to the Golgi in response to CXCR4 activation, leading to the activation of the MAPK pathway and promoting cancer cell migration and invasion (Khater et al., 2021). Thus, the modularity of these pathways allows for a high degree of specificity and flexibility, as different GPCRs can couple to different G-proteins depending on the cell type and context, thereby fine-tuning the cellular response (Meriney and Fanselow, 2019).

4.2 G-Protein-Independent and Non-Canonical Signaling Pathways

Traditionally, GPCRs are known to signal through heterotrimeric G-proteins, which upon activation, dissociate into Gα and Gβγ subunits to regulate various effectors such as adenylyl cyclases, phospholipases, and ion channels. However, emerging studies have highlighted alternative signaling mechanisms that operate independently of G proteins, a few of which are highlighted in **Figure 1.3**. One such mechanism involves β-arrestins, which not only serve to desensitize GPCRs but also initiate distinct signaling cascades that can profoundly influence cardiac function, including contractility and hypertrophy. For instance, β-arrestin-mediated pathways have been shown to regulate cardiac function independently of G proteins, presenting novel therapeutic avenues for treating cardiovascular diseases (Tilley, 2011). Another critical aspect of G-protein independent signaling is the role of cytoplasmic scaffold proteins, which interact with GPCRs to modulate their cellular localization and pharmacological characteristics (Fisyunov, 2012). In the context of taste perception, compounds like denatonium have been shown to activate both G-protein-dependent and independent pathways, with the latter involving calcium release from intracellular stores (Sawano et al., 2005). Metabotropic glutamate receptors (mGluRs) further exemplify this dual signaling capability, as type 1 mGluRs can activate Src-family protein tyrosine kinases independently of G proteins, adding another layer of complexity to synaptic signaling (Heuss et al., 1999). Furthermore, nonGPCR proteins, cytoplasmic interactors possessing Ga-binding and activating (GBA) motifs, have been identified as alternative activators of G-proteins, bypassing the need for GPCRs altogether (Leyme et al., 2017).

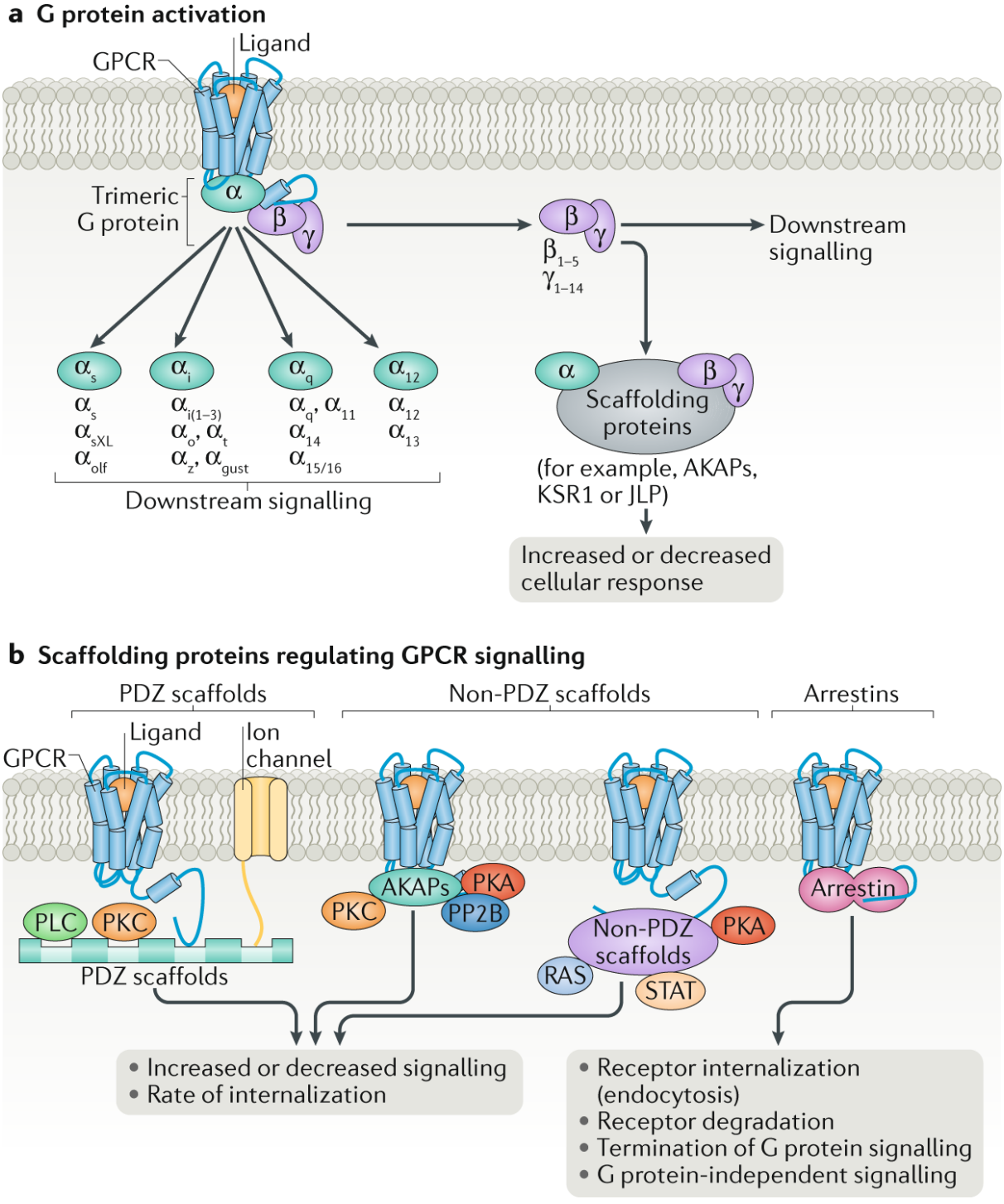

Figure 1.3 GPCR Intracellular Signaling Pathways (taken from Wootten et al. 2018)

a) Canonical GPCR signaling involves interaction with heterotrimeric G proteins (comprising Gα, Gβ, and Gγ subunits). When a GPCR is activated, the Gα and Gβγ subunits separate and can each

initiate downstream signaling pathways. Gα proteins are classified into four primary families, each with distinct signaling characteristics. Additionally, the variety of Gβ and Gγ subunits contributes to a broad range of signaling responses. Gα and Gβγ subunits can also interact with scaffolding proteins that influence their signaling behaviors.

b) G-protein independent signalling requires GPCR scaffolding proteins, which can be categorized into three main types: PDZ scaffolds, which bind to the distal ends of GPCR carboxyl termini and link GPCRs to various signaling molecules such as kinases (e.g., protein kinase C (PKC)), phospholipases (e.g., phospholipase C (PLC)), and ion channels; non-PDZ scaffolds, like A kinase anchor proteins (AKAPs), which attach to the cytoplasmic surface of GPCRs and interact with various signaling partners including kinases (e.g., PKA and PKC), phosphatases (e.g., serine/threonine-protein phosphatase 2B (PP2B)), and intracellular receptors (e.g., inositol 1,4,5-triphosphate receptors (InsP3Rs) in the endoplasmic reticulum, not depicted); and arrestins, which bind to numerous GPCRs, interrupt G protein–GPCR interactions, promote GPCR internalization through endocytosis, and act as scaffolds to enable various interactions between GPCRs and cytoplasmic signaling proteins independently of G proteins. Additionally, GPCRs can function as scaffolding proteins for other membrane proteins, including other GPCRs and receptor-modifying proteins such as receptor activity-modifying proteins (RAMPs) (not illustrated).

5. Regulatory Mechanisms of GPCR Signaling

The intricate and tight regulation of GPCR signaling is orchestrated through numerous post-translational modifications (PTMs) such as phosphorylation, ubiquitination, glycosylation, and palmitoylation, which influence receptor activity, trafficking, and degradation (Patwardhan et al., 2021). Phosphorylation by GPCR kinases (GRKs) and subsequent binding of β-arrestins is a well-established mechanism that terminates G-protein signaling and redirects signaling pathways (Gurevich and Gurevich, 2019). Ubiquitination serves as another chief PTM, guiding GPCRs towards lysosomal degradation and, in some cases, targeting receptors to the proteasome, influencing GPCR signaling and activity (Skieterska et al., 2017). Allosteric regulation by ions, biomolecules, and protein components such as G proteins and β-arrestins, all participate to the fine-tuning GPCR function, with allosteric sites dispersed in various regions of the receptor (Shpakov, 2023). The spatial encoding of GPCR signaling, shaped by receptor organization at the plasma membrane and endocytic pathways, further refines signaling outcomes (Weinberg and Puthenveedu, 2019). Moreover, the discovery of novel pathways for GPCR internalization, such as those involving sorting nexin 9 (SNX9), underscores the complexity of GPCR regulation beyond the classical β-arrestin-dependent mechanisms (Robleto et al., 2023). Furthermore, the role of Regulators of G-protein Signaling (RGS) proteins in terminating GPCR signaling is necessary for maintaining cellular homeostasis, particularly in cardiovascular systems (Lymperopoulos et al., 2022).

5.1 Phosphorylation Codes and GPCR Kinases (GRKs)

Phosphorylation of GPCRs is a critical regulatory mechanism that influences their signaling properties and functional outcomes. The emerging concept of a "phosphorylation code" or "phospho-barcode" offers a sophisticated framework to explain how specific patterns of phosphorylation on GPCRs can direct distinct signaling pathways. This concept is substantiated by a wealth of studies demonstrating the pivotal role of phosphorylation in shaping GPCR functions. For instance, Tobin (2008) discusses multiple phosphorylation sites on GPCRs, positing that the accumulation of bulk negative charge rather than specific sites of phosphorylation, may be significant for receptor regulation, providing a flexible mechanism tailored to tissue-specific physiological processes (Tobin, 2008). Eiger et al. demonstrated that chemokine receptors like CXCR3 exhibit different phosphorylation patterns, or barcodes, which correlate with distinct

signaling outcomes, such as differential activation of G proteins, β-arrestins, and GPCR kinases (GRKs) (Eiger et al., 2023). The complexity of phosphorylation-mediated regulation was recently expanded and described using "bar code" and "flute" models, which explain how arrestin recognizes phosphorylated GPCRs with high specificity. A "QR code" model was also proposed, wherein multiple factors, including ligands and kinases, converge to determine the biological functions of phosphorylated receptors (Chen et al., 2022) (**Figure 1.4**). Yang et al. contribute to this discourse by showing that ligand-specific phosphorylation patterns on GPCRs can direct unique functional outcomes through alterations in arrestin conformations and downstream effector interactions (Yang et al., 2017). Further reinforcing the concept of a phosphorylation code, different phosphorylation patterns on the β2 adrenergic receptor result in distinct β-arrestin conformations and functional outcomes (Nobles et al., 2011). Similarly, with the dopamine D1 receptor, specific phosphorylation sites influence the coupling of G proteins and arrestins, thereby directing signaling towards different pathways such as ERK1/2 or Src activation (Kaya et al., 2020). One cannot overlook the indispensable role of GRKs in generating these phosphorylation patterns, which in turn dictate β-arrestin conformation and subsequent signaling pathways (Liggett, 2011).

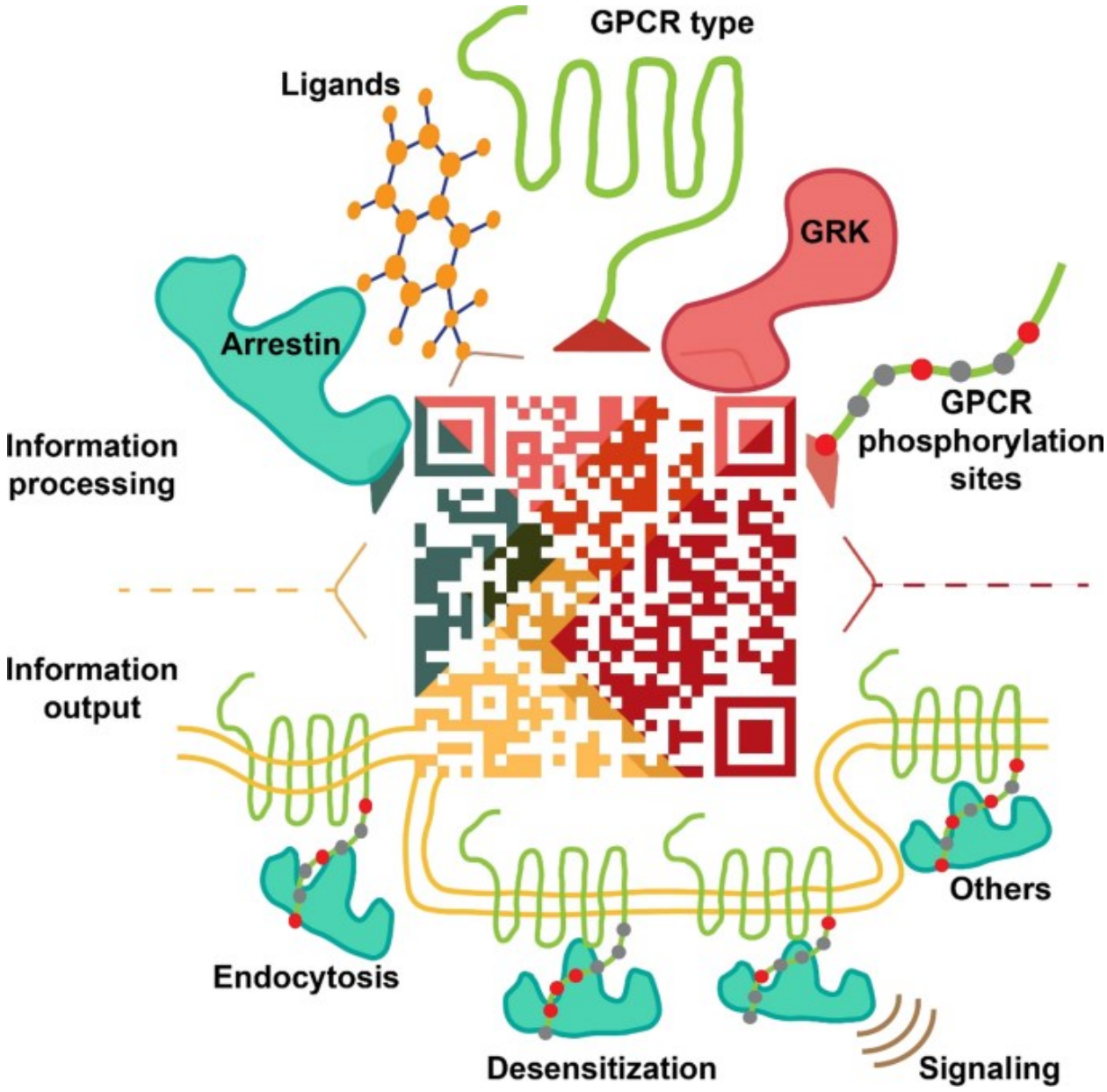

Figure 1.4 Overview of the QR Code Model for GPCR Phosphorylation Recognition (taken from Chen et al. 2022)

Various elements—such as ligands, GPCR types, GRK, arrestin, phosphorylation sites on GPCRs, and other factors—interact to influence the outcomes for phosphorylated receptors. These outcomes can include receptor desensitization, endocytosis, continued signal transmission, or other functional responses.

Studies using HEK293 cells with various GRK knockouts, including single, double, triple, and quadruple knockouts, have underscored the critical roles of GRK2 and GRK3 in facilitating β-arrestin recruitment and receptor internalization for a range of GPCRs, such as the μ-opioid receptor (μ-OR) and D2 dopamine receptor (D2R). For example, cells deficient in GRK2/3 exhibit a marked reduction in β-arrestin2 recruitment and μ-OR internalization, with GRK2 demonstrating a more prominent role than GRK3 (Møller et al., 2020). Similarly, GRK2/3 were found to be essential for maximal agonist-stimulated D2R-β-arrestin interactions, although intriguingly, their kinase activities appear unnecessary, suggesting a non-catalytic, scaffolding role for GRK2 (Sánchez-Soto et al., 2023). Further research has revealed that the interaction between GRK2/3 and G protein βγ-subunits was shown to be critical for β-arrestin2 binding to various GPCRs (Matthees et al., 2024). Interestingly, some GPCRs, such as the chemokine receptor CXCR5, exhibited β-arrestin recruitment and signaling that were dependent on GRK2/3 but independent of receptor phosphorylation, indicating the presence of non-canonical regulatory mechanisms (Crecelius et al., 2024). Furthermore, the creation of combinatorial GRK knockout cell lines has enabled the differentiation of GPCRs into subsets regulated by either GRK2/3 or GRK2/3/5/6, offering insights into the specific roles of different GRKs in GPCR regulation (Drube et al., 2021).

From a broader biological context, the pathological role and therapeutic potential of GRKs has been previously documented. For example, elevated levels of GRK2 and GRK5, for instance, are associated with heart diseases and contribute to the progression of heart failure through their actions in different cellular compartments. Conversely, reducing or inhibiting GRK2 and GRK5 has demonstrated cardioprotective effects, positioning them as promising targets for the development of new treatments for heart failure (Kayki-Mutlu and Koch, 2023).

5.2 Regulators and Activators of G-Protein Signaling (RGS and AGS Proteins)

Activators of G-protein signaling (AGS) and regulators of G-protein signaling (RGS) proteins, though serving different functions, are two sides of the same coin in the modulation of GPCR signaling pathways. AGS proteins, such as AGS3, modulate G-protein signaling independently of GPCRs by acting as guanine nucleotide dissociation inhibitors (GDIs), binding to Gα subunits and thus regulating the release of Gβγ subunits, which in turn influences downstream signaling cascades (Vural and Lanier, 2020; Thotamune et al., 2024). AGS proteins have been implicated in

diverse cellular functions, including asymmetric cell division and membrane protein trafficking, and are expressed in various tissues, including the kidney, where they contribute to blood pressure regulation and endocrine hormone synthesis (Park, 2021).

Conversely, RGS proteins serve as GTPase-activating proteins (GAPs) that accelerate the hydrolysis of GTP on Gα subunits, effectively terminating GPCR signaling. This canonical function is complemented by additional roles in modulating signal transduction through various mechanisms. RGS proteins are categorized into four families—R4, R7, R12, and RZ—based on sequence homology and domain structure, with each family exhibiting specificity towards different Gα subunits (Alqinyah et al., 2019). The involvement of RGS proteins in metabolic functions, such as insulin secretion and insulin resistance, highlights their potential as therapeutic targets for conditions like type 2 diabetes mellitus (T2DM) (McNeill and Zhao, 2023). The mammalian RGS protein superfamily also contributes markedly to physiological regulation of cardiovascular GPCRs. For example, RGS18 is involved in platelet activation by GPCR agonists like thromboxane A2 via prostanoid TP receptors, which stimulate the association of 14-3-3 proteins with RGS18. Similarly, RGS2 is involved in vascular contraction regulation, particularly through the modulation of angiotensin receptors, where it blocks Gαq signaling from AT1R receptors in vascular smooth muscle cells (Lymperopoulos et al., 2022). Furthermore, RGS proteins have been shown to modulate the efficacy of opioid analgesics and are involved in the neural mechanisms underlying addiction and analgesia, suggesting their potential in developing new therapeutic strategies for pain management and addiction treatment (Sakloth et al., 2020). Their role in depression and the action of antidepressants further highlights their significance in neuropsychiatric disorders, affecting both the efficacy of existing treatments and the possibility for new therapeutic approaches (Senese et al., 2018).

5.3 Spatial Regulation of GPCR Signaling

GPCRs, traditionally understood to signal primarily from the plasma membrane, are now recognized to initiate signaling from various intracellular compartments, including endosomes, the Golgi apparatus, and the nucleus, thereby contributing to a wide array of physiological outcomes (Crilly and Puthenveedu, 2021). For instance, opioid receptors (ORs) activated within the Golgi apparatus exhibit distinct downstream effects on transcription and protein phosphorylation

compared to those activated at the plasma membrane, highlighting the role of the lipid environment in location-selective coupling (Radoux-Mergault et al., 2023). The spatial positioning of endosomes, particularly their proximity to the nucleus, has been shown to be crucial for the initiation of cAMP-dependent transcriptional responses, with endosome distance from the nucleus inhibiting these responses due to enhanced phosphodiesterase activity around the plasma membrane (Willette et al., 2023). This spatial encoding of GPCR signaling is further modulated by the dynamic trafficking of receptors, which can alter signaling outcomes through mechanisms such as clathrin-mediated endocytosis and β-arrestin scaffolding (Weinberg and Puthenveedu, 2019). Additionally, the spatial organization within the endomembrane system, encompassing distinct endocytic and exocytic pathways, possess a central role in regulating GPCR signaling, particularly in contexts such as reproduction and pregnancy where cyclical changes in the extracellular environment necessitate precise spatial control of signaling (West and Hanyaloglu, 2015).

5.4 Mechanisms of Desensitization

Desensitization of GPCRs typically involves the phosphorylation of activated receptors by GPCR kinases (GRKs), enhancing their affinity for arrestins, and thus leading to receptor uncoupling from G proteins and subsequent internalization (Sun and Kim, 2021). This canonical mechanism, wherein GRKs phosphorylate serine/threonine residues on the receptors, is well-documented and promotes β-arrestin binding and receptor internalization via clathrin-coated pits. However, GRKs extend their influence beyond this traditional role; they are also involved in β-arrestin-mediated signaling pathways and can phosphorylate non-GPCR substrates, thereby affecting various physiological processes such as cell motility and inflammation (Watari et al., 2014). Interestingly, desensitization can occur through phosphorylation-independent mechanisms, as seen with the β3-adrenergic receptor (β3AR), where GRK2 mediates desensitization via its regulator of G protein signaling (RGS) homology domain rather than its kinase activity; this example illustrates the versatility of GRKs in modulating GPCR function (Echeverría et al., 2020). Furthermore, desensitization mechanisms can be categorized into homologous and heterologous types. Homologous desensitization involves GRK-mediated phosphorylation and β-arrestin recruitment, while heterologous desensitization involves phosphorylation by other kinases like PKC, which can also lead to receptor internalization and desensitization (Carmona-Rosas et al., 2019).

The rapid desensitization of GPCRs, occurring within seconds, is a critical aspect of this regulatory process, with GRK2 and GRK3 playing significant roles by directly interacting with Gq proteins, independent of their kinase activity (Carman et al., 1999). Moreover, the desensitization of GPCRs is not limited to the plasma membrane; it can also involve nuclear trafficking, as seen in the desensitization of dopamine D2-like receptors and β2-adrenoceptors, where arrestin de-ubiquitination and nuclear translocation are crucial (Min et al., 2023). The interplay between GRKs and second messenger-dependent protein kinases introduces another layer of complexity, as different agonists can stabilize distinct receptor conformations that undergo unique desensitization pathways, exemplified by the μ-opioid receptor (Kelly et al., 2008). Additionally, the process of resensitization, whereby desensitized receptors are dephosphorylated and recycled back to the cell membrane, is an essential yet underexplored aspect of GPCR regulation. This dynamic regulation ensures that GPCRs can respond appropriately to continuous or repeated stimuli, maintaining cellular homeostasis. (Gupta et al., 2018).

Collectively, the multifaceted nature of GPCR desensitization involves a range of mechanisms and regulatory proteins that ensure precise control over receptor signaling and cellular responses.

6. Trafficking of GPCRs

6.1 Endocytosis and Internalization

Endocytosis is a multifaceted process that regulates receptor signaling and cellular responsiveness. Traditionally, endocytosis of GPCRs has been understood to occur predominantly via clathrin-mediated pathways, wherein arrestins bind to phosphorylated receptors and recruit them to clathrin-coated pits for internalization. For example, the serotonin1A receptor predominantly undergoes clathrin-mediated endocytosis and recycles back to the plasma membrane via recycling endosomes, a focal pathway given its role in neuropsychiatric disorders (Kumar et al., 2019). This process is heavily influenced by the lipid order of the plasma membrane and the presence of specific cargo, as demonstrated with the β2-adrenergic receptor (β2-AR) (Kumar and Puthenveedu, 2023). However, recent studies have revealed that GPCRs can also internalize via alternative pathways, such as caveolae-dependent and fast endophilin-mediated endocytosis (FEME), underscoring the diversity of mechanisms involved; these processes are depicted in **Figure 1.5** (Moo et al., 2021). Endocytosis is not merely a mechanism to terminate signaling, but

also allows receptors to signal from intracellular compartments, such as endosomes, thereby initiating unique cellular responses distinct from those at the plasma membrane (Jang et al., 2024). For instance, the β2-AR can mediate transcriptional reprogramming via cyclic AMP (cAMP) production from early endosomes, a process that is modulated by the spatial positioning of endosomes within the cell (Fu and Xiang, 2015). The involvement of small GTP-binding proteins and post-translational modifications further adds layers of regulation to GPCR endocytosis, ensuring precise control over receptor function (Zhang and Kim, 2017). The intracellular distribution and trafficking of endogenous G proteins are also critical, with these proteins being present on various endosomal compartments, including early, late, and recycling endosomes, but less abundant on other organelles like the endoplasmic reticulum and mitochondria; this distribution is crucial for the sustained signaling of internalized GPCRs (Jang et al., 2024). Advanced techniques, such as the use of HaloTag for monitoring GPCR internalization and whole-cell ELISA for measuring surface expression, have been developed to study the spatiotemporal dynamics of GPCR signaling and endocytosis, providing deeper insights into the regulatory mechanisms at play (Pandey et al., 2019; Kumagai et al., 2015). Additionally, viral GPCRs (vGPCRs) encoded by herpesviruses viruses like Hepatitis C exploit host cell endocytic pathways, including clathrin-mediated endocytosis, to facilitate entry, infection, immune evasion, and viral dissemination. Constitutive internalization is also a key feature for some vGPCRs like the human cytomegalovirus (HCMV)-encoded US28 receptor, which draws attention to the importance of GPCR endocytosis in various biological contexts (Mavri et al., 2020). To elaborate, the HCMV US28 receptor can scavenge Gαi proteins and impair the function of the host CXCR4 chemokine receptor, disrupting immune cell signaling and trafficking (Lee et al., 2017).

Traditionally, GPCR internalization was viewed as a pathway leading to receptor desensitization, downregulation, recycling and resensitization, but recent studies have revealed that internalized GPCRs can also initiate distinct intracellular signaling cascades, adding a new dimension to our understanding of receptor function (Tang et al., 2022). The internalization process is often mediated by β-arrestins, which not only facilitate receptor endocytosis but also serve as scaffolds for signaling complexes, thereby enabling a “second wave” of signaling from endosomes and other intracellular compartments (Wanka et al., 2022; Foster and Bräuner-Osborne, 2018). While this β-arrestin-dependent internalization is well-documented for class A GPCRs, class C GPCRs, such

as the calcium-sensing receptor (CaSR), also exhibit β-arrestin-dependent internalization, albeit through unique regulatory mechanisms (Mos et al., 2019). GPCR internalization is not solely reliant on β-arrestins; alternative pathways, such as redox-dependent alternative internalization, have been identified, particularly for receptors with low β-arrestin sensitivity like the purinergic P2Y6 receptor (Nishiyama et al., 2022). Interestingly, some GPCRs undergo constitutive internalization, which can be as significant as agonist-induced internalization and is particularly observed with Gq-coupled receptors (Hendrik Schmidt et al., 2020). Moreover, the internalization and subsequent intracellular trafficking of GPCRs to compartments like the trans-Golgi network can activate localized signaling pathways, such as the cAMP/PKA pathway, which are essential for specific cellular responses like CREB phosphorylation and gene transcription (Godbole et al., 2017). Advanced imaging techniques, including near-infrared probes and real-time fluorescence resonance energy transfer (FRET)-based assays, have been developed to monitor GPCR internalization, providing valuable tools for drug discovery and the identification of ligands for orphan receptors (Lesiak et al., 2020). The development of novel assays, such as those based on DnaE intein-mediated reconstitution of luciferase fragments, has enhanced the ability to quantitatively analyze GPCR internalization, making the process more accessible and cost-effective for research and therapeutic applications (Lu et al., 2016).

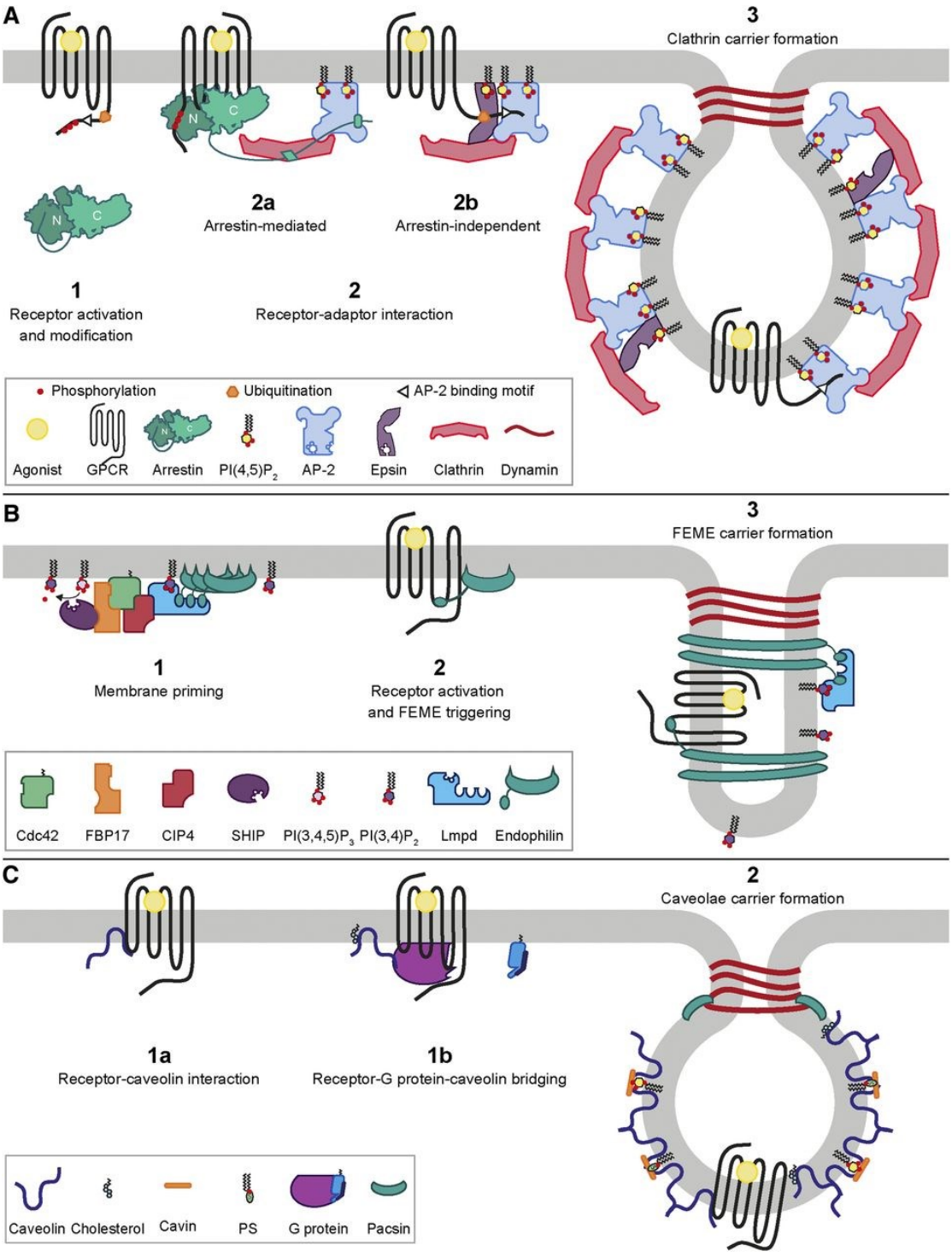
A
3
Clathrin carrier formation
N
C
2a
Arrestin-mediated
2b
Arrestin-independent
1
Receptor activation
and modification
2
Receptor-adaptor interaction
Phosphorylation
Ubiquitination
AP-2 binding motif
Agonist
GPCR
Arrestin
PI(4,5)P2
AP-2
Epsin
Clathrin
Dynamin
B
3
FEME carrier formation
1
Membrane priming
2
Receptor activation
and FEME triggering
Cdc42
FBP17
CIP4
SHIP
PI(3,4,5)P3
PI(3,4)P2
Lmpd
Endophilin
C
2
Caveolae carrier formation
1a
Receptor-caveolin interaction
1b
Receptor-G protein-caveolin bridging
Caveolin
Cholesterol
Cavin
PS
G protein
Pacsin

Figure 1.5 Endocytosis mechanisms involved in GPCR internalization (taken from Moo et al. 2015)

(A) Clathrin-mediated endocytosis of GPCRs: 1) Activation of the receptor by a ligand induces conformational changes, such as the exposure of AP-2 binding motifs on the receptor's C-terminal tail or post-translational modifications like phosphorylation or ubiquitination. 2a) The majority of GPCRs are directed to clathrin-coated pits via arrestins, where the binding of arrestin to the phosphorylated receptor C-tail facilitates the interaction between the arrestin C-tail, AP-2, and clathrin. 2b) Alternatively, receptors may be recruited to clathrin-coated pits independently of arrestins through direct interaction with AP-2 or by binding their polyubiquitinated C-tails to epsins. 3) Clathrin is attracted to the plasma membrane by adaptor proteins such as AP-2 and epsins, which collaborate to form clathrin carriers. This process is completed when dynamin separates the clathrin-coated pits from the plasma membrane.

(B) Fast endophilin-mediated endocytosis (FEME): 1) Endophilin accumulates at the plasma membrane through interaction with lamellipodin (Lmpd), a process dependent on the sequential actions of Cdc42, FBP17, CIP4, and SHIP 1/2. 2) The interaction between an activated GPCR and endophilin initiates FEME. 3) FEME carriers are created when endophilin-stabilized invaginations are separated from the membrane by dynamin.

(C) Caveolae-mediated endocytosis: GPCRs may be recruited to caveolae through direct interaction with caveolin (1a) or via Gαq-mediated interaction with caveolin (1b). Caveolae structures consist of oligomeric caveolin complexes stabilized by cavins and pacsins, which induce membrane curvature. The formation of caveolae carriers is dependent on dynamin to sever the membrane.

6.2 GPCR Recycling

GPCRs undergo a complex recycling process that is vital for maintaining cellular responsiveness and signaling fidelity, as it not only determines receptor availability at the cell surface but also influences downstream signaling pathways and cellular responses (Leslie, 2016). Upon activation by agonists, GPCRs are internalized from the plasma membrane into endosomes, where they face a critical sorting decision: to be recycled back to the cell surface or directed towards lysosomal degradation (Koenig, 2004). This sorting is tightly regulated by specific sequences on the receptors and interacting proteins, distinguishing GPCR recycling from the bulk recycling of other proteins (Bowman and Puthenveedu, 2015). For instance, mu opioid receptor recycling is dynamically regulated by a signaling pathway involving Gβγ, phospholipase C, and protein kinase C, which modulates receptor phosphorylation and endosomal localization (Kunselman et al., 2019). Similarly, β2-AR can switch between sequence-dependent and bulk recycling pathways based on extracellular signals, a process mediated by protein kinase A phosphorylation (Vistein and Puthenveedu, 2013). This sequence-dependent recycling is essential for the spatial encoding of GPCR signaling, as demonstrated by β2-AR's activation of Gαs exclusively in actin/sorting nexin/retromer tubula microdomains within endosomes (Bowman et al., 2016). Additionally, the endothelin receptor type A utilizes a carboxyl-terminal recycling motif that adopts a β-finger conformation, acting as an internal PDZ ligand to facilitate recycling (Paasche et al., 2005). Moreover, the concept of constitutive recycling has been previously described, as exemplified by the delta opioid receptor; its weak expression at the neuronal plasma membrane is regulated by Rab5 and Rab4, which mediate its endocytosis and recycling, respectively (Gendron et al., 2023).

7. Protein-Protein Interactions in GPCR Signaling Networks

7.1 GPCR-Interacting Proteins and the Cytoplasmic Interactome

While GPCRs are integral to numerous physiological processes, they are modulated by a variety of interacting proteins, including PDZ domain-containing proteins and non-PDZ proteins, several examples of which are presented in **Table 1.2**.

PDZ domains, which are modular protein-protein interaction modules, typically recognize short C-terminal sequences of target proteins, facilitating the assembly of macromolecular complexes that regulate various cellular functions (Lee and Zheng, 2010). For instance, the GPCR ADGRV1

interacts with the multi-PDZ protein PDZD7, which is critical for the formation and function of stereocilia in inner ear hair cells. This interaction is mediated by binding of the two N-terminal PDZ domains of PDZD7 to the C-terminal PDZ binding motif of ADGRV1, and mutations in these domains can lead to deafness (Colcombet-Cazenave et al., 2022). Other PDZ proteins such as PSD-95, DlgA, and ZO-1 are known to scaffold GPCRs and other membrane proteins, thereby organizing intracellular signaling machinery and influencing receptor internalization, trafficking, and recycling (Romero et al., 2011). For example, the chemokine receptor CXCR2, four of the somatostatin receptors (SSTRs) and the neuropeptide Y receptor Y2 have been shown to interact with PSD-95, highlighting the broad range of GPCR-PDZ interactions (Møller et al., 2013). Additionally, PDZ proteins like NHERF1 regulate GPCR localization and signaling by clustering receptors such as PTH1R and Fzd, which can lead to diverse signaling outcomes, including G-protein switching and the formation of signaling complexes (Wheeler et al., 2007, 2011). The PrRP receptor also interacts with PDZ domain proteins like GRIP, ABP, and PICK1, which are known to interact with AMPA receptors, suggesting that these interactions could scaffold GPCRs and AMPA receptors together at the synapse (Lin et al., 2001).

GPCRs engage with a diverse array of non-PDZ proteins, each fulfilling purposes towards modulating their signaling, trafficking, and overall function (Walther and Ferguson, 2015). Among these, the 14-3-3 family stands out as a significant group of signal adaptors, known for binding to phosphoserine or phosphothreonine residues on target proteins. These adaptor proteins regulate GPCR trafficking and signaling by either enhancing or inhibiting receptor functions depending on the specific cellular context. For example, 14-3-3 proteins can influence GPCR trafficking by promoting receptor endocytosis or by stabilizing receptors at the cell membrane, thereby affecting the receptor's availability and responsiveness to ligands (Yuan et al., 2019). Furthermore, 14-3-3 proteins have been shown to interact with other key signaling molecules such as Raf-1, extending their role in the broader landscape of GPCR-mediated signal transduction (Li et al., 2016). Another critical non-PDZ protein is the A-kinase anchoring protein (AKAP), which acts as a scaffold, organizing various signaling molecules, including protein kinases and phosphatases, in close proximity to GPCRs. This spatial organization facilitates efficient signal transduction and the fine-tuning of cellular responses. AKAPs, such as AKAP79 and AKAP250, are known to interact with GPCRs like the beta2-adrenergic receptor, orchestrating intricate signaling networks that also

involve interactions with the cytoskeleton and other membrane-associated proteins (Malbon et al., 2004). The Janus kinase 2 (JAK2) is yet another non-PDZ protein that interacts with GPCRs, with previous studies demonstrating that the regulation of Jak/STAT signaling by AT1R relies on its direct interaction with the tyrosine kinase JAK2 (Ali et al., 2000). Additionally, although not part of the cytoplasmic environment, receptor activity-modifying proteins (RAMPs) are single-transmembrane span proteins that also interact with GPCRs, modulating their trafficking, ligand selectivity, and signaling; these interactions are particularly well-documented in class B GPCRs, such as the calcitonin receptor-like (CLR) receptor (Kotliar et al., 2023).

Scaffold Protein	GPCR	Effect
Non-PDZ Proteins		
AKAP79	β_2AR	Phosphorylation ↓
AKAP250	β_2AR	Association with PKA ↑
	β_1AR	Receptor recycling ↑
AKAP5	GPR30	cAMP accumulation ↓
Jak2	AT1R	STAT phosphorylation ↑
14-3-3	FSHR	cAMP accumulation ↓
	PAR4	Plasma membrane transport and signaling ↑
	α_2AR	Ras/Raf signaling ↑
	GPR15	Stability and cell surface expression ↑
PDZ Proteins		
PIST (CAL; GOPC)	mGluR1a	ERK activation ↓
NHERF2	mGluR5	Ca^{2+} signaling ↑
GIPC	β_1AR	ERK activation ↓
MAGI-3		ERK activation ↓
SAP-97		PKA-mediated receptor phosphorylation ↑
PIST		ERK activation ↓
SNX27	β_2AR	Receptor recycling ↑
MAGI-3		ERK activation ↓
NHERF1		Plasma membrane recycling ↑
SNX27	α_2AR	Functional resensitization ↑
Spinophilin		Cell surface expression ↑, phosphorylation ↓, MAPK signaling ↓, Ca^{2+} signaling
MAGI-3	LPA2	ERK activation ↑, ρ activation ↑
NHERF2		Interaction with PLCβ3 ↑, IP3 signaling ↑, ERK activation ↑
MUPP-1	MT1R	Coupling with Gi protein ↑, inhibition of adenylyl cyclase activity ↑
NHERF1 (EBP50)	PTH1R	Coupling to and activation of Gq protein ↑, interaction with β-arrestin-2 ↓, desensitization ↓, cAMP signaling ↑
NHERF2		Interaction with and activation of PLCβ ↑, adenylyl cyclase activity through stimulation of Gi/o proteins
PSD-95	D1R	cAMP signaling ↓
GIPC	D2R	G protein coupling↓
Spinophilin		Signaling ↑

NHERF2	P2Y1R	Interaction with PLCβ ↑, agonist-induced Ca^{2+} signaling ↑
PDS-95	5-HT_{2A}R	IP3 signaling ↑
PDZK1/NHERF3		IP3 signaling ↑
SAP97		IP3 signaling ↑, ERK activation ↑
SAP97/PSD-95	GPR30	cAMP signaling ↓
PDZK1/NHERF3	SSTR5	Interaction with PLCβ3 ↑
PIST (CAL, GOPC)		Trafficking, cell surface expression ↓
SNX27	CRFR1	Receptor recycling ↑
PDZK1/NHERF3		ERK activation ↑
SAP97		ERK activation ↑
GIPC	LHR	ERK activation ↑
PICK1	GHRHR	Cell surface expression ↑, cAMP signaling ↓
Spinophilin	M3R	Signaling ↓
Spinophilin	μ-OR	Endocytosis ↑
PDZK1/NHERF4	IP	Cell surface expression ↑, cAMP signaling ↑

Table 1.2 Examples of Interactions Between GPCRs and PDZ or Non-PDZ Scaffolds (adapted from Dunn and Ferguson, 2015).

7.2 Functional Selectivity

Functional selectivity, also known as biased agonism, is a phenomenon where different ligands binding to the same GPCR can stabilize distinct receptor conformations, thereby selectively activating specific signaling pathways over others. This concept holds profound implications for therapeutic interventions, as it allows for the development of ligands that can selectively activate beneficial signaling pathways while avoiding those associated with adverse side effects. Biased agonists that exhibit functional selectivity towards specific G proteins or β-arrestins are significant pharmacological advancements, with many having progressed to the later phases of clinical development (Wisler et al., 2018). For instance, the study by Cong et al. provides critical insights into how opioid ligands selectively activate the G protein over the β-arrestin pathways through the μ-opioid receptor (μOR), highlighting the dynamic allosteric communications between the ligand-binding pocket and the receptor intracellular domains (Cong et al., 2021). The therapeutic promise of biased ligands is exemplified by a β2-adrenergic receptor agonist that favors Gs coupling over β-arrestin binding, which could lead to novel treatments for obstructive lung diseases (Kim et al., 2022). Interestingly, it has been posited that functional selectivity is involved in mammalian olfactory signal transduction, suggesting that olfactory receptors may also exhibit biased signaling, which could serve as a mechanistic basis for signal integration in olfactory receptor neurons (Ache, 2020).

Several parameters define GPCR signaling, including the proteins that mediate and regulate receptor signaling, the duration of these interactions, and their intracellular localization. These facets of receptor function can vary significantly depending on the activating ligand, contributing to biased signaling (Fernandez et al., 2020). Notably, the concept of “location bias”, where GPCRs can initiate signaling from intracellular membranes, such as the Golgi apparatus, adds another layer of complexity to functional selectivity (Irannejad et al., 2017). Moreover, biased agonism can be variable depending on cell type and experimental constraints, introducing the notion of "biased receptor functionality" to describe differential signaling even with a single agonist (Franco et al., 2018). Further studies have aimed to elucidate the role of specific GPCR domains in contributing to observed biased agonism, which is crucial for understanding functional selectivity at a structural level; for instance, OptoGPCR chimeras have been utilized to identify which domains steer G-protein selectivity, such as the proximal C-terminus and intracellular loop 3.

These chimeric proteins combine elements of light-sensitive opsins with the intracellular signaling domains of GPCRs, allowing for precise control over receptor activity using light, and thus enabling researchers to investigate the dynamics of GPCR signaling in real-time and in specific cellular contexts (Leemann and Kleinlogel, 2023).

7.3 Impact of Differential Tissue Expression of GPCRs and Interacting Proteins

The differential tissue expression of GPCRs and their protein interactors is a critical area of research, influencing cellular responses and consequently, the identification of potential therapeutic targets. The tissue-specific expression of GPCRs and their associated interacting proteins, such as G proteins, GPCR kinases (GRKs), and β-arrestins, are fundamental to their functional regulation and have profound implications for disease mechanisms, including those underlying cancer and neurological disorders (Feigin, 2013; Matthees et al., 2021). High-throughput studies have unveiled considerable variability in GPCR expression across different tissues. For instance, certain GPCRs are uniquely expressed in white and brown adipose tissues, with their expression being altered during adipogenic differentiation and in conditions such as obesity and diabetes (Al Mahri et al., 2023). The construction of tissue-specific interactomes has proven invaluable in identifying drug targets and elucidating disease mechanisms, particularly in neurodegenerative conditions such as Alzheimer's and Parkinson's diseases (Mohammadi and Grama, 2016). In the context of cancer, GPCRs are significantly overrepresented among coding genes with elevated expression in solid tumors, as well as their mRNA signatures correlating with cancer-related pathways, underscoring their potential roles as oncogenes, biomarkers, and therapeutic targets (Wu et al., 2019). The generation of functionally diverse GPCR isoforms, which exhibit distinct signaling properties and tissue-specific expression, adds another layer of complexity to the nuanced landscape of GPCR signaling and drug responses (Prasad et al., 2013). Integrative analyses of genome-wide expression datasets, protein-protein interactions, and functional pathways have highlighted the importance of tissue-specific GPCR signaling; interestingly, only a limited number of GPCRs are expressed in each tissue, where they couple with different G-proteins or β-arrestins to initiate the specific yet broad range of downstream pathways (Hao and Tatonetti, 2016). Moreover, GPCR-interacting proteins (GIPs) are active throughout all stages of the life cycle of GPCRs, facilitating proper folding, targeting to subcellular

compartments, and executing signaling functions, with differential expression of GIPs providing a means to regulate GPCR function in a tissue-specific manner (Maurice et al., 2011).

8. Methodologies for Detection and Characterization of GPCR-Protein Interactions

The study of PPIs involving GPCRs has made substantial strides, driven by the development of various advanced tools and techniques that have significantly enhanced drug discovery and physiological research. Widely-used traditional techniques for identifying protein partners, measuring binding affinity, and characterizing complex structures include yeast two-hybrid analysis, affinity purification mass spectrometry, isothermal titration calorimetry and radiometric assays, have been foundational for the field (Walport et al., 2021). However, the need for high-throughput, sensitive, and special-purpose assays has led to the adoption of newer techniques such as cryo-electron microscopy (cryo-EM), Förster Resonance Energy Transfer (FRET), Bioluminescence Resonance Energy Transfer (BRET), and molecular dynamics simulations, which have gained prominence for their efficiency, cost-effectiveness, and enhanced sensitivity.

Systems based on luminescence or fluorescence, such as those illustrated in **Figure 1.6,** have proven especially effective in cell-based models for *in vitro* studies (Lee, 2011). Techniques such as the Protein-fragment Complementation Assay (PCA), utilizing Renilla Luciferase (Rluc), have been employed to study PPIs in real-time across different model systems, including cancer cells and zebrafish embryos, demonstrating the versatility and sensitivity of these assays (Röck et al., 2015). Techniques like FRET and BRET have become pivotal in analyzing GPCR interactions with various signaling partners, providing insights into the complex signaling pathways that extend beyond classical G-protein-mediated second messenger generation (Guo et al., 2022). Transcriptional assays, including yeast two-hybrid, split ubiquitin, and Tango, convert transient PPIs into stable transgene expression, though they often suffer from high background noise and loss of PPI dynamics. To address these limitations, optimized and advanced methods like PPI-FLARE, which integrates light-gated transcriptional system with high temporal resolution, have been developed to provide more accurate and comprehensive insights (Kim et al., 2017). Additionally, the split-TEV assay, which monitors GPCR activation through β-arrestin 2 recruitment, offers high sensitivity and flexibility across different cell types (Galinski et al., 2018).

Importantly, high-throughput screening (HTS) technologies have revolutionized GPCR drug discovery by enabling the cost-effective screening of large compound libraries (Zhang and Xie, 2012). Computational tools also play a supportive part in studying the interface features that govern protein interactions, with various software aiding in the prediction of physicochemical characteristics, binding sites, and hotspot residues (Schreiber, 2021), and the application of deep learning in PPI analysis is another burgeoning area, with recent advancements used for decrypting biological system dynamics (Chakraborty et al., 2021; Lee, 2023).

8.1 Real Time and Static Endpoint Reporter Assays

Both real-time techniques and static endpoint reporter assays are integral to the study of GPCR-protein interactions, each offering distinct advantages and limitations that make them complementary in the broader context of GPCR research. Real-time techniques, such as the NanoBiT assay, enable continuous monitoring of ligand binding, receptor internalization, and β-arrestin recruitment in living cells, providing dynamic insights into GPCR pharmacology at endogenous expression levels (Edenson, 2020). Similarly, genetically encoded fluorescent biosensors enable the real-time detection of second messengers like cAMP, diacylglycerol (DAG), and Ca2+, offering a temporal resolution that static assays cannot achieve (Tewson et al., 2012). Additionally, optogenetic methods afford precise spatiotemporal control of GPCR signaling pathways, facilitating real-time imaging of downstream effectors such as Gβγ translocation and PIP2 hydrolysis (Meshik and Gautam, 2021).

In contrast, static endpoint assays, including those using radiolabeled GTP analogs or luciferase-based reporter systems, provide valuable data on GPCR-protein interactions and gene transcription modulation, albeit with inherent limitations in capturing dynamic changes (Höring et al., 2020; Azimzadeh et al., 2017). One widely-used method for assessing GPCR activation is the GTPγS binding assay, which measures the binding of a non-hydrolyzable GTP analogue to G proteins, thereby providing a direct readout of GPCR activation. This assay is particularly advantageous due to its simplicity and the flexibility to utilize either radiolabeled ([35S]GTPγS) or non-radioactive (Eu-GTPγS) analogues (Strange, 2010). Another commonly employed endpoint assay is the measurement of intracellular cAMP levels, which serve as indicators of Gs or Gi pathway activation. Techniques such as the GloSensor cAMP assay employ luminescent readouts to

quantify cAMP, offering high sensitivity and adaptability to automated systems, which is especially beneficial for large-scale studies (Wang et al., 2004). In addition to cAMP assays, inositol phosphate accumulation assays are frequently used to monitor Gq-coupled receptor activity by measuring the production of inositol phosphates, key second messengers in the phosphoinositide signaling pathway. These assays often utilize radiolabeled inositol or fluorescent biosensors to detect fluctuations in inositol phosphate levels (Zhang and Xie, 2012). Radioligand binding assays, including saturation, competition, and kinetic binding assays, are essential tools for determining GPCR expression levels, ligand affinity, and receptor-ligand interaction dynamics (Flanagan, 2016). Furthermore, lesser-used noninvasive, label-free assays based on cell-electrode impedance offer a static yet sensitive method to assess GPCR function by measuring changes in cellular morphology, although they lack the temporal resolution of real-time techniques (Yu et al., 2005).

In sum, while real-time techniques offer unparalleled insights into the temporal dynamics of GPCR signaling, static endpoint assays remain valuable for their simplicity and ability to provide specific, quantifiable readouts, making both approaches indispensable in the field of GPCR pharmacology.

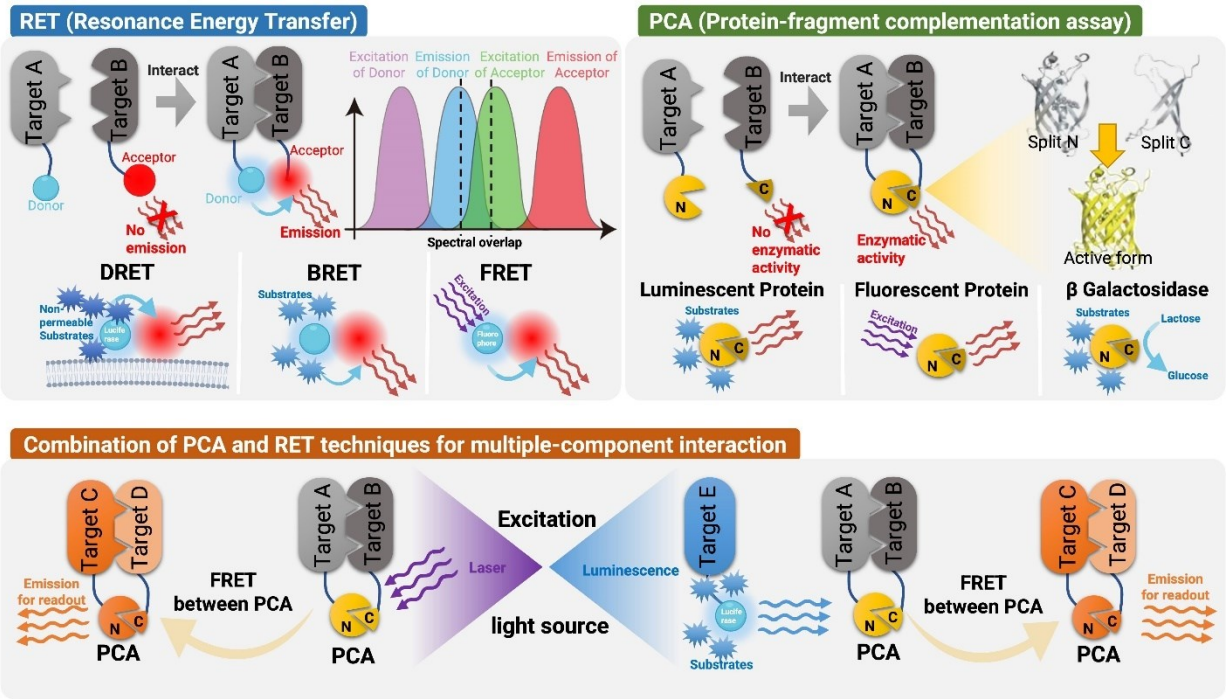

Figure 1.6 Various detection methods used to study GPCR signaling and their spatial distribution (taken from Chen and Obal, 2023).

Resonance energy transfer (RET) is an optical mechanism where energy is conveyed from an excited donor molecule to an acceptor molecule through dipole-dipole coupling. Two prominent forms of RET, Förster resonance energy transfer (FRET) and bioluminescence resonance energy transfer (BRET), are employed to observe biological processes. FRET involves fluorescent molecules, whereas BRET relies on bioluminescent molecules, both of which typically exhibit spectral overlap. Dark Resonance Energy Transfer (DRET) is an emerging energy transfer mechanism that serves as an alternative to traditional methods, utilizing non-fluorescent or weakly fluorescent donors, referred to as “dark donors”, and bright fluorescent acceptors. The fundamental principle behind DRET is the transfer of energy from the dark donor to the bright acceptor without the donor emitting light, minimizing issues associated with background fluorescence and emission leakage that can hinder applications in bioimaging and sensing

In protein-fragment complementation assays (PCA), a reporter protein is divided into inactive fragments, which are then attached to proteins of interest. When these fragments are brought close together, they spontaneously reassemble into an active luminescent protein, fluorescent protein, or

β-galactosidase enzyme. Additionally, combining PCA with RET has been utilized to demonstrate the interactions among multiple components.

8.1.1 Tango Assay

As a static endpoint assay, the Tango assay, as depicted in **Figure 1.7**, stands out as a gold-standard tool in GPCR research, offering a robust method for detecting GPCR activity through the recruitment of β-arrestin2 (Barnea et al., 2008). Unlike traditional GPCR assays that primarily focus on G protein-mediated second messenger generation, the Tango assay capitalizes on the interaction between GPCRs and β-arrestin to measure receptor activity, which can provide insights into functional selectivity. This assay has been further refined for high-throughput screening in the form of the PRESTO-Tango system, which enables the efficient examination of over 300 nonolfactory human GPCRs. Its value is particularly highlighted in its capacity to screen large compound libraries to identify novel drug candidates, which can consequently to enhance their therapeutic efficacy and minimize potential side effects. Moreover, this platform is especially important for the functional characterization and screening of orphan GPCRs, whose endogenous ligands remain unidentified, thereby broadening the scope of drug discovery (Kroeze et al., 2015). The Tango system has proven instrumental in the detailed investigation and high-throughput drug screening of several GPCRs, such as the serotonin 2C receptor (5-HT2CR), which is associated with mental disorders and metabolic abnormalities (Watanabe et al., 2016). Additionally, the application of the Tango assay has been demonstrated in model organisms like Drosophila, where it has been used to detect endogenous GPCR activity and explore physiological and behavioral functions (Katow et al., 2019). Thus, the Tango assay and its derivatives represent an indispensable tool for GPCR research, both for the characterization of GPCRs, as well as the development of targeted therapeutics.

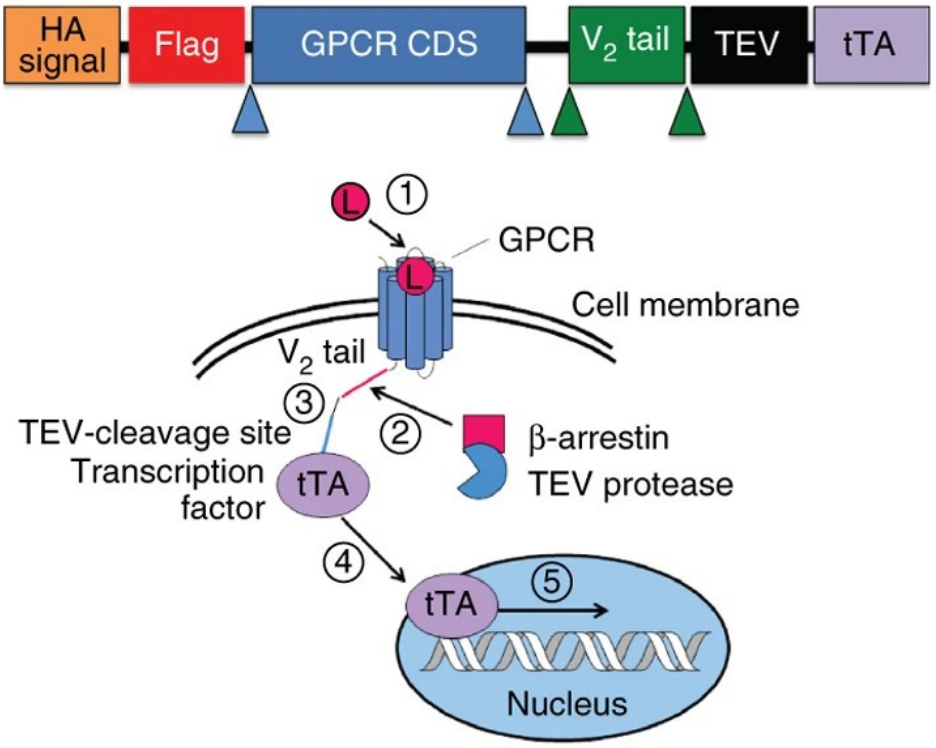

Figure 1.7 Schematic representation of the Tango assay (taken from Kroeze et al., 2015)

The top section illustrates the modular architecture of Tango constructs; the Cla I and Age I restriction sites are indicated by blue and green arrowheads, respectively. The bottom section presents a general overview of the β-arrestin recruitment assay, called Tango. In this process, activation of the GPCR by an agonist (L) (1) triggers the recruitment of β-arrestin to the receptor's C-terminus (2). Subsequently, the GPCR fusion protein is cleaved at the TEV protease cleavage site (3). This cleavage event liberates the tetracycline-controlled transactivator (tTA) transcription factor (4), which then translocates to the nucleus and induces transcription of the luciferase reporter gene (5).

9. Statement of the research problem, rationale, and objectives

Informed by a continuously emerging body of data, current proposed models of GPCR signalling and trafficking are moving beyond the canonical paradigm of ligand-induced signal transduction mediated predominantly by G-proteins and β-arrestin-2. Indeed, the varied outcomes of GPCR activation are finely regulated by a number of elements, including GPCR-interacting proteins (e.g., AKAPs, NHERF1/2, SAP97, PICK1, etc.), isoform diversity (e.g., β-arrestin-1 versus β-arrestin-2, the seven 14-3-3 isoforms), as well as GPCR phosphorylation patterns catalyzed by protein kinases (e.g., AKTs, CK1/2, PKCs, etc.). Moreover, another underexplored source contributing to the pleiotropic signalling of GPCRs emerges from constitutive or basal receptor activity in the absence of ligand stimulation. Thus, to advance our understanding of GPCR signalling and to elucidate the aforementioned components, the development of comprehensive cellular assays and intracellular tools is fundamental, as they reveal valuable information pertaining to the protein identities, their relative abundance, and subcellular localization during dynamic GPCR-protein interactions.

As such, this work has the overall goal of characterizing proximal GPCR-protein interactions at a GPCRome scale, which will be accomplished through the construction of cell-based high-throughput assays to track previously-documented, albeit lesser-studied, GIP interactions and GPCR trafficking, and a multipurpose intracellular biosensor (viz. nanobody) to probe receptor interactomes. It is hypothesized that functional signatures of GPCR activities (e.g., recruitment/dissociation of GPCR-interacting proteins, GPCR internalization, isoform selectivity) will correlate with distinct pharmacological profiles observed between different receptors.

The following two projects will be carried out to address this overarching goal:

Project 1 - Expanding the Tango toolbox: Development of polyvalent platforms for profiling constitutive and ligand-induced GPCR activities.

Specific Aims: Functionally characterize the agonist-induced and constitutive recruitment/dissociation of specific GIPs, specifically β-arrestin1, β-arrestin2, and consequent receptor internalization (Aim 1; Chapter 1), as well as the activities of 14-3-3 isoforms (Aim 2; Chapter 3) at the GPCR-ome level

Project 2 - Development of a V5-tag-directed nanobody and its implementation as an intracellular biosensor of GPCR signalling

Specific Aims: Develop and optimize an in-house V5-tag-targeted nanobody (Aim 1; Chapter 2), which can be utilized to probe proximal V5-tagged GPCR interactors using tried-and-true cellular methodologies, including Tango, BRET and NanoBiT (Aim 2; Chapter 2).

REFERENCES

Ache, B.W. (2020). Position Review: Functional Selectivity in Mammalian Olfactory Receptors. Chem. Senses *45*, 503–508.

Ali, M.S., Sayeski, P.P., and Bernstein, K.E. (2000). Jak2 acts as both a STAT1 kinase and as a molecular bridge linking STAT1 to the angiotensin II AT1 receptor. J. Biol. Chem. *275*, 15586–15593.

Allouche, S., Noble, F., and Marie, N. (2014). Opioid receptor desensitization: Mechanisms and its link to tolerance. Front. Pharmacol. *5*, 121217.

Alqinyah, M., Bodle, C., Dagher, J.B., Chakravarti, B., Choudhuri, S.P., Druey, K.M., Fisher, R.A., Gerber, K.J., Hepler, J.R., Hooks, S.B., et al. (2019). Regulators of G protein Signaling (RGS) proteins (version 2019.4) in the IUPHAR/BPS Guide to Pharmacology Database. IUPHAR/BPS Guid. to Pharmacol. CITE *2019*.

Attwood, T.K., Croning, M.D.R., and Gaulton, A. (2002). Deriving structural and functional insights from a ligand-based hierarchical classification of G protein-coupled receptors. Protein Eng. Des. Sel. *15*, 7–12.

Azimzadeh, P., Olson, J.A., and Balenga, N. (2017). Reporter gene assays for investigating GPCR signaling. Methods Cell Biol. *142*, 89–99.

Azzi, M., Charest, P.G., Angers, S., Rousseau, G., Kohout, T., Bouvier, M., and Piñeyro, G. (2003). β-arrestin-mediated activation of MAPK by inverse agonists reveals distinct active conformations for G protein-coupled receptors. Proc. Natl. Acad. Sci. U. S. A. *100*, 11406–11411.

Barnea, G., Strapps, W., Herrada, G., Berman, Y., Ong, J., Kloss, B., Axel, R., and Lee, K.J. (2008). The genetic design of signaling cascades to record receptor activation. Proc. Natl. Acad. Sci. U. S. A. *105*, 64–69.

Barros-Álvarez, X., Nwokonko, R.M., Vizurraga, A., Matzov, D., He, F., Papasergi-Scott, M.M., Robertson, M.J., Panova, O., Yardeni, E.H., Seven, A.B., et al. (2022). The tethered peptide activation mechanism of adhesion GPCRs. Nat. 2022 6047907 *604*, 757–762.

Begum, K., Mohl, J.E., Ayivor, F., Perez, E.E., and Leung, M.Y. (2020). GPCR-PEnDB: a database of protein sequences and derived features to facilitate prediction and classification of G

protein-coupled receptors. Database J. Biol. Databases Curation *2020*, 1–12.

Bilsky, E.J., Giuvelis, D., Osborn, M.D., Dersch, C.M., Xu, H., and Rothman, R.B. (2010). In Vitro and In Vivo Assessment of Mu Opioid Receptor Constitutive Activity. Methods Enzymol. *484*, 413–443.

Bowman, S.L., and Puthenveedu, M.A. (2015). Postendocytic Sorting of Adrenergic and Opioid Receptors: New Mechanisms and Functions. Prog. Mol. Biol. Transl. Sci. *132*, 189–206.

Bowman, S.L., Shiwarski, D.J., and Puthenveedu, M.A. (2016). Distinct G protein–coupled receptor recycling pathways allow spatial control of downstream G protein signaling. J. Cell Biol. *214*, 797–806.

Carman, C. V., Parent, J.L., Day, P.W., Pronin, A.N., Sternweis, P.M., Wedegaertner, P.B., Gilman, A.G., Benovic, J.L., and Kozasa, T. (1999). Selective regulation of Gα(q/11) by an RGS domain in the G protein- coupled receptor kinase, GRK2. J. Biol. Chem. *274*, 34483–34492.

Carmona-Rosas, G., Alcántara-Hernández, R., and Hernández-Espinosa, D.A. (2019). The role of β-arrestins in G protein-coupled receptor heterologous desensitization: A brief story. Methods Cell Biol. *149*, 195–204.

Chachisvilis, M., Zhang, Y.L., and Frangos, J.A. (2006). G protein-coupled receptors sense fluid shear stress in endothelial cells. Proc. Natl. Acad. Sci. U. S. A. *103*, 15463–15468.

Chakraborty, A., Mitra, S., De, D., Pal, A.J., Ghaemi, F., Ahmadian, A., and Ferrara, M. (2021). Determining Protein-Protein Interaction Using Support Vector Machine: A Review. IEEE Access *9*, 12473–12490.

Chen, H., Zhang, S., Zhang, X., and Liu, H. (2022). QR code model: a new possibility for GPCR phosphorylation recognition. Cell Commun. Signal. *20*, 23.

Colcombet-Cazenave, B., Cordier, F., Zhu, Y., Bouvier, G., Litsardaki, E., Laserre, L., Prevost, M.S., Raynal, B., Caillet-Saguy, C., and Wolff, N. (2022). Deciphering the Molecular Interaction Between the Adhesion G Protein-Coupled Receptor ADGRV1 and its PDZ-Containing Regulator PDZD7. Front. Mol. Biosci. *9*, 923740.

Cong, X., Maurel, D., Déméné, H., Vasiliauskaité-Brooks, I., Hagelberger, J., Peysson, F., Saint-

Paul, J., Golebiowski, J., Granier, S., and Sounier, R. (2021). Molecular insights into the μ-opioid receptor biased signaling. BioRxiv 2021.03.22.436421.

Crecelius, J.M., Manz, A.R., Benzow, S., and Marchese, A. (2024). Receptor Determinants for β-Arrestin Functional Specificity at C-X-C Chemokine Receptor 5. Mol. Pharmacol. *106*, 287–297.

Crilly, S.E., and Puthenveedu, M.A. (2021). Compartmentalized GPCR Signaling from Intracellular Membranes. J. Membr. Biol. *254*, 259–271.

D'Amore, V.M., Conflitti, P., Marinelli, L., and Limongelli, V. (2023). Minute-timescale simulations of G Protein Coupled Receptor A2A activation mechanism reveal a receptor pseudo-active state. BioRxiv 2023.09.14.557711.

Davies, M.N., Gloriam, D.E., Secker, A., Freitas, A.A., Timmis, J., and Flower, D.R. (2011). Present Perspectives on the Automated Classification of the G-Protein Coupled Receptors (GPCRs) at the Protein Sequence Level. Curr. Top. Med. Chem. *11*, 1994–2009.

Dehal, P., and Boore, J.L. (2005). Two rounds of whole genome duplication in the ancestral vertebrate. PLoS Biol. *3*.

Drube, J., Haider, R.S., Matthees, E.S.F., Reichel, M., Zeiner, J., Fritzwanker, S., Ziegler, C., Barz, S., Klement, L., Kliewer, A., et al. (2021). GRK2/3/5/6 knockout: The impact of individual GRKs on arrestin-binding and GPCR regulation. BioRxiv 2021.02.12.430971.

Dunn, H.A., and Ferguson, S.S.G. (2015). PDZ Protein Regulation of G Protein–Coupled Receptor Trafficking and Signaling Pathways. Mol. Pharmacol. *88*, 624–639.

Echeverría, E., Cabrera, M., Burghi, V., Sosa, M., Ripoll, S., Yaneff, A., Monczor, F., Davio, C., Shayo, C., and Fernández, N. (2020). The Regulator of G Protein Signaling Homologous Domain of G Protein-Coupled Receptor Kinase 2 Mediates Short-Term Desensitization of β3-Adrenergic Receptor. Front. Pharmacol. *11*, 508339.

Edenson, S. (2020). Novel Bioluminescent Tools to Study GPCR Pharmacology in Living Cells. FASEB J. *34*, 1–1.

Eiger, D.S., Smith, J.S., Shi, T., Stepniewski, T.M., Tsai, C.F., Honeycutt, C., Boldizsar, N., Gardner, J., Nicora, C.D., Moghieb, A.M., et al. (2023). Phosphorylation barcodes direct biased

chemokine signaling at CXCR3. Cell Chem. Biol. *30*, 362-382.e8.

Fanelli, F., and De Benedetti, P.G. (2006). Inactive and active states and supramolecular organization of GPCRs: insights from computational modeling. J. Comput. Aided. Mol. Des. *20*, 449–461.

Feigin, M.E. (2013). Harnessing the genome for characterization of G-protein coupled receptors in cancer pathogenesis. FEBS J. *280*, 4729–4738.

Fernandez, T.J., De Maria, M., and Lobingier, B.T. (2020). A cellular perspective of bias at G protein-coupled receptors. Protein Sci. *29*, 1345–1354.

Fisyunov, A.I. (2012). Molecular mechanisms of G protein-independent signaling mediated by 7-transmembrane receptors. Neurophysiology *44*, 255–264.

Flanagan, C.A. (2016). GPCR-radioligand binding assays. Methods Cell Biol. *132*, 191–215.

Foster, S.R., and Bräuner-Osborne, H. (2018). Investigating Internalization and Intracellular Trafficking of GPCRs: New Techniques and Real-Time Experimental Approaches. Handb. Exp. Pharmacol. *245*, 41–61.

Foster, S.R., Roura, E., Molenaar, P., and Thomas, W.G. (2015). G protein-coupled receptors in cardiac biology: old and new receptors. Biophys. Rev. *7*, 77–89.

De Francesco, E.M., Sotgia, F., Clarke, R.B., Lisanti, M.P., and Maggiolini, M. (2017). G Protein-Coupled Receptors at the Crossroad between Physiologic and Pathologic Angiogenesis: Old Paradigms and Emerging Concepts. Int. J. Mol. Sci. *18*.

Franco, R., Aguinaga, D., Jiménez, J., Lillo, J., Martínez-Pinilla, E., and Navarro, G. (2018). Biased receptor functionality versus biased agonism in G-protein-coupled receptors. Biomol. Concepts *9*, 143–154.

Fredriksson, R., and Schiöth, H.B. (2006). G Protein-coupled Receptors in the Human Genome. Ligand Des. G Protein-Coupled Recept. *30*, 1–25.

Fredriksson, R., Lagerström, M.C., Lundin, L.-G., and Schiöth, H.B. (2003). The G-protein-coupled receptors in the human genome form five main families. Phylogenetic analysis, paralogon groups, and fingerprints. Mol. Pharmacol. *63*, 1256–1272.

Fu, Q., and Xiang, Y.K. (2015). Trafficking of β-Adrenergic Receptors: Implications in Intracellular Receptor Signaling. Prog. Mol. Biol. Transl. Sci. *132*, 151.

Galinski, S., Wichert, S.P., Rossner, M.J., and Wehr, M.C. (2018). Multiplexed profiling of GPCR activities by combining split TEV assays and EXT-based barcoded readouts. Sci. Rep. *8*, 8137.

Gangal, R., and Kumar, K.K. (2007). Reduced alphabet motif methodology for GPCR annotation. J. Biomol. Struct. Dyn. *25*, 299–310.

Gendron, L., Grastilleur, S., Degrandmaison, J., Laniel, A., Grisé, O., Simard, J., Parent, J.-L., and Lavoie, C. (2023). Constitutive Internalization and Recycling of the Delta opioid Receptor. Authorea Prepr.

George, J.T., Kakkar, R., Marshall, J., Scott, M.L., Finkelman, R.D., Ho, T.W., Veldhuis, J., Skorupskaite, K., Anderson, R.A., McIntosh, S., et al. (2016). Neurokinin B Receptor Antagonism in Women With Polycystic Ovary Syndrome: A Randomized, Placebo-Controlled Trial. J. Clin. Endocrinol. Metab. *101*, 4313–4321.

Glukhova, A., Draper-Joyce, C.J., Sunahara, R.K., Christopoulos, A., Wootten, D., and Sexton, P.M. (2018). Rules of Engagement: GPCRs and G Proteins. ACS Pharmacol. Transl. Sci. *1*, 73–83.

Godbole, A., Lyga, S., Lohse, M.J., and Calebiro, D. (2017). Internalized TSH receptors en route to the TGN induce local Gs-protein signaling and gene transcription. Nat. Commun. 2017 81 *8*, 1–15.

Guo, S., Zhao, T., Yun, Y., and Xie, X. (2022). Recent progress in assays for GPCR drug discovery. Am. J. Physiol. Cell Physiol. *323*, C583–C594.

Gupta, M.K., Mohan, M.L., and Naga Prasad, S. V (2018). G Protein-Coupled Receptor Resensitization Paradigms. Int. Rev. Cell Mol. Biol. *339*, 63–91.

Gurevich, V. V, and Gurevich, E. V (2019). GPCR Signaling Regulation: The Role of GRKs and Arrestins. Front. Pharmacol. *10*, 125.

Hao, Y., and Tatonetti, N.P. (2016). Predicting G protein-coupled receptor downstream signaling by tissue expression. Bioinformatics *32*, 3435.

Hauser, A.S., Kooistra, A.J., Munk, C., Heydenreich, F.M., Veprintsev, D.B., Bouvier, M., Babu, M.M., and Gloriam, D.E. (2021). GPCR activation mechanisms across classes and macro/microscales. Nat. Struct. Mol. Biol. 2021 2811 *28*, 879–888.

Hendrik Schmidt, J., Perslev, M., Bukowski, L., Stoklund, M., Herborg, F., Herlo, R., and Lindegaard Madsen, K. (2020). Constitutive internalization across therapeutically targeted GPCRs correlates with constitutive activity. Basic Clin. Pharmacol. Toxicol. *126 Suppl*, 116–121.

Henstridge, C.M., Balenga, N.A., Schröder, R., Kargl, J.K., Platzer, W., Martini, L., Arthur, S., Penman, J., Whistler, J.L., Kostenis, E., et al. (2010). GPR55 ligands promote receptor coupling to multiple signalling pathways. Br. J. Pharmacol. *160*, 604.

Heuss, C., Scanziani, M., Gähwiler, B.H., and Gerber, U. (1999). G-protein-independent signaling mediated by metabotropic glutamate receptors. Nat. Neurosci. 1999 212 *2*, 1070–1077.

Höring, C., Seibel, U., Tropmann, K., Grätz, L., Mönnich, D., Pitzl, S., Bernhardt, G., Pockes, S., and Strasser, A. (2020). A Dynamic, Split-Luciferase-Based Mini-G Protein Sensor to Functionally Characterize Ligands at All Four Histamine Receptor Subtypes. Int. J. Mol. Sci. 2020, Vol. 21, Page 8440 *21*, 8440.

Iqbal, M.J., Faye, I., and Samir, B.B. (2016). Classification of GPCRs proteins using a statistical encoding method. Proc. Int. Jt. Conf. Neural Networks *2016-October*, 1224–1228.

Irannejad, R., Pessino, V., Mika, D., Huang, B., Wedegaertner, P.B., Conti, M., and Von Zastrow, M. (2017). Functional selectivity of GPCR-directed drug action through location bias. Nat. Chem. Biol. 2017 137 *13*, 799–806.

Iyinikkel, J., and Murray, F. (2018). GPCRs in pulmonary arterial hypertension: tipping the balance. Br. J. Pharmacol. *175*, 3063.

Jacobshagen, M., Niquille, M., Chaumont-Dubel, S., Marin, P., and Dayer, A. (2014). The serotonin 6 receptor controls neuronal migration during corticogenesis via a ligand-independent Cdk5-dependent mechanism. Development *141*, 3370–3377

Jang, W., Senarath, K., Lu, S., and Lambert, N.A. (2024). Visualization of endogenous G proteins on endosomes and other organelles. Elife *13*.

Jobe, A., and Vijayan, R. (2024). Orphan G protein-coupled receptors: the ongoing search for a home. Front. Pharmacol. *15*, 1349097.

Kasai, R.S., Fujiwara, T.K., and Kusumi, A. (2020). Metastable GPCR dimers trigger the basal signal by recruiting G-proteins. BioRxiv 2020.02.10.929588.

Katow, H., Takahashi, T., Saito, K., Tanimoto, H., and Kondo, S. (2019). Tango knock-ins visualize endogenous activity of G protein-coupled receptors in Drosophila. J. Neurogenet. *33*, 44–51.

Kaya, A.I., Perry, N.A., Gurevich, V. V., Iverson, T.M., Iverson, T.M., Iverson, T.M., and Iverson, T.M. (2020). Phosphorylation barcode-dependent signal bias of the dopamine D1 receptor. Proc. Natl. Acad. Sci. U. S. A. *117*, 14139–14149.

Kayki-Mutlu, G., and Koch, W.J. (2023). Novel roles for G protein-coupled receptor kinases in cardiac injury and repair. Biochem. Soc. Trans. *51*, 715–724.

Kelly, E., Bailey, C.P., and Henderson, G. (2008). Agonist-selective mechanisms of GPCR desensitization. Br. J. Pharmacol. *153*, S379–S388.

Khater, M., Wei, Z., Xu, X., Huang, W., Lokeshwar, B.L., Lambert, N.A., and Wu, G. (2021). G protein βγ translocation to the Golgi apparatus activates MAPK via p110γ-p101 heterodimers. J. Biol. Chem. *296*, 100325.

Kim, D., Tokmakova, A., Woo, J.-A.A., An, S.S., Goddard, W.A. 3rd, and Liggett, S.B. (2022). Selective Signal Capture from Multidimensional GPCR Outputs with Biased Agonists: Progress Towards Novel Drug Development. Mol. Diagn. Ther. *26*, 383–396.

Kim, M.W., Wang, W., Sanchez, M.I., Coukos, R., Zastrow, M. Von, and Ting, A.Y. (2017). Time-gated detection of protein-protein interactions with transcriptional readout. BioRxiv 166462.

Kingwell, K. (2017). Picking the pocketome for orphan receptor ligands. Nat. Rev. Drug Discov. 2017 162 *16*, 86–86.

Kleinau, G., Jaeschke, H., Mueller, S., Worth, C.L., Paschke, R., and Krause, G. (2008). Molecular and structural effects of inverse agonistic mutations on signaling of the thyrotropin receptor - A basally active GPCR. Cell. Mol. Life Sci. *65*, 3664–3676.

Kobilka, B.K. (2006). G Protein Coupled Receptor Structure and Activation. Biochim. Biophys. Acta *1768*, 794.

Koenig, J.A. (2004). Assessment of Receptor Internalization and Recycling. Methods Mol. Biol. *259*, 249–273.

Kotliar, I.B., Lorenzen, E., Schwenk, J.M., Hay, D.L., and Sakmar, T.P. (2023). Elucidating the Interactome of G Protein-Coupled Receptors and Receptor Activity-Modifying Proteins. Pharmacol. Rev. *75*, 1–34.

Koutsoukas, A., Torella, R., Drakakis, G., Bender, A., Glen, R.C., and Hurst, W.J. (2013). Relating GPCRs pharmacological space based on ligands chemical similarities. J. Cheminformatics 2013 51 *5*, 1–1.

Kroeze, W.K., Sassano, M.F., Huang, X.-P., Lansu, K., McCorvy, J.D., Giguère, P.M., Sciaky, N., and Roth, B.L. (2015). PRESTO-Tango as an open-source resource for interrogation of the druggable human GPCRome. Nat. Struct. Mol. Biol. *22*, 362–369.

Kumagai, H., Ikeda, Y., Motozawa, Y., Fujishiro, M., Okamura, T., Fujio, K., Okazaki, H., Nomura, S., Takeda, N., Harada, M., et al. (2015). Quantitative Measurement of GPCR Endocytosis via Pulse-Chase Covalent Labeling. PLoS One *10*, e0129394.

Kumar, G.A., and Puthenveedu, M.A. (2023). GPCR cargo modifies lipid order in clathrin-coated pits. J. Pharmacol. Exp. Ther. *385*, 128.

Kumar, G.A., Sarkar, P., Jafurulla, M., Singh, S.P., Srinivas, G., Pande, G., and Chattopadhyay, A. (2019). Exploring Endocytosis and Intracellular Trafficking of the Human Serotonin(1A) Receptor. Biochemistry *58*, 2628–2641.

Kunselman, J.M., Zajac, A.S., Weinberg, Z.Y., and Puthenveedu, M.A. (2019). Homologous regulation of mu opioid receptor recycling by Gβγ, protein kinase C, and receptor phosphorylation. Mol. Pharmacol. *96*, 702–710.

Kurose, H., and Kim, S.G. (2022). Pharmacology of Antagonism of GPCR. Biol. Pharm. Bull. *45*, 669–674.

Lai, H.-T., and Chiang, C.-M. (2013). Bimolecular Fluorescence Complementation (BiFC) Assay

for Direct Visualization of Protein-Protein Interaction in vivo. Bio-Protocol *3*.

Lamichhane, R., Liu, J.J., Pljevaljcic, G., White, K.L., Van Schans, E. Der, Katritch, V., Stevens, R.C., Wüthrich, K., and Millar, D.P. (2015). Single-molecule view of basal activity and activation mechanisms of the G protein-coupled receptor β2 AR. Proc. Natl. Acad. Sci. U. S. A. *112*, 14254–14259.

Lee, M. (2023). Recent Advances in Deep Learning for Protein-Protein Interaction Analysis: A Comprehensive Review. Mol. 2023, Vol. 28, Page 5169 *28*, 5169.

Lee, S. (2011). Platform Technologies for Research on the G Protein Coupled Receptor: Applications to Drug Discovery Research. Biomol. Ther. (Seoul). *19*, 1–8.

Lee, S., Chung, Y.H., and Lee, C. (2017). US28, a Virally-Encoded GPCR as an Antiviral Target for Human Cytomegalovirus Infection. Biomol. Ther. (Seoul). *25*, 69–79.

Lee, H.J., and Zheng, J.J. (2010). PDZ domains and their binding partners: structure, specificity, and modification. Cell Commun. Signal. 2010 81 *8*, 1–18.

Leemann, S., and Kleinlogel, S. (2023). Functional optimization of light-activatable Opto-GPCRs: Illuminating the importance of the proximal C-terminus in G-protein specificity. Front. Cell Dev. Biol. *11*, 1053022.

Leo, L.M., and Abood, M.E. (2021). CB1 Cannabinoid Receptor Signaling and Biased Signaling. Mol. 2021, Vol. 26, Page 5413 *26*, 5413.

Lesiak, L., Zhou, X., Fang, Y., Zhao, J., Beck, J.R., and Stains, C.I. (2020). Imaging GPCR internalization using near-infrared Nebraska red-based reagents. Org. Biomol. Chem. *18*, 2459–2467.

Leslie, M. (2016). Why endosomes recycle GPCRs. J. Cell Biol. *214*, 785–785.

Levitt, E.S., and Williams, J.T. (2018). Desensitization and Tolerance of Mu Opioid Receptors on Pontine Kölliker-Fuse Neurons. Mol. Pharmacol. *93*, 8–13.

Leyme, A., Marivin, A., Maziarz, M., DiGiacomo, V., Papakonstantinou, M.P., Patel, P.P., Blanco-Canosa, J.B., Walawalkar, I.A., Rodriguez-Davila, G., Dominguez, I., et al. (2017). Specific inhibition of GPCR-independent G protein signaling by a rationally engineered protein.

Proc. Natl. Acad. Sci. U. S. A. *114*, E10319–E10328.

Li, H., Eishingdrelo, A., Kongsamut, S., and Eishingdrelo, H. (2016). G-protein-coupled receptors mediate 14-3-3 signal transduction. Signal Transduct. Target. Ther. *1*, 16018.

Liggett, S.B. (2011). Phosphorylation barcoding as a mechanism of directing GPCR signaling. Sci. Signal. *4*, pe36.

Lin, S.H.S., Arai, A.C., Wang, Z., Nothacker, H.P., and Civelli, O. (2001). The Carboxyl Terminus of the Prolactin-Releasing Peptide Receptor Interacts with PDZ Domain Proteins Involved in α-Amino-3-hydroxy-5-methylisoxazole-4-propionic Acid Receptor Clustering. Mol. Pharmacol. *60*, 916–923.

Lovejoy, D.A., Chang, B.S.W., Lovejoy, N.R., and del Castillo, J. (2014). MOLECULAR EVOLUTION OF GPCRS: CRH/CRH receptors. J. Mol. Endocrinol. *52*, T43–T60.

Lu, B., Chen, L., Zhang, Y., Shi, Y., and Zhou, N. (2016). Quantitative analysis of G-protein-coupled receptor internalization using DnaE intein-based assay. Methods Cell Biol. *132*, 293–318.

Lu, S., He, X., Yang, Z., Chai, Z., Zhou, S., Wang, J., Rehman, A.U., Ni, D., Pu, J., Sun, J., et al. (2021). Activation pathway of a G protein-coupled receptor uncovers conformational intermediates as targets for allosteric drug design. Nat. Commun. 2021 121 *12*, 1–15.

Lymperopoulos, A., Suster, M.S., and Borges, J.I. (2022). Cardiovascular GPCR regulation by regulator of G protein signaling proteins. Prog. Mol. Biol. Transl. Sci. *193*, 145–166.

Ma, N., Nivedha, A.K., and Vaidehi, N. (2021). Allosteric communication regulates ligand-specific GPCR activity. FEBS J. *288*, 2502–2512.

Madsen, J.J., Ye, L., Frimurer, T.M., and Olsen, O.H. (2022). Mechanistic basis of GPCR activation explored by ensemble refinement of crystallographic structures. Protein Sci. *31*, e4456.

Mafi, A., Kim, S.K., and Goddard, W.A. (2022). The mechanism for ligand activation of the GPCR-G protein complex. Proc. Natl. Acad. Sci. U. S. A. *119*, e2110085119.

Al Mahri, S., Okla, M., Rashid, M., Malik, S.S., Iqbal, J., Al Ibrahim, M., Dairi, G., Mahmood, A., Muthurangan, M., Yaqinuddin, A., et al. (2023). Profiling of G-Protein Coupled Receptors in Adipose Tissue and Differentiating Adipocytes Offers a Translational Resource for

Obesity/Metabolic Research. Cells *12*, 377.

Malbon, C.C., Tao, J., and Wang, H. (2004). AKAPs (A-kinase anchoring proteins) and molecules that compose their G-protein-coupled receptor signalling complexes. Biochem. J. *379*, 1–9.

Masuho, I., Skamangas, N.K., Muntean, B.S., and Martemyanov, K.A. (2021). Diversity of the Gβγ complexes defines spatial and temporal bias of GPCR signaling. Cell Syst. *12*, 324-337.e5.

Matthees, E.S.F., Haider, R.S., Hoffmann, C., and Drube, J. (2021). Differential Regulation of GPCRs-Are GRK Expression Levels the Key? Front. Cell Dev. Biol. *9*, 687489.

Matthees, E.S.F., Filor, J.C., Jaiswal, N., Reichel, M., Youssef, N., D'Uonnolo, G., Szpakowska, M., Drube, J., König, G.M., Kostenis, E., et al. (2024). GRK specificity and Gβγ dependency determines the potential of a GPCR for arrestin-biased agonism. Commun. Biol. 2024 71 *7*, 1–12.

Maurice, P., Guillaume, J.L., Benleulmi-Chaachoua, A., Daulat, A.M., Kamal, M., and Jockers, R. (2011). GPCR-interacting proteins, major players of GPCR function. Adv. Pharmacol. *62*, 349–380.

Mavri, M., Spiess, K., Rosenkilde, M.M., Rutland, C.S., Vrecl, M., and Kubale, V. (2020). Methods for Studying Endocytotic Pathways of Herpesvirus Encoded G Protein-Coupled Receptors. Molecules *25*.

McNeill, S.M., and Zhao, P. (2023). The roles of RGS proteins in cardiometabolic disease. Br. J. Pharmacol.

Meriney, S.D., and Fanselow, E.E. (2019). Metabotropic g-protein-coupled receptors and their cytoplasmic signaling pathways. Synaptic Transm. 245–273.

Meshik, X., and Gautam, N. (2021). Live Cell Imaging and Optogenetics-Based Assays for GPCR Activity. Methods Mol. Biol. *2268*, 207–221.

Mestek, A., Hurley, J.H., Bye, L.S., Campbell, A.D., Chen, Y., Tian, M., Liu, J., Schulman, H., and Yu, L. (1995). The human mu opioid receptor: modulation of functional desensitization by calcium/calmodulin-dependent protein kinase and protein kinase C. J. Neurosci. *15*, 2396–2406.

Min, X., Sun, N., Wang, S., Zhang, X., and Kim, K.M. (2023). Sequestration of Gβγ by deubiquitinated arrestins into the nucleus as a novel desensitization mechanism of G protein–

coupled receptors. Cell Commun. Signal. *21*, 1–20.

Mohammadi, S., and Grama, A. (2016). A convex optimization approach for identification of human tissue-specific interactomes. Bioinformatics *32*, i243–i252.

Møller, T.C., Wirth, V.F., Roberts, N.I., Bender, J., Bach, A., Jacky, B.P.S., Strømgaard, K., Deussing, J.M., Schwartz, T.W., and Martinez, K.L. (2013). PDZ Domain-Mediated Interactions of G Protein-Coupled Receptors with Postsynaptic Density Protein 95: Quantitative Characterization of Interactions. PLoS One *8*, e63352.

Møller, T.C., Pedersen, M.F., van Senten, J.R., Seiersen, S.D., Mathiesen, J.M., Bouvier, M., and Bräuner-Osborne, H. (2020). Dissecting the roles of GRK2 and GRK3 in μ-opioid receptor internalization and β-arrestin2 recruitment using CRISPR/Cas9-edited HEK293 cells. Sci. Rep. *10*, 17395.

Moo, E. Von, van Senten, J.R., Bräuner-Osborne, H., and Møller, T.C. (2021). Arrestin-Dependent and -Independent Internalization of G Protein-Coupled Receptors: Methods, Mechanisms, and Implications on Cell Signaling. Mol. Pharmacol. *99*, 242–255.

Mos, I., Jacobsen, S.E., Foster, S.R., and Bräuner-Osborne, H. (2019). Calcium-Sensing Receptor Internalization Is β-Arrestin-Dependent and Modulated by Allosteric Ligands. Mol. Pharmacol. *96*, 463–474.

Nakliang, P., Lazim, R., Chang, H., and Choi, S. (2020). Multiscale Molecular Modeling in G Protein-Coupled Receptor (GPCR)-Ligand Studies. Biomolecules *10*.

Nishiyama, K., Nishimura, A., Shimoda, K., Tanaka, T., Kato, Y., Shibata, T., Tanaka, H., Kurose, H., Azuma, Y.T., Ihara, H., et al. (2022). Redox-dependent internalization ofthe purinergic P2Y6 receptor limits colitis progression. Sci. Signal. *15*, eabj0644.

Niv, M.Y., Skrabanek, L., Filizola, M., and Weinstein, H. (2006). Modeling activated states of GPCRs: The rhodopsin template. J. Comput. Aided. Mol. Des. *20*, 437–448.

Nobles, K.N., Xiao, K., Ahn, S., Shukla, A.K., Lam, C.M., Rajagopal, S., Strachan, R.T., Huang, T.Y., Bressler, E.A., Hara, M.R., et al. (2011). Distinct phosphorylation sites on the β(2)-adrenergic receptor establish a barcode that encodes differential functions of β-arrestin. Sci. Signal. *4*.

Paasche, J.D., Attramadal, T., Kristiansen, K., Oksvold, M.P., Johansen, H.K., Huitfeldt, H.S., Dahl, S.G., and Attramadal, H. (2005). Subtype-Specific Sorting of the ETA Endothelin Receptor by a Novel Endocytic Recycling Signal for G Protein-Coupled Receptors. Mol. Pharmacol. *67*, 1581–1590.

Pandey, S., Roy, D., and Shukla, A.K. (2019). Measuring surface expression and endocytosis of GPCRs using whole-cell ELISA. Methods Cell Biol. *149*, 131–140.

Park, F. (2021). Activators of G -
Protein Signaling in the Normal and Diseased Kidney. GPCRs as Ther. Targets *2*, 767–803.

Park, P.S.H., Lodowski, D.T., and Palczewski, K. (2008). Activation of G Protein–Coupled Receptors: Beyond Two-State Models and Tertiary Conformational Changes. Annu. Rev. Pharmacol. Toxicol. *48*, 107.

Parrill, A.L., and Bautista, D.L. (2010). GPCR Conformations: Implications for Rational Drug Design. Pharm. 2011, Vol. 4, Pages 7-43 *4*, 7–43.

Patwardhan, A., Cheng, N., and Trejo, J. (2021). Post-Translational Modifications of G Protein-Coupled Receptors Control Cellular Signaling Dynamics in Space and Time. Pharmacol. Rev. *73*, 120–151.

Pizzoni, A., Zhang, X., and Altschuler, D.L. (2024). From membrane to nucleus: A three-wave hypothesis of cAMP signaling. J. Biol. Chem. *300*, 105497.

Powers, A.S., Khan, A., Paggi, J.M., Latorraca, N.R., Souza, S., Salvo, J. Di, Lu, J., Soisson, S.M., Johnston, J.M., Weinglass, A.B., et al. (2023). A non-canonical mechanism of GPCR activation. BioRxiv 2023.08.14.553154.

Prague, J.K., Roberts, R.E., Comninos, A.N., Clarke, S., Jayasena, C.N., Mohideen, P., Lin, V.H., Stern, T.P., Panay, N., Hunter, M.S., et al. (2018). Neurokinin 3 receptor antagonism rapidly improves vasomotor symptoms with sustained duration of action. Menopause *25*, 862.

Prasad, S., Zeug, A., and Ponimaskin, E. (2013). Analysis of Receptor–Receptor Interaction by Combined Application of FRET and Microscopy. Methods Cell Biol. *117*, 243–265.

Prosser, R.S., Ye, L., Pandey, A., and Orazietti, A. (2017). Activation processes in ligand-activated

G protein-coupled receptors: A case study of the adenosine A2A receptor. BioEssays *39*, 1700072.

Qin, J., Cai, Y., Xu, Z., Ming, Q., Ji, S.Y., Wu, C., Zhang, H., Mao, C., Shen, D.D., Hirata, K., et al. (2022). Molecular mechanism of agonism and inverse agonism in ghrelin receptor. Nat. Commun. 2022 131 *13*, 1–11.

Radoux-Mergault, A., Oberhauser, L., Aureli, S., Gervasio, F.L., and Stoeber, M. (2023). Subcellular location defines GPCR signal transduction. Sci. Adv. *9*.

Rajagopal, S., and Ponnusamy, M. (2018). Overview of G-Protein Coupled Receptor. Metabotropic GPCRs TGR5 P2Y Recept. Heal. Dis. 1–18.

Robleto, V., Zhuo, Y., Crecelius, J., and Marchese, A. (2023). Regulation of GPCR Signaling by Sorting Nexins. J. Pharmacol. Exp. Ther. *385*, 529.

Röck, R., Bachmann, V., Bhang, H.E.C., Malleshaiah, M., Raffeiner, P., Mayrhofer, J.E., Tschaikner, P.M., Bister, K., Aanstad, P., Pomper, M.G., et al. (2015). In-vivo detection of binary PKA network interactions upon activation of endogenous GPCRs. Sci. Reports 2015 51 *5*, 1–11.

Roettger, B.F., Ghanekar, D., Rao, R., Toledo, C., Yingling, J., Pinon, D., and Miller, L.J. (1997). Antagonist-stimulated internalization of the G protein-coupled cholecystokinin receptor. Mol. Pharmacol. *51*, 357–362.

Romero, G., von Zastrow, M., and Friedman, P.A. (2011). Role of PDZ proteins in regulating trafficking, signaling, and function of GPCRs: means, motif, and opportunity. Adv. Pharmacol. *62*, 279–314.

Routledge, S.J., Ladds, G., and Poyner, D.R. (2017). The effects of RAMPs upon cell signalling. Mol. Cell. Endocrinol. *449*, 12–20.

Russell, I.C., Zhang, X., Bumbak, F., McNeill, S.M., Josephs, T.M., Leeming, M.G., Christopoulos, G., Venugopal, H., Flocco, M.M., Sexton, P.M., et al. (2024). Lipid-Dependent Activation of the Orphan G Protein-Coupled Receptor, GPR3. Biochemistry *63*, 625–631.

Sakloth, F., Polizu, C., Bertherat, F., and Zachariou, V. (2020). Regulators of G Protein Signaling in Analgesia and Addiction. Mol. Pharmacol. *98*, 739–750.

Sánchez-Soto, M., Boldizsar, N.M., Schardien, K.A., Madaras, N.S., Willette, B.K.A., Inbody,

L.R., Dasaro, C., Moritz, A.E., Drube, J., Haider, R.S., et al. (2023). G Protein-Coupled Receptor Kinase 2 Selectively Enhances β-Arrestin Recruitment to the D2 Dopamine Receptor through Mechanisms That Are Independent of Receptor Phosphorylation. Biomolecules *13*, 1552.

Sawano, S., Seto, E., Mori, T., and Hayashi, Y. (2005). G-Protein-Dependent and -Independent Pathways in Denatonium Signal Transduction. Biosci. Biotechnol. Biochem. *69*, 1643–1651.

Scheerer, P., Heck, M., Goede, A., Jung, H.P., Choe, H.W., Ernst, O.P., Hofmann, K.P., and Hildebrand, P.W. (2009). Structural and kinetic modeling of an activating helix switch in the rhodopsin-transducin interface. Proc. Natl. Acad. Sci. U. S. A. *106*, 10660–10665.

Schihada, H., Shekhani, R., and Schulte, G. (2021). Quantitative assessment of constitutive G protein–coupled receptor activity with BRET-based G protein biosensors. Sci. Signal. *14*, 1653.

Scholz, N., Langenhan, T., and Schöneberg, T. (2019). Revisiting the classification of adhesion GPCRs. Ann. N. Y. Acad. Sci. *1456*, 80–95.

Schöneberg, T., and Liebscher, I. (2021). Mutations in G Protein–Coupled Receptors: Mechanisms, Pathophysiology and Potential Therapeutic Approaches. Pharmacol. Rev. *73*, 89–119.

Schreiber, G. (2021). CHAPTER 1: Protein-Protein Interaction Interfaces and their Functional Implications. RSC Drug Discov. Ser. *2021-January*, 1–24.

Seibel-Ehlert, U., Plank, N., Inoue, A., Bernhardt, G., and Strasser, A. (2021). Label-free investigations on the g protein dependent signaling pathways of histamine receptors. Int. J. Mol. Sci. *22*, 9739.

Seifert, R., and Wenzel-Seifert, K. (2002a). Constitutive activity of G-protein-coupled receptors: cause of disease and common property of wild-type receptors. Naunyn. Schmiedebergs. Arch. Pharmacol. *366*, 381–416.

Seifert, R., and Wenzel-Seifert, K. (2002b). Constitutive activity of G-proteins-coupled receptors: Cause of disease and common property of wild-type receptors. Naunyn. Schmiedebergs. Arch. Pharmacol. *366*, 381–416.

Seifert, R., and Wieland, T. (2006). G Protein-Coupled Receptors as Drug Targets: Analysis of

Activation and Constitutive Activity. G Protein-Coupled Recept. as Drug Targets Anal. Act. Const. Act. *24*, 1–275.

Senese, N.B., Rasenick, M.M., and Traynor, J.R. (2018). The Role of G-proteins and G-protein Regulating Proteins in Depressive Disorders. Front. Pharmacol. *9*, 1289.

Shpakov, A.O. (2023). Allosteric Regulation of G-Protein-Coupled Receptors: From Diversity of Molecular Mechanisms to Multiple Allosteric Sites and Their Ligands. Int. J. Mol. Sci. *24*.

Siehler, S. (2009). Regulation of RhoGEF proteins by G12/13-coupled receptors. Br. J. Pharmacol. *158*, 41–49.

Skieterska, K., Rondou, P., and Van Craenenbroeck, K. (2017). Regulation of G Protein-Coupled Receptors by Ubiquitination. Int. J. Mol. Sci. *18*.

Skorupskaite, K., George, J.T., Veldhuis, J.D., Millar, R.P., and Anderson, R.A. (2018). Neurokinin 3 Receptor Antagonism Reveals Roles for Neurokinin B in the Regulation of Gonadotropin Secretion and Hot Flashes in Postmenopausal Women. Neuroendocrinology *106*, 148–157.

Smrcka, A. V (2008). G protein βγ subunits: central mediators of G protein-coupled receptor signaling. Cell. Mol. Life Sci. *65*, 2191–2214.

Spiegel, A.M., and Weinstein, L.S. (2004). Inherited diseases involving g proteins and g protein-coupled receptors. Annu. Rev. Med. *55*, 27–39.

Stein, R.S.L., and Ehlert, F.J. (2015). A kinetic model of GPCRs: analysis of G protein activity, occupancy, coupling and receptor-state affinity constants. J. Recept. Signal Transduct. *35*, 269–283.

Stoddart, L.A., White, C.W., Nguyen, K., Hill, S.J., and Pfleger, K.D.G. (2016). Fluorescence- and bioluminescence-based approaches to study GPCR ligand binding. Br. J. Pharmacol. *173*, 3028–3037.

Strange, P.G. (2010). Use of the GTPγS ([35S]GTPγS and Eu-GTPγS) binding assay for analysis of ligand potency and efficacy at G protein-coupled receptors. Br. J. Pharmacol. *161*, 1238–1249.

Sun, N., and Kim, K.-M. (2021). Mechanistic diversity involved in the desensitization of G

protein-coupled receptors. Arch. Pharm. Res. *44*, 342–353.

Taddese, B., Simpson, L.M., Wall, I.D., Blaney, F.E., and Reynolds, C.A. (2013). Modeling Active GPCR Conformations. Methods Enzymol. *522*, 21–35.

Tang, X., Bian, J., and Li, Z. (2022). Posttranslational modifications in GPCR internalization. Am. J. Physiol. Cell Physiol. *323*, C84–C94.

Tao, Y.X. (2008). Constitutive Activation of G Protein-Coupled Receptors and Diseases: Insights into Mechanisms of Activation and Therapeutics. Pharmacol. Ther. *120*, 129.

Tewson, P., Westenberg, M., Zhao, Y., Campbell, R.E., Quinn, A.M., and Hughes, T.E. (2012). Simultaneous detection of Ca2+ and diacylglycerol signaling in living cells. PLoS One *7*, 42791.

Thompson, M.D., Hendy, G.N., Percy, M.E., Bichet, D.G., and Cole, D.E.C. (2014). G protein-coupled receptor mutations and human genetic disease. Methods Mol. Biol. *1175*, 153–187.

Thotamune, W., Ubeysinghe, S., Rajarathna, C., Kankanamge, D., Olupothage, K., Chandu, A., Copits, B.A., and Karunarathne, A. (2024). AGS3-based optogenetic GDI induces GPCR-independent Gβγ signaling and macrophage migration. BioRxiv 2024.06.04.597473.

Tilley, D.G. (2011). G protein-dependent and G protein-independent signaling pathways and their impact on cardiac function. Circ. Res. *109*, 217–230.

Tobin, A.B. (2008). G-protein-coupled receptor phosphorylation: where, when and by whom. Br. J. Pharmacol. *153*, S167–S176.

Tobin, A.B., Butcher, A.J., and Kong, K.C. (2008). Location, location, location…site-specific GPCR phosphorylation offers a mechanism for cell-type-specific signalling. Trends Pharmacol. Sci. *29*, 413.

Ulloa-Aguirre, A., Zariñán, T., and Jardón-Valadez, E. (2021). Misfolded G Protein-Coupled Receptors and Endocrine Disease. Molecular Mechanisms and Therapeutic Prospects. Int. J. Mol. Sci. *22*.

Vaudry, H. (2014). MOLECULAR EVOLUTION OF GPCRS: What we know and what the future holds. J. Mol. Endocrinol. *52*, E1–E2.

Vistein, R., and Puthenveedu, M.A. (2013). Reprogramming of G protein-coupled receptor

recycling and signaling by a kinase switch. Proc. Natl. Acad. Sci. U. S. A. *110*, 15289–15294.

Vural, A., and Lanier, S.M. (2020). Intersection of two key signal integrators in the cell: activator of G-protein signaling 3 and dishevelled-2. J. Cell Sci. *133*.

Walport, L.J., Low, J.K.K., Matthews, J.M., and MacKay, J.P. (2021). The characterization of protein interactions – what, how and how much? Chem. Soc. Rev. *50*, 12292–12307.

Walther, C., and Ferguson, S.S.G. (2015). Minireview: Role of intracellular scaffolding proteins in the regulation of endocrine G protein-coupled receptor signaling. Mol. Endocrinol. *29*, 814–830.

Wang, T., Li, Z., Cvijic, M.E., Zhang, L., and Sum, C.S. (2004). Measurement of cAMP for G(αs)- and G(αi) Protein-Coupled Receptors (GPCRs). S. Markossian, A. Grossman, K. Brimacombe, M. Arkin, D. Auld, C. Austin, J. Baell, T.D.Y. Chung, N.P. Coussens, J.L. Dahlin, et al., eds. (Bethesda (MD)), p.

Wanka, L., Behr, V., and Beck-Sickinger, A.G. (2022). Arrestin-dependent internalization of rhodopsin-like G protein-coupled receptors. Biol. Chem. *403*, 133–149.

Watanabe, Y., Tsujimura, A., Aoki, M., Taguchi, K., and Tanaka, M. (2016). Development of the 5-HT2CR-Tango System Combined with an EGFP Reporter Gene. J. Mol. Neurosci. *58*, 162–169.

Watari, K., Nakaya, M., and Kurose, H. (2014). Multiple functions of G protein-coupled receptor kinases. J. Mol. Signal. *9*.

Watkins, L.R., and Orlandi, C. (2021). In vitro profiling of orphan G protein coupled receptor (GPCR) constitutive activity. Br. J. Pharmacol. *178*, 2963–2975.

Weinberg, Z.Y., and Puthenveedu, M.A. (2019). Regulation of G protein-coupled receptor signaling by plasma membrane organization and endocytosis. Traffic *20*, 121–129.

Weis, W.I., and Kobilka, B.K. (2018). The Molecular Basis of G Protein-Coupled Receptor Activation. Annu. Rev. Biochem. *87*, 897–919.

West, C., and Hanyaloglu, A.C. (2015). Minireview: Spatial Programming of G Protein-Coupled Receptor Activity: Decoding Signaling in Health and Disease. Mol. Endocrinol. *29*, 1095–1106.

Wheeler, D., Sneddon, W.B., Wang, B., Friedman, P.A., and Romero, G. (2007). NHERF-1 and

the cytoskeleton regulate the traffic and membrane dynamics of G protein-coupled receptors. J. Biol. Chem. *282*, 25076–25087.

Wheeler, D.S., Barrick, S.R., Grubisha, M.J., Brufsky, A.M., Friedman, P.A., and Romero, G. (2011). Direct interaction between NHERF1 and Frizzled regulates β-catenin signaling. Oncogene *30*, 32.

Willette, B.K.A., Zhang, J.F., Zhang, J., and Tsvetanova, N.G. (2023). Endosome positioning coordinates spatially selective GPCR signaling. Nat. Chem. Biol. 2023 202 *20*, 151–161.

Wisler, J.W., Rockman, H.A., and Lefkowitz, R.J. (2018). Biased G protein-coupled receptor signaling: Changing the paradigm of drug discovery. Circulation *137*, 2315–2317.

Wright, S.C., Avet, C., Gaitonde, S.A., Muneta-Arrate, I., Gouill, C. Le, Hogue, M., Breton, B., Koutsilieri, S., Alarcia, R.D.-, Héroux, M., et al. (2024). Conformation- and activation-based BRET sensors differentially report on GPCR–G protein coupling. Sci. Signal. *17*.

Wu, V., Yeerna, H., Nohata, N., Chiou, J., Harismendy, O., Raimondi, F., Inoue, A., Russell, R.B., Tamayo, P., and Gutkind, J.S. (2019). Illuminating the Onco-GPCRome: Novel G protein-coupled receptor-driven oncocrine networks and targets for cancer immunotherapy. J. Biol. Chem. *294*, 11062–11086.

Xiao, J.Y., Ruiz, G.V., Whorton, M.R., Rasmussen, S.G.F., DeVree, B.T., Deupi, X., Sunahara, R.K., and Kobilka, B. (2009). The effect of ligand efficacy on the formation and stability of a GPCR-G protein complex. Proc. Natl. Acad. Sci. U. S. A. *106*, 9501–9506.

Xie, X.Q., and Chowdhury, A. (2013). Advances in Methods to Characterize Ligand-Induced Ionic Lock and Rotamer Toggle Molecular Switch in G Protein-Coupled Receptors. Methods Enzymol. *520*, 153–174.

Yang, Z., Yang, F., Zhang, D., Liu, Z., Lin, A., Liu, C., Xiao, P., Yu, X., and Sun, J.P. (2017). Phosphorylation of G Protein-Coupled Receptors: From the Barcode Hypothesis to the Flute Model. Mol. Pharmacol. *92*, 201–210.

Yu, N., Atienza, J.M., Bernard, J., Blanc, S., Zhu, J., Wang, X., Xu, X., and Abassi, Y.A. (2005). Real-Time Monitoring of Morphological Changes in Living Cells by Electronic Cell Sensor Arrays: An Approach To Study G Protein-Coupled Receptors. Anal. Chem. *78*, 35–43.

Yuan, L., Barbash, S., Kongsamut, S., Eishingdrelo, A., Sakmar, T.P., and Eishingdrelo, H. (2019). 14-3-3 signal adaptor and scaffold proteins mediate GPCR trafficking. Sci. Rep. *9*, 11156.

Zhang, R., and Xie, X. (2012). Tools for GPCR drug discovery. Acta Pharmacol. Sin. *33*, 372–384.

Zhang, X., and Kim, K.-M. (2017). Multifactorial Regulation of G Protein-Coupled Receptor Endocytosis. Biomol. Ther. (Seoul). *25*, 26–43.

Zhang, X.C., Zhou, Y., and Cao, C. (2016). Thermodynamics of GPCR activation. Biophys. Reports *1*, 115.

Zhao, M., Wang, Z., Yang, M., Ding, Y., Zhao, M., Wu, H., Zhang, Y., and Lu, Q. (2021). The Roles of Orphan G Protein-Coupled Receptors in Autoimmune Diseases. Clin. Rev. Allergy Immunol. 2021 602 *60*, 220–243.

Zhou, Q., Yang, D., Wu, M., Guo, Y., Guo, W., Zhong, L., Cai, X., Dai, A., Jang, W., Shakhnovich, E., et al. (2019). Common activation mechanism of class a GPCRs. Elife *8*.

CHAPTER 2: Profiling of constitutive and ligand-dependent GPCR activities by means of a polyvalent cell-based high-throughput platform

Profiling of basal and ligand-dependent GPCR activities by means of a polyvalent cell-based high-throughput platform

Manel Zeghal[1], Geneviève Laroche[1], Julia Douglas Freitas[1], Rebecca Wang[1], Patrick M. Giguère[1,2*]

[1] Department of Biochemistry, Microbiology and Immunology, University of Ottawa, Ottawa, ON, K1H8M5, Canada
[2] Brain and Mind Research Institute, University of Ottawa, Ottawa, ON, K1H8M5, Canada
*Correspondence to Patrick M. Giguère. Email: patrick.giguere@uottawa.ca

ABSTRACT

Representing the most attractive and successful druggable receptors of the proteome, GPCRs regulate a myriad of physiological and pathophysiological functions. Although over half of present pharmaceuticals target GPCRs, the advancement of drug discovery is hampered by a lack of adequate screening tools, the majority of which are limited to probing agonist-induced G-protein and β-arrestin-2-mediated events as a measure of receptor activation. Here, we develop Tango-Trio, a comprehensive cell-based high-throughput platform comprising cumate-inducible expression of transducers, capable of the parallelized profiling of both basal and agonist-dependent GPCR activities. We capture the functional diversity of GPCRs, reporting β-arrestin-1/2 couplings, selectivities, and receptor internalization signatures across the GPCRome. Moreover, we present the construction of cumate-induced basal activation curves at approximately 200 receptors, including over 50 orphans. Overall, Tango-Trio's robustness is well-suited for the functional characterization and screening of GPCRs, especially for parallel interrogation, and is a valuable addition to the pharmacological toolbox.

INTRODUCTION

As central orchestrators of cellular and physiological processes, G protein-coupled receptors (GPCRs) mediate the transduction of extracellular stimuli into conformationally-driven intracellular signals. Comprised of more than 800 members in the human genome, the diversity of this superfamily of membrane proteins is shaped by both the multiplicity of ligands they respond to, as well as the diverse array of signalling pathways they coordinate[1–3]. Moreover, GPCRs function in conjunction with protein interactors, whose identities and abundances vary by virtue of tissue- and/or cellular-specific expression[4].

The dynamism of GPCR signaling events is due to the receptors' conformational and locational changes throughout their life cycle, including activation, desensitization, internalization and resensitization. Although there is great diversity of ligands among them, GPCRs share a common fundamental mechanism of receptor activation. GPCRs in their inactive conformation are coupled to a heterotrimeric G-proteins complex, formed of a Gα subunit bound to GDP and Gβγ dimer stabilizing the inactive conformation of the heterotrimer. Activation of the GPCR results in conformational changes which enable the exchange of bound GDP by Gα for GTP, resulting in the dissociation of Gα-GTP and Gβγ-subunits from the receptor, which transduce different downstream signalling cascades depending on the nature of the GPCR and the subclasses of the G-protein subunits, composing the basis of G-protein dependent signalling[5,6]. This classical paradigm posits that activation can be induced not only by agonist binding, but also by virtue of GPCRs' ability to spontaneously adopt active conformations in the absence of agonist, termed constitutive activity[7]. Although it is now widely recognized that all GPCRs exhibit spontaneous activation, albeit at varying degrees, a large-scale quantification of constitutive activity across the GPCRome, including druggable and orphan receptors, has yet to be conducted.

To prevent overstimulation, active GPCRs can be desensitized, wherein kinases such as GRKs phosphorylate the receptor at specific serine/threonine residues, typically C-terminal or intracellular loop 3 (IL3) sites[5]. Phosphorylation in turn leads to the recruitment of arrestins, the most well-known and characterized scaffold proteins comprising four isoforms, the two visual arrestins, arrestin-1 and arrestin-4, that are confined to retinal cones and rods, and the ubiquitously expressed nonvisual arrestins, β-arrestin-1 and -2[8]. While nonvisual arrestins have been shown to bind to hundreds of different GPCR members, the vast majority of demonstrations have been conducted with β-arrestin-2, with few studies addressing the contributions of the relevant but often forgotten β-arrestin-1 isoform[9]. Besides inducing receptor desensitization through steric hindrance of the G-protein binding site, arrestins also redirect GPCR signalling to alternative G-protein independent pathways such as MAPKs, JNKs, and Src [10]. Additionally, the engagement of arrestin initiates receptor internalization via dynamin- and clathrin-dependent endocytosis[11]. Besides canonical arrestin-mediated endocytosis, increasing evidence has emerged describing GPCRs internalizing independently of arrestins[12].

Herein, we describe a comprehensive screening and interrogation platform evolved from the PRESTO-Tango, capable of the simultaneous interrogation of β-arrestin-2 recruitment at approximately 300 non-olfactory druggable GPCRs[13]. The reconstruction of this system was sought in part to increase the dynamic range and sensitivity of the original system, specifically improving the TRE promoter and TEV protease elements, and to expand its versatility beyond monitoring β-arrestin-2. Indeed, our platform, named Tango-Trio, includes monoclonal cell lines expressing trackers of β-arrestin-2, β-arrestin-1, and FYVE domain for internalization, all sharing the common luciferase reporter lineage. Moreover, their cumate-inducible nature enables the study of the various GPCR state-dependent and independent activities. Hereafter, we refer to the following states: the manifest agonist-induced active state; the constitutive active state, which represents ligand-independent activated receptor; steady-state, which refers to state-independent interaction level; and the basal level, which includes the steady-state plus constitutively active receptor pool, which cannot be discriminated in most cases. We are revealing divergent basal versus agonist-dependent β-arrestin-1/2 couplings, selectivities, and receptor endocytosis signatures across the GPCRome. We report the basal sigmoidal-fitted activities of more than 200 class A GPCRs, including approximately 50 orphans. Our findings represent a step towards uncovering the differences behind the mechanisms of constitutive versus agonist-induced activation, as well as state-independent activity. Moreover, we believe the Tango-Trio platform could facilitate the development of new GPCR-acting drugs and deorphanization efforts.

RESULTS

Development of the Tango-Trio and its comparison to the PRESTO-Tango

The PRESTO-Tango has a number of advantages, including selective read-out as the response is specific to the target receptor, sensitivity due to signal integration to produce a read-out, and the ability to study a multitude of GPCRs as the assay is independent of the G protein family the receptor signals through[13]. As such, we exploited these strategic features to undergird the development of the Tango-Trio platform, while addressing its original limitations, chiefly the tetracycline-response element (TRE) promoter and tobacco etch virus (TEV) protease.

To stringently control gene expression, tTA binding to tetO7 permits transcriptional activation of the luciferase reporter[14]. However, the main limitation to the Tet system is the leakiness due to the strong positional effects on the tetO7 minimal promoter[15], resulting in relatively high background transcription. In turn, this would lead to basal expression that would not be dependent on the tTA, which is intended to be cleaved from the GPCR by the β-arrestin2-TEV fusion protein. The second-generation promoter called TRE-Tight (Clonetech), redesigned tetO7 to remove potential bindings sites of endogenous transcription factors within the operon such as ISRE and GATA, renders this promoter virtually silent in the absence of induction[16]. As expected, lower RLU counts were obtained with TRE-Tight, but the induction factor remained higher for the TRE-Tight promoter (4.5 fold) compared to TRE (2.7 fold) (**Fig. 2.1a**); the dopamine D2 receptor (DRD2) Tango receptor was used as it is a strong β-arrestin2 recruiter[13]. Thus, the minimal basal leakage and increased fold window suggest TRE-Tight to be an improved promoter for Tango-Trio and reduce potential arrestin-independent modulation of the reporter activity.

Based on these observations, we generated a monoclonal TRE-Tight Luciferase reporter cell line for the Tango-Trio platform as an improvement over the HTL (HEK293T cells stably expressing TRE-Luc) cells of the original Tango assay (**Fig. 2.1b**). Although it is unknown whether Luc or Luc+ was used in creating the HTL cell line, we opted to clone TRE-Tight upstream the Luc2 gene (Promega), a markedly improved variant over its predecessors with significantly lower levels of cryptic transcription from the coding region and codon optimized expression[17]. Henceforth referred to as HTTL (HEK293T TRE-Tight-Luc), our reporter cell line had a comparable level of maximal expression to HTL but possessed a much lower baseline compared to its counterpart, resulting in a larger induction factor.

The Tango system involves a protein fusion consisting of β-arrestin-2 with TEV, which cleaves the engineered GPCR following β-arrestin-2 recruitment to the receptor to release the tTA. However, one limitation of the WT TEV is that it undergoes self-cleavage, generating a truncated protease with greatly diminished activity[18]. A variant of the WT, S219V-stop (TEV219), carries a stabilizing point mutation and was truncated to remove the auto-inhibitory C-terminal tail[19]. Given previous reports of this variant being 100-fold more stable than the full-length TEV and a more efficient catalyst, TEV219 was tested as a replacement for the WT TEV (**Fig. 2.1c**). TEV219

significantly lowered the baseline while producing maximal induced expression similar to that observed with the original protease, resulting in a signal ratio more than double (3.3-fold) that of TEV (1.3-fold).

Based on the aforementioned findings, β-arrestin-1, β-arrestin-2, and FYVE, a domain used to probe endocytosis given its high binding affinity and specificity to phosphatidylinositol 3-phosphate (PI3P)-enriched early endosomes[20], were cloned to the chosen TEV219 protease. These trackers were subsequently transferred into the pcDH cumate-inducible destination lentivector, providing robust and reversible expression of genes, and adjustable expression levels by titrating the amount of cumate added to cell medium[21]. The effect of its addition in cumate-independent systems was assessed in the PRESTO-Tango, with negligeable changes to the basal signal in untransfected HTLA (**Supplementary Fig. 2.1a**), as well as at the arbitrary Tango-receptors tested (**Supplementary Fig. 2.1b**); nonetheless, considering that certain receptors produce weak maximum signals in Tango-based platforms, it is recommended that users test to confirm that cumate does not produce any significant agonistic or antagonistic behavior at the receptors they are employing. HTTL was used as the host cells for the subsequent generation of double stable cell lines, ensuring uniform genetic and reporter background. Monoclonal cell lines for β-arrestin1-, β-arrestin2-, and FYVE-TEV219, henceforth referred to as HTTL-B1, HTTL-B2 and HTTL-F respectively, were screened by functional assay and the final selection was based on pharmacological parameters, including baseline, efficacy, potency, and fold change (E_{max}/E_0). Seeing as the basal signal varies across the three different HTTL cell lines in the absence of receptor expression (**Supplementary Fig. 2.2**), the baseline was henceforth defined for each independent experiment and dose-curve construction, specifically as the mean luminescence readings of the three lowest drug dilution concentrations. Following selection, the amelioration of Tango-Trio over the PRESTO-Tango was assayed by comparing the original HTLA (HTL cells stably expressing β-Arrestin-2-TEV) cell line to our corresponding HTTL-B2.

While both GATA and ISRE are present in the TRE, the redesign of TRE-Tight saw the removal of only ISRE, with GATA still present as it is overlapping with tetO[22]. Based on previous work revealing that phorbol 12-myristate 13-acetate (PMA) activates the ISRE-Luc reporter and induces

JAK-STAT signal transduction[23], we postulated that activators of the Jak/Stat pathway would have an impact on the TRE promoter, but not TRE-Tight.

Corroborating this hypothesis, stimulation of HTLA and HTTL-B2 cells with PMA induced a significant response at 5-HT2A- and 5-HT2B-Tango receptors (2.6 and 8.6 fold, respectively) in the HTLA, but was absent in the latter, an effect that could be reversed in HTLA with the addition of Jak Inhibitor I (**Figs. 2.1d-2.1h**)[24]. In the same vein, confirmation of the higher specificity of HTTL-B2 over HTLA is exemplified by the lack of activation observed following stimulation of transfected 5-HT2A-Tango receptor with untreated and heat-inactivated FBS, as well as with dialyzed FBS, sera with removed serotonin to prevent nonspecific activity at GPCRs[25]. This effect was also minimally observed with 5-HT2B-Tango, yet absent in the untransfected cells, and negligeable at 5-HT1B-Tango and at other GPCRs that activate the Jak/STAT Pathway, such as CXCR4- and F2R-Tango receptors[26]; interestingly, this artifactual response in HTLA was absent following stimulation with Tet-approved FBS (**Figs. 2.1o-2.1r**). We believe that subtraction of external control of the TRE-Tight promoter compared to the original TRE explains the difference observed for β-arrestin-2 recruitment at some receptors. Hence, some factors present in the serum might artificially enhance promoter activity as shown for DRD2-, HTR5A-, CHRM4-, OPRM1-, ADRB3-, and PTGDR-Tango receptors (**Figs. 2.1i-2.1n**).

To validate cumate induction, time-course and dose-response experiments were conducted on all three of our established cell lines using prototypical GPCR-Tango receptors covering the main subtypes of G-protein primary couplings: AVPR2 (G_s), ADRB2 (G_s), DRD2 (G_i), and CHRM1 (G_q)[27]. To confirm the control of gene expression was dose-dependent, monoclonal cell lines were transfected without cumate, and then stimulated with a cumate concentration-curve starting from 40 µg/mL with 2-fold dilutions (**Figs. 2.2a-2.2f**). Based on the EC50 values of tested receptors, maximal activation is achieved at approximately 10 µg/mL, corroborating other studies that have also used the cumate switch system[28]. Cumate induction was also confirmed to have minimal impact on the basal signals and fold windows of the three HTTL cell lines after reaching maximal activation, yet a slight decrease was generally observed for both parameters at the highest tested induction concentration (**Supplementary Fig. 2.3**). The time-course experiments consisted of adding cumate at the different time points and maintaining it in the cell medium from then on,

ranging from as long as 5 days total cumate exposure to a minimum of 18 hours throughout (**Figs. 2.2g-2.2r**). In general, the best response was observed following approximately 3 days of total cumate exposure, which we expected as the developers of the cumate-gene switch previously observed a maximal expression after 72 hours[21]. Overall, Tango-Trio presents greater dynamic range, sensitivity, specificity, and versatility over the original tried-and-true Tango system.

Tango-Trio generates a compendium of GPCRome basal and agonist-dependent activities

With our established monoclonal cell lines forming the foundations of the Tango-Trio HTS platform, parallel interrogations of the GPCRome were conducted by transfecting a panel of 350 GPCR PRESTO-Tango constructs in arrayed format, the large majority of which consist of Class A members[29]. To investigate proximal GPCR-arrestin interactions and receptor endocytosis at the two possible activated receptor states, agonist-induced activities were screened for in presence of selective agonist at approximately 150 non-orphan GPCRs, while basal activity was probed for using the presence of cumate. Based on initial hit thresholds set to <-2 and >2 log2, fold-changes (E_{max}/E_0) were visualized as heatmaps to depict contrasts between the couplings of arrestin isoforms and corresponding GPCR internalization efficiencies (**Figs. 2.3a-2.3e** and **Figs. 2.4a-2.4f**). Based on NC-IUPHAR classification, heatmaps were constructed for each of the four branches of the non-olfactory class A members (α, β, γ and δ), for orphan class A members, and one covering a select number of receptors spanning the B, C, and adhesion classes, illustrating the diversity within the GPCR superfamily[27,30].

Consistent for both screenings, the similitudes of profiles amongst receptor members of the same subfamily varied on a case-by-case basis. Drawing on examples from the α branch, the Alpha-1 adrenergic-Tango receptors (ADRA1A, 1B, 1D) all preferentially recruited β-arrestin-1 over β-arrestin-2 (approximately 2-3 fold difference) at the basal level, whereas in the case of the Prostaglandin EP-Tango subfamily (PTGER1-4), different basal arrestin selectivity profiles were observed among members, such as PTGER2-Tango's marked selectivity towards β-arrestin-2 and that of PTGER4-Tango towards β-arrestin-1 (**Fig. 2.4a**). These marked differences in arrestin selectivity profiles between receptor subfamilies could be due to the differences in their C-terminal tail and intracellular loop sequences which dictate different phosphorylation codes, influencing the isoform type and degree of arrestin recruitment. It is also important to note however that these selectivity findings must be interpreted with the understanding that all Tango receptors are fused

to a "V2 tail", originating from the C-terminus of AVPR2. Such a phospho-peptide addition is also present in other b-arrestin recruitment assays such as the PathHunter assay[31]. The V2 tail was originally added given its high affinity for β-arrestin2 and for its ability to stabilize the interaction between a given receptor and the recruited arrestin; this addition is indispensable for those of low-affinity or for transient β-arrestin recruitment at many GPCRs. The stabilization of the interaction allows efficient cleavage by the TEV protease but also generates a detectable basal level, resulting in an increased assay quality (z-factor), which is strongly affected when RLU are too low; this is particularly important when performing parallel interrogation or high-throughput screening. When working on a single or a select set of receptors, the V2-tail can easily be removed and experimental conditions adjusted to achieve an acceptable level of RLU counts, if possible. However, for some receptors, the interaction of β-arrestin is of low affinity or transient such that it cannot be accurately detected using a protease-dependent reporter assay. In such cases, the V2 tail should be retained or an alternative assay such as BRET should be envisaged. To further compare GPCR-Tango constructs used in Tango-Trio and unmodified wildtype counterparts, a supplementary table comprising the agonist-induced β-arrestin-1/2 recruitments observed from the EMTA studies and our Tango-Trio work was compiled (**Supplementary Table 2.1**). Although a large number of receptors behave similarly toward β-arrestin-1/2 recruitment, several discrepancies were noted. For example, Tango-Trio detects β-arrestin recruitment at HTR1D-, PTGER1-, GNRGR- and MTNR1B-Tango receptors, while the EMTA biosensors were unsuccessful, or oppositely, β-arrestin recruitment at F2R, LPAR1, LPAR2 and VIPR1 was observed with EMTA but not with Tango-Trio. Moreover, a stronger proclivity for β-arrestin-2 over β-arrestin-1 was also observed in Tango-Trio for certain receptors, such as AGTR1-, PTGER4-, HCRTR2-, and AVPR2-Tango receptors. Similarly, another facet to consider is the influence of the V2-tail on the changes of the arrestin-independent and dependent internalization patterns of GPCRs. For example, based on the HTTL-F agonist-dependent screen (**Fig 2.3**), ADRB1-, 5-HT2A-, ADRA2A-, CHRM3-, CHRM4-Tango receptors all exhibited significant internalization following agonist stimulation, all of which have been previously reported to undergo arrestin-independent internalization; however, other reported GPCRs exhibiting this behaviour such as DRD3, DRD4, UTS2R, AGTR1, ENDRA, EDNRB and APJ were not among our hits. It is not surprising to observe a certain degree of inconsistency between two heterologous systems[32]. Numerous possibilities could thus contribute to the inconsistency observed, especially for β-arrestin recruitment, which requires receptor

phosphorylation by endogenous kinases. In addition to endogenous modulators, such as kinases, the fusion of the receptor and β-arrestins with functionalized proteins tags can affect the recruitment and/or stability of the complexes. The presence of the phosphopeptide (V2 tail) could also contribute to some divergences, but the significant difference in the duration of the experiments (<1 vs. 18 hours) is probably a major factor, especially for efficacy, which is strongly dependent on cell surface receptor abundance. Notwithstanding these discrepancies, we are confident that comparing EC50 (potency) and Emax (efficacy) to an internal reference will provide an accurate differential measure, but as is the case for any artificial system, we cannot rule out that β-arrestin recruitment is over/underestimated compared to endogenous recruitment in a physiological context. The main advantage of our Tango-Trio assay remains the ease of performing parallel high-content or high-throughput screening.

Across the array of interrogated GPCRs, it is obvious that β-arrestin-1/2 are quite promiscuous; however, similarly to Avet et al. who reported that 22% of receptors investigated did not recruit arrestins beyond their established threshold[33], we also observed a significant pool of receptors which exhibited no β-arrestin-1/2 translocation at either basal or agonist-induced states. It should be noted however that very few GPCRs lacked arrestin interactions at both of these states. Additionally, as seen in **Figs. 2.3 and 2.4**, there is little overlap between basal and agonist-induced signatures across the GPCRome; for example, very strong agonist-induced arrestin recruitment at SSTR5-Tango did not correspond to high basal activity (**Figs. 2.3c and 2.4c**). This implies that there are different mechanisms at play that regulate internalization and arrestin activities between an agonist-stabilized GPCR versus basal activity in the absence of agonist[34], as discussed below.

The representation of our screens as heat maps allows one to easily identify receptors with the strongest basal activities, such as CHRM5-, 5-HT1E-, 5-HT5-, NTSR1-, CXCR4-, and MRGPRD-Tango. To exclude the possibility of cumate addition contributing to marked increase of receptor expression, an ELISA was conducted to evaluate receptor surface expression on a select subset of constitutive hits (**Supplementary Fig. 2.4**). No significant differences between non-treated cells versus those with the addition of saturating cumate concentration, compared to the drastic fold-differences observed in the constitutive screen, corroborated that detected hits were a result of bona fide constitutive activities; for example, a modest 1.2-fold difference in receptor expression

was observed in HTTL-B2 cells transfected with CXCR4-Tango, compared to the 67-fold change in constitutive β-arrestin-2 recruitment. The lack of correlation between receptor expression and apparent basal activity was also confirmed across a larger panel of receptors including a wide range of basal arrestin recruitment profiles (**Supplementary Fig. 2.5**). Finally, absolute receptor expression levels were not found to affect constitutive activity, as titrating Tango construct DNA did not generally reduce the cumate-induced fold change (**Supplementary Fig. 2.6**).

Validation of GPCR internalization, β-arrestin-1/2 coupling and selectivity profiles

Secondary screening of top potential hits was carried out in a dose-dependent manner (agonist or cumate, accordingly) to validate our platform's high-throughput performance (**Figs. 2.5a-2.5o** and **2.6a-2.6o**). With the primary screen findings in agreement with our concentration-response profiles, thus confirming the platform's reproducibility, we exploited Tango-Trio to perform more detailed analyses of the arrestin selectivities and corresponding GPCR endocytosis patterns observed. This was accomplished by producing the β-arrestin-1/2 and internalization dose-response curves for approximately 150 non-orphan GPCRs, and most important, presenting for the first-time dose dependent constitutive activation curves at approximately 200 receptors, including more than 50 orphans (**Supplementary Figures 2.11-2.26**). Many of our high-basal and agonist-dependent findings are in agreement with previous studies, such as high constitutive activity at GPR182-Tango receptor (**Fig. 2.6i**)[35,36]. Moreover, Tango-Trio was able to detect activity at GPCRs that could not be validated in PRESTO-Tango[13], including BAM-22 at MRGRPX2-Tango (**Fig. 2.5m**), and β-Alanine at MRGPRD-Tango (**Fig. 2.5n**).

While HTTL-B1 and HTTL-B2 captures the nuanced differences between arrestin couplings and selectivities at receptors, our internalization measures are not as robust. Especially in our HTTL-F agonist-dependent screen, very few hits were detected, with the majority of receptors producing the strongest agonist-induced internalization belonging to the β branch, such as GPBA-, NMBR-, CCKBR-, GHSR-, and HCRTR2-Tango receptors (**Fig. 2.5i** and **2.5j**). On the other hand, our HTTL-F is better-suited for studying constitutive endocytosis, seeing as considerably more receptors had stronger constitutive internalization profiles, such as GPR126-, GPR87-, and CHRM5-Tango (**Fig. 2.6c**, **2.6g** and **2.6k**). As discussed below, the selectivity of FYVE-targeted early endosome trafficking should be re-evaluated.

Based on our validation of hits from our β-arrestin-1, β-arrestin-2, and FYVE screens, distinct GPCR selectivity profiles towards the arrestin isoforms were observed. Regarding constitutive activity, receptors can be clustered into three distinct functional classes, specifically those that interact fairly equally with both isoforms, those that preferentially recruit β-arrestin-1 over β-arrestin-2, and vice versa. Based on constitutive activity curves, it seems that the constitutive internalization at a given receptor corresponds to the profile of one of the β-arrestin isoforms, such as those observed at 5-HT1D-, CHRM5-, OXTR-, SCTR-, and GPRC5A-Tango receptors, amongst others (**Figs. 2.6a**, **2.6c**, **2.6e**, **2.6l** and **2.6n**). This observation follows the widely accepted classical paradigm of how arrestins play a central role in GPCR endocytosis via the predominant clathrin-mediated pathway. However, this is not a uniform correlation, involving exceptions where either significant constitutive internalization is observed in the absence of arrestin activities, for example in the case of GPR126- and VIPR2-Tango (**Figs. 2.6k and 2.6m**) or oppositely, strong β-arrestin-1 and/or β-arrestin-2 recruitment but negligeable receptor internalization, such as the case of GPR37L1- and MRGPRD-Tango (**Figs. 2.6f and 2.6h**). Indeed, these findings confirm that GPCR endocytic pathways are more diverse than originally defined, as an increasing number of receptors are found to be endocytosed via alternate pathways besides clathrin-mediated, including the caveolae-dependent and fast endophilin-mediated endocytosis (FEME) pathways, as well as another 30 known examples of GPCRs have been found to internalize independently of arrestins altogether[32].

As for agonist-dependent activity, although similar arrestin selectivity profiles were also observed, the vast majority fell under two functional classes, equal (e.g., **Figs. 2.5c, 2.5d and 2.5j**) or preferential (e.g., **Figs. 2.5b, 2.5g and 2.5m**) recruitment of β-arrestin-2 over β-arrestin-1. Our results parallel those of Oakley et al. who delineated two major classes of receptors based on the 10 GPCRs that they studied, namely "Class A" receptors which bound β-arrestin2 with higher affinity than β-arrestin1, and "Class B" receptors which bound both β-arrestin isoforms with similar high affinities[37]. Similar subsets were observed in Avet et al.'s recent publication profiling the engagement of different G-protein families at 100 therapeutically relevant GPCRs, including β-arrestin1 and β-arrestin2 following agonist stimulation[33]. Orthogonal validation of GPCRs with pronounced arrestin isoform selectivities was conducted in BRET2, which revealed discrepancies between the two systems (**Supplementary Fig. 2.7**). For example, β-arrestin1 is recruited at a

much lower efficacy compared to β-arrestin2 at AGTR1 in Tango-Trio (**Fig. 2.5b**). In BRET however, this selectivity is not observed, with very little difference in recruitment observed between the two isoforms (**Supplementary Fig. 2.7e**). Given that BRET experiments occur over a short duration, the results obtained are based on the amount of receptor present at the time of adding the ligand, and thus, other factors such as receptor internalization, the role of the intracellular pool, and binding kinetic profiles will have minimal effects, whereas the Tango-Trio, being a signal amplification system, may disproportionately magnify efficacies due to the aforementioned factors. Nonetheless, both systems have different limitations and are useful in their own respects for the purposes of screening and pharmacological characterization and should not be interpreted as a measure of endogenous recruitment, but rather as a pharmacological tool to compare drug activity towards a reference compound.

Thus, by using Tango-Trio to screen the GPCRome and distinguishing functional subsets of GPCRs, this might give molecular insight into structural interface positions common among these related receptors, which could be involved in recruitment and internalization.

Mechanistic insights into basal GPCR activities revealed by Tango-Trio

Besides the wealth of basal and agonist-induced activation profiles generated with Tango-Trio, additional explorations of the applications of this platform were undertaken, including studying inverse agonists and their relative abilities to subdue constitutive activity versus steady-state recruitment. Seeing as inverse agonism may appear differently based on cell phenotypes[38], we chose a panel of drugs classified as either inverse agonists or antagonists to target GPCRs exhibiting high constitutive β-arrestin-1 and/or β-arrestin-2 recruitment (**Figs. 2.7a-2.7m**)[39]. A spectrum of inverse agonistic properties was validated, albeit no drug was able to completely ablate the basal activity observed. For example, O-1918 reduced the response observed at GPR55-Tango by almost half in both HTTL-B1 and HTTL-B2 (**Figs. 2.7a-2.7b**)[40], while at HRH1-Tango, stimulation with Mepyramine reduced constitutive activity only for β-arrestin-2, unlike its counterpart Cetirizine which could inhibit activities in both cell lines (**Figs. 2.7c-2.7d**). Furthermore, certain compounds previously designated as antagonists/inverse agonists, such as FC-131 at CXCR4-[41] (**Figs. 2.7e-2.7f**) and Tolvaptan at AVPR2-Tango (**Figs. 2.7g-2.7h**), increased the constitutive translocation of β-arrestin-1 and β-arrestin-2 in our system. Thus, our

platform, nor other arrestin-based assays, are not entirely suitable for quantifying measurements of inverse agonism given the range of arrestin activities observed. For instance, in both PRESTO-Tango and Tango-Trio, Tolvaptan increased arrestin recruitment at AVPR2-Tango, while Pindolol resulted in a depletion of arrestin recruitment at the 5-HT1B-Tango (**Supplementary Fig. 2.8b and 2.8e**). To exclude the possibility of artifacts arising due to endogenous cleavage GPCR-Tango fusion constructs, the same receptors were co-transfected with β-arrestin-2 in HTTL, with no arrestin recruitment detected (**Supplementary Fig. 2.9**). Thus, although the identification of inverse agonists is not possible with arrestin-based assays per say, Tango-Trio is valuable for their characterization, more specifically providing novel information about their effects on constitutive arrestin recruitment and receptor internalization. It seems that G-protein uncoupling using inverse agonist is clearly a different receptor pool or receptor state and cannot be directly translated toward β-arrestin activity. We cannot rule out that G-protein uncoupling could result in β-arrestin recruitment for some receptors, as seen for CXCR4- (FC131-treated) and AVPR2- (Tolvaptan-treated) Tango receptors.

Tango-Trio HTS produces variegated snapshots of the arrestin couplings of GPCRs and their corresponding internalization efficacies, suggesting that the mechanisms of endocytosis among GPCR members are more heterogeneous than originally conceived, especially those of constitutive nature. To further this point, the dominant-negative dynaminK44A was co-transfected in HTTL-F cells with select GPCRs exhibiting strong constitutive internalization. As expected, various degrees of inhibition were observed, from partial inhibition in the case of 5-HT4-Tango (**Fig. 2.7p**), to complete blocking of GPR87-Tango endocytosis (**Fig. 2.7n**), suggesting a greater dynamin-dependence involved during its constitutive internalization process. Intriguingly, overexpressing dynaminK44A resulted in a substantial increase in constitutive CHRM5-Tango endocytosis (**Fig. 2.7o**), bringing to light the possibility of multiple compensatory internalization mechanisms at play at a given receptor. Expanding this idea, β-arrestin-1/2 knockdown was performed to evaluate the arrestin dependence at certain GPCRs with high constitutive internalization, confirming partially arrestin-independent endocytosis at CHRM5- and CD97-Tango receptors (**Supplementary Fig. 2.10a and 2.10e**).

A recent appreciation has grown for GPCR-interacting proteins, with emerging findings supporting how they modulate GPCR expression at the cell surface, signal transduction, and receptor endocytosis, amongst others[42]. Of particular note are the protein kinases that phosphorylate specific sites on the intracellular loops and C-terminal tail of GPCRs, inducing specific arrestin roles and varying functional consequences for the modified receptors[43]. Given limited literature exploring the distinct functions of kinases and their contributions to constitutive activity, we examined the Human Protein Atlas (HPA) consensus tissue-specific expression levels of serine/threonine-specific protein kinases (ST kinases) previously reported to phosphorylate GPCRs, such as GRKs, PKAs, and PKCs amongst other[43], as well as the expression levels of β-arrestin-1/2 and of select receptors with high constitutive selectivity for one arrestin isoform over the other. We postulated that the kinases and receptors of similar tissue expression profiles may have overlapping activities. Our generated PCA plots revealed varying signatures for each of ST kinase families, some of which forming clusters with our constitutively active GPCRs based on shared expression patterns (**Fig. 2.8**). Based on the GRK plot, it seems that GRK2, GRK6 and β-arrestin-2 might share a functional network[44], especially at CXCR4[45] and PTGER2, which were found to be highly selective for β-arrestin-2 at constitutively active receptors (**Fig. 2.8a**). A dense cluster including GRK5 also leads us to speculate a greater involvement of this GRK at constitutively active receptors selective for β-arrestin-1, such as AGTR2, ADRA2A, PTGER3, and SUNCR1. The restricted expression profile of GRK4 also suggests that this might be the predominant GRK acting at receptors such as MC1R. Despite a lack of research into the lesser-reported kinases capable of phosphorylating GPCRs, certain interactions could be confirmed from past studies, such as the role of PIMs at CRCR4 (**Fig. 2.8e**)[46,47]. Thus, our analyses may also reveal novel functions at these ST kinases GPCRs; for example, we hypothesize that Ca^{2+}/calmodulin-dependent kinases, including CAMKI, CAMKII and CAMKIV complexes, might significantly contribute to the phosphorylation and subsequent recruitment of β-arrestin-1 to GPCRs, although this has yet to be experimentally investigated (**Fig. 2.8h**).

DISCUSSION

The functional heterogeneity of GPCRs is attributed in part to their spectral activation states, desensitization, and internalization, accounting for their multifaceted signalling processes.

Towards establishing accurate and comprehensive functional profiles, this study developed Tango-Trio, a polyvalent screening platform consisting of a triad of stable cell lines, capable of interrogating constitutive and agonist-activated GPCRome activities. The foundation of the platform, the HTTL reporter cell line, stably expresses a luciferase gene under the control of an improved low-background and sensitive TRE-Tight promoter compared to the original PRESTO-Tango[16]. To increase the versatility of this system, Tango-Trio monitors the translocation of β-arrestin1, β-arrestin2, and GPCR internalization using a FYVE domain, all of which were cloned to the truncated TEV219 protease for its enhanced signal-noise ratio[19]; these chosen elements provide valuable insight into crucial stages in the GPCR life cycle. Despite sharing a high degree of structural and sequence similarity, the non-visual arrestin isoforms have been reported to accomplish disparate roles[9]. For example, one study demonstrated that silencing β-arrestin2 reduced agonist-induced PAC1R and C3aR receptor internalization, whereas silencing β-arrestin1 had no effects[48,49]. Given its implications in signal regulation, desensitization, resensitization, and ligand scavenging functions of some receptors, our measurements of GPCR internalization also contribute to our account of the diversity of GPCR-dependent dynamics[50].

The scope of our platform is broadened further by the controlling the expression of these multiple probes using a cumate-controlled lentiviral vector[21], enabling the interrogation of not only at the agonist-induced state, but also monitoring basal activities in a dose-dependent manner by adjusting the expression level of the fusion proteins, which is not feasible with existing HTS technologies. Two aspects affect the magnitude of basal activity, specifically a receptor's conformational flexibility from the inactive to active states in the absence of ligand, and state-independent GPCR-effector coupling. Previous quantifications of constitutive activity have been extracted based on the latter factor, specifically constructing receptor-density response curves by regulating the amount of receptor expression and measure resultant increases in the basal responses[38]. Tango-Trio is one of the first of its kind to modulate GPCR-effector coupling stoichiometry not through changing receptor density, but by tuning the density of cytoplasmic effectors, specifically β-arrestin1, β-arrestin2, and FYVE, to probe basal activity. Moreover, seeing as continuous overexpression of engineered proteins could potentially give rise to spurious GPCR dynamics[51], titratable induction of Tango-Trio fusion proteins enables greater management of the cellular

environment to one more reflective of the native in vivo setting if desired, by tuning the intensity of gene expression during profiling of agonist-stimulated receptors.

Following establishment of our stable cell lines, we conducted HTS of the GPCRome to shed light into how β-arrestin1 and β-arrestin2 differ in their couplings and selectivity at GPCRs, and provide insight on how this arrestin selectivity may play a role in GPCR trafficking properties. After validating select hits from our primary screen, we sought to further characterize constitutive and ligand-dependent dynamics. Given the inability to capture pharmacological parameters (EC_{50}, E_{max}/E_0, etc.) regarding basal activities in general, as well as the lack of information regarding ligand-induced β-arrestin1 recruitment and internalization across the GPCRome, we profiled approximately 200 GPCRs, including over 50 orphans, in cumate and/or agonist dose-response fashion. Interestingly, we observed distinct functional signatures between basal and agonist-dependent activities observed at GPCRs, suggesting different mechanisms in play at these different activation states[34]. Although the promiscuity of couplings detected for both isoforms is supported by the fact that these non-visual β-arrestins are ubiquitously expressed to regulate hundreds of GPCRs within the human body[8], we observed a significantly larger percentage of receptors which were more selective towards β-arrestin2 over β-arrestin1 at both basal and agonist-activated states. From a structural standpoint, β-arrestin2 has less defined secondary structure within its C-terminal basket, resulting in increased flexibility and adaptability to the structural differences of GPCRs[52], which may attribute why it is less selective and couples preferentially to more receptors compared to β-arrestin1. Thus, Tango-Trio may be useful for future development and testing of arrestin-isoform biased compounds, if there are positive functional outcomes that are shown to emerge from favouring β-arrestin1 versus β-arrestin2 recruitment; although few reports of this nature of functional selectivity have been explored, a couple of existing agonists have been demonstrated to favour one arrestin isoform over another, such as 2-arachidonoylglycerol and anandamide[53]. Addedly, the original PRESTO-Tango platform interrogates only the recruitment of β-arrestin2, one of the two non-visual arrestins expressed in vertebrates. While it has been previously demonstrated that β-arrestin1 is the most prevalent isoform in most cells, comprising more than 90% of the total arrestin complement[54], few studies have investigated its recruitment to GPCRs on a larger scale; Tango-Trio enables such an interrogation, and simultaneous comparison to β-arrestin2 selectivity. Finally, some receptors lacked interactions with either isoform, which has

been typically attributed to the lack of consensus sequences for GRKs[55]. Nonetheless, a growing body of evidence has indicated that arrestin recruitment is not entirely dependent on phosphorylation by GRKs specifically, but also by other serine/threonine kinases[43], as we explored later on. Moreover, arrestin recruitment is a biphasic process that involves the partial engagement of the phosphorylated GPCR's C-tail with arrestin and a fully engaged complex where the receptor core interacts with the arrestin finger loops[56]. As a highly sensitive reporter assay, we cannot exclude that Tango-Trio can detect partially engaged complexes to phosphorylated and non-phosphorylated receptors. Given that interaction with the receptor core requires complete activation of the receptor and G-protein dissociation, the constitutive interaction observed is probably highly dependent on receptor C-tail phosphorylation and thus highly dependent on kinases present within the cellular system used[57]. It will be interesting in futures studies to measure the changes in this receptor constitutive distribution while overexpressing a specific kinase.

Unfortunately, one caveat to Tango-Trio is that the dynamic window of GPCR internalization is smaller than that observed with arrestin activity. This could be attributed to multiple reasons but we believe that the range of observed internalization across the GPCRome is not as expansive as the range of arrestin activities. Moreover, the transit of the receptor to early endosomes could be too fast for efficient TEV cleavage or may lead to weak tTA translocation into the nucleus. Another potential pitfall of using the FYVE domain to track GPCR internalization is the known PI3K activation by some GPCRs, which in turn will increase phosphatidylinositol 3-phosphate (PIP3) at the cell membrane and endosomes, possibly contributing to biased results. Another important distinction is that for HTTL-B1 and HTTL-B2, it is the expression of arrestin effector proteins that is affected by cumate induction, hence tuning the process of GPCR-arrestin coupling itself, whereas for HTTL-F, titratable cumate addition does not influence the process of receptor internalization, but rather only changes the expression of the FYVE probe that tracks it. Finally, the FYVE domain directly interacts with the inositol polar heads of PIP3, which is present on the surface of the endosome but also at the plasma membrane. It has been proposed that dimerization of FYVE-domain containing protein amplifies the weak binding of individual FYVE fingers to the phospholipid. We cannot exclude that the TEV219 fusion disrupts dimerization, nor that the expression of only the FYVE-domain has a very low affinity, thus reducing sensitivity. We do not exclude to test other fusion proteins such as EEA1 containing the FYVE domain and the adjacent

dimerization coiled-coil region[58]. Overall, the use of FYVE domain fusion protein for tracking GPCR internalization should be used with caution; nonetheless, the variety of responses observed in our GPCRome screening highlights some interesting observations that will require further investigation.

Tango-Trio is especially valuable for studying orphan receptors, whose lack of identified endogenous ligands presents a challenge to studying said receptors[59]. Seeing as existing tools have focused on detecting classical G-protein signalling, Tango-Trio's ability to quantify activity independent of G-proteins is a suitable tool for deorphanization efforts[60]. By using the Tango-Trio to investigate the internalization profiles and potential biases of orphan receptors towards different isoforms of β-arrestin, we hope our platform can identify novel ligands for orphans that would not be detected by G-protein dependent changes, especially given that Tango-Trio represents, to our knowledge, one of the first assay which is able to concurrently quantify and compare the degree of constitutive β-arrestin1/2 translocation and internalization at a GPCRome-wide level, and is also capable of profiling orphan activity in a dose-dependent manner.

Interestingly, none of the inverse agonists tested in our study was able to completely block the basal arrestin recruitment. For this reason, we defined the basal activity as the summation of state-dependent constitutive activity and state-independent activity (steady-state). We cannot exclude that amplification systems, including the Tango assay, fail to accurately detect constitutive activity, which represent a small percentage within the ensemble of a receptor's conformational landscape[61]. Given that basal activity is highly cell-dependent as it influenced by the basal phosphorylation of GPCRs[57], it is difficult to discriminate between basal and constitutive activity in our system apart from using inverse agonists. Thus, the partial decrease in arrestin recruitment observed for certain compounds, such as O-1918, Cetirizine, and Thiothixene, could be attributed to their effects on the small population of constitutively active receptors, but they cannot blunt the level of basal arrestin recruitment. Nonetheless, if this were the case, further studies would be warranted to explain why a significant enhancement in arrestin recruitment was observed for other inverse agonists, such as FC131 and Fluspirilene. It is becoming more evident that receptor activation follows a multistate model in which G-proteins and arrestins stabilize specific conformations. Each of these conformations can be further stabilized by different ligands, leading

to a broad intrinsic efficacy landscape, which in certain cases, can be opposite to each other when comparing two signaling pathways[62]. Finally, for some receptors, the uncoupling of G-proteins with an inverse agonist could facilitate b-arrestin recruitment. Another important consideration is that in vitro assays may fail to capture the true potency and efficacy of certain drugs with slow on-rates[63].

While Tango-Trio's ability to measure basal activity supports the discovery and study of inverse agonists in vitro, whose properties can be assessed based on the depression of constitutive arrestin translocation, it should be complemented with G-protein dependent profiling, especially since constitutive activity, by definition, is observed due to spontaneous G-protein activation[7]. Indeed, several inverse agonists profiled in our study produced either no change or an enhancement in constitutive arrestin recruitment, and a previous study saw no arrestin recruitment occurring in the presence of the GHSR inverse agonist SPA[61]. Therefore, given the diversity of responses we observed based on the type of inverse agonist tested, arrestin activities should not be the sole measure of the inverse agonistic properties of a compound. Although assays such as BRET will capture the direct effect of most drugs onto the conformational landscape of the receptors, some have a more complex pharmacology, acting as allosteric modulators, bitopic ligands, protean agonists, pharmacochaperones, or even a mixed pharmacological profile depending on receptor subpopulation. Moreover, the overall resultant activity, when used in vivo, is a summation of all effects of the drug toward the receptor when used for an extended period and thus, must also include its impact on receptor abundance and receptor post-translational modification. These effects are rather slow and require prolonged incubation of the drug onto the cell expressing the target receptor. In those cases, a reporter system such as the Tango-Trio, which involves incubation with drugs for >8 hrs, may capture pharmacological behavior not detected with short term incubation (<1h).

By using the dynaminK44A loss-of-function mutant, we were also able to determine the extent of dynamin dependence during internalization[64]. However, given the numerous dynamin-dependent (e.g., clathrin-mediated, FEME,) and -independent pathways (e.g., CLIC/GEEC, micropinocytosis), further investigations into the other mediators of endocytosis are needed to elucidate the specific type of endocytosis mechanism employed at a given receptor. Of notable

distinction is FEME, which has been shown to cargo several amine GPCRs, including ADRB1, ADRA2A, DRD4, and CHRM4, caveolae mechanisms observed for ADRB2, AGTR1, ENDRA, and GLP2R, and of course, the canonical clathrin-dependent endocytosis such as at APJ, DRD3, and CHRM3[32,65]. Arrestin-dependence of either isoform during the internalization of a given GPCR can also be orthogonally assayed used dominant negative arrestins[66].

While Tango-Trio uses modified GPCR constructs, the findings presented herein demonstrate that the addition of the V2-tail itself cannot fully account for differences between our Tango-based platform and those that employ unmodified WT GPCRs, such as the EMTA system. With regard to the V2 tail, while its original purpose was to increase basal β-arrestin2 recruitment and thus may artificially enhance its detection, seeing as it was added to all the receptors found in the PRESTO-Tango kit, any artificial increases in the Tango signal would still be proportional amongst all. Furthermore, PRESTO-Tango developers tested the effects of removing the V2 tail for some receptors and found variable results; notably, the removal of the V2 tail decreased the ligand-induced responses of some, e.g., the FFAR2 free fatty acid receptor, and had little effect on the ligand-induced responses of others e.g., the LTBR4 leukotriene receptor[1]. Another factor that could also contribute to the discrepancies in results between EMTA and Tango-based methods is the effect of receptor internalization when β-arrestin1/2 are overexpressed, especially considering the difference in the duration of the experiments. Overexpression of β-arrestin1/2 could contribute to increased internalization for certain receptors, which could account for the extent of arrestin recruitment, such as the case with OPRM1; agonists will also vary in their capacity to induce endocytosis of a given receptor; e.g., DAMGO at OPRM1 promotes rapid internalization, as opposed to morphine[67]. On the other hand, given that EMTA experiments occur over a short duration, the result obtained is based on the amount of receptor present at the time of adding the ligand, and thus, other factors such as receptor internalization will have minimal effects unlike in Tango-based. Finally, one of the biggest factors that limit comparisons between systems is that the EMTA method, as like other systems which use unmodified GPCRs, requires overexpression of GRK2 to examine β-arrestin-1/2 interactions, a limitation which could influence the cellular context, stoichiometry and levels of expression of GRKs, possibly leading to potential artifactual downstream signalling/arrestin recruitment measurements obtained. For example, the EMTA method found that among the receptors able to recruit β-arrestins, only a very small number

selectively recruited β-arrestin-1 (1.3%) or β-arrestin-2 (6.4%), most of them recruiting both β-arrestins in the presence of GRK2 (92.3%)[33]. Tango-Trio does not require the overexpression of GRKs, so is preferable in that regard, and the level of expression of β-arrestin-1/2 and Fyve fusion proteins is modifiable using cumate induction, to be as close to the native environment/context as possible. If GRK2 or other kinases were overexpressed in Tango-Trio, we believe that several of the GPCRs with weak/no arrestin signals would also be detected in our system, and the degree of preferential β-arrestin isoform recruitment may also shift. In short, it must be underscored that both systems may artificially increase arrestin recruitment, either using modified GPCR constructs such as in Tango-Trio or using WT GPCRs but with the addition of a kinase such as in EMTA. Nonetheless, based on the intended purpose of an experiment, these methods have their own advantages and disadvantages and thus one system cannot truly replace the other, but rather both should be used as a complement.

One limitation to the profiles captured by Tango-Trio is that they may not be portable from different tissues, as the level of expression and identities of GPCR interactors directly influence the regulation of receptor signalling, localization and trafficking[4]. One study demonstrated that the constitutive activity of glutamate metabotropic receptors is depressed in the presence of Homer 3 scaffold protein[68]. Another example reports that of the GRK family members, GRK4 exclusively mediates the constitutive phosphorylation of DRD1[69]. Relevant to Tango-Trio, mRNA expression analysis of endogenously expressed GPCR-related proteins reveals that while HEK293 cells, the cell lineage upon which our platform was established, express numerous isoforms and full repertoires of numerous GPCR-interacting proteins, such as PKA and PKCs, they also do not express significant levels of certain essential effectors, such as GRK2[70], thereby impairing complete profiling at certain GPCRs dependent on GRK2 phosphorylation. The importance of GRK specificity is epitomized by a study in which GRK2 and GRK3 phosphorylation of their tested receptors (ADRB2 and CHRM2) was agonist-dependent, whereas GRK5 and GRK6 were able to phosphorylate in the absence of agonists[71]. Despite the challenge introduced by tissue-specific variations, Tango-Trio is a rich resource of arrestin coupling, selectivity and internalization profiles of hundreds of GPCRs, which can be confirmed and supplemented using orthogonal assays.

Studying GPCR activities and differences between signaling events is crucial for expanding our mechanistic understanding of GPCR signaling, and in turn, advancing the development of improved GPCR-targeted therapeutics. Towards these efforts, our wealth of data will help to functionally characterize GPCRs based on their β-arrestin1 and β-arrestin2 couplings, selectivities, and internalization efficacies. On a larger scale, the versatility and robustness of our platform is well-suited to illuminating the big picture on the elements governing GPCRome pharmacological activities. We envision Tango-Trio to spur a transformational change on the study of basal and constitutive GPCR activities, and to promote research into GPCR constitutive versus agonist-induced activation mechanisms.

METHODS

Cell culture

Human Embryonic Kidney cells (HEK293T) were maintained in Dulbecco's modified Eagle's medium (DMEM) supplemented with 5% fetal bovine serum (FBS), 5% bovine calf serum (BCS), and 100 µg/mL of penicillin-streptomycin at 37°C in a humidified atmosphere containing 5% CO_2. HTL (HEK293T stably expressing a luciferase reporter gene) and HTLA cells (HTL cells stably expressing a human β-arrestin-2 fused to Tobacco Etch Virus protease), both kindly provided by Dr. Richard Axel, were maintained in DMEM supplemented with 5% FBS, 5% BCS, 100 µg/mL of penicillin-streptomycin, 2.5 µg/mL of puromycin and 50 µg/mL of hygromycin.

HTTL were generated by transfection of HEK293T with modified pNLCoI1 vector (Promega) containing the luciferase2 (luc2) coding sequence under the control of the TRE-Tight promoter. Cells were transfected using PEI transfection method[72] and selected with hygromycin at 100 µg/mL. Colonies were picked, expanded, eventually duplicated, and further tested in 6-well format by transient transfection of a receptor and β-arrestin2-TEV219/pcDNA3.1+. The best clone was selected based on growth and β-arrestin2 recruitment at different GPCRs, which were previously validated by PRESTO-Tango[13].

HTLL-B1, -B2 and -F were generated by lentiviral infection of pCDH-CuO-MCS-EF1α-CymR-T2A-Bleo3 SparQ plasmid encoding β-arrestin2-TEV219, β-arrestin1-TEV219 or FYVE-TEV219 as per supplier instructions and selected using zeocin at 200 µg/mL. Colonies were picked, expanded, eventually duplicated, and further tested in 6-well format by transient transfection of a

given receptor. The best clone was selected based on growth and β-arrestin1/2 recruitment or internalization at previously validated GPCRs.

Tango-Trio cell lines generated herein (HTTL, HTTL-B1, HTTL-B2, HTTL-F) are maintained continuously on dishes coated with 5 μg/mL collagen (Gibco). Tango-Trio cell lines are readily available and free of charge from the corresponding author upon request.

Transfection

Cell transfections were performed using a modified polyethyleneimine (PEI) transfection method[72]. Briefly, $1.5x10^6$ cells were plated in a collagen-coated well of a 6-well plate with 2 mL of complete growth medium. 2 μg of DNA was mixed with 200 μL of Opti-MEM medium followed by addition of 6 μL of PEI (Polysciences) reagent stock solution (1 mg/mL, pH 7.0). The mixture was added dropwise to cells after 20 minutes incubation at room temperature. Medium was changed the next day and replaced with complete fresh medium. For stable cell line generation, antibiotics were added 48-hours post-transfection.

Tango β-arrestin recruitment assay

Assays were performed using modifications of the original Tango assay, as detailed below[13,29]. Cells were plated on collagen-coated dishes and transfected by the PEI precipitation method as described above. The day following transfection, the cells were plated in DMEM supplemented with 1% dialyzed FBS into collagen-coated 384-well white clear bottom cell culture plates at a density of 20,000 cells/well (or 16,000 cells/well for same-day transfection) in a total volume of 40 μL. The following day or the same day 5 hours after seeding, ligand solutions were prepared in filtered assay buffer (20 mM HEPES, 1× Hanks' balanced salt solution (HBSS), pH 7.40) at 3X and added to cells (20 μL per well) for overnight incubation (16-20 hours). Cumate, at indicated concentrations, was directly added in the complete medium from a water-soluble stock solution (10,000X in 95% ethanol). For most experiments, cumate was added at the time of cell plating (a day before transfection) and kept throughout the experiment. For time-dependent experiments, cumate was added as indicated in the text. The following day, media and drug solutions were removed, and 20 μL per well of homemade luciferase detection reagent (108 mM Tris–HCl; 42 mM Tris-Base, 75 mM NaCl, 3 mM MgCl2, 5 mM Dithiothrei-tol (DTT), 0.2 mM

Coenzyme A, 0.14 mg/ml D-Luciferin, 1.1 mM ATP, 0.25% v/v Triton X-100, 2 mM Sodium hydrosulfite) was added. Plates were incubated for 10 minutes at room temperature in the dark before counting using Synergy Neo2 microplate reader (BioTek Instruments) and collected using Gen5 software v3.11 (BioTek Instruments). Data were subjected to non-linear least-squares regression analysis using the sigmoidal dose-response function (3-parameters modeled using Y=Bottom + (Top-Bottom)/(1+10^((LogEC50-X))); 4-parameters modeled using Y=Bottom + (X^Hillslope)*(Top-Bottom)/(X^HillSlope + EC50^HillSlope)) provided in GraphPad Prism v9.5.1. Data is presented as Relative Luminescence Units (RLU) and was processed (calculation of mean, SD or SEM, baseline correction as percentage difference using 100* (Value-Baseline)/Baseline) as indicated in figure legends. Parallel interrogation was performed as previously published by us[29].

Measurement of cell surface expression by ELISA

HTTL-B1, HTTL-B2 and HTTL-F were plated in collagen-coated 6-wells either with or without 30 µg/mL cumate. 24 hours later, cells were transfected with a select number of validated GPCR hits from the constitutive HTS. Transfected cells were subsequently re-plated in 384-well plates at 30,000 cells/well and fixed for 10 minutes using 20 µL/well of 4% paraformaldehyde. Blocking was performed by incubating cells for 30 minutes with 20 µL/well of 5% normal goat serum in PBS, followed by the addition of 20 µL/well of 1/10,000 diluted anti-FLAG-HRP conjugated antibody (MilliporeSigma) for 1 hour and two washes of 80 µL/well PBS. Supersignal ELISA Femto Substrate (Thermo Fisher Scientific) was applied per well, and luminescence was subsequently read with Synergy Neo2 microplate reader (BioTek Instruments).

Principal Component Analysis and visualization of RNA tissue-specific expression data

Human Protein Atlas (HPA) RNA consensus tissue gene data (version 21.0 and Ensembl version 103.38., accessed at https://www.proteinatlas.org/about/download) summarizing the expression levels in 55 tissues was extracted for β-arrestin-1 and -2 (ARRB1 and ARRB2), for select receptors with significant constitutive selectivity for at least one arrestin isoform (GPR182, AGTR2, ADRA2A, GPR37L1, SCTR, ADRB3, PTGER4, SUNCR1, PTGER3, MRGPRG,

NPY5R, NPY1R, GLP1R, FPR1, MC1R, FPR3, 5-HT5, MRGPRD, GPR87, CXCR4, HRH1, AVPR2, 5-HT4, 5-HT2A, NTSR1, GLP2R, 5-HT1D, CXCR2, 5-HT1B, 5-HT1E, PTGER2, 5-HT2B, PTGDR), and the following serine/threonine kinases: GRKs (GRK2, GRK3, GRK5 GRK6), PKA (PRKACA, PRKACB, PRKACC), PKCs, PKNs, and PKDs (PRKCA, PRKCB, PRKCG, PRKCD, PRKCE, PRKCH, PRKCQ, PRKCI, PRKCZ, PKN1, PKN2, PKN3, PKD1, PKD2, PKD3), PKGs (PRKG1-2), PIMs (PIM1-3), AKTs (AKT1-3), GSK3 (GSK3A, GSK3B), CAMKI, CAMKII, and CAMIV (CAMK1D, CAMK1G, CAMK2A, CAMK2B, CAMK2D, CAMK2G, CAMK1, CAMK4, PNCK), CK1s and CK2s (CSNK1A1, CSNK1D, CSNK1E, CSNK1G1, CSNK1G2, CSNK1G3, CSNK2A1, CSNK2A2, CSNK2A3, CSNK2B). Despite protein levels not always equating to RNA expression levels, the latter was used as it was more complete than the existing protein expression data. The data was analyzed using principal component analysis (PCA) on our standardized data ($X_{standardized} = (X_{raw} - \bar{X})/sx$, where $\bar{X}$ is the mean and sx is the standard deviation of the variable value). The number of PCs were selected using GraphPad Prism v9.5.1's Parallel Analysis Approach (n=1000 Monte Carlo simulations; PC1 and PC2 selected with eigenvalues greater than the 95th percentile of simulated counterparts), and subsequently visualized as loading plots.

Bioluminescence resonance energy transfer (BRET2) measurements

HEK293T cells were seeded in 6 well plates at $1.2x10^6$ cells per well and were transfected with 0.5 µg of GPRC-RLuc8 construct and 0.5 µg of β-arrestin1/2-GFP2 using Jetprime (PolyPlus transfection). Following transfection, cells were detached and split on PLL-coated white 96-well assay plates (Perkin Elmer). 24 hours later, spent medium was aspirated and replaced with 60 µL of 1X HBSS buffer, followed by 30 µL of serial dilutions of agonist at 3X concentration. Plates were incubated as 37°C for 30 minutes, and 10 µL of Coelenterazine 400a (Nanolight Technologies) at 50 µM was added to each well, for a final concentration of 5 µM. Plates were incubated for 10-15 minutes at room temperature to allow the signal to stabilize, and subsequently read using the Hidex Sense Beta Plus microplate reader (Gamble Technologies) with 405 nm (RLuc8-Coelenterazine 400a) and 500 nm (GFP2) emission filters, at 1 second/well integration times.

shRNA knockdown, RNA isolation and RT-qPCR assay

Lentiviral β-arrestin-1 and -2 shRNA plasmids, obtained from the High-Throughput Screening Lab at the Children's Hospital of Eastern Ontario Research Institute, were transfected in HEK293T cells, along with psPAX2 and VSV-G vectors. The medium was replaced the following day with complete growth medium, and lentiviral shRNA medium was collected following 48 hours transfection. For the knockdown experiment, HTTL-F cells were seeded in either complete medium or in the previously prepared lentiviral β-arrestin-1 and -2 shRNA medium (combined at a 1:1 ratio), with infection of cells facilitated with polybrene at 8 μg/mL.

Total RNA was isolated from transduced HTTL-F cells using the RNeasy Mini Kit (Qiagen) and quantified using the NanoDrop 2000 spectrophotometer (Thermo Fisher Scientific). First strand cDNA was synthesized with 900 ng of extracted RNA using the TransStart IV Reverse Transcriptase Kit (TransGen) according to the manufacturer's protocol. Human Actin (sense: 5'-CATGTACGTTGCTATCCAGGC-3'; antisense: 5'- CTCCTTAATGTCACGCACGAT-3'), β-arrestin-1 (sense: 5'- CCTGACCTTTCGCAAGGACC-3'; antisense: 5'-CAAGCCTTCCCCGTGTCTTC-3') and β-arrestin-2 (sense: 5'-AAGCTCACCGTGTACTTGGG-3'; antisense: 5'-AGGGTCACAAACACTACAGGG-3') primers were synthesized by IDT, Inc. Quantitative real time PCR experiments were performed with 2 μL of the synthesized cDNA in a total volume of 20 μL using the SYBR™ Green PCR Master Mix (Thermo Fisher Scientific), with the following cycling parameters: 95°C for 10 minutes, followed by 40 cycles of 95°C for 30 second, 60°C for 30 seconds and 72°C for 30 seconds. Data was analyzed using the comparative Ct (ΔΔCT) method, with the relative degree of response determined by $2^{-(\Delta\Delta CT)}$.

Molecular Biology

TRE-Tight-Luc2 expression plasmid was constructed using the pNLCoI1[luc2-P2A-NlucP/Hygro] Vector (Promega) as backbone vector (Accession no. KM359771), and a stop codon was added using QuikChange mutagenesis (Agilent) at the end of luc2 gene. This vector was chosen because it contains a synthetic poly(A) transcription pause site before the promoter, which reduces background and does not contain any SV40 ori, which is not compatible with the large T antigen expression in HEK293T. TRE-Tight promoter was PCR amplified from

pTRETightBI-RY-0, which was a gift from Phil Sharp (Addgene plasmid # 31463) and cloned at NheI-HindIII restriction sites.
Codon optimized β-arrestin1-TEV219 was initially synthesized (Bio Basic) and cloned in pcDNA3.1+ (Thermo Fisher Scientific). β-arrestin2 was PCR amplified from pLX317-β-arrestin2 and the FYVE domain from pLX317-ZFYVE16 (Endofin) both from the MISSION TRC3 Human LentiORF Collection (MilliporeSigma). Both were cloned into the β-arrestin1-TEV219/pcDNA3.1+ at HindIII-BamHI sites. The PURO resistance gene in the all-in-one lentivector pCDH-CuO-MCS-EF1α-CymR-T2A-PURO SparQ (System Biosciences, QM800A-1) was changed for the BLEO3 resistance using PCR amplification and restriction site cloning (EcoRI-SalI). β-arrestin1-TEV219, β-arrestin2-TEV219, and FYVE-TEV219 were PCR amplified from the pcDNA3.1+ plasmid and cloned at NheI-SwaI restriction sites. Sequence maps for the aforementioned constructs can be found in the Supplementary Information.
GPCR-RLuc8 constructs for BRET2 experiments were cloned by PCR amplifying RLuc8 and cloned into Tango constructs at AgeI-XbaI site. β-arrestin1-GFP2 and β-arrestin2-GFP2 were cloned by PCR amplifying GFP2 and cloned at BamHI-XbaI sites of β-arrestin1-TEV219 and β-arrestin2-TEV219 in pcDNA3.1+.

The Roth Lab PRESTO-Tango GPCR Kit was from Dr. Bryan Roth and is available through Addgene (www.addgene.org/kits/roth-gpcr-presto-tango/).

DATA AVAILABILITY

All data generated or analyzed during this study, including data underlying **Figures 2.1-2.8** and all Supplementary Figures, are provided as a Source Data file, accessible at the Figshare repository. Human Protein Atlas (HPA) RNA consensus tissue gene data (version 21.0 and Ensembl version 103.38.) used for the production of **Figure 2.8** was accessed at https://www.proteinatlas.org/about/. EMTA data compared in **Supplementary Table 2.1**, including Emax (in % of vehicle response) and absolute pEC50 values, was downloaded from https://cdn.elifesciences.org/articles/74101/elife-74101-supp2-v2.xlsx.

REFERENCES

1. Kroeze, W. K., Sheffler, D. J. & Roth, B. L. G-protein-coupled receptors at a glance. *J. Cell Sci.* **116**, 4867–9 (2003).
2. Pierce, K. L., Premont, R. T. & Lefkowitz, R. J. Seven-transmembrane receptors. *Nat. Rev. Mol. Cell Biol.* **3**, 639–650 (2002).
3. Lynch, J. R. & Wang, J. Y. G Protein-Coupled Receptor Signaling in Stem Cells and Cancer. *Int. J. Mol. Sci.* **17**, (2016).
4. Ritter, S. L. & Hall, R. A. Fine-tuning of GPCR activity by receptor-interacting proteins. *Nature Reviews Molecular Cell Biology* vol. 10 819–830 (2009).
5. Black, J. B., Premont, R. T. & Daaka, Y. Feedback regulation of G protein-coupled receptor signaling by GRKs and arrestins. *Semin. Cell Dev. Biol.* **50**, 95–104 (2016).
6. Draper-Joyce, C. & Furness, S. G. B. Conformational Transitions and the Activation of HeterotrimericG Proteins by G Protein-Coupled Receptors. *ACS Pharmacol. Transl. Sci.* **2**, 285 (2019).
7. Rosenbaum, D. M., Rasmussen, S. G. F. & Kobilka, B. K. The structure and function of G-protein-coupled receptors. *Nature* **459**, 356–363 (2009).
8. Smith, J. S. & Rajagopal, S. The β-Arrestins: Multifunctional Regulators of G Protein-coupled Receptors. *J. Biol. Chem.* **291**, 8969–77 (2016).
9. Kohout, T. A., Lin, F.-T., Perry, S. J., Conner, D. A. & Lefkowitz, R. J. β-Arrestin 1 and 2 differentially regulate heptahelical receptor signaling and trafficking. *Proc. Natl. Acad. Sci.* **98**, 1601–1606 (2001).
10. Tilley, D. G. G protein-dependent and G protein-independent signaling pathways and their impact on cardiac function. *Circ. Res.* **109**, 217–30 (2011).
11. Thomsen, A. R. B., Jensen, D. D., Hicks, G. A. & Bunnett, N. W. Therapeutic Targeting of Endosomal G-Protein-Coupled Receptors. *Trends Pharmacol. Sci.* **39**, 879–891 (2018).
12. Van Koppen, C. J. & Jakobs, K. H. Arrestin-independent internalization of G protein-coupled receptors. *Mol. Pharmacol.* **66**, 365–367 (2004).
13. Kroeze, W. K. *et al.* PRESTO-Tango as an open-source resource for interrogation of the druggable human GPCRome. *Nat. Struct. Mol. Biol. 2015 225* **22**, 362–369 (2015).
14. Blau, H. M. & Rossi, F. M. Tet B or not tet B: advances in tetracycline-inducible gene expression. *Proc. Natl. Acad. Sci. U. S. A.* **96**, 797–9 (1999).

15. Jaisser, F. Inducible Gene Expression and Gene Modification in Transgenic Mice. *J. Am. Soc. Nephrol.* **11**, (2000).
16. Liu, B., Wang, S., Brenner, M., Paton, J. F. R. & Kasparov, S. Enhancement of cell-specific transgene expression from a Tet-Off regulatory system using a transcriptional amplification strategy in the rat brain. *J. Gene Med.* **10**, 583–92 (2008).
17. Vopálenský, V. *et al.* Firefly luciferase gene contains a cryptic promoter. *RNA* **14**, 1720–9 (2008).
18. Parks, T. D., Howard, E. D., Wolpert, T. J., Arp, D. J. & Dougherty, W. G. Expression and Purification of a Recombinant Tobacco Etch Virus NIa Proteinase: Biochemical Analyses of the Full-Length and a Naturally Occurring Truncated Proteinase Form. *Virology* **210**, 194–201 (1995).
19. Kapust, R. B. *et al.* Tobacco etch virus protease: mechanism of autolysis and rational design of stable mutants with wild-type catalytic proficiency. *Protein Eng.* **14**, 993–1000 (2001).
20. Seet, L.-F. & Hong, W. Endofin, an Endosomal FYVE Domain Protein. *J. Biol. Chem.* **276**, 42445–42454 (2001).
21. Mullick, A. *et al.* The cumate gene-switch: A system for regulated expression in mammalian cells. *BMC Biotechnol.* **6**, 43 (2006).
22. Gould, D. J. & Chernajovsky, Y. Endogenous GATA Factors Bind the Core Sequence of the tetO and Influence Gene Regulation with the Tetracycline System. *Mol. Ther.* **10**, 127–138 (2004).
23. Cohen, S., Dovrat, S., Sarid, R., Huberman, E. & Salzberg, S. JAK–STAT signaling involved in phorbol 12-myristate 13-acetate- and dimethyl sulfoxide-induced 2′-5′ oligoadenylate synthetase expression in human HL-60 leukemia cells. *Leuk. Res.* **29**, 923–931 (2005).
24. Pedranzini, L. *et al.* Pyridone 6, A Pan-Janus–Activated Kinase Inhibitor, Induces Growth Inhibition of Multiple Myeloma Cells. *Cancer Res.* **66**, 9714–9721 (2006).
25. Saucier, C., Morris, S. J. & Albert, P. R. Endogenous serotonin-2A and -2C receptors in Balb/c-3T3 cells revealed in serotonin-free medium: Desensitization and down-regulation by serotonin. *Biochem. Pharmacol.* **56**, 1347–1357 (1998).
26. Bousoik, E. & Montazeri Aliabadi, H. “Do We Know Jack” About JAK? A Closer Look

at JAK/STAT Signaling Pathway. *Front. Oncol.* **8**, 287 (2018).

27. Alexander, S. P. H. *et al.* THE CONCISE GUIDE TO PHARMACOLOGY 2021/22: G protein-coupled receptors. *Br. J. Pharmacol.* **178**, S27–S156 (2021).
28. Seo, S. O. & Schmidt-Dannert, C. Development of a synthetic cumate-inducible gene expression system for Bacillus. *Appl. Microbiol. Biotechnol.* **103**, 303–313 (2019).
29. Zeghal, M., Laroche, G. & Giguère, P. M. Parallel Interrogation of β-Arrestin2 Recruitment for Ligand Screening on a GPCR-Wide Scale using PRESTO-Tango Assay. *JoVE (Journal Vis. Exp.* **2020**, e60823 (2020).
30. Rinne, M., Tanoli, Z. U. R., Khan, A. & Xhaard, H. Cartography of rhodopsin-like G protein-coupled receptors across vertebrate genomes. *Sci. Reports 2019 91* **9**, 1–16 (2019).
31. Zhao, X. *et al.* A homogeneous enzyme fragment complementation-based beta-arrestin translocation assay for high-throughput screening of G-protein-coupled receptors. *J. Biomol. Screen.* **13**, 737–747 (2008).
32. Moo, E. Von, van Senten, J. R., Bräuner-Osborne, H. & Møller, T. C. Arrestin-Dependent and -Independent Internalization of G Protein-Coupled Receptors: Methods, Mechanisms, and Implications on Cell Signaling. *Mol. Pharmacol.* **99**, 242–255 (2021).
33. Avet, C. *et al.* Effector membrane translocation biosensors reveal G protein and Parrestin coupling profiles of 100 therapeutically relevant GPCRs. *Elife* **11**, (2022).
34. Zhou, Q. *et al.* Common activation mechanism of class a GPCRs. *Elife* **8**, (2019).
35. Lu, S., Jang, W., Inoue, A. & Lambert, N. A. Constitutive G protein coupling profiles of understudied orphan GPCRs. *PLoS One* **16**, (2021).
36. Watkins, L. R. & Orlandi, C. In vitro profiling of orphan G protein coupled receptor (GPCR) constitutive activity. *Br. J. Pharmacol.* **178**, 2963–2975 (2021).
37. Oakley, R. H., Laporte, S. A., Holt, J. A., Caron, M. G. & Barak, L. S. Differential affinities of visual arrestin, beta arrestin1, and beta arrestin2 for G protein-coupled receptors delineate two major classes of receptors. *J. Biol. Chem.* **275**, 17201–10 (2000).
38. Berg, K. A. & Clarke, W. P. Making Sense of Pharmacology: Inverse Agonism and Functional Selectivity. *Int. J. Neuropsychopharmacol.* **21**, 962–977 (2018).
39. Harding, S. D. *et al.* The IUPHAR/BPS guide to PHARMACOLOGY in 2022: curating pharmacology for COVID-19, malaria and antibacterials. *Nucleic Acids Res.* **50**, D1282–D1294 (2022).

40. Simcocks, A. C. *et al.* Atypical cannabinoid ligands O-1602 and O-1918 administered chronically in diet-induced obesity. *Endocr. Connect.* **8**, 203 (2019).
41. Thiele, S., Mungalpara, J., Steen, A., Rosenkilde, M. M. & Våbenø, J. Determination of the binding mode for the cyclopentapeptide CXCR4 antagonist FC131 using a dual approach of ligand modifications and receptor mutagenesis. *Br. J. Pharmacol.* **171**, 5313–5329 (2014).
42. Magalhaes, A. C., Dunn, H. & Ferguson, S. S. G. Regulation of GPCR activity, trafficking and localization by GPCR-interacting proteins. *Br. J. Pharmacol.* **165**, 1717 (2012).
43. Yang, Z. *et al.* Phosphorylation of G Protein-Coupled Receptors: From the Barcode Hypothesis to the Flute Model. *Mol. Pharmacol.* **92**, 201–210 (2017).
44. Drube, J. *et al.* GRK2/3/5/6 knockout: The impact of individual GRKs on arrestin-binding and GPCR regulation. *bioRxiv* 2021.02.12.430971 (2021) doi:10.1101/2021.02.12.430971.
45. Busillo, J. M. *et al.* Site-specific phosphorylation of CXCR4 is dynamically regulated by multiple kinases and results in differential modulation of CXCR4 signaling. *J. Biol. Chem.* **285**, 7805–7817 (2010).
46. Białopiotrowicz, E. *et al.* Microenvironment-induced PIM kinases promote CXCR4-triggered mTOR pathway required for chronic lymphocytic leukaemia cell migration. *J. Cell. Mol. Med.* **22**, 3548–3559 (2018).
47. Decker, S. *et al.* PIM Kinases Are Essential for Chronic Lymphocytic Leukemia Cell Survival (PIM2/3) and CXCR4-Mediated Microenvironmental Interactions (PIM1). *Mol. Cancer Ther.* **13**, 1231–1245 (2014).
48. Shintani, Y. *et al.* β-Arrestin1 and 2 differentially regulate PACAP-induced PAC1 receptor signaling and trafficking. *PLoS One* **13**, e0196946 (2018).
49. Vibhuti, A., Gupta, K., Subramanian, H., Guo, Q. & Ali, H. Distinct and Shared Roles of β-Arrestin-1 and β-Arrestin-2 on the Regulation of C3a Receptor Signaling in Human Mast Cells. *PLoS One* **6**, e19585 (2011).
50. Levoye, A. *et al.* A broad G protein-coupled receptor internalization assay that combines SNAP-tag labeling, diffusion-enhanced resonance energy transfer, and a highly emissive terbium cryptate. *Front. Endocrinol. (Lausanne).* **6**, 167 (2015).
51. Moriya, H. Quantitative nature of overexpression experiments. *Mol. Biol. Cell* **26**, 3932

(2015).

52. Peterson, Y. K. & Luttrell, L. M. The Diverse Roles of Arrestin Scaffolds in G Protein–Coupled Receptor Signaling. *Pharmacol. Rev.* **69**, 256–297 (2017).
53. Miljuš, T. *et al.* Diverse chemotypes drive biased signaling by cannabinoid receptors. *bioRxiv* 2020.11.09.375162 (2020) doi:10.1101/2020.11.09.375162.
54. Gurevich, E. V., Benovic, J. L. & Gurevich, V. V. Arrestin2 expression selectively increases during neural differentiation. *J. Neurochem.* **91**, 1404–1416 (2004).
55. Komolov, K. E. & Benovic, J. L. G protein-coupled receptor kinases: Past, present and future. *Cell. Signal.* **41**, 17 (2018).
56. Kumari, P. *et al.* Core engagement with β-arrestin is dispensable for agonist-induced vasopressin receptor endocytosis and ERK activation. *Mol. Biol. Cell* **28**, 1003 (2017).
57. Tobin, A. B. G-protein-coupled receptor phosphorylation: where, when and by whom. *Br. J. Pharmacol.* **153**, S167 (2008).
58. Stenmark, H., Aasland, R. & Driscoll, P. C. The phosphatidylinositol 3-phosphate-binding FYVE finger. *FEBS Lett.* **513**, 77–84 (2002).
59. Roth, B. L. Impossible or Merely Difficult? Two Grand Challengesfrom a Biologist's Perspective. *ACS Med. Chem. Lett.* **4**, 316 (2013).
60. Ngo, T. *et al.* Identifying ligands at orphan GPCRs: current status using structure-based approaches. *Br. J. Pharmacol.* **173**, 2934–2951 (2016).
61. Mary, S. *et al.* Ligands and signaling proteins govern the conformational landscape explored by a G protein-coupled receptor. *Proc. Natl. Acad. Sci. U. S. A.* **109**, 8304–8309 (2012).
62. Azzi, M. *et al.* Beta-arrestin-mediated activation of MAPK by inverse agonists reveals distinct active conformations for G protein-coupled receptors. *Proc. Natl. Acad. Sci. U. S. A.* **100**, 11406–11411 (2003).
63. Williams, C. & Hill, S. J. GPCR signaling: understanding the pathway to successful drug discovery. *Methods Mol. Biol.* **552**, 39–50 (2009).
64. Huber, M., Brabec, M., Bayer, N., Blaas, D. & Fuchs, R. Elevated endosomal pH in HeLa cells overexpressing mutant dynamin can affect infection by pH-sensitive viruses. *Traffic* **2**, 727–736 (2001).
65. Casamento, A. & Boucrot, E. Molecular mechanism of Fast Endophilin-Mediated

Endocytosis. *Biochem. J.* **477**, 2327 (2020).

66. Orsini, M. J. & Benovic, J. L. Characterization of dominant negative arrestins that inhibit beta2-adrenergic receptor internalization by distinct mechanisms. *J. Biol. Chem.* **273**, 34616–34622 (1998).
67. Al-Hasani, R. & Bruchas, M. R. Molecular mechanisms of opioid receptor-dependent signaling and behavior. *Anesthesiology* **115**, 1363–1381 (2011).
68. Chung, G. & Kim, S. J. Sustained Activity of Metabotropic Glutamate Receptor: Homer, Arrestin, and Beyond. *Neural Plast.* **2017**, 5125624 (2017).
69. Rankin, M. L. *et al.* The D1 dopamine receptor is constitutively phosphorylated by G protein-coupled receptor kinase 4. *Mol. Pharmacol.* **69**, 759–769 (2006).
70. Atwood, B. K., Lopez, J., Wager-Miller, J., Mackie, K. & Straiker, A. Expression of G protein-coupled receptors and related proteins in HEK293, AtT20, BV2, and N18 cell lines as revealed by microarray analysis. *BMC Genomics* **12**, 14 (2011).
71. Li, L. *et al.* G Protein-coupled Receptor Kinases of the GRK4 Protein Subfamily Phosphorylate Inactive G Protein-coupled Receptors (GPCRs). *J. Biol. Chem.* **290**, 10775 (2015).
72. Longo, P. A., Kavran, J. M., Kim, M. S. & Leahy, D. J. Transient mammalian cell transfection with polyethylenimine (PEI). *Methods Enzymol.* **529**, 227–240 (2013).

ACKNOWLEDGEMENTS

MZ is supported by the Alexander Graham Bell Canada Graduate Scholarships-Doctoral Program (CGS-D3) from Natural Sciences and Engineering Research Council of Canada. This work was funded by the Canadian Institutes of Health Research (CIHR grant #MOP142219) and Natural Sciences and Engineering Research Council of Canada (NSERC RGPIN-2017-06151).

The authors also wish to thank Dr. Mario Tiberi for his assistance and providing several of our tested inverse agonists and antagonists.

AUTHOR CONTRIBUTIONS

PMG conceived the overall concept; MZ and GL designed and performed all experiments; JDF assisted with validation of primary screen findings; RW prepared the arrayed agonist and PRESTO-Tango DNA plates for the primary screen; MZ, GL, and PMG analyzed the data and wrote the manuscript.

COMPETING INTERESTS

The authors declare no competing interests.

MAIN FIGURES

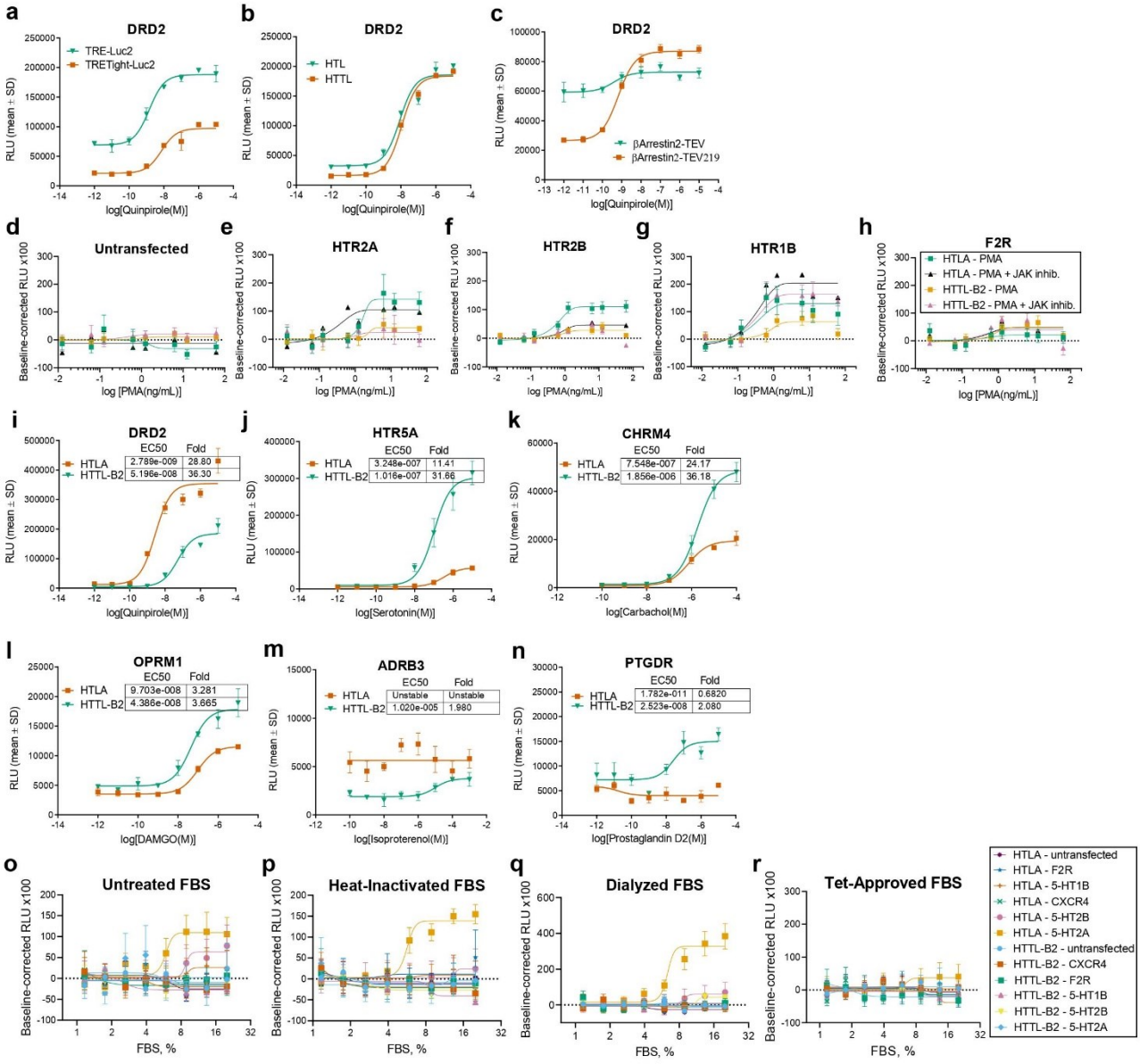

Figure 2.1. Optimization of the dynamic range, sensitivity, and specificity of the Tango-Trio platform. (a) Comparison of TRE and TRE-Tight. Promoters were cloned upstream luc2, and expression vectors were transfected in HEK293T cells along with the β-arrestin2-TEV fusion protein and DRD2. Transfected cells were stimulated with the DRD2 specific agonist quinpirole. (b) Selection and pharmacological characterization of the monoclonal reporter cell line HTTL (HEK293T-TRE-Tight-Luc2) compared to the original HTL (HEK293T-TRE-Luc) cell line. (c)

Comparison of TEV and TEV219 proteases. β-arrestin2 was cloned to both proteases, and transfected in HTL cells with DRD2. Transfected cells were stimulated with the DRD2 specific agonist quinpirole. (d-h) HTTL-B2 and HTLA were transfected with HTR2A (e), HTR2B (f), HTR1B (g), and F2R (h) and stimulated, along with untransfected cells (d), with dose-response curve of PMA and in presence/absence of 10 μM JAK inhibitor I. (i-n) HTTL-B2 and HTLA dose-response curves at various targets: DRD2 to quinpirole (i), HTR5A to serotonin (j), CHRM4 to carbachol (k), OPRM1 to DAMGO (l), ADRB3 to isoproterenol (m), and PTGDR to prostaglandin D2 (n). (o-r) Comparison of the specificity of HTTL-B2 and HTLA readouts. Cell lines were transfected with GPCRs that activate the Jak/STAT Pathway and stimulated with serial dilutions of untreated FBS (o), heat-inactivated (p), dialyzed (q), and Tet-System Approved (r) sera.
HTTL-B2 was maintained in cumate-containing media throughout. Dose- response curves were built using XY analysis for non-linear regression curve and the 3-parameters dose-response stimulation function. Data are presented as mean values, with error bars representing SD. Data are representative of 2 biological replicates, with 3 technical replicates each. Generic receptor codes refer to the GPCR-Tango constructs.

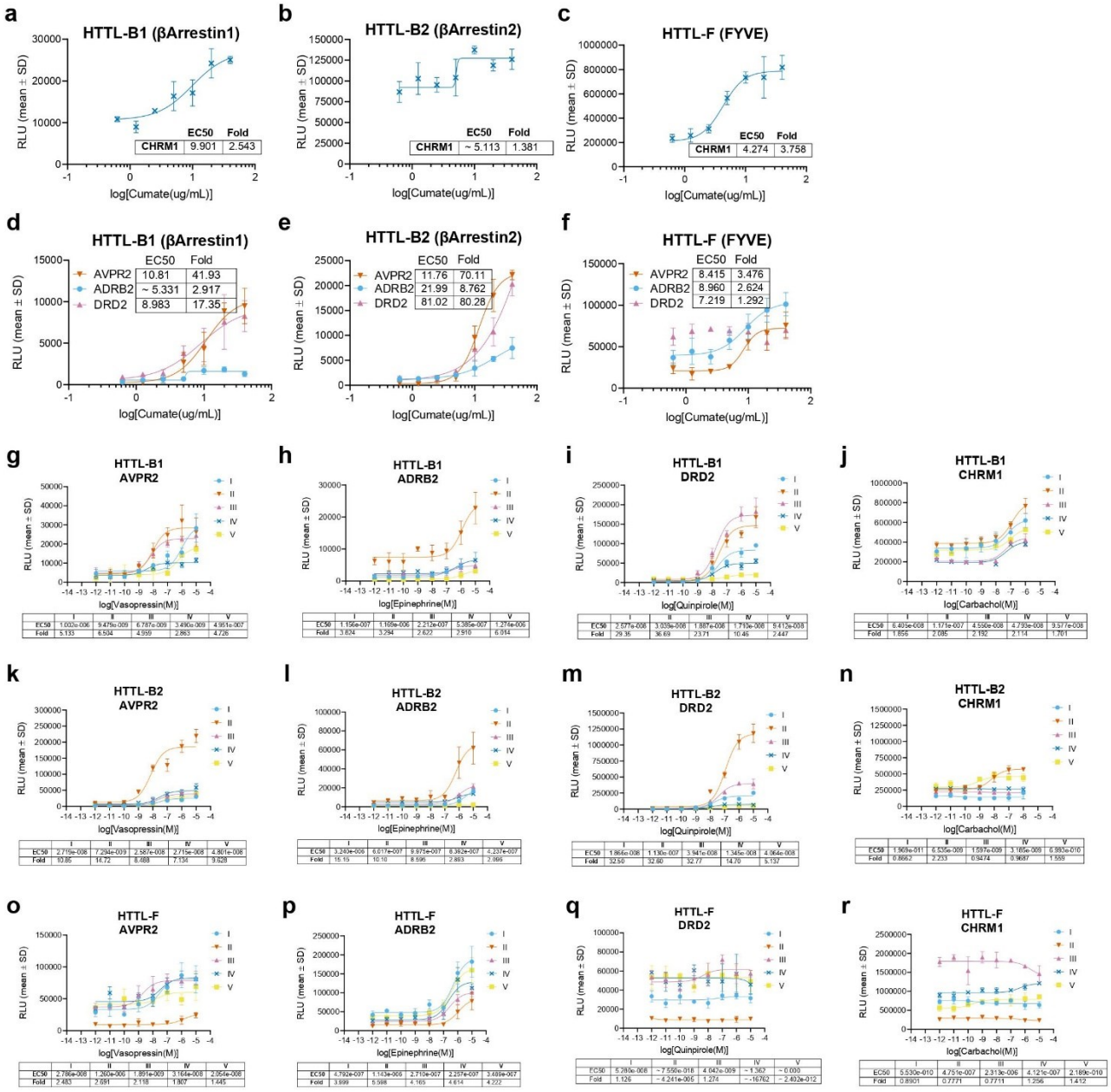

Figure 2.2. Dose-response and time-course verification of cumate-induced expression. (a-f) Validation of fusion protein induction initiated by cumate dose-responses in HTTL-B1 (a, d), HTTL-B2 (b, e), and HTTL-F (c, f) cell lines. Cells were transfected with AVPR2, ADRB2, DRD2 and CHRM1 Tango receptors and stimulated with a cumate dose-curve starting from 40 µg/mL with 2-fold dilutions. (g-r) Timing optimization of fusion protein induction in HTTL-B1 (g-j), HTTL-B2 (k-n), and HTTL-F (o-r) cell lines. Cells were transfected with AVPR2, ADRB2, DRD2 and CHRM1 Tango receptors and stimulated with receptor selective agonist. Cumate (30 µg/mL)

was added at the following time points and maintained in the cell medium thenceforth: I - 5 days; II - 3 days; III - 2 days; IV - 24 hours; V - 18 hrs total cumate exposure. Dose- response curves were built using XY analysis for non-linear regression curve and the 3-parameters dose-response stimulation function. Data are presented as mean values, with error bars representing SD. Data are representative of 2 biological replicates, with 3 technical replicates each. Generic receptor codes refer to the GPCR-Tango constructs.

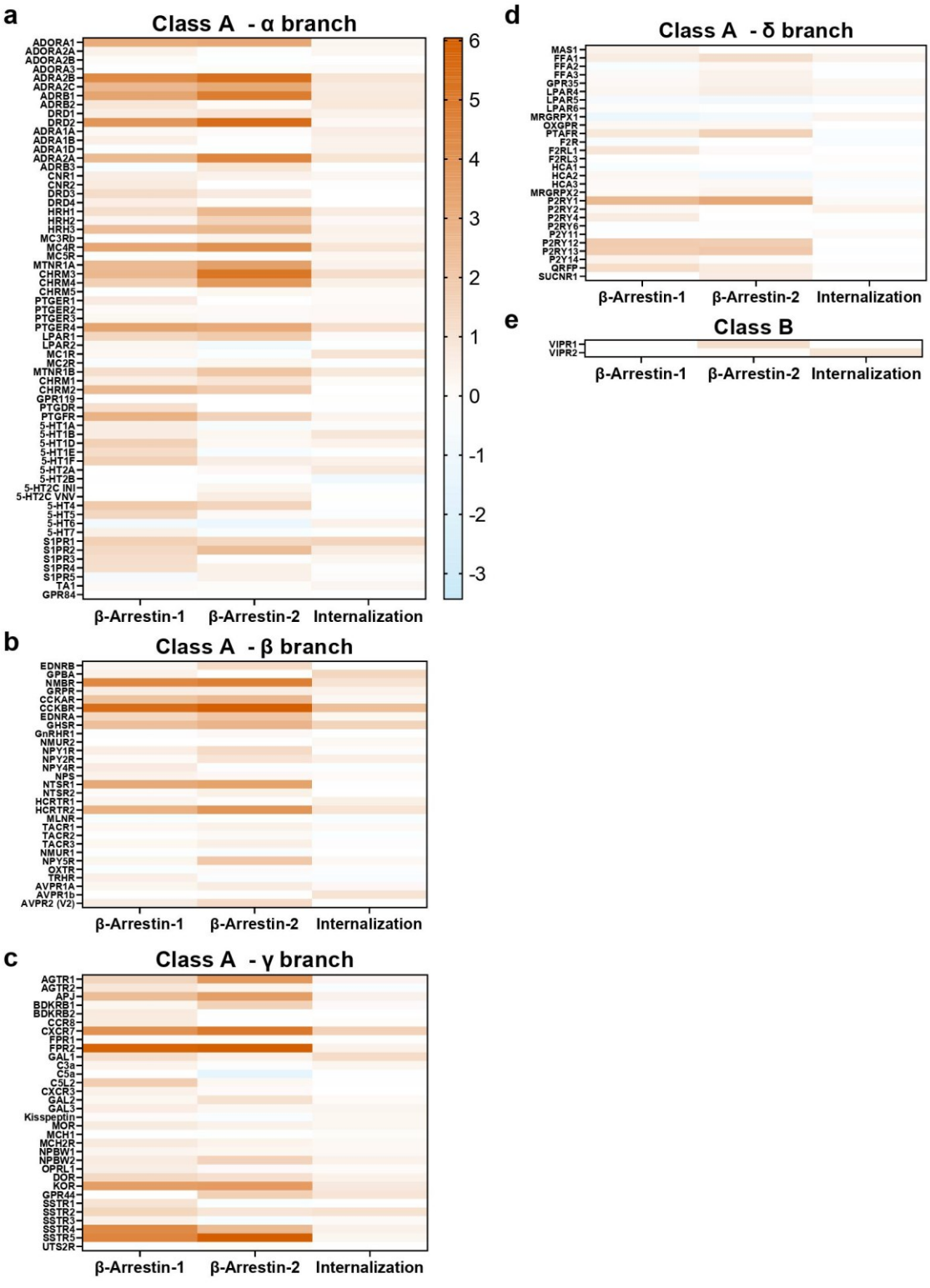
a
Class A - α branch
ADORA1
ADORA2A
ADORA2B
ADORA3
ADRA2B
ADRA2C
ADRB1
ADRB2
DRD1
DRD2
ADRA1A
ADRA1B
ADRA1D
ADRA2A
ADRB3
CNR1
CNR2
DRD3
DRD4
HRH1
HRH2
HRH3
MC3Rb
MC4R
MC5R
MTNR1A
CHRM3
CHRM4
CHRM5
PTGER1
PTGER2
PTGER3
PTGER4
LPAR1
LPAR2
MC1R
MC2R
MTNR1B
CHRM1
CHRM2
GPR119
PTGDR
PTGFR
5-HT1A
5-HT1B
5-HT1D
5-HT1E
5-HT1F
5-HT2A
5-HT2B
5-HT2C INI
5-HT2C VNV
5-HT4
5-HT5
5-HT6
5-HT7
S1PR1
S1PR2
S1PR3
S1PR4
S1PR5
TA1
GPR84
6
5
4
3
2
1
0
-1
-2
-3
β-Arrestin-1
β-Arrestin-2
Internalization
b
Class A - β branch
EDNRB
GPBA
NMBR
GRPR
CCKAR
CCKBR
EDNRA
GHSR
GnRHR1
NMUR2
NPY1R
NPY2R
NPY4R
NPS
NTSR1
NTSR2
HCRTR1
HCRTR2
MLNR
TACR1
TACR2
TACR3
NMUR1
NPY5R
OXTR
TRHR
AVPR1A
AVPR1b
AVPR2 (V2)
β-Arrestin-1
β-Arrestin-2
Internalization
c
Class A - γ branch
AGTR1
AGTR2
APJ
BDKRB1
BDKRB2
CCR8
CXCR7
FPR1
FPR2
GAL1
C3a
C5a
C5L2
CXCR3
GAL2
GAL3
Kisspeptin
MOR
MCH1
MCH2R
NPBW1
NPBW2
OPRL1
DOR
KOR
GPR44
SSTR1
SSTR2
SSTR3
SSTR4
SSTR5
UTS2R
β-Arrestin-1
β-Arrestin-2
Internalization
d
Class A - δ branch
MAS1
FFA1
FFA2
FFA3
GPR35
LPAR4
LPAR5
LPAR6
MRGRPX1
OXGPR
PTAFR
F2R
F2RL1
F2RL3
HCA1
HCA2
HCA3
MRGRPX2
P2RY1
P2RY2
P2RY4
P2RY6
P2Y11
P2RY12
P2RY13
P2Y14
QRFP
SUCNR1
β-Arrestin-1
β-Arrestin-2
Internalization
e
Class B
VIPR1
VIPR2
β-Arrestin-1
β-Arrestin-2
Internalization

Figure 2.3. Heatmap representation of hits identified from agonist-dependent HTS. To analyze agonist-induced activities within the GPCRome, HTTL-B1, HTTL-B2 and HTTL-F cells were plated in cumate-containing (30 μg/mL) medium and transfected with a library of 162 non-orphan GPCR Tango constructs. Transfected cells were stimulated either with HBSS-Hepes buffer or with a panel of selective agonists. Log2 fold changes in agonist-dependent arrestin recruitment/dissociation or GPCR internalization was calculated between the wells in the absence or presence of agonist and plotted as heat maps, grouping class A α (a), β (b), γ (c), and δ (d) branches, and class B receptors (e). Log2 values are the means calculated from quadruplicate conditions, generated from two separate screens (n = 8, 2 biological measurements with 4 technical replicates each). Generic receptor codes refer to the GPCR-Tango constructs.

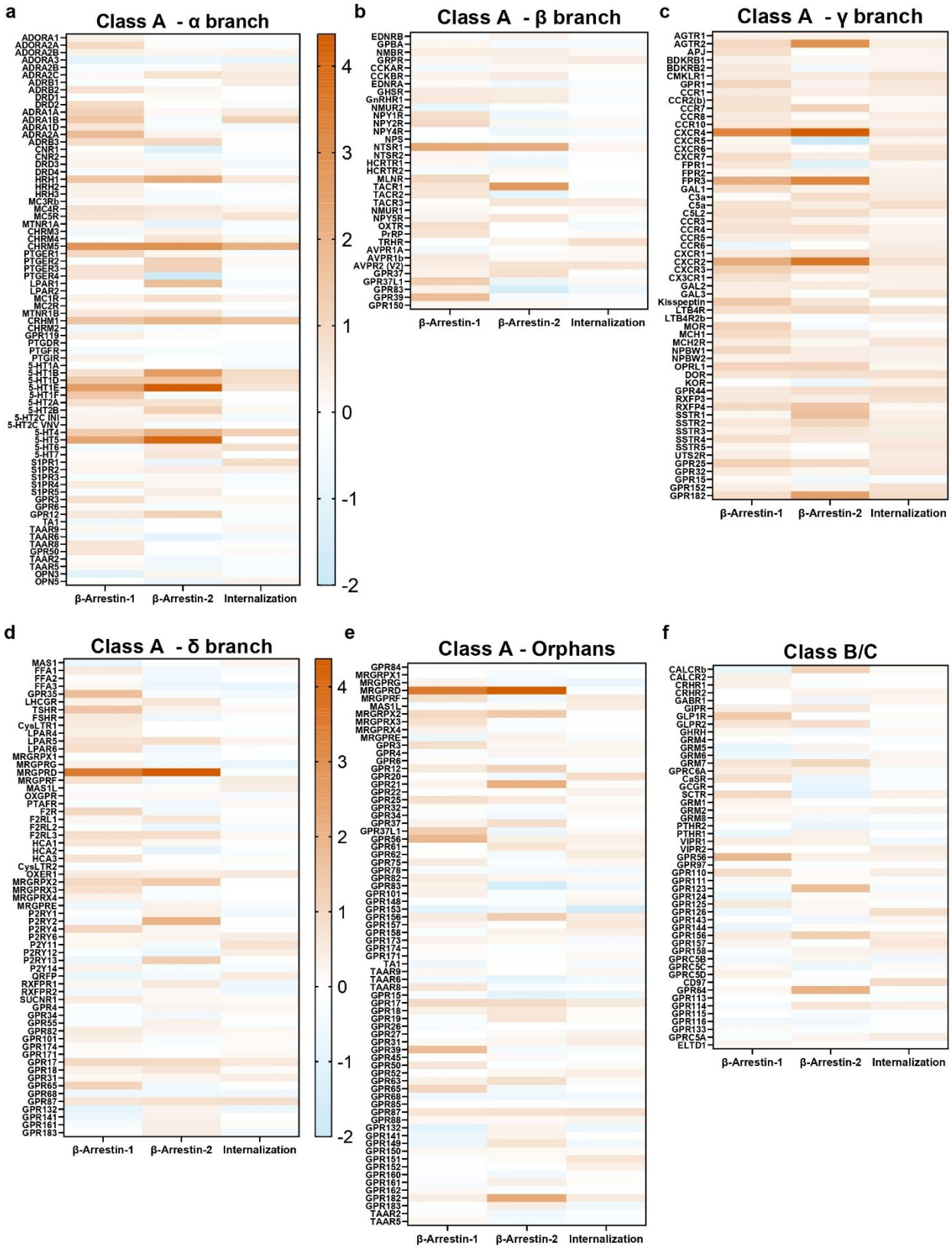
a
Class A - α branch
ADORA1
ADORA2A
ADORA2B
ADORA3
ADRA2B
ADRA2C
ADRB1
ADRB2
DRD1
DRD2
ADRA1A
ADRA1B
ADRA1D
ADRA2A
ADRB3
CNR1
CNR2
DRD3
DRD4
HRH1
HRH2
HRH3
MC3Rb
MC4R
MC5R
MTNR1A
CHRM3
CHRM4
CHRM5
PTGER1
PTGER2
PTGER3
PTGER4
LPAR1
LPAR2
MC1R
MC2R
MTNR1B
CHRM1
CHRM2
GPR119
PTGDR
PTGFR
PTGIR
5-HT1A
5-HT1B
5-HT1D
5-HT1E
5-HT1F
5-HT2A
5-HT2B
5-HT2C INI
5-HT2C VNV
5-HT4
5-HT5
5-HT6
5-HT7
S1PR1
S1PR2
S1PR3
S1PR4
S1PR5
GPR3
GPR6
GPR12
TA1
TAAR9
TAAR6
TAAR8
GPR50
TAAR2
TAAR5
OPN3
OPN5
β-Arrestin-1
β-Arrestin-2
Internalization
4
3
2
1
0
-1
-2
b
Class A - β branch
EDNRB
GPBA
NMBR
GRPR
CCKAR
CCKBR
EDNRA
GHSR
GnRHR1
NMUR2
NPY1R
NPY2R
NPY4R
NPS
NTSR1
NTSR2
HCRTR1
HCRTR2
MLNR
TACR1
TACR2
TACR3
NMUR1
NPY5R
OXTR
PrRP
TRHR
AVPR1A
AVPR1B
AVPR2 (V2)
GPR37
GPR37L1
GPR83
GPR39
GPR150
β-Arrestin-1
β-Arrestin-2
Internalization
c
Class A - γ branch
AGTR1
AGTR2
APJ
BDKRB1
BDKRB2
CMKLR1
GPR1
CCR1
CCR2(b)
CCR7
CCR8
CCR10
CXCR4
CXCR5
CXCR6
CXCR7
FPR1
FPR2
FPR3
GAL1
C3a
C5a
C5L2
CCR3
CCR4
CCR5
CCR6
CXCR1
CXCR2
CXCR3
CX3CR1
GAL2
GAL3
Kisspeptin
LTB4R
LTB4R2b
MOR
MCH1
MCH2R
NPBW1
NPBW2
OPRL1
DOR
KOR
GPR44
RXFP3
RXFP4
SSTR1
SSTR2
SSTR3
SSTR4
SSTR5
UTS2R
GPR25
GPR32
GPR15
GPR152
GPR182
β-Arrestin-1
β-Arrestin-2
Internalization
d
Class A - δ branch
MAS1
FFA1
FFA2
FFA3
GPR35
LHCGR
TSHR
FSHR
CysLTR1
LPAR4
LPAR5
LPAR6
MRGRPX1
MRGPRG
MRGPRD
MRGPRF
MAS1L
OXGPR
PTAFR
F2R
F2RL1
F2RL2
F2RL3
HCA1
HCA2
HCA3
CysLTR2
OXER1
MRGRPX2
MRGPRX3
MRGPRX4
MRGPRE
P2RY1
P2RY2
P2RY4
P2RY6
P2Y11
P2RY12
P2RY13
P2Y14
QRFP
RXFPR1
RXFPR2
SUCNR1
GPR4
GPR34
GPR55
GPR82
GPR101
GPR174
GPR171
GPR17
GPR18
GPR31
GPR65
GPR68
GPR87
GPR132
GPR141
GPR161
GPR183
β-Arrestin-1
β-Arrestin-2
Internalization
4
3
2
1
0
-1
-2
e
Class A - Orphans
GPR84
MRGPRX1
MRGPRG
MRGPRD
MRGPRF
MAS1L
MRGPRX2
MRGPRX3
MRGPRX4
MRGPRE
GPR3
GPR4
GPR6
GPR12
GPR20
GPR21
GPR22
GPR25
GPR32
GPR34
GPR37
GPR37L1
GPR56
GPR61
GPR62
GPR75
GPR78
GPR82
GPR83
GPR101
GPR148
GPR153
GPR156
GPR157
GPR158
GPR173
GPR174
GPR171
TA1
TAAR9
TAAR6
TAAR8
GPR15
GPR17
GPR18
GPR19
GPR26
GPR27
GPR31
GPR39
GPR45
GPR50
GPR52
GPR63
GPR65
GPR68
GPR85
GPR87
GPR88
GPR132
GPR141
GPR149
GPR150
GPR151
GPR152
GPR160
GPR161
GPR162
GPR182
GPR183
TAAR2
TAAR5
β-Arrestin-1
β-Arrestin-2
Internalization
f
Class B/C
CALCRb
CALCR2
CRHR1
CRHR2
GABR1
GIPR
GLP1R
GLPR2
GHRH
GRM4
GRM5
GRM6
GRM7
GPRC6A
CaSR
GCGR
SCTR
GRM1
GRM2
GRM8
PTHR2
PTHR1
VIPR1
VIPR2
GPR98
GPR97
GPR110
GPR111
GPR123
GPR124
GPR125
GPR126
GPR143
GPR144
GPR156
GPR157
GPR158
GPRC5B
GPRC5C
GPRC5D
CD97
GPR64
GPR113
GPR114
GPR115
GPR116
GPR133
GPRC5A
ELTD1
β-Arrestin-1
β-Arrestin-2
Internalization

Figure 2.4. Heatmap representation of hits identified from basal activity HTS. To analyze basal activities within the GPCRome, HTTL-B1, HTTL-B2 and HTTL-F cells were plated alternating rows with or without cumate (30 μg/mL). Cells were transfected with a library of 350 GPCR Tango constructs, including approximately 100 orphan receptors. Log2 fold changes in basal arrestin recruitment/dissociation or GPCR internalization was calculated between the wells in the absence or presence of cumate and plotted as heat maps, grouping class A α (a), β (b), γ (c), and δ (d) branches, class A orphans (e) and class B/C receptors (f). Log2 values are the means calculated from quadruplicate conditions, generated from two separate screens (n = 8, 2 biological measurements with 4 technical replicates each). Generic receptor codes refer to the GPCR-Tango constructs.

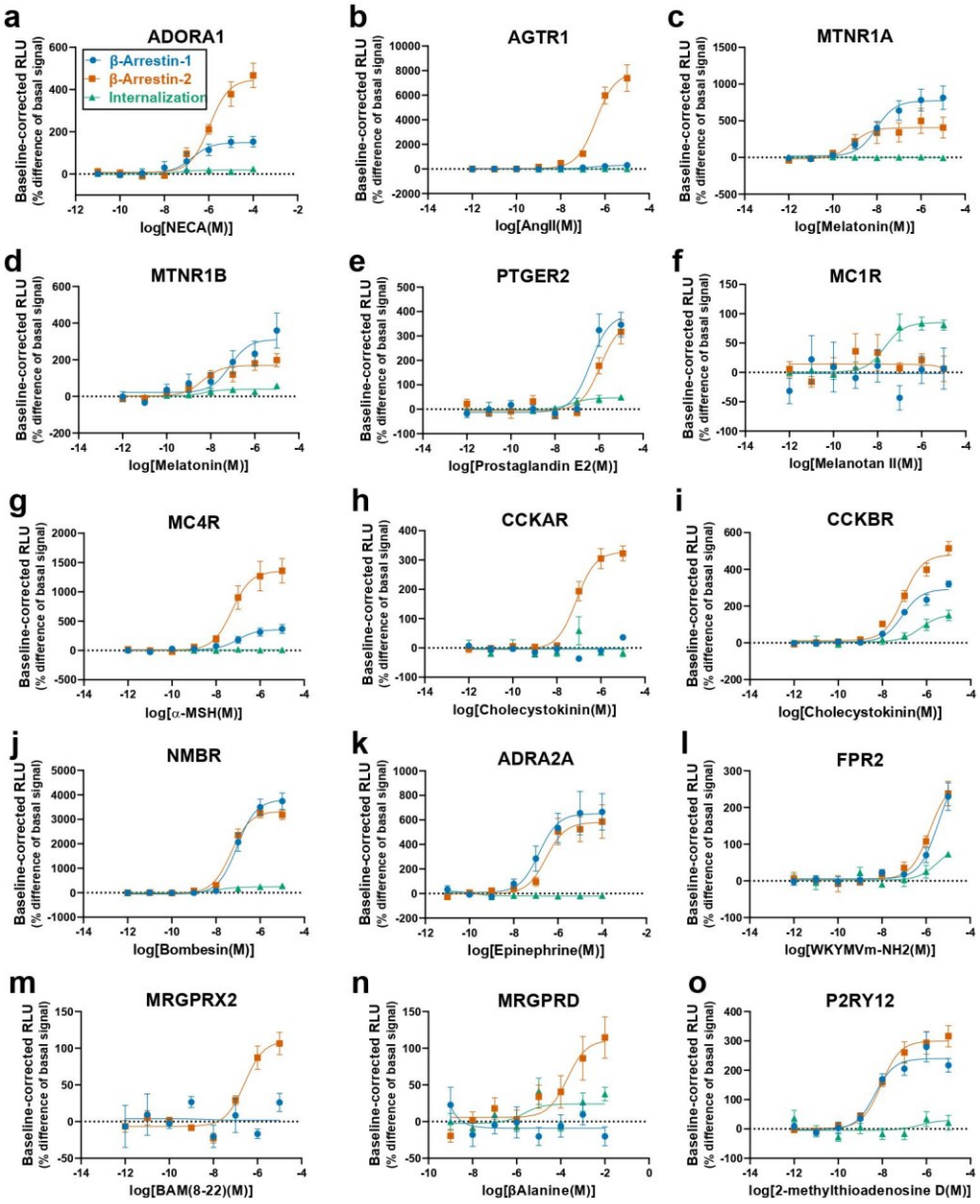

Figure 2.5. Validation of compiled positive hits from agonist-dependent HTS in dose-response. HTTL-B1, HTTL-B2 and HTTL-F cells were plated in cumate-containing (30 µg/mL) medium and transfected with potential GPCR hits identified from the agonist-dependent HTS. Transfected cells were stimulated with the receptor specific agonist and dose- response curves were built using XY analysis for non-linear regression curve and the 3-parameters dose-response stimulation function, followed by baseline correction. Data are presented as mean values, with error bars representing SEM. Data are representative of 2 biological replicates, with 3 technical replicates each. Generic receptor codes refer to the GPCR-Tango constructs.

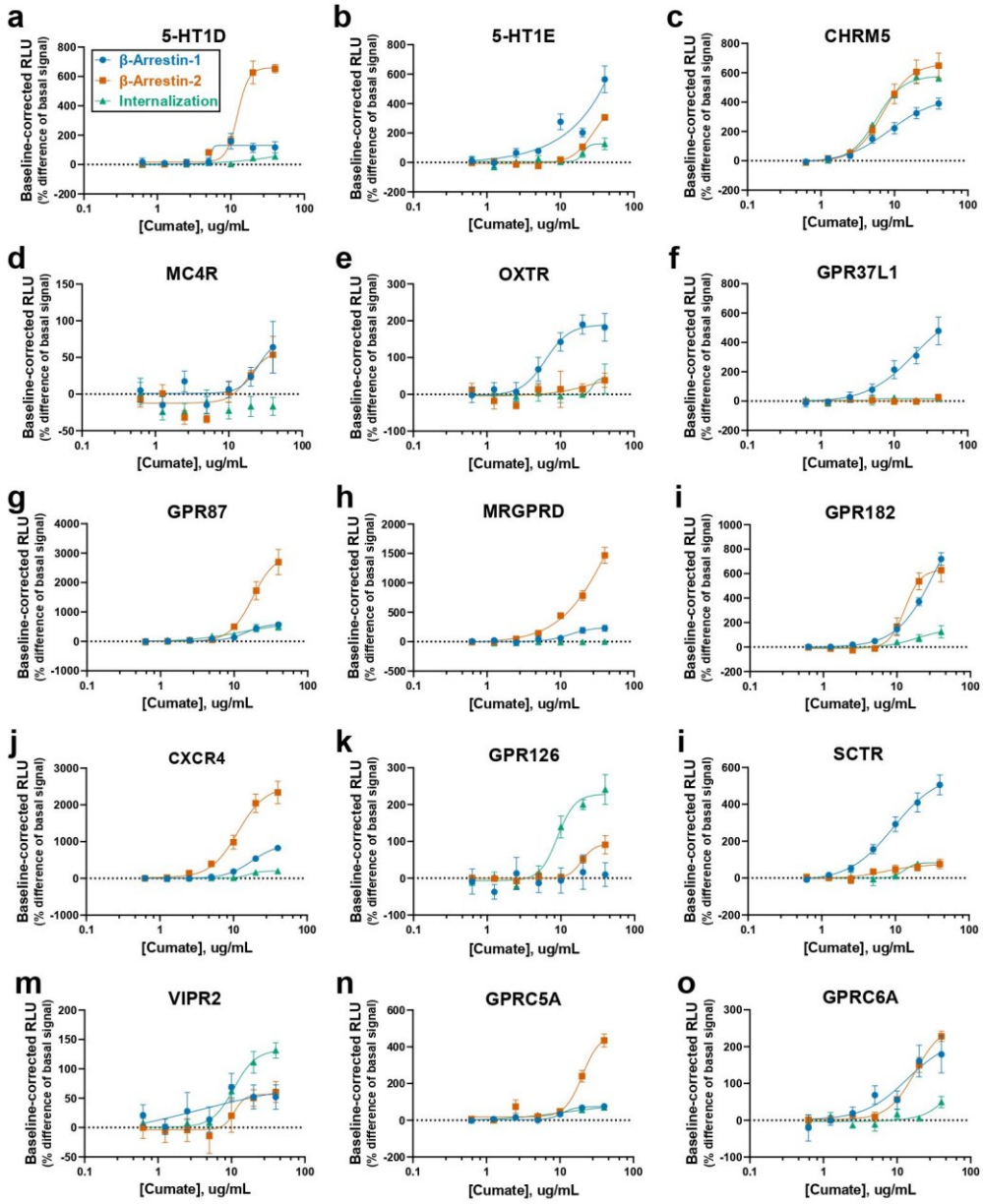

Figure 2.6. Validation of compiled positive hits from basal activity HTS in dose-response. HTTL-B1, HTTL-B2 and HTTL-F cells were transfected with potential GPCR hits identified from the basal HTS. Transfected cells were stimulated with cumate, and dose- response curves were built using XY analysis for non-linear regression curve and the 4-parameters dose-response stimulation function, followed by baseline correction. Data are presented as mean values, with error bars representing SEM. Data are representative of 2 biological replicates, with 3 technical replicates each. Generic receptor codes refer to the GPCR-Tango constructs.

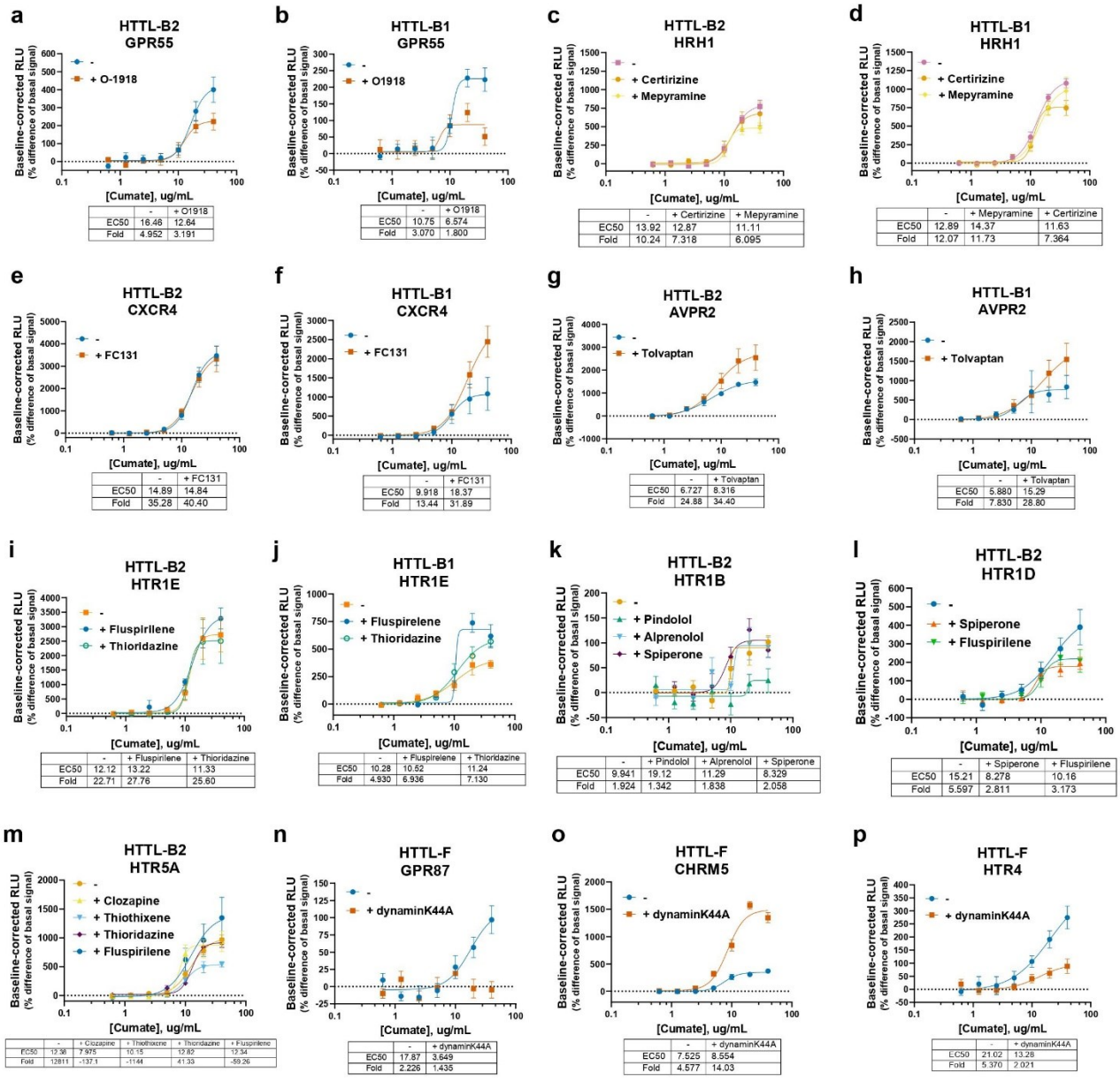

Figure 2.7. Applications and further investigations into basal activities revealed by Tango-Trio. HTTL-B1 and HTTL-B2 were transfected with GPCRs exhibiting strong basal arrestin recruitment. Transfected cells were stimulated as cumate dose-response in the presence or absence of the following inverse agonists/antagonists at saturating (EC80) concentrations: O-1918 at GPR55 (a-b), Cetirizine and Mepyramine at HRH1 (c-d), FC131 at CXCR4 (e-f), Tolvaptan at AVPR2 (g-h), Fluspirelene and Thioridazine at HTR1E (i-j), Pindolol, Alprenolol and Spiperone at HTR1B (k), Spiperone and Fluspirelene at HTR1D (l), and Clozapine, Thiothexene, Thioridazine and Fluspirelene at HTR5A (m). Dynamin-dependence of high basal internalization

was tested by co-transfecting HTTL-F cells with GPR87 (n), CHRM5 (o), and HTR4 (p) with/without dynaminK44A. Transfected cells were stimulated as a cumate dose-response, and stimulation curves were built using XY analysis for non-linear regression curve and the 4-parameters dose-response stimulation function, followed by baseline correction. Data are presented as mean values, with error bars representing SEM. Data are representative of 2 biological replicates, with 3 technical replicates each. Generic receptor codes refer to the GPCR-Tango constructs.

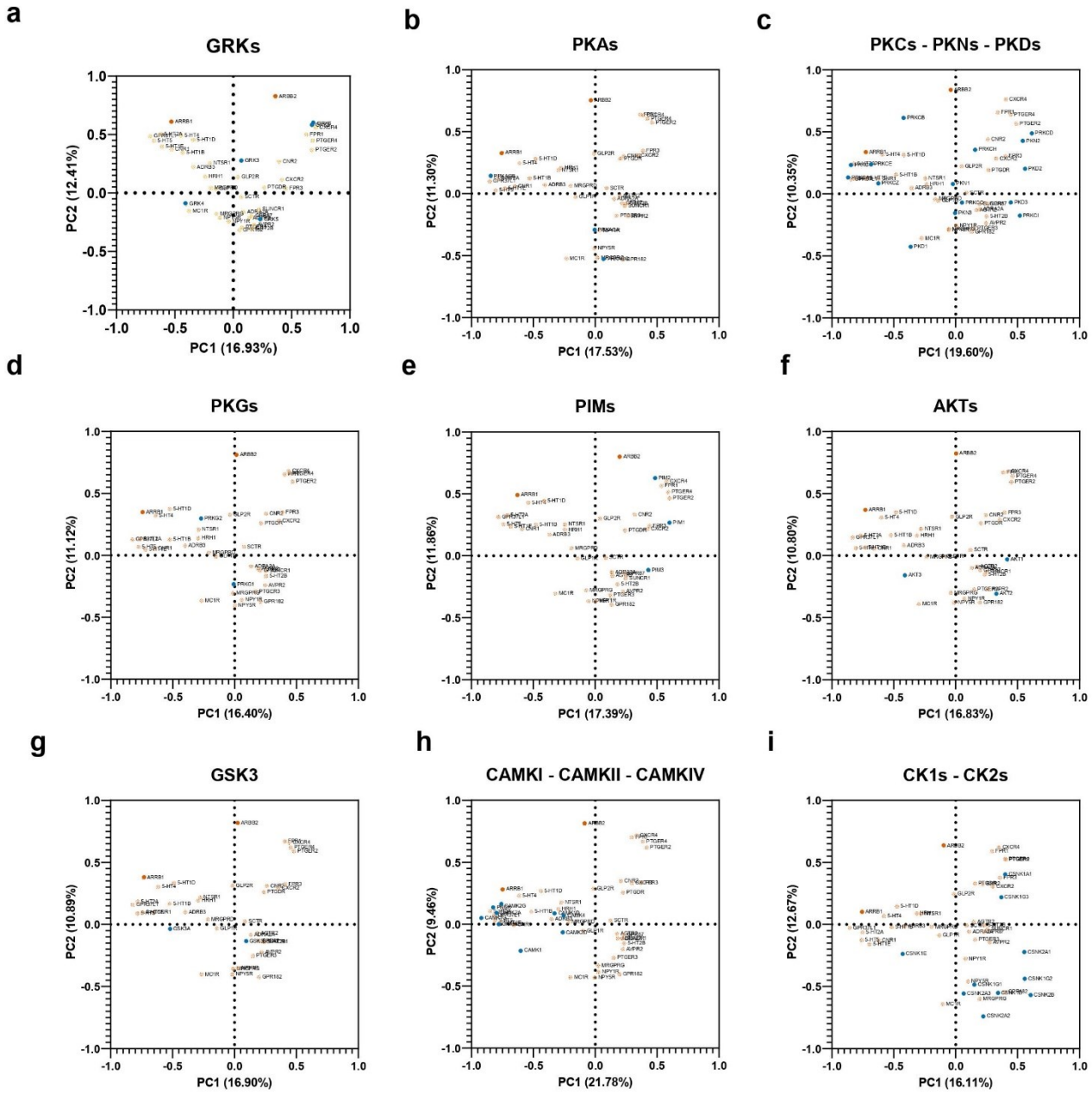

Figure 2.8. Visualization of tissue-specific expression levels of select GPCRs with high basal activities, serine/threonine kinases, β-arrestin-1 and β-arrestin -2. Human Protein Atlas (HPA) RNA consensus tissue gene data (version 21.0 and Ensembl version 103.38.) summarizing the expression levels in 55 tissues was extracted for β-arrestin-1 and -2 (ARRB1 and ARRB2), select receptors with high constitutive selectivity for one arrestin isoform over the other (GPR182, AGTR2, ADRA2A, GPR37L1, SCTR, ADRB3, PTGER4, SUNCR1, PTGER3, MRGPRG, NPY5R, NPY1R, GLP1R, FPR1, MC1R, FPR3, 5-HT5, MRGPRD, GPR87, CXCR4, HRH1,

AVPR2, 5-HT4, 5-HT2A, NTSR1, GLP2R, 5-HT1D, CXCR2, 5-HT1B, 5-HT1E, PTGER2, 5-HT2B, PTGDR), and either GRKs (a), PKA (b), PKCs, PKNs, and PKDs (c), PKGs (d), PIMs (e), AKTs (f), GSK3 (g), CAMKI, CAMKII, and CAMIV (h), CK1s and CK2s (i). The data was analyzed using principal component analysis; β-arrestin-1 and -2 are denoted with red, ST kinases with blue, and GPCRs with orange symbols. Generic receptor codes refer to the GPCR-Tango constructs.

Supplementary Information for

Profiling of basal and ligand-dependent GPCR activities by means of a polyvalent cell-based high-throughput platform

Manel Zeghal[1], Geneviève Laroche[1], Julia Douglas Freitas[1], Rebecca Wang[1], Patrick M. Giguère[1,2*]

[1] Department of Biochemistry, Microbiology and Immunology, University of Ottawa, Ottawa, ON, K1H8M5, Canada
[2] Brain and Mind Research Institute, University of Ottawa, Ottawa, ON, K1H8M5, Canada
*Correspondence to Patrick M. Giguère. Email: patrick.giguere@uottawa.ca

Supplemental Figures

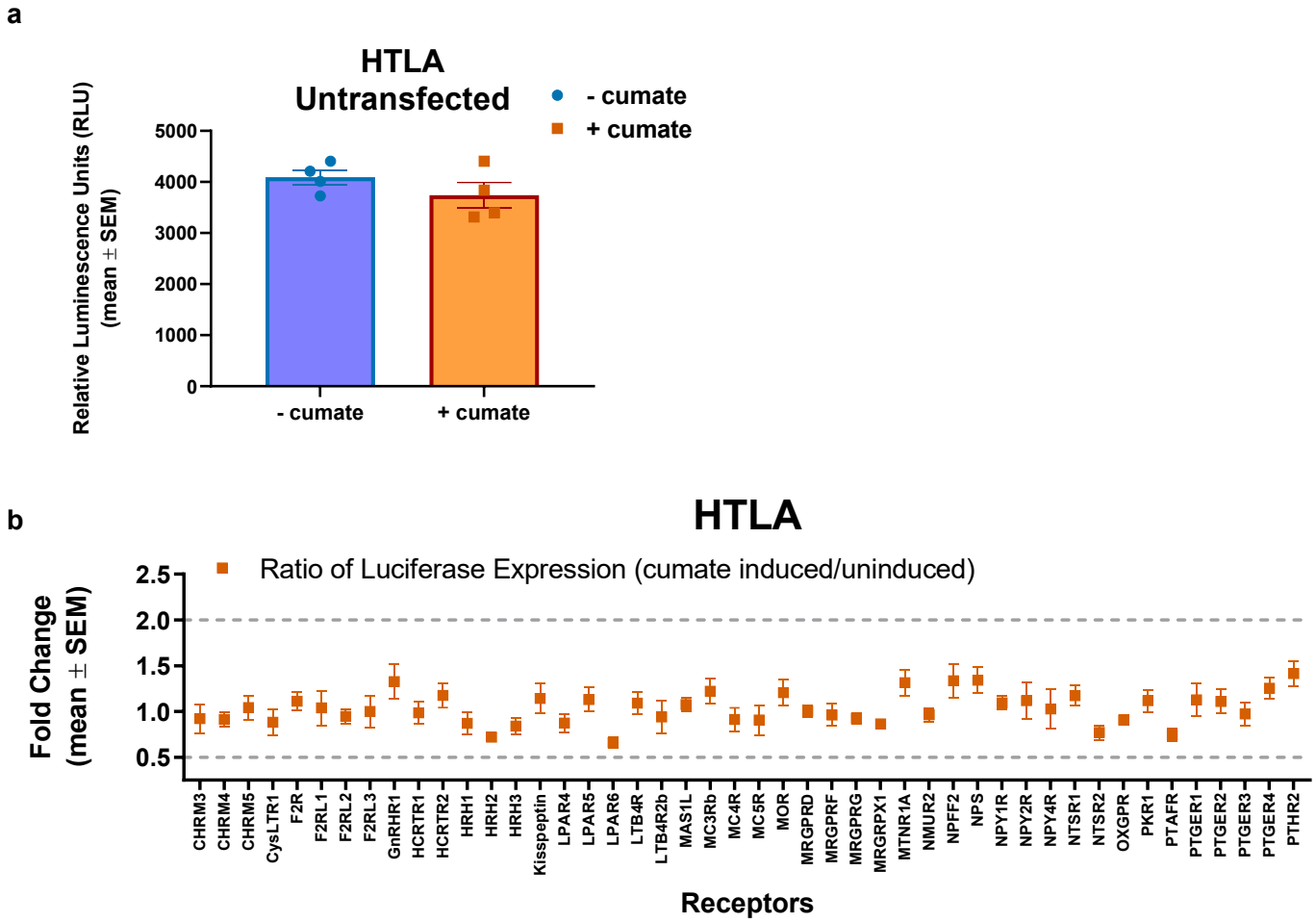

Supplementary Figure 2.1. Assessment of the effect of cumate in the PRESTO-Tango (cumate-independent system). To confirm that cumate itself does not possess any agonistic or antagonistic properties in a cumate-independent system, HTLA cells from the PRESTO-Tango platform were plated in the presence and absence of cumate (30 µg/mL) (a) and were transfected with a panel of diverse GPCR Tango constructs (b). 96 hours following its initial addition, fold changes in basal arrestin recruitment were calculated between the wells in the absence or presence of cumate. Data are presented as mean values, with error bars representing SEM (Supplementary Fig 1A: n = 12, with 3 technical replicates from 4 biological samples; Supplementary Fig 1B: n = 4, with 4 technical replicates from one biological sample). Generic receptor codes refer to the GPCR-Tango constructs.

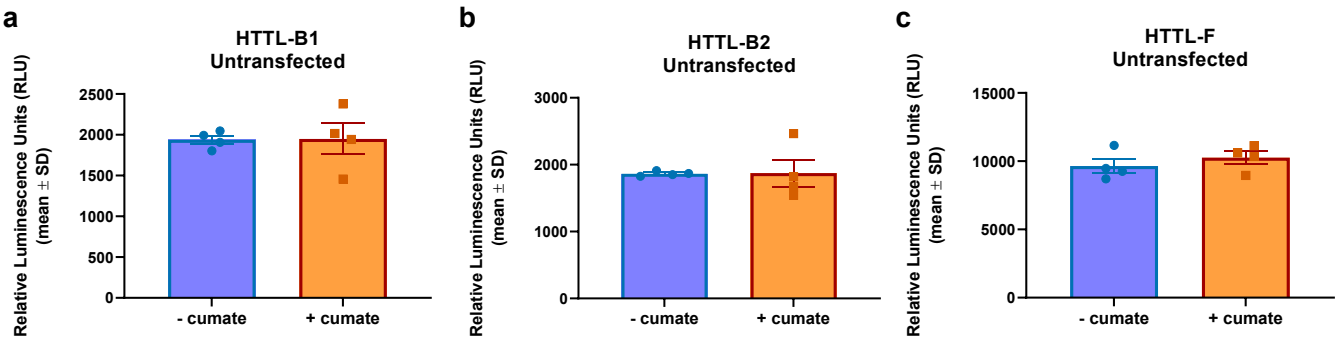

Supplementary Figure 2.2. Baseline signal of Tango-Trio cell lines. HTTL-B1, HTTL-B2, and HTTL-F cells were plated in the presence or absence of cumate (30 µg/mL), which was maintained throughout (totalling approximately 72 hours). As per standard protocol, cells were serum starved for the last 24 hours of the experiment, and luminescence was subsequently read to compare the differences in baseline signal of untransfected cells. Data are presented as mean values, with error bars representing SD (n = 12, with 3 technical replicates from 4 biological samples).

a

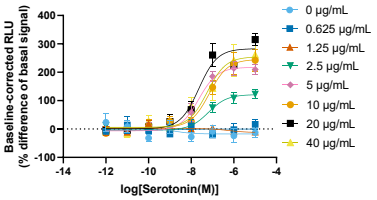

	EC50	Fold
0 µg/mL	1.522e-009	0.7986
0.625 µg/mL	6.476e-009	1.032
1.25 µg/mL	5.666e-007	0.8598
2.5 µg/mL	6.493e-008	2.302
5 µg/mL	2.277e-008	3.396
10 µg/mL	7.106e-008	3.305
20 µg/mL	2.281e-008	3.797
40 µg/mL	5.685e-008	3.347

b

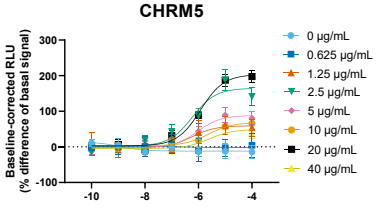

	EC50	Fold
0 µg/mL	1.261e-009	0.7768
0.625 µg/mL	2.616e-007	0.9735
1.25 µg/mL	5.848e-007	1.630
2.5 µg/mL	5.948e-007	2.585
5 µg/mL	9.187e-007	1.923
10 µg/mL	2.424e-006	1.626
20 µg/mL	1.187e-006	2.952
40 µg/mL	2.552e-006	1.560

c

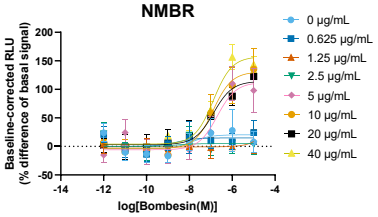

	EC50	Fold
0 µg/mL	1.333e-008	1.255
0.625 µg/mL	2.705e-009	1.146
1.25 µg/mL	0.1617	Unstable
2.5 µg/mL	2.063e-009	1.053
5 µg/mL	2.005e-007	2.256
10 µg/mL	1.295e-007	2.403
20 µg/mL	1.348e-007	2.077
40 µg/mL	1.316e-007	2.475

d

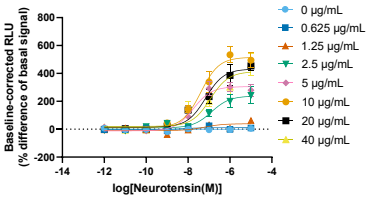

	EC50	Fold
0 µg/mL	0.03127	Unstable
0.625 µg/mL	5.844e-009	1.140
1.25 µg/mL	6.036e-008	1.545
2.5 µg/mL	1.300e-007	3.099
5 µg/mL	1.779e-008	4.610
10 µg/mL	4.025e-008	5.504
20 µg/mL	6.903e-008	4.617
40 µg/mL	1.153e-007	4.251

e

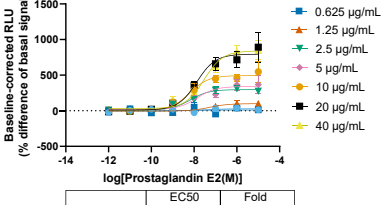

	EC50	Fold
0 µg/mL	5.024e-008	1.309
0.625 µg/mL	2.567e-009	1.143
1.25 µg/mL	5.236e-008	2.099
2.5 µg/mL	6.696e-009	3.636
5 µg/mL	1.387e-008	3.731
10 µg/mL	6.337e-009	5.511
20 µg/mL	1.327e-008	8.103
40 µg/mL	2.933e-008	7.132

f

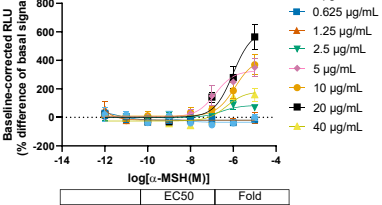

	EC50	Fold
0 µg/mL	2.220e-009	0.6302
0.625 µg/mL	4.753e-012	0.5670
1.25 µg/mL	2.018e-015	Unstable
2.5 µg/mL	2.823e-007	1.864
5 µg/mL	1.459e-007	4.093
10 µg/mL	1.204e-006	4.687
20 µg/mL	9.759e-007	7.012
40 µg/mL	4.858e-007	3.775

g

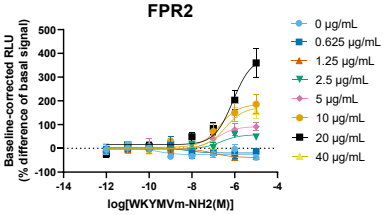

	EC50	Fold
0 µg/mL	2.372e-010	0.7269
0.625 µg/mL	5.153e-009	0.7824
1.25 µg/mL	1.013e-007	0.6304
2.5 µg/mL	2.296e-007	1.621
5 µg/mL	1.377e-007	1.970
10 µg/mL	1.981e-007	2.739
20 µg/mL	8.317e-007	4.177
40 µg/mL	3.618e-007	2.758

h

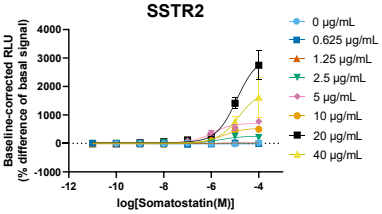

	EC50	Fold
0 µg/mL	1.306e-007	0.9568
0.625 µg/mL	1.517e-010	0.7628
1.25 µg/mL	2.058e-006	1.253
2.5 µg/mL	2.399e-006	3.481
5 µg/mL	1.086e-006	7.144
10 µg/mL	2.812e-006	7.369
20 µg/mL	1.202e-005	24.43
40 µg/mL	1.403e-005	16.52

i

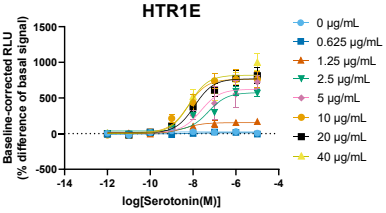

	EC50	Fold
0 µg/mL	6.643e-011	1.347
0.625 µg/mL	9.436e-009	1.154
1.25 µg/mL	4.096e-009	2.500
2.5 µg/mL	5.166e-008	4.929
5 µg/mL	2.304e-008	6.100
10 µg/mL	5.882e-009	7.516
20 µg/mL	1.179e-008	7.945
40 µg/mL	6.688e-009	8.827

j

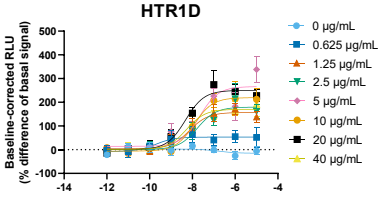

	EC50	Fold
0 µg/mL	1.711e-007	0.8261
0.625 µg/mL	1.945e-010	1.660
1.25 µg/mL	7.274e-009	2.478
2.5 µg/mL	1.703e-008	2.768
5 µg/mL	2.194e-008	3.205
10 µg/mL	1.199e-008	3.403
20 µg/mL	4.799e-009	3.491
40 µg/mL	5.383e-009	2.669

k

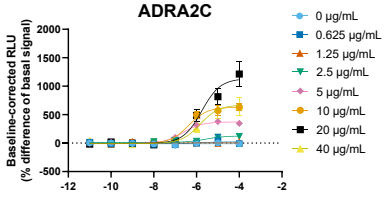

	EC50	Fold
0 µg/mL	6.870e-010	0.8535
0.625 µg/mL	1.161e-006	1.332
1.25 µg/mL	6.461e-016	Unstable
2.5 µg/mL	2.674e-006	2.013
5 µg/mL	2.320e-007	4.982
10 µg/mL	4.337e-007	7.992
20 µg/mL	1.761e-006	12.92
40 µg/mL	1.491e-006	8.250

l

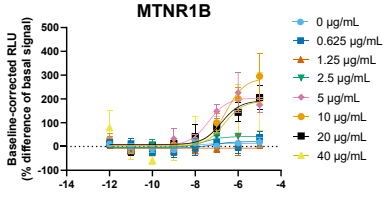

	EC50	Fold
0 µg/mL	8.045e-009	1.165
0.625 µg/mL	6.530e-008	1.287
1.25 µg/mL	90711713	Unstable
2.5 µg/mL	2.453e-008	1.478
5 µg/mL	4.129e-008	2.906
10 µg/mL	2.752e-007	3.653
20 µg/mL	1.686e-007	2.702
40 µg/mL	2.283e-007	2.870

Supplementary Figure 2.3. Changes in baseline signals and fold windows due to cumate induction. HTTL-B1, HTTL-B2 and HTTL-F cells were plated in increasing concentrations of cumate (0, 0.625, 1.25, 2.5, 5, 10, 20, and 40 μg/mL), which was maintained throughout the entire experiment, and were transfected with select GPCRs: HTR4 (a), CHRM5 (b), and NMBR (c) in HTTL-F; NTSR1 (d), PTGER4 (e), MC4R (f), FPR2 (g), and SSTR2 (h) in HTTL-B2; HTR1E (i), HTR1D (j), ADRA2C (k), and MTNR1B (l) in HTTL-B1. Transfected cells were stimulated with the receptor specific agonist and dose-response curves were built using XY analysis for non-linear regression curve and the 3-parameters dose-response stimulation function, followed by baseline correction. Data are presented as mean values, with error bars representing SEM (n = 3, with three technical replicates from one biological sample). Generic receptor codes refer to the GPCR-Tango constructs.

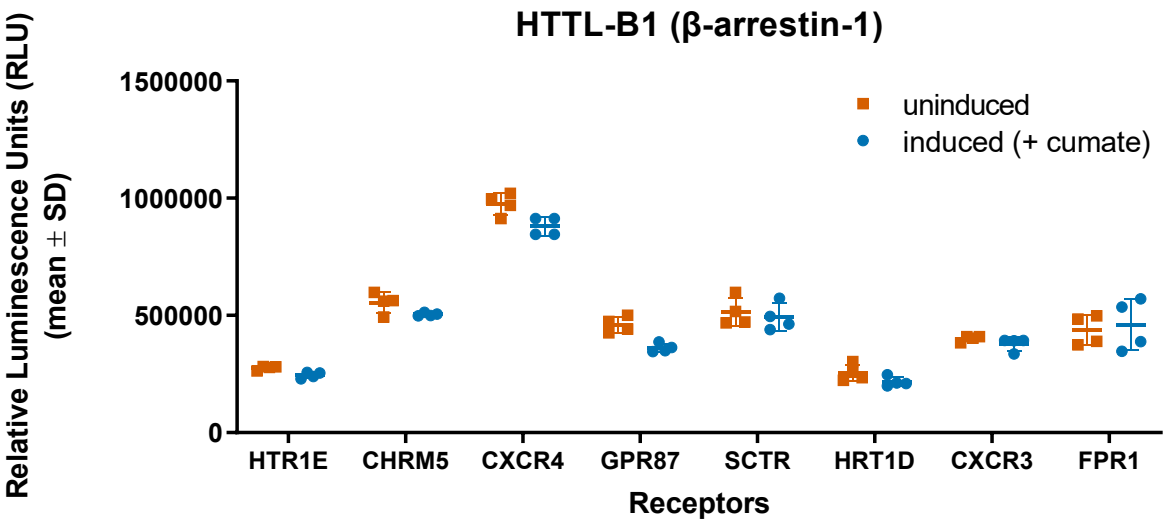
HTTL-B1 (β-arrestin-1)
Relative Luminescence Units (RLU)
(mean ± SD)
1500000
1000000
500000
0
uninduced
induced (+ cumate)
HTR1E
CHRM5
CXCR4
GPR87
SCTR
HRT1D
CXCR3
FPR1
Receptors

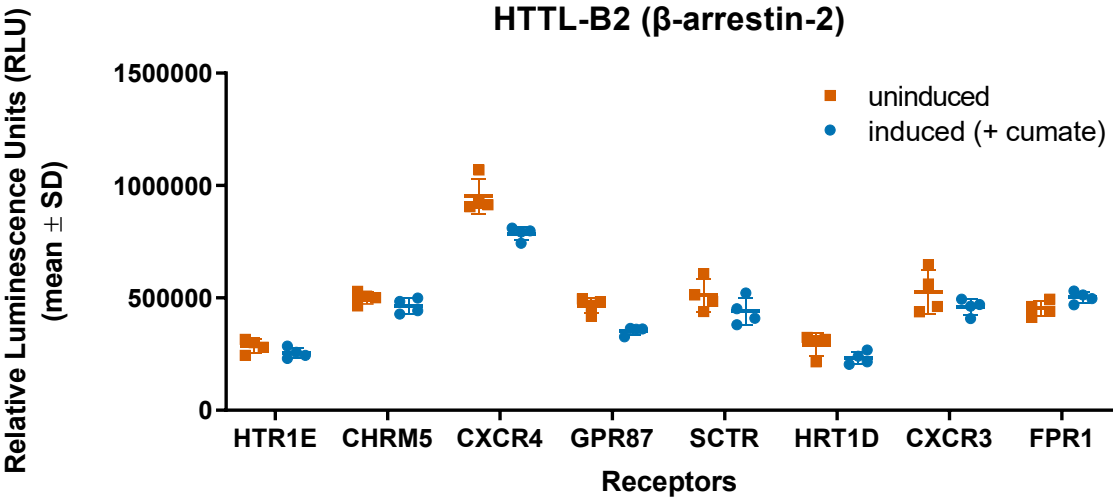
HTTL-B2 (β-arrestin-2)
Relative Luminescence Units (RLU)
(mean ± SD)
1500000
1000000
500000
0
uninduced
induced (+ cumate)
HTR1E
CHRM5
CXCR4
GPR87
SCTR
HRT1D
CXCR3
FPR1
Receptors

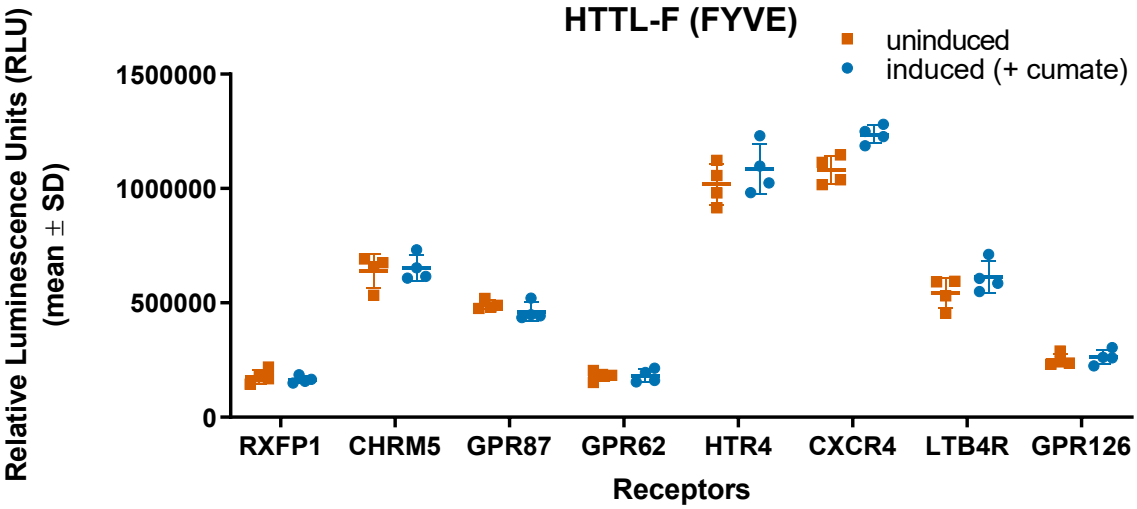
HTTL-F (FYVE)
Relative Luminescence Units (RLU)
(mean ± SD)
1500000
1000000
500000
0
uninduced
induced (+ cumate)
RXFP1
CHRM5
GPR87
GPR62
HTR4
CXCR4
LTB4R
GPR126
Receptors

Supplementary Figure 2.4. Receptor surface expression following cumate induction of fusion protein expression HTTL-B1, HTTL-B2 and HTTL-F were plated in the presence or absence of cumate (30 μg/mL) and were transfected with a select number of positive GPCR hits from the constitutive HTS. ELISA experiments were subsequently carried out on transfected cells to determine receptor surface expression. Data are presented as mean values, with error bars representing SD (n = 4, with four technical replicates from one biological sample). Generic receptor codes refer to the GPCR-Tango constructs.

a

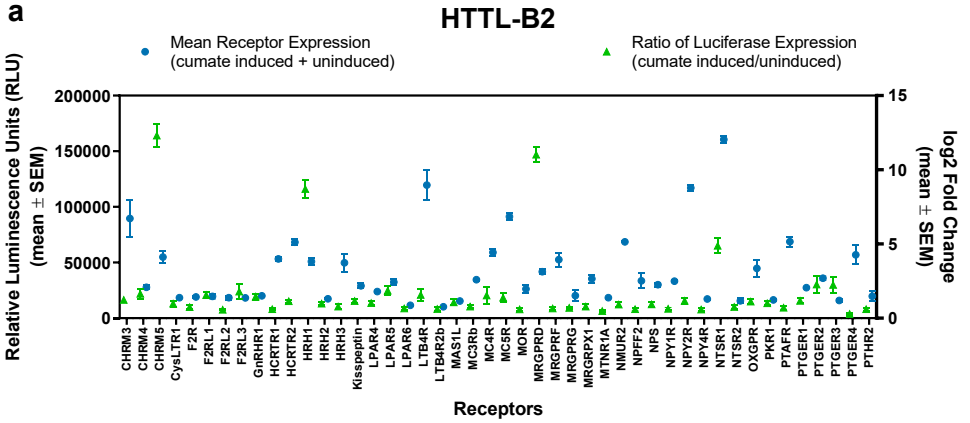

Pearson r	
r	0.2084
95% confidence interval	-0.08714 to 0.4703
R squared	0.04344
P value	
P (two-tailed)	0.1645
P value summary	ns
Significant? (alpha = 0.05)	No
Number of XY Pairs	46

b

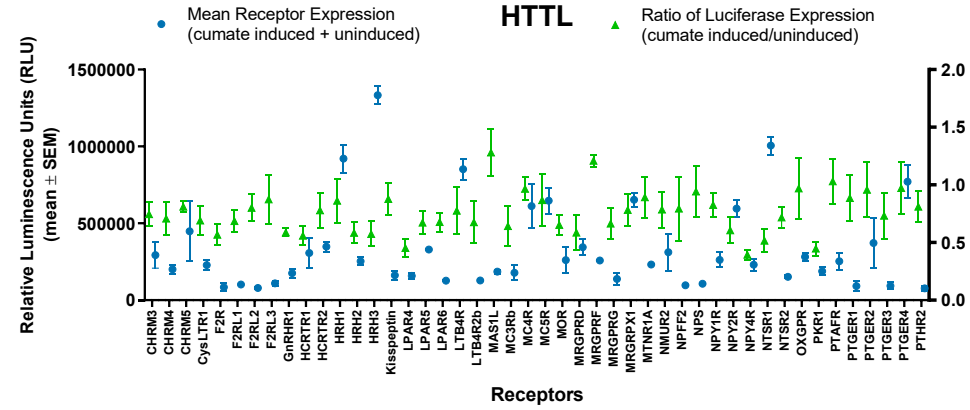

Pearson r	
r	-0.03125
95% confidence interval	-0.3187 to 0.2614
R squared	0.0009767
P value	
P (two-tailed)	0.8366
P value summary	ns
Significant? (alpha = 0.05)	No
Number of XY Pairs	46

c

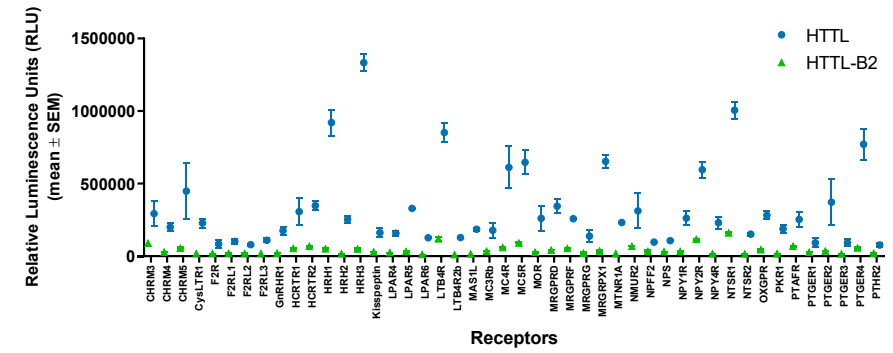

Pearson r	
r	0.6659
95% confidence interval	0.4656 to 0.8013
R squared	0.4434
P value	
P (two-tailed)	<0.0001
P value summary	****
Significant? (alpha = 0.05)	Yes
Number of XY Pairs	46

d

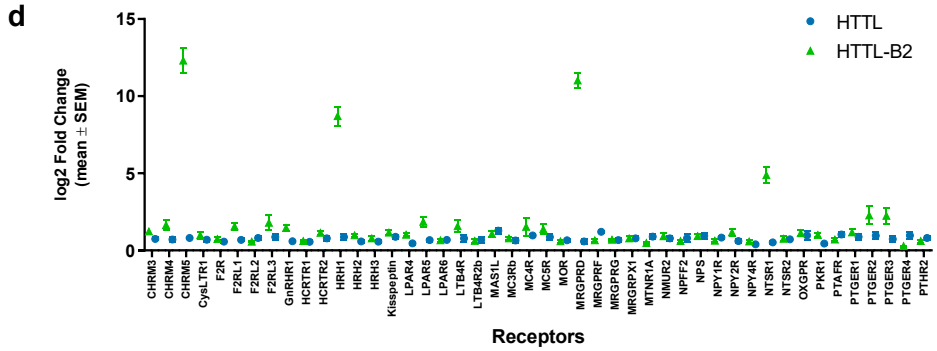

Pearson r	
r	-0.04866
95% confidence interval	-0.3342 to 0.2451
R squared	0.002368
P value	
P (two-tailed)	0.7481
P value summary	ns
Significant? (alpha = 0.05)	No
Number of XY Pairs	46

Supplementary Figure 2.5. Comparison of receptor expression and constitutive activity across panel of GPCRs. HTTL-B2 (a) and HTTL (b) were plated in the presence or absence of cumate (30 μg/mL) and were transfected with a panel of GPCRs with a varying range of constitutive activities. ELISA experiments were subsequently carried out on transfected cells to determine receptor surface expression, and log2 fold changes in constitutive arrestin recruitment were calculated between the wells in the absence or presence of cumate. Mean receptor expression (c) and log2 fold changes in constitutive arrestin recruitment (d) were also compared between the HTTL and HTTL-B2 cell lines. Pearson correlation coefficients (r) and corresponding p values (two-tailed) were computed between data sets using GraphPad Prism. Data are presented as mean values, with error bars representing SEM (n = 4, with four technical replicates from one biological sample). Generic receptor codes refer to the GPCR-Tango constructs.

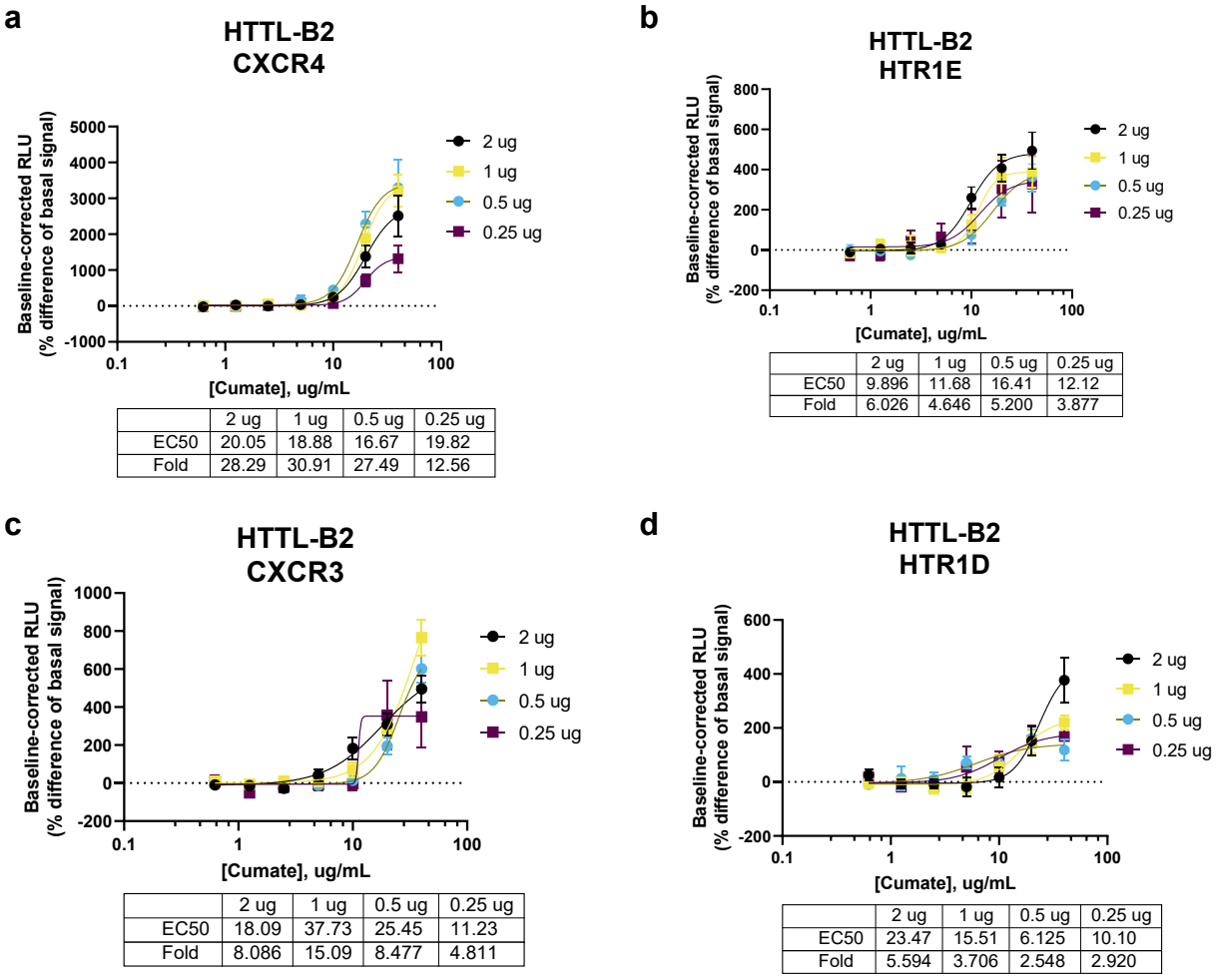

	2 ug	1 ug	0.5 ug	0.25 ug
EC50	20.05	18.88	16.67	19.82
Fold	28.29	30.91	27.49	12.56

	2 ug	1 ug	0.5 ug	0.25 ug
EC50	9.896	11.68	16.41	12.12
Fold	6.026	4.646	5.200	3.877

	2 ug	1 ug	0.5 ug	0.25 ug
EC50	18.09	37.73	25.45	11.23
Fold	8.086	15.09	8.477	4.811

	2 ug	1 ug	0.5 ug	0.25 ug
EC50	23.47	15.51	6.125	10.10
Fold	5.594	3.706	2.548	2.920

Supplementary Figure 2.6. Titration of GPCR Tango DNA and consequent effects on constitutive activity. HTTL-B2 cells were seeded in 6-well plates and transfected with various amount of CXCR4 (a), HTR1E (b), CXCR3 (c), and HTR1D (d) Tango DNA, ranging from 0.25 ug – 2 ug total per well. Transfected cells were stimulated with cumate, and dose- response curves were built using XY analysis for non-linear regression curve and the 4-parameters dose-response stimulation function, followed by baseline correction. Data are presented as mean values, with error bars representing SEM (n = 3, with three technical replicates from one biological sample). Generic receptor codes refer to the GPCR-Tango constructs.

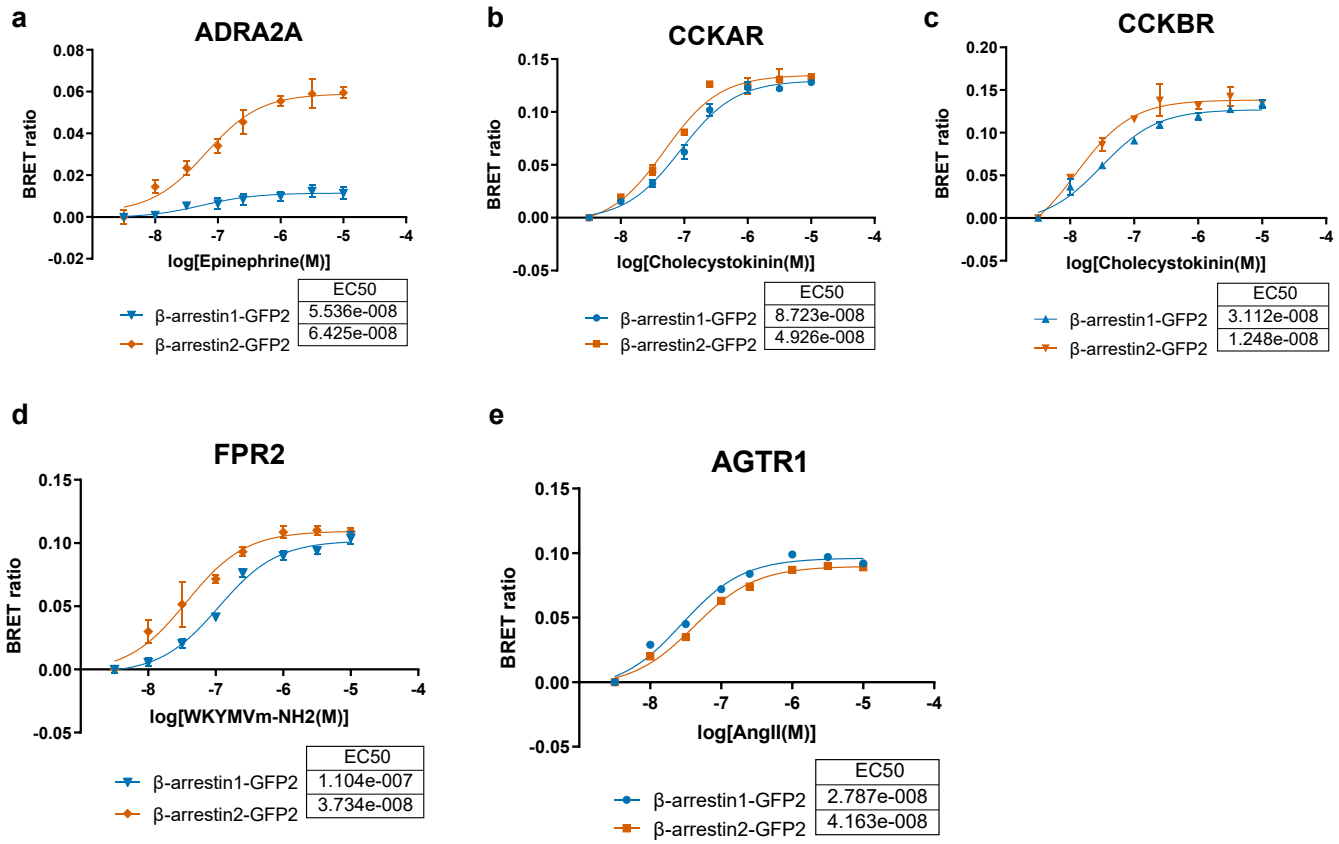

Supplementary Figure 2.7. Orthogonal determination of arrestin isoform selectivity using BRET2. HEK293T cells were transfected with β-arrestin1/2-GFP2, as well as the following GPCRs: ADRA2A (a), CCKAR (b), CCKBR (c), FPR2 (d), AGTR1 (e). Following transfection, cells were stimulated with serial dilutions of selective agonist, and read with 405 nm (RLuc8-Coelenterazine 400a) and 500 nm (GFP2) emission filters. Dose- response curves were built using XY analysis for non-linear regression curve and the 3-parameters dose-response stimulation function, followed by baseline correction. Data are presented as mean values, with error bars representing SEM (n = 2, with two technical replicates from one biological sample). Generic receptor codes refer to the GPCR-Rluc8 constructs.

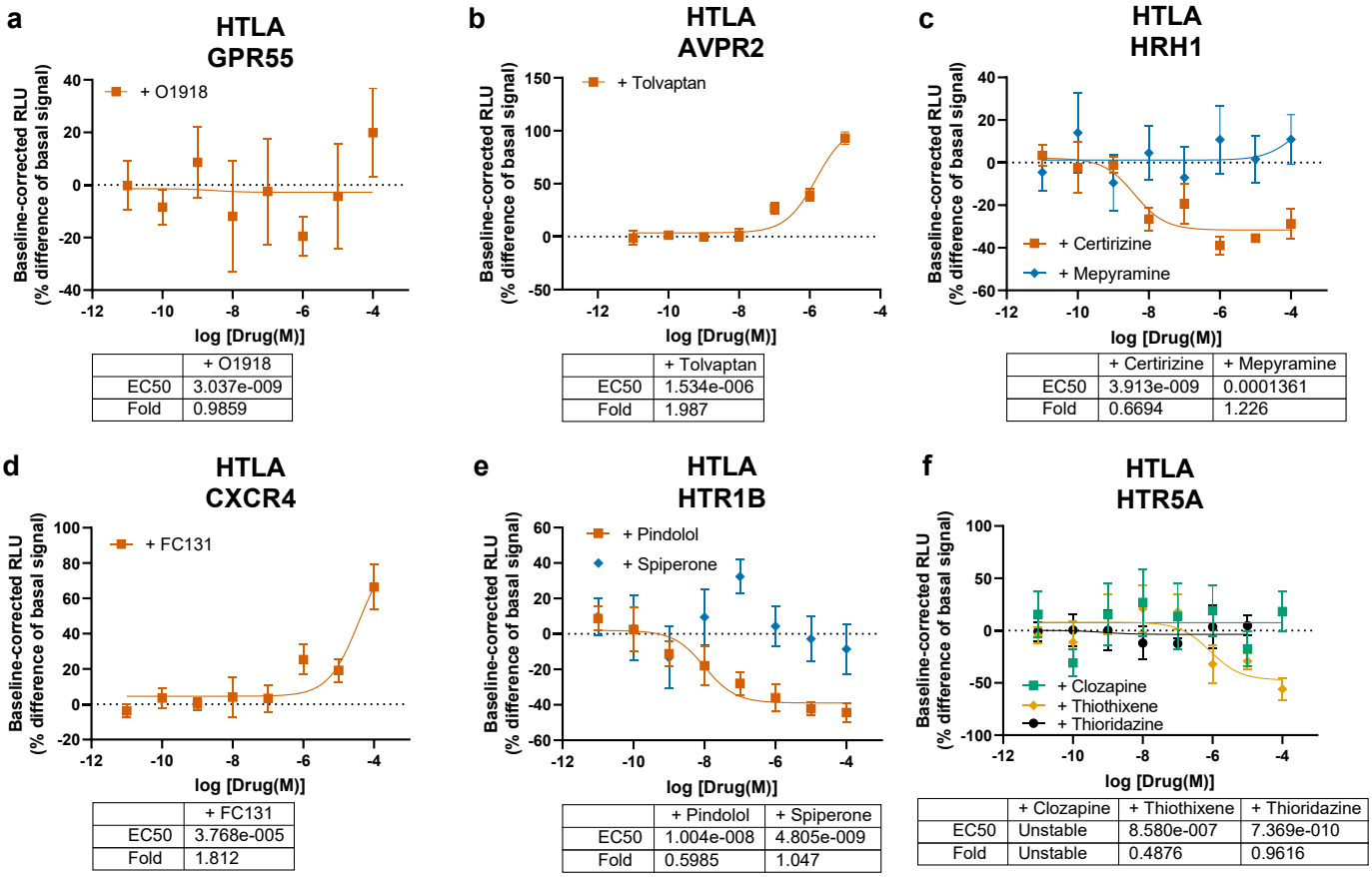

	+ O1918
EC50	3.037e-009
Fold	0.9859

	+ Tolvaptan
EC50	1.534e-006
Fold	1.987

	+ Certirizine	+ Mepyramine
EC50	3.913e-009	0.0001361
Fold	0.6694	1.226

	+ FC131
EC50	3.768e-005
Fold	1.812

	+ Pindolol	+ Spiperone
EC50	1.004e-008	4.805e-009
Fold	0.5985	1.047

	+ Clozapine	+ Thiothixene	+ Thioridazine
EC50	Unstable	8.580e-007	7.369e-010
Fold	Unstable	0.4876	0.9616

Supplementary Figure 2.8. Orthogonal characterization of select inverse agonists and antagonists using PRESTO-Tango. HTLA cells were transfected with GPCRs exhibiting strong constitutive arrestin recruitment from the primary Tango-Trio screen, serving to validate the findings shown in Figure 7. Transfected cells were stimulated with a dose-response curve using the following inverse agonists/antagonists: O-1918 at GPR55 (a), Tolvaptan at AVPR2 (b), Cetirizine and Mepyramine at HRH1 (c), FC131 at CXCR4 (d), Pindolol and Spiperone at HTR1E (e), and Clozapine, Thiothexene, and Thioridazine at HTR5A (f). Stimulation curves were built using XY analysis for non-linear regression curve and the 3-parameters dose-response stimulation function, followed by baseline correction. Data are presented as mean values, with error bars representing SEM (Supplementary Figs 8a, 8c-f: n = 3, with three technical replicates from one biological sample; Supplementary Fig 8b: n = 6, with three technical replicates from two biological samples). Generic receptor codes refer to the GPCR-Tango constructs.

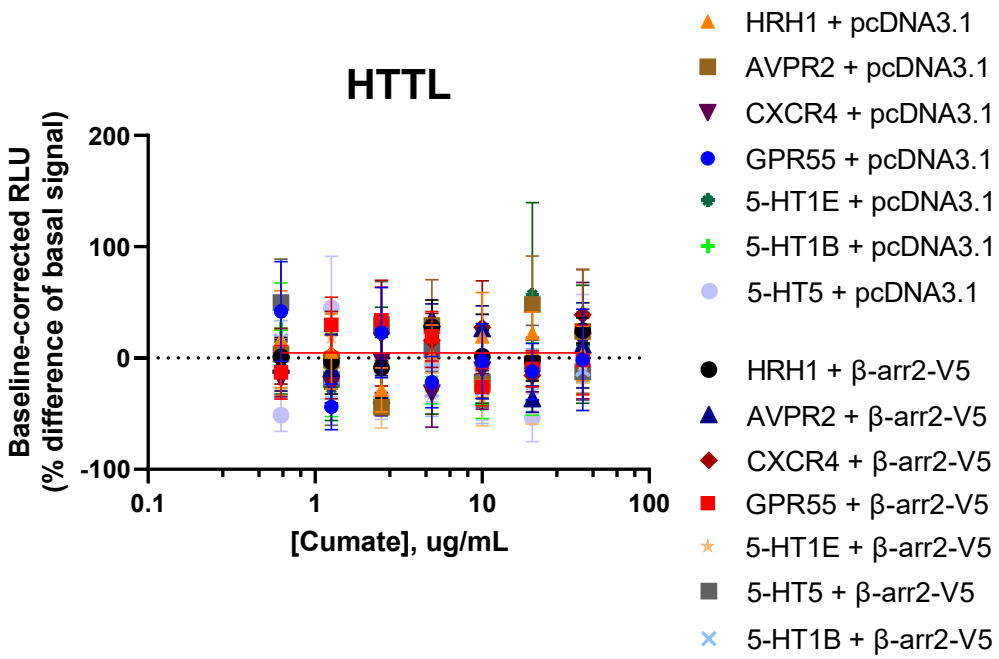

Supplementary Figure 2.9. Expression of GPCR-Tango constructs in the absence of TEV protease. HTTL cells were co-transfected with select GPCR constructs (tested with antagonists/inverse agonists from Fig 7), and either β-arrestin-2 (not tagged to TEV protease) or pcDNA3.1 as a control. Transfected cells were stimulated as a cumate dose-response, and stimulation curves were built using XY analysis for non-linear regression curve and the 4-parameters dose-response stimulation function, followed by baseline correction. Data are presented as mean values, with error bars representing SEM (n = 3, with three technical replicates from one biological sample). Generic receptor codes refer to the GPCR-Tango constructs.

a

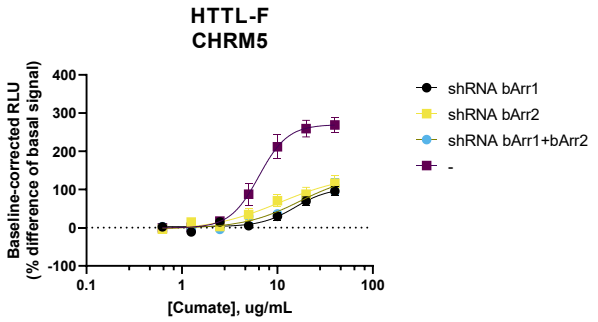

	EC50	logEC50	Span	Fold
shRNA bArr1	15.38	1.187	459303	1.993
shRNA bArr2	10.60	1.025	669083	2.622
shRNA bArr1+bArr2	17.20	1.236	564353	2.461
-	6.405	0.8065	139806	3.725

b

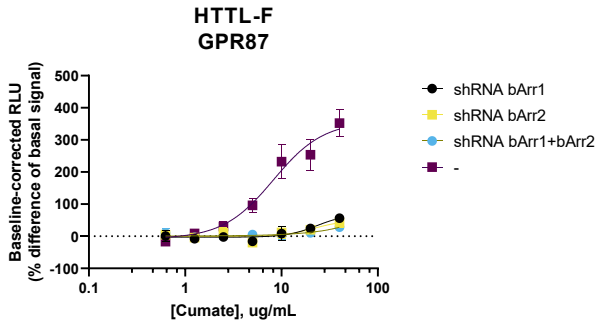

	EC50	logEC50	Span	Fold
shRNA bArr1	23.39	1.369	30849	1.744
shRNA bArr2	21.66	1.336	29759	1.513
shRNA bArr1+bArr2	557592	5.746	Unstable	Unstable
-	8.221	0.9149	48577	4.983

c

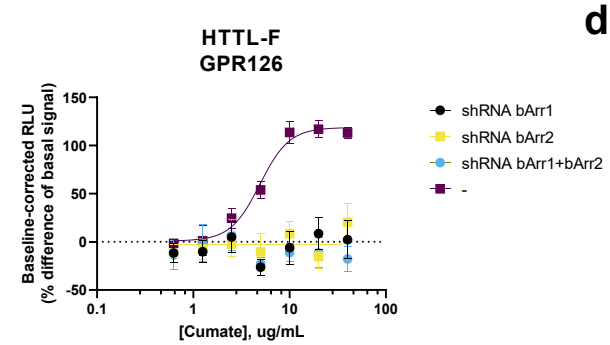

	EC50	logEC50	Span	Fold
shRNA bArr1	3.069	0.4871	30035	1.651
shRNA bArr2	42.20	1.625	Unstable	Unstable
shRNA bArr1+bArr2	3.419	0.5339	21766	1.486
-	4.921	0.6920	38098	2.169

d

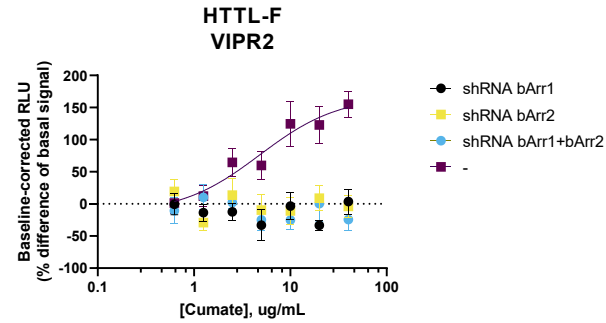

	EC50	logEC50	Span	Fold
shRNA bArr1	8.957	0.9522	63180	1.713
shRNA bArr2	4.508	0.6540	46960	1.685
shRNA bArr1+bArr2	3.386	0.5297	43671	1.472
-	4.821	0.6831	57025	3.172

e

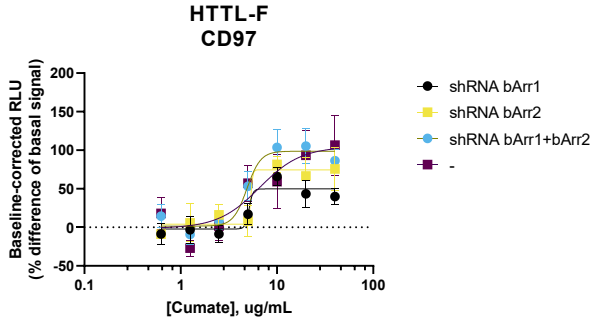

	EC50	logEC50	Span	Fold
shRNA bArr1	5.126	0.7098	59654	1.532
shRNA bArr2	5.352	0.7285	71885	1.678
shRNA bArr1+bArr2	4.878	0.6883	94061	1.956
-	6.606	0.8200	67253	2.072

f

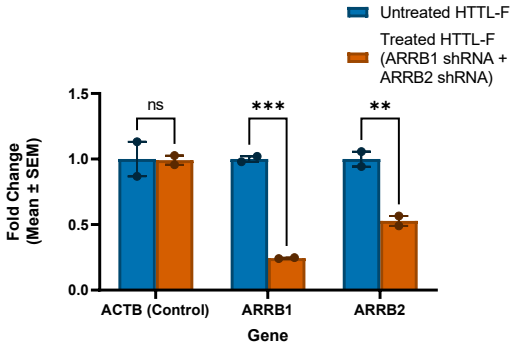

	ACTB (Control)	ARRB1	ARRB2
P value	0.930008	0.000147	0.001847
Mean of Untreated HTTL-F	1.000	1.000	1.000
Mean of Column B	0.9918	0.2444	0.5285
Difference	0.008163	0.7556	0.4715
SE of difference	0.08913	0.08913	0.08913
t ratio	0.09159	8.477	5.290
df	6.000	6.000	6.000
Adjusted P Value	0.930008	0.000442	0.003691

Supplementary Figure 2.10. Internalization of GPCRs in HTTL-F following β-arrestin-1 and β-arrestin-2 knockdown. Lentiviral β-arrestin-1 and -2 shRNA plasmids were transfected in HEK293T cells, along with psPAX2 and VSV-G vectors. The medium was replaced the following day with complete fresh medium, and lentiviral shRNA medium was collected following 48 hours transfection. For the knockdown experiment, HTTL-F cells were seeded in either complete medium or in the previously prepared lentiviral β-arrestin-1 and -2 shRNA medium (combined at a 1:1 ratio), with infection of cells facilitated with polybrene at 8 μg/mL. HTTL-F cells were transfected with GPCRs demonstrating high constitutive internalization: CHRM5 (a), GPR87 (b), GPR126 (c), VIPR2 (d), and CD97 (e). Transfected cells were stimulated as a cumate dose-response, and stimulation curves were built using XY analysis for non-linear regression curve and the 4-parameters dose-response stimulation function, followed by baseline correction. Data are presented as mean values, with error bars representing SEM (n = 3, with three technical replicates from one biological sample), and generic receptor codes refer to the GPCR-Tango constructs. qPCR was performed on untreated and infected HTTL-F cells to confirm sufficient knockdown of β-arrestin-1 and -2 (f). Data are presented as mean values, with error bars representing SEM. Fold change of gene expression and corresponding p values (two-tailed) were assessed with multiple unpaired t test using the FDR method of Benjamini & Yekutieli (n = 2, with two technical replicates from one biological sample).

Supplementary Figure 2.11. Basal profiles of β-arrestin-1 and β-arrestin-2 translocation, and receptor internalization generated using Tango-Trio (Class A, α-branch). To profile basal activities, HTTL-B1, HTTL-B2 and HTTL-F cells were transfected with GPCR Tango constructs. Transfected cells were stimulated with cumate in a dose-dependent manner. Dose-response curves were built using XY analysis for non-linear regression curve and the 4-parameters dose-response stimulation function, followed by baseline correction. Data are presented as mean values, with error bars representing SEM (n = 3, with 3 technical replicates from one biological sample). Generic receptor codes refer to the GPCR-Tango constructs.

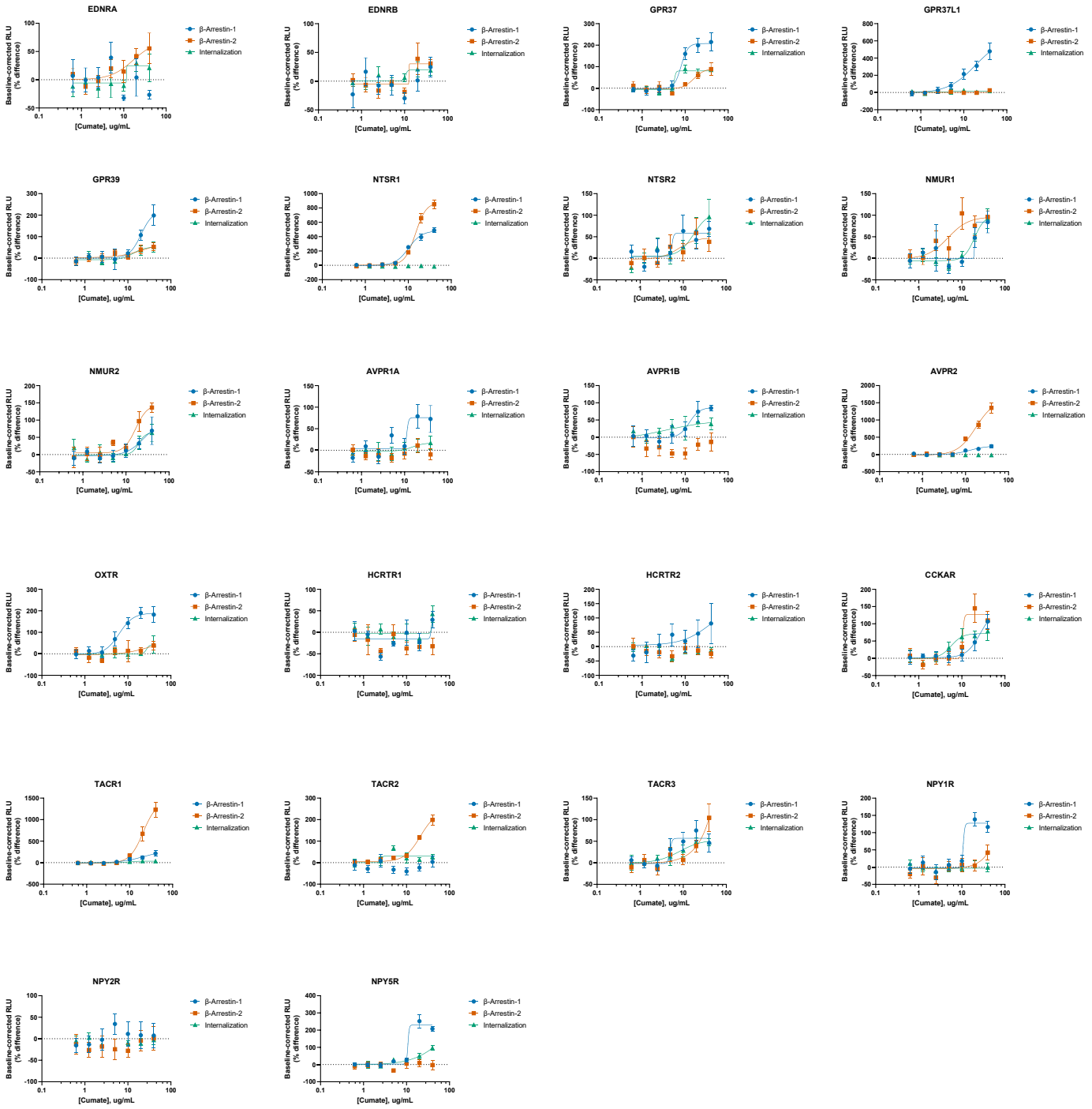

Supplementary Figure 2.12. Basal profiles of β-arrestin-1 and β-arrestin-2 translocation, and receptor internalization generated using Tango-Trio (Class A, β-branch). To profile basal activities, HTTL-B1, HTTL-B2 and HTTL-F cells were transfected with GPCR Tango constructs. Transfected cells were stimulated with cumate in a dose-dependent manner. Dose-response curves were built using XY analysis for non-linear regression curve and the 4-parameters dose-response stimulation function, followed by baseline correction. Data are presented as mean values, with error bars representing SEM (n = 3, with 3 technical replicates from one biological sample). Generic receptor codes refer to the GPCR-Tango constructs.

Supplementary Figure 2.13. Basal profiles of β-arrestin-1 and β-arrestin-2 translocation, and receptor internalization generated using Tango-Trio (Class A, γ-branch). To profile basal activities, HTTL-B1, HTTL-B2 and HTTL-F cells were transfected with GPCR Tango constructs. Transfected cells were stimulated with cumate in a dose-dependent manner. Dose-response curves were built using XY analysis for non-linear regression curve and the 4-parameters dose-response stimulation function, followed by baseline correction. Data are presented as mean values, with error bars representing SEM (n = 3, with 3 technical replicates from one biological sample). Generic receptor codes refer to the GPCR-Tango constructs.

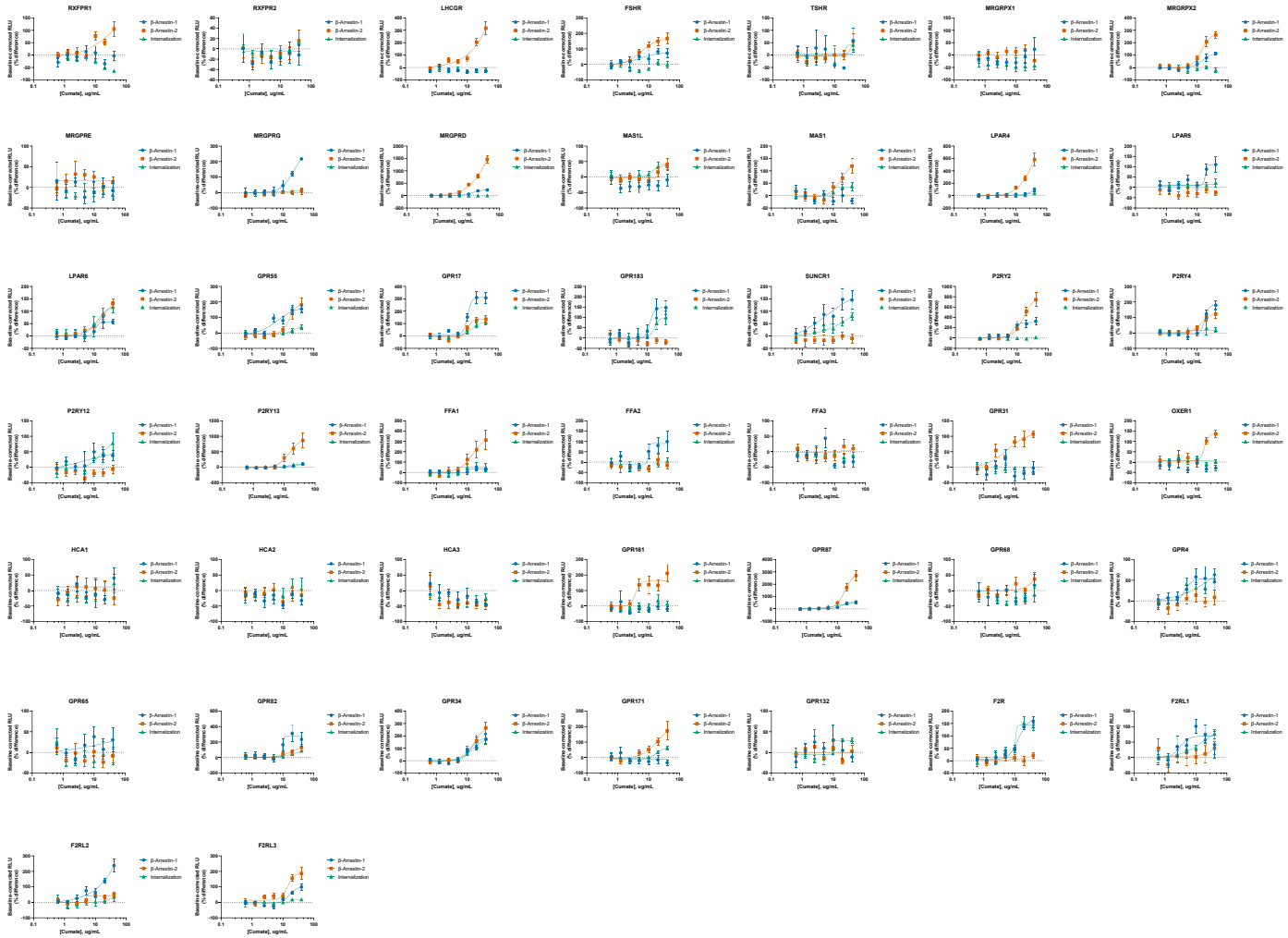

Supplementary Figure 2.14. Basal profiles of β-arrestin-1 and β-arrestin-2 translocation, and receptor internalization generated using Tango-Trio (Class A, δ-branch). To profile basal activities, HTTL-B1, HTTL-B2 and HTTL-F cells were transfected with GPCR Tango constructs. Transfected cells were stimulated with cumate in a dose-dependent manner. Dose-response curves were built using XY analysis for non-linear regression curve and the 4-parameters dose-response stimulation function, followed by baseline correction. Data are presented as mean values, with error bars representing SEM (n = 3, with 3 technical replicates from one biological sample). Generic receptor codes refer to the GPCR-Tango constructs.

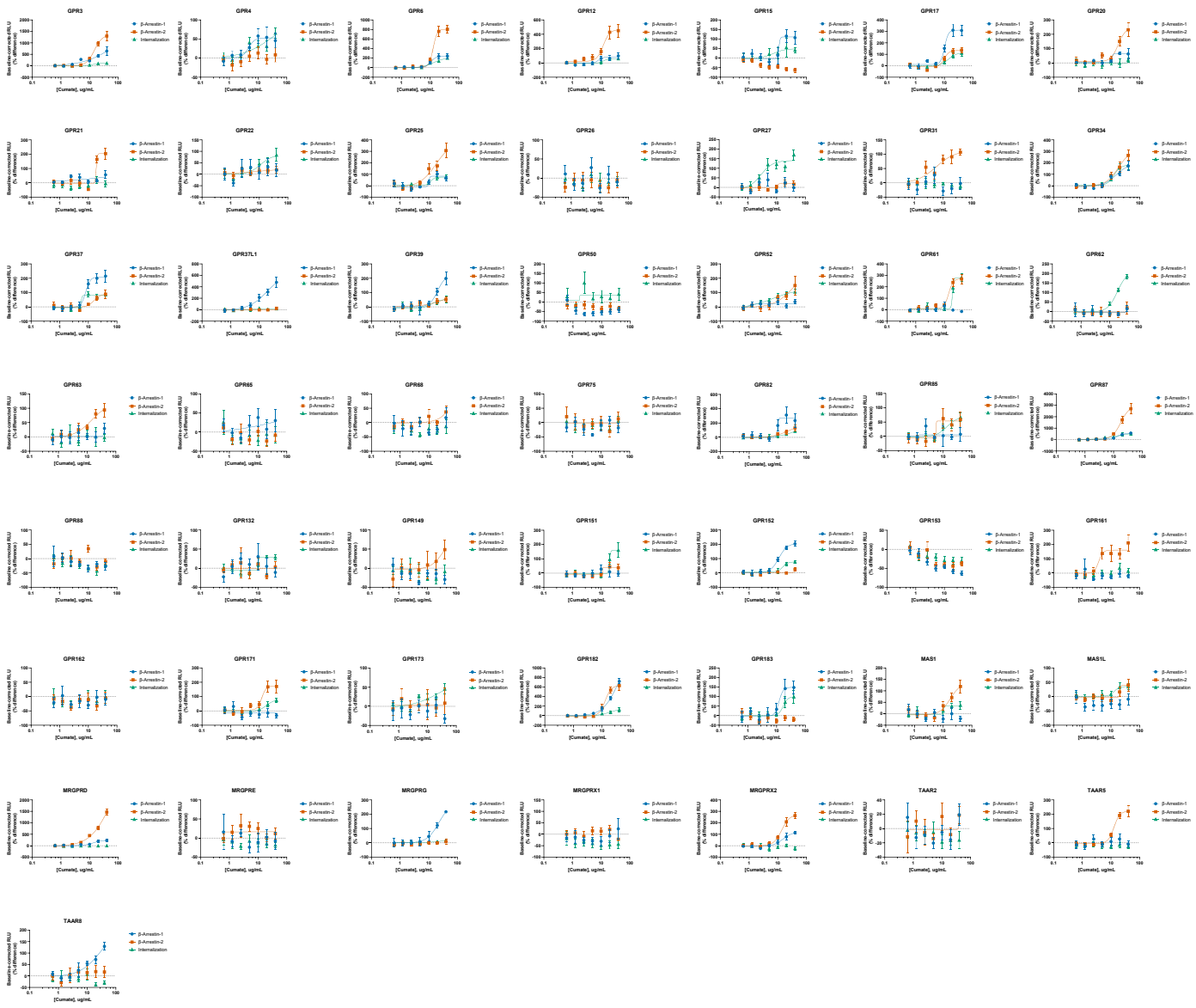

Supplementary Figure 2.15. Basal profiles of β-arrestin-1 and β-arrestin-2 translocation, and receptor internalization generated using Tango-Trio (Class A, orphan receptors). To profile basal activities, HTTL-B1, HTTL-B2 and HTTL-F cells were transfected with GPCR Tango constructs. Transfected cells were stimulated with cumate in a dose-dependent manner. Dose-response curves were built using XY analysis for non-linear regression curve and the 4-parameters dose-response stimulation function, followed by baseline correction. Data are presented as mean values, with error bars representing SEM (n = 3, with 3 technical replicates from one biological sample). Generic receptor codes refer to the GPCR-Tango constructs.

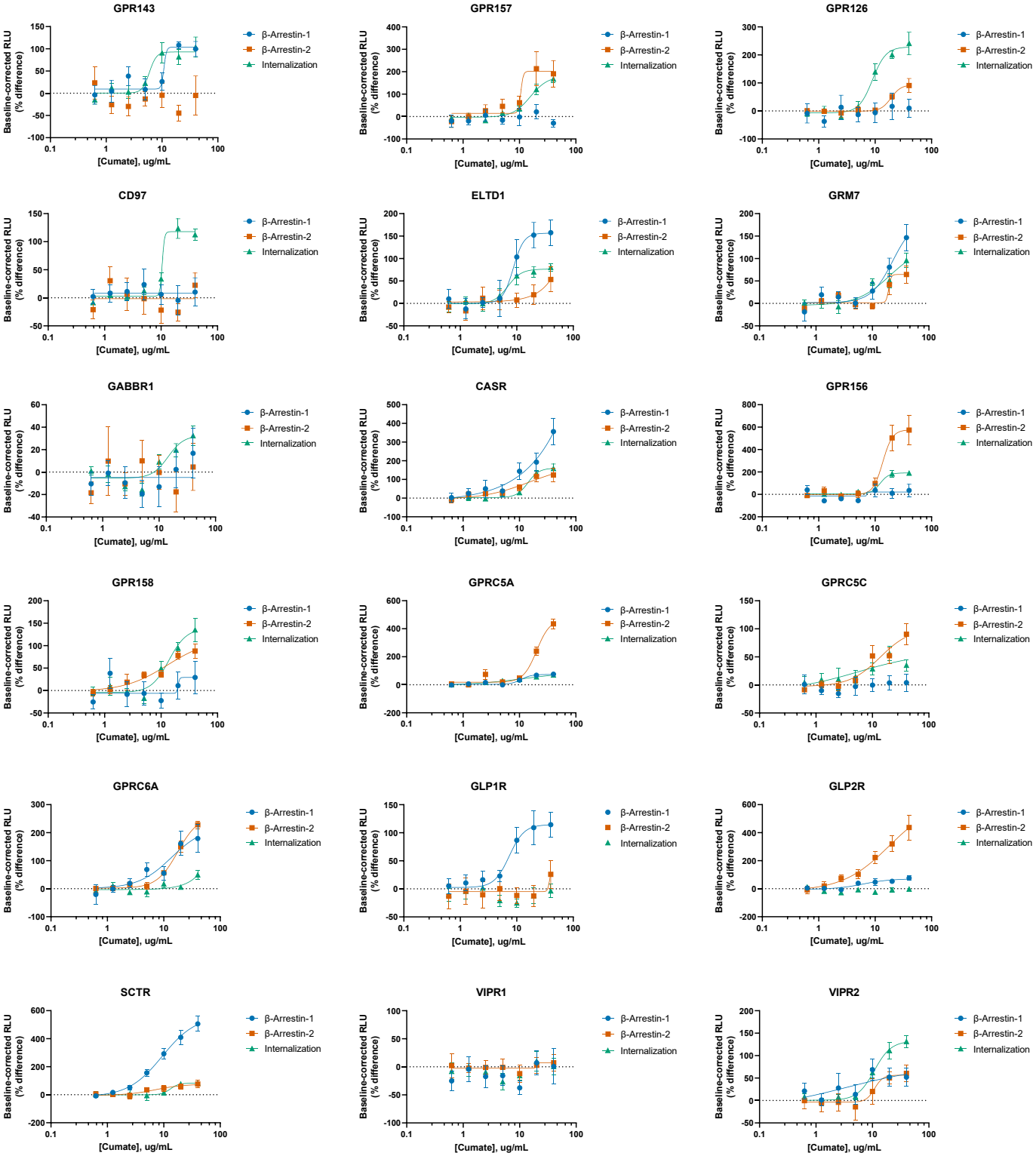
GPR143
GPR157
GPR126
CD97
ELTD1
GRM7
GABBR1
CASR
GPR156
GPR158
GPRC5A
GPRC5C
GPRC6A
GLP1R
GLP2R
SCTR
VIPR1
VIPR2
β-Arrestin-1
β-Arrestin-2
Internalization
Baseline-corrected RLU (% difference)
[Cumate], ug/mL

Supplementary Figure 2.16. Basal profiles of β-arrestin-1 and β-arrestin-2 translocation, and receptor internalization generated using Tango-Trio (Class B/C). To profile basal activities, HTTL-B1, HTTL-B2 and HTTL-F cells were transfected with GPCR Tango constructs. Transfected cells were stimulated with cumate in a dose-dependent manner. Dose-response curves were built using XY analysis for non-linear regression curve and the 4-parameters dose-response stimulation function, followed by baseline correction. Data are presented as mean values, with error bars representing SEM (n = 3, with 3 technical replicates from one biological sample). Generic receptor codes refer to the GPCR-Tango constructs.


MTNR1A
log[Melatonin(M)]
MTNR1B
log[Melatonin(M)]
GPR119
log[AS-1269574(M)]
PTGER3
log[Prostaglandin E2(M)]
PTGER1
log[Prostaglandin E2(M)]
PTGER2
log[Prostaglandin E2(M)]
PTGDR
log[Prostaglandin D2(M)]
PTGER4
log[Prostaglandin E2(M)]
ADORA3
log[NECA(M)]
ADORA2A
log[NECA(M)]
DRD1
log[Dihydrexidine HCl(M)]
DRD2
log[Quinpirole(M)]
DRD3
log[Quinpirole(M)]
DRD4
log[Quinpirole(M)]
5-HT6
log[Serotonin(M)]
HRH2
log[HTMT dimaleate(M)]
5-HT4
log[Serotonin(M)]
ADRB1
log[Isoproterenol(M)]
ADRB1
log[Isoproterenol(M)]
ADRB3
log[Isoproterenol(M)]
5-HT7
log[Serotonin(M)]
5-HT5
log[Serotonin(M)]
5-HT1B
log[Serotonin(M)]
5-HT1D
log[Serotonin(M)]
5-HT1E
log[Serotonin(M)]
5-HT1F
log[Serotonin(M)]
5-HT2A
log[Serotonin(M)]
5-HT2B
log[Serotonin(M)]
5-HT2C
log[Serotonin(M)]
ADRA2A
log[Epinephrine(M)]
ADRA2B
log[Norepinephrine(M)]
ADRA2C
log[Epinephrine(M)]
ADRA1A
log[Epinephrine(M)]
ADRA1B
log[Epinephrine(M)]
ADRA1D
log[Epinephrine(M)]
HRH1
log[HTMT dimaleate(M)]
HRH3
log[(R)-(-)-α-Methylhistamine dihydrobromide(M)]
HRH4
log[Histamine dihydrochloride(M)]
CHRM1
log[Carbachol(M)]
CHRM2
log[Carbachol(M)]
CHRM3
log[Carbachol(M)]
CHRM4
log[Carbachol(M)]
CHRM5
log[Carbachol(M)]
TAAR1
log[Tyramine(M)]
S1PR1
log[SIP(M)]
S1PR2
log[SIP(M)]
S1PR3
log[SIP(M)]
S1PR4
log[SIP(M)]
S1PR5
log[AS71432(M)]
LPAR1
log[LPA(M)]
LPAR2
log[LPA(M)]
MC1R
log[Melanotan II(M)]
MC2R
log[ACTH(M)]
MC4R
log[α-MSH(M)]
MC5R
log[Melanotan II(M)]
MC3R
log[α-MSH(M)]
GPR119
log[Oleylethanolamide(M)]
ADORA1
log[NECA(M)]
ADORA2B
log[NECA(M)]
β-Arrestin-1
β-Arrestin-2
Internalization
Baseline-corrected RLU
(% difference)

Supplementary Figure 2.17. Agonist-induced profiles of β-arrestin-1 and β-arrestin-2 translocation, and receptor internalization generated using Tango-Trio (Class A, α-branch). To quantify agonist-dependent activities, HTTL-B1, HTTL-B2 and HTTL-F cells were plated in cumate-containing (30 μg/mL) medium and transfected with non-orphan GPCR Tango constructs. Transfected cells were stimulated with the receptor-specific agonist, and dose-response curves were built using XY analysis for non-linear regression curve and the 3-parameters dose-response stimulation function, followed by baseline correction. Data are presented as mean values, with error bars representing SEM (n = 3, with 3 technical replicates from one biological sample). Generic receptor codes refer to the GPCR-Tango constructs.

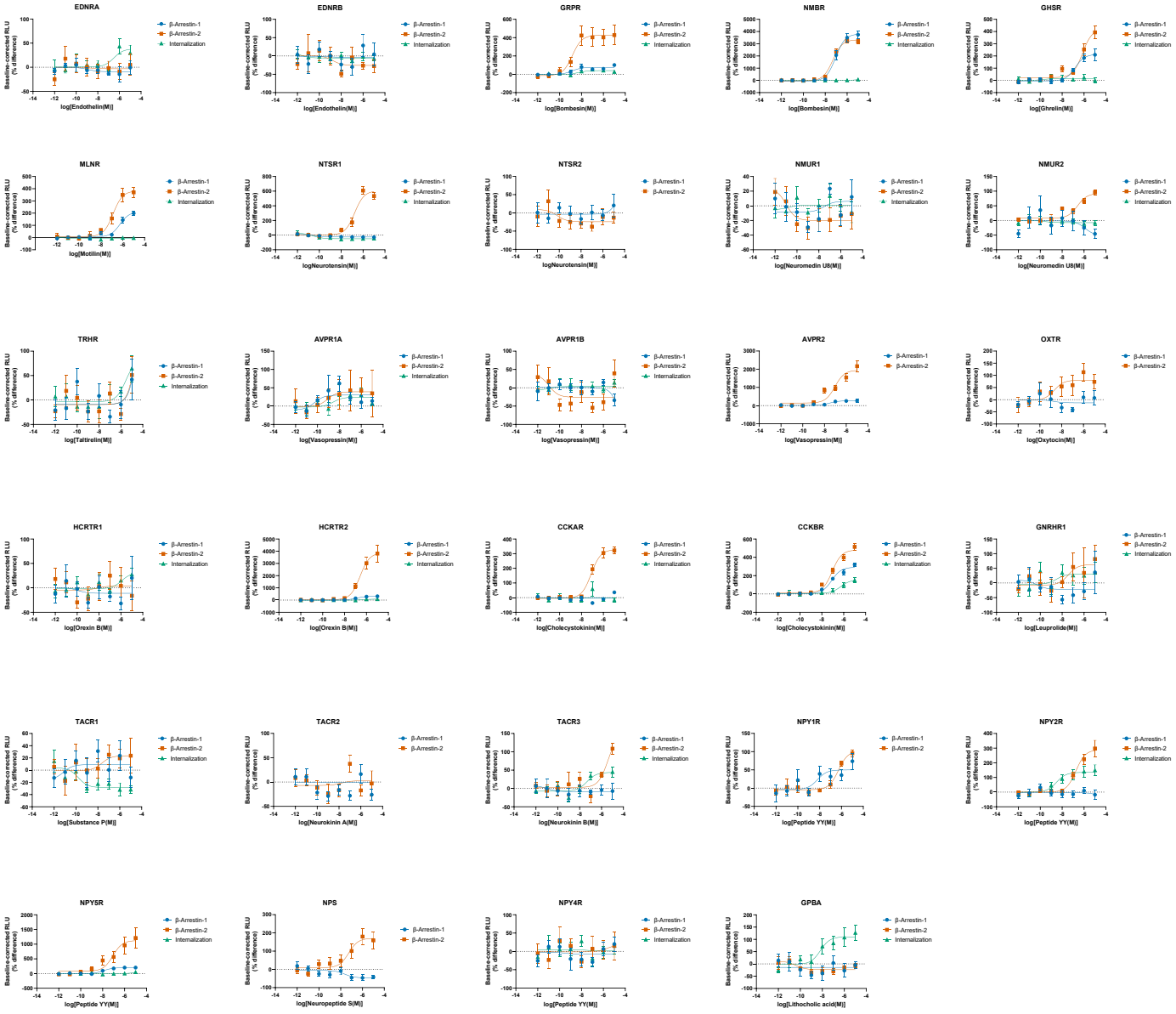

Supplementary Figure 2.18. Agonist-induced profiles of β-arrestin-1 and β-arrestin-2 translocation, and receptor internalization generated using Tango-Trio (Class A, β-branch). To quantify agonist-dependent activities, HTTL-B1, HTTL-B2 and HTTL-F cells were plated in cumate-containing (30 µg/mL) medium and transfected with non-orphan GPCR Tango constructs. Transfected cells were stimulated with the receptor-specific agonist, and dose-response curves were built using XY analysis for non-linear regression curve and the 3-parameters dose-response stimulation function, followed by baseline correction. Data are presented as mean values, with error bars representing SEM (n = 3, with 3 technical replicates from one biological sample). Generic receptor codes refer to the GPCR-Tango constructs.

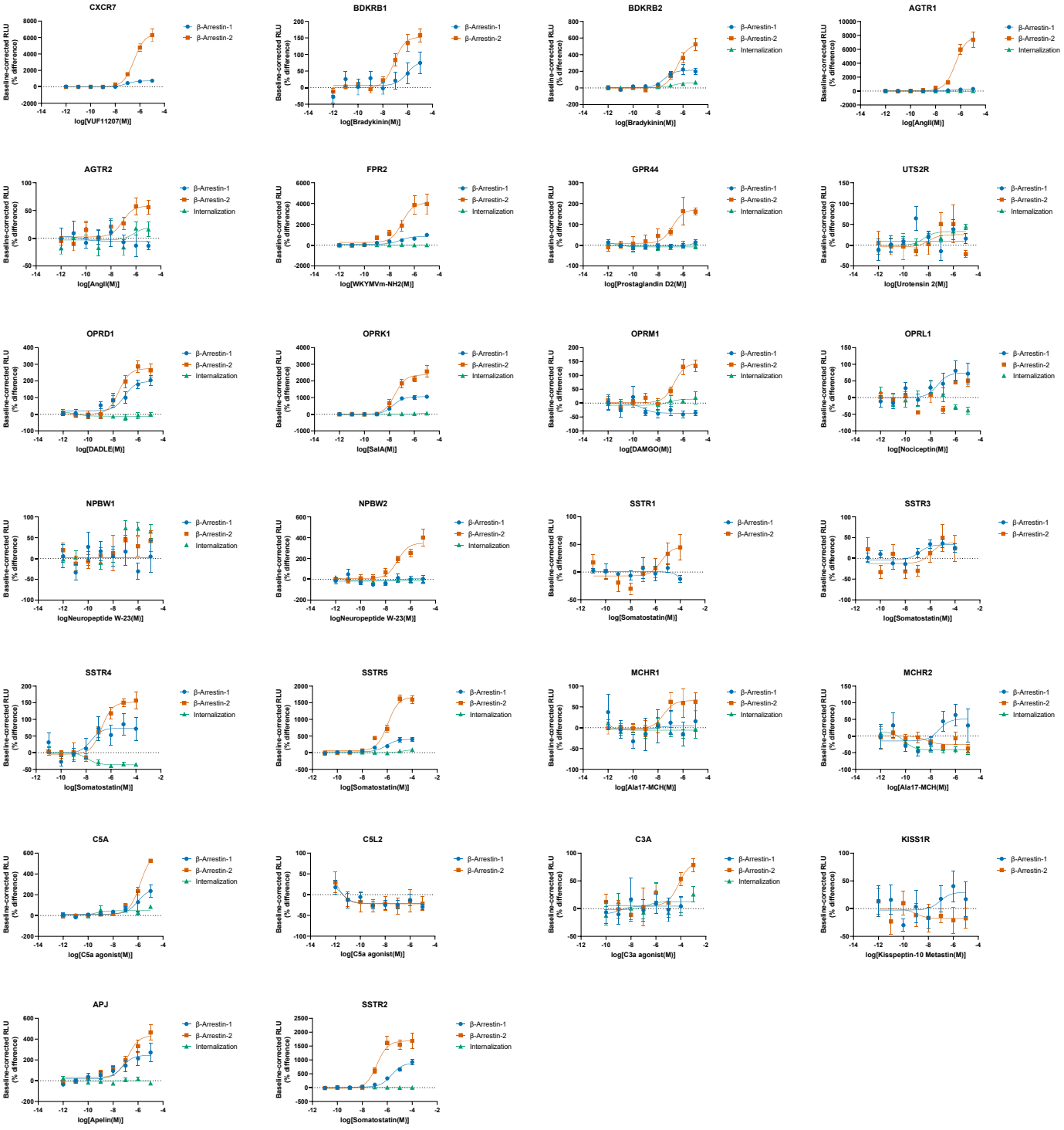
CXCR7
Baseline-corrected RLU (% difference)
log[VUF11207(M)]
β-Arrestin-1
β-Arrestin-2
BDKRB1
log[Bradykinin(M)]
BDKRB2
log[Bradykinin(M)]
Internalization
AGTR1
log[AngII(M)]
AGTR2
log[AngII(M)]
FPR2
log[WKYMVm-NH2(M)]
GPR44
log[Prostaglandin D2(M)]
UTS2R
log[Urotensin 2(M)]
OPRD1
log[DADLE(M)]
OPRK1
log[SalA(M)]
OPRM1
log[DAMGO(M)]
OPRL1
log[Nociceptin(M)]
NPBW1
logNeuropeptide W-23(M)]
NPBW2
logNeuropeptide W-23(M)]
SSTR1
log[Somatostatin(M)]
SSTR3
log[Somatostatin(M)]
SSTR4
log[Somatostatin(M)]
SSTR5
log[Somatostatin(M)]
MCHR1
log[Ala17-MCH(M)]
MCHR2
log[Ala17-MCH(M)]
C5A
log[C5a agonist(M)]
C5L2
log[C5a agonist(M)]
C3A
log[C3a agonist(M)]
KISS1R
log[Kisspeptin-10 Metastin(M)]
APJ
log[Apelin(M)]
SSTR2
log[Somatostatin(M)]

Supplementary Figure 2.19. Agonist-induced profiles of β-arrestin-1 and β-arrestin-2 translocation, and receptor internalization generated using Tango-Trio (Class A, γ-branch). To quantify agonist-dependent activities, HTTL-B1, HTTL-B2 and HTTL-F cells were plated in cumate-containing (30 μg/mL) medium and transfected with non-orphan GPCR Tango constructs. Transfected cells were stimulated with the receptor-specific agonist, and dose-response curves were built using XY analysis for non-linear regression curve and the 3-parameters dose-response stimulation function, followed by baseline correction. Data are presented as mean values, with error bars representing SEM (n = 3, with 3 technical replicates from one biological sample). Generic receptor codes refer to the GPCR-Tango constructs.

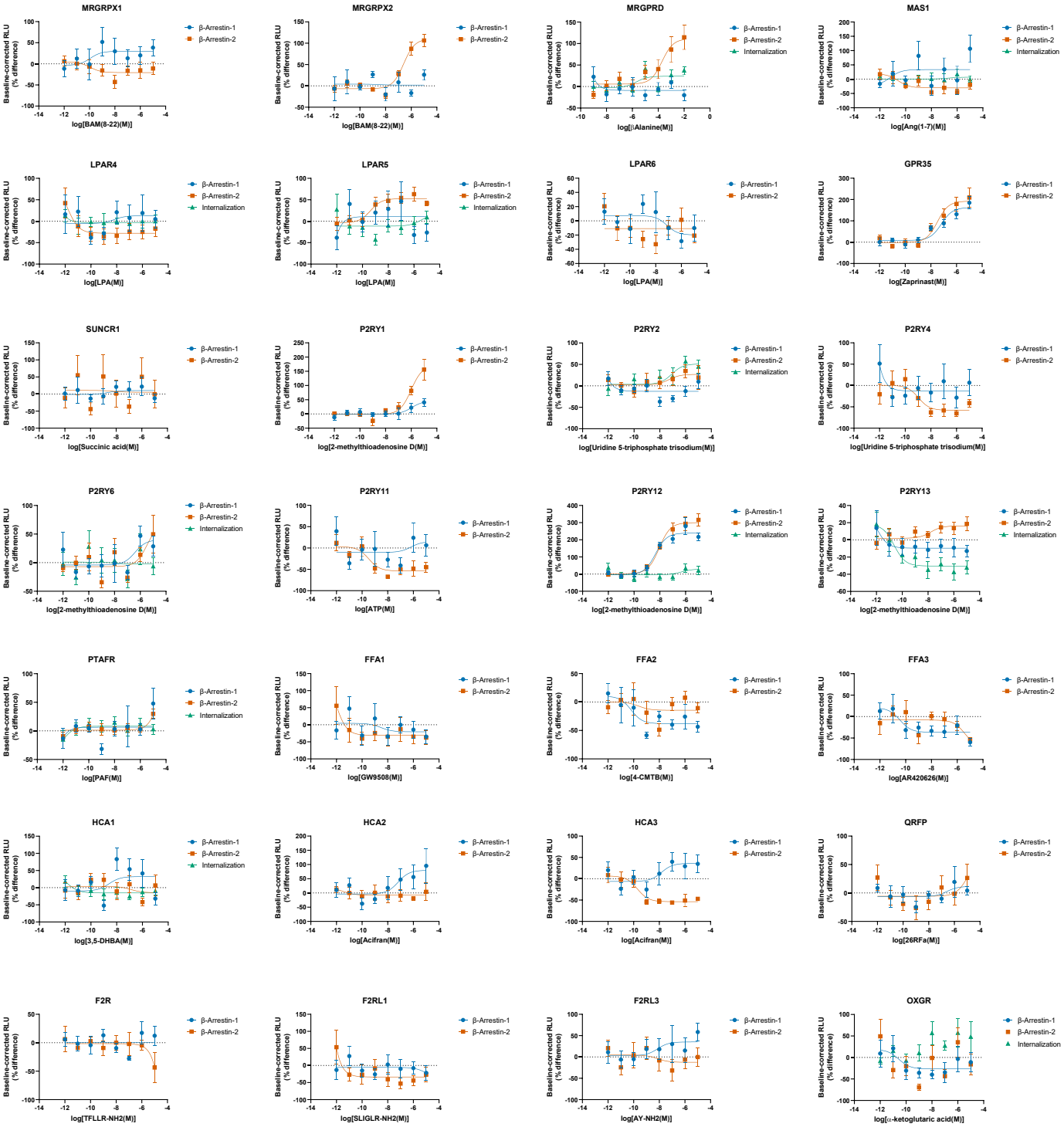
MRGRPX1
log[BAM(8-22)(M)]
MRGRPX2
log[BAM(8-22)(M)]
MRGPRD
log[βAlanine(M)]
MAS1
log[Ang(1-7)(M)]
LPAR4
log[LPA(M)]
LPAR5
log[LPA(M)]
LPAR6
log[LPA(M)]
GPR35
log[Zaprinast(M)]
SUNCR1
log[Succinic acid(M)]
P2RY1
log[2-methylthioadenosine D(M)]
P2RY2
log[Uridine 5-triphosphate trisodium(M)]
P2RY4
log[Uridine 5-triphosphate trisodium(M)]
P2RY6
log[2-methylthioadenosine D(M)]
P2RY11
log[ATP(M)]
P2RY12
log[2-methylthioadenosine D(M)]
P2RY13
log[2-methylthioadenosine D(M)]
PTAFR
log[PAF(M)]
FFA1
log[GW9508(M)]
FFA2
log[4-CMTB(M)]
FFA3
log[AR420626(M)]
HCA1
log[3,5-DHBA(M)]
HCA2
log[Acifran(M)]
HCA3
log[Acifran(M)]
QRFP
log[26RFa(M)]
F2R
log[TFLLR-NH2(M)]
F2RL1
log[SLIGLR-NH2(M)]
F2RL3
log[AY-NH2(M)]
OXGR
log[α-ketoglutaric acid(M)]
Baseline-corrected RLU (% difference)
β-Arrestin-1
β-Arrestin-2
Internalization

Supplementary Figure 2.20. Agonist-induced profiles of β-arrestin-1 and β-arrestin-2 translocation, and receptor internalization generated using Tango-Trio (Class A, δ-branch). To quantify agonist-dependent activities, HTTL-B1, HTTL-B2 and HTTL-F cells were plated in cumate-containing (30 μg/mL) medium and transfected with non-orphan GPCR Tango constructs. Transfected cells were stimulated with the receptor-specific agonist, and dose-response curves were built using XY analysis for non-linear regression curve and the 3-parameters dose-response stimulation function, followed by baseline correction. Data are presented as mean values, with error bars representing SEM (n = 3, with 3 technical replicates from one biological sample). Generic receptor codes refer to the GPCR-Tango constructs.

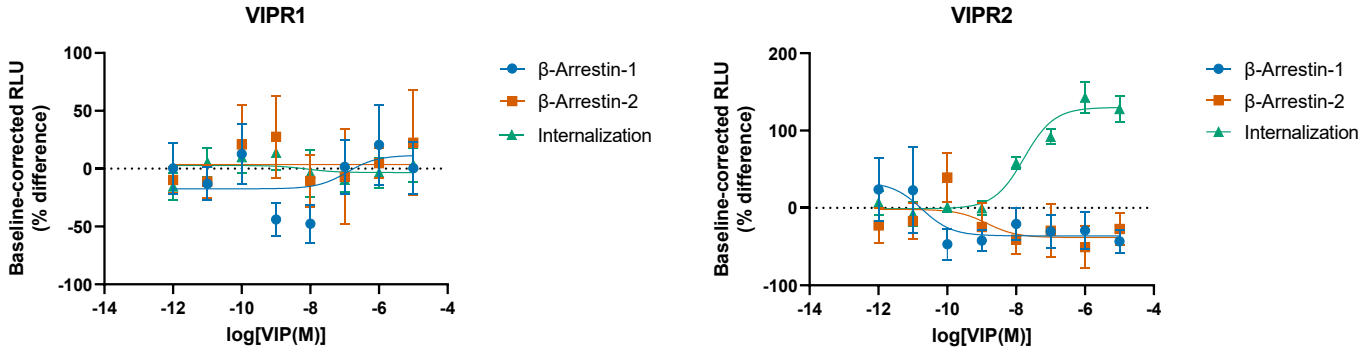

Supplementary Figure 2.21. Agonist-induced profiles of β-arrestin-1 and β-arrestin-2 translocation, and receptor internalization generated using Tango-Trio (Class B/C). To quantify agonist-dependent activities, HTTL-B1, HTTL-B2 and HTTL-F cells were plated in cumate-containing (30 µg/mL) medium and transfected with non-orphan GPCR Tango constructs. Transfected cells were stimulated with the receptor-specific agonist, and dose-response curves were built using XY analysis for non-linear regression curve and the 3-parameters dose-response stimulation function, followed by baseline correction. Data are presented as mean values, with error bars representing SEM (n = 3, with 3 technical replicates from one biological sample). Generic receptor codes refer to the GPCR-Tango constructs.

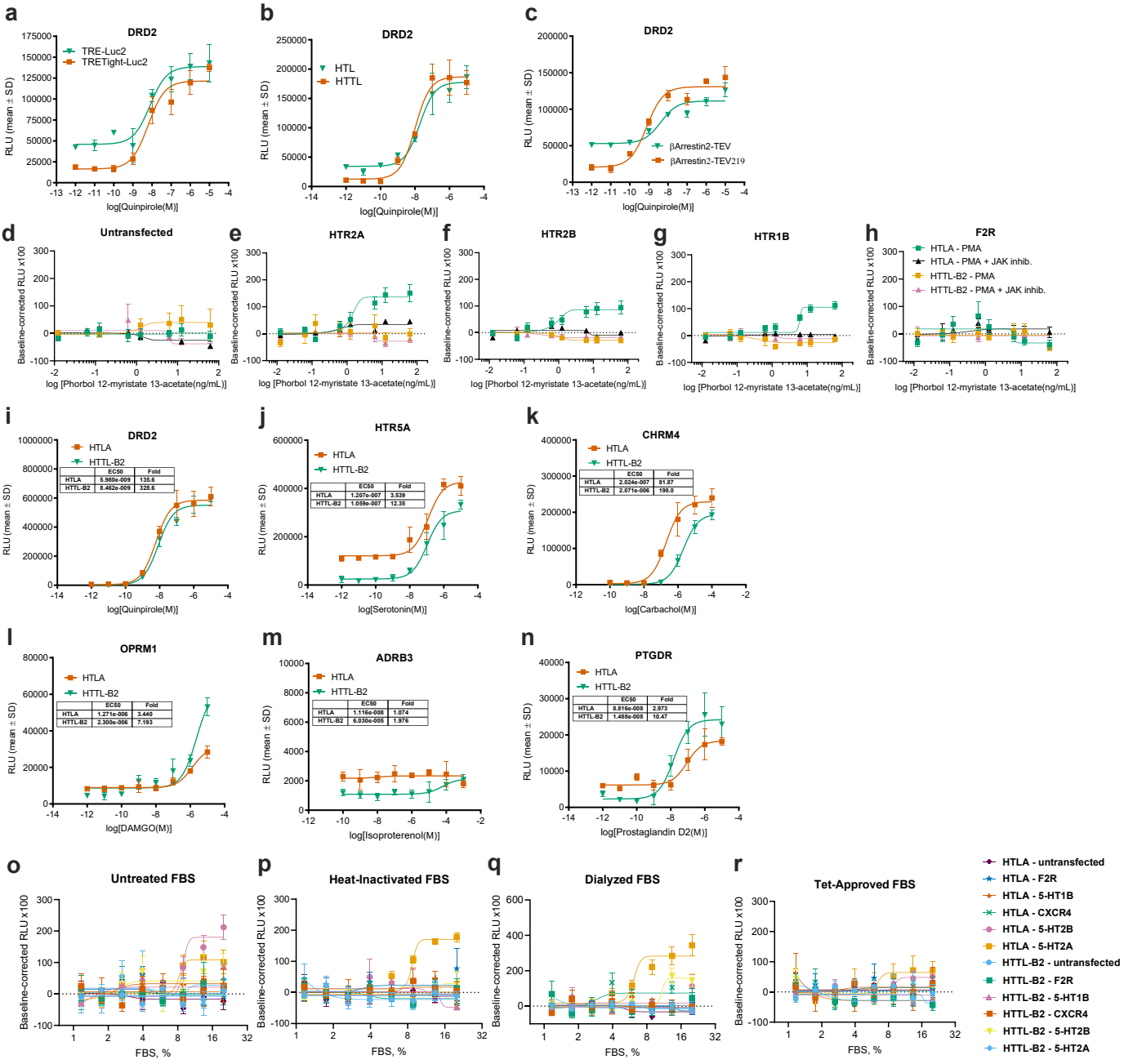

Supplementary Figure 2.22. Optimization of the dynamic range, sensitivity, and specificity of the Tango-Trio platform - independent biological replicate of the main manuscript Figure 1. Data are representative of 2 biological replicates, with 3 technical replicates each.

a HTTL-B1 (βArrestin1)

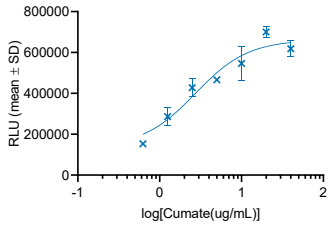

	CHRM1
EC50	2.736
Fold	4.821

b HTTL-B2 (βArrestin2)

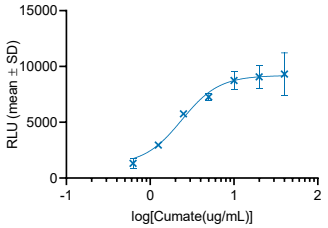

	CHRM1
EC50	2.378
Fold	7.682

c HTTL-F (FYVE)

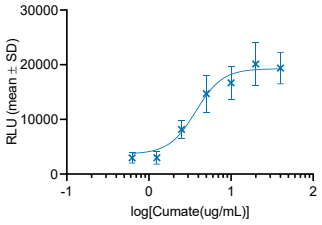

	CHRM1
EC50	3.722
Fold	5.273

d HTTL-B1 (βArrestin1)

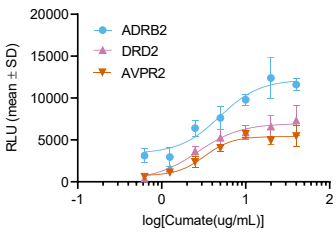

	AVPR2	ADRB2	DRD2
EC50	3.253	4.904	2.712
Fold	7.515	3.624	29.51

e HTTL-B2 (βArrestin2)

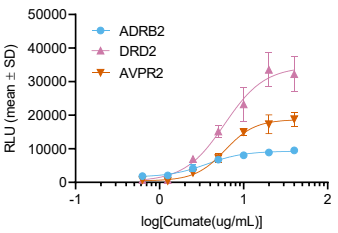

	AVPR2	ADRB2	DRD2
EC50	6.015	3.643	5.947
Fold	41.84	5.936	149.9

f HTTL-F (FYVE)

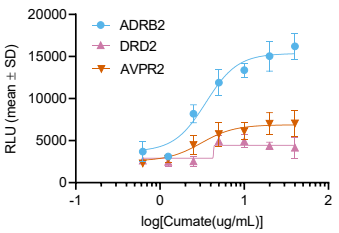

	AVPR2	ADRB2	DRD2
EC50	3.094	3.507	~ 4.328
Fold	2.693	4.171	~ 1.532

g HTTL-B1 AVPR2

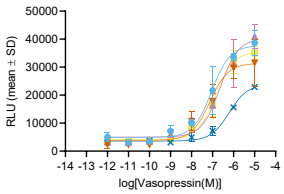

	EC50	Fold
I	9.071e-008	7.630
II	7.444e-008	8.169
III	2.299e-007	8.001
IV	6.147e-007	6.607
V	1.422e-007	8.551

h HTTL-B1 ADRB2

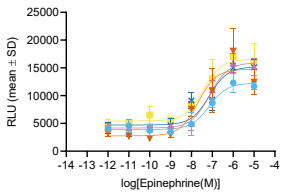

	EC50	Fold
I	7.146e-008	3.137
II	2.072e-008	5.343
III	7.349e-008	3.808
IV	7.287e-008	3.216
V	3.743e-008	3.041

i HTTL-B1 DRD2

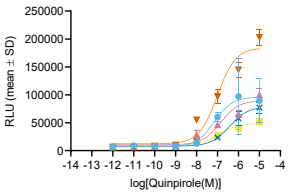

	EC50	Fold
I	7.025e-008	14.31
II	9.855e-008	15.18
III	1.410e-007	8.674
IV	3.766e-007	9.855
V	1.119e-007	5.311

j HTTL-B1 CHRM1

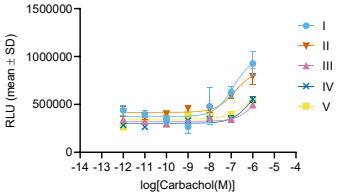

	EC50	Fold
I	1.282e-007	2.664
II	1.441e-007	2.032
III	2.072e-006	2.608
IV	8.548e-007	2.528
V	4.036e-007	1.790

k HTTL-B2 AVPR2

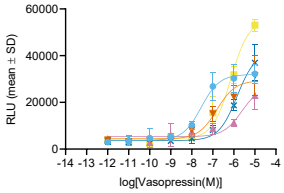

	EC50	Fold
I	2.792e-008	8.642
II	1.552e-007	6.720
III	2.365e-006	5.057
IV	1.427e-006	11.39
V	7.205e-007	12.74

l HTTL-B2 ADRB2

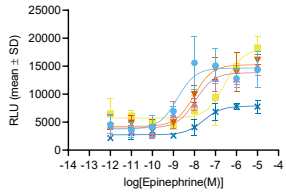

	EC50	Fold
I	1.538e-009	3.887
II	9.604e-009	3.590
III	1.129e-008	3.504
IV	2.785e-008	2.875
V	2.878e-007	3.163

m HTTL-B2 DRD2

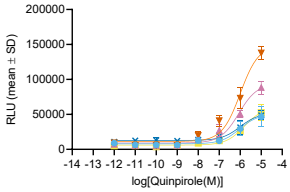

	EC50	Fold
I	9.339e-007	6.346
II	1.010e-006	13.10
III	8.610e-007	10.36
IV	9.850e-007	4.053
V	1.561e-006	9.810

n HTTL-B2 CHRM1

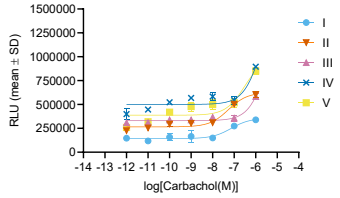

	EC50	Fold
I	7.266e-008	2.498
II	5.417e-008	2.352
III	4.336e-006	5.100
IV	2.258e-006	3.572
V	3.019e-007	2.550

o HTTL-F AVPR2

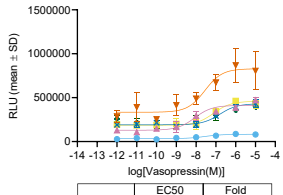

	EC50	Fold
I	2.786e-008	2.483
II	2.786e-008	2.483
III	8.515e-009	3.194
IV	1.576e-007	2.260
V	7.677e-008	2.463

p HTTL-F ADRB2

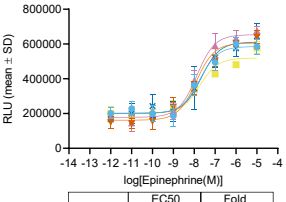

	EC50	Fold
I	1.803e-008	2.906
II	1.242e-008	3.745
III	1.305e-008	3.664
IV	2.178e-008	3.024
V	1.830e-008	2.596

q HTTL-F DRD2

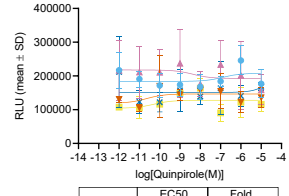

	EC50	Fold
I	1.297e-007	1.131
II	2.274e-011	1.231
III	4.310e-009	0.8847
IV	~ 0.6455	~ 6739
V	5.073e-011	1.224

r HTTL-F CHRM1

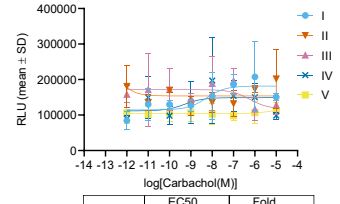

	EC50	Fold
I	5.467e-009	1.587
II	~ 6.878e-018	~ 4.130e-005
III	5.793e-007	0.6826
IV	5.126e-010	1.334
V	4.013e-006	1.112

Supplementary Figure 2.23. Dose-response and time-course verification of cumate-induced expression - independent biological replicate of the main manuscript Figure 2. Data are representative of 2 biological replicates, with 3 technical replicates each.

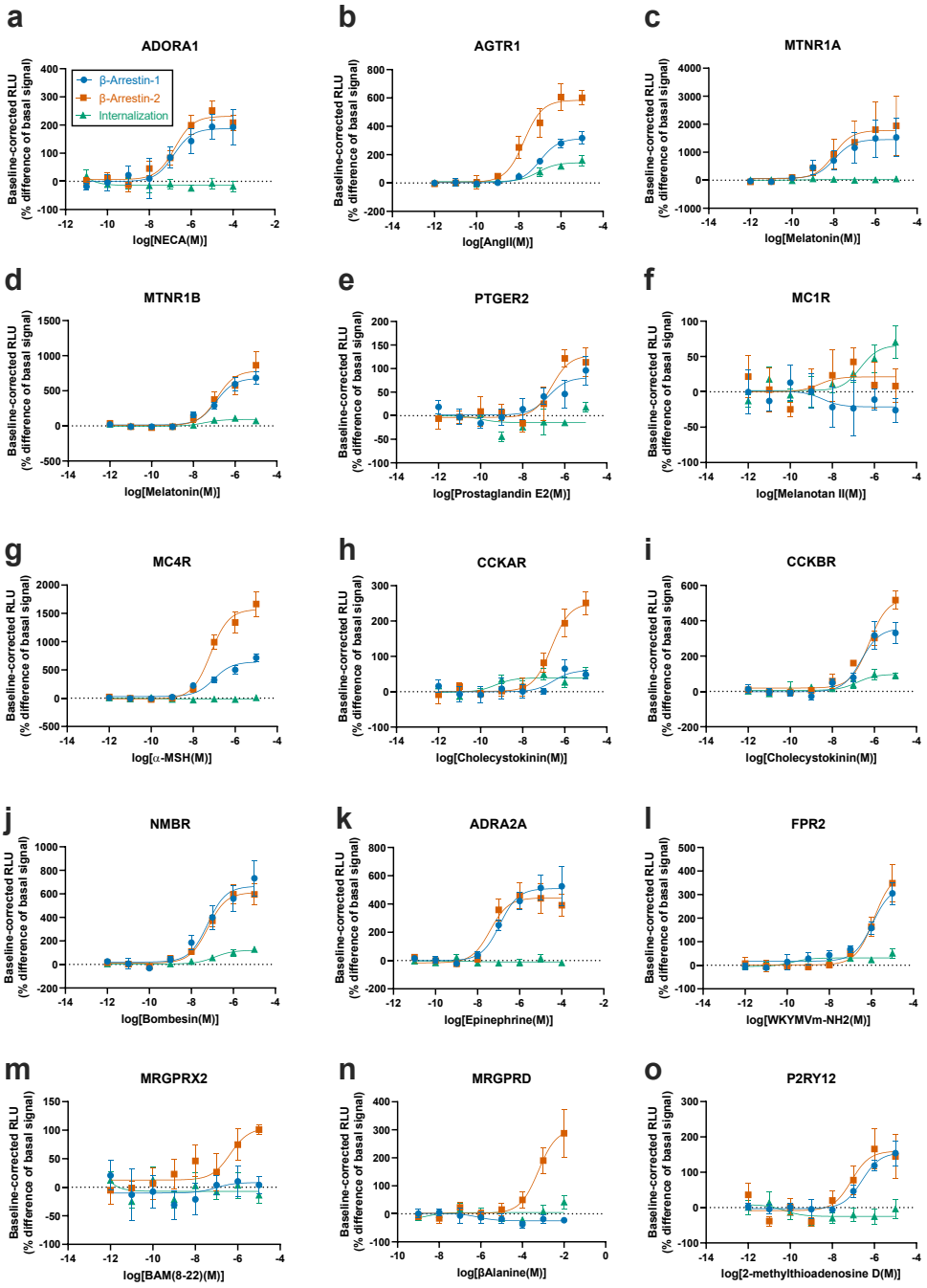

Supplementary Figure 2.24. Validation of compiled positive hits from agonist-dependent HTS in dose response - independent biological replicate of the main manuscript Figure 5. Data are representative of 2 biological replicates, with 3 technical replicates each.

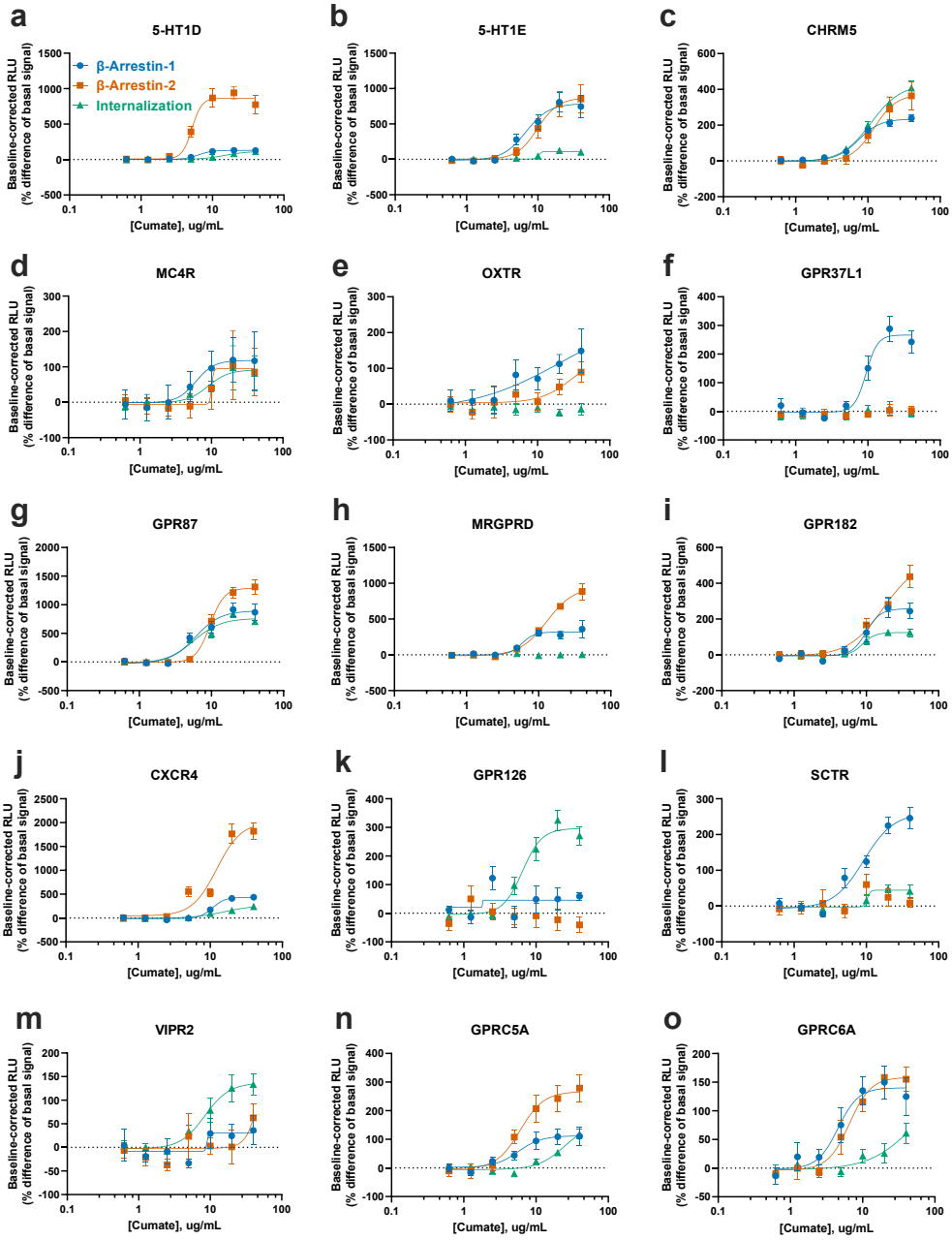

Supplementary Figure 2.25. Validation of compiled positive hits from basal activity HTS in dose-response - independent biological replicate of the main manuscript Figure 6. Data are representative of 2 biological replicates, with 3 technical replicates each.

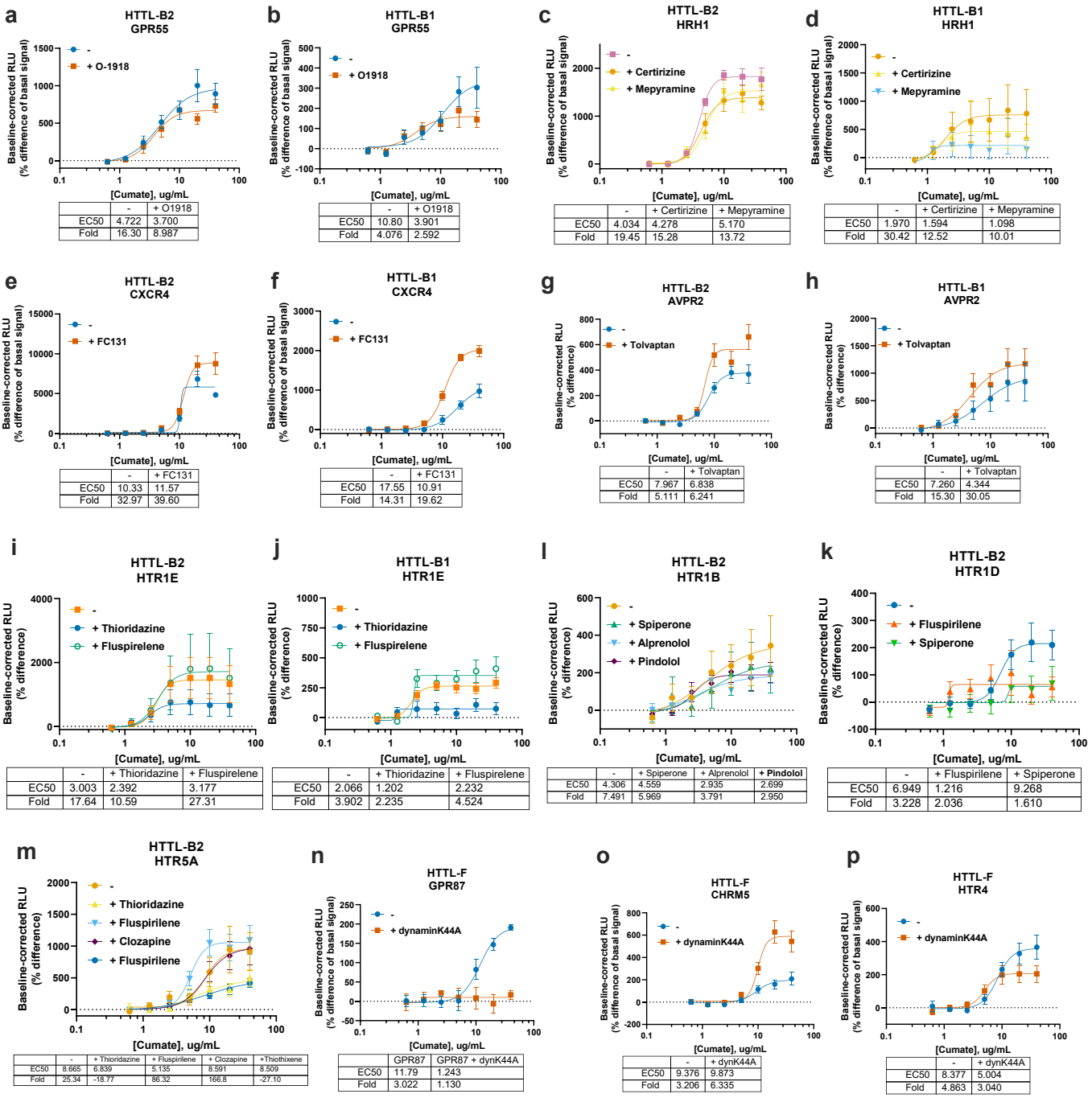

Supplementary Figure 2.26. Applications and further investigations into basal activities revealed by Tango-Trio - independent biological replicate of the main manuscript Figure 7. Data are representative of 2 biological replicates, with 3 technical replicates each.

Supplemental Tables

Supplementary Table 2.1. Comparison of the pharmacological parameters extracted from EMTA and Tango-Trio. Absolute pEC50 and Emax values of β-arrestin-1/2 activity at GPCRs stimulated with common ligands were extracted from EMTA (Avet et al. 2022) and Tango-Trio studies. Tango-Trio pEC50 data was extracted from the non-linear least-squares regression analysis using the sigmoidal dose-response function (3-parameters modeled using Y=Bottom + (Top-Bottom)/(1+10^((LogEC50-X))) and Emax values from the baseline correction as percentage difference using 100* (Value-Baseline)/Baseline), both provided in GraphPad Prism 9.5.1. (n = 3, with three technical replicates from one biological sample). Generic receptor codes refer to the GPCR-Tango constructs.

		pEC50				Emax (in % of vehicle response for EMTA & % difference from baseline for Tango-Trio)			
Receptor (Gene Name)	**Ligand**	**βArrestin1 /GRK2 EMTA**	**βArrestin1 Tango-Trio**	**βArrestin2 /GRK2 EMTA**	**β-Arrestin2 Tango-Trio**	**βArrestin1 /GRK2 EMTA**	**βArrestin1 Tango-Trio**	**βArrestin2 /GRK2 EMTA**	**β-Arrestin2 Tango-Trio**
HTR1B	Serotonin	7.6	6.96	7.685	6.49	36.35	490	57.78	393.4
HTR1D	Serotonin		7.66		6.89		-14.78		347.9
HTR2A	Serotonin	6.709	8.22	7.028	5.76	518.1	24.81	778.6	29.24
HTR2B	Serotonin	7.809	6.5	8.168	11.31	171.6	80.54	247.2	-26.67
HTR2C	Serotonin	7.995	8.76	8.456	9.33	1564	-28.38	705	14.12
AGTR1	Angiotensin II	8.64	6.62	8.84	6.41	207.8	289.2	220.6	7802
CCKAR	Cholecystokinin	8.329	unstable	8.721	7.11	1374	unstable	1520	332.9
PTGER1	PGE2		6.95		unstable		71.02		unstable
PTGER2	PGE2	6.515	6.38	6.925	5.95	107.8	400.8	100.5	363
PTGER3	PGE2		8.53		6.324		-24.13		19.44
PTGER4	PGE2	8.921	8.62	9.25	8.35	251.5	326.9	146.8	1192
EDNRA	Endothelin-1	8.232	8.9	8.381	8.7	588.1	-8.86	1581	-2.98
GHSR	Ghrelin	8.249	6.81	8.515	6.14	68.41	217.8	169.6	396.8
GNRHR	GnRH		10.32		7.43		-31.52		70.49
GPBAR1	Litocholic acid		unstable		10.41		unstable		-34.66
LPAR1	O-LPA	7.528	11.93	7.464	11.21	289.4	-90.04	232	-32.09
LPAR2	O-LPA	6.773	6.13	7.078	11.33	715.2	-41.64	938.9	-64.29
MC4R	α-MSH		7.01	7.449	7.28		346.3	76.44	1351
OPRM1	DAMGO	7.099	9.19	7.424	6.7	1008	-35.21	1198	142.9
MTNR1A	Melatonin	8.937	8.03	8.75	9.11	78.64	754.1	157.5	425.5
MTNR1B	Melatonin		7.12		8.38		290		168
OPRL1	Nociceptin	8.249	6.15	8.716	6.17	147.5	73.78	238.1	-50.64
OXTR	Oxytocin	8.091	8.78	8.6	8.67	128.3	-13.08	229.8	82.31
HCRTR2	Orexin-A	8.471	6.9	8.558	6.58	852.9	315.7	863.9	3850
P2RY2	UTP	5.235	unstable	5.36	7.29	184.7	unstable	94.68	24.6
F2R	TFLLR-NH2	5.082	unstable	5.177	-2.55	445.5	unstable	469.5	unstable
S1PR1	Sphingosine 1-phosphate	7.269	6.47	7.459	6.5	477	233.6	557.1	182.8
SSTR2	Somatostatin	8.815	5.66	8.918	6.83	2867	866	1820	1714
AVPR1A	AVP	7.743	10.25	7.824	9.08	890.1	40.7	934.7	40.67
AVP2R	AVP	7.603	7.52	7.846	7.03	353.3	258.6	334.2	1804
VIPR1	VIP	9.109	6.92	9.254	unstable	1367	28.97	1060	unstable
NPY1R	NPY		8.2	8.815	6.28		53.76	42.09	106.1
NPY5R	NPY		7.92		7.07		210.3		1046

CHAPTER 3: Development of a V5-tag–directed nanobody and its implementation as an intracellular biosensor of GPCR signaling

Development of a V5-tag-directed nanobody and its implementation as an intracellular biosensor of GPCR signalling

Manel Zeghal[1*], Kevin Matte[1*], Angelica Venes[1], Shivani Patel[1], Geneviève Laroche[1], Sabina Sarvan[1,2], Monika Joshi[1,2], Jean-Christophe Rain[3], Jean-François Couture[1,2], Patrick M. Giguère[1,4]✉

From the [1]Department of Biochemistry, Microbiology and Immunology, Faculty of Medicine, University of Ottawa, Ottawa, ON, K1H 8M5, Canada; [2]Ottawa Institute of Systems Biology, University of Ottawa, Ottawa, ON K1H 8M5, Canada; [3]Hybrigenics Services, 91000 Évry-Courcouronnes, France; [4]Brain and Mind Research Institute, University of Ottawa, Ottawa, ON, K1H 8M5, Canada

** Contributed equally to the work*

✉*Correspondence and requests for materials should be addressed to Patrick M. Giguère (Email : patrick.giguere@uottawa.ca).*

ABSTRACT

Protein-protein interactions (PPIs) form the foundation of any cell signaling network. Considering that PPIs are highly dynamic processes, cellular assays are often essential for their study because they closely mimic the biological complexities of cellular environments. However, incongruity may be observed across different PPI assays when investigating a protein partner of interest; these discrepancies can be partially attributed to the fusion of different large functional moieties, such as fluorescent proteins or enzymes, which can yield disparate perturbations to the protein's stability, subcellular localization, and interaction partners depending on the given cellular assay. Owing to their smaller size, epitope tags may exhibit a diminished susceptibility to instigate such perturbations. However, while they have been widely used for detecting or manipulating proteins in vitro, epitope tags lack the in vivo traceability and functionality needed for intracellular biosensors. Herein, we develop NbV5, an intracellular nanobody binding the V5-tag, which is suitable for use in cellular assays commonly used to study PPIs such as BRET, NanoBiT, and Tango. The NbV5:V5 tag system has been applied to interrogate G protein-coupled receptor signaling, specifically by replacing larger functional moieties attached to the protein interactors, such as fluorescent or luminescent

proteins (~30kDa), by the significantly smaller V5-tag peptide (1.4kDa), and for microscopy imaging which is successfully detected by NbV5-based biosensors. Therefore, the NbV5:V5 tag system presents itself as a versatile tool for live-cell imaging and a befitting adaptation to existing cellular assays dedicated to probing PPIs.

RUNNING TITLE: Optimization of a V5-tag-directed intracellular nanobody.

KEYWORDS: protein-protein interaction, single-domain antibody (sdAb, nanobody), crystal structure, G protein-coupled receptor (GPCR), bioluminescence resonance energy transfer (BRET), protease-dependent reporter assay (Tango), nanoluciferase binary technology (NanoBiT).

INTRODUCTION

Nestled at the heart of the study of molecular biology, protein-protein interaction (PPI) assays stand as heralded experimental techniques used to investigate the interactions between two or more proteins, often informing drug discovery and development, such as for G-protein coupled receptor (GPCR) signaling (1, 2). Cell-based assays also find particular relevance in unraveling PPIs from a physiological context, shedding light on their roles in biological processes, their implications within cellular environments, and the consequences of their dysregulation in disease (3). Considering the varying strengths and limitations inherent to each approach, the selection of an appropriate PPI assay is contingent upon the specific research question being addressed (4). Earlier experimental methodologies, such as pull-down and immunoprecipitation techniques, were commonly employed to detect or isolate protein complexes. However, these approaches exhibit disruptive tendencies towards larger complexes, particularly those involving membrane-spanning proteins (5). A pivotal subset of cell-based assays comes in the form of biosensor-based techniques, which offer indispensable insights into PPIs within the realm of living cells. By utilizing fluorescent/luminescent molecules or functional moieties to label two proteins of interest, the biosensor-based technique enables monitoring their interaction within a cellular milieu. Moreover, these cellular biosensors can measure both high- and low-affinity interactions and transient and stable

complexes using endpoint or live assay (6, 7). With respect to GPCR signaling, the most common cellular systems employing such biosensors include the protease-dependent reporter assays such as the Tobacco Etch protease-dependent assay (TANGO), Bioluminescence Resonance Energy Transfer (BRET), and Nanoluciferase Binary Technology (NanoBiT) (8). Despite the value of these biosensor-based cellular techniques, the imbroglio of the protein interactome can complicate the execution of its study, and investigations of PPIs at a scaled-up level have been limited thus far. Moreover, PPI assays, such as resonance energy transfer or binary complementation, require cloning of each component in all possible and permissive orientations, specifically at the C- or N-terminus of the protein, which could translate into over twelve different combinations to be tested (9). Finally, while approaches such as Tango, BRET, and NanoBiT, have been designed to provide an understanding of different PPIs, all involve the fusion of large, functionalized tags (TEV, GFP2, LgBiT, respectively) to the proteins of interest (10).

Considering the aforementioned limitations, the adoption of short peptide or epitope tags offers a reasonable possibility to probe PPIs. Less than 20 residues in length, epitope tags (e.g., HA, Flag, Myc and V5) are commonplace in protein purification and localization/detection such as microscopy, but less so for monitoring dynamic interactions (11). However, although fluorophores (e.g., GFP, mCherry) and other polypeptides (e.g., MBP, GST) are popularly used for probing recombinant proteins in a cellular context, including live cell imaging, reporter assays, and resonance energy transfer, the smaller size of epitope tags could be preferable for these purposes, as the fusion of bulkier fluorophores and polypeptides could interfere with the native behaviour and functions of the protein of interest, especially interactions that are particularly proximity- or location-dependent (12). Besides avoiding cross-reactions within the native proteome, epitope tags obviate the need for custom antibody generation for every protein of interest and give rise to the possibility of multiplexing orthogonal peptide tags within the same experiment (11, 13).

Given the indispensability of these peptides, antibodies have continually been developed to recognize existing and newly developed epitope tags. Although conventional antibodies have proven to be robust workhorses in various cell biology research fields, their large size and complex architecture preclude them from functioning within living cells (14, 15). These limitations spurred advances in engineering novel recombinant antibody constructs, termed intracellular antibodies or intrabodies. Although their biophysical properties are unlike the conventional monoclonal antibodies, intrabodies retain the capacities for recognition and/or neutralization with similarly high specificities and affinities, with the added conferred ability to bind specific targets expressed within the same living cell that houses it, typically within the cytoplasm of eukaryotic cells (16). Despite intense efforts, minimal antigen-binding fragments such as single-chain variable fragments (scFvs) or F(ab)-type fragments remain highly unstable in a cellular environment and have limited activity in an intracellular milieu (17-19). The challenges for intrabodies to be expressed in their functional forms are partly due to their aggregation propensity and the reducing environment of the cytoplasm, which prevents intradomain disulfide bond formation (20, 21).

Of greater promise are single-domain antibodies (sdAbs), also referred to as VHHs or nanobodies (Nbs), which are the smallest antibody derivatives (12-15 kDa). Although originally derived from members of the *Camelidae* and *Chondrichthyes* family, human-derived sdAbs have also been engineered from conventional human IgGs (22). Epitope-specific Nbs can be selected by various approaches, including display-based panning or synthetic libraries generated *in vitro* using predesigned scaffolds that undergo CDR codon randomization (23). Moreover, retrieved Nbs can be affinity-matured to further improve upon the original pharmacological features (24). Structurally, these non-canonical antibodies are more compact, consisting exclusively of shortened heavy chains with three interspersed complementarity-determining regions (CDRs) that form their antigen-binding domain. Devoid of the hydrophobic interface between heavy and light chains and stabilized by only a single internal disulfide bond, Nbs rival conventional IgGs given their low immunogenicity, enhanced solubility, and stability, all while retaining high binding affinities towards their targets, and

thereby are more successfully expressed in the cytosol of mammalian cells (25). In terms of binding performance, Nbs have an enhanced ability to target sterically hindered and/or concave epitopes given their slightly convex-shaped paratope (26). As such, the physicochemical and pharmacological properties of Nbs offer a multitude of possibilities for live-cell applications, such as elucidating signalling pathways and PPIs in live cells, targeting proteins or protein complexes formerly inaccessible to biologics, fusing to other functional effectors such as proteases and fluorophores, visualizing and localizing proteins of interest using conventional and advanced microscopy (27). Moreover, Nbs targeting intracellular targets are plentiful, the majority of which target various cytosolic proteins, and more recently, short peptide or epitope tags (28-41). However, Nbs recognizing these small peptide fragments are still scarce, in part due to conformational difficulties of the cleft-like paratope of Nbs for recognizing linear peptides and the needed strength of Nb-peptide tag interaction; based on existing literature, less than 10 peptide-targeted Nbs have been identified, specifically against the EPEA (42), SPOT (43, 44), 6E (45), Moon (46, 47), Myc (48), BC2 (43, 49) and ALFA tags (50, 51). Only two of these antibody-peptide pairs retained binding in cells, the Moon and ALFA tag, allowing for the possibility of multiplexing (52).

Therefore, the paucity of tag-targeted intrabodies is a bottleneck for intracellular interrogations, especially given the pre-existing arrayed or pooled tag-encoded cDNA and ORF libraries for overexpression studies. For example, while there are comprehensive human genome-wide and fully annotated V5-tagged libraries developed from the ORFeome project (53) and the Drosophila genome-wide V5-tagged library (54), these open resources are mainly limited to phenotypic screenings for living cellular assay or microscopy for in vitro assay on fixed tissues. As for the peptide itself, the V5 tag is a universal epitope that has been extensively used since its introduction roughly 30 years ago (55), and has desirable characteristics suitable for intracellular use. More specifically, the V5 tag is of small size (1.42 kDa), possesses an equal number of positively and negatively charged residues exhibiting a pI of 5.85 and no net charge at physiological pH (56, 57), is of prokaryotic origin which circumvents possible background signals when expressed in mammalian and insect cell host, as well as being

resistant to cleavage by their endogenous proteases (51). Thus, the development of intracellular Nb recognizing the small peptide V5-tag and its functionalization would be highly amenable to cellular studies of a broader nature using the genome-wide V5-tagged ORF library, as well as more directed investigations of gene function and genetic rescues, and protein-protein interactions such as dynamic receptor-protein interfaces, with minimal interference.

To this end, we introduce the NbV5, a novel nanobody that interacts with the V5-tag, serving as the foundation of our multipurpose intracellular nanobody-based biosensors. Our work demonstrates that the NbV5:V5 tag system is suitable for monitoring dynamic PPIs in various adapted cellular assays, specifically in the context of GPCR signalling, and for microscopic imaging techniques.

RESULTS

Generation of a nanobody directed against the V5-tag –The first generation of selective nanobodies recognizing the V5-tag was identified using the Hybribody approach, a two-pronged screening strategy involving synthetic VHHs phage-display and yeast two-hybrid (Y2H). Peptide phage display was first performed against a purified HaloTag protein harboring a duplicate copy of the V5-tag to select for a synthetic VHH against the V5-tag (sequence in **Fig. 3.1A**). Following the first round of the phage display screening process, the VHHs demonstrating an interaction for the V5-tag were subsequently cloned into a yeast prey vector to execute the second yeast-two hybrid (58, 59), yielding 52 distinct VHHs with redundancies ranging from 1 to 37. Among this repertoire of VHHs, the top 20 clones that exhibited the highest degrees of redundancy were selected, and subsequently cloned into mammalian expression vector fused at the C-terminus with the TEV219. This integrated approach and the utilization of the highly diverse humanized library NaLi-H1 (60), promoted the enrichment of stable and soluble intracellular-targeting nanobodies; the overall process is illustrated in **Fig. 3.1B-C**.

To interrogate their binding capabilities and specificities, the potential VHHs were subsequently evaluated using the TANGO-based assay, specifically by using the mu-opioid receptor (μ-OR) and Angiotensin II receptor type 1 (AT1R) and independently testing each clone using increasing concentrations of the μ-OR agonist DAMGO and AT1R agonist angiotensin II. To maximize the detection of β-arrestin recruitment at these receptors, two variants of tagged-β-arrestin-2 were utilized, either carrying a N- or C-terminal V5-tag (V5-β-arrestin-2 and β-arrestin-2-V5, respectively). The overall schematic of the nanobody-based TANGO assay is depicted in **Fig. 3.2A**. Based on these preliminary findings, a particular clone, designated as NbA1, exhibited a robust response with β-arrestin-2-V5, while displaying a barely detectable response with N-terminally tagged V5-β-arrestin-2. Furthermore, codon optimization for human expression, enhanced the original nanobody's expression level threefold and thus was selected for further experiments in human cells (**Fig. 3.2B-C**).

Crystal structure of the NbA1 – To address the suboptimal activity of NbA1 toward the N-terminally tagged β-arrestin-2, a computer-aided affinity maturation strategy was opted for. Towards this aim, we initially solved the V5-bound structure of NbA1 at a resolution of 2Å. Structural analysis revealed that NbA1 adopts a typical V-shaped IgG fold connected by a disulfide bond, while the V5 peptide lacks any secondary structures (**Fig. 3.3A**) (61). The paratope responsible for V5 peptide interaction is primarily mediated by the CDR2 and CDR3 regions, a common feature of nanobodies (62). Nbs compensate for their reduced number of CDRs compared to conventional antibodies through distinctive CDR structures and antigen-binding modes; for example, many Nbs possess elongated CDR3 loops to provide a larger antigen interaction surface (43), as observed in NbV5 (**Fig. 3.3A**). The V5 peptide makes multiple polar and hydrophobic contacts with NbA1 and is oriented at 90 degrees to the central axis of the nanobody. Out of the 14 residues of the tag, 11 directly interact with NbA1 (**Fig. 3.3B**). The lateral chains of two residues, Lys 2 and Ile 4, point outward but their backbones make water-mediated hydrogen bonds with NbA1. As shown in **Fig. 3.3C**, the interaction is largely mediated by hydrophobic residues, suggesting a strong contribution of entropic forces by the Nb:V5 interfaces (63). Numerous reports have documented the greater paratope

diversity of nanobodies compared to the classical Ab VH domain (63), which was exemplified in this study by the distinct recognition mode of NbA1:V5 compared to the NbALFA:ALFA-tag interaction, which involves contacts with all three CDRs and is oriented parallel to the central axis (**Suppl. Fig. 3.1**) of the nanobody. Finally, three residues (Gln57, Gly58, Asp59) within the CDR2 loop are disordered and were unresolved (**Fig. 3.3A** and **Suppl. Fig. 3.1**). The primary coding sequence of NbA1 is shown in **Fig. 3.3D**.

Maturation of the NbA1 – A primary objective driving our research was to advance the study of PPIs utilizing a versatile nanobody-based sensor. While NbA1 demonstrates intracellular functionality, it exhibits a marked preference for the C-terminally tagged β-arrestin-2. This partiality can potentially be attributed to the lack of interactions with the last two residues of the V5 tag. To improve the overall affinity, particularly for the N-terminus of the V5 tag, *in silico* affinity maturation was performed using the Rosetta modelling software. The generated models were assessed based on their corresponding scores and binding energy metrics, resulting in ten designed mutants harboring degenerated mutations, which were subsequently synthesized and tested using the TANGO assay. Based on the functional evaluation, it was deduced that two mutations (ΔD59 and S60K) resulted in better activity compared to NbA1, especially for the N-terminal V5-tagged arrestin. Consequently, an optimized nanobody was generated to incorporate only those two mutations, called NbV5. As shown in **Fig. 3.3E**, the maturated NbV5 can recognize both N- or C-terminally tagged β-arrestin-2. In the case of AT1R, no discernible disparity was observed between the two orientations of the tag. However, in the context of μ-OR, a slight reduction in the recognition of β-arrestin-2-V5 was noted; nevertheless, this was compensated by a significant gain of function towards V5-β-arrestin-2 (N-terminal tag) (**Fig. 3.3E**). Although the precise mode of interaction remains to be elucidated, this optimized NbV5 variant exhibited a notable improvement in its overall behavior within our functional TANGO assay, warranting its selection for further development of our nanobody-based biosensors.

Determination of the apparent KD of NbV5 was carried out using yeast surface display in the EBY100 yeast strain. Using the Gap-repair method, NbV5 was cloned in a yeast display vector (pYD1-Halo) derived from pCTCON2 (64), resulting in the construct NbV5-AGAP2-Halo-myc in N-terminal to C-terminal orientation. Efficient display of the nanobody was verified using flow cytometry (FACS), utilizing Halo-Alexa 488 as the labeling agent (**Suppl. Fig. 3.2A-C**). As for the antigen, we opted for the 1N3R Tau protein isoform (NP_001190180.1) with a V5 insertion between E73 and A74, and labeled with Alexa Fluor 488 succinimidyl ester. This unstructured protein is well-suited for displaying linear epitopes (65), avoiding any bias related to the N-terminal or C-terminal Tag-V5 presentation. Assessment of binding was conducted by FACS, specifically using serial dilutions of labeled Tau-V5 ranging from 500 nM to 0.98 nM. The findings, as presented in **Supplementary Figure 3.2D**, indicated an estimated affinity of 29 nM for NbV5. Nevertheless, it is important to emphasize that *in vitro* affinity measurements may not accurately reflect cellular affinity or activity.

Protein-protein interaction assays – PPIs lie at the core of cellular processes, wherein there is a reciprocal and dynamic interplay between two proteins, often generalized as the "bait" and "prey". In our NbV5:V5 system, the bait represents a membrane receptor from the G protein-coupled receptor (GPCR) family. Notably, due to the inherent membrane configuration of GPCRs, their fusion is limited to the C-terminal region. Conversely, the prey protein represents any protein of interest tagged with the V5 epitope, which can be positioned at the C-terminus, N-terminus, or even within the protein sequence itself. As a proof-of-concept, we utilized the well-established GPCR interactors, β-arrestin-1 and β-arrestin-2, as the prey proteins. Within this tripartite system, the NbV5-based biosensor acts as a molecular bridge, reconstituting a functional cell-based assay by orchestrating the interaction between the V5-tagged prey protein and the bait receptor, which carries the complementary functional moiety. Importantly, this setup ensures minimal disruption of the native complex formation and preserves the intrinsic functionality of the prey protein.

The initial characterization of our platform with GPCRs enabled tunable regulation of the interaction dynamics through the utilization of an agonist and, thus, a more precise assessment of biosensor efficiency. Subsequent experiments were conducted using two distinct GPCRs, namely the AT1R and μ-OR, both of which are widely studied receptors in our laboratory and thus would serve well as targets for the characterization of the Nb-V5 biosensors.

NbV5-based protease-dependent reporter assay (TANGO) – The first functional assay adapted as a tripartite NbV5:V5 system was the Tobacco Etch protease-dependent TANGO assay. Renowned for its high sensitivity and permissibility, previous efforts have successfully exploited this platform to investigate β-arrestin recruitment at specific GPCRs or to conduct high-throughput screenings of the entire class A GPCR-ome simultaneously (66-68). The TANGO assay leverages a modified GPCR, termed TANGO-ized GPCR, which carries a transcription factor, tTA (tetracycline-controlled transactivator), fused at its C-terminus and preceded by a tobacco etch virus endopeptidase (TEV) cleavage site. Upon recruitment of the β-arrestin protein fused with TEV protease (β-arrestin-TEV) to the receptor, the TEV protease cleaves its recognition site, liberating the tTA transcription factor. Subsequently, the translocated tTA engages the nucleus and activates a reporter gene under the control of the tTA-response element (TRE). Our study selected an optimized version of the TEV protease, TEV219, which exhibits enhanced efficiency and avoids self-inactivation (69), to improve further the GPCR-TANGO platform's performance (70).

Assessment of the NbV5 biosensors within the TANGO assay was conducted using μ-OR and AT1R. Interestingly, a robust dose-response relationship was observed for both β-arrestin-1 and β-arrestin-2, regardless of the position of the V5-tag (**Fig. 3.4A and B**). It is noteworthy to highlight that the obtained EC50 values were comparable to those obtained from our updated TANGO assay featuring a direct fusion of TEV219 at the C-terminus of the β-arrestins (**Fig. 3.4C**). The inter-assay reproducibility of the TANGO assay is presented in **Supplementary Figure 3.3A**, where data from multiple biological replicates were normalized toward the top-performing conditions and pooled. These findings substantiate the suitability and efficacy of

our NbV5 biosensors in conjunction with the TANGO-based assay, further affirming their potential as valuable tools in PPI studies.

NbV5-based Bioluminescence Resonance Energy Transfer (BRET) – Biophysical techniques involving resonance energy transfer enable monitoring of the formation of dynamic complexes in living cells (71), with their use being well-established and remaining a gold standard in GPCR signaling (8). In the second generation of BRET (BRET2), the receptor is fused at the C-terminus with the Renilla Luciferase variant 2 or 8 (RLuc2 or 8) (72) while the nanobody is fused at either N- or C-terminus with the GFP2 acceptor (**Fig. 3.5A**) (73, 74). The underlying principle involves the generation of a resonance energy transfer signal when there is sufficient spectral overlap between the acceptor and donor molecules in close proximity, leading to dipole-dipole coupling. Importantly, the extended working distance range afforded by the BRET2 system enables the study of larger protein systems, including GPCR-protein interactor assemblies.

In a manner analogous to the adaptation of the TANGO system, various configurations involving β-arrestin-1 and β-arrestin-2 fused at the N- or C-terminus with the V5-tag were assessed, alongside the reference ALFA-tag, which served as a benchmark due to the well-characterized performance of the corresponding NbALFA intrabody with different tag placements (N-term, C-term, and internal). As depicted in **Figure 3.5B-D**, all configurations exhibited a robust signal; however, it was observed that the C-terminally tagged NbV5 (NbV5-GFP2) yielded a superior BRET2 ratio, while the impact on NbALFA was comparatively less pronounced. One possibility behind this intriguing observation could be explained by the distinct binding orientation of NbALFA, which is oriented at a 90-degree angle relative to NbV5, as illustrated in **Supplementary Figure 3.1**. Notably, the tag placement within the prey protein did not substantially influence the receptor-β-arrestin coupling under investigation. For the AT1R receptor specifically, both isoforms of β-arrestin were well recruited, with a slight preference observed for β-arrestin-2 within this particular assay. However, it is worth highlighting that we failed to detect a significant β-arrestin BRET signal at the μ-OR receptor,

even in the presence of GRK2. While BRET has frequently been employed to quantify β-arrestin2 recruitment at the μ-OR receptor, it is noteworthy that the BRET ratio is always weaker compared to other GPCRs, including the closely related kappa opioid receptor, which worked in our Nb-V5 adapted BRET assay. The reasons underlying the ineffectiveness of the μ-OR receptor in this assay remain unclear; however, we speculate that the overall conformation of the μ-OR receptor may not be conducive to efficient resonance energy transfer. Notwithstanding this observation, we successfully detected β-arrestin recruitment utilizing the other two assays presented in this study. Consequently, our NbV5-based biosensors demonstrate substantial promise for implementation in BRET assays, but adding a tripartite constituent might not be favorable to efficient resonance energy transfer with specific pairs.

NbV5-based Nanoluciferase Binary Technology (NanoBiT) – The NanoBiT assay represents a versatile structural complementation reporter system, harnessing the unique properties of a Large BiT (LgBiT; 18 kDa) subunit and its corresponding Small BiT (SmBiT; 11 amino acids) peptide, specifically engineered to exhibit a low affinity for LgBiT. When these two proteins interact, the subunits assemble into an active enzyme which, in the presence of its substrate, furimazine, produces a luminescent signal in living cells, enabling real-time kinetic measurements of protein interaction dynamics (75). In the context of GPCRs, it is conventionally advantageous to fuse the SmBiT peptide to the C-terminus of the receptor, likely minimizing perturbations to the receptor's native state or ligand-induced complexes.

As depicted in **Figure 3.6**, various configurations of β-arrestin fusions (V5-β-arrestin and β-arrestin-V5) and nanobody fusions (Nbs-LgBiT and LgBiT-Nbs) were compared to evaluate their respective functional performances. In contrast to the BRET2 experiment (**Figure 3.5**), LgBiT-NbV5 produced a superior response compared to NbV5-LgBiT, underscoring the importance of evaluating both orientations to achieve optimal response and sensitivity. Interestingly, the NanoBiT assay revealed a pronounced preference for β-arrestin-1 over β-arrestin-2 at the AT1 receptor, a trend also observed with the ALFA-tag system, thereby

confirming that the choice of tag system does not significantly influence the outcomes (**Supp. Fig. 3.2A**). To detect reasonable recruitment at the μ-OR receptor, the co-expression of G protein-coupled receptor kinase 2 (GRK2) is often necessary, particularly considering its absence at endogenous levels in HEK293 cells (76). As shown in **Figures 3.6E and F**, β-arrestin-1 was favored over β-arrestin-2 at the μ-OR receptor, with the N-terminally V5-tagged β-arrestins and N-terminal LgBiT-NbV5 identified as the optimal orientations for tripartite interaction at this receptor. **Supplementary Figure 3.3B** displays the inter-assay reproducibility of the NanoBiT assay, wherein data from various biological replicates were normalized relative to the most optimal conditions and then pooled.

The NanoBiT assay offers notable advantages, particularly its suitability and ease for performing live experiments. While it can be employed for endpoint assays on a microplate reader, using an appropriate real-time kinetic reader, such as the FLIPR-TETRA, can reveal additional information in live settings. This aspect holds particular relevance for GPCRs, as it is often assumed that all interactions occur under equilibrium conditions, despite it being well-established that the interactions are transitory in nature, especially in the case of heterotrimeric G proteins (77). Thus, to study GPCR signaling under non-equilibrium conditions, kinetic experiments, and appropriate models should be favored (78). In light of this, we present a live kinetics experiment in **Figures 3.6D and G**, wherein the recruitment of V5-tagged β-arrestin at the μ-OR and AT1R receptors is examined at a single concentration of 1 μM selective agonist.

The ability of NbV5 to recognize an internally positioned V5-tag was also evaluated, specifically using the inhibitory G protein GαoA with the V5-tag inserted at position 92. It is well established that inhibitory G proteins tolerate such insertions, commonly employed for the introduction of fluorescent proteins or RLuc8 for BRET experiments. **Figure 3.6H** illustrates the employed approach, where SmBiT was fused at the N-terminus of the Gγ2 subunit and co-expressed with Gβ3, thereby facilitating the assembly of the obligatory Gβγ dimer that interacts with the inactive GDP-bound GαoA. Upon activation by the Gαi/o-coupled

μ-OR receptor, G protein activation can be detected through the dissociation of the heterotrimer. As depicted in **Figure 3.6I**, activation of the μ-OR receptor by its agonist, DAMGO induces the dissociation of the trimer, which can be monitored using NbV5 fused with LgBiT at the N- or C-terminus. Hence, our Nb-based sensor enables the measurement of G protein activation through the internal insertion of the V5 sequence, thereby minimizing the potential impact on overall G protein regulation. Furthermore, based on previous experiments conducted in our laboratory, it has been determined that NanoBiT complementary subunits are not well-tolerated when placed internally, further reinforcing the advantage of utilizing the NbV5:V5 tag system.

With regard to epitope tags, these incorporations are highly favourable as they avoid the need to generate custom antibodies for each protein of interest and allow orthogonal peptide tags to be multiplexed within the same experiment (11, 13); thus, the selectivity of the nanobody toward its target peptide tag is of paramount importance. As demonstrated in **Supplementary Figure 3.4B**, NbV5 exhibits remarkable specificity for the V5 epitope while displaying no detectable activity towards the ALFA-tag. This finding underscores the potential for simultaneous utilization of both tags broadening the experimental possibilities of our nanobody-based framework. To illustrate the application for a multiplexing experiment, the C-terminally V5-tagged AT1R was used to bridge the NbV5 carrying the SmBiT to the LgBiT-tagged NbALFA, detecting the recruitment of ALFA-tagged β-arrestin1. All combinations were permissive, but the SmBiT-NbV5 resulted in the best fold-over baseline compared to NbV5-SmBiT. Interestingly, while the fold-over baseline was substantially reduced, a gain into EC50 was observed from ~10nM to ~1nM (**Suppl. Fig. 3.4A** vs. **Suppl. Fig. 3.4C**). We do not have a definitive explanation for the observed increase, as the SmBiT-tag (11 aa) is approximatively the same size as the V5-tag (14 aa). However, the higher affinity of both nanobodies for their respective tags compared to SmBiT-LgBit interaction could account for this gain or alternatively, it could be attributed to a more favorable spatial orientation of the complex. Together, **Suppl. Fig. 3.2B and 3.2C** strongly support the selectivity of each tag system and their application for multiplexing configurations.

Nanobodies as fluorescence trackers for microscopy – To explore the potential application of NbV5 as a genetically-encoded tracker, we conducted experiments involving the co-expression of γ-actin tagged with a V5 epitope at its C-terminus (γ-actin-V5) along with NbV5 fused with the constitutive fluorescent protein eGFP. As shown in **Fig. 3.7**, the NbV5-eGFP fusion protein diffuses within the cell when expressed with the control pcDNA3.1, but selectively associates with γ-actin-V5 in its presence. Importantly, discernable actin-related structures like stress fibers and lamellipodia can be observed, indicating that the NbV5-eGFP (green) could efficiently interact with a dynamic protein such as γ-actin without interfering with its natural localization. The selectivity of the interaction is shown by the colocalization (yellow) between γ-actin-V5:NbV5-eGFP staining (green) and direct staining using the phalloidin-568 (red), which is a high-affinity F-actin probe. While the phalloidin selectively stains the actin filaments (F-actin), the γ -actin-V5:NbV5-eGFP also stains the globular actin (G-actin). Therefore, NbV5-based biosensors could be used to track protein remodeling or trafficking in a live-cell-based experiment.

DISCUSSION

Existing biotechnological methodologies used for the characterization and validation of putative drug targets and as the elucidation of physiological and pathophysiological cellular processes necessitate a wealth of information pertaining to the abundance, localization, and dynamic interactions of cellular constituents (79). Consequently, the development of intracellular traceable proteins for both endpoint investigations and real-time kinetics diagnostics assumes paramount significance, particularly in light of increasing efforts to acquire a more comprehensive understanding of cellular PPIs, and thus extending the applicability of such intracellular tracers to encompass a genome-wide even to an organism (-omics-) scale.

In this study, we contribute to this endeavor by developing and characterizing a V5-tag targeted nanobody named NbV5 alongside a suite of NbV5-based intracellular biosensors with multipurpose functionalities. The premise of our approach was to avoid the fusion of a large, functionalized tag to a protein while taking advantage the vast repertoire of C-terminally V5-tagged genome-wide open source ORFs. The V5 epitope, an established and widely employed peptide tag for over three decades, assumes a pivotal role in our investigation. This 14-mer peptide is devoid of net charge under physiological pH conditions and does not have any predicted secondary structures, albeit featuring quite an ordered core owing to the presence of three proline residues. The inherent rigidity is posited to reduce the multidimensional complexity of the conformational landscape, thereby mitigating the impact of environmentally induced secondary structures and conferring stability in solution (80).

Multiple peptide tags have emerged, each bearing its own set of advantages and disadvantages, yet few tags have corresponding functional intrabodies that are thoroughly characterized, as done in this study. While it is worth noting the exceptions of the NbALFA:ALFA-tag (51) and Moon-tag (46, 47), it is crucial to highlight that neither of these were thoroughly characterized for PPI studies as showcased herein with the NbV5; nonetheless, the availability of these tag systems could capitalize on through simultaneous multiplexing implementations in conjunction with the NbV5:V5. Unique to the V5-tag is the associated commercially available V5-tagged genome-wide ORF library, thereby paving the way for the prospect of large-scale PPI investigations. Furthermore, it must be underscored that among the numerous available nanobody structures, only a handful involve those complexed with linear peptide tags, namely ALFA (PDB: 6I2G), BC2 (PDB: 5IVO), and the V5 tag (reported herein). One avenue for future investigation is evaluating whether advanced protein modeling programs, such as Alphafold2, Alphafold Multimer or IgFold, can provide accurate predictions of nanobody-peptide tag structures (81), which would help inform the development of novel optimize future nanobody scaffolds with an increased propensity for intracellular stability. Recently, Dingus et al. have developed a general consensus framework derived from the most highly conserved positional residues across a large group of intracellularly stable nanobodies, which would also

be a valuable asset for increasing the intracellular stability of nanobodies through targeted mutagenesis without compromising target binding (15).

The majority of nanobodies available to date have been developed by animal immunization, but the utilization of synthetic *in vitro* platforms, as exemplified in our study, holds immense promise. The Hybribody methodology employed combines peptide phage display and intracellular yeast-two-hybrid techniques, as well as the selection of nanobodies wherein the folding of the paratope is independent of disulfide bonds, thus significantly enhancing the enrichment and identification of viable intrabodies (60, 82). This screening approach isolated a cohort of prospective nanobodies, among which clone NbA1 emerged as the preeminent candidate as an intrabody. Initial investigations unveiled a low expression level for all nanobodies, circumvented through codon optimization tailored for a human expression system. Subsequent characterization in the TANGO assay revealed that NbA1 exhibited suboptimal recognition of the N-terminally positioned V5-tag on β-arrestin2. To address this limitation, we sought to resolve its crystal structure, which would provide insight into the binding interface of NbA1:V5 tag. Consequently, NbA1 was purified from the periplasm of SHuffle bacteria, which are best suited for the purification of proteins containing disulfide bonds (83), and the purified NbA1 was then co-crystallized with the V5-tag. The resultant crystal structure served as the foundation for computer-aided maturation, aimed at refining the functionality of the nanobody. The maturation process was confined to the three CDRs, with no discernible mutants predicted to induce significant changes in binding energy. Based on the mutants tested in TANGO experiments, it was determined that two specific mutations conferred improved recognition of the V5-tag. The key distinguishing feature of NbV5 vis-à-vis NbA1 lies in its interaction with the N-terminally situated V5-tag, as shown in **Fig. 3.3E**. Given that these two key mutations, ΔD59 and S60K, are juxtaposed within a disordered loop in CDR2 (**Suppl. Fig. 3.1**), the deletion of a single residue is postulated to confer stability to this region, while Lys60 establishes direct contacts with the CDR2 loop, thereby further stabilizing this region (**Suppl. Fig. 3.1B, C**). While it is generally accepted that CDR3 is the most critical region for antigen recognition and binding due to its longer length and higher variability, several reports and as

demonstrated herein, demonstrate that mutations in CDR1 or CDR2 may optimize affinity or stability, particularly if these regions are directly involved in the paratope interaction (84). Thus, comprehensive optimization strategies should involve exploring mutations in all three CDRs to assess their combined impact on nanobody performance.

Having delineated the general mode of interaction between the nanobody and V5 tag, we proceeded to construct NbV5-based biosensors for versatile applications in the most widely used cellular PPI assays, namely Tango, BRET, and NanoBit assays. As shown herein, our biosensors probed the recruitment of both β-arrestin-1 and β-arrestin-2 at two well-characterized GPCRs, the μ-OR, and the AT1R. The μ-OR serves as the primary target for the most prescribed analgesics such as morphine and fentanyl (85). As for AT1R, this receptor is important for controlling vasocontraction, with AT1R antagonists (ARBs) being prescribed for the treatment of hypertension, congestive heart failure, and diabetic nephropathy (86). Although both receptors are known to engage both β-arrestin isoforms, there exists conflicting data regarding isoform selectivity and, more importantly, the intrinsic drug efficacy. As the measurement of the direct interaction between the receptor and its effector is a key aspect for accurately determining intrinsic drug efficacy (87), the use of smaller tags should mitigate some distortions caused by larger functional tags. With regard to GPCRs, the fusion of a large moiety to its C-terminus may introduce artifacts that lead to impaired signaling, altered ligand binding, mislocalization and affect trafficking, and changes to their stability and expression levels, likely due to steric hindrance or altered receptor conformation caused by the GFP fusion (88). Therefore, tag systems such as V5 would enable a more faithful characterization of receptor-effector interactions.

This work's adaptation of common cellular-based PPI assays involved the integration of NbV5-based biosensors, commencing with the TEV-dependent reporter assay (Tango), given its permissibility and sensitivity. Subsequently, our efforts extended to the adaptation of two widely employed PPI assays, namely BRET and NanoBiT. Intriguingly, a discrepancy between BRET and NanoBiT assays surfaced when investigating the selective recruitment of β-arrestin

isoforms at the AT1R receptor, with a distinct preference for β-arrestin-1 over β-arrestin-2 observed solely in the NanoBiT assay, while BRET2 and TANGO assays yielded no such disparity. The underlying reasons behind this observation remain unknown. Still, it is plausible to consider that the size and orientation of the tag may exert differential influences contingent upon the assay employed. In essence, these effects could manifest as alterations in the kinetics of PPIs or literal steric hindrance during complex formation. Another layer of complexity emerges from the intrinsic principles governing each assay: BRET, being highly conformationally dependent, necessitates optimal distance and spatial orientation for effective dipole-dipole coupling to facilitate efficient resonance energy transfer (89). One plausible explanation is that the measured BRET2 signal represents an average of recruitment and conformational changes (multi-states). Conversely, in binary complementation assays like NanoBiT, the two complementary fragments must assume a favorable spatial arrangement to facilitate complex formation. Moreover, binary complementation assays solely capture newly recruited β-arrestin or a single conformational state of the complex, precluding the monitoring of spatial rearrangements (90). In the case of TANGO, the prolonged stimulation and slower kinetics, due to the inherent proteolytic activity of TEV (69), might mitigate any detrimental kinetic effects stemming from tag size or orientation, albeit steric hindrance remains a pertinent consideration. While the implementation of a tag system has the potential to alleviate the impact of steric hindrance or particular arrangements of interacting partners during complex formation, the tag system itself may influence the sensitivity of the assay under specific circumstances. This phenomenon was evidenced within our system, as NbV5 failed to detect arrestin recruitment to the μ-OR in the BRET2 assay while performing well for AT1R. It should also be noted that during the optimization process, diverse sizes of flexible linkers (ranging from 5 to 70 amino acids) were explored to ensure the optimal distance between functional moieties (91); however, varying linker size did not improve the lack of detected at μ-OR. While a modest effect on the observed activity was noted at AT1R, the small (GGGGS)2x fusion linker was ultimately chosen as the optimal peptide for the NbV5-based biosensors.

While the current work primarily focused on utilizing GPCRs as a means to characterize the NbV5-based system, future efforts will be consecrated to expanding the applicability of the NbV5:V5 system to a broad range of PPIs, such as other membrane receptor-protein and protein-protein interactions. Thus, the authors hope that the versatility and adaptability of the NbV5:V5 platform will contribute to probing and unraveling the intricate dynamics of various interaction networks.

CONCLUSION

Herein, we engineered a novel nanobody that recognizes the V5-tag epitope, a widely employed peptide tag in many expression vectors, including the MISSION TRC3 human genome-wide ORF library. Said nanobody was selected and maturated to optimize its functionality in the intracellular environment, culminating in the development of NbV5. Our NbV5 intrabody offers a broad range of applications, including biosensors in cellular-based PPI assays, such as NanoBiT, TANGO, and $BRET^2$, and for microscopic imaging purposes. Moreover, the potential of NbV5 extends beyond its current scope and can be further expanded to adapt other existing PPI assays. In summary, NbV5 represents a unique tool that offers traceability of intracellular binding proteins with minimal disturbance to the native cellular milieu.

EXPERIMENTAL PROCEDURES

Cell culture

Human embryonic kidney 293T (HEK293T) and HT1080 cells were obtained from the American Type Culture Collection (ATCC) and maintained in Dulbecco's modified Eagle's medium (DMEM) supplemented with 5% fetal bovine serum (Fisher Scientific), 5% bovine calf serum (Fisher Scientific) and 1X Pen-Strep (100 U/ml penicillin, and 100 µg/ml streptomycin) (Fisher Scientific). HEK293T cells stably expressing MOR-SmBiT (MOR-SmBiT/HEK293T) were generated by transduction with lentivirus particles, which had been

produced in HEK293T cells by transiently co-transfecting the lentiviral packaging plasmid psPAX2 (Addgene #12260), a lentiviral vector encoding μ-OR-SmBiT (pLenti-Blast Addgene #17451), and the envelope plasmid pCMV-VSV-G (gift from Marceline Côté) at a 1:1:1 ratio using PEI transfection reagent. The following day, media was changed, and the supernatant was harvested at 48h post transfection. Cells were then transduced with lentivirus in standard growth media containing 5 μg/ml polybrene and the next day, selected with blasticidin at 5μg/ml. All cells were cultured at 37°C in a humidified atmosphere containing 5% CO_2.

Plasmids and cloning

All plasmid DNA used in this publication were fully sequenced and are available upon request or through Addgene repository (https://www.addgene.org/Patrick_Giguere/). Plasmid encoding ɣ-Actin-V5 was extracted from the MISSION TRC3 Human LentiORF Puromycin library (MilliporeSigma). V5-βArrestin1, V5-βArrestin2, βArrestin1-V5, βArrestin2-V5, βArrestin2-ALFA, ALFA-βArrestin2, βArrestin1-ALFA and ALFA-βArrestin1 were amplified by PCR, including the V5 tag within the primer, and subsequently cloned into pcDNA3.1$^+$ at the HindIII-XbaI restriction sites. GαoA with internal V5-tag at position 92 was synthesized by IDT (Integrated DNA Technologies) and cloned at HindIII-XbaI sites in pcDNA3.1$^+$. BRET^2 constructs: AT_1R-RLuc8, μ-OR-RLuc8, NbV5-GFP2, GFP2-NbV5, βArrestin2-GFP2, βArrestin2-ALFA-GFP2 were amplified by PCR and cloned in pcDNA3.1$^+$ using NEB HiFi DNA Assembly (New England Biolabs). Gβ3 and Gɣ2-GFP2 were generously gifted by Dr. Asuka Inoue (TOHOKU University). NanoBiT constructs: μ-OR-SmBiT and AT_1R-SmBiT were amplified by PCR by including the SmBiT tag within the primer preceded by a $(GGGGS)_{2x}$ linker. NbV5-LgBiT, LgBiT-NbV5, NbALFA-LgBiT and LgBiT-NbALFA were amplified by PCR and cloned in pcDNA3.1$^+$ using NEB HiFi DNA Assembly (New England Biolabs). Gɣ2-SmBiT was generously gifted by Dr. Asuka Inoue (TOHOKU University). TANGO constructs: μ-OR-TANGO and AT_1R-TANGO are from the original PRESTO-TANGO library (29-31). Aforementioned nanobodies fused to the TEV219 were cloned by PCR at restriction sites HindIII-BamHI in pcDNA3.1$^+$-X-TEV219 vector. NbV5-

eGFP was generated by PCR amplification of NbV5 and cloned into pEGFP-N1 (Clontech) at the HindIII-BamHI sites.

Nanobody development

To identify nanobodies that bind to a linear target and that could be expressed from inside the cell (as intrabodies), phage display selection was conducted with the Nali-H1 synthetic library (57), by Hybrigenics Services (Paris, France), using a His-Halo protein fused with three successive V5-tags (Halo-3xV5). The naïve library was first depleted using another antigen fused in the same Halo vector and selected on magnetic streptavidin beads with the biotinylated Halo-3xV5. With the first round presenting a complexity of $3x10^6$ colonies, the DNA extracted from the first round were used to construct a Yeast-Two-Hybrid prey library by PCR and Gap repair. The VHH selected after one round of phage display against V5 tag-Biotin were cloned into the pP9 yeast prey vector, which is derived from the original pGADGH plasmid; the library had $2.6x10^5$ independent clones in yeast. A single V5 tag, as well as two tandem V5 tags, were cloned into pB27 as a C- terminal fusion to LexA (LexA-V5); pB27 is derived from the original pBTM116 plasmid (92). The constructs were verified by sequencing the insert and used as baits to screen the V5-specific VHH library For the screen, clones were vetted using a mating approach with YHGX13 (Y187 ade2-101:loxP-kanMX-loxP, matα) and L40ΔGal4 (mata) yeast strains as previously described (59). Moreover, the library has been screened at saturation by cell-to-cell mating (59). A total of 264 His+ colonies were selected on a medium lacking tryptophan, leucine and histidine supplemented with 0.5 mM 3-AT, obtaining 52 different VHH with redundancies from 1 to 37.

Protein purification

The NbA1 was cloned into the expression vector pET26b (+) (Novagen) at NcoI-XhoI restriction sites to generate the pelB leader-NbA1-His_6 construct. The plasmid was transformed in SHuffle T7 Competent E. coli (New England BioLabs), and the NbA1 was subsequently purified from the periplasm of SHuffle T7 cells. Bacteria were then grown at 30°C in Terrific Broth and, after reaching an OD600 of ~0.6-0.8, were induced with 1mM IPTG (Isopropyl β-

d-1-thiogalactopyranoside, ThermoFisher) at 25°C for approximately 16 hours. Bacteria were then pelleted and resuspended in a solution of lysis buffer (0.5 M sucrose, 0.2 M Tris pH 8, 0.5 mM EDTA) and water at a ratio of 1:2 to create an osmotic shock. The lysate was then frozen and thawed for more efficient purification. Followingly, the mixture was stirred for 45 minutes at 4 °C and brought to a concentration of 150 mM NaCl, 2 mM $MgCl_2$, and 20 mM imidazole and centrifuged at 20,000xg for 30 min at 4 °C. The supernatant was then filtered through a 0,22 µm filter. After filtration, the supernatant was added to a gravity column containing 4 mL of Ni-NTA (Qiagen). Beads were washed with a high salt buffer (20 mM HEPES pH 7.5, 500 mM NaCl, 20 mM Imidazole) and washed three times with low salt buffer (20 mM HEPES pH7.5, 100 mM NaCl, 20 mM imidazole). The nanobodies were then eluted (20 mM HEPES pH 7.5, 100 mM NaCl, 400 mM imidazole) and dialyzed into physiological buffer solution (10 mM HEPES pH 7.4, 140 mM KCl, 10 mM NaCl) and purified using FPLC (Fast protein liquid chromatography, AKTA GE) on an S75 prep size-exclusion column.

Crystallization, data collection and structure determination

Purified NbA1 (30mg/mL) was incubated with the V5 peptide in a 1:3 ratio (protein: peptide). The protein complex was crystallized via the sitting drop vapour diffusion method at 4°C with a mother liquor composed of Bis-Tris pH 6.5, 19% (w/v) PEG 3350 and 20% (v/v) ethylene glycol. The crystals were flash-frozen in liquid nitrogen, and a full data set was collected using a Rigaku MicroMax-007HF equipped with a copper anode. Images were collected using an R-Axis IV++ detector (Rigaku) and processed using Structure Studio (Rigaku). The structure was solved by molecular replacement using the structure of NbALFA (PDB 6I2G) as search model and Phaser (50). Following several rounds of NbA1 building and refinement using COOT and Phenix, respectively, V5 was built in the positive Fourier map. The model was completed by adding the molecules and truncating side chains for which no electronic density could be observed. Ramachandran statistics: Non-glycine Ramachandran outliers; 0%, Non-glycine Ramachandran favored; 100%, Molprobity score : 1.65. Statistics of data collection and refinement are summarized in Table1. All structural figures were prepared in PyMOL.

Nanobody maturation

To optimize the NbA1 sequence and potentially increase the affinity of the antibody towards V5, Rosetta single-state design protocol was performed using the Rosetta Software Suite on the crystal structure of the NbA1 complex. The structure of NbA1 was prepared for antibody affinity maturation for Rosetta by manually editing the PDB file in PyMOL. PyMOL command prompts were used to delete the unwanted water molecules and all non-essential ligands and chains. An extra processing step was also performed to remove any protein atoms that are not involved in the antibody-antigen interface; chains were also renamed and reordered to help differentiate the antibody residues from the antigen residues. Next, a resfile (python script) was generated to identify the residues that were within a distance of specified residues that define the NbA1 protein interface. The side-chain conformations were optimized using the repacking and relaxing feature in Rosetta protein design, which was performed to minimize backbone phi-phi angles to relieve small clashes between side chains. The relaxed model was then used to generate ten designed models through RosettaScripts XML file, which contains a design protocol that uses a single round of fixed backbone design. As a control, the same protocol was repeated to generate ten control models without designing any residues. These control models were generated to compare the scores and the binding energies of the designed models to the native sequence during the analysis stage. The designed sequences were then analyzed by looking at the score, binding energy, and the binding density of the models. The analysis of the metrics was plotted using RosettaScripts which plots the score and the binding energy of the designed models against the control models. Subsequently, specific mutations were identified that resulted in the improvement of the NbA1 complex based on corresponding findings from functional assay experiments (as shown in **Figure 3.1**). Finally, a sequence logo was generated from the designed models in order to determine which mutations were made and their frequencies.

BRET^2 assay

HEK293T cells were plated in 6-well plates at 1.2x10^6 cells and subsequently transfected using the PEI precipitation method with BRET^2 constructs at a total of 3 µg of DNA per well.

Transfected cells were detached and seeded on PLL-coated white 96-well assay plates (ThermoFisher). The following day, spent medium was removed and replaced with 60 µL of 1X HBSS buffer, followed by the addition of 10 µL of Coelenterazine 400a (Nanolight Technologies) at 50 µM to each well, for a final concentration of 5 µM. After incubating the plates away from light for 8 minutes, 30 µL of serial dilutions of agonists at 3X concentration was added. Plates were subsequently read 4 times after 2 minutes, 10 minutes, 20 minutes, and 30 minutes using the Hidex Sense Beta Plus microplate reader (Gamble Technologies) with 405 nm (RLuc8-Coelenterazine 400a) and 500 nm (GFP2) emission filters, at 1 second/well integration times. Figures shown in the manuscript account for the reads after 20-minute incubations with agonist (and correspondingly, approximately 30-minute incubations with Coelenterazine 400a). Data were extracted using the integrated software and subjected to non-linear least-squares regression analysis using the sigmoidal dose-response function provided in GraphPad Prism 9.0. Data of 3 independent experiments (N=3) performed in quadruplicate are presented as $BRET^2$ ratio (acceptor/donor) as indicated in figure legends.

NanoBiT assay

µ-OR-SmBiT/HEK293T and HEK293T cells were plated in 6-well plates at $1.2x10^6$ cells and then transfected using the PEI precipitation method with the NanoBiT constructs the next day at a total of 3 µg of DNA per well. Transfected cells were detached and seeded on PLL-coated white 384-well assay plates (ThermoFisher) in starvation media (DMEM, 1% FBS, 1x Pen-Strep), The next day, media was removed and replaced with 20µL of 1X HBSS buffer containing 5 µM furimazine and incubated for a total of 10 minutes at room temperature before reading on Fluorescent Imaging Plate Reader (FLIPR) Tetra system (Molecular Devices). Baseline measurements were initially read before drugs were added into their respective wells (concentration and different drugs in Figure legends). The subsequent changes in relative luminescence signals (RLU) were recorded over time. Data were extracted using the integrated ScreenWorks software and subjected to non-linear least-squares regression analysis using the sigmoidal dose-response function provided in GraphPad Prism 9.0. Data of 3 independent

experiments (N=3) performed in quadruplicate are presented as Relative Luminescence Units (RLU) or normalized as indicated in figure legends.

TANGO assay

HTTL (HEK293T stably expressing a luciferase reporter gene under the TRE-Tight promoter) cells, an in-house developed reporter cell line (70), were seeded in 6-well plates at $1.2x10^6$ cells and were transfected with TANGO-ized constructs using the PEI precipitation method. Twenty hours later, the transfected cells were plated in DMEM supplemented with 1% dialyzed FBS into PLL coated 384-well white clear bottom cell culture plates at a density of 30,000 cells/well in a total volume of 40 µL for 5 hours to ensure proper attachment of cells. Agonist solutions, previously prepared at 3X concentration in sterilized assay buffer (20 mM HEPES, 1× Hanks' balanced salt solution (HBSS), pH 7.4), were added to the cells at 20 µL per well. Following overnight incubation, media was removed and 20 µL per well of homemade luciferase detection reagent (108 mM Tris–HCl; 42 mM Tris-Base, 75 mM NaCl, 3 mM $MgCl_2$, 5 mM Dithiothreitol (DTT), 0.2 mM Coenzyme A, 0.14 mg/ml D-Luciferin, 1.1 mM ATP, 0.25% v/v Triton X-100, 2 mM Sodium hydrosulfite) was added to all wells (68). After 10 minutes of incubation in the dark at room temperature, plates were read using the Hidex Sense Beta Plus microplate reader (Gamble Technologies). Data were subjected to non-linear least-squares regression analysis using the sigmoidal dose-response function provided in GraphPad Prism 9.0. Data of 3 independent experiments (N=3) performed in quadruplicate are presented as Relative Luminescence Units (RLU) or normalized as indicated in figure legends.

Fluorescence imaging

HT1080 were seeded in an ibiTreat chambered coverslip (Ibidi) in complete medium to obtain a 50% confluency the following day. The next day, cells were transiently cotransfected using JetPRIME (Polyplus Transfection) with ɣ-actin-V5/pLX307 or pcDNA3 and NbV5-eGFP/pcDNA3.1+. Twenty-four hours post-transfection, cells were fixed for 10 min in PBS containing 4% (w/v) paraformaldehyde, then washed three times in PBS and incubated 30 min in PBS containing 0.1% Triton (v/v). The cells were then incubated with Alexa Fluor 568

Phalloidin (ThermoFisher) (1:200 dilution) for 45 min and washed three times, followed by an incubation with 2mM Hoechst 33342 (ThermoFisher) for 15 min at room temperature. The coverslips were then washed with PBS, drained, and mounted with permafluor mounting media (Epredia). Cells were imaged on a GE Delta Vision Elite microscope using a 60x, 1.4NA, oil, Plan-Apo N objective. The images were analyzed using ImageJ software.

Affinity measurement

Yeast Display: pYD1-Halo is derived from the pCTCON2 plasmid, while retaining the AGAP2 and Gal4 inducible system. The nanobody is first encoded into the strain EBY100 (64), followed by the Agap2 and the Halo-Tag (pHTC, Promega Corp.). Pre-culture was performed in drop-out media minus tryptophane, with glycerol (1%), lactate (1%), and non-repressible media with a trace amount of glucose (0.05%) overnight. Subsequently, galactose (2% final concentration) was used to induce the system for 6 hours. PBS 1X with 1% BSA was utilized for binding and washing, and readings were taken using a Novocyte Flow Cytometer (Agilent Scientific) as per the manufacturer's instructions.

Antigen: The cDNA of the 1N3R Tau protein isoform7 (NP_001190180.1) with a V5-tag inserted between E73 and A74 was cloned in the pET15b vector, and purification was carried out following the protocol described previously (93). Labelling was realized using Alexa Fluor 488 NHS ester (ThermoFisher Scientific), with a molecular ratio of 2:1 for NHS Alexa:Tau-V5. Binding analysis was performed using FACS, with serial diluations of labeled Tau-V5 ranging from 500 nM to 0.98 nM. Data were subjected to non-linear least-squares regression analysis using the sigmoidal dose-response function provided in GraphPad Prism 9.0. Data presented are representative of one biological replicates (n=1) in triplicate and represents the mean of % fraction bound.

DATA AVAILIBITY

Crystal structure is available from Protein Data Bank (https://www.rcsb.org/), PDB # 8SKJ. The data that support the findings of this study are available from the corresponding authors upon reasonable request.

SUPPORTING INFORMATION

This article contains supporting information.

CONFLICT OF INTERESTS

The authors declare no competing interests.

ACKNOWLEDGMENTS

We would like to acknowledge technical support from the Protein Biophysics Core Facility and uOttawa Cell Biology and Image Acquisition (CBIA) Core Facility. We would like to thank Dr. Asuka Inoue for his generous gift of different plasmids, as highlighted in the Material and Methods. Thank you to Hybrigenics (Gard, France) for performing the nanobody selection and Y2H. We would also like to thank the uOttawa CBIA core (RRID: SCR_021845) and core staff, Dr. Chloë van Oostende.

Funding and additional information

KM is supported by a graduate scholarship from the Natural Sciences and Engineering Research Council of Canada. MZ is supported by the Alexander Graham Bell Canada Graduate Scholarships-Doctoral Program (CGS-D3) from Natural Sciences and Engineering Research Council of Canada. This work was supported by the Canadian Institutes of Health Research (CIHR grant #MOP142219) and Natural Sciences and Engineering Research Council of Canada (NSERC RGPIN-2017-06151).

Author contributions

P.M.G. Supervision, Conceptualization, Methodology, Writing - Review & Editing; **M.Z.** Writing - Original Draft, Investigation, Validation; **K.M.** Investigation, Validation, Formal analysis; **G.L.** Investigation, Validation, Visualization, Resources, Formal analysis; **A.V.** Validation; **S.P.** Investigation, Software; **J.C.R**. Investigation, Validation; **S.S., M.J., J.F.C.,** Investigation, Software, Data Curation.

REFERENCES

1. Milligan, G., and White, J. H. (2001) Protein-protein interactions at G-protein-coupled receptors Trends Pharmacol Sci **22**, 513-518 10.1016/s0165-6147(00)01801-0
2. Seychell, B. C., and Beck, T. (2021) Molecular basis for protein-protein interactions Beilstein J Org Chem **17**, 1-10 10.3762/bjoc.17.1
3. Kuzmanov, U., and Emili, A. (2013) Protein-protein interaction networks: probing disease mechanisms using model systems Genome Med **5**, 37 10.1186/gm441
4. Rao, V. S., Srinivas, K., Sujini, G. N., and Kumar, G. N. (2014) Protein-protein interaction detection: methods and analysis Int J Proteomics **2014**, 147648 10.1155/2014/147648
5. Bell, M. R., Engleka, M. J., Malik, A., and Strickler, J. E. (2013) To fuse or not to fuse: what is your purpose? Protein Sci **22**, 1466-1477 10.1002/pro.2356
6. Newman, R. H., Fosbrink, M. D., and Zhang, J. (2011) Genetically encodable fluorescent biosensors for tracking signaling dynamics in living cells Chem Rev **111**, 3614-3666 10.1021/cr100002u
7. Villalobos, V., Naik, S., and Piwnica-Worms, D. (2007) Current state of imaging protein-protein interactions in vivo with genetically encoded reporters Annu Rev Biomed Eng **9**, 321-349 10.1146/annurev.bioeng.9.060906.152044
8. Guo, S., Zhao, T., Yun, Y., and Xie, X. (2022) Recent progress in assays for GPCR drug discovery Am J Physiol Cell Physiol **323**, C583-C594 10.1152/ajpcell.00464.2021
9. Sun, Y., Rombola, C., Jyothikumar, V., and Periasamy, A. (2013) Forster resonance energy transfer microscopy and spectroscopy for localizing protein-protein interactions in living cells Cytometry A **83**, 780-793 10.1002/cyto.a.22321
10. Wade, M., Mendez, J., Coussens, N. P., Arkin, M. R., and Glicksman, M. A. (2004) Inhibition of Protein-Protein Interactions: Cell-Based Assays In Assay Guidance Manual, Markossian S, Grossman A, Brimacombe K, Arkin M, Auld D, Austin C, et al., eds. Bethesda (MD)

11. Kimple, M. E., Brill, A. L., and Pasker, R. L. (2013) Overview of affinity tags for protein purification Curr Protoc Protein Sci **73**, 9 9 1-9 9 23 10.1002/0471140864.ps0909s73
12. Kuey, C., Larocque, G., Clarke, N. I., and Royle, S. J. (2019) Unintended perturbation of protein function using GFP nanobodies in human cells J Cell Sci **132**, 10.1242/jcs.234955
13. Zhao, X., Li, G., and Liang, S. (2013) Several affinity tags commonly used in chromatographic purification J Anal Methods Chem **2013**, 581093 10.1155/2013/581093
14. Brilhante-da-Silva, N., de Oliveira Sousa, R. M., Arruda, A., Dos Santos, E. L., Marinho, A. C. M., Stabeli, R. G. *et al.* (2021) Camelid Single-Domain Antibodies for the Development of Potent Diagnosis Platforms Mol Diagn Ther **25**, 439-456 10.1007/s40291-021-00533-7
15. Dingus, J. G., Tang, J. C. Y., Amamoto, R., Wallick, G. K., and Cepko, C. L. (2022) A general approach for stabilizing nanobodies for intracellular expression Elife **11**, 10.7554/eLife.68253
16. Marschall, A. L., Dubel, S., and Boldicke, T. (2015) Specific in vivo knockdown of protein function by intrabodies MAbs **7**, 1010-1035 10.1080/19420862.2015.1076601
17. Bates, A., and Power, C. A. (2019) David vs. Goliath: The Structure, Function, and Clinical Prospects of Antibody Fragments Antibodies (Basel) **8**, 10.3390/antib8020028
18. Hudson, P. J., and Kortt, A. A. (1999) High avidity scFv multimers; diabodies and triabodies J Immunol Methods **231**, 177-189 10.1016/s0022-1759(99)00157-x
19. Kabayama, H., Takeuchi, M., Tokushige, N., Muramatsu, S. I., Kabayama, M., Fukuda, M. *et al.* (2020) An ultra-stable cytoplasmic antibody engineered for in vivo applications Nat Commun **11**, 336 10.1038/s41467-019-13654-9
20. Guglielmi, L., Denis, V., Vezzio-Vie, N., Bec, N., Dariavach, P., Larroque, C. *et al.* (2011) Selection for intrabody solubility in mammalian cells using GFP fusions Protein Eng Des Sel **24**, 873-881 10.1093/protein/gzr049

21. Kvam, E., Sierks, M. R., Shoemaker, C. B., and Messer, A. (2010) Physico-chemical determinants of soluble intrabody expression in mammalian cell cytoplasm Protein Eng Des Sel **23**, 489-498 10.1093/protein/gzq022
22. Goldman, E. R., Liu, J. L., Zabetakis, D., and Anderson, G. P. (2017) Enhancing Stability of Camelid and Shark Single Domain Antibodies: An Overview Front Immunol **8**, 865 10.3389/fimmu.2017.00865
23. Flicker, S., Zettl, I., and Tillib, S. V. (2020) Nanobodies-Useful Tools for Allergy Treatment? Front Immunol **11**, 576255 10.3389/fimmu.2020.576255
24. Muyldermans, S. (2021) A guide to: generation and design of nanobodies FEBS J **288**, 2084-2102 10.1111/febs.15515
25. Steeland, S., Vandenbroucke, R. E., and Libert, C. (2016) Nanobodies as therapeutics: big opportunities for small antibodies Drug Discov Today **21**, 1076-1113 10.1016/j.drudis.2016.04.003
26. Soetens, E., Ballegeer, M., and Saelens, X. (2020) An Inside Job: Applications of Intracellular Single Domain Antibodies Biomolecules **10**, 10.3390/biom10121663
27. de Beer, M. A., and Giepmans, B. N. G. (2020) Nanobody-Based Probes for Subcellular Protein Identification and Visualization Front Cell Neurosci **14**, 573278 10.3389/fncel.2020.573278
28. Che, T., English, J., Krumm, B. E., Kim, K., Pardon, E., Olsen, R. H. J. *et al.* (2020) Nanobody-enabled monitoring of kappa opioid receptor states Nat Commun **11**, 1145 10.1038/s41467-020-14889-7
29. Galli, V., Sebastian, R., Moutel, S., Ecard, J., Perez, F., and Roux, A. (2017) Uncoupling of dynamin polymerization and GTPase activity revealed by the conformation-specific nanobody dynab Elife **6**, 10.7554/eLife.25197
30. Gulati, S., Jin, H., Masuho, I., Orban, T., Cai, Y., Pardon, E. *et al.* (2018) Targeting G protein-coupled receptor signaling at the G protein level with a selective nanobody inhibitor Nat Commun **9**, 1996 10.1038/s41467-018-04432-0

31. Jullien, D., Vignard, J., Fedor, Y., Bery, N., Olichon, A., Crozatier, M. *et al.* (2016) Chromatibody, a novel non-invasive molecular tool to explore and manipulate chromatin in living cells J Cell Sci **129**, 2673-2683 10.1242/jcs.183103
32. Keller, L., Bery, N., Tardy, C., Ligat, L., Favre, G., Rabbitts, T. H. *et al.* (2019) Selection and Characterization of a Nanobody Biosensor of GTP-Bound RHO Activities Antibodies (Basel) **8**, 10.3390/antib8010008
33. Kruse, A. C., Ring, A. M., Manglik, A., Hu, J., Hu, K., Eitel, K. *et al.* (2013) Activation and allosteric modulation of a muscarinic acetylcholine receptor Nature **504**, 101-106 10.1038/nature12735
34. Livingston, K. E., Mahoney, J. P., Manglik, A., Sunahara, R. K., and Traynor, J. R. (2018) Measuring ligand efficacy at the mu-opioid receptor using a conformational biosensor Elife **7**, 10.7554/eLife.32499
35. Morgenstern, T. J., Park, J., Fan, Q. R., and Colecraft, H. M. (2019) A potent voltage-gated calcium channel inhibitor engineered from a nanobody targeted to auxiliary Ca(V)beta subunits Elife **8**, 10.7554/eLife.49253
36. Schenck, S., Kunz, L., Sahlender, D., Pardon, E., Geertsma, E. R., Savtchouk, I. *et al.* (2017) Generation and Characterization of Anti-VGLUT Nanobodies Acting as Inhibitors of Transport Biochemistry **56**, 3962-3971 10.1021/acs.biochem.7b00436
37. Singh, S., Murillo, G., Chen, D., Parihar, A. S., and Mehta, R. G. (2018) Suppression of Breast Cancer Cell Proliferation by Selective Single-Domain Antibody for Intracellular STAT3 Breast Cancer (Auckl) **12**, 1178223417750858 10.1177/1178223417750858
38. Staus, D. P., Wingler, L. M., Strachan, R. T., Rasmussen, S. G., Pardon, E., Ahn, S. *et al.* (2014) Regulation of beta2-adrenergic receptor function by conformationally selective single-domain intrabodies Mol Pharmacol **85**, 472-481 10.1124/mol.113.089516
39. Truttmann, M. C., Wu, Q., Stiegeler, S., Duarte, J. N., Ingram, J., and Ploegh, H. L. (2015) HypE-specific nanobodies as tools to modulate HypE-mediated target AMPylation J Biol Chem **290**, 9087-9100 10.1074/jbc.M114.634287

40. Van Impe, K., Bethuyne, J., Cool, S., Impens, F., Ruano-Gallego, D., De Wever, O. *et al.* (2013) A nanobody targeting the F-actin capping protein CapG restrains breast cancer metastasis Breast Cancer Res **15**, R116 10.1186/bcr3585
41. Wilton, E. E., Opyr, M. P., Kailasam, S., Kothe, R. F., and Wieden, H. J. (2018) sdAb-DB: The Single Domain Antibody Database ACS Synth Biol **7**, 2480-2484 10.1021/acssynbio.8b00407
42. De Genst, E. J., Guilliams, T., Wellens, J., O'Day, E. M., Waudby, C. A., Meehan, S. *et al.* (2010) Structure and properties of a complex of alpha-synuclein and a single-domain camelid antibody J Mol Biol **402**, 326-343 10.1016/j.jmb.2010.07.001
43. Braun, M. B., Traenkle, B., Koch, P. A., Emele, F., Weiss, F., Poetz, O. *et al.* (2016) Peptides in headlock--a novel high-affinity and versatile peptide-binding nanobody for proteomics and microscopy Sci Rep **6**, 19211 10.1038/srep19211
44. Virant, D., Traenkle, B., Maier, J., Kaiser, P. D., Bodenhofer, M., Schmees, C. *et al.* (2018) A peptide tag-specific nanobody enables high-quality labeling for dSTORM imaging Nat Commun **9**, 930 10.1038/s41467-018-03191-2
45. Cabalteja, C. C., Sachdev, S., and Cheloha, R. W. (2022) Characterization of a Nanobody-Epitope Tag Interaction and Its Application for Receptor Engineering ACS Chem Biol **17**, 2296-2303 10.1021/acschembio.2c00407
46. Boersma, S., Khuperkar, D., Verhagen, B. M. P., Sonneveld, S., Grimm, J. B., Lavis, L. D. *et al.* (2019) Multi-Color Single-Molecule Imaging Uncovers Extensive Heterogeneity in mRNA Decoding Cell **178**, 458-472 e419 10.1016/j.cell.2019.05.001
47. Lutje Hulsik, D., Liu, Y. Y., Strokappe, N. M., Battella, S., El Khattabi, M., McCoy, L. E. *et al.* (2013) A gp41 MPER-specific llama VHH requires a hydrophobic CDR3 for neutralization but not for antigen recognition PLoS Pathog **9**, e1003202 10.1371/journal.ppat.1003202
48. Jin-jing LI, F. X., Yan-wei JI,Mei SHU,Zhui TU,Jin-heng FU (2018) Biopanning of Anti c-Myc-tag Nanobodies and Its Application for Bioimaging China Biotechnology **38**, 61-67 10.13523/j.cb.20180209

49. Traenkle, B., Emele, F., Anton, R., Poetz, O., Haeussler, R. S., Maier, J. *et al.* (2015) Monitoring interactions and dynamics of endogenous beta-catenin with intracellular nanobodies in living cells Mol Cell Proteomics **14**, 707-723 10.1074/mcp.M114.044016
50. Cheloha, R. W., Harmand, T. J., Wijne, C., Schwartz, T. U., and Ploegh, H. L. (2020) Exploring cellular biochemistry with nanobodies J Biol Chem **295**, 15307-15327 10.1074/jbc.REV120.012960
51. Gotzke, H., Kilisch, M., Martinez-Carranza, M., Sograte-Idrissi, S., Rajavel, A., Schlichthaerle, T. *et al.* (2019) The ALFA-tag is a highly versatile tool for nanobody-based bioscience applications Nat Commun **10**, 4403 10.1038/s41467-019-12301-7
52. Vigano, M. A., Ell, C. M., Kustermann, M. M. M., Aguilar, G., Matsuda, S., Zhao, N. *et al.* (2021) Protein manipulation using single copies of short peptide tags in cultured cells and in Drosophila melanogaster Development **148**, 10.1242/dev.191700
53. Yang, X., Boehm, J. S., Yang, X., Salehi-Ashtiani, K., Hao, T., Shen, Y. *et al.* (2011) A public genome-scale lentiviral expression library of human ORFs Nat Methods **8**, 659-661 10.1038/nmeth.1638
54. Sarov, M., Barz, C., Jambor, H., Hein, M. Y., Schmied, C., Suchold, D. *et al.* (2016) A genome-wide resource for the analysis of protein localisation in Drosophila Elife **5**, e12068 10.7554/eLife.12068
55. Hanke, T., and Randall, R. E. (1995) Variable domain sequences of mAb with high affinity for a linear oligopeptide Immunogenetics **42**, 442-443 10.1007/BF00179415
56. Hanke, T., Szawlowski, P., and Randall, R. E. (1992) Construction of solid matrix-antibody-antigen complexes containing simian immunodeficiency virus p27 using tag-specific monoclonal antibody and tag-linked antigen J Gen Virol **73 (Pt 3)**, 653-660 10.1099/0022-1317-73-3-653
57. Randall, R. E., Young, D. F., Goswami, K. K., and Russell, W. C. (1987) Isolation and characterization of monoclonal antibodies to simian virus 5 and their use in revealing antigenic differences between human, canine and simian isolates J Gen Virol **68 (Pt 11)**, 2769-2780 10.1099/0022-1317-68-11-2769

58. Bartel, P. L., and Fields, S. (1995) Analyzing protein-protein interactions using two-hybrid system Methods Enzymol **254**, 241-263 10.1016/0076-6879(95)54018-0
59. Fromont-Racine, M., Rain, J. C., and Legrain, P. (1997) Toward a functional analysis of the yeast genome through exhaustive two-hybrid screens Nat Genet **16**, 277-282 10.1038/ng0797-277
60. Moutel, S., Bery, N., Bernard, V., Keller, L., Lemesre, E., de Marco, A. *et al.* (2016) NaLi-H1: A universal synthetic library of humanized nanobodies providing highly functional antibodies and intrabodies Elife **5**, 10.7554/eLife.16228
61. Padlan, E. A. (1994) Anatomy of the antibody molecule Mol Immunol **31**, 169-217 10.1016/0161-5890(94)90001-9
62. Miura, N., Miyamoto, K., Ohtani, Y., Yaginuma, K., Aburaya, S., Kitagawa, Y. *et al.* (2019) Domain swapping of complementarity-determining region in nanobodies produced by Pichia pastoris AMB Express **9**, 107 10.1186/s13568-019-0833-2
63. Mitchell, L. S., and Colwell, L. J. (2018) Analysis of nanobody paratopes reveals greater diversity than classical antibodies Protein Eng Des Sel **31**, 267-275 10.1093/protein/gzy017
64. Chao, G., Lau, W. L., Hackel, B. J., Sazinsky, S. L., Lippow, S. M., and Wittrup, K. D. (2006) Isolating and engineering human antibodies using yeast surface display Nat Protoc **1**, 755-768 10.1038/nprot.2006.94
65. Danis, C., Dupre, E., Zejneli, O., Caillierez, R., Arrial, A., Begard, S. *et al.* (2022) Inhibition of Tau seeding by targeting Tau nucleation core within neurons with a single domain antibody fragment Mol Ther **30**, 1484-1499 10.1016/j.ymthe.2022.01.009
66. Kroeze, W. K., Sassano, M. F., Huang, X. P., Lansu, K., McCorvy, J. D., Giguere, P. M. *et al.* (2015) PRESTO-Tango as an open-source resource for interrogation of the druggable human GPCRome Nat Struct Mol Biol **22**, 362-369 10.1038/nsmb.3014
67. Laroche, G., and Giguere, P. M. (2019) Measurement of beta-Arrestin Recruitment at GPCRs Using the Tango Assay Methods Mol Biol **1947**, 257-267 10.1007/978-1-4939-9121-1_14

68. Zeghal, M., Laroche, G., and Giguere, P. M. (2020) Parallel Interrogation of beta-Arrestin2 Recruitment for Ligand Screening on a GPCR-Wide Scale using PRESTO-Tango Assay J Vis Exp 10.3791/60823
69. Kim, M. W., Wang, W., Sanchez, M. I., Coukos, R., von Zastrow, M., and Ting, A. Y. (2017) Time-gated detection of protein-protein interactions with transcriptional readout Elife **6**, 10.7554/eLife.30233
70. Zeghal, M., Laroche, G., Freitas, J. D., Wang, R., and Giguere, P. M. (2023) Profiling of basal and ligand-dependent GPCR activities by means of a polyvalent cell-based high-throughput platform Nat Commun **14**, 3684 10.1038/s41467-023-39132-x
71. Sun, S., Yang, X., Wang, Y., and Shen, X. (2016) In Vivo Analysis of Protein-Protein Interactions with Bioluminescence Resonance Energy Transfer (BRET): Progress and Prospects Int J Mol Sci **17**, 10.3390/ijms17101704
72. Loening, A. M., Fenn, T. D., Wu, A. M., and Gambhir, S. S. (2006) Consensus guided mutagenesis of Renilla luciferase yields enhanced stability and light output Protein Eng Des Sel **19**, 391-400 10.1093/protein/gzl023
73. Bertrand, L., Parent, S., Caron, M., Legault, M., Joly, E., Angers, S. *et al.* (2002) The BRET2/arrestin assay in stable recombinant cells: a platform to screen for compounds that interact with G protein-coupled receptors (GPCRS) J Recept Signal Transduct Res **22**, 533-541 10.1081/rrs-120014619
74. Jensen, A. A., Hansen, J. L., Sheikh, S. P., and Brauner-Osborne, H. (2002) Probing intermolecular protein-protein interactions in the calcium-sensing receptor homodimer using bioluminescence resonance energy transfer (BRET) Eur J Biochem **269**, 5076-5087 10.1046/j.1432-1033.2002.03218.x
75. Dixon, A. S., Schwinn, M. K., Hall, M. P., Zimmerman, K., Otto, P., Lubben, T. H. *et al.* (2016) NanoLuc Complementation Reporter Optimized for Accurate Measurement of Protein Interactions in Cells ACS Chem Biol **11**, 400-408 10.1021/acschembio.5b00753

76. Nickolls, S. A., Humphreys, S., Clark, M., and McMurray, G. (2013) Co-expression of GRK2 reveals a novel conformational state of the micro-opioid receptor PLoS One **8**, e83691 10.1371/journal.pone.0083691
77. Wan, Q., Okashah, N., Inoue, A., Nehme, R., Carpenter, B., Tate, C. G. *et al.* (2018) Mini G protein probes for active G protein-coupled receptors (GPCRs) in live cells J Biol Chem **293**, 7466-7473 10.1074/jbc.RA118.001975
78. Culhane, K. J., Gupte, T. M., Madhugiri, I., Gadgil, C. J., and Sivaramakrishnan, S. (2022) Kinetic model of GPCR-G protein interactions reveals allokairic modulation of signaling Nat Commun **13**, 1202 10.1038/s41467-022-28789-5
79. Wagner, T. R., and Rothbauer, U. (2020) Nanobodies Right in the Middle: Intrabodies as Toolbox to Visualize and Modulate Antigens in the Living Cell Biomolecules **10**, 10.3390/biom10121701
80. Stadler, C., Rexhepaj, E., Singan, V. R., Murphy, R. F., Pepperkok, R., Uhlen, M. *et al.* (2013) Immunofluorescence and fluorescent-protein tagging show high correlation for protein localization in mammalian cells Nat Methods **10**, 315-323 10.1038/nmeth.2377
81. Ruffolo, J. A., Chu, L. S., Mahajan, S. P., and Gray, J. J. (2023) Fast, accurate antibody structure prediction from deep learning on massive set of natural antibodies Nat Commun **14**, 2389 10.1038/s41467-023-38063-x
82. McMahon, C., Baier, A. S., Pascolutti, R., Wegrecki, M., Zheng, S., Ong, J. X. *et al.* (2018) Yeast surface display platform for rapid discovery of conformationally selective nanobodies Nat Struct Mol Biol **25**, 289-296 10.1038/s41594-018-0028-6
83. Lobstein, J., Emrich, C. A., Jeans, C., Faulkner, M., Riggs, P., and Berkmen, M. (2012) SHuffle, a novel Escherichia coli protein expression strain capable of correctly folding disulfide bonded proteins in its cytoplasm Microb Cell Fact **11**, 56 10.1186/1475-2859-11-56
84. Rabia, L. A., Desai, A. A., Jhajj, H. S., and Tessier, P. M. (2018) Understanding and overcoming trade-offs between antibody affinity, specificity, stability and solubility Biochem Eng J **137**, 365-374 10.1016/j.bej.2018.06.003

85. Pathan, H., and Williams, J. (2012) Basic opioid pharmacology: an update Br J Pain **6**, 11-16 10.1177/2049463712438493
86. Dasgupta, C., and Zhang, L. (2011) Angiotensin II receptors and drug discovery in cardiovascular disease Drug Discov Today **16**, 22-34 10.1016/j.drudis.2010.11.016
87. Salahudeen, M. S., and Nishtala, P. S. (2017) An overview of pharmacodynamic modelling, ligand-binding approach and its application in clinical practice Saudi Pharm J **25**, 165-175 10.1016/j.jsps.2016.07.002
88. Milligan, G. (1999) Exploring the dynamics of regulation of G protein-coupled receptors using green fluorescent protein Br J Pharmacol **128**, 501-510 10.1038/sj.bjp.0702824
89. El Khamlichi, C., Reverchon-Assadi, F., Hervouet-Coste, N., Blot, L., Reiter, E., and Morisset-Lopez, S. (2019) Bioluminescence Resonance Energy Transfer as a Method to Study Protein-Protein Interactions: Application to G Protein Coupled Receptor Biology Molecules **24**, 10.3390/molecules24030537
90. Wouters, E., Vasudevan, L., Crans, R. A. J., Saini, D. K., and Stove, C. P. (2019) Luminescence- and Fluorescence-Based Complementation Assays to Screen for GPCR Oligomerization: Current State of the Art Int J Mol Sci **20**, 10.3390/ijms20122958
91. Chen, X., Zaro, J. L., and Shen, W. C. (2013) Fusion protein linkers: property, design and functionality Adv Drug Deliv Rev **65**, 1357-1369 10.1016/j.addr.2012.09.039
92. Vojtek, A. B., and Hollenberg, S. M. (1995) Ras-Raf interaction: two-hybrid analysis Methods Enzymol **255**, 331-342 10.1016/s0076-6879(95)55036-4
93. Danis, C., Despres, C., Bessa, L. M., Malki, I., Merzougui, H., Huvent, I. *et al.* (2016) Nuclear Magnetic Resonance Spectroscopy for the Identification of Multiple Phosphorylations of Intrinsically Disordered Proteins J Vis Exp 10.3791/55001

FIGURES

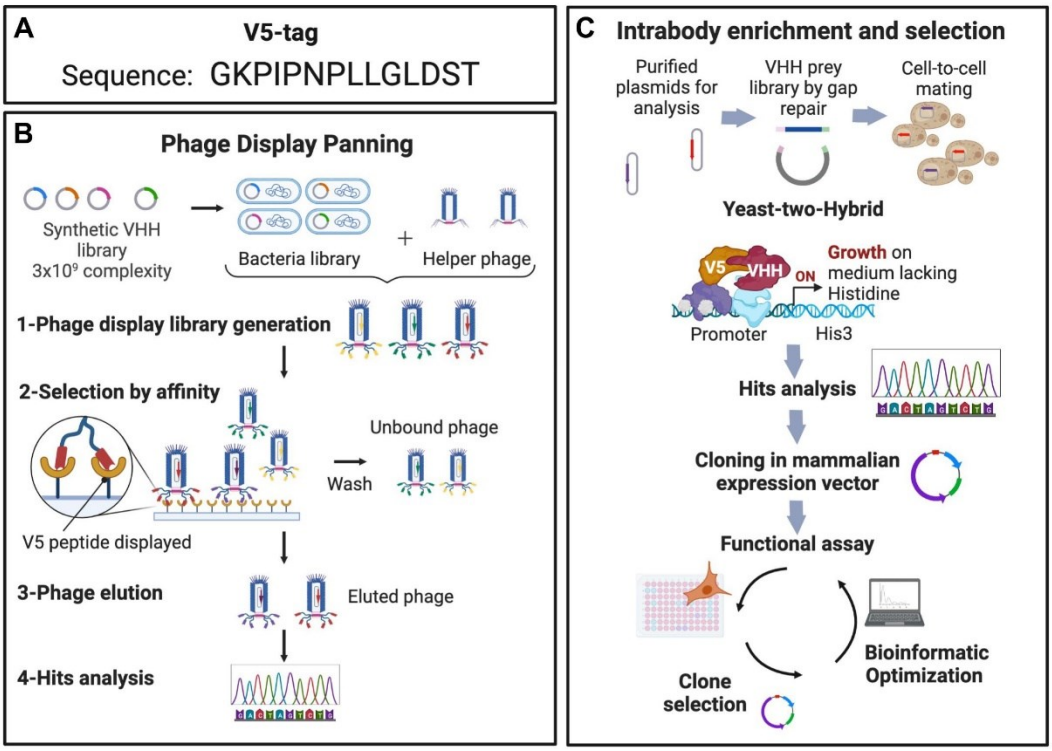

Figure 3.1: Overview of the selection of a synthetic nanobody interacting with the V5-tag.

A, Sequence of the V5-tag. **B**, Schematic of the phage-display panning for the enrichment of nanobodies interacting with the V5-peptide tag. **C**, Schematic of the yeast-two-hybrid screening (Y2H) for the enrichment of nanobodies interacting with the V5-peptide tag in an intracellular environment (intrabody).

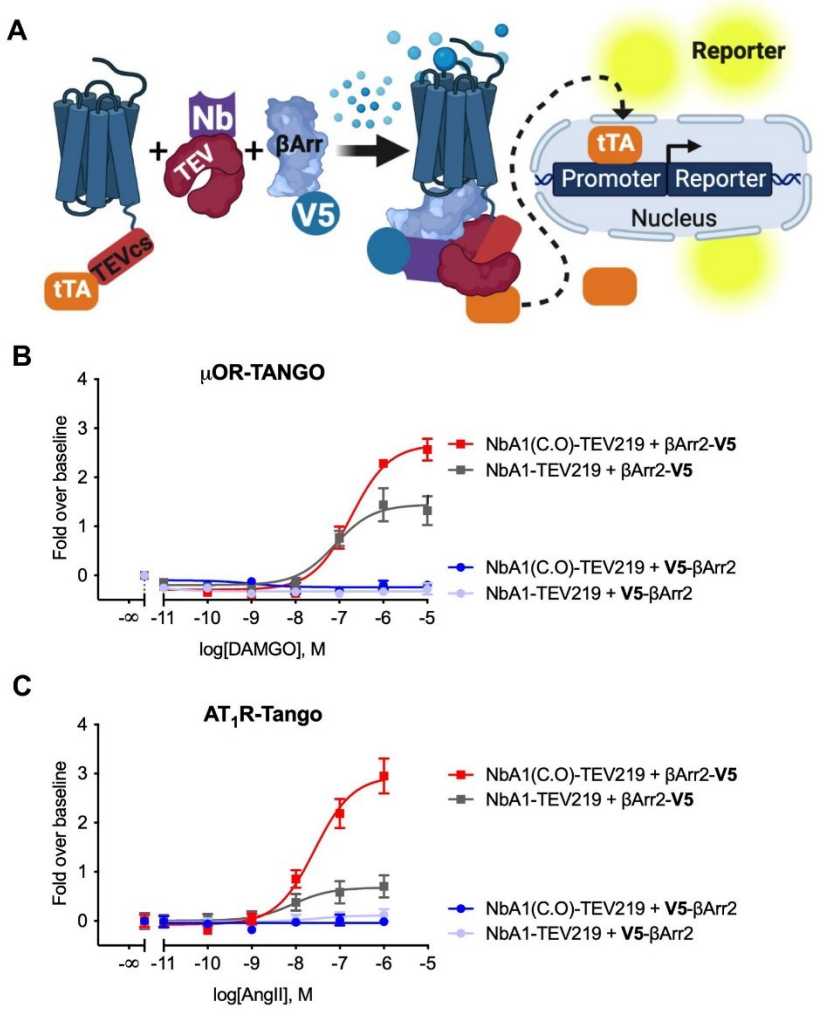

Figure 3.2: The first generation of the anti-V5 nanobody (NbA1) only recognizes the C-terminal positioned V5-tag.

A, Schematic of the protease-dependent cell-based assay (TANGO) used to assay the anti-V5 nanobodies. The original NbA1 clone selected from the Y2H screening was fused with the TEV219 protease and cloned into a eukaryotic expression vector. The initial assessment revealed that the nanobody was not well expressed in HEK293 and codon optimization (NbA1(C.O)) increased its expression and consequently its functional activity. The μ-OR-TANGO (**B**) and AT_1R-TANGO (**C**) were co-transfected with β-arrestin2 carrying a C- or N-

terminal V5-peptide tag along with either the NbA1-TEV219 or NbA1(C.O)-TEV219 fusion protein the receptor stimulated with dose-response agonists, DAMGO for μ-OR and Angiotensin II (AngII) for AT_1R. The original NbA1 clone only recognizes the C-terminally tagged β-arrestin2 (β-arrestin2-V5). Dose-response curves were built using XY analysis for non-linear regression curve and the 3-parameters dose-response stimulation function from GraphPad Prism. Baseline corrected curves were built using the "Remove baseline and column math" function (Value-Baseline/Baseline). Wells in absence of ligand were used as the baseline for each condition. All error bars represent SD of 3 or 4 technical replicates. Data presented are representative of 3 biological replicates.

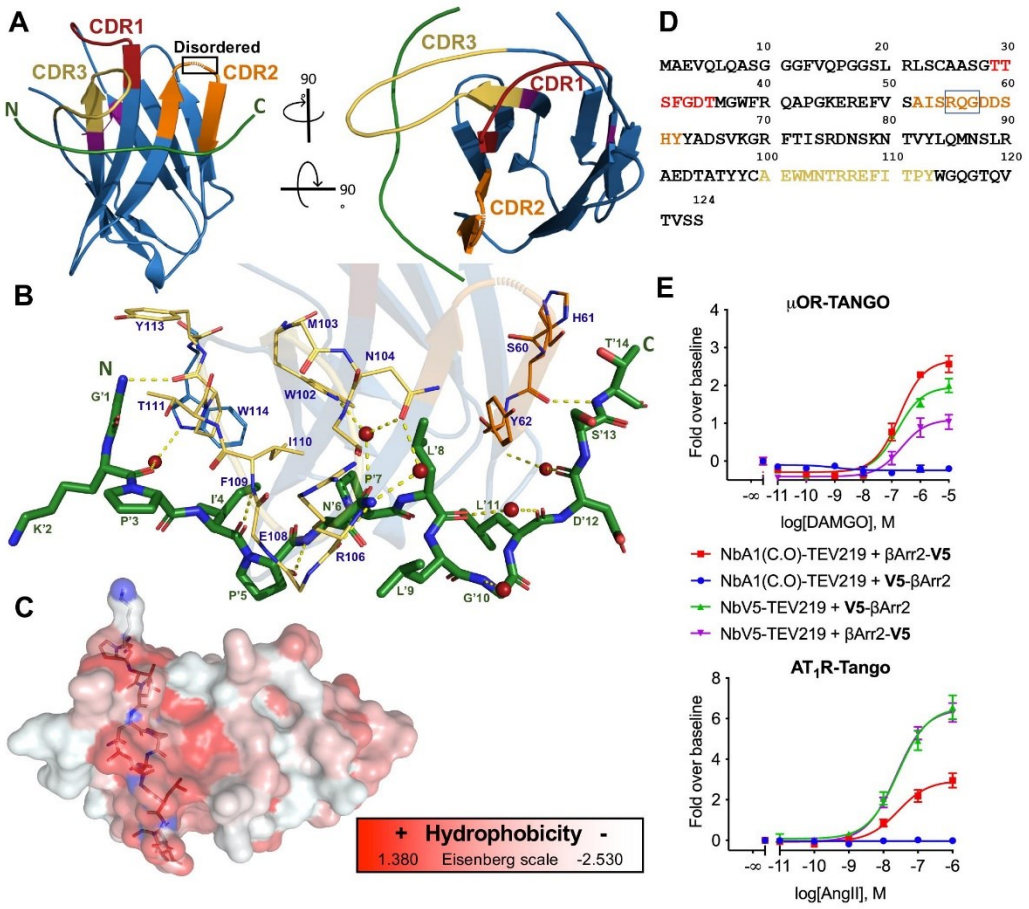

Figure 3.3: Structure of the NbA1 bound to the V5 peptide.

A, Overview of the NbA1:V5 peptide complex shown as cartoon representation. NbA1 is colored in blue with CDRs 1-3 colored in red, orange, and yellow, respectively. Three residues from the CDR2 were not resolved in the refined structure. The V5 peptide is coloured green. **B**, Close-up view of the polar interactions within the complex including water-bridged interaction. The V5-peptide (green) is shown as stick representation with the N-terminal on the left. Interacting residues from the paratope are labeled in blue while the peptide labels are green and marked with a prime symbol. H-bonds are shown as yellow-dashed lines and water

molecules as red spheres. **C**, The NbA1:V5 peptide complex shown as surface representation and colored using the color_h script based on the Eisenberg hydrophobicity scale [64]. **D**, Sequence of NbA1 with CDRs 1-3 colored in red, orange, and yellow, respectively. The square highlights the RQG tripeptide that is disordered in the CDR2 loop. **E**, The μ-OR-TANGO and AT_1R-TANGO were co-transfected with β-arrestin2 carrying a C- or N-terminal V5-peptide tag along with either the NbV5-TEV219 or codon optimized NbA1(C.O)-TEV219 fusion protein the receptor stimulated with dose-response agonists, DAMGO for μ-OR and Angiotensin II (AngII) for AT_1R. The NbV5 recognizes the N- or C-terminally V5-tagged β-arrestin2 with similar logistic parameters (potency and efficacy) while the original NbA1 clone only recognizes the C-terminally tagged β-arrestin2 (β-arrestin2-V5). Dose-response curves were built using XY analysis for non-linear regression curve and the 3-parameters dose-response stimulation function from GraphPad Prism. Baseline correction was performed using the "Remove baseline and column math" function (Value-Baseline/Baseline). Wells in absence of ligand were used as the baseline for each condition. All error bars represent SD of 3 or 4 technical replicates. Data presented are representative of 3 biological replicates.

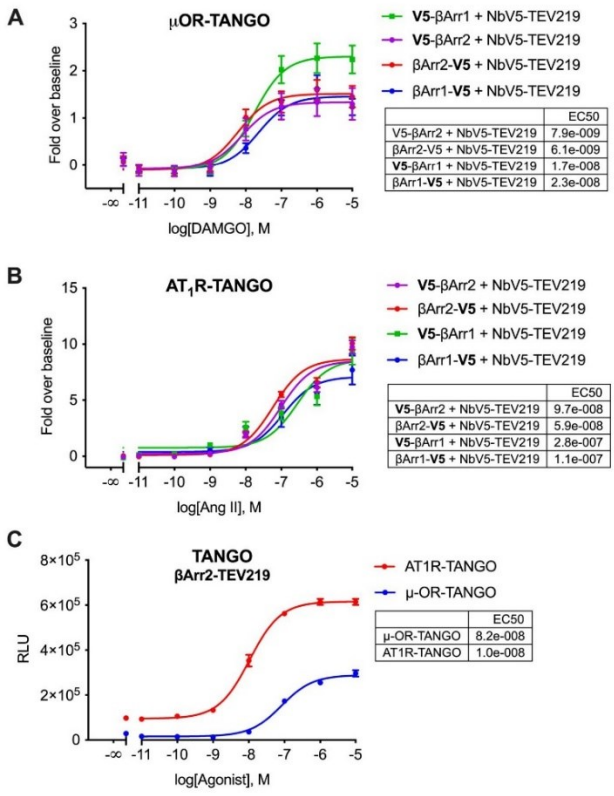

Figure 3.4: NbV5 as a versatile nanobody-based biosensor: application in protease-dependent cell-based assay (TANGO).

The μ-OR-TANGO (**A**) and AT_1R-TANGO (**B**) were co-transfected with β-arrestin1 or β-arrestin2 carrying a C- or N-terminal V5-peptide tag along with the NbV5-TEV219 fusion protein. Dose-response agonist treatments demonstrate the recruitment of β-arrestin in all configurations tested. (**C**) The μ-OR-TANGO and AT_1R-TANGO were co-transfected with β-arrestin2-TEV219 and stimulated with agonists showing that EC50 obtained using the original TANGO is similar to the NbV5-adapted TANGO. Dose-response curves were built using XY analysis for non-linear regression curve and the 3-parameters dose-response stimulation function from GraphPad Prism. Baseline corrected curves were constructed using the "Remove baseline and column math" function (Value-Baseline/Baseline). Wells in absence of ligand were used as the baseline for each condition. All error bars represent SD of 3 or 4 technical replicates. Data presented are representative of 3 biological replicates.

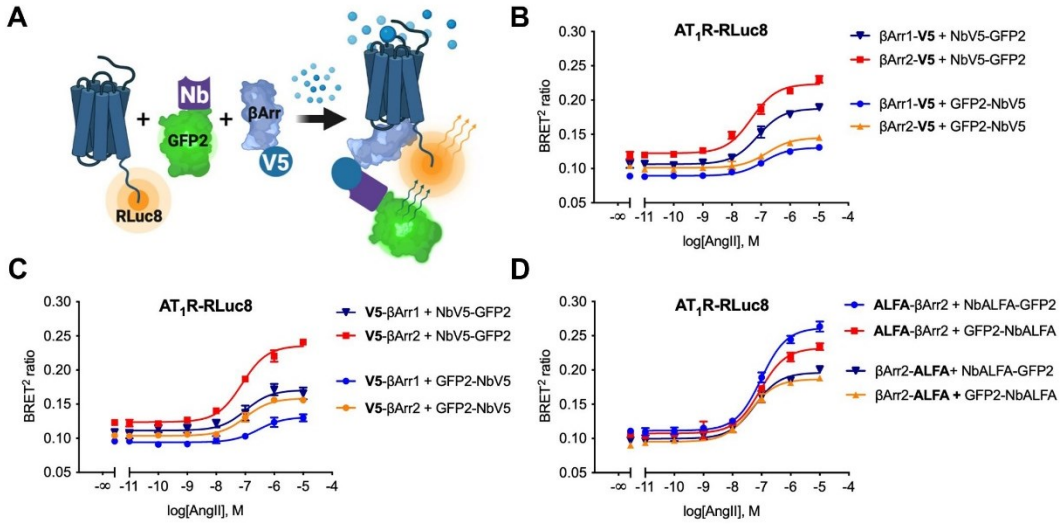

Figure 3.5: NbV5 as a versatile nanobody-based biosensor: application in *B*ioluminescence *R*esonance *E*nergy *T*ransfer (BRET^2).

A, Schematic of the BRET^2 cell-based assay used to evaluate the NbV5. The recruitment of the β-arrestin-NbV5-GFP2 complex to the receptor fused to RLuc8 allows the energy transfer between the *Renilla reniformis* Luciferase mutant (RLuc8) and the green fluorescence protein mutant GFP2 in the presence of the RLuc8 substrate Coelenterazine 400a. **B-C,** NbV5-based detection of β-arrestin1 and β-arrestin2 recruitment at the AT$_1$R-RLuc8. N- and C-terminally V5-tagged β-arrestins were tested as well as both N- and C-terminally GFP2-tagged NbV5. Dose-response curve treatment with angiotensin II reveals equivalent recruitment of β-arrestin1 and 2 at the AT$_1$R. **D**, Similar results were obtained with the nanobody that recognizes the synthetic ALFA-tag (NbALFA). Dose-response curves were built using XY analysis for non-linear regression curve and the 3-parameters dose-response stimulation function. All error bars represent SD of 3 biological replicates with 2 technical replicates (n=6).

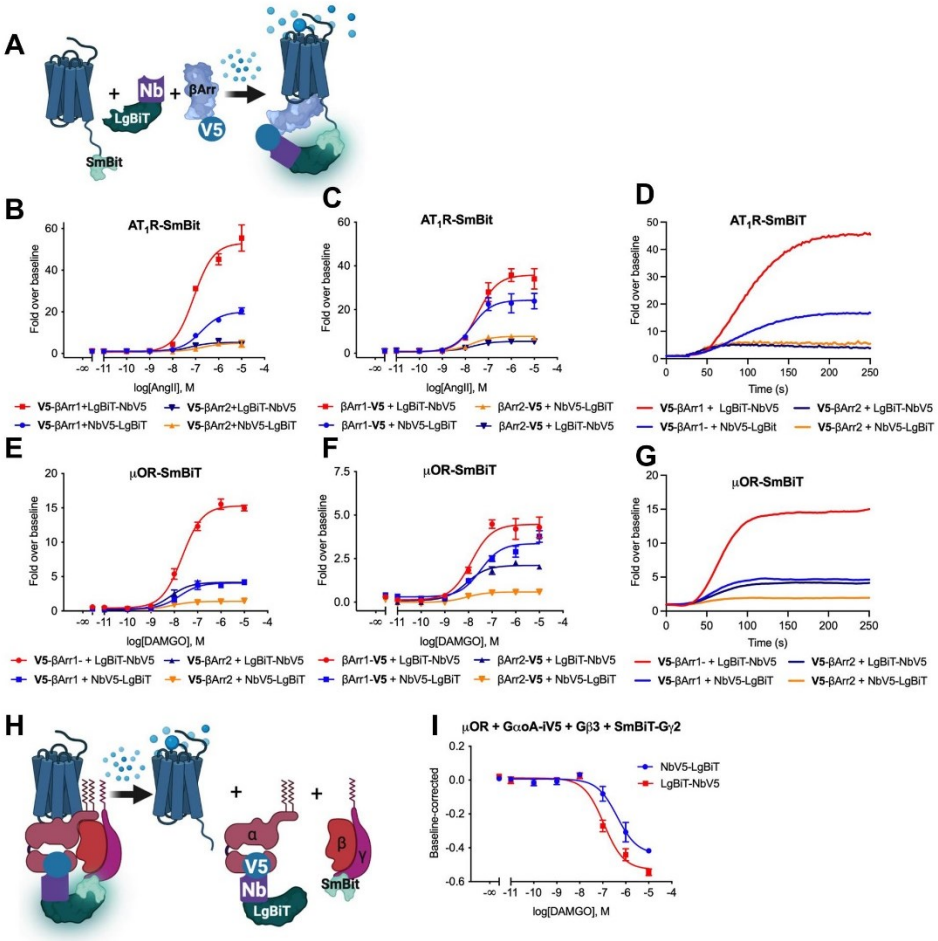

Figure 3.6: NbV5 as a versatile nanobody-based biosensor: application in *Nano*luciferase *Bi*nary *T*echnology (NanoBiT).

A, Schematic of the NanoBiT cell-based assay used to evaluate the NbV5. NbV5-based detection of β-arrestin1 and β-arrestin2 recruitment at the AT_1R-SmBiT (**B,C,D**) and μ-OR-SmBiT (**E,F,G**) was assayed. N- and C-terminally V5-tagged β-arrestin was tested as well as both N- and C-terminally LgBiT-tagged NbV5. (**D,G**), Live kinetic trace at 1 μM agonist are shown in (**D**) for the AT1R and (**G**) for the μ-OR. The trace represents the mean of a quadruplicate experiment. **H**, Schematic of the NanoBiT cell-based assay used to assess the internal V5-tag. **I**, Functional recognition of an internal localized V5-tag was also assayed by NanoBiT by incorporating the V5-tag at position 92 of the GαoA (GαoA-iV5) and measuring

the dissociation from the Gβ3 and SmBiT-Gγ2 dimer upon μ-OR activation with DAMGO. (**B,C,E,F,I**), Dose-response curves were built using XY analysis for non-linear regression curve and the 3-parameters dose-response stimulation function from GraphPad Prism. Baseline correction was performed using the "Remove baseline and column math" function, calculated as Value-Baseline/Baseline **(B-G)**, or Value-Baseline (**I**). Wells in absence of ligand were used as the baseline for each condition. All error bars represent SD of 3 or 4 technical replicates. Data presented are representative of 3 biological replicates.

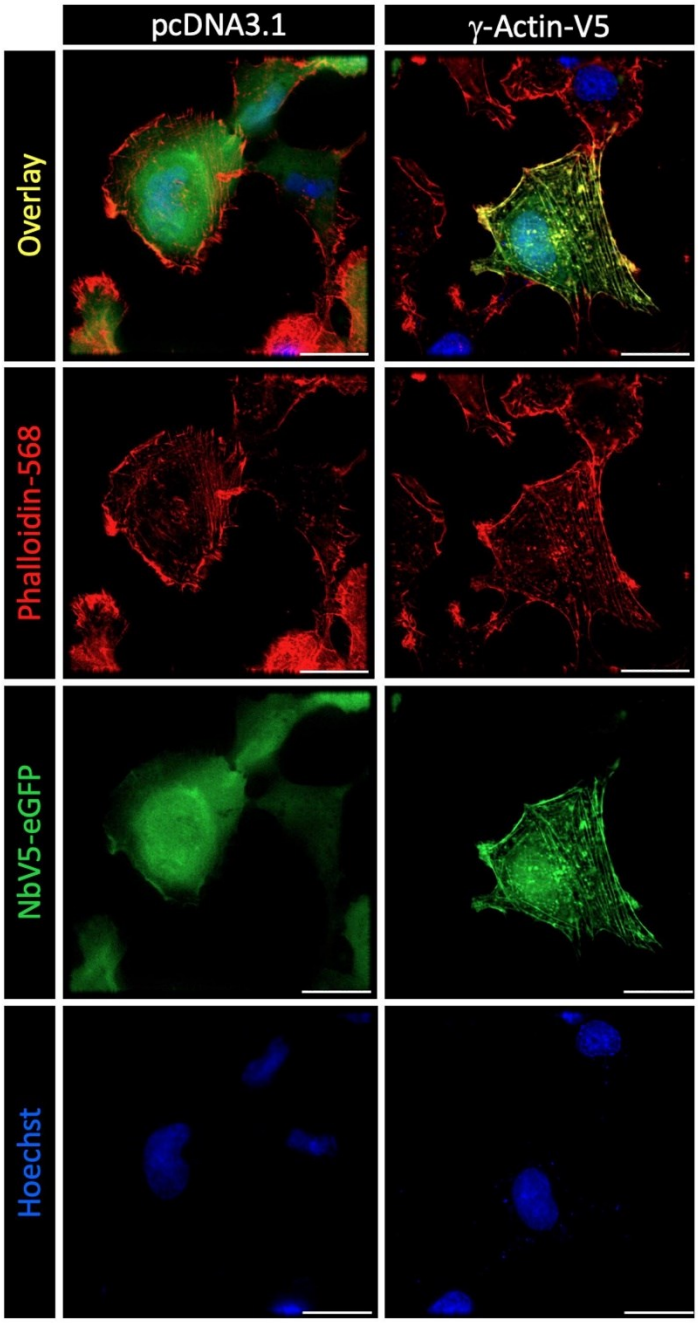
pcDNA3.1
γ-Actin-V5
Overlay
Phalloidin-568
NbV5-eGFP
Hoechst

Figure 3.7: NbV5-based detection of V5-tagged proteins by cell imaging.

Fluorescence imaging of HT1080 cells expressing NbV5-eGFP and ɣ-Actin-V5 or pcDNA3.1+ as a negative control. In the absence of ɣ-Actin-V5, NbV5-eGFP (green) is diffuse throughout the cell while in the presence of ɣ-Actin-V5, NbV5-eGFP is enriched in actin-rich protrusions and structures. Cells were co-stained with the F-actin probe Alexa Fluor 568 phalloidin (red) and the blue DNA stain Hoechst. The overlay is shown on the top panel. Images are representative of 25 cells from three independent experiments. Scale bars are 25 µm.

SUPPORTING INFORMATION

Development of a V5-tag-directed nanobody and its implementation as an intracellular biosensor of GPCR signalling

Manel Zeghal[1]*, Kevin Matte[1]*, Angelica Venes[1], Shivani Patel[1], Geneviève Laroche[1], Sabina Sarvan[1,2], Monika Joshi[1,2], Jean-Christophe Rain[3], Jean- François Couture[1,2], Patrick M. Giguère[1,4]

From the [1]Department of Biochemistry, Microbiology and Immunology, Faculty of Medicine, University of Ottawa, Ottawa, ON, K1H 8M5, Canada; [2]Ottawa Institute of Systems Biology, University of Ottawa, Ottawa, ON K1H 8M5, Canada; [3]Hybrigenics Services, 91000 Évry-Courcouronnes, France; [4]Brain and Mind Research Institute, University of Ottawa, Ottawa, ON, K1H 8M5, Canada

* Contributed equally to the work

Correspondence and requests for materials should be addressed to Patrick M. Giguère (Email : patrick.giguere@uottawa.ca).

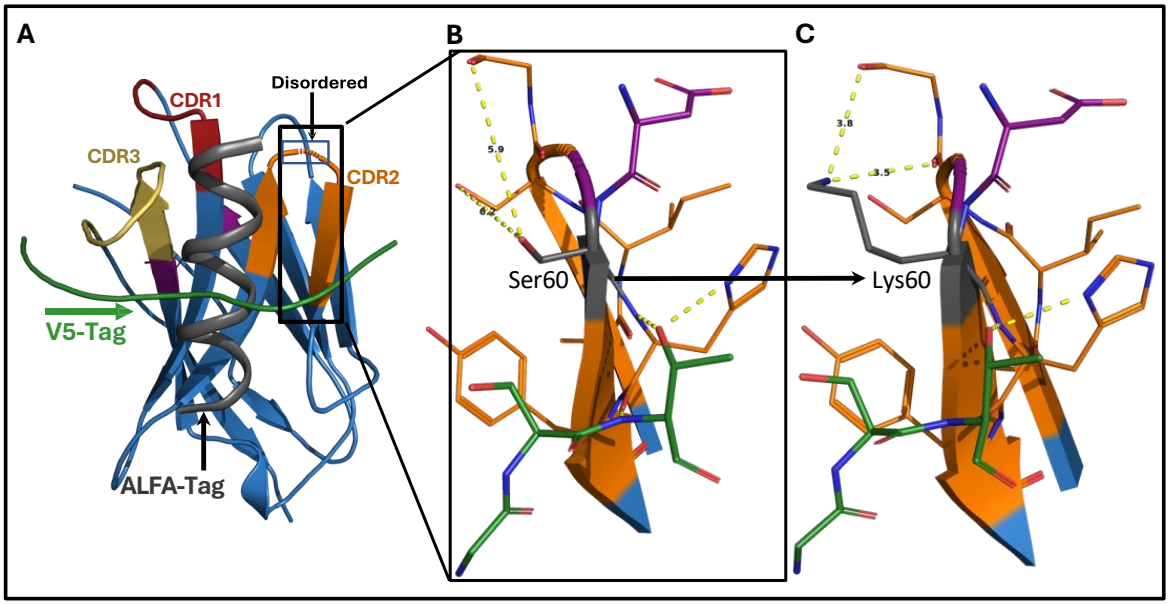

Supplementary Figure 3.1: Structure of the NbA1 bound to the V5 peptide.

A, Overlay of the NbA1:V5 structure with the NbALFA:ALFA (PDB: 6I2G) structure. The NbALFA structure was omitted for simplicity and to present the binding pose of the ALFA-tag, which is at 90 degrees compared with the V5-tag. Using *in silico* maturation and functional studies assessment, the mutations ΔAsp^{59}, Ser^{60}Lys were discovered to substantially improve the behavior of the nanobody. B, Close-up view of the Asp^{59} and Ser^{60} of the CDR2 loop that are juxtaposed to the disordered tripeptide RQG. The Ser^{60} is not involved in any interaction and the distance with the closest residues is shown with a dash line. C, It is hypothesized that mutations ΔAsp59 and Ser^{60}Lys could favorize new intramolecular polar interactions within the CDR2 loop which might stabilize it by reducing entropy.

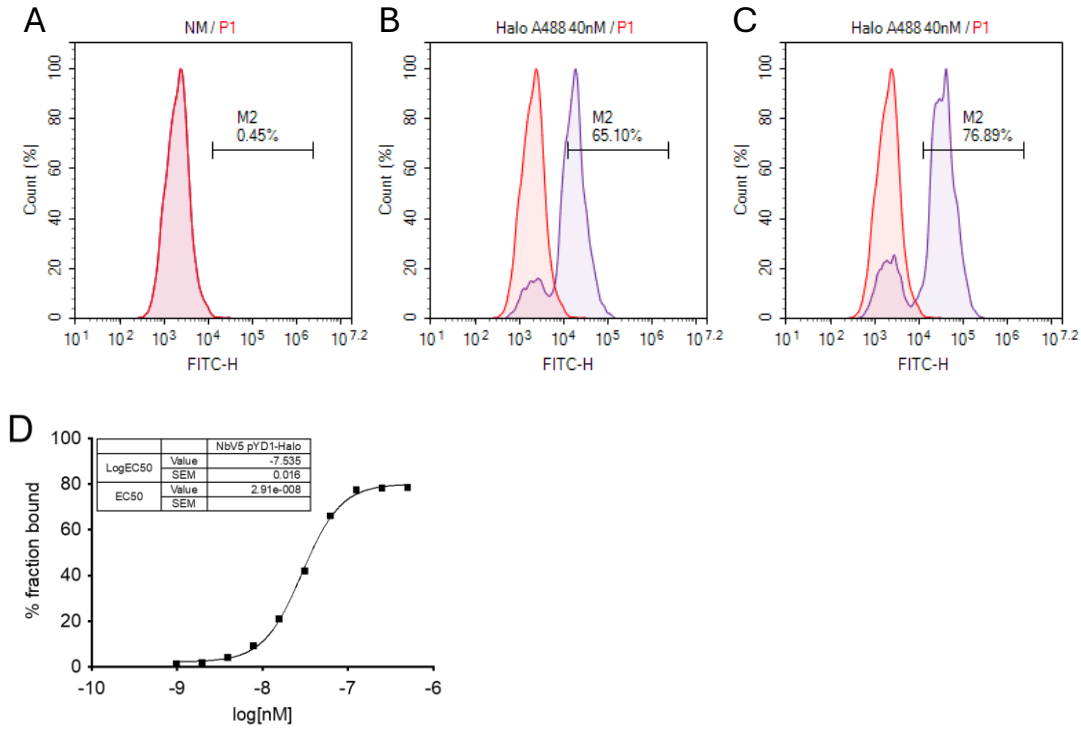

Supplementary Figure 3.2: Affinity measurement of NbV5 by yeast display.

A-C, NbV5 is displayed in pYD1-Halo: A) Unlabelled nanobody, B) Control anti-strep nanobody labeled with 40 nM Halo Alexa Fluor 488, C) NbV5 labeled with 40 nM Halo Alexa Fluor 488. D, Apparent KD measurement of NbV5 determined by yeast surface display. A-C, Data presented are representative of one biological replicates (n=1). D, Data presented are representative of one biological replicates (n=1) in triplicate and represents the mean of % fraction bound.

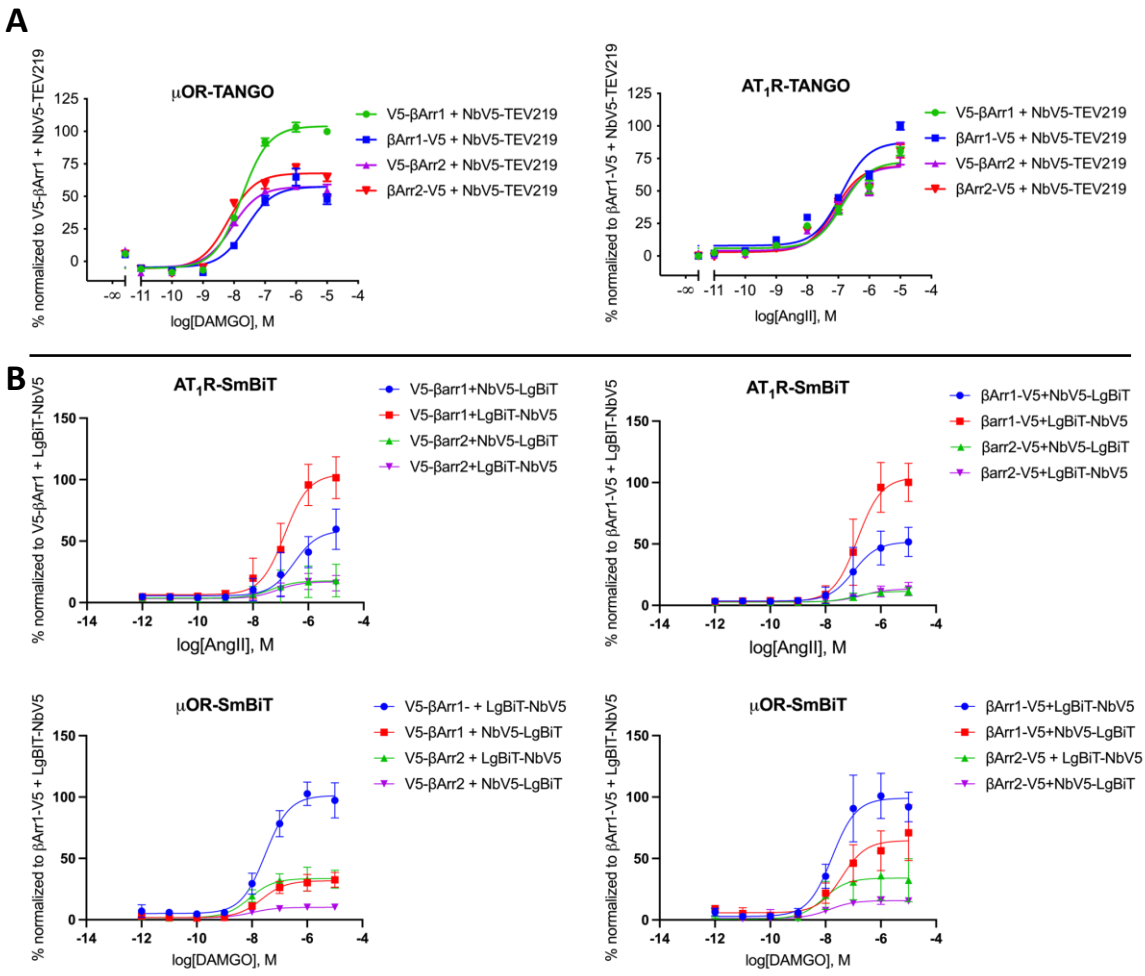

Supplementary Figure 3.3: Reproducibility of NbV5-based biosensor measurements.

Biological replicates from Figure 4 (A) and Figure 6 (B) were normalized and presented as % of the best-fitted curve for each experiment to display the inter- reproducibility. Dose-response curves were built using XY analysis for non-linear regression curve and the 3-parameters dose-response stimulation function from GraphPad Prism. Baseline corrected curved were produced using the "Remove baseline and column math" function (Value-Baseline/Baseline). Wells in absence of ligand were used as the baseline for each condition. Data was normalized using the Normalize function from GraphPad Prism, defining the highest Fold-over- baseline condition as the 100% for all data sets and the minimum of the same experiment as the 0% for all data sets. Data are presented as the % of the best

responding condition. All error bars represent SD of 3 or 4 technical replicates. Data presented are from a minimum of 3 biological replicates.

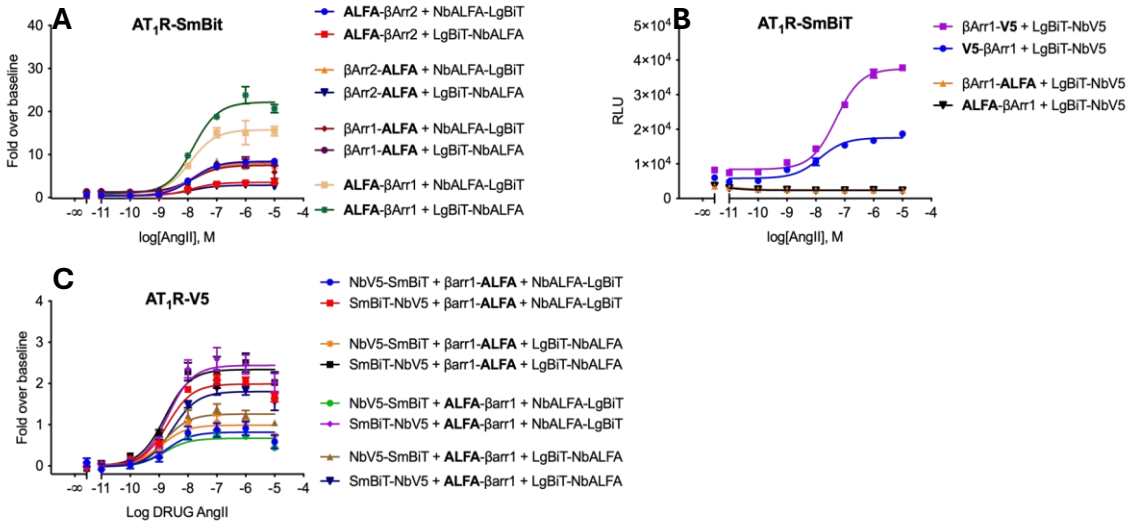

Supplementary Figure 3.4: NbV5 as a versatile nanobody-based biosensor for application in NanoBit.

A, By way of comparison, similar results shown with NbV5 were obtained with the nanobody that recognizes the synthetic ALFA-tag (NbALFA) at the AT1R- SmBiT. NbV5-based detection of β-arrestin1 and β-arrestin2 recruitment at the AT1R-SmBiT was assayed using N- and C-terminally ALFA-tagged β-arrestin, as well as both N- and C-terminally LgBiT-tagged NbALFA. B, The selectivity of NbV5 toward the V5-tag over ALFA-tag was confirmed using NanoBiT. N- and C-terminally V5- or ALFA-tagged β-arrestin1 recruitment at the AT1R-SmBiT using N- and C-terminally LgBiT-tagged NbV5 is shown. C, The multiplexing of the NbV5 with NbALFA was tested using NanoBit. The C-terminally V5-tagged AT1R (AT1R-V5) was co-transfected with N- or C-terminally SmBiT-tagged NbV5, N- or C-terminally ALFA-tagged β -arrestin1 and N- or C-terminally LgBiT tagged NbALFA. A-C, The receptor was stimulated with a serial dilution of the selective agonist Angiotensin II (AngII) and maximum relative light unit (RLU) extracted. Dose-response curves were built using XY analysis for non-linear regression curve and the 3-parameters dose-response stimulation function from GraphPad Prism. Baseline correction was calculated using the "Remove baseline and column math" function (Value-Baseline/Baseline). Wells in absence of ligand were used as the baseline for each condition. All error bars represent SD of 3 or 4 technical replicates. Data presented are representative of 3 biological replicates.

CHAPTER 4: The protean nature of 14-3-3 proteins in GPCR signaling: highlighting selectivity and dynamic interactions at the NK3 receptor interface

The protean nature of 14-3-3 proteins in GPCR signaling: highlighting selectivity and dynamic interactions at the NK3 receptor interface

Manel Zeghal[1], Danylo Aloshyn[1], Samantha K. Rogers[1], Geneviève Laroche[1],Patrick M. Giguère[1,2,3*]

From the [1]Department of Biochemistry, Microbiology and Immunology, Faculty of Medicine, University of Ottawa, Ottawa, ON, K1H 8M5, Canada; [2]Ottawa Institute of Systems Biology, University of Ottawa, Ottawa, ON K1H 8M5, Canada; [3]Brain and Mind Research Institute, University of Ottawa, Ottawa, ON, K1H 8M5, Canada

*Correspondence and requests for materials should be addressed to Patrick M. Giguère (Email: patrick.giguere@uottawa.ca).

ABSTRACT

Informed by a continuously emerging body of data, current proposed models of GPCR signalling and trafficking are moving beyond the canonical paradigm of ligand-induced signal transduction mediated predominantly by G-proteins and β-arrestins. Indeed, the various outcomes of GPCR activation are precisely regulated by a number of elements, including GPCR-interacting proteins, isoform diversity, as well as GPCR phosphorylation patterns catalyzed by kinases. One underexplored source contributing to the pleiotropic activities of GPCRs emerges from the dynamic recruitment and dissociation of 14-3-3 proteins, a family of ubiquitously expressed adaptor proteins that modulate key cellular processes. Recent studies have demonstrated that GPCR-14-3-3 protein interactions are isoform-specific and can be modulated in a spatiotemporal manner by ligands; however, there has yet to be an investigation of 14-3-3 dynamics across all seven human isoforms and across a large panel of GPCRs. As such, this work is the first characterization of proximal GPCR-14-3-3 protein interactions at a GPCRome scale, which was accomplished through the construction of stable reporter cell lines expressing all human 14-3-3 isoforms and performing cell-based high-throughput screening to probe approximately 100 GPCR interactomes. Among the notable findings from this screen, the NK3 receptor emerged as a promising candidate for in-depth examination of 14-3-3 protein modulation of GPCR activity, especially considering that scant literature exists regarding NK3 signalling, including in relation to G-proteins or β-arrestins. Our findings suggest different combinations of hetero- and homodimers of 14-3-3 isoforms result in different functional outcomes at NK3, such as the

upregulation of NK3 surface expression by 14-3-3γ. Furthermore, 14-3-3γ was found to modulate canonical signalling pathways by attenuating G-protein dissociation and increasing β-arrestin recruitment signals.

INTRODUCTION

G protein-coupled receptors (GPCRs) are pivotal mediators of cellular signaling, interacting with a plethora of intracellular proteins to orchestrate diverse physiological responses. Canonically, GPCRs engage G-proteins and β-arrestins to propagate and regulate signaling pathways. However, burgeoning evidence underscores the significance of the broader interactome, comprising proteins recruited to or situated in close proximity to the receptor, thereby modulating GPCR function and cellular outcomes(Kotliar et al., 2023). These cytoplasmic scaffolding proteins, which include postsynaptic density 95/disc large/zona occludens-1 (PDZ) domain-containing proteins (PDZ proteins), and non-PDZ proteins, act as molecular organizers, bringing together multiple proteins to form functional complexes that regulate various aspects of GPCR signaling(Magalhaes et al., 2012). PDZ proteins, including Synapse-associated protein 97 (SAP97), Postsynaptic-density protein 95 (PSD-95), Sorting nexin 27 (SNX27), and Multiple PDZ domain protein (MUPP-1), have been implicated in the regulation of ERK1/2 activation, G protein-mediated signaling, and interactions with other signaling molecules like phospholipase C (PLC) and Rho GTPases(Walther and Ferguson, 2015). For example, the somatostatin receptor subtype 5 (SSTR5) interacts with SNX27, facilitating receptor recycling back to the plasma membrane and contributing to the availability of functional receptors for agonist binding(Bauch et al., 2014). Additionally, non-PDZ proteins interact with GPCRs and contribute to the regulation of downstream signaling cascades. These proteins, such as A-kinase anchor proteins (AKAPs) and Janus kinase (Jak)-2, coordinate the subcellular localization of signaling molecules such as PKA and Jak/STAT, thereby modulating GPCR signaling in a spatially and temporally controlled manner(Walther and Ferguson, 2015).

One important family of non-PDZ proteins are 14-3-3 proteins, comprised of seven mammalian isoforms (β, γ, ε, ζ, η, θ and σ) which interact with various GPCRs such as the FSH receptor and

PAR-4, modulating receptor trafficking, stability, and signaling properties(Cohen et al., 2004)(Cunningham et al., 2012)(Pennington et al., 2018). Central to the functionality of 14-3-3 proteins is their predisposition to form homo- and heterodimers, facilitating interactions with an extensive array of cellular proteins via their distinctive phosphoserine/phosphothreonine-binding activity. This binding activity has been historically elucidated through the identification of phosphorylation-dependent interactions, notably via binding motifs I (RXX[pS/pT]X[P/G]) and II (RX[F/Y]X[pS/pT]X[P/G])(Johnson et al., 2010). However, it has been demonstrated that 14-3-3 proteins also exhibit interactions with diverse phosphorylated serine/threonine motifs that deviate from these motifs, lacking an arginine at the −3 position and a proline/glycine at the +2 position, such as the 14-3-3ζ complex with phosphorylated proapoptotic protein BAD(Srdanović et al., 2022),(Sluchanko et al., 2021). Moreover, 14-3-3 interactions can also occur independent of phosphorylation, such as the interaction between 14-3-3ζ and exoenzyme S, underscoring the complex regulatory landscape governing 14-3-3 protein interactions (Ottmann et al., 2007).

Interestingly, 14-3-3 isoforms exhibit differential expression across tissues, suggesting specific roles tailored to individual cellular contexts. In neuronal tissues, 14-3-3 isoforms such as ζ and γ are often abundantly expressed, reflecting roles in neuronal signaling and synaptic function. Conversely, in cardiac tissues, isoforms such as τ and ϵ exhibit higher expression levels, indicating possible involvement in cardiac muscle contraction, ion channel regulation, and cardiomyocyte physiology, whereas the σ is most prominently expressed in skin tissues, potentially contributing to processes such as epithelial cell proliferation, differentiation, and wound healing(Gogl et al., 2021). Finally, dysregulation of 14-3-3 signalling is often implicated in various diseases, including cancer, neurodegenerative disorders such as Alzheimer's disease, Parkinson's disease, Huntington's disease, and metabolic conditions such as diabetes and obesity(McFerrin et al., 2017).

Experimental techniques such as yeast two-hybrid, *in vitro* and *in vivo* pull-down, and affinity binding techniques have identified a number of 14-3-3-GPCR complexes. Moreover, the LinkLight assay has been employed to study these dynamic interactions in living cells, pharmacologically characterizing 36 GPCR-14-3-3 interactions, specifically with 14-3-3ε and 14-3-3γ(Yuan et al., 2019; Kongsamut and Eishingdrelo, 2023). Importantly, the recruitment or dissociation of 14-3-3 isoforms at a given receptor is isoform-selective, such as how the

recruitment of 14-3-3γ but dissociation of 14-3-3ε was observed at the delta-opioid receptor (DOR)(Eishingdrelo et al., 2022). Different ligands can also regulate GPCR-14-3-3 interactions in a spatiotemporal manner. For example, Eishingdrelo et al. (2022) demonstrated that adrenaline-induced ADRA2A-14-3-3γ and ADRA2A-β-arrestin-2 signals quickly decreased, whereas lofexidine-induced ADRA2A-14-3-3γ and ADRA2A-β-arrestin-2 signals were long-lasting(Eishingdrelo et al., 2022).

One key knowledge gap however is that these existing reported interactions have focused on one or two isoforms of 14-3-3 proteins, neglecting the complexity introduced by the seven distinct isoforms, each with unique tissue-specific expression patterns. Moreover, the effect of 14-3-3 interactions must also be taken into account in relation to other signalling pathways, such as canonical G-protein and β-arrestin activity. The interplay between 14-3-3 proteins and other intracellular partners, such as G-proteins and arrestins, has been somewhat described, but further characterization is warranted. As such, this study aimed to address this by systematically probing interactions between GPCRs and all seven isoforms of 14-3-3 proteins at a large scale. Additionally, we focused our work by further delineating 14-3-3 interactions at a select receptor, tachykinin receptor 3 (NK3), by examining the functional outcomes of homo- and heterodimerization, identifying and studying potential 14-3-3 binding sites, and investigating the potential interplay between 14-3-3 isoforms, and G-proteins and arrestins, thereby highlighting the multifaceted nature of 14-3-3 proteins in GPCR signaling.

RESULTS

In the context of expanding the Tango assay, which is widely used to track β-arrestin2 recruitment to GPCRs, a reporter cell line of HEK293T background carrying a luciferase gene under the control of the TRE-Tight promoter, dubbed HTTL cells, was formerly established(Zeghal et al., 2023). In the same vein as the Tango-Trio platform, HTTL cells were chosen for the foundation of reporter cell lines that would stably express all seven 14-3-3 isoforms, which were transduced with cumate-inducible pcDH lentiviral vectors encoding 14-3-3-TEV219 fusion proteins. Prior to selecting monoclonal cell lines by functional assay, Tango-fused GPCRs that have previously documented interactions with 14-3-3 isoforms were assessed for their propensity to recruit or dissociate the

seven different isoforms, including CHRM1, CHRM3, DRD2, ADRB2, SSTR4, CNR1, and OPRK1(Kongsamut and Eishingdrelo, 2023). As shown in **Suppl. Fig. 4.1A**, the Cannabinoid receptor type 1 (CNR1-Tango) receptor exhibited interactions with all 14-3-3 isoforms, including 14-3-3σ; this novel finding is especially noteworthy, as prior to our work, all isoforms except σ have been shown biochemically to interact with GPCRs(Li et al., 2016). Corroborating a previous paper by Yuan et al. (2019), we also observed a dissociation signal at CNR1 at not only 14-3-3ε, but across all 7 isoforms(Yuan et al., 2019). Selected as the superior candidate for screening purposes, we proceeded to create stable cell lines in HTTL lineage expressing 14-3-3-TEV219 for each of the isoforms, subjecting potential clones to transient transfection with CNR1-Tango; final cell lines were selected based on suitable pharmacological parameters, including baseline ("bottom", E0), efficacy ("top", Emax), potency (EC50), and fold change (Emax/E0), as depicted in **Suppl. Fig. 4.1B**. Using the established monoclonal cell lines, parallel interrogations were achieved at a GPCRome scale using a panel of approximately 100 GPCR Tango constructs, investigating proximal 14-3-3 activities at the ligand-activated receptor state. Agonist screenings, illustrated as a heat map in **Fig. 4.1A**, unveiled varying patterns within GPCR subfamilies; some consistently displayed uniform responses across all isoforms, as exemplified by the widespread dissociation for the alpha-adrenergic receptors or recruitment for galanin receptors, while others exhibited receptor-specific differences, such as within the 5-HT family where dissociation signals were detected at all isoforms for 5-HT2C, whereas recruitment was primarily detected at 5-HT4. Moreover, as previously reported, GPCRs can selectively recruit certain isoforms while dissociating others, a dichotomy that underscores the nuanced interplay between receptor conformational states and isoform-specific interactions with 14-3-3 proteins. For example, the majority of isoforms exhibited agonist-induced signal increases at PTAFR, but a significant decrease was observed for 14-3-3ζ. While our panel of selected GPCRs contains receptors that have already documented 14-3-3 interactions to corroborate existing work, such as recruitment of 14-3-3ε at KISSR and dissociation at C5AR1(Yuan et al., 2019), the large majority of our findings have not been previously reported given the extensive number of GPCRs screened and the utilization of 14-3-3 probes of all isoforms. As previously mentioned, the screening identifies novel findings regarding the interaction of sigma isoform with several GPCRs, a phenomenon previously unexplored; for instance, 14-3-3σ was found to be significantly present in the interfaces of MC2R and SUNCR1 receptors. Validation of top hits from these screens was carried out in

dose-response curve with selective agonists, confirming the diversity observed spanning several GPCRs and 14-3-3 isoforms (**Fig. 4.1B**). Receptors used for secondary screening included those with previously reported interactions, such as CHRM1, as well as novel hits, such as MAS1. Among these, TACR3, also known as the neurokinin or tachykinin 3 receptor (NK3), emerged as a source of intrigue, primarily by its robust recruitment of all 14-3-3 isoforms, and yet, no similar parallels with TACR1 and TACR2 despite its high homology with these receptors(Steinhoff et al., 2014). NK3, predominantly activated by the neuropeptide neurokinin B (NKB), is involved in various physiological processes, including the regulation of the reproductive system and central nervous system, such as modulation of mood, anxiety, and stress responses(Chu et al., 2020). The selection of NK3 as a focal point for subsequent investigations with 14-3-3 is also advantageous given the paucity of literature regarding its pharmacological characterization and signaling dynamics but also given the recently approved (May 23, 2023) NK3 antagonist, Fezolinetant, to treat moderate to severe hot flashes in menopausal women(Wright et al., 2023).

The propensity of 14-3-3 proteins to dimerize, owing to the numerous hydrophobic and electrostatic interactions at the interface between the N-terminal domains of monomers, is crucial for their roles as cellular modulators(Obsilova and Obsil, 2022). However, different 14-3-3 isoforms have been shown to possess varying abilities to form homo- and heterodimers, largely due to the varying number of salt bridges at the interface of the dimers. For example, 14-3-3σ has been shown to predominantly form homodimers, in contrast to 14-3-3ε, which largely forms heterodimers with any isoform (excluding 14-3-3σ); the other isoforms do not exhibit substantial preference and can form either hetero- or homodimers(Gardino et al., 2006). Previous studies of 14-3-3 and GPCR interactions have yet to investigate the functional consequences of different homo- or heterodimer pairs with regard to signalling consequences. Overexpressing a single 14-3-3 isoform, may lead to a disproportionate representation of homodimers or limited heterodimer formation with endogenous 14-3-3 isoforms in the host cell line. This consideration should not be neglected, as certain 14-3-3 binding partners exhibit selective interactions with specific homo- or heterodimers, such as how 14-3-3ζ/τ heterodimers specifically regulate phosphatase Slingshot (SSH1) activity in keratinocytes(Kligys et al., 2009), or the specific heterodimer of 14-3-3β/ε for aldosterone regulation of the epithelial sodium channel (ENaC)(Liang et al., 2008). Thus, to investigate the potential implications of different dimer configurations on 14-3-3 recruitment and

dissociation, NK3 was transiently transfected in the previously established 14-3-3-TEV219 stable lines, along with the individual overexpression of 14-3-3-V5 isoforms and pcDNA3.1 as a control (**Fig. 4.2**). Western blot analysis confirmed the expression of all 14-3-3-V5 constructs (**Suppl. Fig. 4.2**). Our findings reveal nuanced effects of isoform overexpression and consequent dimer formations on 14-3-3 recruitment dynamics. Interestingly, a substantial increase in the baseline signal was observed when overexpressing 14-3-3γ in the majority of stable cell lines. It is hypothesized that 14-3-3γ increases basal dimer interactions in the absence of agonist stimulation, or this isoform promotes NK3 cell surface expression; the latter hypothesis was confirmed by ELISA (**Suppl. Fig 4.3**). Certain isoforms, specifically β, ε, and σ, exhibited minimal variation in potency and fold change compared to the control. This indicates either that only the homodimer is formed with the stably expressed 14-3-3-TEV219 proteins (and overexpression of 14-3-3V5s have no effect), such as presumed for 14-3-3σ, or that homo- and/or heterodimers are equally formed with no preference, such as the case for 14-3-3β. However, overexpression of 14-3-3τ or 14-3-3γ in conjunction with ζ, τ, γ, and η isoforms resulted in increased recruitment of the 14-3-3-TEV219 fusion construct to the receptor, and thus increased fold changes. The results depicted in **Fig. 4.2** suggest that heterodimers 14-3-3ζ/γ, 14-3-3η/γ, 14-3-3 τ/γ, and 14-3-3η/τ are selectively recruited to NK3 receptor. Despite observing these effects at NK3, overexpression of different 14-3-3-V5 isoforms failed to display similar augmented recruitments at NK1 and NK2, as evidenced in **Suppl. Fig. 4.4**.

To elucidate the molecular determinants involved with 14-3-3 binding at NK3, we employed bioinformatics tools to identify potential binding sites within TACR3. PhosphoSitePlus® and 14-3-3-Pred software identified five putative critical residues involved in the NK3 binding sites of 14-3-3, specifically S399, T404, and T410 (PhosphoSitePlus®), as well as T118 and S444 (14-3-3Pred)(Hornbeck et al., 2012)(Madeira et al., 2015). To identify which of the aforementioned residues contribute to binding, site-directed mutagenesis was carried out on NK3-Tango receptor, switching the putative phosphorylation sites serine/threonine to alanine, and the mutated constructs were tested in functional assay compared to the WT receptor. As confirmed by Western Blot, all tested NK3 receptors harboring said mutations retained surface expression (**Suppl. Fig. 4.3**). As shown in **Fig. 4.3A**, TACR3-Tango mutant harboring the T118A mutation largely decreased or for certain isoforms such as γ, completely disrupted 14-3-3 binding; the other mutated residues did

not have any similar effect. Interestingly, NK3-T118A mutant receptor dose-response profiles had significantly higher baselines compared to WT and all other mutants. Similarly to the effect observed in the 14-3-3-TEV219 stable cell lines, T118A mutation diminished but did not completely abolish β-arrestin recruitment signal, suggesting a multifaceted role for T118 residue in multiple signalling pathways (**Fig. 4.3B**). This residue was the only predicted site that is not located on the receptor's C-terminus; moreover, the site closely resembles binding motif I, albeit it is not entirely conventional as it lacks a proline/glycine at the +2 position. Interestingly, Hauser et al. (2018) previously reported this residue (2.37x37) as a site of natural genetic variation, specifically T118I (Hauser et al., 2018). This mutation was listed to be probably damaging, with inferred arrestin interaction; moreover, this site was predicted to have high surface accessibility based on ScanSite4.0. Seeing as 14-3-3γ overexpression resulted in increased cell surface expression of NK3, it is hypothesized that T118 might be implicated in the trafficking dynamics of the receptor, seeing as its mutation completely abolished 14-3-3γ recruitment.

Regarding the association of 14-3-3 and canonical G-protein and β-arrestin signalling, previous literature has determined that agonist-induced GPCR and β-arrestin interactions occur at an earlier timeframe than with 14-3-3 (Yuan et al., 2019). Motivated by this paradigm, we sought to elucidate the functional consequences of 14-3-3 overexpression on β-arrestin recruitment. Employing the NanoBiT assay, we investigated the recruitment dynamics of β-arrestin alone versus β-arrestin in conjunction with 14-3-3 τ and/or γ isoforms. As depicted in **Fig. 4.4**, the addition of 14-3-3 proteins, particularly γ isoform, results in an increased β-arrestin detection signal, suggesting 14-3-3 proteins facilitate in their recruitment. As for the G-protein-mediated pathway, 14-3-3 was previously shown to modulate RGS proteins, which act as GTPase activating proteins, more specifically, 14-3-3 prevents RGS from interacting with Gα, and ultimately indirectly prolonging G-protein signaling(Gerber et al., 2018). Leveraging the bioluminescence resonance energy transfer (BRET) method, G-protein dissociation was monitored at NK3, firstly by testing different combinations of Gα/β/γ probes from the TRUPATH system, arriving at Gαq/β3/γ9 as the most optimal array for the best detectable signal (**Suppl. Fig 4.6**), aligning with the established findings of NK3 as a primarily Gαq-coupled receptor (Laniyonu et al., 1988). Subsequent analyses, depicted in **Fig. 4.5A**, reveal additional insights into the regulatory role of 14-3-3 proteins on G-protein signaling dynamics. The addition of 14-3-3 proteins elicited a decrease in basal BRET,

accompanied by a reduction in the net BRET ratio. These findings suggest that 14-3-3 proteins do not competitively inhibit G-protein binding, but rather are indicative of attenuated G-protein dissociation, corroborating previous work. To gain further insight into the effects of 14-3-3 on the canonical G-protein pathway, downstream G-protein signalling was indirectly measured using the GloSensor™ cAMP assay. As shown in **Fig. 4.5B**, the pattern observed parallels those obtained by BRET2, in that 14-3-3 addition causes a decrease in cAMP production, and thus reduction in G-protein activation. Seeing as how the GloSensor system monitors activation of Gαi or Gαs-coupled receptors, these results suggest the cAMP activation downstream of NK3 is reliant upon Gβ/γ, as NK3 primarily signals through Gαq and does not couple to Gαi or Gαs (Laniyonu et al., 1988;Oury-Donat et al., 1995).

DISCUSSION

G protein-coupled receptors (GPCRs) mediate the transduction of extracellular stimuli into conformationally-driven intracellular signals, in turn regulating a multitude of biological processes. These transduction machineries interact with various cytosolic and transmembrane proteins throughout their life cycle, by which they regulate GPCR function, including expression at the cell surface, receptor-ligand specificity, endocytosis, and recycling, as well as fine-tuning GPCR signalling. 14-3-3 proteins are prevalent members of the proximal interactome of the majority of GPCRs, however, the role of these interactions is not well characterized, especially at an isoform-specific level.

By establishing cumate-inducible reporter stable cell lines expressing 14-3-3-TEV219 fusion proteins of all seven human isoforms, we assessed the interaction propensities of these isoforms with various Tango-fused GPCRs previously documented to interact with 14-3-3 proteins, as well as a large array of unreported receptors. The selection of potential monoclonal stable cell lines for all 7 14-3-3 isoforms was completed, with pharmacological parameters verified in a Tango-based functional assay using the previously determined partner CNR1; a dissociation of all 14-3-3 isoforms was observed, corroborating past studies demonstrating equivalent activity with the 14-3-3ε isoform. Given the few reports of GPCR-14-3-3 interactions, we sought to extend these works

and perform parallel interrogations at a GPCRome scale using these established monoclonal cell lines. Proximal 14-3-3 activities were screened at ligand-activated receptors using a panel of approximately 100 GPCR Tango constructs, revealing diverse patterns of 14-3-3 recruitment and dissociation within different subfamilies, such as uniform dissociation, uniform association, or receptor-specific differences within a given subfamily, or the specific recruitment of certain 14-3-3 isoforms while others are dissociated at certain GPCRs; these results underscore the selective nature of GPCR and 14-3-3 isoform interactions. GPCRome screening also revealed that 14-3-3 interactions are a common phenomenon, which corroborates previous bioinformatic analyses that revealed approximately 90% of GPCRs contain at least one putative 14-3-3 binding motif. Strikingly, certain GPCRs were found to interact with 14-3-3σ, marking a novel discovery as this isoform had not been previously shown to interact with GPCRs biochemically.

Validation of agonist-induced hits, specifically to confirm if potential GPCR-14-3-3 interactions are isoform- selective or promiscuous among multiple or all 7 isoforms, confirmed NK3 to be an interesting hit, as it recruits all seven 14-3-3 isoforms to a robust degree; despite its high homology with TACR1 and TACR2, these receptors did not display similar interactions. This receptor's involvement in regulating mood, anxiety, and stress responses, along with its critical role in the reproductive system, underscores its importance in further investigations given the potential therapeutic applications, especially given the lack of work done regarding its signalling dynamics.

The propensity of 14-3-3 proteins to form homo- and heterodimers, which is influenced by the number of salt bridges at the dimer interface, plays a significant role in their function as cellular modulators. However, research often focuses on one or two isoforms of 14-3-3 proteins, thus the functional consequences of 14-3-3 dimerization on signalling outcomes, be it homo- or heterodimerization, remain largely underexplored. With NK3 chosen as the linchpin of subsequent investigations, overexpression of specific 14-3-3 isoforms in our stable cell lines demonstrated nuanced effects on 14-3-3 recruitment dynamics, particularly with 14-3-3γ, which increased baseline signals in the majority of stable cell lines. This suggests a potential role for 14-3-3γ in enhancing basal dimer interactions or promoting NK3 cell surface expression. Our findings from Figure 2 reveal isoform-specific dimerization preferences at NK3, as evidenced by the increased recruitment of heterodimers containing the γ isoforms, such as 14-3-3ζ/γ, 14-3-3η/γ and 14-3-3τ/γ.

It should be noted that one limitation of this study is the unknown extent of dimerization, as it is possible that not all binding sites are saturated, or that the observed effects are merely due to increased levels of overexpressed protein without the actual formation of dimers.

Identification of critical residues within NK3 and the functional implications of 14-3-3 activity is crucial, as this would provide a foundation for future research into therapeutic targeting of these interactions. On that account, five critical residues within NK3 were identified to be potentially involved in 14-3-3 binding using bioinformatics tools. Site-directed mutagenesis confirmed the significance of T118 in mediating these interactions, as its mutation disrupted 14-3-3 binding and diminished β-arrestin recruitment, suggesting a multifaceted role in signaling pathways. This site was predicted with high confidence by the consensus sequence prediction tool 14-3-3 Site Finder, which was developed using machine learning to account for intrinsic protein disorder and unbiased mass spectrometry identification rate. With regard to critical residues, a notion to consider is that 14-3-3 proteins may exhibit promiscuous binding, capable of engaging multiple sites within the receptor structure. If one preferred binding site is compromised, compensatory interactions at alternate sites may sustain 14-3-3 association, suggesting potential adaptability of these protein-protein interactions and thus adding another layer of regulatory complexity.

Delving into the functional ramifications of T118 mutation, we postulate its potential impact on receptor recycling dynamics and consequent surface expression. Alterations in TACR3 trafficking, driven by mutations at T118, could influence receptor availability at the cell surface, thereby modulating subsequent interactions with both arrestin and 14-3-3 proteins, suggesting a multifaceted role for this residue in receptor signaling modulation. It should be noted that there is high homology between NK1, NK2, and NK3 in the region encompassing T118, specifically within the intracellular loop 1 (ICL1) and transmembrane domain 2 (TM2), however, these receptors were shown to not substantially exhibit 14-3-3 interactions in our system.

Finally, exploring the functional consequences of 14-3-3 overexpression on β-arrestin recruitment using the NanoBiT assay revealed that 14-3-3 proteins, especially the γ isoform, enhance β-arrestin detection signals. Additionally, our results suggest that 14-3-3 proteins modulate G-protein signaling by attenuating G-protein dissociation and cAMP production, aligning with their known

role in regulating RGS proteins; indeed, multiple studies have confirmed the interactions of 14-3-3 proteins with several types of RGS proteins, including RGS3, RGS4, RGS5, RGS7, RGS16 and RGS18 (Benzing et al., 2000; Niu et al., 2002; Louwette et al., 2012). Thus, we hypothesize that 14-3-3 can modulate the specificity of NK3 signalling in a variety of manners, including sequestering RGS proteins to hinder the dissociation of trimeric G proteins, as well as potentiating receptor recycling, thereby increasing the pool of receptors at the cell surface available for subsequent β-arrestin binding, explaining the increased β-arrestin signals observed in 14-3-3 overexpression. Given that previous literature has established that certain GPCR/14-3-3 complexes can form at the cell membrane in an agonist-independent fashion, while others occur in endosomes in an agonist-dependent manner, the subcellular localization of these interactions, especially those involving the 14-3-3γ isoform, should also be confirmed in future experiments, for example via NanoBiT with FYVE domain to identify endosomes(Reyes-Alcaraz et al., 2022).

Therefore, the composite effect of the wide array of G-protein interacting proteins, such as β-arrestin and 14-3-3 isoforms, as well as receptor type and the type of ligand, must be collectively considered to inform the diversified consequences of GPCR signal transduction. Towards these efforts, by focusing on the multifacetedness of 14-3-3 interactions, especially NK3, we hope this work will aid in establishing more comprehensive pharmacological profiles.

METHODS

Molecular biology

Initial cloning involved the creation of a template 14-3-3-TEV219 construct into pcDNA3.1+ (ThermoFisher), which was accomplished through a double PCR technique. Using pLX307-14-3-3ζ-V5 (MilliporeSigma) as the template, this isoform was amplified by PCR with primers containing NheI-BamHI restriction sites. The TEV219 segment from a β-arrestin2-TEV219/pcDNA3.1+ construct was amplified using primers with BamHI-SwaI restriction sites. The 14-3-3ζ and TEV219 fragments were then fused by combining equal amounts of gel-purified fragments and performing PCR. The pcDNA3.1 vector was digested with NheI-SwaI and ligated with 14-3-3ζ-TEV219, followed by transformation into DH5α bacterial cells, with positive clones identified through Sanger sequencing.

The all-in-one lentivector pCDH-CuO-MCS-EF1α-CymR-T2A-PURO SparQ was from System Biosciences and the PURO resistance gene was previously changed for the BLEO3 resistance using PCR amplification and restriction site cloning (EcoRI-SalI). 14-3-3ζ-TEV219 was swapped into the pcDH vector at NheI-SwaI restriction sites, followed by transformation into XL-10 cells, with positive clones identified through Sanger sequencing. Subsequent cloning of 14-3-3 σ, ε, γ, η, β and τ isoforms was done by PCR amplification, with primers containing NheI-BamHI restriction sites. pcDH-14-3-3ζ-TEV219 was digested with NheI-BamHI to replace 14-3-3ζ with 14-3-3 σ, ε, γ, or τ, followed by transformation into XL-10 cells, and confirmation of positive clones using Sanger sequencing.

pLX307-14-3-3-V5 constructs of ζ, ε, γ, η, and β isoforms are from the MISSION TRC3 Human LentiORF Collection (MilliporeSigma). pLX307-14-3-3τ-V5 and pLX307-14-3-3σ-V5 were purchased through DNASU plasmid repository.

TACR3-Tango DNA, as well as all other GPCR-Tango constructs, were taken from the PRESTO-Tango GPCR Kit, which was gifted from Dr. Bryan Roth and is available through Addgene (www.addgene.org/kits/roth-gpcr-presto-tango/).

The NanoBiT receptor construct TACR3-SmBiT was amplified by PCR by including the SmBiT tag within the primer preceded by a (GGGGS)2x linker. β-Arrestin1-LgBiT and β-Arrestin2-LgBiT were amplified by PCR and previously cloned in pcDNA3.1+ using NEB HiFi DNA Assembly (New England Biolabs).

BRET2 constructs were acquired from the TRUPATH BRET2 biosensor kit available through Addgene (https://www.addgene.org/kits/roth-trupath/).

Cell culture

Human Embryonic Kidney cells (HEK293T) and HTLL cells were cultured in Dulbecco's Modified Eagle Medium (DMEM) with the addition of 5% fetal bovine serum (FBS), 5% bovine calf serum (BCS), and 100 µg/mL penicillin and streptomycin; HTTL cells were also cultured with 2.5 µg/mL of puromycin and 50 µg/mL of hygromycin. The cells were maintained at 37°C in a humidified environment with 5% CO2.

HTTL-pcDH-14-3-3-TEV219 stable cell lines were generated by lentiviral infection of each of the seven pcDH-14-3-3-TEV219 constructs into HTTL reporter cells as per supplier instruction and selected using zeocin at 200 mg/mL. Colonies were picked, expanded, eventually duplicated and

further tested in 6-well format by transient transfection with CNR1-Tango, with the best clones of each isoform selected based on growth and 14-3-3 dissociation.

HTTL and HTTL-pcDH-14-3-3-TEV219 stable cell lines were maintained on collagen-coated dishes. Rat-tail collagen is diluted within 20 mM acetic acid according to the manufacturer's instructions to obtain a concentration of 5 µg/mL (Gibco).

Transfection

Cell transfections were conducted using a modified polyethyleneimine (PEI) method. $1.2x10^6$ cells were seeded in a well of a 6-well plate containing 2 mL of complete growth medium. A solution of a total of 3 µg of DNA in 200 µL of Opti-MEM medium was prepared, to which 9 µL of PEI (Polysciences) reagent stock solution (1 mg/mL, pH 7.0) was added. After incubating the mixture for 20 minutes at room temperature, it was added to the cells. The following day, the medium was replaced with fresh complete medium.

Tango β-arrestin recruitment assay

As detailed previously, functional assays were conducted using modified versions of the original Tango assay. Cells were transfected using the PEI precipitation method described earlier. The day after transfection, cells were plated in DMEM supplemented with 1% dialyzed FBS in Poly-L-Lysine (PLL) coated 384-well white clear bottom cell culture plates at a density of 20,000 cells per well, in a total volume of 40 µL. Ligand solutions were prepared in filtered assay buffer (20 mM HEPES, 1× Hank's balanced salt solution (HBSS), pH 7.40) at 3X concentration and added to the cells (20 µL per well) either the following day or 5 hours after seeding, for overnight incubation (16-20 hours). A stock solution of cumate was prepared at 300 mg/mL in 95% ethanol, and was directly added to the complete medium for a final concentration of 30 µg/mL. Cumate was added during cell plating (a day before transfection) and maintained throughout the experiment. The next day, media and drug solutions were removed, and 20 µL per well of homemade Glo reagent (108 mM Tris-HCl; 42 mM Tris-Base, 75 mM NaCl, 3 mM MgCl2, 5 mM Dithiothreitol (DTT), 0.2 mM Coenzyme A, 0.14 mg/ml D-Luciferin, 1.1 mM ATP, 0.25% v/v Triton X-100, 2 mM Sodium hydrosulfite) was added. Plates were incubated in the dark at room temperature for 10 minutes before being counted using a Hidex Sense Beta Plus (Gamble Technologies, ON). The data were analyzed using non-linear least-squares regression with the

sigmoidal dose-response function in GraphPad Prism 9.0. Data from independent experiments are presented as Relative Luminescence Units (RLU) or normalized as specified in the figure legends. Parallel analysis was performed as previously published.

Measurement of cell surface expression by ELISA

HEK293T cells were seeded in 6-well plates and transfected with pcDNA3.1+, TACR3-Tango (containing the FLAG tag), and 14-3-3-V5 constructs, as described in **Suppl. Fig. 4.5.** The transfected cells were then re-plated in 384-well plates at a density of 30,000 cells per well and fixed with 20 µL of 4% paraformaldehyde for 10 minutes. The cells were blocked using 20 µL of 5% normal goat serum in PBS for 30 minutes. Following the blocking step, 20 µL of an anti-FLAG-HRP conjugated antibody (Sigma), diluted 1:10,000, was added and incubated for 1 hour. The wells were then washed twice with 80 µL of PBS. To read luminescence, Supersignal ELISA Femto Substrate (Fisher) was added. Error bars represent standard deviation (SD) based on four measurements.

NanoBiT assay

HEK293T cells were plated in 6-well plates at a density of $1.0x10^6$ cells per well. The following day, the cells were transfected with the NanoBiT constructs and pLX307-14-3-3-V5 using a total of 3 µg of DNA per well. After transfection, the cells were detached and reseeded on Poly-L-Lysine (PLL) coated white 384-well assay plates (ThermoFisher) in starvation media (DMEM, 1% FBS, 1x Pen-Strep). The next day, the media was replaced with 20 µL of 1X HBSS buffer containing 5 µM furimazine, and the cells were incubated for 10 minutes at room temperature. Luminescence was measured using the Fluorescent Imaging Plate Reader (FLIPR) Tetra system (Molecular Devices). Baseline readings were taken before adding the drugs to their respective wells (concentrations and types of drugs are detailed in the figure legends). Changes in relative luminescence signals (RLU) were recorded over time. Data were extracted using the integrated ScreenWorks software and analyzed using non-linear least-squares regression with the sigmoidal dose-response function in GraphPad Prism 9.0.

Bioluminescence resonance energy transfer (BRET) assay

HEK293T cells were plated in 6-well plates at 1.0×10^6 cells per well and subsequently transfected the next day using the PEI transfection reagent with BRET2 constructs at a total of 2 μg of DNA per well. The DNA ratio of the transfected constructs was as follows: NK3-SmBit : Gαq-Rluc8 : Gβ3 : Gγ9-GFP2 – (3:1:3:3). To assess the effect of 14-3-3 γ/τ in the BRET2, we transfected the following amount of mentioned DNA constructs: 14-3-3 γ (400 ng), 14-3-3 τ (400 ng), and 14-3-3 γ/τ dimer (200 ng each). pcDNA3.1 vector was used to bring the final DNA amount to 2 μg in the control condition.

On the following day after transfection, cells were detached and seeded on poly-L-lysine (PLL)-coated white 96-well assay plates (Thermo Fisher Scientific). The next day, spent medium was removed and replaced with 60 μl of 1× Hanks' balanced salt solution (HBSS) buffer, followed by the addition of 30 μl of serial dilutions of Neurokinin B at 3× concentration. After incubation for 2 minutes with the agonist, 10 μl of Coelenterazine 400a (NanoLight Technologies) was added at 50 μM to each well, for a final concentration of 5 μM and incubated for 5 minutes in the dark.

Plates were subsequently read 4 times after 5 minutes, 10 minutes, 30 minutes, and 45 minutes using the Hidex Sense Beta Plus microplate reader (Gamble Technologies) with 405 nm (RLuc8-Coelenterazine 400a) and 500 nm (GFP2) emission filters, at 1 second/well integration times.

GloSensor assay

A GloSensor/HEK293T stable cell line was generated using the Promega Glosensor plasmid. The cells were plated in 6 well plates at $1x10^6$ cells. The following day, the cells were transfected using jetPRIME transfection protocol (Polyplus) at 2μg total DNA per well. After 24 hours, the transfected cells were detached and split into a PLL-coated white 384 well plate (ThermoFisher) in starvation media (DMEM, 1% FBS, 1x Pen-Strep). The next day, the media was replaced with 20 μL of 1 mg/mL luciferin (GoldBio) in HBSS pH 7.4 and left to equilibrate at room temperature in the dark for 30 minutes. After incubation, 5 μL of a 5X solution of drug in HBSS pH7.4 was added to each well. Subsequent changes in luminescence (relative luminescence units) were recorded using a Hidex sense microplate reader (Hidex). The data collected was subjected to non-linear regression analysis using the sigmoidal dose-response function provided by GraphPad Prism. Data of three independent experiments (n=3) performed in triplicate are presented as RLUs.

Western Blot

Cells were washed with PBS then lysed with cold lysis buffer (1% Triton X-100, 0.5% deoxycholate, 0.1% SDS, 150 mM NaCl, 50 mM Tris pH 8.0) containing protease inhibitors. The proteins were resolved by SDS-page using a NuPAGE 4-12% Bis-Tris gel (Invitrogen). Proteins were then transferred to polyvinylidenedifluoride (PVDF) membranes and then blocked for 1 hour in a blocking buffer (5% skim milk powder in 25mM Tris, pH 7.5, 150mM NaCl, and 0.1% Tween 20 [TBST]). The membrane was then incubated overnight at 4C with the primary monoclonal antibody (V5 tag [SV5-Pk1], Abcam; ANTI-FLAG M2-perioxidase (HRP), Sigma; Anti-β-Actin, Sigma), washed with TBST then incubated for 1 hour with the secondary antibody (Anti-mouse IgG HRP-linked, Cell Signalling Technology). The membrane was washed again with TBST then visualised using chemiluminescence (Bio-RAD Clarity ECL substrate).

ACKNOWLEDGEMENTS

MZ is supported by the Alexander Graham Bell Canada Graduate Scholarships-Doctoral Program (CGS-D3) from Natural Sciences and Engineering Research Council of Canada. This work was supported by the Canadian Institutes of Health Research (CIHR grant #MOP142219) and Natural Sciences and Engineering Research Council of Canada (NSERC RGPIN-2017-06151).

AUTHOR CONTRIBUTIONS

MZ and PMG conceived the overall concept; MZ, DA, SKR, and GL performed all functional experiments and analyzed the data. MZ and PMG wrote the manuscript.

DECLARATION OF INTERESTS

The authours declare no competing interests.

REFERENCES

Bauch, C., Koliwer, J., Buck, F., Hönck, H.H., and Kreienkamp, H.J. (2014). Subcellular Sorting of the G-Protein Coupled Mouse Somatostatin Receptor 5 by a Network of PDZ-Domain Containing Proteins. PLoS One *9*:.

Benzing, T., Yaffe, M.B., Arnould, T., Sellin, L., Schermer, B., Schilling, B., et al. (2000). 14-3-3 interacts with regulator of G protein signaling proteins and modulates their activity. J Biol Chem *275*: 28167–28172.

Chu, Y.X., Zhang, W.W., and Wang, Y. (2020). Tacr3/NK3R: Beyond Their Roles in Reproduction. ACS Chem Neurosci *11*: 2935–2943.

Cohen, B.D., Nechamen, C.A., and Dias, J.A. (2004). Human follitropin receptor (FSHR) interacts with the adapter protein 14-3-3τ. Mol Cell Endocrinol *220*: 1–7.

Cunningham, M.R., McIntosh, K.A., Pediani, J.D., Robben, J., Cooke, A.E., Nilsson, M., et al. (2012). Novel Role for Proteinase-activated Receptor 2 (PAR2) in Membrane Trafficking of Proteinase-activated Receptor 4 (PAR4). J Biol Chem *287*: 16656.

Dunn, H.A., and Ferguson, S.S.G. (2015). PDZ Protein Regulation of G Protein–Coupled Receptor Trafficking and Signaling Pathways. Mol Pharmacol *88*: 624–639.

Eishingdrelo, H., Qin, X., Yuan, L., Kongsamut, S., and Yu, L. (2022). Ligands can differentially and temporally modulate GPCR interaction with 14-3-3 isoforms. Current Research in Pharmacology and Drug Discovery *3*: 100123.

Gardino, A.K., Smerdon, S.J., and Yaffe, M.B. (2006). Structural determinants of 14-3-3 binding specificities and regulation of subcellular localization of 14-3-3-ligand complexes: a comparison of the X-ray crystal structures of all human 14-3-3 isoforms. Semin Cancer Biol *16*: 173–182.

Gerber, K.J., Squires, K.E., and Hepler, J.R. (2018). 14-3-3γ binds regulator of G protein signaling 14 (RGS14) at distinct sites to inhibit the RGS14:Gαi–AlF4− signaling complex and RGS14 nuclear localization. J Biol Chem *293*: 14616.

Gogl, G., Tugaeva, K. V., Eberling, P., Kostmann, C., Trave, G., and Sluchanko, N.N. (2021). Hierarchized phosphotarget binding by the seven human 14-3-3 isoforms. Nature Communications 2021 12:1 *12*: 1–12.

Hauser, A.S., Chavali, S., Masuho, I., Jahn, L.J., Martemyanov, K.A., Gloriam, D.E., et al. (2018). Pharmacogenomics of GPCR Drug Targets. Cell *172*: 41-54.e19.

Hornbeck, P. V., Kornhauser, J.M., Tkachev, S., Zhang, B., Skrzypek, E., Murray, B., et al. (2012). PhosphoSitePlus: a comprehensive resource for investigating the structure and function of experimentally determined post-translational modifications in man and mouse. Nucleic Acids Res *40*:.

Johnson, C., Crowther, S., Stafford, M.J., Campbell, D.G., Toth, R., and MacKintosh, C. (2010). Bioinformatic and experimental survey of 14-3-3-binding sites. Biochemical Journal *427*: 69.

Kligys, K., Yao, J., Yu, D., and Jones, J.C.R. (2009). 14-3-3ζ/τ heterodimers regulate Slingshot activity in migrating keratinocytes. Biochem Biophys Res Commun *383*: 450.

Kongsamut, S., and Eishingdrelo, H. (2023). Modulating GPCR and 14-3-3 protein interactions: Prospects for CNS drug discovery. Drug Discov Today *28*: 103641.

Kotliar, I.B., Lorenzen, E., Schwenk, J.M., Hay, D.L., and Sakmar, T.P. (2023). Elucidating the Interactome of G Protein-Coupled Receptors and Receptor Activity-Modifying Proteins. Pharmacol Rev *75*: 1–34.

Laniyonu, A., Sliwinski-Lis, E., and Fleming, N. (1988). Different tachykinin receptor subtypes are coupled to the phosphoinositide or cyclic AMP signal transduction pathways in rat submandibular cells. FEBS Lett *240*: 186–190.

Li, H., Eishingdrelo, A., Kongsamut, S., and Eishingdrelo, H. (2016). G-protein-coupled receptors mediate 14-3-3 signal transduction. Signal Transduct Target Ther *1*: 16018.

Liang, X., Butterworth, M.B., Peters, K.W., Walker, W.H., and Frizzell, R.A. (2008). An Obligatory Heterodimer of 14-3-3β and 14-3-3ε Is Required for Aldosterone Regulation of the Epithelial Sodium Channel. J Biol Chem *283*: 27418.

Louwette, S., Geet, C. Van, and Freson, K. (2012). Regulators of G protein signaling: role in hematopoiesis, megakaryopoiesis and platelet function. J Thromb Haemost *10*: 2215–2222.

Madeira, F., Tinti, M., Murugesan, G., Berrett, E., Stafford, M., Toth, R., et al. (2015). 14-3-3-Pred: improved methods to predict 14-3-3-binding phosphopeptides. Bioinformatics *31*: 2276.

Magalhaes, A.C., Dunn, H., and Ferguson, S.S. (2012). Regulation of GPCR activity, trafficking and localization by GPCR-interacting proteins. Br J Pharmacol *165*: 1717–1736.

McFerrin, M.B., Chi, X., Cutter, G., and Yacoubian, T.A. (2017). Dysregulation of 14-3-3 proteins in neurodegenerative diseases with Lewy body or Alzheimer pathology. Ann Clin Transl Neurol *4*: 466.

Niu, J., Scheschonka, A., Druey, K.M., Davis, A., Reed, E., Kolenko, V., et al. (2002). RGS3 interacts with 14-3-3 via the N-terminal region distinct from the RGS (regulator of G-protein signalling) domain. Biochem J *365*: 677–684.

Obsilova, V., and Obsil, T. (2022). Structural insights into the functional roles of 14-3-3 proteins. Front Mol Biosci *9*: 1016071.

Ottmann, C., Yasmin, L., Weyand, M., Veesenmeyer, J.L., Diaz, M.H., Palmer, R.H., et al. (2007). Phosphorylation-independent interaction between 14-3-3 and exoenzyme S: from structure to pathogenesis. EMBO J *26*: 902–913.

Oury-Donat, F., Carayon, P., Thurneyssen, O., Pailhon, V., Emonds-Alt, X., Soubrié, P., et al. (1995). Functional characterization of the nonpeptide neurokinin3 (NK3) receptor antagonist, SR142801 on the human NK3 receptor expressed in Chinese hamster ovary cells. Journal of Pharmacology and Experimental Therapeutics *274*:.

Pennington, K., Chan, T., Torres, M., and Andersen, J. (2018). The dynamic and stress-adaptive signaling hub of 14-3-3: emerging mechanisms of regulation and context-dependent protein–protein interactions. Oncogene 2018 37:42 *37*: 5587–5604.

Reyes-Alcaraz, A., Lucero Garcia-Rojas, E.Y., Merlinsky, E.A., Seong, J.Y., Bond, R.A., and McConnell, B.K. (2022). A NanoBiT assay to monitor membrane proteins trafficking for drug discovery and drug development. Commun Biol *5*: 212.

Sluchanko, N.N., Tugaeva, K. V., Gushchin, I., Remeeva, A., Kovalev, K., and Cooley, R.B. (2021). Crystal structure of human 14-3-3ζ complexed with the noncanonical phosphopeptide from proapoptotic BAD. Biochem Biophys Res Commun *583*: 100–105.

Srdanović, S., Wolter, M., Trinh, C.H., Ottmann, C., Warriner, S.L., and Wilson, A.J. (2022). Understanding the interaction of 14-3-3 proteins with hDMX and hDM2: a structural and biophysical study. FEBS J *289*: 5341–5358.

Steinhoff, M.S., Mentzer, B. von, Geppetti, P., Pothoulakis, C., and Bunnett, N.W. (2014). Tachykinins and Their Receptors: Contributions to Physiological Control and the Mechanisms of Disease. Physiol Rev *94*: 265.

Walther, C., and Ferguson, S.S.G. (2015). Minireview: Role of intracellular scaffolding proteins in the regulation of endocrine G protein-coupled receptor signaling. Mol Endocrinol *29*: 814–30.

Wright, A.C., Beaudoin, F.L., McQueen, R.B., Yeung, K., Moradi, A., Herron-Smith, S., et al. (2023). The effectiveness and value of fezolinetant for moderate-to-severe vasomotor symptoms associated with menopause: A summary from the Institute for Clinical and Economic Review's Midwest Public Advisory Council. J Manag Care Spec Pharm *29*: 692–698.

Yuan, L., Barbash, S., Kongsamut, S., Eishingdrelo, A., Sakmar, T.P., and Eishingdrelo, H. (2019). 14-3-3 signal adaptor and scaffold proteins mediate GPCR trafficking. Sci Rep *9*: 11156.

Zeghal, M., Laroche, G., Freitas, J.D., Wang, R., and Giguère, P.M. (2023). Profiling of basal and ligand-dependent GPCR activities by means of a polyvalent cell-based high-throughput platform. Nat Commun *14*:.

FIGURES

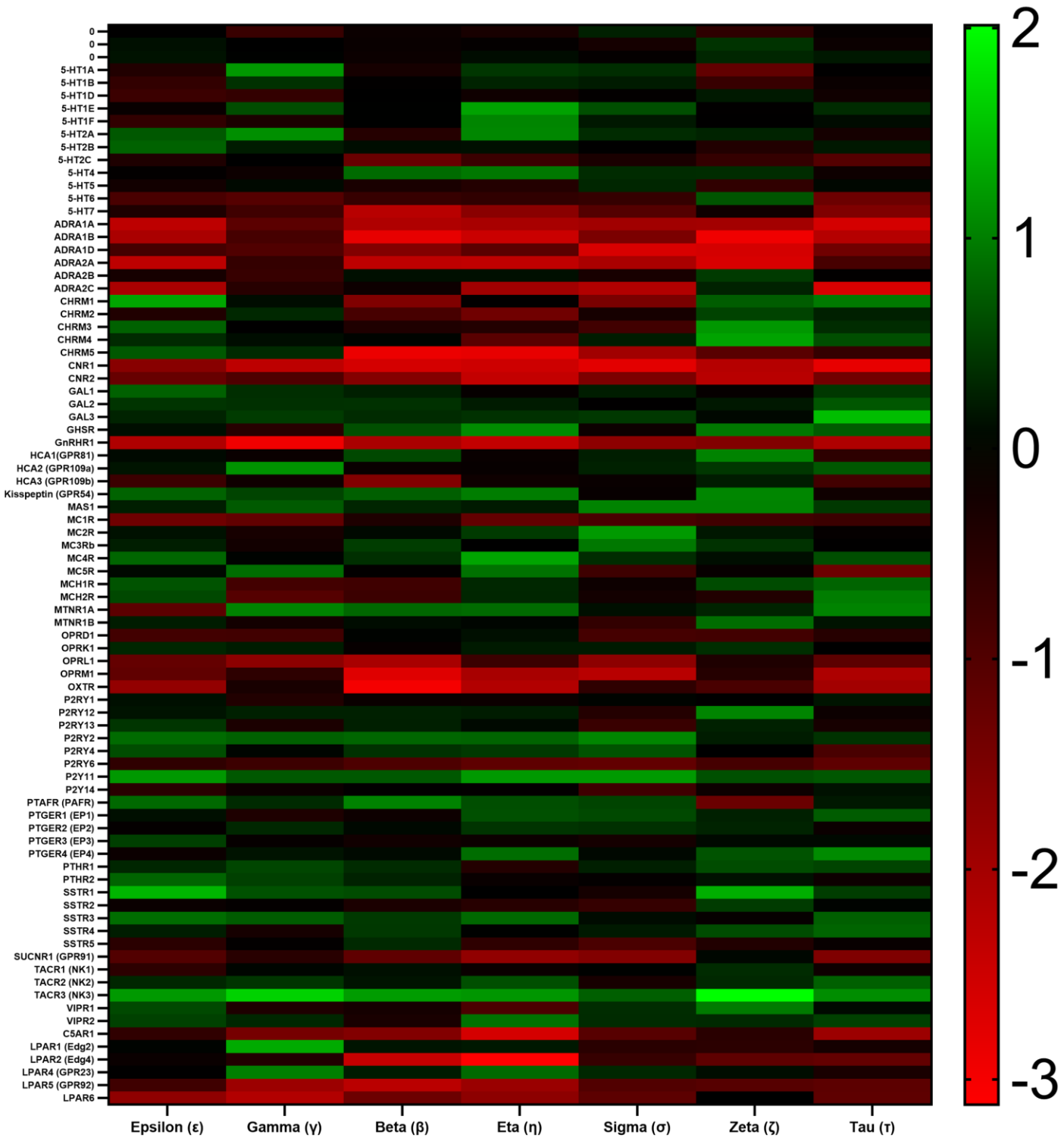

Figure 4.1A. Heatmap representation of select GPCR-14-3-3 interactions identified from agonist-dependent HTS.

To analyze agonist-induced 14-3-3 dissociation/association within the GPCRome, HTTL monoclonal cell lines stably expressing each of the 7 14-3-3 isoforms were plated in cumate-containing (30 µg/mL) medium and

transfected with a panel of approximately 100 non-orphan GPCR Tango constructs. Transfected cells were stimulated either with HBSS-Hepes buffer or with a panel of selective agonists. Log2 fold changes in agonist-dependent 14-3-3 recruitment/dissociation was calculated between the wells in the absence or presence of agonist. Log2 values are the means calculated from quadruplicate conditions, generated from one screen (n = 8, two biological measurement with 4 technical replicates each). Generic receptor codes refer to the GPCR-Tango constructs.

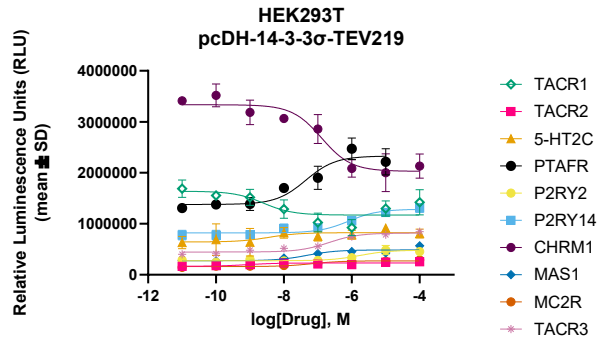

	Bottom	Top	LogEC50	EC50	Fold
TACR1	1638575	1171323	-8.600	2.509e-009	0.7148
TACR2	166892	230865	-9.068	8.556e-010	1.383
TACR3	446449	818273	-6.668	2.148e-007	1.833
5-HT2C	643321	825118	-8.441	3.619e-009	1.283
PTAFR	1379168	2328741	-7.353	4.433e-008	1.689
P2RY2	275552	482567	-5.756	1.755e-006	1.751
P2RY14	821201	1285146	-6.086	8.202e-007	1.565
CHRM1	3334456	2029482	-6.887	1.299e-007	0.6086
MAS1	275961	487041	-7.313	4.860e-008	1.765
MC2R	160955	272973	-7.173	6.715e-008	1.696

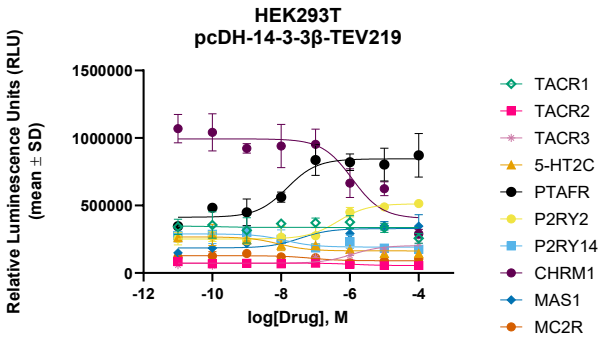

	Bottom	Top	LogEC50	EC50	Fold
TACR1	347420	337491	-9.738	1.828e-010	0.9714
TACR2	73323	54840	-5.871	1.346e-006	0.7479
TACR3	71768	203968	-5.933	1.167e-006	2.842
5-HT2C	267390	163730	-8.067	8.576e-009	0.6123
PTAFR	413014	845517	-7.828	1.487e-008	2.047
P2RY2	251781	512547	-6.350	4.463e-007	2.036
P2RY14	289271	191937	-7.869	1.352e-008	0.6635
CHRM1	993458	403060	-5.933	1.166e-006	0.4057
MAS1	185770	328993	-7.443	3.603e-008	1.771
MC2R	128104	90706	-7.113	7.708e-008	0.7081

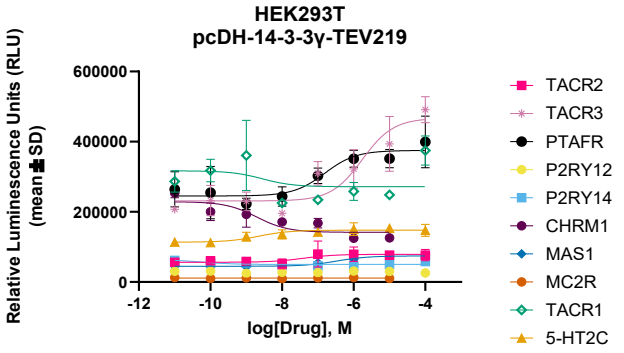

	Bottom	Top	LogEC50	EC50	Fold
TACR1	316848	271542	-8.549	2.825e-009	0.8570
TACR2	56307	78871	-7.409	3.902e-008	1.401
TACR3	231044	467155	-5.758	1.745e-006	2.022
5-HT2C	113524	147706	-8.649	2.244e-009	1.301
PTAFR	245263	375035	-6.805	1.568e-007	1.529
P2RY12	Unstable	-5.363e+077	Unstable	Unstable	Unstable
P2RY14	63589	50161	-10.24	5.803e-011	0.7888
CHRM1	228917	141682	-8.707	1.962e-009	0.6189
MAS1	44920	74325	-6.476	3.340e-007	1.655
MC2R	11278	Unstable	Unstable	Unstable	Unstable

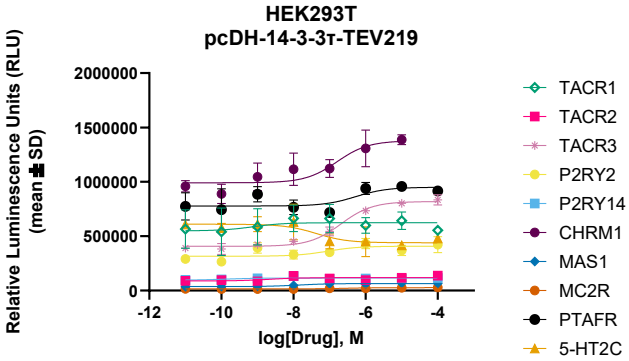

	Bottom	Top	LogEC50	EC50	Fold
TACR1	549268	624063	-9.123	7.525e-010	1.136
TACR2	88198	118795	-8.683	2.075e-009	1.347
TACR3	406978	819030	-6.683	2.076e-007	2.012
5-HT2C	610282	439796	-7.369	4.273e-008	0.7206
PTAFR	777935	950081	-6.272	5.350e-007	1.221
P2RY2	315996	407953	-7.062	8.663e-008	1.291
P2RY14	95556	115042	-9.880	1.319e-010	1.204
CHRM1	991403	1378170	-6.792	1.613e-007	1.390
MAS1	36796	64601	-7.870	1.348e-008	1.756
MC2R	15081	26737	-6.589	2.574e-007	1.773

Figure 4.1B. Secondary screening of compiled hits from agonist-dependent HTS in dose-response. To validate hits from Fig 1A, HTTL monoclonal cell lines stably expressing each of the 7 14-3-3 isoforms were plated in cumate-containing (30 µg/mL) medium and transfected with potential GPCR hits identified from the agonist-dependent HTS. Transfected cells were stimulated with the receptor specific agonist and dose- response curves were built using XY analysis for non-linear regression curve and the 3-parameters dose-response stimulation function. All error bars represent SEM (n = 3 technical replicates). Generic receptor codes refer to the GPCR-Tango constructs.

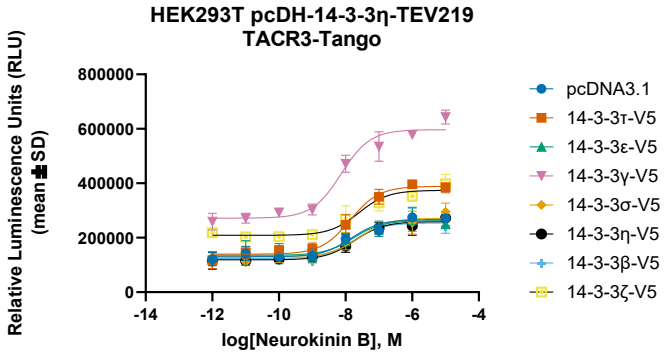

	Bottom	Top	LogEC50	EC50	Fold
pcDNA3.1	129928	266837	-7.825	1.495e-008	2.054
14-3-3τ-V5	139445	388875	-7.866	1.363e-008	2.789
14-3-3ε-V5	135409	262928	-7.764	1.720e-008	1.942
14-3-3γ-V5	271729	596924	-8.133	7.359e-009	2.197
14-3-3σ-V5	130536	271561	-7.580	2.628e-008	2.080
14-3-3η-V5	118675	259026	-7.732	1.855e-008	2.183
14-3-3β-V5	123599	254218	-7.770	1.700e-008	2.057
14-3-3ζ-V5	208747	374116	-7.603	2.496e-008	1.792

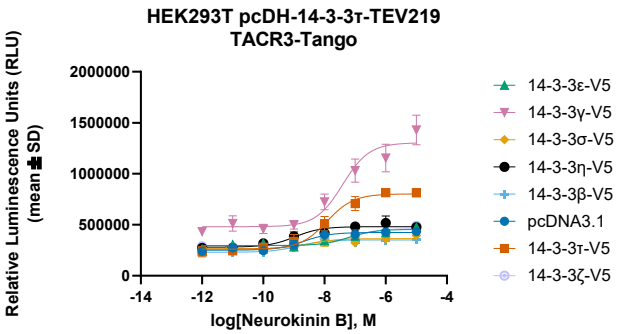

	Bottom	Top	LogEC50	EC50	Fold
pcDNA3.1	250645	424700	-8.680	2.090e-009	1.694
14-3-3τ-V5	260904	802701	-7.922	1.196e-008	3.077
14-3-3ε-V5	296204	454808	-7.208	6.200e-008	1.535
14-3-3γ-V5	480906	1303959	-7.409	3.899e-008	2.711
14-3-3σ-V5	264845	363710	-8.474	3.355e-009	1.373
14-3-3η-V5	280595	481401	-8.970	1.072e-009	1.716
14-3-3β-V5	230680	351417	-8.865	1.364e-009	1.523
14-3-3ζ-V5	296922	463015	-7.108	7.794e-008	1.559

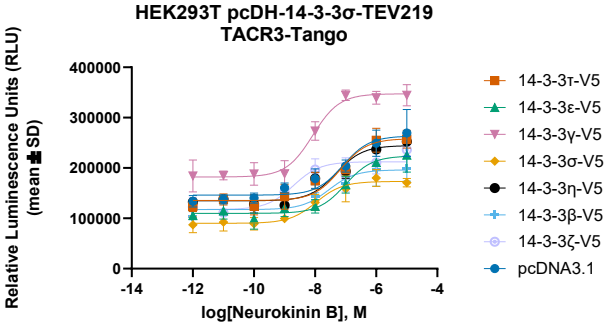

	Bottom	Top	LogEC50	EC50	Fold
pcDNA3.1	146043	263578	-7.091	8.118e-008	1.805
14-3-3τ-V5	135414	258214	-7.174	6.699e-008	1.907
14-3-3ε-V5	109921	223981	-7.008	9.818e-008	2.038
14-3-3γ-V5	182129	347365	-8.076	8.386e-009	1.907
14-3-3σ-V5	90121	173309	-7.969	1.074e-008	1.923
14-3-3η-V5	134800	244493	-7.310	4.897e-008	1.814
14-3-3β-V5	117376	196232	-7.546	2.843e-008	1.672
14-3-3ζ-V5	117525	212350	-8.710	1.952e-009	1.807

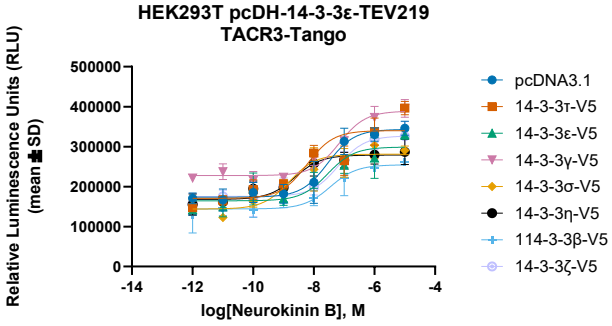

	Bottom	Top	LogEC50	EC50	Fold
pcDNA3.1	173566	343207	-7.541	2.875e-008	1.977
14-3-3τ-V5	170533	340080	-8.226	5.948e-009	1.994
14-3-3ε-V5	164445	298954	-7.545	2.853e-008	1.818
14-3-3γ-V5	227635	388886	-7.162	6.883e-008	1.708
14-3-3σ-V5	143886	281042	-8.807	1.560e-009	1.953
14-3-3η-V5	167898	278876	-8.622	2.387e-009	1.661
14-3-3β-V5	144100	254556	-7.458	3.487e-008	1.767
14-3-3ζ-V5	175397	326852	-7.197	6.347e-008	1.863

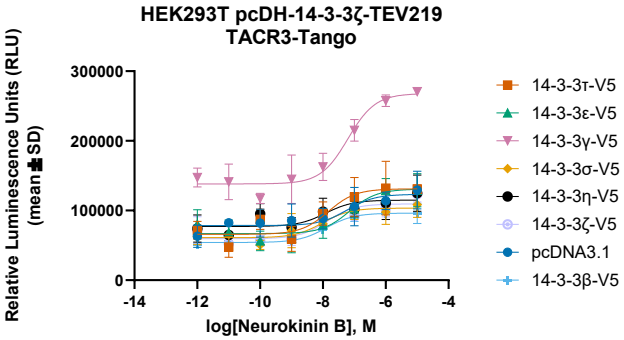

	Bottom	Top	LogEC50	EC50	Fold
pcDNA3.1	78494	123271	-7.221	6.005e-008	1.570
14-3-3τ-V5	65810	131137	-7.829	1.483e-008	1.993
14-3-3ε-V5	66859	130738	-7.156	6.988e-008	1.955
14-3-3γ-V5	138188	267946	-7.202	6.279e-008	1.939
14-3-3σ-V5	60996	103451	-8.014	9.684e-009	1.696
14-3-3η-V5	77106	114913	-7.920	1.203e-008	1.490
14-3-3β-V5	54119	96248	-7.889	1.291e-008	1.778
14-3-3ζ-V5	59580	109473	-7.878	1.323e-008	1.837

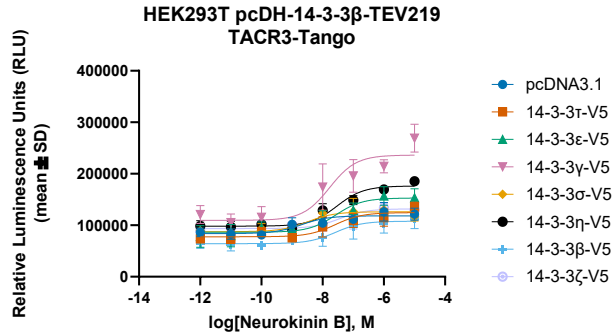

	Bottom	Top	LogEC50	EC50	Fold
pcDNA3.1	83815	118269	-8.690	2.041e-009	1.411
14-3-3τ-V5	77631	124539	-7.590	2.572e-008	1.604
14-3-3ε-V5	86489	152909	-7.578	2.642e-008	1.768
14-3-3γ-V5	109596	236297	-7.774	1.682e-008	2.156
14-3-3σ-V5	87567	126111	-8.479	3.319e-009	1.440
14-3-3η-V5	98250	176228	-7.531	2.943e-008	1.794
14-3-3β-V5	64273	107869	-7.585	2.602e-008	1.678
14-3-3ζ-V5	93637	131797	-7.446	3.577e-008	1.408

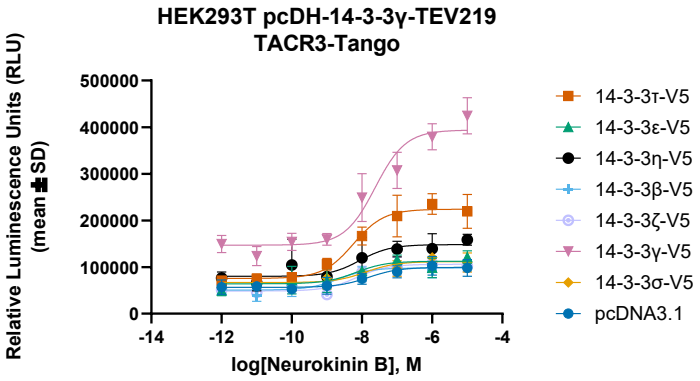

	Bottom	Top	LogEC50	EC50	Fold
pcDNA3.1	56431	99330	-7.809	1.552e-008	1.760
14-3-3τ-V5	75584	223985	-8.240	5.749e-009	2.963
14-3-3ε-V5	64095	112483	-8.176	6.663e-009	1.755
14-3-3γ-V5	146941	393790	-7.622	2.387e-008	2.680
14-3-3σ-V5	66772	111644	-7.893	1.281e-008	1.672
14-3-3η-V5	80014	148129	-8.060	8.703e-009	1.851
14-3-3β-V5	50600	98001	-8.671	2.135e-009	1.937
14-3-3ζ-V5	48609	105935	-8.159	6.929e-009	2.179

Figure 4.2. **Effects of 14-3-3 Isoform Overexpression on β-arrestin-2 Recruitment at NK3 receptor.** To explore the impact of 14-3-3 homo- and heterodimer configurations on GPCR signaling, TACR3-Tango was transiently transfected into the HTTL/14-3-3-TEV219 stable cell lines, alongside the individual overexpression of 14-3-3-V5 isoforms or pcDNA3.1 as the negative control. Transfected cells were stimulated with the receptor specific agonist neurokinin B and dose- response curves were built using XY analysis for non-linear regression curve and the 3-parameters dose-response stimulation function. All error bars represent SEM (n = 3 technical replicates).

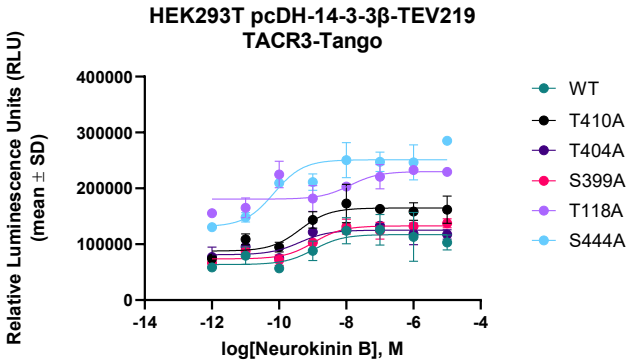

	Bottom	Top	LogEC50	EC50	Fold
WT	63587	117330	-8.970	1.072e-009	1.845
T410A	87745	164848	-9.374	4.231e-010	1.879
S399A	73732	132823	-8.970	1.070e-009	1.801
T404A	81167	125194	-9.391	4.064e-010	1.542
T118A	180707	230072	-7.892	1.283e-008	1.273
S444A	131337	251190	-10.16	6.977e-011	1.913

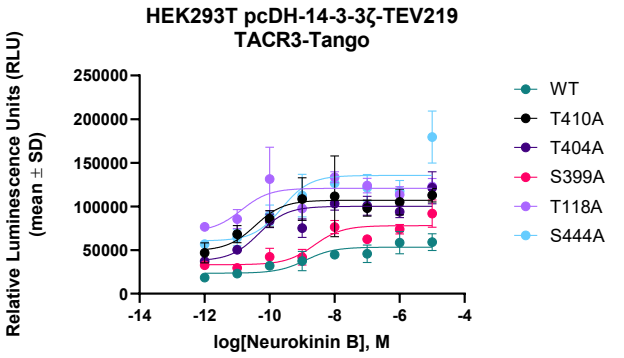

	Bottom	Top	LogEC50	EC50	Fold
WT	23447	53296	-8.891	1.284e-009	2.273
T410A	49045	107056	-10.44	3.637e-011	2.183
S399A	33202	77945	-8.625	2.369e-009	2.348
T404A	37503	100094	-10.33	4.670e-011	2.669
T118A	70810	120770	-10.87	1.353e-011	1.706
S444A	60429	135494	-9.626	2.367e-010	2.242

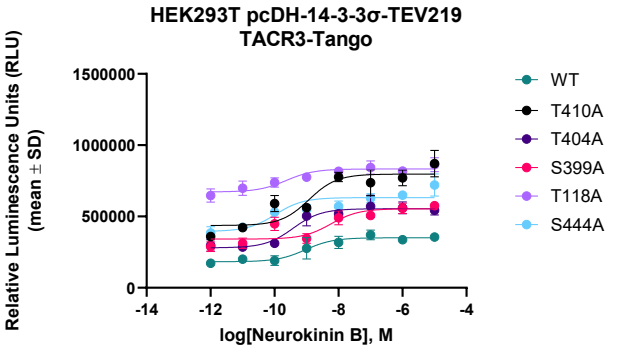

	Bottom	Top	LogEC50	EC50	Fold
WT	182669	350661	-9.034	9.239e-010	1.920
T410A	436800	797129	-8.928	1.182e-009	1.825
S399A	341346	553831	-8.238	5.781e-009	1.622
T404A	279965	554175	-9.420	3.798e-010	1.979
T118A	672069	832746	-9.633	2.328e-010	1.239
S444A	395073	632200	-9.975	1.059e-010	1.600

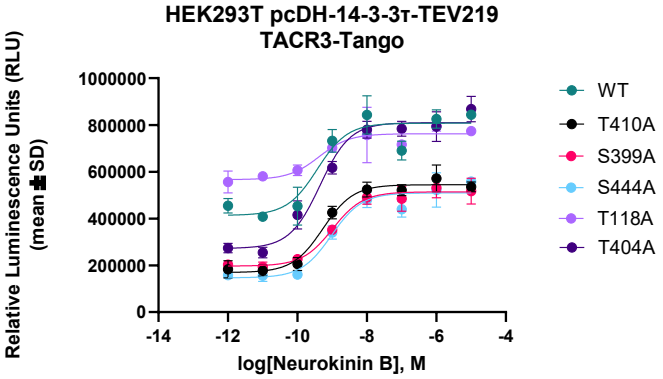

	Bottom	Top	LogEC50	EC50	Fold
WT	413518	807586	-9.429	3.725e-010	1.953
T410A	169272	544449	-9.264	5.444e-010	3.216
S399A	196806	513946	-8.989	1.025e-009	2.611
T404A	272006	809839	-9.351	4.457e-010	2.977
T118A	566268	762305	-9.375	4.218e-010	1.346
S444A	146649	509421	-9.018	9.587e-010	3.474

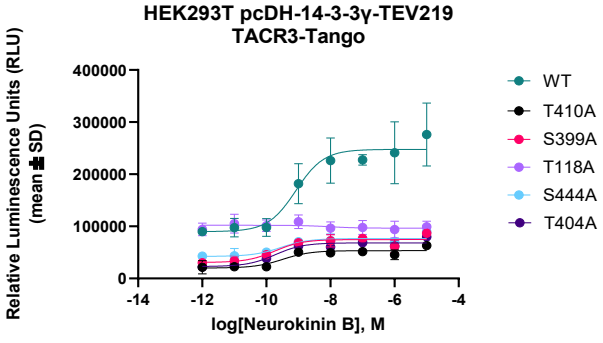

	Bottom	Top	LogEC50	EC50	Fold
WT	89824	247629	-9.076	8.389e-010	2.757
T410A	20042	53340	-9.489	3.240e-010	2.661
S399A	30711	74672	-9.731	1.856e-010	2.431
T404A	22951	68272	-9.721	1.901e-010	2.975
T118A	102022	96539	-8.028	9.367e-009	0.9463
S444A	42333	76609	-9.547	2.835e-010	1.810

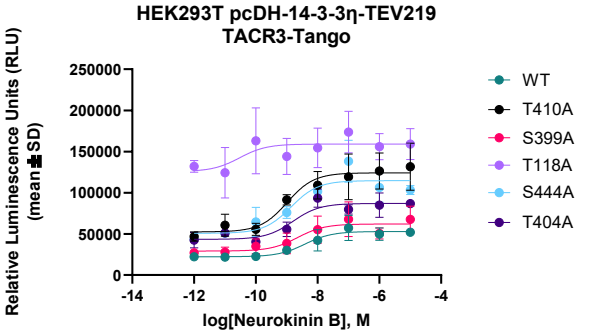

	Bottom	Top	LogEC50	EC50	Fold
WT	22225	52885	-8.409	3.896e-009	2.379
T410A	52377	124119	-8.983	1.040e-009	2.370
S399A	29131	61990	-8.646	2.261e-009	2.128
T404A	43373	86959	-8.799	1.589e-009	2.005
T118A	125677	159086	-10.52	2.994e-011	1.266
S444A	50669	114645	-8.857	1.390e-009	2.263

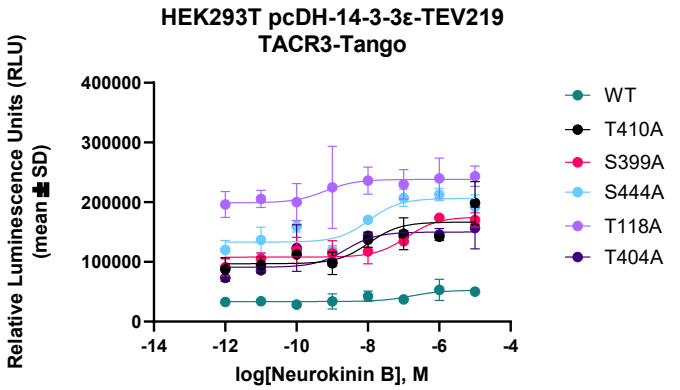

	Bottom	Top	LogEC50	EC50	Fold
WT	33624	52520	-6.765	1.718e-007	1.562
T410A	96967	166685	-7.968	1.076e-008	1.719
S399A	107998	175190	-6.909	1.233e-007	1.622
T404A	90964	150030	-8.621	2.393e-009	1.649
T118A	198918	238125	-9.205	6.238e-010	1.197
S444A	133133	206278	-7.969	1.073e-008	1.549

Figure 4.3A. Evaluation of serine/threonine residue mutations in NK3 on 14-3-3 isoform recruitment.

Site-directed mutagenesis was performed on the NK3-Tango receptor to assess the role of specific serine/threonine residues in 14-3-3 binding, specifically T410A, S399A, S444A, T118A, and T404A. HTTL monoclonal cell lines stably expressing each of the 7 14-3-3 isoforms were plated in cumate-containing (30 µg/mL) medium and transfected with the mutant NK3-Tango receptors, along with the WT. Transfected cells were stimulated with the receptor specific agonist neurokinin B and dose- response curves were built using XY analysis for non-linear regression curve and the 3-parameters dose-response stimulation function. All error bars represent SEM (n = 3 technical replicates).

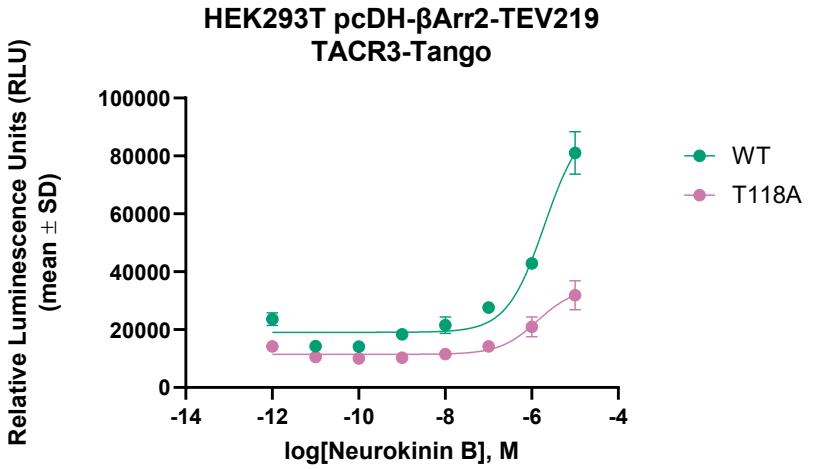

	Bottom	Top	LogEC50	EC50	Fold
WT	19074	92887	-5.708	1.958e-006	4.870
T118A	11456	34576	-5.869	1.353e-006	3.018

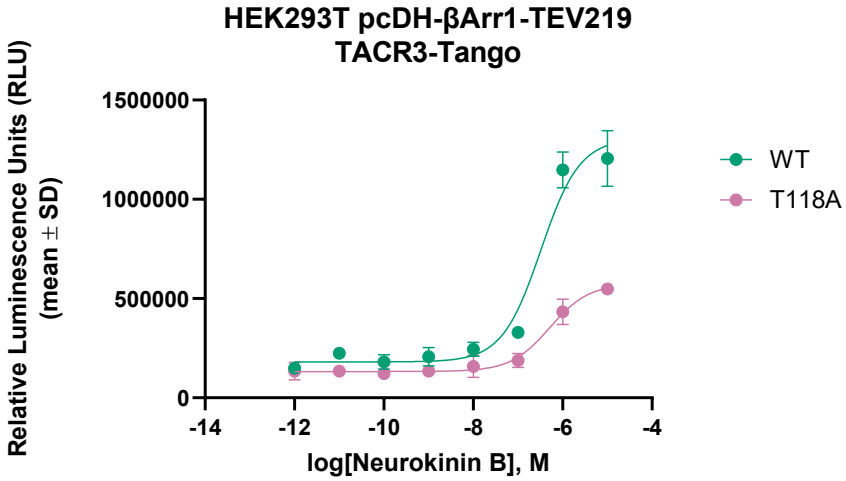

	Bottom	Top	LogEC50	EC50	Fold
WT	180808	1306383	-6.488	3.251e-007	7.225
T118A	132387	573611	-6.290	5.124e-007	4.333

Figure 4.3B. Impact of T118A Mutation on β-arrestin-1/2 recruitment at NK3-Tango Receptor.

HTTL monoclonal cell lines stably expressing β-arrestin-1/-TEV219 were plated in cumate-containing (30 µg/mL) medium and transfected with either WT NK3 or NK3-Tango T118. Transfected cells were stimulated with the receptor specific agonist neurokinin B and dose- response curves were built using XY analysis for non-linear regression curve and the 3-parameters dose-response stimulation function. All error bars represent SEM (n = 3 technical replicates).

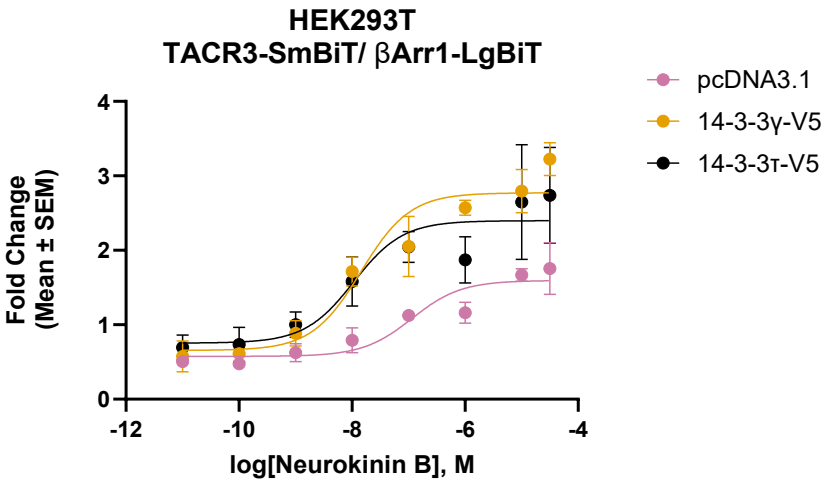

	LogEC50	EC50	Fold
pcDNA3.1	-6.939	1.151e-007	2.772
14-3-3γ-V5	-7.842	1.440e-008	4.229
14-3-3τ-V5	-7.969	1.073e-008	3.182

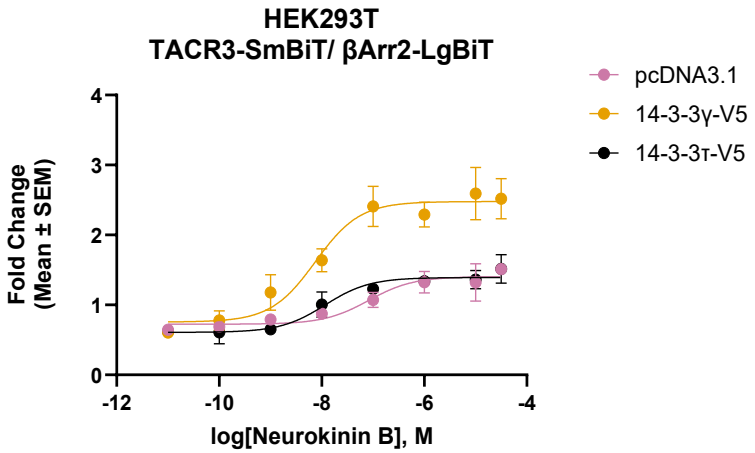

	LogEC50	EC50	Fold
pcDNA3.1	-7.084	8.233e-008	1.939
14-3-3γ-V5	-8.126	7.489e-009	3.280
14-3-3τ-V5	-7.934	1.164e-008	2.290

Figure 4.4. β-arrestin recruitment dynamics to NK3 receptor in the presence of 14-3-3 τ or γ isoforms. HEK293T cells were transfected with 3 µg total of NanoBiT constructs and either pLX307-14-3-3-V5 DNA or pcDNA3.1 (at a 1:1:1 ratio). After detachment, cells were reseeded onto PLL-coated white 384-well plates in starvation media. Following a 10-minute incubation with furimazine, luminescence was measured using the FLIPR Tetra system. Baseline readings were recorded prior to drug treatment, and changes in relative luminescence units (RLU) were monitored over time. Data were analyzed using non-linear regression with the sigmoidal dose-response function in GraphPad Prism 9.0. All error bars represent SEM (n = 3 technical replicates).

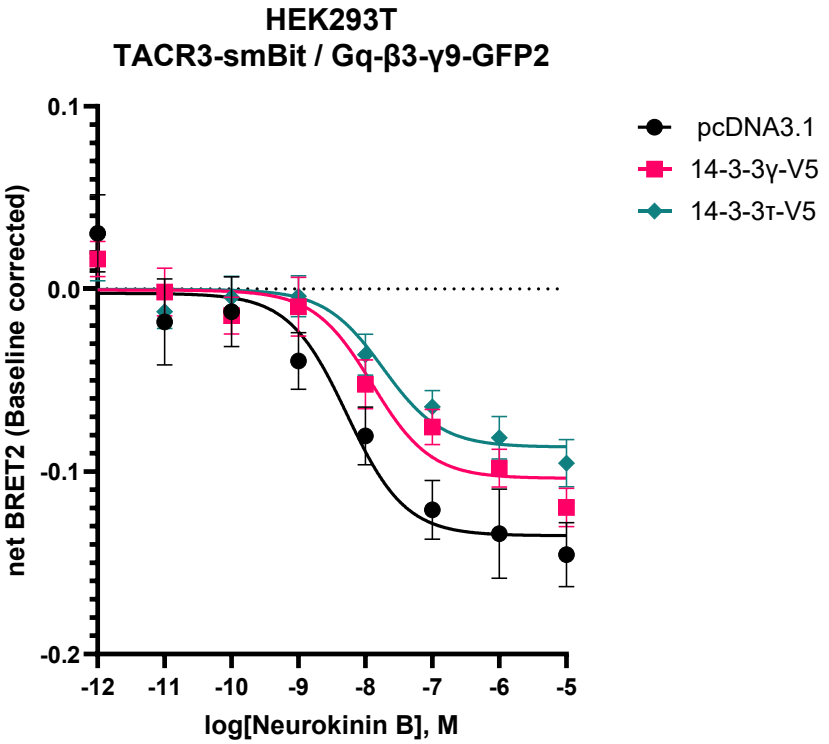

	EC50
pcDNA3.1	5.313e-009
14-3-3γ-V5	1.262e-008
14-3-3τ-V5	1.832e-008

Figure 4.5A. Changes in G-protein dissociation at NK3 receptor in the presence of 14-3-3 τ or γ isoforms. HEK293T cells were co-transfected with BRET2 constructs alongside 14-3-3 γ, 14-3-3 τ, or pcDNA3.1. Cells were seeded on PLL-coated 96-well plates and treated with serial dilutions of Neurokinin B. Following stimulation, luminescence was measured at emission wavelengths of 405 nm and 500 nm. Data were collected at multiple time points post-Coelenterazine 400a addition and analyzed for the effect of 14-3-3 isoforms on the net BRET2 signal; data represent mean netBRET2 (baseline corrected) values from the 30-minute time point.

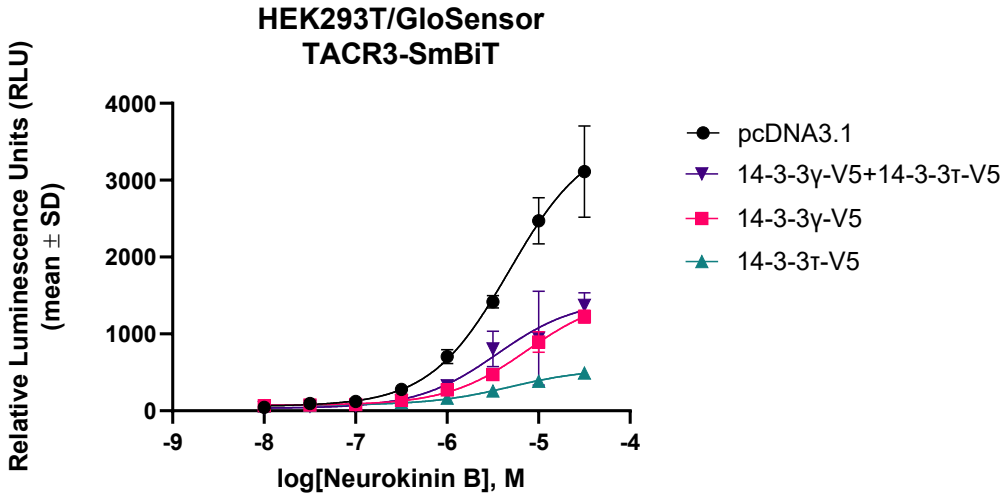

	Bottom	Top	LogEC50	EC50	Fold
pcDNA3.1	57.85	3582	-5.321	4.772e-006	61.92
14-3-3γ-V5	72.18	1497	-5.127	7.462e-006	20.74
14-3-3τ-V5	72.58	549.3	-5.313	4.869e-006	7.568
14-3-3γ-V5+14-3-3τ-V5	31.82	1449	-5.452	3.529e-006	45.53

Figure 4.5B. Changes in cAMP production following activation of NK3 receptor in the presence of 14-3-3 τ and/or γ isoforms. HEK293T cells stably expressing yhe Glosensor construct were transfected with 2 µg of total DNA per well using jetPRIME. Following a 24-hour incubation, cells were transferred to PLL-coated white 384-well plates in starvation media. Luminescence was recorded after incubation with luciferin and subsequent addition of Neurokinin B serial dilutions. The data represent relative luminescence units (RLUs) recorded over three independent experiments (n=3), each performed in triplicate.

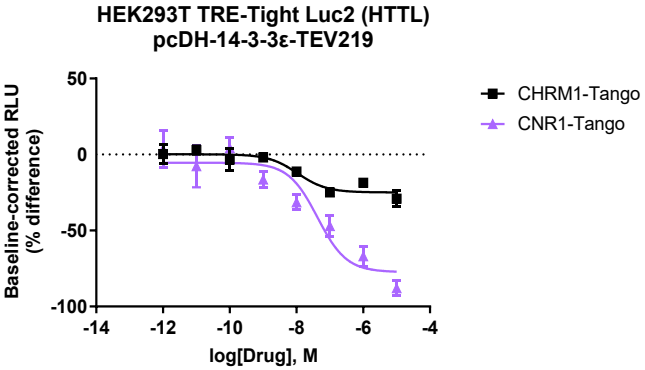

	LogEC50	EC50	Fold
CHRM1-Tango	-7.965	1.083e-008	0.7495
CNR1-Tango	-7.370	4.268e-008	0.2391

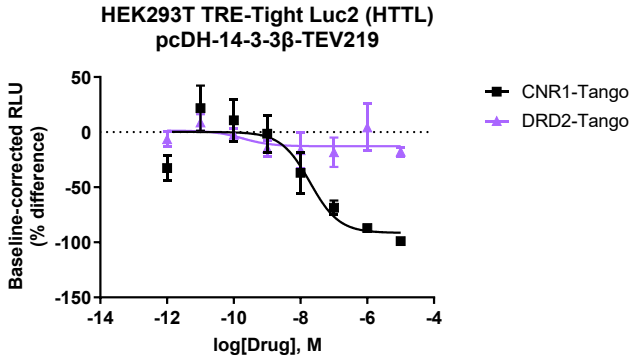

	LogEC50	EC50	Fold
CNR1-Tango	-7.714	1.933e-008	0.08530
DRD2-Tango	-9.732	1.853e-010	0.8596

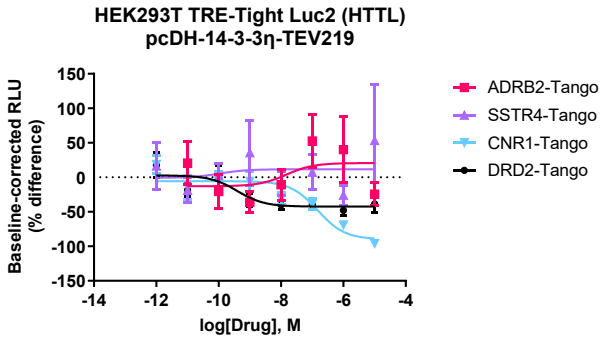

	LogEC50	EC50	Fold
ADRB2-Tango	-7.828	1.484e-008	1.386
SSTR4-Tango	-9.964	1.086e-010	1.123
CNR1-Tango	-6.824	1.501e-007	0.1069
DRD2-Tango	-9.403	3.958e-010	0.5600

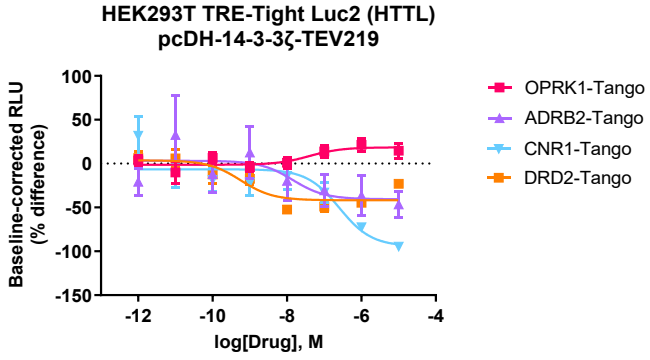

	LogEC50	EC50	Fold
OPRK1-Tango	-7.422	3.787e-008	1.206
ADRB2-Tango	-7.843	1.434e-008	0.5757
CNR1-Tango	-6.594	2.545e-007	0.06023
DRD2-Tango	-9.244	5.704e-010	0.5610

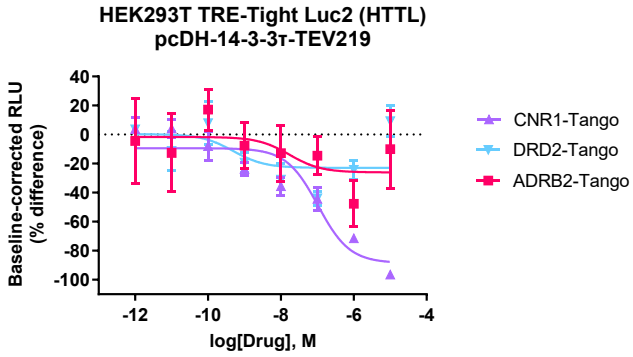

	LogEC50	EC50	Fold
ADRB2-Tango	-7.757	1.749e-008	0.7485
CNR1-Tango	-6.979	1.049e-007	0.1268
DRD2-Tango	-9.310	4.900e-010	0.7683

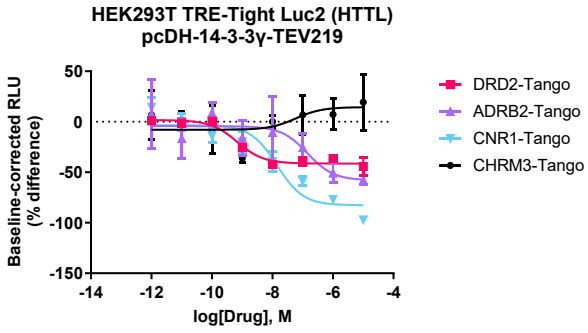

	LogEC50	EC50	Fold
DRD2-Tango	-9.171	6.749e-010	0.5765
ADRB2-Tango	-6.844	1.433e-007	0.4387
CNR1-Tango	-7.852	1.405e-008	0.1793
CHRM3-Tango	-7.228	5.912e-008	1.244

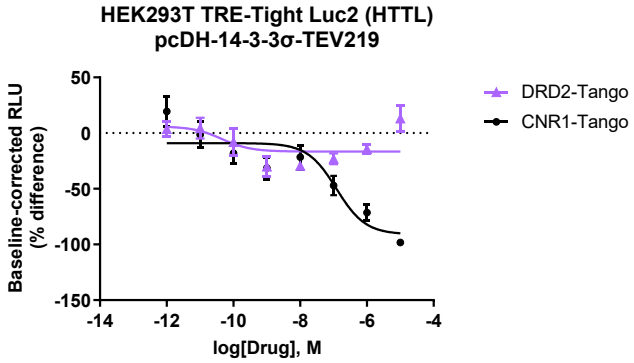

	LogEC50	EC50	Fold
CNR1-Tango	-6.913	1.221e-007	0.09924
DRD2-Tango	-10.35	4.486e-011	0.7869

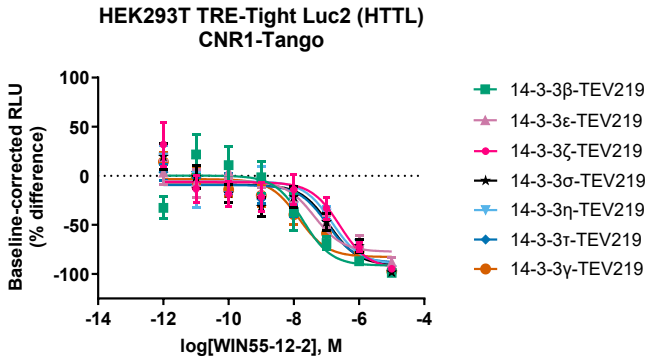

	LogEC50	EC50	Fold
14-3-3ε-TEV219	-7.370	4.268e-008	0.2391
14-3-3β-TEV219	-7.714	1.933e-008	0.08530
14-3-3η-TEV219	-6.824	1.501e-007	0.1069
14-3-3ζ-TEV219	-6.594	2.545e-007	0.06023
14-3-3τ-TEV219	-6.979	1.049e-007	0.1268
14-3-3γ-TEV219	-7.852	1.405e-008	0.1793
14-3-3σ-TEV219	-6.913	1.221e-007	0.09924

Supplementary Figure 4.1A. Interaction of CNR1-Tango Receptor with 14-3-3 Isoforms in HTTL Cells. GPCRs previously reported to interact with 14-3-3 proteins, including CHRM1, CHRM3, DRD2, ADRB2, SSTR4, CNR1, and OPRK1, were evaluated in HTTL cells for their ability to recruit or dissociate the seven different 14-3-3 isoforms. HTTL cells were transduced with supernatant containing cumate-inducible pcDH lentiviral vectors encoding 14-3-3-TEV219 fusion proteins; expression was induced by the addition of 30 µg/mL cumate, which was kept for the duration of the experiment. This preliminary work was used to determine CNR1-Tango as the ideal candidate for the monoclonal cell line selection process, given its interactions of all 14-3-3 isoforms. Transfected cells were stimulated with the receptor specific agonist and dose- response curves were built using XY analysis for non-linear regression curve and the 3-parameters dose-response stimulation function, followed by baseline correction. All error bars represent SEM (n = 3 technical replicates).

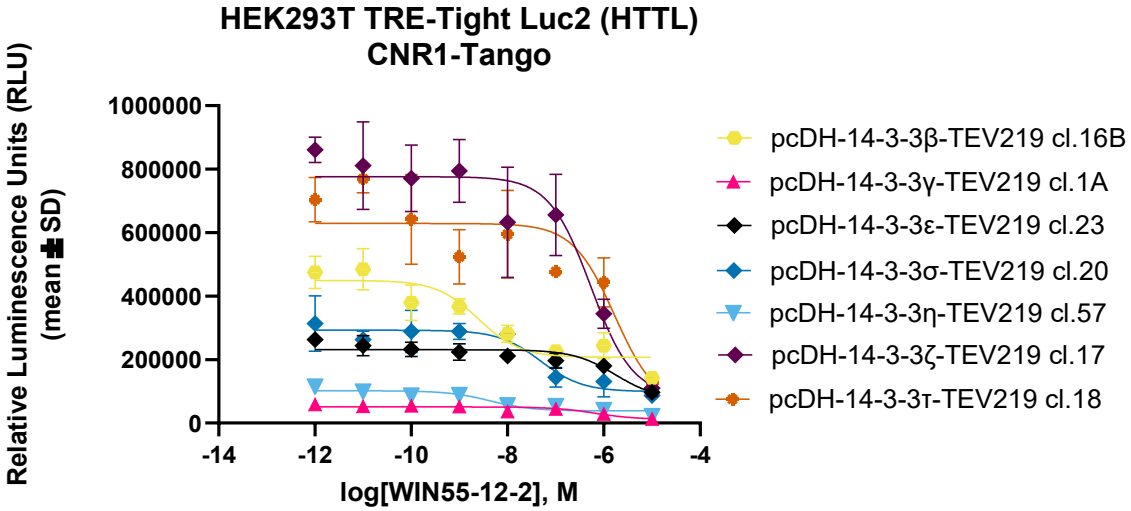

	Bottom	Top	LogEC50	EC50	Fold
pcDH-14-3-3γ-TEV219 cl.1A	50774	11294	-6.184	6.543e-007	0.2224
pcDH-14-3-3ε-TEV219 cl.23	231023	74983	-5.770	1.700e-006	0.3246
pcDH-14-3-3β-TEV219 cl.16B	449465	207031	-8.608	2.465e-009	0.4606
pcDH-14-3-3η-TEV219 cl.57	101685	38334	-8.363	4.335e-009	0.3770
pcDH-14-3-3ζ-TEV219 cl.17	776272	83149	-6.270	5.371e-007	0.1071
pcDH-14-3-3σ-TEV219 cl.20	292573	98989	-7.317	4.818e-008	0.3383
pcDH-14-3-3τ-TEV219 cl.18	628823	50371	-5.778	1.667e-006	0.08010

Supplementary Figure 4.1B. Selection of monoclonal cell lines expressing cumate-inducible 14-3-3-TEV219 probes.

14-3-3β, η, ε, γ, τ, σ and ζ fused to TEV219 were cloned in the pcDH lentiviral destination vector encoding a zeocin selection gene. Lentiviruses expressing these constructs were prepared in HEK293T cells, and the resulting lentiviral medium was collected, filtered and added to the host reporter cell line HTTL (HEK293T stably expressing TRE-Tight-controlled Luc2). Selection was performed for three weeks with zeocin, followed by the isolation of single colonies into 48-well plates. Clones were subsequently expanded to 6-well plates for testing in Tango and henceforth maintained in a saturating concentration of 30 µg/mL cumate to induce fusion protein expression. All clones were transiently transfected with CNR1-Tango and transfected cells were stimulated with the receptor specific agonist WIN55-12-2. Luciferase expression was read the following day, and dose-response curves were built in GraphPad Prism software using XY analysis for non-linear regression curve and the 3-parameters dose-response stimulation function.

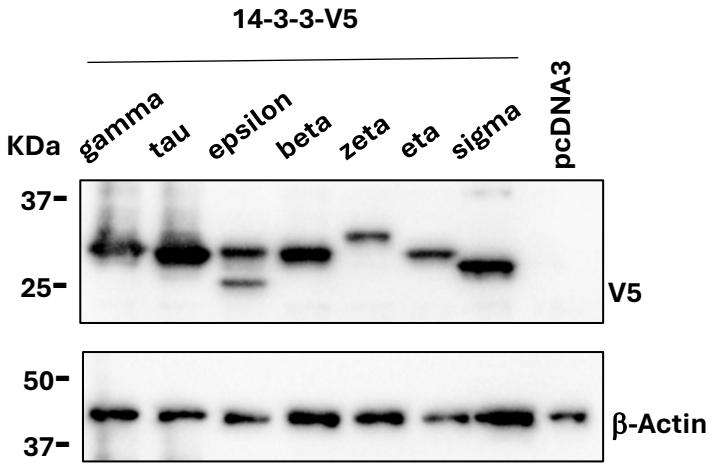

Supplementary Figure 4.2. Validation of 14-3-3 Protein Expression Using Western Blotting

Representative Western blot of HEK293T cell lysates, illustrating the detection of the seven V5-tagged 14-3-3 isoforms with a V5 tag primary antibody; pcDNA3 was used as a negative control. The proteins were separated using a 4-12% Bis-Tris gel, transferred to PVDF membranes, and detected using HRP-conjugated secondary antibodies. β-Actin served as a loading control to ensure equivalent protein loading across samples.

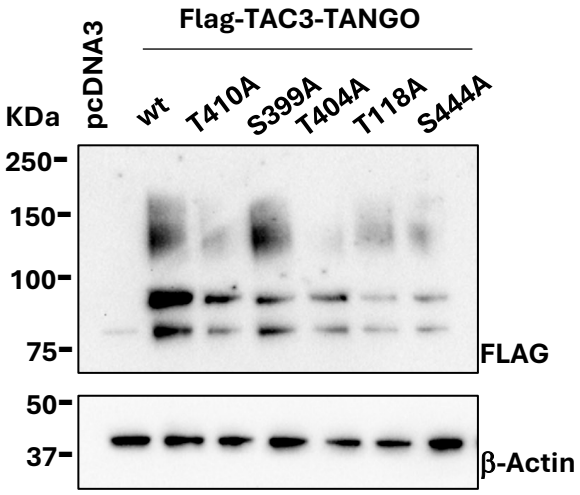

Supplementary Figure 4.3. Western Blot Analysis of TACR3 Mutant Receptor Expression

HEK293T cells were transfected with either WT TACR3 receptor, or T410A, S399A, T404A, T118A, or S444A mutant receptors. Lysates were subsequently prepared and subjected to SDS-PAGE on a NuPAGE 4-12% Bis-Tris gel, followed by transfer to a PVDF membrane. The membrane was probed with a primary V5 tag antibody (Abcam), and a secondary HRP-conjugated anti-mouse IgG antibody (Cell Signaling Technology). Protein bands were visualized using Bio-RAD Clarity ECL substrate. β-Actin was used as a loading control.

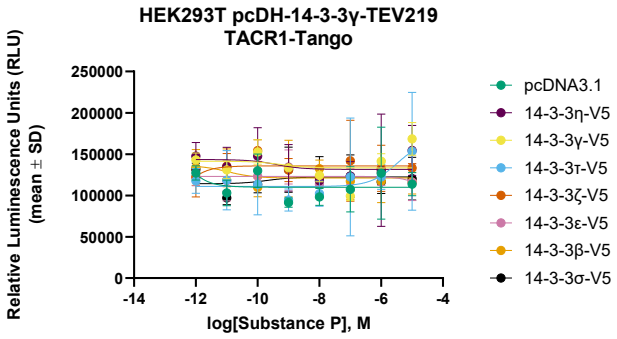

	Bottom	Top	LogEC50	EC50	Fold
pcDNA3.1	Unstable	109924	-16.95	1.116e-017	Unstable
14-3-3γ-V5	141437	133335	-9.229	5.900e-010	0.9427
14-3-3τ-V5	110855	167513	-5.473	3.364e-006	1.511
14-3-3η-V5	143457	131577	-9.398	3.997e-010	0.9172
14-3-3ζ-V5	Unstable	135828	-16.66	2.196e-017	Unstable
14-3-3ε-V5	123109	Unstable	0.003329	1.008	Unstable
14-3-3β-V5	136380	121066	-10.96	1.093e-011	0.8877
14-3-3σ-V5	114117	122312	-9.680	2.089e-010	1.072

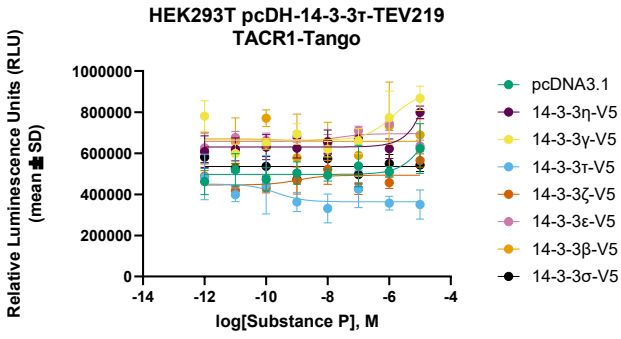

	Bottom	Top	LogEC50	EC50	Fold
pcDNA3.1	497067	898767	-4.659	2.194e-005	1.808
14-3-3γ-V5	663953	895038	-5.891	1.286e-006	1.348
14-3-3τ-V5	450204	363500	-9.657	2.205e-010	0.8074
14-3-3η-V5	630208	Unstable	-2.334	0.004631	Unstable
14-3-3ζ-V5	445661	492685	-8.981	1.044e-009	1.106
14-3-3ε-V5	657663	695182	-7.664	2.167e-008	1.057
14-3-3β-V5	669400	657682	-9.421	3.793e-010	0.9825
14-3-3σ-V5	Unstable	535042	Unstable	Unstable	Unstable

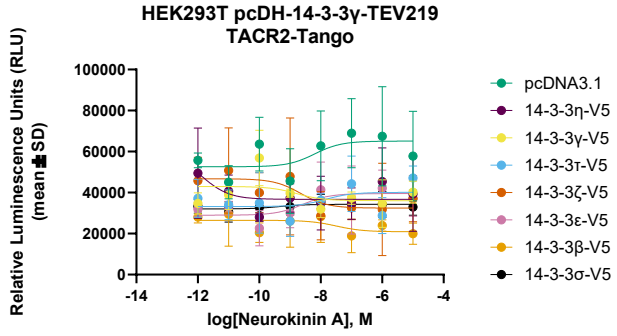

	Bottom	Top	LogEC50	EC50	Fold
pcDNA3.1	52591	65109	-8.197	6.359e-009	1.238
14-3-3γ-V5	42983	36070	-8.788	1.629e-009	0.8392
14-3-3τ-V5	33202	40113	-7.854	1.399e-008	1.208
14-3-3η-V5	58179	36725	-11.83	1.473e-012	0.6312
14-3-3ζ-V5	46739	32446	-8.651	2.234e-009	0.6942
14-3-3ε-V5	28986	39531	-8.583	2.612e-009	1.364
14-3-3β-V5	26486	20905	-7.490	3.237e-008	0.7893
14-3-3σ-V5	32013	34283	-9.365	4.311e-010	1.071

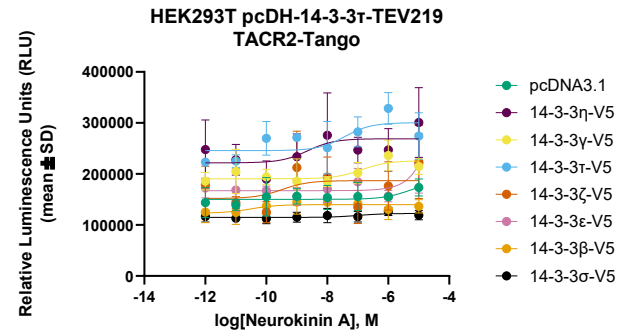

	Bottom	Top	LogEC50	EC50	Fold
pcDNA3.1	150309	185048	-5.304	4.961e-006	1.231
14-3-3γ-V5	190624	225841	-6.869	1.351e-007	1.185
14-3-3τ-V5	245764	300481	-7.428	3.731e-008	1.223
14-3-3η-V5	221803	268985	-8.644	2.272e-009	1.213
14-3-3ζ-V5	151860	186885	-9.486	3.265e-010	1.231
14-3-3ε-V5	167304	4524319299	-0.06233	0.8663	27042
14-3-3β-V5	123062	139892	-10.51	3.124e-011	1.137
14-3-3σ-V5	114825	122556	-6.990	1.022e-007	1.067

Supplementary Figure 4.4. Effects of 14-3-3 Isoform Overexpression on β-arrestin-2 Recruitment at NK1 and NK2 receptors. To explore the impact of 14-3-3 homo- and heterodimer configurations on GPCR signaling, TACR1 and TACR2-Tango were transiently transfected into the HTTL/14-3-3-TEV219 stable cell lines, alongside the individual overexpression of 14-3-3-V5 isoforms or pcDNA3.1 as the negative control. Transfected cells were stimulated with the receptor specific agonists substance P and neurokinin A, respectively, and dose-response curves were built using XY analysis for non-linear regression curve and the 3-parameters dose-response stimulation function. All error bars represent SEM (n = 3 technical replicates).

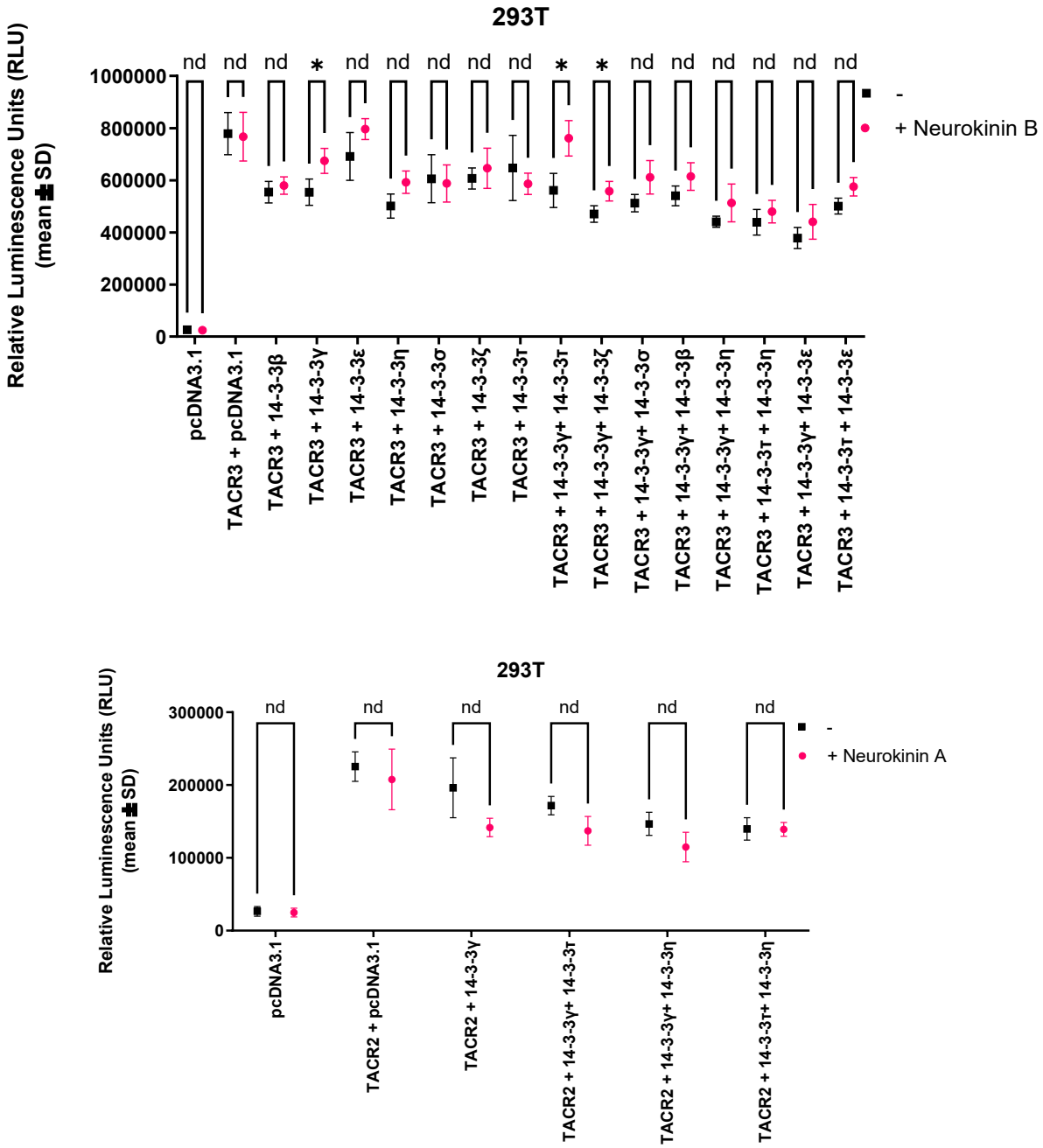

Supplementary Figure 4.5. Comparison of Cell Surface Expression Changes in TACR3 and TACR2 Following Overexpression of 14-3-3 τ and/or γ Isoforms.

HEK293T cells were transfected with pcDNA3.1+, TACR3-Tango and TACR2-Tango (FLAG-tagged), and 14-3-3-V5 constructs or pcDNA3.1 as a negative control. Cells were subsequently re-plated in 384-well plates and fixed with 4% paraformaldehyde. Following fixation, cells were blocked with 5% normal goat serum in PBS and incubated with an anti-FLAG-HRP conjugated antibody. Luminescence was measured after the addition of Supersignal ELISA Femto Substrate. Data are presented as mean ± SD from four independent measurements.

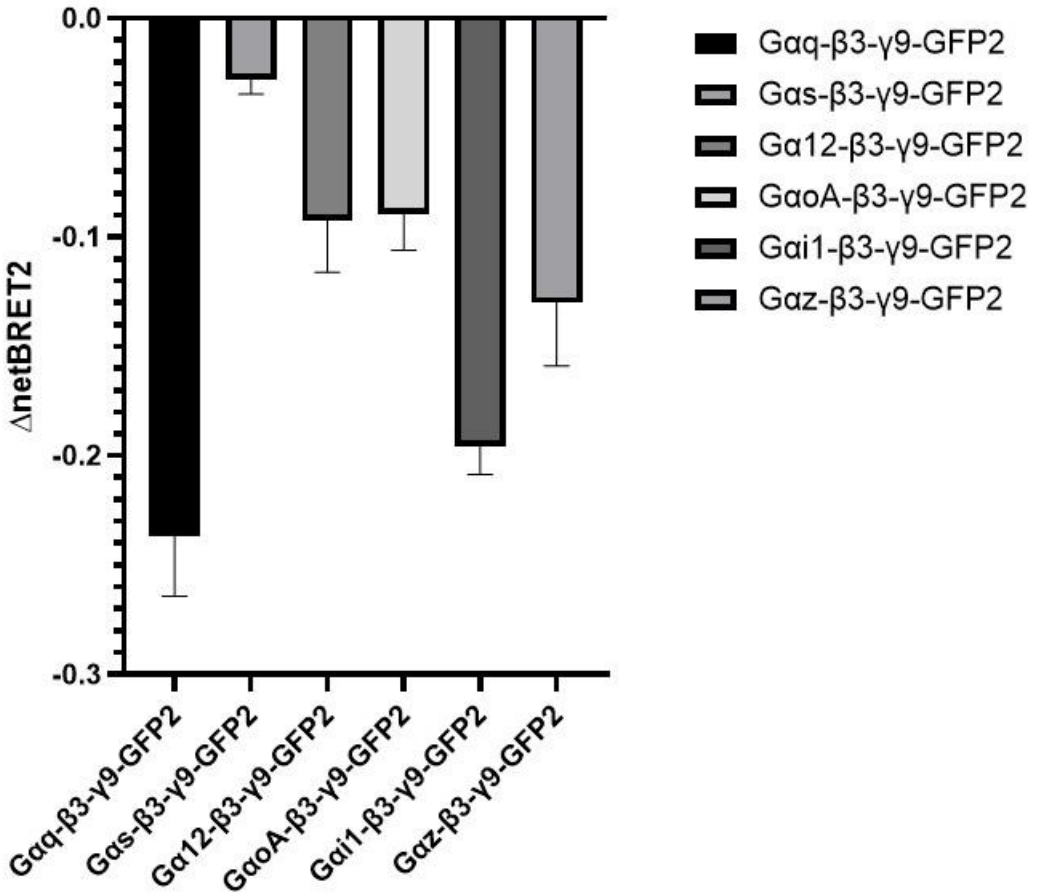

Supplementary Figure 4.6. Evaluating the performance of Gα subunit-Rluc8 constructs for NK3.

HEK293T cells were transfected with a 2 µg mixture of BRET2 constructs (NK3-SmBit: Gα-Rluc8 : Gβ3 : Gγ9-GFP2 in a 3:1:3:3 ratio) using PEI. Cells were seeded on PLL-coated 96-well plates and treated with Neurokinin B. After incubation, luminescence was recorded at 405 nm (RLuc8-Coelenterazine 400a) and 500 nm (GFP2) using the Hidex Sense Beta Plus microplate reader. Data represent mean values from the 30-minute time point following the addition of Coelenterazine 400a.

CHAPTER 5: Discussion and Conclusions

True to their name, G protein-coupled receptors (GPCRs) transiently associate with heterotrimeric G-proteins to propagate their conformational changes into downstream signalling events. In concert with G-proteins, the scaffolding protein β-arrestin2 binds to hundreds of GPCRs, typifying the canonical interactome of GPCRs. However, this oversimplified presentation of the communication interface of GPCRs has led to the "Streetlight Effect", which could negatively impact a comprehensive characterization of receptors, as well as the development of effective drugs. For example, in the study of functional selectivity, seminal work by Schmid et al. (2017) demonstrated a strong correlation between the relative signaling bias of compounds at MOR and their therapeutic windows, giving rise to the possibility of developing safer opioids by favouring certain pathways. In sum, β-arrestin2-biased compounds, such as fentanyl, were more likely to induce side effects, while G-protein-biased agonists resulted in more efficacious analgesia. However, discrepancies to this theory continue to be brought to light; for example, morphine-induced (morphine is an unbiased opioid) addiction was substantially enhanced in β-arrestin2 KO mice, and a recent publication demonstrated that morphine-induced respiratory depression is independent of β-arrestin2 signalling. This suggests that in vitro profiling of functional selectivity solely at G-protein vs. β-arrestin2 pathways does not truly well define the in vivo therapeutic potential of a drug. To overcome the knowledge gap surrounding pharmacological profiling of GPCRs, defining the role of other neighboring and interacting partners, termed GPCR interacting proteins (GIPs), has began to slowly gain momentum, shedding light on how GIPs can modulate receptor ligand specificity (e.g. RAMPs), receptor endocytosis (e.g. Arf6, RalA, phospholipase D2), expression at the cell surface (e.g. PSD95), and receptor recycling (e.g. 14-3-3, SAP97).

As such, this project had the overall goal of identifying, at the GPCRome level, overlapping and distinct functional signatures of GPCR activity, especially the role of lesser-studied GIPs. It was hypothesized that the interactome of GPCRs and the activities occurring throughout their life cycle (including but not limited to recruitment and dissociation of particular GIPs, functional selectivity of ligands, and GPCR internalization) will correlate with the pharmacological profiles observed between different receptors.

In this dissertation, the aforementioned goal was approached two different ways, specifically by developing cell-based platforms capable of high-throughput screening of a small set of GIPs at hundreds of non-olfactory class A GPCRs, simultaneously or not, (Chapters 1 and 3), and by creating an intrabody biosensor capable of probing a wide range of proteins found in the proximal cytoplasmic interactome of select GPCRs (Chapter 2).

Chapter 1 presents a high-throughput platform for profiling basal and ligand-dependent GPCR activities using a polyvalent cell-based assay based on the PRESTO-Tango platform. Dubbed Tango-Trio, the application of the aforementioned platform comprised the simultaneous interrogation of β-arrestin2, β-arrestin1, and internalization of non-olfactory druggable GPCRs. Multiple hits were identified from both agonist-dependent and basal activity high-throughput screenings, showcasing significant log2 fold changes in arrestin recruitment and GPCR internalization across various receptor constructs, with heat maps constructed to group different classes to identify class-specific activity patterns. The heat maps revealed that β-arrestin2 generally had higher recruitment compared to β-arrestin1 across various GPCRs, which was particularly evident in the agonist-dependent activity screen, suggesting that the presence of an agonist can significantly influence the recruitment dynamics of the two arrestin isoforms and diverging activation mechanisms between basal-activated and ligand-activated receptors. Additionally, class A receptors had a notable trend of substantially higher β-arrestin2 recruitment, such as the AGRT1 receptor, compared to class B, which displayed more balanced signalling overall. For the basal screening, orphan receptors displayed variable recruitment patterns, highlighting the diverse nature of these receptors. Taking advantage of the unique cumate-inducible nature of the Tango-Trio system to quantify basal activity, a range of potential inverse agonists were validated; interestingly, no drug was able to completely ablate the basal activity observed. Moreover, inverse agonists acted differently on the arrestin isoforms, such as Mepyramine reducing basal activity only for β-arrestin2 at histamine H1 receptor (HRH1)-Tango, while Cetirizine inhibited activities for both isoforms. Interestingly, some compounds previously designated as antagonists or inverse agonists, such as FC-131 at CXCR4-Tango and Tolvaptan at AVPR2-Tango, unexpectedly increased the constitutive translocation of arrestins as well. This work also highlighted the heterogeneous nature of endocytosis mechanisms among GPCR members, especially those with basal activity. For instance, the dominant-negative dynaminK44A was used to show varying degrees of inhibition in

GPCR internalization, suggesting multiple compensatory internalization mechanisms. Constitutive internalization at a given receptor sometimes corresponded to the profile of one of the arrestin isoforms. For example, 5-HT1D and CHRM5 showed significant constitutive internalization corresponding to arrestin activities, while GPR126 and VIPR2 exhibited constitutive internalization in the absence of arrestin activities. However, the use of the FYVE domain to track GPCR internalization has limitations, such as potential PI3K activation leading to biased results and weak binding affinity, which may reduce sensitivity. Alternative fusion proteins like EEA1 could be considered for better results and to validate Tango-Trio findings in future work.

One of the most significant advances of the Tango-Trio system is its ability to investigate orphan receptors and quantify their activation independent of G-protein involvement. One of the initial steps in the de-orphanization of an oGPCR is identifying the intracellular pathways it signals through. This provides a crucial functional readout for developing screening platforms to evaluate receptor activation by potential endogenous or synthetic ligands. However, the absence of known ligands poses a significant challenge, restricting the experimental approaches available for interrogating oGPCRs (Jobe and Vijayan, 2024). A less commonly employed strategy to tackle this challenge involves assessing the receptor's constitutive activity (Watkins and Orlandi, 2021); therefore, Tango-Trio has the potential to advance deorphanization initiatives in future studies and broadening the therapeutic landscape.

Moreover, Tango-Trio addresses the existing research challenge of capturing pharmacological parameters related to basal activities, as well as the paucity of data on ligand-induced β-arrestin1 recruitment and internalization across the GPCRome. This work highlighted the limited comprehension of the distinctions in GPCR activities between basal and ligand-dependent states, suggesting the presence of disparate mechanisms in these activation contexts. As such, further exploration is warranted into the structural and functional nuances between β-arrestin1 and β-arrestin2, particularly concerning their coupling dynamics and selectivity at GPCRs; for example, future studies should be devoted to comparing the structural interface positions common among related receptors to gain molecular insights into recruitment of β-arrestin1 vs β-arrestin2. One limitation observed was the discrepancies when comparing the Tango-Trio and EMTA ebBRET system, where differences in outcomes due to the overexpression of GRKs affects arrestin recruitment levels, underscoring the importance of kinases and other tissue-specific GIPs in the

life cycle and signalling consequences of GPCRs. Moreover, the phenomenon of biased signalling, presents another fertile ground for future experimentation, particularly the differential recruitment of β-arrestin isoforms. The distinct roles of β-arrestin1 and β-arrestin2 in modulating receptor function and downstream signaling pathways are areas of burgeoning interest as well, such as at cannabinoid receptors. β-arrestin1 and β-arrestin2 play distinct and sometimes overlapping roles in CB1 signaling, internalization, and behavioral effects, with their functions varying based on ligand type and brain region, and this complexity influences acute and chronic responses to cannabinoids. With regard to signalling dynamics, β-arrestin1 promotes slower, sustained ERK1/2 phosphorylation localized to endosomes, affecting cytoskeletal dynamics and protein translation, while β-arrestin2 facilitates receptor internalization and has a lesser role in ERK1/2 signaling. Moreover, these translate to behavioural effects, such as how β-arrestin1 contributes to cannabinoid-induced analgesia and hypothermia, while β-arrestin2 often has a regulatory role (Leo and Abood, 2021). Utilizing the Tango Trio assay to dissect the nuances of β-arrestin1 vs. β-arrestin2 recruitment and their subsequent signaling outcomes could provide critical insights into the biased agonism paradigm. For example, different cannabinoids preferentially recruit β-arrestin isoforms: CP55940 favors β-arrestin1, while THC favors β-arrestin2 (Leo and Abood, 2021). This would not only enhance our comprehension of GPCR signaling specificity but also inform the design of ligands that preferentially engage one β-arrestin isoform over the other, potentially leading to more targeted and refined therapeutic strategies.

Chapter 2 introduces NbV5, a novel nanobody designed to interact with the V5-tag, enabling the advancement of intracellular biosensors for monitoring dynamic protein-protein interactions, particularly within the context of GPCR signaling and microscopic imaging techniques. The NbV5-based biosensors were effectively implemented in various cellular assays, including Tango, BRET, and NanoBiT, showcasing their utility in studying GPCR signaling pathways with minimal interference. Generated through a Hybribody approach involving synthetic VHHs phage display and yeast two-hybrid screening, NbA1 emerged from a pool of 52 distinct VHHs, each displaying high specificity for the V5-tag. Structural analysis revealed that NbA1 primarily engages the V5 peptide via the CDR2 and CDR3 regions, forming multiple polar and hydrophobic contacts, thus ensuring precise and tight interaction between epitope and nanobody. Codon optimization for human expression was carried out to significantly enhance the expression level of the nanobody,

increasing its functional activity threefold in our mammalian cells. Seeing that original NbA1 clone only recognized C-terminally tagged β-arrestin2, an *in silico* affinity maturation strategy was employed using the Rosetta modeling software, generating ten mutants that were tested in functional assay. Two mutations, ΔD59 and S60K, were identified as resulting in better activity than NbA1, especially for the N-terminal V5-tagged arrestin, and consequently, an optimized nanobody dubbed NbV5 was created by incorporating said mutations. NbV5 was adapted as a biosensor in three major PPI assays, specifically Tango, BRET, and NanoBit assays, using μ-OR and AT1R as proof-of-concept receptors. The NbV5-adapted Tango assay showed similar EC50 values to the original Tango assay, indicating that the adaptation did not alter the assay's sensitivity. In the BRET system, μ-OR was ineffective, possibly due to its conformation not being conducive to efficient resonance energy transfer; however, arrestin recruitment was successfully detected using AT1R, confirming NbV5's application in a BRET system. NbV5-based biosensors were also capable of detecting arrestin recruitment at both receptors in the NanoBiT assay and demonstrated functional recognition of an internally localized V5-tag, showing versatility in different configurations. Additionally, NbV5 demonstrated potential as a genetically encoded tracker, selectively interacting with V5-tagged γ-actin, thereby facilitating the visualization of actin-related structures in live cells.

This work addresses a significant gap in the availability of nanobodies that recognize small peptide fragments, particularly epitope tags like V5. The scarcity of tag-targeted intrabodies has hindered comprehensive studies on protein-protein interactions, despite the existence of tag-encoded cDNA libraries, such as the TRC3 ORF V5-tagged library. However, several significant obstacles exist towards creating functional intrabodies, including the propensity for aggregation and the reducing conditions of the cytoplasm, the limited activity of these fragments in an intracellular milieu, attributed to the absence of intradomain disulfide bond formation. The potential applications of NbV5 stand to be greatly expanded, especially broadening its application to encompass a wider array of G-protein-interacting proteins (GIPs), such as 14-3-3 and SAP97. Conducting a genome-wide screen involving key receptors like the μ-OR presents an exciting frontier for exploration, enabling a comprehensive profiling of the entire repertoire of GIPs that are recruited or dissociated upon ligand binding to this receptor. For instance, a genome-wide screen to fish for novel interactors could be conducted using Bimolecular Fluorescence Complementation (BiFC). This approach leverages fluorescence for fluorescence-activated cell sorting (FACS) and benefits from

the high strength and irreversible nature of the interactions, direct visualization in live cells, and sensitive readout to detect PPIs at low expression levels similar to those of endogenous proteins (Lai and Chiang, 2013). In this setup, the target receptor, such as μ-OR, would be fused to the C-terminal half of the Venus fluorescence protein (VC), while NbV5 would be attached to the N-terminal half of Venus (VN). Using the TRC3 ORF V5-tagged library, if a protein is part of the receptor's proximal interactome, NbV5 will bind to it, leading to the reconstitution and folding of the Venus fluorescence protein, thereby generating detectable fluorescence with a 528 nm emission. To validate these interactions, complementary techniques such as BRET, FRET, NanoBiT, or Tango assays could be employed. However, potential limitations such as protein orientation and steric hinderance must be considered. The identification of these dynamic protein interactions could have profound implications for drug discovery and development, particularly in the context of pain management and addiction therapy, such as the development of biased ligands towards certain GIPs that exhibit reduced negative side effects. Moreover, future work will be dedicated to expanding the applicability of the NbV5:V5 system to a broad range of PPIs beyond GPCRs, including other membrane receptor-protein interactions.

Chapter 3 delves into the dynamics of 14-3-3 proteins at the NK3 receptor interface within GPCR signaling, emphasizing isoform-specific effects that have not been fully investigated in previous studies. This work marks the first comprehensive characterization of GPCR-14-3-3 interactions on a GPCRome scale, revealing novel insights into the recruitment and dissociation patterns of 14-3-3 isoforms across different GPCRs, especially uncovering the critical role of 14-3-3γ in influencing canonical signaling pathways at NK3. Our findings revealed how overexpression of specific isoforms can significantly alter recruitment dynamics, particularly enhancing recruitment fold changes at the NK3 receptor following the overexpression of 14-3-3γ and 14-3-3τ isoforms. Moreover, the interplay between 14-3-3 proteins and other intracellular partners is discussed, specifically how the aforementioned isoforms were found to modulate canonical signaling pathways by attenuating G-protein dissociation and enhancing β-arrestin recruitment, as confirmed in orthogonal NanoBit and BRET systems.

The NK3 receptor, given its involvement in regulating mood, anxiety, stress responses, and its critical role in the reproductive system, has importance for future therapeutic investigations. For example, NK3 is known to play a critical role in the regulation of the reproductive axis, particularly

in the modulation of gonadotropin-releasing hormone (GnRH) release. 14-3-3 interactions with NK3 could be involved in stabilizing or regulating activity in the hypothalamus, thereby influencing reproductive outcomes. Future experiments could involve Fezolinetant (MLE4901), a non-hormonal antagonist selectively targeting NK3 which has been investigated for its potential in alleviating menopausal symptoms, particularly hot flashes (Skorupskaite et al., 2017). A few studies have demonstrated that NK3 receptor antagonism can reduce luteinizing hormone (LH) levels in individuals, which is relevant for managing menopausal symptoms (George et al., 2016). This suggests that blocking the NK3 receptor, which is involved in the regulation of gonadotropin-releasing hormone (GnRH) secretion, can alleviate menopausal symptoms (Skorupskaite et al., 2017). A phase 2 randomized, double-blind, placebo-controlled trial found that Fezolinetant significantly reduced the frequency and severity of hot flashes in postmenopausal women compared to placebo (Prague et al., 2017). However, the full spectrum of its pharmacological effects remains to be fully elucidated. By investigating how Fezolinetant influences the recruitment and dissociation of 14-3-3 isoforms, as well as G-protein and arrestin signalling, we can gain a more comprehensive understanding of its mechanism of action and identify which pathways contribute to its therapeutic efficacy. However, it is important to note that although Fezolinetant may inhibit G-protein signalling at NK3, it does not necessarily mean that the same effect will be observed for 14-3-3. Certain antagonists and inverse agonists have been shown to challenge the classical models of receptor activation and inhibition, such as promoting processes such as receptor endocytosis and stabilizing specific receptor states capable of engaging β-arrestin, which is typically associated with agonists (Roettger et al., 1997). For example, such as ICI118551 and propranolol have been to shown to exhibit partial agonist efficacy on the β-arrestin-dependent MAPK pathway (Azzi et al., 2003).

Identification of critical residues within NK3 and the functional implications of 14-3-3 activity is should also be considered for future research for therapeutic targeting of these interactions. In the context of this dissertation, determining functional consequences of T118 mutation in NK3, its impact on receptor recycling dynamics, and surface expression modulation is warranted for a comprehensive understanding of receptor signaling modulation. Finally, future studies will be conducted to confirm subcellular localization of 14-3-3 interactions, especially with the 14-3-3γ isoform, in order to better understand their role in enhancing 14-3-3 dimer interactions or promoting NK3 cell surface expression.

In sum, the composite effect of the wide array of G-protein interacting proteins, such as β-arrestin and 14-3-3 isoforms, GPCR phosphorylation catalyzed by kinases, as well as receptor type, the absence or presence and type of ligand, must be collectively considered to inform the diversified consequences of GPCR signal transduction, such as desensitization, endocytosis, recycling, or the continuation of signal transmission. Towards these efforts, I hope that the cell-based screening platforms and nanobody probe developed in this dissertation will aid in establishing accurate and comprehensive pharmacological profiles.

Appendix I: Scholarly Contributions

Publications

1. **Manel Zeghal,** Geneviève Laroche, Julia Douglas Freitas, Rebecca Wang, Patrick M. Giguère (2023). *Profiling of constitutive and ligand-dependent GPCR activities by means of a polyvalent cell-based high-throughput platform.* Nature Communications, DOI: 10.1038/s41467-023-39132-x.
2. **Manel Zeghal*,** Kevin Matte*, Angelica Venes, Shivani Patel, Geneviève Laroche, Sabina Sarvan, Monika Joshi, Jean-Christophe Rain, Jean-François Couture, Patrick M. Giguère (2023). *Development of a V5-tag-directed nanobody and its implementation as an intracellular biosensor of GPCR signalling.* Journal of Biological Chemistry, DOI: 10.1016/j.jbc.2023.105107
3. Abdulhamid O. Mohamud*, **Manel Zeghal*,** Shivani Patel, Geneviève Laroche, Nuria Blgacim, Patrick M. Giguère (2022). *Functional characterization of sodium channel inhibitors at the delta-opioid receptor.* ACS Omega, DOI: 10.1021/acsomega.1c07226.
4. **Manel Zeghal**, Geneviève Laroche, Patrick M. Giguère (2020). *Parallel Interrogation of β-Arrestin2 Recruitment for Ligand Screening on a GPCR-Wide Scale using PRESTO-TANGO assay.* J. Vis. Exp, DOI:10.3791/60823.
5. Louis Gendron, Karim Nagi, **Manel Zeghal**, Patrick M. Giguère, Graciela Pineyro (2019). *Molecular aspects of delta opioid receptors.* Vitamins and Hormones, DOI: 10.1016/bs.vh.2019.06.001

   * Contributed equally

In preparation

1. **Manel Zeghal,** Danylo Aloshyn, Samantha K. Rogers, Geneviève Laroche,Patrick M. Giguère (2024). *The protean nature of 14-3-3 proteins in GPCR signaling: highlighting selectivity and dynamic interactions at the NK3 receptor interface.* [In preparation for submission to ACS Pharmacology & Translational Science].

Conferences

1. **Manel Zeghal,** Kevin Matte, Angelica Venes, Shivani Patel, Geneviève Laroche, Sabina Sarvan, Monika Joshi, Jean-Christophe Rain, Jean-François Couture, Patrick M. Giguère. *Development of a V5-tag–directed nanobody and its implementation as an intracellular biosensor of GPCR signaling.* **Poster presentation** at the 22nd Great Lakes GPCR Retreat 2023, Montebello, Quebec, Canada (November 2-4, 2023)
2. **Manel Zeghal**, Geneviève Laroche, Julia Douglas Freitas, Rebecca Wang, Patrick M. Giguère. *Profiling of constitutive and ligand-dependent GPCR activities by means of a polyvalent cell-based high-throughput platform.* **Poster presentation** at the 21st Great Lakes GPCR Retreat 2022, Niagara-on-the-Lake, Ontario, Canada (May 12-14, 2022)

Appendix II: Appended Publications and Permissions to Republish

nature communications

Article

https://doi.org/10.1038/s41467-023-39132-x

Profiling of basal and ligand-dependent GPCR activities by means of a polyvalent cell-based high-throughput platform

Received: 14 August 2022

Accepted: 25 May 2023

Published online: 05 July 2023

Check for updates

Manel Zeghal[1], Geneviève Laroche[1], Julia Douglas Freitas[1], Rebecca Wang[1] & Patrick M. Giguère[1,2]

Representing the most attractive and successful druggable receptors of the proteome, GPCRs regulate a myriad of physiological and pathophysiological functions. Although over half of present pharmaceuticals target GPCRs, the advancement of drug discovery is hampered by a lack of adequate screening tools, the majority of which are limited to probing agonist-induced G-protein and β-arrestin-2-mediated events as a measure of receptor activation. Here, we develop Tango-Trio, a comprehensive cell-based high-throughput platform comprising cumate-inducible expression of transducers, capable of the parallelized profiling of both basal and agonist-dependent GPCR activities. We capture the functional diversity of GPCRs, reporting β-arrestin-1/2 couplings, selectivities, and receptor internalization signatures across the GPCRome. Moreover, we present the construction of cumate-induced basal activation curves at approximately 200 receptors, including over 50 orphans. Overall, Tango-Trio's robustness is well-suited for the functional characterization and screening of GPCRs, especially for parallel interrogation, and is a valuable addition to the pharmacological toolbox.

As central orchestrators of cellular and physiological processes, G protein-coupled receptors (GPCRs) mediate the transduction of extracellular stimuli into conformationally-driven intracellular signals. Comprised of more than 800 members in the human genome, the diversity of this superfamily of membrane proteins is shaped by both the multiplicity of ligands they respond to, as well as the diverse array of signaling pathways they coordinate[1–3]. Moreover, GPCRs function in conjunction with protein interactors, whose identities and abundances vary by virtue of tissue- and/or cellular-specific expression[4].

The dynamism of GPCR signaling events is due to the receptors' conformational and locational changes throughout their life cycle, including activation, desensitization, internalization and resensitization. Although there is great diversity of ligands among them, GPCRs share a common fundamental mechanism of receptor activation. GPCRs in their inactive conformation are coupled to a heterotrimeric G-proteins complex, formed of a Gα subunit bound to GDP and Gβγ dimer stabilizing the inactive conformation of the heterotrimer. Activation of the GPCR results in conformational changes which enable the exchange of bound GDP by Gα for GTP, resulting in the dissociation of Gα-GTP and Gβγ-subunits from the receptor, which transduce different downstream signaling cascades depending on the nature of the GPCR and the subclasses of the G-protein subunits, composing the basis of G-protein dependent signaling[5,6]. This classical paradigm posits that activation can be induced not only by agonist binding, but also by virtue of GPCRs' ability to spontaneously adopt active conformations in the absence of agonist, termed constitutive activity[7]. Although it is now widely recognized that all GPCRs exhibit spontaneous activation, albeit at varying degrees, a large-scale quantification of constitutive activity across the GPCRome, including druggable and orphan receptors, has yet to be conducted.

To prevent overstimulation, active GPCRs can be desensitized, wherein kinases such as GRKs phosphorylate the receptor at specific

[1]Department of Biochemistry, Microbiology and Immunology, University of Ottawa, Ottawa, ON K1H8M5, Canada. [2]Brain and Mind Research Institute, University of Ottawa, Ottawa, ON K1H8M5, Canada. e-mail: patrick.giguere@uottawa.ca

serine/threonine residues, typically C-terminal or intracellular loop 3 (IL3) sites[5]. Phosphorylation in turn leads to the recruitment of arrestins, the most well-known and characterized scaffold proteins comprising four isoforms, the two visual arrestins, arrestin-1 and arrestin-4, that are confined to retinal cones and rods, and the ubiquitously expressed nonvisual arrestins, β-arrestin-1 and −2[8]. While nonvisual arrestins have been shown to bind to hundreds of different GPCR members, the vast majority of demonstrations have been conducted with β-arrestin-2, with few studies addressing the contributions of the relevant but often forgotten β-arrestin-1 isoform[9]. Besides inducing receptor desensitization through steric hindrance of the G-protein binding site, arrestins also redirect GPCR signaling to alternative G-protein independent pathways such as MAPKs, JNKs, and Src[10]. Additionally, the engagement of arrestin initiates receptor internalization via dynamin- and clathrin-dependent endocytosis[11]. Besides canonical arrestin-mediated endocytosis, increasing evidence has emerged describing GPCRs internalizing independently of arrestins[12].

Herein, we describe a comprehensive screening and interrogation platform evolved from the PRESTO-Tango, capable of the simultaneous interrogation of β-arrestin-2 recruitment at ~300 non-olfactory druggable GPCRs[13]. The reconstruction of this system was sought in part to increase the dynamic range and sensitivity of the original system, specifically improving the TRE promoter and TEV protease elements, and to expand its versatility beyond monitoring β-arrestin-2. Indeed, our platform, named Tango-Trio, includes monoclonal cell lines expressing trackers of β-arrestin-2, β-arrestin-1, and FYVE domain for internalization, all sharing the common luciferase reporter lineage. Moreover, their cumate-inducible nature enables the study of the various GPCR state-dependent and independent activities. Hereafter, we refer to the following states: the manifest agonist-induced active state; the constitutive active state, which represents ligand-independent activated receptor; steady-state, which refers to state-independent interaction level; and the basal level, which includes the steady-state plus constitutively active receptor pool, which cannot be discriminated in most cases. We are revealing divergent basal versus agonist-dependent β-arrestin-1/2 couplings, selectivities, and receptor endocytosis signatures across the GPCRome. We report the basal sigmoidal-fitted activities of more than 200 class A GPCRs, including ~50 orphans. Our findings represent a step towards uncovering the differences behind the mechanisms of constitutive versus agonist-induced activation, as well as state-independent activity. Moreover, we believe the Tango-Trio platform could facilitate the development of new GPCR-acting drugs and deorphanization efforts.

Results

Development of the Tango-Trio and its comparison to the PRESTO-Tango

The PRESTO-Tango has a number of advantages, including selective read-out as the response is specific to the target receptor, sensitivity due to signal integration to produce a read-out, and the ability to study a multitude of GPCRs as the assay is independent of the G protein family the receptor signals through[13]. As such, we exploited these strategic features to undergird the development of the Tango-Trio platform, while addressing its original limitations, chiefly the tetracycline-response element (TRE) promoter and tobacco etch virus (TEV) protease.

To stringently control gene expression, tTA binding to tetO7 permits transcriptional activation of the luciferase reporter[14]. However, the main limitation to the Tet system is the leakiness due to the strong positional effects on the tetO7 minimal promoter[15], resulting in relatively high background transcription. In turn, this would lead to basal expression that would not be dependent on the tTA, which is intended to be cleaved from the GPCR by the β-arrestin2-TEV fusion protein. The second-generation promoter called TRE-Tight (Clonetech), redesigned tetO7 to remove potential bindings sites of endogenous transcription factors within the operon such as ISRE and GATA, renders this promoter virtually silent in the absence of induction[16]. As expected, lower RLU counts were obtained with TRE-Tight, but the induction factor remained higher for the TRE-Tight promoter (4.5 fold) compared to TRE (2.7 fold) (Fig. 1a); the dopamine D2 receptor (DRD2) Tango receptor was used as it is a strong β-arrestin2 recruiter[13]. Thus, the minimal basal leakage and increased fold window suggest TRE-Tight to be an improved promoter for Tango-Trio and reduce potential arrestin-independent modulation of the reporter activity.

Based on these observations, we generated a monoclonal TRE-Tight Luciferase reporter cell line for the Tango-Trio platform as an improvement over the HTL (HEK293T cells stably expressing TRE-Luc) cells of the original Tango assay (Fig. 1b). Although it is unknown whether Luc or Luc+ was used in creating the HTL cell line, we opted to clone TRE-Tight upstream the Luc2 gene (Promega), a markedly improved variant over its predecessors with significantly lower levels of cryptic transcription from the coding region and codon optimized expression[17]. Henceforth referred to as HTTL (HEK293T TRE-Tight-Luc), our reporter cell line had a comparable level of maximal expression to HTL but possessed a much lower baseline compared to its counterpart, resulting in a larger induction factor.

The Tango system involves a protein fusion consisting of β-arrestin-2 with TEV, which cleaves the engineered GPCR following β-arrestin-2 recruitment to the receptor to release the tTA. However, one limitation of the WT TEV is that it undergoes self-cleavage, generating a truncated protease with greatly diminished activity[18]. A variant of the WT, S219V-stop (TEV219), carries a stabilizing point mutation and was truncated to remove the auto-inhibitory C-terminal tail[19]. Given previous reports of this variant being 100-fold more stable than the full-length TEV and a more efficient catalyst, TEV219 was tested as a replacement for the WT TEV (Fig. 1c). TEV219 significantly lowered the baseline while producing maximal induced expression similar to that observed with the original protease, resulting in a signal ratio more than double (3.3-fold) that of TEV (1.3-fold).

Based on the aforementioned findings, β-arrestin-1, β-arrestin-2, and FYVE, a domain used to probe endocytosis given its high binding affinity and specificity to phosphatidylinositol 3-phosphate (PI3P)-enriched early endosomes[20], were cloned to the chosen TEV219 protease. These trackers were subsequently transferred into the pcDH cumate-inducible destination lentivector, providing robust and reversible expression of genes, and adjustable expression levels by titrating the amount of cumate added to cell medium[21]. The effect of its addition in cumate-independent systems was assessed in the PRESTO-Tango, with negligeable changes to the basal signal in untransfected HTLA (Supplementary Fig. 1a), as well as at the arbitrary Tango-receptors tested (Supplementary Fig. 1b); nonetheless, considering that certain receptors produce weak maximum signals in Tango-based platforms, it is recommended that users test to confirm that cumate does not produce any significant agonistic or antagonistic behavior at the receptors they are employing. HTTL was used as the host cells for the subsequent generation of double stable cell lines, ensuring uniform genetic and reporter background. Monoclonal cell lines for β-arrestin1-, β-arrestin2-, and FYVE-TEV219, henceforth referred to as HTTL-B1, HTTL-B2 and HTTL-F respectively, were screened by functional assay and the final selection was based on pharmacological parameters, including baseline, efficacy, potency, and fold change (E_{max}/E_O). Seeing as the basal signal varies across the three different HTTL cell lines in the absence of receptor expression (Supplementary Fig. 2), the baseline was henceforth defined for each independent experiment and dose-curve construction, specifically as the mean luminescence readings of the three lowest drug dilution concentrations. Following selection, the amelioration of Tango-Trio over the

PRESTO-Tango was assayed by comparing the original HTLA (HTL cells stably expressing β-Arrestin-2-TEV) cell line to our corresponding HTTL-B2.

While both GATA and ISRE are present in the TRE, the redesign of TRE-Tight saw the removal of only ISRE, with GATA still present as it is overlapping with tetO[22]. Based on previous work revealing that phorbol 12-myristate 13-acetate (PMA) activates the ISRE-Luc reporter and induces JAK-STAT signal transduction[23], we postulated that activators of the Jak/Stat pathway would have an impact on the TRE promoter, but not TRE-Tight.

Corroborating this hypothesis, stimulation of HTLA and HTTL-B2 cells with PMA induced a significant response at 5-HT2A- and 5-HT2B-Tango receptors (2.6 and 8.6 fold, respectively) in the HTLA, but was absent in the latter, an effect that could be reversed in HTLA with the addition of Jak Inhibitor I (Fig. 1d–h)[24]. In the same vein, confirmation of the higher specificity of HTTL-B2 over HTLA is exemplified by the lack of activation observed following stimulation of transfected 5-HT2A-Tango receptor with untreated and heat-inactivated FBS, as well as with dialyzed FBS, sera with removed serotonin to prevent nonspecific activity at GPCRs[25]. This effect was

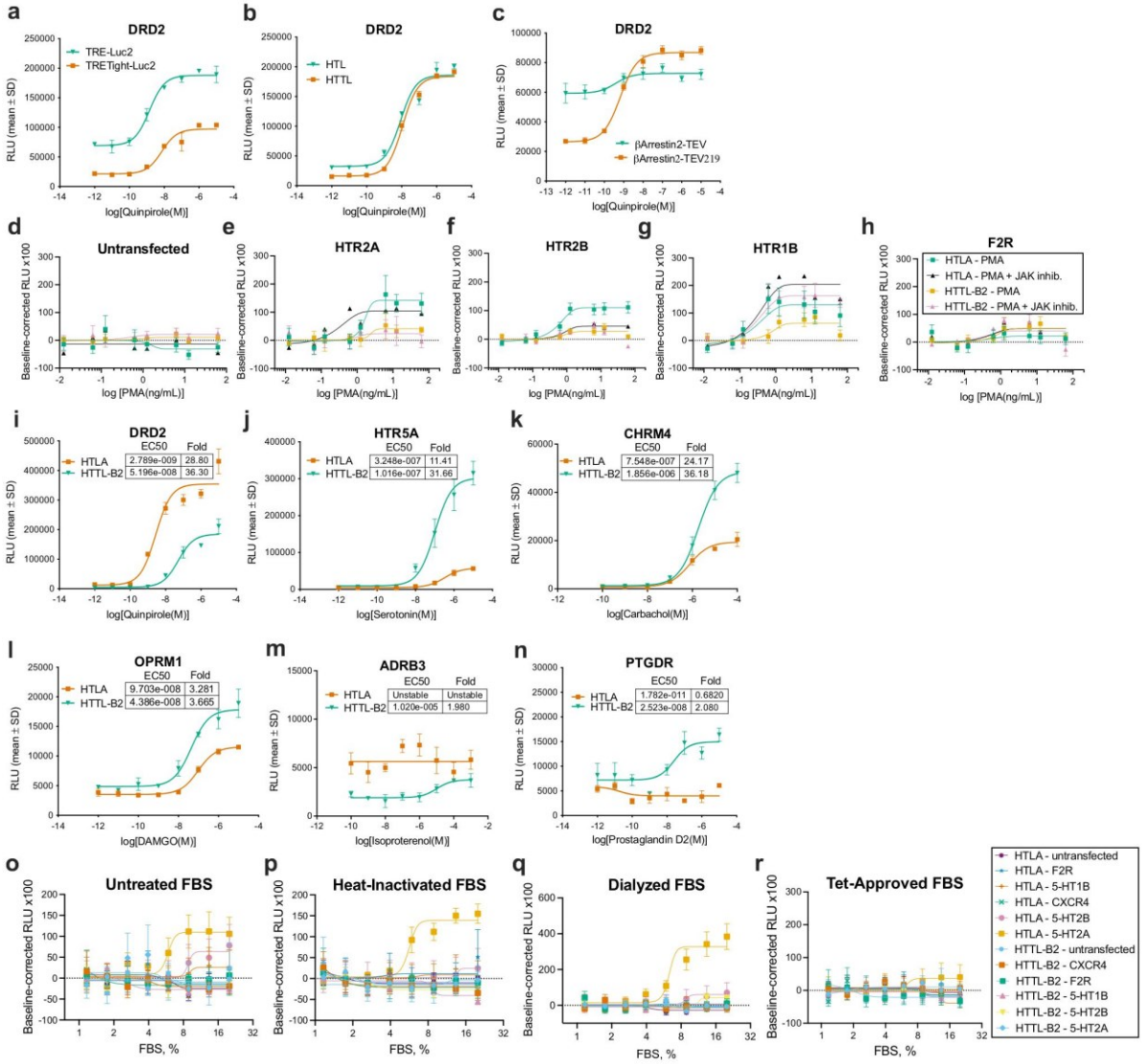

Fig. 1 | Optimization of the dynamic range, sensitivity, and specificity of the Tango-Trio platform. a Comparison of TRE and TRE-Tight. Promoters were cloned upstream luc2, and expression vectors were transfected in HEK293T cells along with the β-arrestin2-TEV fusion protein and DRD2. Transfected cells were stimulated with the DRD2 specific agonist quinpirole. **b** Selection and pharmacological characterization of the monoclonal reporter cell line HTTL (HEK293T-TRE-Tight-Luc2) compared to the original HTL (HEK293T-TRE-Luc) cell line. **c** Comparison of TEV and TEV219 proteases. β-arrestin2 was cloned to both proteases, and transfected in HTL cells with DRD2. Transfected cells were stimulated with the DRD2 specific agonist quinpirole. HTTL-B2 and HTLA were transfected with HTR2A (**e**), HTR2B (**f**), HTR1B (**g**), and F2R (**h**) and stimulated, along with untransfected cells (**d**), with dose-response curve of PMA and in presence/absence of 10 μM JAK inhibitor I. HTTL-B2 and HTLA dose-response curves at various targets: DRD2 to quinpirole (**i**), HTR5A to serotonin (**j**), CHRM4 to carbachol (**k**), OPRM1 to DAMGO (**l**), ADRB3 to isoproterenol (**m**), and PTGDR to prostaglandin D2 (**n**). **o**–**r** Comparison of the specificity of HTTL-B2 and HTLA readouts. Cell lines were transfected with GPCRs that activate the Jak/STAT Pathway and stimulated with serial dilutions of untreated FBS (**o**), heat-inactivated (**p**), dialyzed (**q**), and Tet-System Approved (**r**) sera. HTTL-B2 was maintained in cumate-containing media throughout. Dose- response curves were built using XY analysis for non-linear regression curve and the 3-parameters dose-response stimulation function. Data are presented as mean values, with error bars representing SD. Data are representative of 2 biological replicates, with 3 technical replicates each. Generic receptor codes refer to the GPCR-Tango constructs.

https://doi.org/10.1038/s41467-023-39132-x

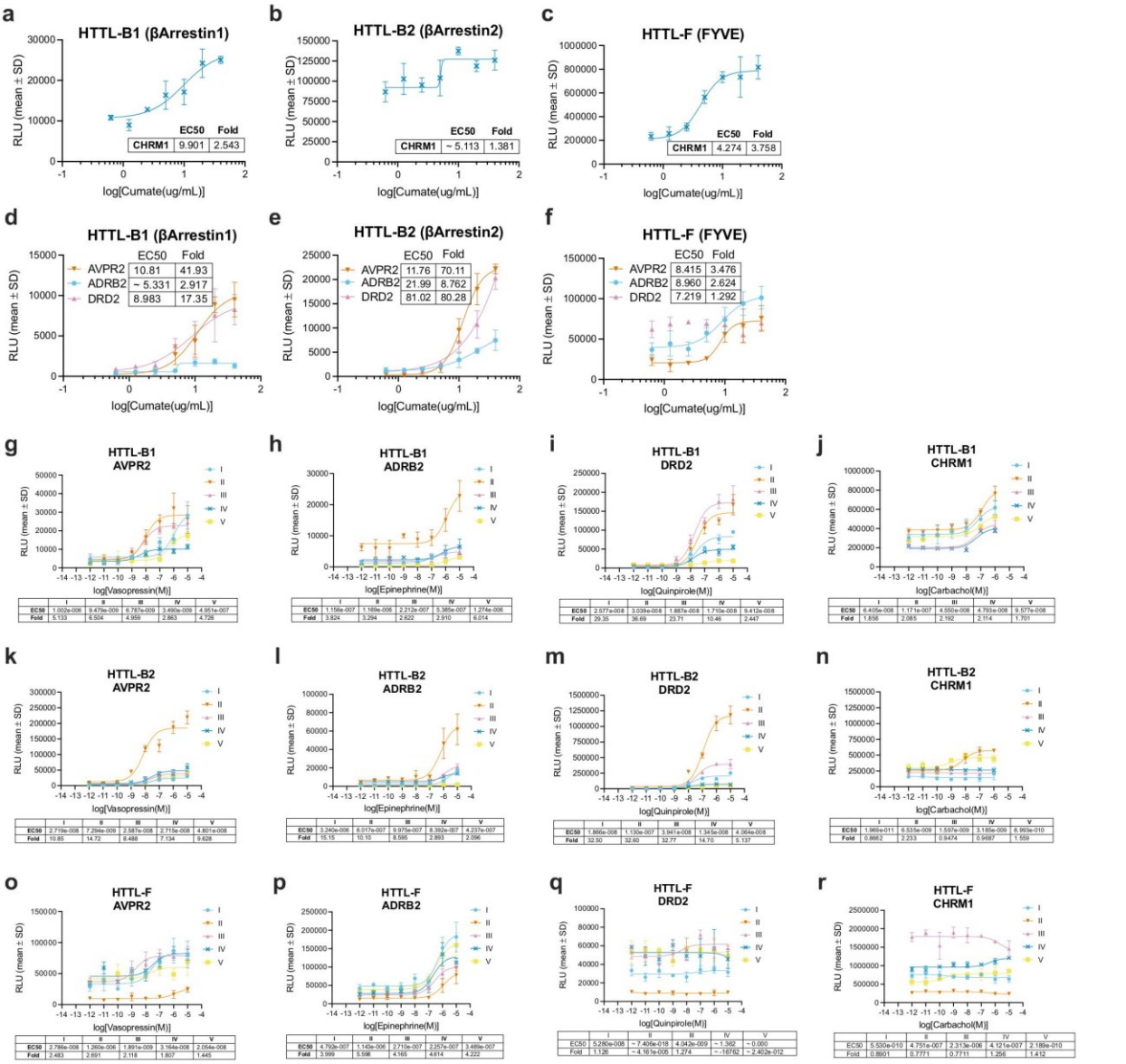

Fig. 2 | Dose-response and time-course verification of cumate-induced expression. Validation of fusion protein induction initiated by cumate dose-responses in HTTL-B1 (**a**, **d**), HTTL-B2 (**b**, **e**), and HTTL-F (**c**, **f**) cell lines. Cells were transfected with AVPR2, ADRB2, DRD2 and CHRM1 Tango receptors and stimulated with a cumate dose-curve starting from 40 μg/mL with 2-fold dilutions. Timing optimization of fusion protein induction in HTTL-B1 (**g**–**j**), HTTL-B2 (**k**–**n**), and HTTL-F (**o**–**r**) cell lines. Cells were transfected with AVPR2, ADRB2, DRD2 and CHRM1 Tango receptors and stimulated with receptor selective agonist. Cumate (30 μg/mL) was added at the following time points and maintained in the cell medium thenceforth: I − 5 days; II − 3 days; III − 2 days; IV − 24 h; V − 18 h total cumate exposure. Dose- response curves were built using XY analysis for non-linear regression curve and the 3-parameters dose-response stimulation function. Data are presented as mean values, with error bars representing SD. Data are representative of 2 biological replicates, with 3 technical replicates each. Generic receptor codes refer to the GPCR-Tango constructs.

also minimally observed with 5-HT2B-Tango, yet absent in the untransfected cells, and negligeable at 5-HT1B-Tango and at other GPCRs that activate the Jak/STAT Pathway, such as CXCR4- and F2R-Tango receptors[26]; interestingly, this artifactual response in HTLA was absent following stimulation with Tet-approved FBS (Fig. 1o–r). We believe that subtraction of external control of the TRE-Tight promoter compared to the original TRE explains the difference observed for β-arrestin-2 recruitment at some receptors. Hence, some factors present in the serum might artificially enhance promoter activity as shown for DRD2-, HTR5A-, CHRM4-, OPRM1-, ADRB3-, and PTGDR-Tango receptors (Fig. 1i–n).

To validate cumate induction, time-course and dose-response experiments were conducted on all three of our established cell lines using prototypical GPCR-Tango receptors covering the main subtypes of G-protein primary couplings: AVPR2 (G_s), ADRB2 (G_s), DRD2 (G_i), and CHRM1 (G_q)[27]. To confirm the control of gene expression was dose-dependent, monoclonal cell lines were transfected without cumate, and then stimulated with a cumate concentration-curve starting from 40 μg/mL with 2-fold dilutions (Fig. 2a–f). Based on the EC50 values of tested receptors, maximal activation is achieved at ~10 μg/mL, corroborating other studies that have also used the cumate switch system[28]. Cumate induction was also confirmed to have minimal impact on the

basal signals and fold windows of the three HTTL cell lines after reaching maximal activation, yet a slight decrease was generally observed for both parameters at the highest tested induction concentration (Supplementary Fig. 3). The time-course experiments consisted of adding cumate at the different time points and maintaining it in the cell medium from then on, ranging from as long as 5 days total cumate exposure to a minimum of 18 h throughout (Fig. 2g–r). In general, the best response was observed following ~3 days of total cumate exposure, which we expected as the developers of the cumate-gene switch previously observed a maximal expression after 72 h[21]. Overall, Tango-Trio presents greater dynamic range, sensitivity, specificity, and versatility over the original tried-and-true Tango system.

Tango-Trio generates a compendium of GPCRome basal and agonist-dependent activities

With our established monoclonal cell lines forming the foundations of the Tango-Trio HTS platform, parallel interrogations of the GPCRome were conducted by transfecting a panel of 350 GPCR PRESTO-Tango constructs in arrayed format, the large majority of which consist of Class A members[29]. To investigate proximal GPCR-arrestin interactions and receptor endocytosis at the two possible activated receptor states, agonist-induced activities were screened for in presence of selective agonist at ~150 non-orphan GPCRs, while basal activity was probed for using the presence of cumate. Based on initial hit thresholds set to <−2 and >2 log2, fold-changes (E_{max}/E_0) were visualized as heatmaps to depict contrasts between the couplings of arrestin isoforms and corresponding GPCR internalization efficiencies (Figs. 3a–e and 4a–f). Based on NC-IUPHAR classification, heatmaps were constructed for each of the four branches of the non-olfactory class A members (α, β, γ and δ), for orphan class A members, and one covering a select number of receptors spanning the B, C, and adhesion classes, illustrating the diversity within the GPCR superfamily[27,30].

Consistent for both screenings, the similitudes of profiles amongst receptor members of the same subfamily varied on a case-by-case basis. Drawing on examples from the α branch, the Alpha-1 adrenergic-Tango receptors (ADRA1A, 1B, 1D) all preferentially recruited β-arrestin-1 over β-arrestin-2 (~2-3 fold difference) at the basal level, whereas in the case of the Prostaglandin EP-Tango subfamily (PTGER1–4), different basal arrestin selectivity profiles were observed among members, such as PTGER2-Tango's marked selectivity towards β-arrestin-2 and that of PTGER4-Tango towards β-arrestin-1 (Fig. 4a). These marked differences in arrestin selectivity profiles between receptor subfamilies could be due to the differences in their C-terminal tail and intracellular loop sequences which dictate different phosphorylation codes, influencing the isoform type and degree of arrestin recruitment. It is also important to note however that these selectivity findings must be interpreted with the understanding that all Tango receptors are fused to a "V2 tail", originating from the C-terminus of AVPR2. Such a phospho-peptide addition is also present in other β-arrestin recruitment assays such as the PathHunter assay[31]. The V2 tail was originally added given its high affinity for β-arrestin2 and for its ability to stabilize the interaction between a given receptor and the recruited arrestin; this addition is indispensable for those of low-affinity or for transient β-arrestin recruitment at many GPCRs. The stabilization of the interaction allows efficient cleavage by the TEV protease but also generates a detectable basal level, resulting in an increased assay quality (z-factor), which is strongly affected when RLU are too low; this is particularly important when performing parallel interrogation or high-throughput screening. When working on a single or a select set of receptors, the V2-tail can easily be removed and experimental conditions adjusted to achieve an acceptable level of RLU counts, if possible. However, for some receptors, the interaction of β-arrestin is of low affinity or transient such that it cannot be accurately detected using a protease-dependent reporter assay. In such cases, the V2 tail should be retained or an alternative assay such as BRET should be envisaged. To further compare GPCR-Tango constructs used in Tango-Trio and unmodified wildtype counterparts, a supplementary table comprising the agonist-induced β-arrestin-1/2 recruitments observed from the EMTA studies and our Tango-Trio work was compiled (Supplementary Table 1). Although a large number of receptors behave similarly toward β-arrestin-1/2 recruitment, several discrepancies were noted. For example, Tango-Trio detects β-arrestin recruitment at HTR1D-, PTGER1-, GNRGR- and MTNR1B-Tango receptors, while the EMTA biosensors were unsuccessful, or oppositely, β-arrestin recruitment at F2R, LPAR1, LPAR2 and VIPR1 was observed with EMTA but not with Tango-Trio. Moreover, a stronger proclivity for β-arrestin-2 over β-arrestin-1 was also observed in Tango-Trio for certain receptors, such as AGTR1-, PTGER4-, HCRTR2-, and AVPR2-Tango receptors. Similarly, another facet to consider is the influence of the V2-tail on the changes of the arrestin-independent and dependent internalization patterns of GPCRs. For example, based on the HTTL-F agonist-dependent screen (Fig. 3), ADRB1-, 5-HT2A-, ADRA2A-, CHRM3-, CHRM4-Tango receptors all exhibited significant internalization following agonist stimulation, all of which have been previously reported to undergo arrestin-independent internalization; however, other reported GPCRs exhibiting this behavior such as DRD3, DRD4, UTS2R, AGTR1, ENDRA, EDNRB and APJ were not among our hits. It is not surprising to observe a certain degree of inconsistency between two heterologous systems[32]. Numerous possibilities could thus contribute to the inconsistency observed, especially for β-arrestin recruitment, which requires receptor phosphorylation by endogenous kinases. In addition to endogenous modulators, such as kinases, the fusion of the receptor and β-arrestins with functionalized proteins tags can affect the recruitment and/or stability of the complexes. The presence of the phosphopeptide (V2 tail) could also contribute to some divergences, but the significant difference in the duration of the experiments (<1 vs. 18 h) is probably a major factor, especially for efficacy, which is strongly dependent on cell surface receptor abundance. Notwithstanding these discrepancies, we are confident that comparing EC50 (potency) and Emax (efficacy) to an internal reference will provide an accurate differential measure, but as is the case for any artificial system, we cannot rule out that β-arrestin recruitment is over/underestimated compared to endogenous recruitment in a physiological context. The main advantage of our Tango-Trio assay remains the ease of performing parallel high-content or high-throughput screening.

Across the array of interrogated GPCRs, it is obvious that β-arrestin-1/2 are quite promiscuous; however, similarly to Avet et al. who reported that 22% of receptors investigated did not recruit arrestins beyond their established threshold[33], we also observed a significant pool of receptors which exhibited no β-arrestin-1/2 translocation at either basal or agonist-induced states. It should be noted however that very few GPCRs lacked arrestin interactions at both of these states. Additionally, as seen in Figs. 3 and 4, there is little overlap between basal and agonist-induced signatures across the GPCRome; for example, very strong agonist-induced arrestin recruitment at SSTR5-Tango did not correspond to high basal activity (Figs. 3c and 4c). This implies that there are different mechanisms at play that regulate internalization and arrestin activities between an agonist-stabilized GPCR versus basal activity in the absence of agonist[34], as discussed below.

The representation of our screens as heat maps allows one to easily identify receptors with the strongest basal activities, such as CHRM5-, 5-HT1E-, 5-HT5-, NTSR1-, CXCR4-, and MRGPRD-Tango. To exclude the possibility of cumate addition contributing to marked increase of receptor expression, an ELISA was conducted to evaluate receptor surface expression on a select subset of constitutive hits (Supplementary Fig. 4). No significant differences between non-treated cells versus those with the addition of saturating cumate concentration, compared to the drastic fold-differences observed in the constitutive screen, corroborated that detected hits were a result

https://doi.org/10.1038/s41467-023-39132-x

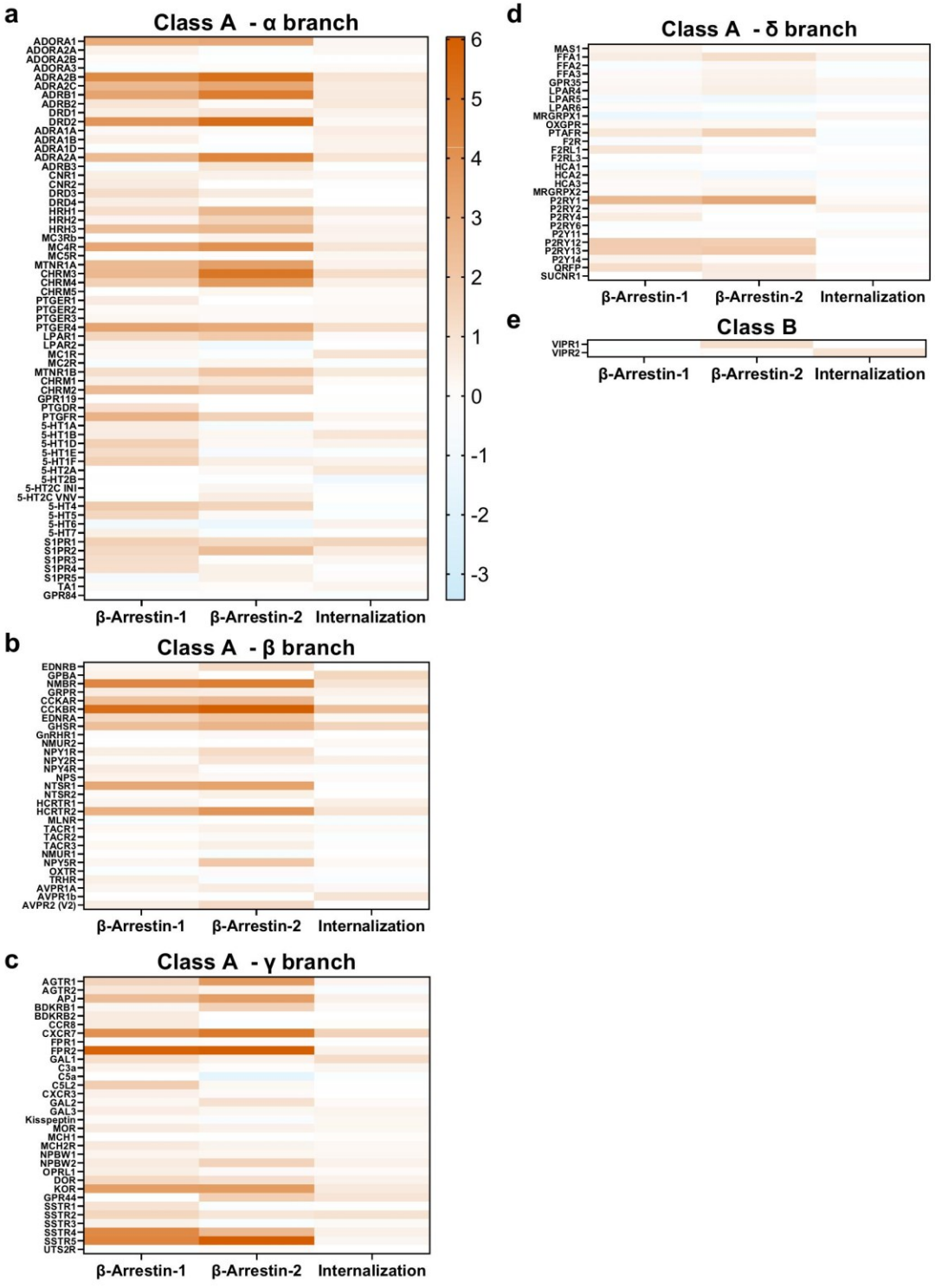

Fig. 3 | Heatmap representation of hits identified from agonist-dependent HTS. To analyze agonist-induced activities within the GPCRome, HTTL-B1, HTTL-B2 and HTTL-F cells were plated in cumate-containing (30 μg/mL) medium and transfected with a library of 162 non-orphan GPCR Tango constructs. Transfected cells were stimulated either with HBSS-Hepes buffer or with a panel of selective agonists. Log2 fold changes in agonist-dependent arrestin recruitment/dissociation or GPCR internalization was calculated between the wells in the absence or presence of agonist and plotted as heat maps, grouping class A α (**a**), β (**b**), γ (**c**), and δ (**d**) branches, and class B receptors (**e**). Log2 values are the means calculated from quadruplicate conditions, generated from two separate screens ($n = 8$, 2 biological measurements with 4 technical replicates each). Generic receptor codes refer to the GPCR-Tango constructs.

https://doi.org/10.1038/s41467-023-39132-x

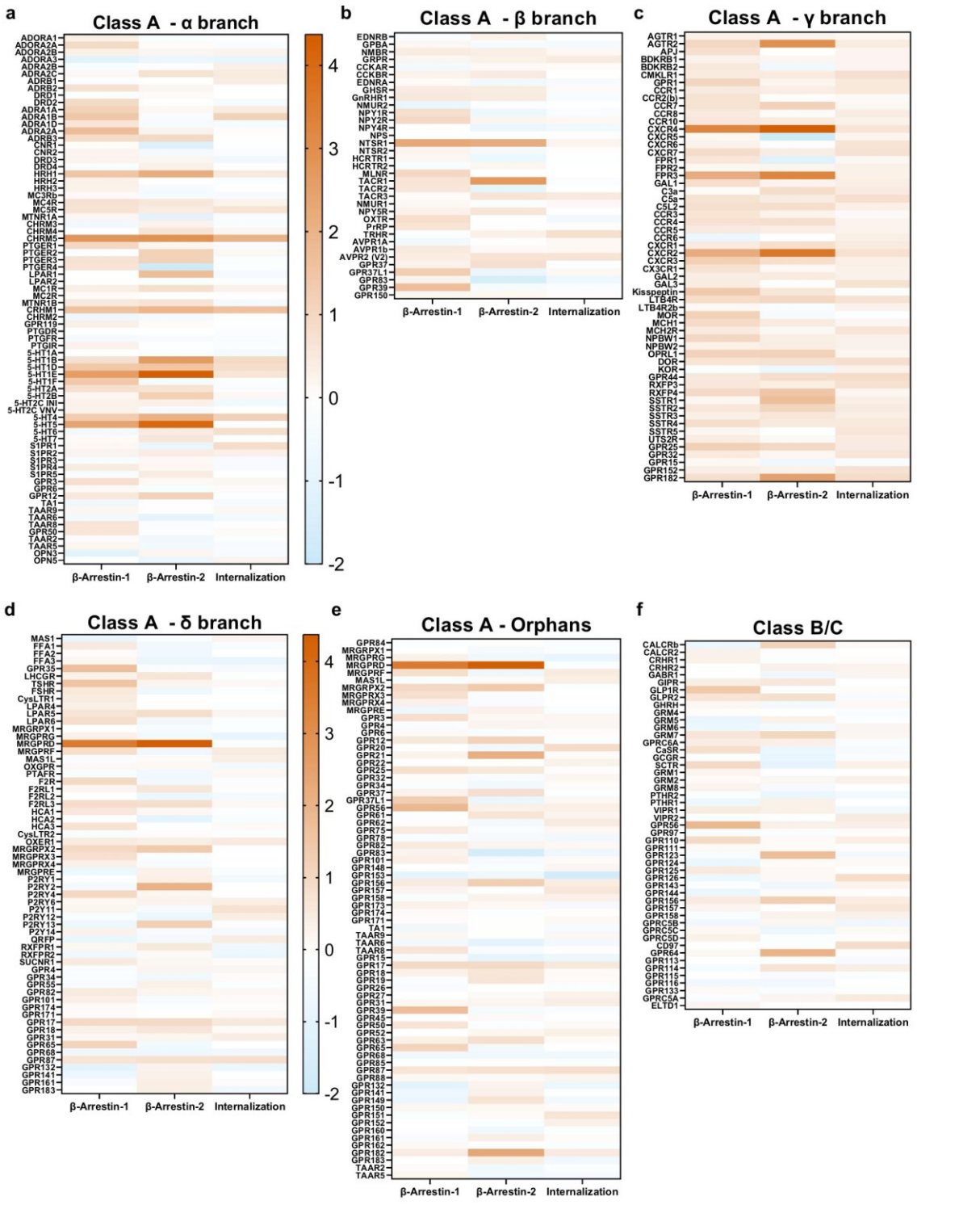

Fig. 4 | Heatmap representation of hits identified from basal activity HTS. To analyze basal activities within the GPCRome, HTTL-B1, HTTL-B2 and HTTL-F cells were plated alternating rows with or without cumate (30 μg/mL). Cells were transfected with a library of 350 GPCR Tango constructs, including ~100 orphan receptors. Log2 fold changes in basal arrestin recruitment/dissociation or GPCR internalization was calculated between the wells in the absence or presence of cumate and plotted as heat maps, grouping class A α (**a**), β (**b**), γ (**c**), and δ (**d**) branches, class A orphans (**e**) and class B/C receptors (**f**). Log2 values are the means calculated from quadruplicate conditions, generated from two separate screens ($n = 8$, 2 biological measurements with 4 technical replicates each). Generic receptor codes refer to the GPCR-Tango constructs.

https://doi.org/10.1038/s41467-023-39132-x

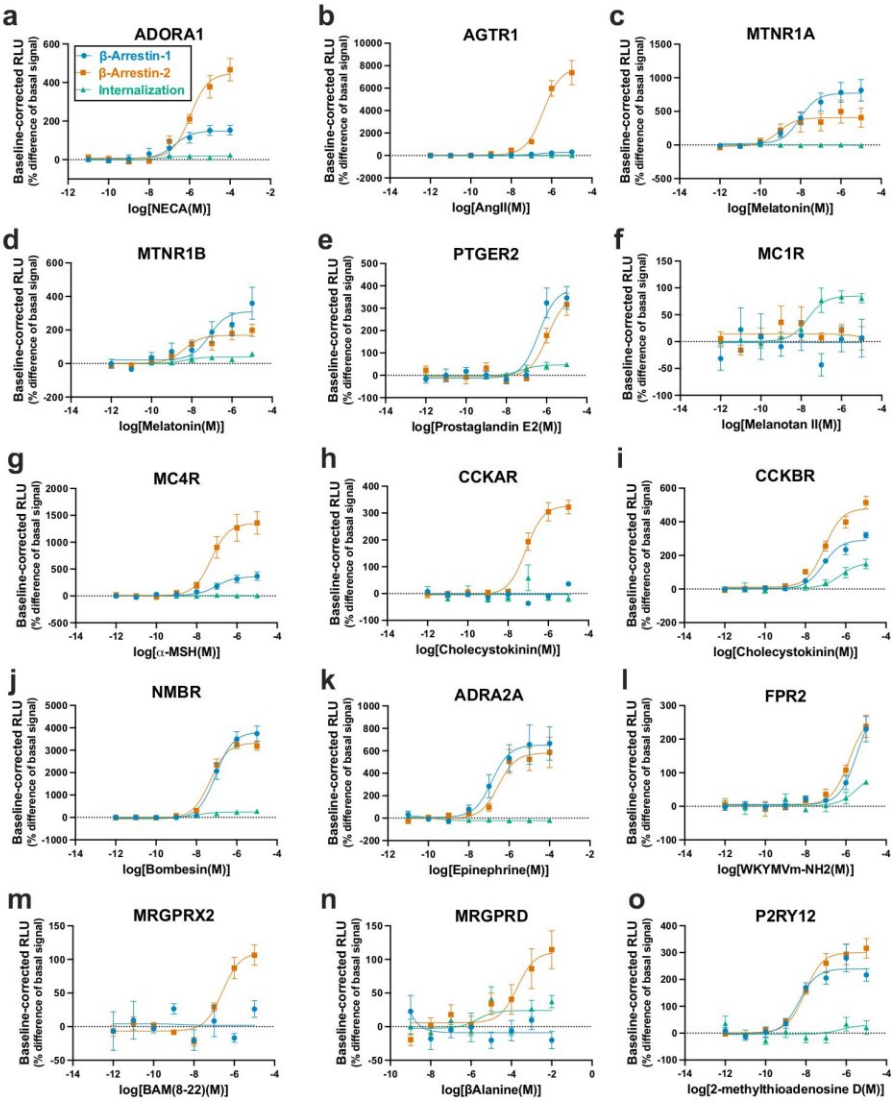

Fig. 5 | Validation of compiled positive hits from agonist-dependent HTS in dose-response. a–o HTTL-B1, HTTL-B2 and HTTL-F cells were plated in cumate-containing (30 μg/mL) medium and transfected with potential GPCR hits identified from the agonist-dependent HTS. Transfected cells were stimulated with the receptor specific agonist and dose- response curves were built using XY analysis for non-linear regression curve and the 3-parameters dose-response stimulation function, followed by baseline correction. Data are presented as mean values, with error bars representing SEM. Data are representative of 2 biological replicates, with 3 technical replicates each. Generic receptor codes refer to the GPCR-Tango constructs.

of bona fide constitutive activities; for example, a modest 1.2-fold difference in receptor expression was observed in HTTL-B2 cells transfected with CXCR4-Tango, compared to the 67-fold change in constitutive β-arrestin-2 recruitment. The lack of correlation between receptor expression and apparent basal activity was also confirmed across a larger panel of receptors including a wide range of basal arrestin recruitment profiles (Supplementary Fig. 5). Finally, absolute receptor expression levels were not found to affect constitutive activity, as titrating Tango construct DNA did not generally reduce the cumate-induced fold change (Supplementary Fig. 6).

Validation of GPCR internalization, β-arrestin-1/2 coupling and selectivity profiles

Secondary screening of top potential hits was carried out in a dose-dependent manner (agonist or cumate, accordingly) to validate our platform's high-throughput performance (Figs. 5a–o and 6a–o). With the primary screen findings in agreement with our concentration-response profiles, thus confirming the platform's reproducibility, we exploited Tango-Trio to perform more detailed analyses of the arrestin selectivities and corresponding GPCR endocytosis patterns observed. This was accomplished by producing the β-arrestin-1/2 and internalization dose-response curves for ~150 non-orphan GPCRs, and most important, presenting for the first-time dose dependent constitutive activation curves at ~200 receptors, including more than 50 orphans (Supplementary Figs. 11–26). Many of our high-basal and agonist-dependent findings are in agreement with previous studies, such as high constitutive activity at GPR182-Tango receptor (Fig. 6i)[35,36]. Moreover, Tango-Trio was able to detect activity at GPCRs that could not be validated in PRESTO-Tango[13], including BAM-22 at MRGRPX2-Tango (Fig. 5m), and β-Alanine at MRGPRD-Tango (Fig. 5n).

https://doi.org/10.1038/s41467-023-39132-x

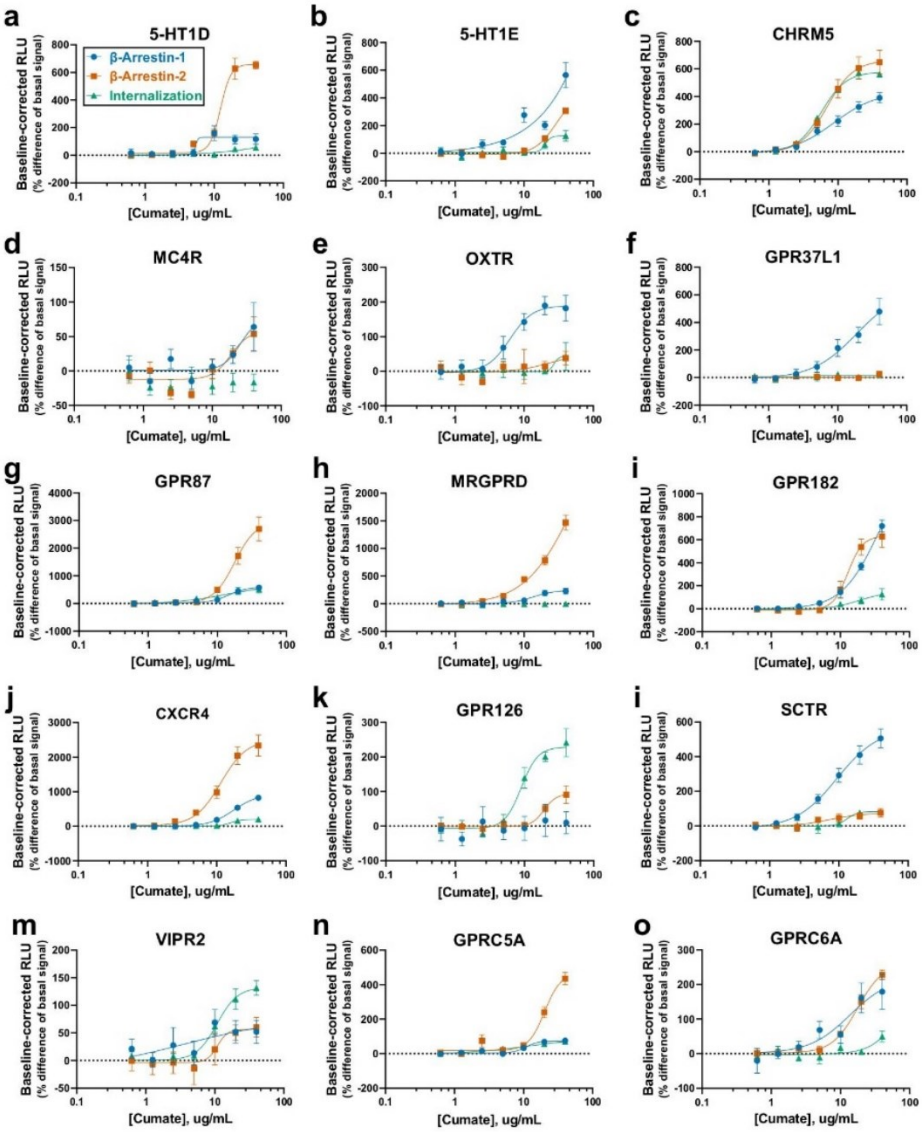

Fig. 6 | Validation of compiled positive hits from basal activity HTS in dose-response. a–o HTTL-B1, HTTL-B2 and HTTL-F cells were transfected with potential GPCR hits identified from the basal HTS. Transfected cells were stimulated with cumate, and dose- response curves were built using XY analysis for non-linear regression curve and the 4-parameters dose-response stimulation function, followed by baseline correction. Data are presented as mean values, with error bars representing SEM. Data are representative of 2 biological replicates, with 3 technical replicates each. Generic receptor codes refer to the GPCR-Tango constructs.

While HTTL-B1 and HTTL-B2 captures the nuanced differences between arrestin couplings and selectivities at receptors, our internalization measures are not as robust. Especially in our HTTL-F agonist-dependent screen, very few hits were detected, with the majority of receptors producing the strongest agonist-induced internalization belonging to the β branch, such as GPBA-, NMBR-, CCKBR-, GHSR-, and HCRTR2-Tango receptors (Fig. 5i, j). On the other hand, our HTTL-F is better-suited for studying constitutive endocytosis, seeing as considerably more receptors had stronger constitutive internalization profiles, such as GPR126-, GPR87-, and CHRM5-Tango (Fig. 6c, g, k). As discussed below, the selectivity of FYVE-targeted early endosome trafficking should be re-evaluated.

Based on our validation of hits from our β-arrestin-1, β-arrestin-2, and FYVE screens, distinct GPCR selectivity profiles towards the arrestin isoforms were observed. Regarding constitutive activity, receptors can be clustered into three distinct functional classes, specifically those that interact fairly equally with both isoforms, those that preferentially recruit β-arrestin-1 over β-arrestin-2, and vice versa. Based on constitutive activity curves, it seems that the constitutive internalization at a given receptor corresponds to the profile of one of the β-arrestin isoforms, such as those observed at 5-HT1D-, CHRM5-, OXTR-, SCTR-, and GPRC5A-Tango receptors, amongst others (Fig. 6a, c, e, l, n). This observation follows the widely accepted classical paradigm of how arrestins play a central role in GPCR endocytosis via the predominant clathrin-mediated pathway. However, this is not a uniform correlation, involving exceptions where either significant constitutive internalization is observed in the absence of arrestin activities, for example in the case of GPR126- and VIPR2-Tango (Fig. 6k, m) or oppositely, strong β-arrestin-1 and/or β-arrestin-2 recruitment but negligeable receptor internalization, such as the case of GPR37L1- and MRGPRD-Tango (Fig. 6f, h). Indeed, these findings confirm that GPCR endocytic pathways are more diverse than originally defined, as an increasing number

of receptors are found to be endocytosed via alternate pathways besides clathrin-mediated, including the caveolae-dependent and fast endophilin-mediated endocytosis (FEME) pathways, as well as another 30 known examples of GPCRs have been found to internalize independently of arrestins altogether[32].

As for agonist-dependent activity, although similar arrestin selectivity profiles were also observed, the vast majority fell under two functional classes, equal (e.g., Fig. 5c, d, j) or preferential (e.g., Fig. 5b, g, m) recruitment of β-arrestin-2 over β-arrestin-1. Our results parallel those of Oakley et al. who delineated two major classes of receptors based on the 10 GPCRs that they studied, namely "Class A" receptors which bound β-arrestin2 with higher affinity than β-arrestin1, and "Class B" receptors which bound both β-arrestin isoforms with similar high affinities[37]. Similar subsets were observed in Avet et al.'s recent publication profiling the engagement of different G-protein families at 100 therapeutically relevant GPCRs, including β-arrestin1 and β-arrestin2 following agonist stimulation[33]. Orthogonal validation of GPCRs with pronounced arrestin isoform selectivities was conducted in BRET2, which revealed discrepancies between the two systems (Supplementary Fig. 7). For example, β-arrestin1 is recruited at a much lower efficacy compared to β-arrestin2 at AGTR1 in Tango-Trio (Fig. 5b). In BRET however, this selectivity is not observed, with very little difference in recruitment observed between the two isoforms (Supplementary Fig. 7e). Given that BRET experiments occur over a short duration, the results obtained are based on the amount of receptor present at the time of adding the ligand, and thus, other factors such as receptor internalization, the role of the intracellular pool, and binding kinetic profiles will have minimal effects, whereas the Tango-Trio, being a signal amplification system, may disproportionately magnify of efficacies due to the aforementioned factors. Nonetheless, both systems have different limitations and are useful in their own respects for the purposes of screening and pharmacological characterization and should not be interpreted as a measure of endogenous recruitment, but rather as a pharmacological tool to compare drug activity towards a refence compound.

Thus, by using Tango-Trio to screen the GPCRome and distinguishing functional subsets of GPCRs, this might give molecular insight into structural interface positions common among these related receptors, which could be involved in recruitment and internalization.

Mechanistic insights into basal GPCR activities revealed by Tango-Trio

Besides the wealth of basal and agonist-induced activation profiles generated with Tango-Trio, additional explorations of the applications of this platform were undertaken, including studying inverse agonists and their relative abilities to subdue constitutive activity versus steady-state recruitment. Seeing as inverse agonism may appear differently based on cell phenotypes[38], we chose a panel of drugs classified as either inverse agonists or antagonists to target GPCRs exhibiting high constitutive β-arrestin-1 and/or β-arrestin-2 recruitment (Fig. 7a–m)[39]. A spectrum of inverse agonistic properties was validated, albeit no drug was able to completely ablate the basal activity observed. For example, O-1918 reduced the response observed at GPR55-Tango by almost half in both HTTL-B1 and HTTL-B2 (Fig. 7a, b)[40], while at HRH1-Tango, stimulation with Mepyramine reduced constitutive activity only for β-arrestin-2, unlike its counterpart Cetirizine which could inhibit activities in both cell lines (Fig. 7c, d). Furthermore, certain compounds previously designated as antagonists/inverse agonists, such as FC-131 at CXCR4-[41] (Fig. 7e, f) and Tolvaptan at AVPR2-Tango (Fig. 7g, h), increased the constitutive translocation of β-arrestin-1 and β-arrestin-2 in our system. Thus, our platform, nor other arrestin-based assays, are not entirely suitable for quantifying measurements of inverse agonism given the range of arrestin activities observed. For instance, in both PRESTO-Tango and Tango-Trio, Tolvaptan increased arrestin recruitment at AVPR2-Tango, while Pindolol resulted in a depletion of arrestin recruitment at the 5-HT1B-Tango (Supplementary Fig. 8b, e). To exclude the possibility of artifacts arising due to endogenous cleavage GPCR-Tango fusion constructs, the same receptors were co-transfected with β-arrestin-2 in HTTL, with no arrestin recruitment detected (Supplementary Fig. 9). Thus, although the identification of inverse agonists is not possible with arrestin-based assays per say, Tango-Trio is valuable for their characterization, more specifically providing information about their effects on constitutive arrestin recruitment and receptor internalization. It seems that G-protein uncoupling using inverse agonist is clearly a different receptor pool or receptor state and cannot be directly translated toward β-arrestin activity. We cannot rule out that G-protein uncoupling could result in β-arrestin recruitment for some receptors, as seen for CXCR4- (FC131-treated) and AVPR2- (Tolvaptan-treated) Tango receptors.

Tango-Trio HTS produces variegated snapshots of the arrestin couplings of GPCRs and their corresponding internalization efficacies, suggesting that the mechanisms of endocytosis among GPCR members are more heterogeneous than originally conceived, especially those of constitutive nature. To further this point, the dominant-negative dynaminK44A was co-transfected in HTTL-F cells with select GPCRs exhibiting strong constitutive internalization. As expected, various degrees of inhibition were observed, from partial inhibition in the case of 5-HT4-Tango (Fig. 7p), to complete blocking of GPR87-Tango endocytosis (Fig. 7n), suggesting a greater dynamin-dependence involved during its constitutive internalization process. Intriguingly, overexpressing dynaminK44A resulted in a substantial increase in constitutive CHRM5-Tango endocytosis (Fig. 7o), bringing to light the possibility of multiple compensatory internalization mechanisms at play at a given receptor. Expanding this idea, β-arrestin-1/2 knockdown was performed to evaluate the arrestin dependence at certain GPCRs with high constitutive internalization, confirming partially arrestin-independent endocytosis at CHRM5- and CD97-Tango receptors (Supplementary Fig. 10a, e).

A recent appreciation has grown for GPCR-interacting proteins, with emerging findings supporting how they modulate GPCR expression at the cell surface, signal transduction, and receptor endocytosis, amongst others[42]. Of particular note are the protein kinases that phosphorylate specific sites on the intracellular loops and C-terminal tail of GPCRs, inducing specific arrestin roles and varying functional consequences for the modified receptors[43]. Given limited literature exploring the distinct functions of kinases and their contributions to constitutive activity, we examined the HPA consensus tissue-specific expression levels of serine/threonine-specific protein kinases (ST kinases) previously reported to phosphorylate GPCRs, such as GRKs, PKAs, and PKCs amongst other[43], as well as the expression levels of β-arrestin-1/2 and of select receptors with high constitutive selectivity for one arrestin isoform over the other. We postulated that the kinases and receptors of similar tissue expression profiles may have overlapping activities. Our generated PCA plots revealed varying signatures for each of ST kinase families, some of which forming clusters with our constitutively active GPCRs based on shared expression patterns (Fig. 8). Based on the GRK plot, it seems that GRK2, GRK6 and β-arrestin-2 might share a functional network[44], especially at CXCR4[45] and PTGER2, which were found to be highly selective for β-arrestin-2 at constitutively active receptors (Fig. 8a). A dense cluster including GRK5 also leads us to speculate a greater involvement of this GRK at constitutively active receptors selective for β-arrestin-1, such as AGTR2, ADRA2A, PTGER3, and SUNCR1. The restricted expression profile of GRK4 also suggests that this might be the predominant GRK acting at receptors such as MC1R. Despite a lack of research into the lesser-reported kinases capable of phosphorylating GPCRs, certain interactions could be confirmed from past studies, such as the role of PIMs at CRCR4 (Fig. 8e)[46,47]. Thus, our analyses may also reveal functions at these ST kinases GPCRs; for example, we hypothesize that Ca^{2+}/calmodulin-dependent kinases, including CAMKI, CAMKII and CAMKIV

https://doi.org/10.1038/s41467-023-39132-x

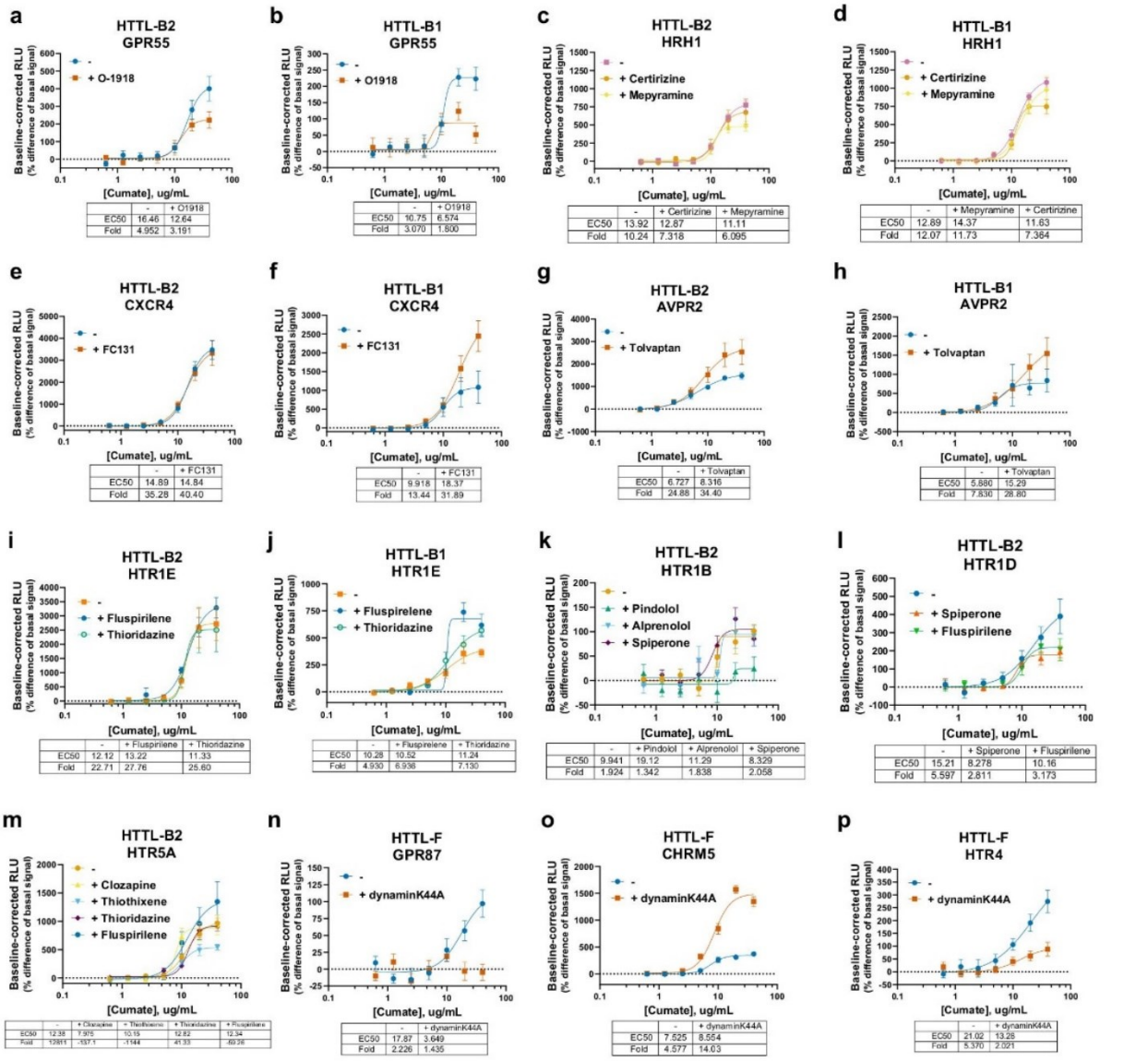

Fig. 7 | Applications and further investigations into basal activities revealed by Tango-Trio. HTTL-B1 and HTTL-B2 were transfected with GPCRs exhibiting strong basal arrestin recruitment. Transfected cells were stimulated as cumate dose-response in the presence or absence of the following inverse agonists/antagonists at saturating (EC80) concentrations: O-1918 at GPR55 (**a**, **b**), Cetirizine and Mepyramine at HRH1 (**c**, **d**), FC131 at CXCR4 (**e**, **f**), Tolvaptan at AVPR2 (**g**, **h**), Fluspirelene and Thioridazine at HTR1E (**i**, **j**), Pindolol, Alprenolol and Spiperone at HTR1B (**k**), Spiperone and Fluspirelene at HTR1D (**l**), and Clozapine, Thiothexene, Thioridazine and Fluspirelene at HTR5A (**m**). Dynamin-dependence of high basal internalization was tested by co-transfecting HTTL-F cells with GPR87 (**n**), CHRM5 (**o**), and HTR4 (**p**) with/without dynaminK44A. Transfected cells were stimulated as a cumate dose-response, and stimulation curves were built using XY analysis for non-linear regression curve and the 4-parameters dose-response stimulation function, followed by baseline correction. Data are presented as mean values, with error bars representing SEM. Data are representative of 2 biological replicates, with 3 technical replicates each. Generic receptor codes refer to the GPCR-Tango constructs.

complexes, might significantly contribute to the phosphorylation and subsequent recruitment of β-arrestin-1 to GPCRs, although this has yet to be experimentally investigated (Fig. 8h).

Discussion

The functional heterogeneity of GPCRs is attributed in part to their spectral activation states, desensitization, and internalization, accounting for their multifaceted signaling processes. Towards establishing accurate and comprehensive functional profiles, this study developed Tango-Trio, a polyvalent screening platform consisting of a triad of stable cell lines, capable of interrogating constitutive and agonist-activated GPCRome activities. The foundation of the platform, the HTTL reporter cell line, stably expresses a luciferase gene under the control of an improved low-background and sensitive TRE-Tight promoter compared to the original PRESTO-Tango[16]. To increase the versatility of this system, Tango-Trio monitors the translocation of β-arrestin1, β-arrestin2, and GPCR internalization using a FYVE domain, all of which were cloned to the truncated TEV219 protease for its enhanced signal-noise ratio[19]; these chosen elements provide valuable insight into crucial stages in the GPCR life cycle. Despite sharing a high degree of structural and sequence similarity, the non-visual arrestin isoforms have been reported to accomplish disparate roles[9]. For example, one study

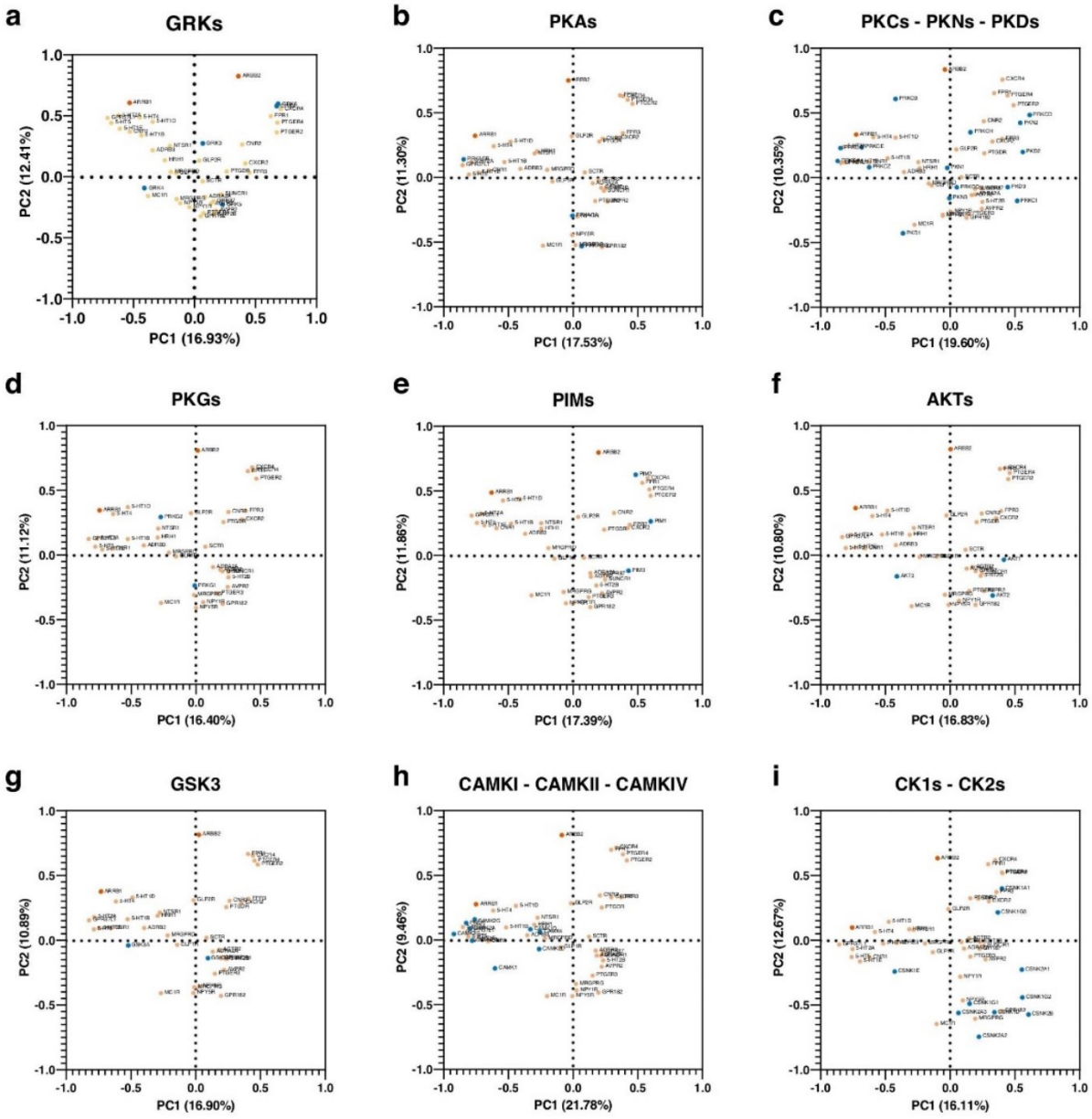

Fig. 8 | Visualization of tissue-specific expression levels of select GPCRs with high basal activities, serine/threonine kinases, β-arrestin-1 and β-arrestin−2. Human Protein Atlas (HPA) RNA consensus tissue gene data (version 21.0 and Ensembl version 103.38.) summarizing the expression levels in 55 tissues was extracted for β-arrestin-1 and −2 (ARRB1 and ARRB2), select receptors with high constitutive selectivity for one arrestin isoform over the other (GPR182, AGTR2, ADRA2A, GPR37L1, SCTR, ADRB3, PTGER4, SUNCR1, PTGER3, MRGPRG, NPY5R, NPY1R, GLP1R, FPR1, MC1R, FPR3, 5-HT5, MRGPRD, GPR87, CXCR4, HRH1, AVPR2, 5-HT4, 5-HT2A, NTSR1, GLP2R, 5-HT1D, CXCR2, 5-HT1B, 5-HT1E, PTGER2, 5-HT2B, PTGDR), and either and either GRKs (**a**), PKA (**b**), PKCs, PKNs, and PKDs (**c**), PKGs (**d**), PIMs (**e**), AKTs (**f**), GSK3 (**g**), CAMKI, CAMKII, and CAMIV (**h**), CK1s and CK2s (**i**). The data was analyzed using principal component analysis; β-arrestin-1 and −2 are denoted with red, ST kinases with blue, and GPCRs with orange symbols. Generic receptor codes refer to the GPCR-Tango constructs.

demonstrated that silencing β-arrestin2 reduced agonist-induced PAC1R and C3aR receptor internalization, whereas silencing β-arrestin1 had no effects[48,49]. Given its implications in signal regulation, desensitization, resensitization, and ligand scavenging functions of some receptors, our measurements of GPCR internalization also contribute to our account of the diversity of GPCR-dependent dynamics[50].

The scope of our platform is broadened further by the controlling the expression of these multiple probes using a cumate-controlled lentiviral vector[21], enabling the interrogation of not only at the agonist-induced state, but also monitoring basal activities in a dose-dependent manner by adjusting the expression level of the fusion proteins, which is not feasible with existing HTS technologies. Two aspects affect the magnitude of basal activity, specifically a receptor's conformational flexibility from the inactive to active states in the absence of ligand, and state-independent GPCR-effector coupling. Previous quantifications of constitutive activity have been extracted based on the latter factor, specifically constructing receptor-density response curves by regulating the amount of receptor expression and measure resultant

increases in the basal responses[38]. Tango-Trio modulates GPCR-effector coupling stoichiometry not through changing receptor density, but by tuning the density of cytoplasmic effectors, specifically β-arrestin1, β-arrestin2, and FYVE, to probe basal activity. Moreover, seeing as continuous overexpression of engineered proteins could potentially give rise to spurious GPCR dynamics[51], titratable induction of Tango-Trio fusion proteins enables greater management of the cellular environment to one more reflective of the native in vivo setting if desired, by tuning the intensity of gene expression during profiling of agonist-stimulated receptors.

Following establishment of our stable cell lines, we conducted HTS of the GPCRome to shed light into how β-arrestin1 and β-arrestin2 differ in their couplings and selectivity at GPCRs, and provide insight on how this arrestin selectivity may play a role in GPCR trafficking properties. After validating select hits from our primary screen, we sought to further characterize constitutive and ligand-dependent dynamics. Given the inability to capture pharmacological parameters (EC_{50}, E_{max}/E_O, etc.) regarding basal activities in general, as well as the lack of information regarding ligand-induced β-arrestin1 recruitment and internalization across the GPCRome, we profiled ~200 GPCRs, including over 50 orphans, in cumate and/or agonist dose-response fashion. Interestingly, we observed distinct functional signatures between basal and agonist-dependent activities observed at GPCRs, suggesting different mechanisms in play at these different activation states[34]. Although the promiscuity of couplings detected for both isoforms is supported by the fact that these non-visual β-arrestins are ubiquitously expressed to regulate hundreds of GPCRs within the human body[8], we observed a significantly larger percentage of receptors which were more selective towards β-arrestin2 over β-arrestin1 at both basal and agonist-activated states. From a structural standpoint, β-arrestin2 has less defined secondary structure within its C-terminal basket, resulting in increased flexibility and adaptability to the structural differences of GPCRs[52], which may attribute why it is less selective and couples preferentially to more receptors compared to β-arrestin1. Thus, Tango-Trio may be useful for future development and testing of arrestin-isoform biased compounds, if there are positive functional outcomes that are shown to emerge from favouring β-arrestin1 versus β-arrestin2 recruitment; although few reports of this nature of functional selectivity have been explored, a couple of existing agonists have been demonstrated to favor one arrestin isoform over another, such as 2-arachidonoylglycerol and anandamide[53]. Addedly, the original PRESTO-Tango platform interrogates only the recruitment of β-arrestin2, one of the two non-visual arrestins expressed in vertebrates. While it has been previously demonstrated that β-arrestin1 is the most prevalent isoform in most cells, comprising more than 90% of the total arrestin complement[54], few studies have investigated its recruitment to GPCRs on a larger scale; Tango-Trio enables such an interrogation, and simultaneous comparison to β-arrestin2 selectivity. Finally, some receptors lacked interactions with either isoform, which has been typically attributed to the lack of consensus sequences for GRKs[55]. Nonetheless, a growing body of evidence has indicated that arrestin recruitment is not entirely dependent on phosphorylation by GRKs specifically, but also by other serine/threonine kinases[43], as we explored later on. Moreover, arrestin recruitment is a biphasic process that involves the partial engagement of the phosphorylated GPCR's C-tail with arrestin and a fully engaged complex where the receptor core interacts with the arrestin finger loops[56]. As a highly sensitive reporter assay, we cannot exclude that Tango-Trio can detect partially engaged complexes to phosphorylated and non-phosphorylated receptors. Given that interaction with the receptor core requires complete activation of the receptor and G-protein dissociation, the constitutive interaction observed is probably highly dependent on receptor C-tail phosphorylation and thus highly dependent on kinases present within the cellular system used[57]. It will be interesting in futures studies to measure the changes in this receptor constitutive distribution while overexpressing a specific kinase.

Unfortunately, one caveat to Tango-Trio is that the dynamic window of GPCR internalization is smaller than that observed with arrestin activity. This could be attributed to multiple reasons but we believe that the range of observed internalization across the GPCRome is not as expansive as the range of arrestin activities. Moreover, the transit of the receptor to early endosomes could be too fast for efficient TEV cleavage or may lead to weak tTA translocation into the nucleus. Another potential pitfall of using the FYVE domain to track GPCR internalization is the known PI3K activation by some GPCRs, which in turn will increase phosphatidylinositol 3-phosphate (PIP3) at the cell membrane and endosomes, possibly contributing to biased results. Another important distinction is that for HTTL-B1 and HTTL-B2, it is the expression of arrestin effector proteins that is affected by cumate induction, hence tuning the process of GPCR-arrestin coupling itself, whereas for HTTL-F, titratable cumate addition does not influence the process of receptor internalization, but rather only changes the expression of the FYVE probe that tracks it. Finally, the FYVE domain directly interacts with the inositol polar heads of PIP3, which is present on the surface of the endosome but also at the plasma membrane. It has been proposed that dimerization of FYVE-domain containing protein amplifies the weak binding of individual FYVE fingers to the phospholipid. We cannot exclude that the TEV219 fusion disrupts dimerization, nor that the expression of only the FYVE-domain has a very low affinity, thus reducing sensitivity. We do not exclude to test other fusion proteins such as EEA1 containing the FYVE domain and the adjacent dimerization coiled-coil region[58]. Overall, the use of FYVE domain fusion protein for tracking GPCR internalization should be used with caution; nonetheless, the variety of responses observed in our GPCRome screening highlights some interesting observations that will require further investigation.

Tango-Trio is especially valuable for studying orphan receptors, whose lack of identified endogenous ligands presents a challenge to studying said receptors[59]. Seeing as existing tools have focused on detecting classical G-protein signaling, Tango-Trio's ability to quantify activity independent of G-proteins is a suitable tool for deorphanization efforts[60]. By using the Tango-Trio to investigate the internalization profiles and potential biases of orphan receptors towards different isoforms of β-arrestin, we hope our platform can identify ligands for orphans that would not be detected by G-protein dependent changes, especially given that Tango-Trio represents an assay which is able to concurrently quantify and compare the degree of constitutive β-arrestin1/2 translocation and internalization at a GPCRome-wide level, and is also capable of profiling orphan activity in a dose-dependent manner.

Interestingly, none of the inverse agonists tested in our study was able to completely block the basal arrestin recruitment. For this reason, we defined the basal activity as the summation of state-dependent constitutive activity and state-independent activity (steady-state). We cannot exclude that amplification systems, including the Tango assay, fail to accurately detect constitutive activity, which represent a small percentage within the ensemble of a receptor's conformational landscape[61]. Given that basal activity is highly cell-dependent as it influenced by the basal phosphorylation of GPCRs[57], it is difficult to discriminate between basal and constitutive activity in our system apart from using inverse agonists. Thus, the partial decrease in arrestin recruitment observed for certain compounds, such as O-1918, Cetirizine, and Thiothixene, could be attributed to their effects on the small population of constitutively active receptors, but they cannot blunt the level of basal arrestin recruitment. Nonetheless, if this were the case, further studies would be warranted to explain why a significant enhancement in arrestin recruitment was observed for other inverse agonists, such as FC131 and Fluspirilene. It is becoming more evident that receptor activation follows a multistate model in which G-proteins

and arrestins stabilize specific conformations. Each of these conformations can be further stabilized by different ligands, leading to a broad intrinsic efficacy landscape, which in certain cases, can be opposite to each other when comparing two signaling pathways[62]. Finally, for some receptors, the uncoupling of G-proteins with an inverse agonist could facilitate β-arrestin recruitment. Another important consideration is that in vitro assays may fail to capture the true potency and efficacy of certain drugs with slow on-rates[63].

While Tango-Trio's ability to measure basal activity supports the discovery and study of inverse agonists in vitro, whose properties can be assessed based on the depression of constitutive arrestin translocation, it should be complemented with G-protein dependent profiling, especially since constitutive activity, by definition, is observed due to spontaneous G-protein activation[7]. Indeed, several inverse agonists profiled in our study produced either no change or an enhancement in constitutive arrestin recruitment, and a previous study saw no arrestin recruitment occurring in the presence of the GHSR inverse agonist SPA[61]. Therefore, given the diversity of responses we observed based on the type of inverse agonist tested, arrestin activities should not be the sole measure of the inverse agonistic properties of a compound. Although assays such as BRET will capture the direct effect of most drugs onto the conformational landscape of the receptors, some have a more complex pharmacology, acting as allosteric modulators, bitopic ligands, protean agonists, pharmacochaperones, or even a mixed pharmacological profile depending on receptor subpopulation. Moreover, the overall resultant activity, when used in vivo, is a summation of all effects of the drug toward the receptor when used for an extended period and thus, must also include its impact on receptor abundance and receptor post-translational modification. These effects are rather slow and require prolonged incubation of the drug onto the cell expressing the target receptor. In those cases, a reporter system such as the Tango-Trio, which involves incubation with drugs for >8 hrs, may capture pharmacological behavior not detected with short term incubation (<1 h).

By using the dynaminK44A loss-of-function mutant, we were also able to determine the extent of dynamin dependence during internalization[64]. However, given the numerous dynamin-dependent (e.g., clathrin-mediated, FEME,) and -independent pathways (e.g., CLIC/GEEC, micropinocytosis), further investigations into the other mediators of endocytosis are needed to elucidate the specific type of endocytosis mechanism employed at a given receptor. Of notable distinction is FEME, which has been shown to cargo several amine GPCRs, including ADRB1, ADRA2A, DRD4, and CHRM4, caveolae mechanisms observed for ADRB2, AGTR1, ENDRA, and GLP2R, and of course, the canonical clathrin-dependent endocytosis such as at APJ, DRD3, and CHRM3[32,65]. Arrestin-dependence of either isoform during the internalization of a given GPCR can also be orthogonally assayed used dominant negative arrestins[66].

While Tango-Trio uses modified GPCR constructs, the findings presented herein demonstrate that the addition of the V2-tail itself cannot fully account for differences between our Tango-based platform and those that employ unmodified WT GPCRs, such as the EMTA system. With regard to the V2 tail, while its original purpose was to increase basal β-arrestin2 recruitment and thus may artificially enhance its detection, seeing as it was added to all the receptors found in the PRESTO-Tango kit, any artificial increases in the Tango signal would still be proportional amongst all. Furthermore, PRESTO-Tango developers tested the effects of removing the V2 tail for some receptors and found variable results; notably, the removal of the V2 tail decreased the ligand-induced responses of some, e.g., the FFAR2 free fatty acid receptor, and had little effect on the ligand-induced responses of others e.g., the LTBR4 leukotriene receptor[1]. Another factor that could also contribute to the discrepancies in results between EMTA and Tango-based methods is the effect of receptor internalization when β-arrestin1/2 are overexpressed, especially considering the difference in the duration of the experiments. Overexpression of β-arrestin1/2 could contribute to increased internalization for certain receptors, which could account for the extent of arrestin recruitment, such as the case with OPRM1; agonists will also vary in their capacity to induce endocytosis of a given receptor; e.g., DAMGO at OPRM1 promotes rapid internalization, as opposed to morphine[67]. On the other hand, given that EMTA experiments occur over a short duration, the result obtained is based on the amount of receptor present at the time of adding the ligand, and thus, other factors such as receptor internalization will have minimal effects unlike in Tango-based. Finally, one of the biggest factors that limit comparisons between systems is that the EMTA method, as like other systems which use unmodified GPCRs, requires overexpression of GRK2 to examine β-arrestin-1/2 interactions, a limitation which could influence the cellular context, stoichiometry and levels of expression of GRKs, possibly leading to potential artifactual downstream signaling/arrestin recruitment measurements obtained. For example, the EMTA method found that among the receptors able to recruit β-arrestins, only a very small number selectively recruited β-arrestin-1 (1.3%) or β-arrestin-2 (6.4%), most of them recruiting both β-arrestins in the presence of GRK2 (92.3%)[33]. Tango-Trio does not require the overexpression of GRKs, so is preferable in that regard, and the level of expression of β-arrestin-1/2 and Fyve fusion proteins is modifiable using cumate induction, to be as close to the native environment/context as possible. If GRK2 or other kinases were overexpressed in Tango-Trio, we believe that several of the GPCRs with weak/no arrestin signals would also be detected in our system, and the degree of preferential β-arrestin isoform recruitment may also shift. In short, it must be underscored that both systems may artificially increase arrestin recruitment, either using modified GPCR constructs such as in Tango-Trio or using WT GPCRs but with the addition of a kinase such as in EMTA. Nonetheless, based on the intended purpose of an experiment, these methods have their own advantages and disadvantages and thus one system cannot truly replace the other, but rather both should be used as a complement.

One limitation to the profiles captured by Tango-Trio is that they may not be portable from different tissues, as the level of expression and identities of GPCR interactors directly influence the regulation of receptor signaling, localization and trafficking[4]. One study demonstrated that the constitutive activity of glutamate metabotropic receptors is depressed in the presence of Homer 3 scaffold protein[68]. Another example reports that of the GRK family members, GRK4 exclusively mediates the constitutive phosphorylation of DRD1[69]. Relevant to Tango-Trio, mRNA expression analysis of endogenously expressed GPCR-related proteins reveals that while HEK293 cells, the cell lineage upon which our platform was established, express numerous isoforms and full repertoires of numerous GPCR-interacting proteins, such as PKA and PKCs, they also do not express significant levels of certain essential effectors, such as GRK2[70], thereby impairing complete profiling at certain GPCRs dependent on GRK2 phosphorylation. The importance of GRK specificity is epitomized by a study in which GRK2 and GRK3 phosphorylation of their tested receptors (ADRB2 and CHRM2) was agonist-dependent, whereas GRK5 and GRK6 were able to phosphorylate in the absence of agonists[71]. Despite the challenge introduced by tissue-specific variations, Tango-Trio is a rich resource of arrestin coupling, selectivity and internalization profiles of hundreds of GPCRs, which can be confirmed and supplemented using orthogonal assays.

Studying GPCR activities and differences between signaling events is crucial for expanding our mechanistic understanding of GPCR signaling, and in turn, advancing the development of improved GPCR-targeted therapeutics. Towards these efforts, our wealth of data will help to functionally characterize GPCRs based on their β-arrestin1 and β-arrestin2 couplings, selectivities, and internalization efficacies. On a larger scale, the versatility and robustness of our platform is

well-suited to illuminating the big picture on the elements governing GPCRome pharmacological activities. We envision Tango-Trio to spur a transformational change on the study of basal and constitutive GPCR activities, and to promote research into GPCR constitutive versus agonist-induced activation mechanisms.

Methods

Cell culture

Human Embryonic Kidney cells (HEK293T) were maintained in Dulbecco's modified Eagle's medium (DMEM) supplemented with 5% fetal bovine serum (FBS), 5% bovine calf serum (BCS), and 100 µg/mL of penicillin-streptomycin at 37 °C in a humidified atmosphere containing 5% CO_2.

HTL (HEK293T stably expressing a luciferase reporter gene) and HTLA cells (HTL cells stably expressing a human β-arrestin-2 fused to Tobacco Etch Virus protease), both kindly provided by Dr. Richard Axel, were maintained in DMEM supplemented with 5% FBS, 5% BCS, 100 µg/mL of penicillin-streptomycin, 2.5 µg/mL of puromycin and 50 µg/mL of hygromycin.

HTTL were generated by transfection of HEK293T with modified pNLCoI1 vector (Promega) containing the luciferase2 (luc2) coding sequence under the control of the TRE-Tight promoter. Cells were transfected using PEI transfection method[72] and selected with hygromycin at 100 µg/mL. Colonies were picked, expanded, eventually duplicated, and further tested in 6-well format by transient transfection of a receptor and β-arrestin2-TEV219/pcDNA3.1+. The best clone was selected based on growth and β-arrestin2 recruitment at different GPCRs, which were previously validated by PRESTO-Tango[13].

HTLL-B1, -B2 and -F were generated by lentiviral infection of pCDH-CuO-MCS-EF1α-CymR-T2A-Bleo3 SparQ plasmid encoding β-arrestin2-TEV219, β-arrestin1-TEV219 or FYVE-TEV219 as per supplier instructions and selected using zeocin at 200 µg/mL. Colonies were picked, expanded, eventually duplicated, and further tested in 6-well format by transient transfection of a given receptor. The best clone was selected based on growth and β-arrestin1/2 recruitment or internalization at previously validated GPCRs.

Tango-Trio cell lines generated herein (HTTL, HTTL-B1, HTTL-B2, HTTL-F) are maintained continuously on dishes coated with 5 µg/mL collagen (Gibco). Tango-Trio cell lines are readily available and free of charge from the corresponding author upon request.

Transfection

Cell transfections were performed using a modified polyethyleneimine (PEI) transfection method[72]. Briefly, 1.5×10^6 cells were plated in a collagen-coated well of a 6-well plate with 2 mL of complete growth medium. 2 µg of DNA was mixed with 200 µL of Opti-MEM medium followed by addition of 6 µL of PEI (Polysciences) reagent stock solution (1 mg/mL, pH 7.0). The mixture was added dropwise to cells after 20 min incubation at room temperature. Medium was changed the next day and replaced with complete fresh medium. For stable cell line generation, antibiotics were added 48-hours post-transfection.

Tango β-arrestin recruitment assay

Assays were performed using modifications of the original Tango assay, as detailed below[13,29]. Cells were plated on collagen-coated dishes and transfected by the PEI precipitation method as described above. The day following transfection, the cells were plated in DMEM supplemented with 1% dialyzed FBS into collagen-coated 384-well white clear bottom cell culture plates at a density of 20,000 cells/well (or 16,000 cells/well for same-day transfection) in a total volume of 40 µL. The following day or the same day 5 h after seeding, ligand solutions were prepared in filtered assay buffer (20 mM HEPES, 1× Hanks' balanced salt solution (HBSS), pH 7.40) at 3X and added to cells (20 µL per well) for overnight incubation (16–20 h). Cumate, at indicated concentrations, was directly added in the complete medium from a water-soluble stock solution (10,000X in 95% ethanol). For most experiments, cumate was added at the time of cell plating (a day before transfection) and kept throughout the experiment. For time-dependent experiments, cumate was added as indicated in the text. The following day, media and drug solutions were removed, and 20 µL per well of homemade luciferase detection reagent (108 mM Tris–HCl; 42 mM Tris-Base, 75 mM NaCl, 3 mM MgCl2, 5 mM Dithiothrei-tol (DTT), 0.2 mM Coenzyme A, 0.14 mg/ml D-Luciferin, 1.1 mM ATP, 0.25% v/v Triton X-100, 2 mM Sodium hydrosulfite) was added. Plates were incubated for 10 min at room temperature in the dark before counting using Synergy Neo2 microplate reader (BioTek Instruments) and collected using Gen5 software v3.11 (BioTek Instruments). Data were subjected to non-linear least-squares regression analysis using the sigmoidal dose-response function (3-parameters modeled using Y = Bottom + (Top-Bottom)/(1 + 10^((LogEC50-X))); 4-parameters modeled using Y = Bottom + (X^Hillslope)*(Top-Bottom)/(X^HillSlope + EC50^HillSlope)) provided in GraphPad Prism v9.5.1. Data is presented as Relative Luminescence Units (RLU) and was processed (calculation of mean, SD or SEM, baseline correction as percentage difference using 100* (Value-Baseline)/Baseline) as indicated in figure legends. Parallel interrogation was performed as previously published by us[29].

Measurement of cell surface expression by ELISA

HTTL-B1, HTTL-B2 and HTTL-F were plated in collagen-coated 6-wells either with or without 30 µg/mL cumate. 24 h later, cells were transfected with a select number of validated GPCR hits from the constitutive HTS. Transfected cells were subsequently re-plated in 384-well plates at 30,000 cells/well and fixed for 10 min using 20 µL/well of 4% paraformaldehyde. Blocking was performed by incubating cells for 30 min with 20 µL/well of 5% normal goat serum in PBS, followed by the addition of 20 µL/well of 1/10,000 diluted anti-FLAG-HRP conjugated antibody (MilliporeSigma) for 1 h and two washes of 80 µL/well PBS. Supersignal ELISA Femto Substrate (Thermo Fisher Scientific) was applied per well, and luminescence was subsequently read with Synergy Neo2 microplate reader (BioTek Instruments).

Principal component analysis and visualization of RNA tissue-specific expression data

Human Protein Atlas (HPA) RNA consensus tissue gene data (version 21.0 and Ensembl version 103.38., accessed at https://www.proteinatlas.org/about/download) summarizing the expression levels in 55 tissues was extracted for β-arrestin-1 and −2 (ARRB1 and ARRB2), for select receptors with significant constitutive selectivity for at least one arrestin isoform (GPR182, AGTR2, ADRA2A, GPR37L1, SCTR, ADRB3, PTGER4, SUNCR1, PTGER3, MRGPRG, NPY5R, NPY1R, GLP1R, FPR1, MC1R, FPR3, 5-HT5, MRGPRD, GPR87, CXCR4, HRH1, AVPR2, 5-HT4, 5-HT2A, NTSR1, GLP2R, 5-HT1D, CXCR2, 5-HT1B, 5-HT1E, PTGER2, 5-HT2B, PTGDR), and the following serine/threonine kinases: GRKs (GRK2, GRK3, GRK5 GRK6), PKA (PRKACA, PRKACB, PRKACC), PKCs, PKNs, and PKDs (PRKCA, PRKCB, PRKCG, PRKCD, PRKCE, PRKCH, PRKCQ, PRKCI, PRKCZ, PKN1, PKN2, PKN3, PKD1, PKD2, PKD3), PKGs (PRKG1-2), PIMs (PIM1-3), AKTs (AKT1-3), GSK3 (GSK3A, GSK3B), CAMKI, CAMKII, and CAMIV (CAMK1D, CAMK1G, CAMK2A, CAMK2B, CAMK2D, CAMK2G, CAMK1, CAMK4, PNCK), CK1s and CK2s (CSNK1A1, CSNK1D, CSNK1E, CSNK1G1, CSNK1G2, CSNK1G3, CSNK2A1, CSNK2A2, CSNK2A3, CSNK2B). Despite protein levels not always equating to RNA expression levels, the latter was used as it was more complete than the existing protein expression data. The data was analyzed using principal component analysis (PCA) on our standardized data (Xstandardized = (Xraw − $\bar{X}$)/sx, where $\bar{X}$ is the mean and sx is the standard deviation of the variable value). The number of PCs were selected using GraphPad Prism v9.5.1's Parallel Analysis Approach ($n = 1000$ Monte Carlo simulations; PC1 and PC2 selected with eigenvalues greater than the 95th percentile of simulated counterparts), and subsequently visualized as loading plots.

Bioluminescence resonance energy transfer (BRET2) measurements

HEK293T cells were seeded in 6 well plates at 1.2×10^6 cells per well and were transfected with 0.5 μg of GPRC-RLuc8 construct and 0.5 μg of β-arrestin1/2-GFP2 using Jetprime (PolyPlus transfection). Following transfection, cells were detached and split on PLL-coated white 96-well assay plates (Perkin Elmer). 24 h later, spent medium was aspirated and replaced with 60 μL of 1X HBSS buffer, followed by 30 μL of serial dilutions of agonist at 3X concentration. Plates were incubated as 37 °C for 30 min, and 10 μL of Coelenterazine 400a (Nanolight Technologies) at 50 μM was added to each well, for a final concentration of 5 μM. Plates were incubated for 10–15 min at room temperature to allow the signal to stabilize, and subsequently read using the Hidex Sense Beta Plus microplate reader (Gamble Technologies) with 405 nm (RLuc8-Coelenterazine 400a) and 500 nm (GFP2) emission filters, at 1 s/well integration times.

shRNA knockdown, RNA isolation and RT-qPCR assay

Lentiviral β-arrestin-1 and −2 shRNA plasmids, obtained from the High-Throughput Screening Lab at the Children's Hospital of Eastern Ontario Research Institute, were transfected in HEK293T cells, along with psPAX2 and VSV-G vectors. The medium was replaced the following day with complete growth medium, and lentiviral shRNA medium was collected following 48 h transfection. For the knockdown experiment, HTTL-F cells were seeded in either complete medium or in the previously prepared lentiviral β-arrestin-1 and −2 shRNA medium (combined at a 1:1 ratio), with infection of cells facilitated with polybrene at 8 μg/mL.

Total RNA was isolated from transduced HTTL-F cells using the RNeasy Mini Kit (Qiagen) and quantified using the NanoDrop 2000 spectrophotometer (Thermo Fisher Scientific). First strand cDNA was synthesized with 900 ng of extracted RNA using the TransStart IV Reverse Transcriptase Kit (TransGen) according to the manufacturer's protocol. Human Actin (sense: 5′- CATGTACGTT GCTATCCAGGC-3′; antisense: 5′- CTCCTTAATGTCACGCACGAT-3′), β-arrestin-1 (sense: 5′- CCTGACCTTTCGCAAGGACC-3′; antisense: 5′-CAAGCCTTCCCCGTGTCTTC-3′) and β-arrestin-2 (sense: 5′-AAGCT CACCGTGTACTTGGG-3′; antisense: 5′-AGGGTCACAAACACTACAG GG-3′) primers were synthesized by IDT, Inc. Quantitative real time PCR experiments were performed with 2 μL of the synthesized cDNA in a total volume of 20 μL using the SYBR™ Green PCR Master Mix (Thermo Fisher Scientific), with the following cycling parameters: 95 °C for 10 min, followed by 40 cycles of 95 °C for 30 s, 60 °C for 30 s and 72 °C for 30 s. Data was analyzed using the comparative Ct (ΔΔCT) method, with the relative degree of response determined by $2^{-(\Delta\Delta CT)}$.

Molecular biology

TRE-Tight-Luc2 expression plasmid was constructed using the pNLCoI[luc2-P2A-NlucP/Hygro] Vector (Promega) as backbone vector (Accession no. KM359771), and a stop codon was added using QuikChange mutagenesis (Agilent) at the end of luc2 gene. This vector was chosen because it contains a synthetic poly(A) transcription pause site before the promoter, which reduces background and does not contain any SV40 ori, which is not compatible with the large T antigen expression in HEK293T. TRE-Tight promoter was PCR amplified from pTRETightBI-RY-0, which was a gift from Phil Sharp (Addgene plasmid # 31463) and cloned at NheI-HindIII restriction sites.

Codon optimized β-arrestin1-TEV219 was initially synthesized (Bio Basic) and cloned in pcDNA3.1+ (Thermo Fisher Scientific). β-arrestin2 was PCR amplified from pLX317-β-arrestin2 and the FYVE domain from pLX317-ZFYVE16 (Endofin) both from the MISSION TRC3 Human LentiORF Collection (MilliporeSigma). Both were cloned into the β-arrestin1-TEV219/pcDNA3.1+ at HindIII-BamHI sites. The PURO resistance gene in the all-in-one lentivector pCDH-CuO-MCS-EF1α-CymR-T2A-PURO SparQ (System Biosciences, QM800A-1) was changed for the BLEO3 resistance using PCR amplification and restriction site cloning (EcoRI-SalI). β-arrestin1-TEV219, β-arrestin2-TEV219, and FYVE-TEV219 were PCR amplified from the pcDNA3.1+ plasmid and cloned at NheI-SwaI restriction sites. Sequence maps for the aforementioned constructs can be found in the Supplementary Information.

GPCR-RLuc8 constructs for BRET2 experiments were cloned by PCR amplifying RLuc8 and cloned into Tango constructs at AgeI-XbaI site. β-arrestin1-GFP2 and β-arrestin2-GFP2 were cloned by PCR amplifying GFP2 and cloned at BamHI-XbaI sites of β-arrestin1-TEV219 and β-arrestin2-TEV219 in pcDNA3.1+.

The Roth Lab PRESTO-Tango GPCR Kit was from Dr. Bryan Roth and is available through Addgene [www.addgene.org/kits/roth-gpcr-presto-tango/].

Reporting summary

Further information on research design is available in the Nature Portfolio Reporting Summary linked to this article.

Data availability

The data that support this study are available from the corresponding authors upon request. All data generated or analyzed during this study, including data underlying Figs. 1–8 and all Supplementary Figures are provided as a Source Data file accessible at the Figshare repository [https://doi.org/10.6084/m9.figshare.22802948]. Human Protein Atlas (HPA) RNA consensus tissue gene data (version 21.0 and Ensembl version 103.38.) used for the production of Fig. 8 was accessed at [https://www.proteinatlas.org/about/]. EMTA data compared in Supplementary Table 1, including Emax (in % of vehicle response) and absolute pEC50 values, was downloaded from [https://cdn.elifesciences.org/articles/74101/elife-74101-supp2-v2.xlsx].

References

1. Kroeze, W. K., Sheffler, D. J. & Roth, B. L. G-protein-coupled receptors at a glance. *J. Cell Sci.* **116**, 4867–9 (2003).
2. Pierce, K. L., Premont, R. T. & Lefkowitz, R. J. Seven-transmembrane receptors. *Nat. Rev. Mol. Cell Biol.* **3**, 639–650 (2002).
3. Lynch, J. R. & Wang, J. Y. G protein-coupled receptor signaling in stem cells and cancer. *Int. J. Mol. Sci.* **17**, 707 (2016).
4. Ritter, S. L. & Hall, R. A. Fine-tuning of GPCR activity by receptor-interacting proteins. *Nat. Rev. Mol. Cell Biol.* **10**, 819–830 (2009).
5. Black, J. B., Premont, R. T. & Daaka, Y. Feedback regulation of G protein-coupled receptor signaling by GRKs and arrestins. *Semin. Cell Dev. Biol.* **50**, 95–104 (2016).
6. Draper-Joyce, C. & Furness, S. G. B. Conformational transitions and the activation of heterotrimeric G proteins by G protein-coupled receptors. *ACS Pharmacol. Transl. Sci.* **2**, 285 (2019).
7. Rosenbaum, D. M., Rasmussen, S. G. F. & Kobilka, B. K. The structure and function of G-protein-coupled receptors. *Nature* **459**, 356–363 (2009).
8. Smith, J. S. & Rajagopal, S. The β-Arrestins: multifunctional regulators of G protein-coupled receptors. *J. Biol. Chem.* **291**, 8969–77 (2016).
9. Kohout, T. A., Lin, F.-T., Perry, S. J., Conner, D. A. & Lefkowitz, R. J. β-Arrestin 1 and 2 differentially regulate heptahelical receptor signaling and trafficking. *Proc. Natl Acad. Sci.* **98**, 1601–1606 (2001).
10. Tilley, D. G. G protein-dependent and G protein-independent signaling pathways and their impact on cardiac function. *Circ. Res.* **109**, 217–30 (2011).
11. Thomsen, A. R. B., Jensen, D. D., Hicks, G. A. & Bunnett, N. W. Therapeutic targeting of endosomal G-protein-coupled receptors. *Trends Pharmacol. Sci.* **39**, 879–891 (2018).
12. Van Koppen, C. J. & Jakobs, K. H. Arrestin-independent internalization of G protein-coupled receptors. *Mol. Pharmacol.* **66**, 365–367 (2004).

13. Kroeze, W. K. et al. PRESTO-Tango as an open-source resource for interrogation of the druggable human GPCRome. *Nat. Struct. Mol. Biol.* **22**, 362–369 (2015).
14. Blau, H. M. & Rossi, F. M. Tet B or not tet B: advances in tetracycline-inducible gene expression. *Proc. Natl Acad. Sci. USA.* **96**, 797–9 (1999).
15. Jaisser, F. Inducible gene expression and gene modification in transgenic mice. *J. Am. Soc. Nephrol.* **11**, S95–S100 (2000).
16. Liu, B., Wang, S., Brenner, M., Paton, J. F. R. & Kasparov, S. Enhancement of cell-specific transgene expression from a Tet-Off regulatory system using a transcriptional amplification strategy in the rat brain. *J. Gene Med.* **10**, 583–92 (2008).
17. Vopálenský, V. et al. Firefly luciferase gene contains a cryptic promoter. *RNA* **14**, 1720–9 (2008).
18. Parks, T. D., Howard, E. D., Wolpert, T. J., Arp, D. J. & Dougherty, W. G. Expression and purification of a recombinant tobacco etch virus NIa proteinase: biochemical analyses of the full-length and a naturally occurring truncated proteinase form. *Virology* **210**, 194–201 (1995).
19. Kapust, R. B. et al. Tobacco etch virus protease: mechanism of autolysis and rational design of stable mutants with wild-type catalytic proficiency. *Protein Eng.* **14**, 993–1000 (2001).
20. Seet, L.-F. & Hong, W. Endofin, an endosomal FYVE domain protein. *J. Biol. Chem.* **276**, 42445–42454 (2001).
21. Mullick, A. et al. The cumate gene-switch: a system for regulated expression in mammalian cells. *BMC Biotechnol.* **6**, 43 (2006).
22. Gould, D. J. & Chernajovsky, Y. Endogenous GATA factors bind the core sequence of the tetO and influence gene regulation with the tetracycline system. *Mol. Ther.* **10**, 127–138 (2004).
23. Cohen, S., Dovrat, S., Sarid, R., Huberman, E. & Salzberg, S. JAK–STAT signaling involved in phorbol 12-myristate 13-acetate- and dimethyl sulfoxide-induced 2′–5′ oligoadenylate synthetase expression in human HL-60 leukemia cells. *Leuk. Res.* **29**, 923–931 (2005).
24. Pedranzini, L. et al. Pyridone 6, A Pan-Janus–activated kinase inhibitor, induces growth inhibition of multiple myeloma cells. *Cancer Res.* **66**, 9714–9721 (2006).
25. Saucier, C., Morris, S. J. & Albert, P. R. Endogenous serotonin-2A and −2C receptors in Balb/c-3T3 cells revealed in serotonin-free medium: Desensitization and down-regulation by serotonin. *Biochem. Pharmacol.* **56**, 1347–1357 (1998).
26. Bousoik, E. & Montazeri Aliabadi, H. "Do We Know Jack" About JAK? A Closer Look at JAK/STAT Signaling Pathway. *Front. Oncol.* **8**, 287 (2018).
27. Alexander, S. P. H. et al. THE CONCISE GUIDE TO PHARMACOLOGY 2021/22: G protein-coupled receptors. *Br. J. Pharmacol.* **178**, S27–S156 (2021).
28. Seo, S. O. & Schmidt-Dannert, C. Development of a synthetic cumate-inducible gene expression system for Bacillus. *Appl. Microbiol. Biotechnol.* **103**, 303–313 (2019).
29. Zeghal, M., Laroche, G. & Giguère, P. M. Parallel interrogation of β-arrestin2 recruitment for ligand screening on a GPCR-wide scale using PRESTO-Tango assay. *J. Vis. Exp.* **2020**, e60823 (2020).
30. Rinne, M., Tanoli, Z. U. R., Khan, A. & Xhaard, H. Cartography of rhodopsin-like G protein-coupled receptors across vertebrate genomes. *Sci. Rep. 2019 91* **9**, 1–16 (2019).
31. Zhao, X. et al. A homogeneous enzyme fragment complementation-based beta-arrestin translocation assay for high-throughput screening of G-protein-coupled receptors. *J. Biomol. Screen.* **13**, 737–747 (2008).
32. Moo, E. Von, van Senten, J. R., Bräuner-Osborne, H. & Møller, T. C. Arrestin-dependent and -independent internalization of G protein-coupled receptors: methods, mechanisms, and implications on cell signaling. *Mol. Pharmacol.* **99**, 242–255 (2021).
33. Avet, C. et al. Effector membrane translocation biosensors reveal G protein and Parrestin coupling profiles of 100 therapeutically relevant GPCRs. *Elife* **11**, e74101 (2022).
34. Zhou, Q. et al. Common activation mechanism of class a GPCRs. *Elife* **8**, e50279 (2019).
35. Lu, S., Jang, W., Inoue, A. & Lambert, N. A. Constitutive G protein coupling profiles of understudied orphan GPCRs. *PLoS One* **16**, e0247743 (2021).
36. Watkins, L. R. & Orlandi, C. In vitro profiling of orphan G protein coupled receptor (GPCR) constitutive activity. *Br. J. Pharmacol.* **178**, 2963–2975 (2021).
37. Oakley, R. H., Laporte, S. A., Holt, J. A., Caron, M. G. & Barak, L. S. Differential affinities of visual arrestin, beta arrestin1, and beta arrestin2 for G protein-coupled receptors delineate two major classes of receptors. *J. Biol. Chem.* **275**, 17201–10 (2000).
38. Berg, K. A. & Clarke, W. P. Making sense of pharmacology: inverse agonism and functional selectivity. *Int. J. Neuropsychopharmacol.* **21**, 962–977 (2018).
39. Harding, S. D. et al. The IUPHAR/BPS guide to PHARMACOLOGY in 2022: curating pharmacology for COVID-19, malaria and antibacterials. *Nucleic Acids Res.* **50**, D1282–D1294 (2022).
40. Simcocks, A. C. et al. Atypical cannabinoid ligands O-1602 and O-1918 administered chronically in diet-induced obesity. *Endocr. Connect* **8**, 203 (2019).
41. Thiele, S., Mungalpara, J., Steen, A., Rosenkilde, M. M. & Våbenø, J. Determination of the binding mode for the cyclopentapeptide CXCR4 antagonist FC131 using a dual approach of ligand modifications and receptor mutagenesis. *Br. J. Pharmacol.* **171**, 5313–5329 (2014).
42. Magalhaes, A. C., Dunn, H. & Ferguson, S. S. G. Regulation of GPCR activity, trafficking and localization by GPCR-interacting proteins. *Br. J. Pharm.* **165**, 1717 (2012).
43. Yang, Z. et al. Phosphorylation of G protein-coupled receptors: from the barcode hypothesis to the flute model. *Mol. Pharmacol.* **92**, 201–210 (2017).
44. Drube, J. et al. GRK2/3/5/6 knockout: the impact of individual GRKs on arrestin-binding and GPCR regulation. *bioRxiv* https://doi.org/10.1101/2021.02.12.430971 (2021).
45. Busillo, J. M. et al. Site-specific phosphorylation of CXCR4 is dynamically regulated by multiple kinases and results in differential modulation of CXCR4 signaling. *J. Biol. Chem.* **285**, 7805–7817 (2010).
46. Białopiotrowicz, E. et al. Microenvironment-induced PIM kinases promote CXCR4-triggered mTOR pathway required for chronic lymphocytic leukaemia cell migration. *J. Cell. Mol. Med.* **22**, 3548–3559 (2018).
47. Decker, S. et al. PIM kinases are essential for chronic lymphocytic leukemia cell survival (PIM2/3) and CXCR4-mediated microenvironmental interactions (PIM1). *Mol. Cancer Ther.* **13**, 1231–1245 (2014).
48. Shintani, Y. et al. β-Arrestin1 and 2 differentially regulate PACAP-induced PAC1 receptor signaling and trafficking. *PLoS One* **13**, e0196946 (2018).
49. Vibhuti, A., Gupta, K., Subramanian, H., Guo, Q. & Ali, H. Distinct and shared roles of β-Arrestin-1 and β-Arrestin-2 on the regulation of C3a receptor signaling in human mast cells. *PLoS One* **6**, e19585 (2011).
50. Levoye, A. et al. A broad G protein-coupled receptor internalization assay that combines SNAP-tag labeling, diffusion-enhanced resonance energy transfer, and a highly emissive terbium cryptate. *Front. Endocrinol.* **6**, 167 (2015).
51. Moriya, H. Quantitative nature of overexpression experiments. *Mol. Biol. Cell* **26**, 3932 (2015).

52. Peterson, Y. K. & Luttrell, L. M. The diverse roles of arrestin scaffolds in G protein–coupled receptor signaling. *Pharmacol. Rev.* **69**, 256–297 (2017).
53. Miljuš, T. et al. Diverse chemotypes drive biased signaling by cannabinoid receptors. *bioRxiv* https://doi.org/10.1101/2020.11.09.375162, (2020).
54. Gurevich, E. V., Benovic, J. L. & Gurevich, V. V. Arrestin2 expression selectively increases during neural differentiation. *J. Neurochem* **91**, 1404–1416 (2004).
55. Komolov, K. E. & Benovic, J. L. G protein-coupled receptor kinases: past, present and future. *Cell. Signal.* **41**, 17 (2018).
56. Kumari, P. et al. Core engagement with β-arrestin is dispensable for agonist-induced vasopressin receptor endocytosis and ERK activation. *Mol. Biol. Cell* **28**, 1003 (2017).
57. Tobin, A. B. G-protein-coupled receptor phosphorylation: where, when and by whom. *Br. J. Pharm.* **153**, S167 (2008).
58. Stenmark, H., Aasland, R. & Driscoll, P. C. The phosphatidylinositol 3-phosphate-binding FYVE finger. *FEBS Lett.* **513**, 77–84 (2002).
59. Roth, B. L. Impossible or merely difficult? Two grand challenges-from a biologist's perspective. *ACS Med. Chem. Lett.* **4**, 316 (2013).
60. Ngo, T. et al. Identifying ligands at orphan GPCRs: current status using structure-based approaches. *Br. J. Pharmacol.* **173**, 2934–2951 (2016).
61. Mary, S. et al. Ligands and signaling proteins govern the conformational landscape explored by a G protein-coupled receptor. *Proc. Natl Acad. Sci. USA.* **109**, 8304–8309 (2012).
62. Azzi, M. et al. Beta-arrestin-mediated activation of MAPK by inverse agonists reveals distinct active conformations for G protein-coupled receptors. *Proc. Natl Acad. Sci. USA.* **100**, 11406–11411 (2003).
63. Williams, C. & Hill, S. J. GPCR signaling: understanding the pathway to successful drug discovery. *Methods Mol. Biol.* **552**, 39–50 (2009).
64. Huber, M., Brabec, M., Bayer, N., Blaas, D. & Fuchs, R. Elevated endosomal pH in HeLa cells overexpressing mutant dynamin can affect infection by pH-sensitive viruses. *Traffic* **2**, 727–736 (2001).
65. Casamento, A. & Boucrot, E. Molecular mechanism of fast endophilin-mediated endocytosis. *Biochem. J.* **477**, 2327 (2020).
66. Orsini, M. J. & Benovic, J. L. Characterization of dominant negative arrestins that inhibit beta2-adrenergic receptor internalization by distinct mechanisms. *J. Biol. Chem.* **273**, 34616–34622 (1998).
67. Al-Hasani, R. & Bruchas, M. R. Molecular mechanisms of opioid receptor-dependent signaling and behavior. *Anesthesiology* **115**, 1363–1381 (2011).
68. Chung, G. & Kim, S. J. Sustained activity of metabotropic glutamate receptor: homer, arrestin, and beyond. *Neural Plast.* **2017**, 5125624 (2017).
69. Rankin, M. L. et al. The D1 dopamine receptor is constitutively phosphorylated by G protein-coupled receptor kinase 4. *Mol. Pharmacol.* **69**, 759–769 (2006).
70. Atwood, B. K., Lopez, J., Wager-Miller, J., Mackie, K. & Straiker, A. Expression of G protein-coupled receptors and related proteins in HEK293, AtT20, BV2, and N18 cell lines as revealed by microarray analysis. *BMC Genom.* **12**, 14 (2011).
71. Li, L. et al. G protein-coupled receptor kinases of the GRK4 protein subfamily phosphorylate inactive G protein-coupled receptors (GPCRs). *J. Biol. Chem.* **290**, 10775 (2015).
72. Longo, P. A., Kavran, J. M., Kim, M. S. & Leahy, D. J. Transient mammalian cell transfection with polyethylenimine (PEI). *Methods Enzymol.* **529**, 227–240 (2013).

Acknowledgements

M.Z. is supported by the Alexander Graham Bell Canada Graduate Scholarships-Doctoral Program (CGS-D3) from Natural Sciences and Engineering Research Council of Canada. This work was funded by the Canadian Institutes of Health Research (CIHR grant #MOP142219) and Natural Sciences and Engineering Research Council of Canada (NSERC RGPIN-2017-06151). The authors also wish to thank Dr. Mario Tiberi for his assistance and providing several of our tested inverse agonists and antagonists.

Author contributions

P.M.G. conceived the overall concept; M.Z. and G.L. designed and performed all experiments; J.D.F. assisted with validation of primary screen findings; R.W. prepared the arrayed agonist and PRESTO-Tango DNA plates for the primary screen; M.Z., G.L., and P.M.G. analyzed the data and wrote the manuscript.

Competing interests

The authors declare no competing interests.

Additional information

Supplementary information The online version contains supplementary material available at https://doi.org/10.1038/s41467-023-39132-x.

Correspondence and requests for materials should be addressed to Patrick M. Giguère.

Peer review information *Nature Communications* thanks David Reiner-Link and the other, anonymous, reviewer(s) for their contribution to the peer review of this work.

Your contacts to obtain permission for the reuse of material from:

- books: bookpermissions@springernature.com
- journals: journalpermissions@springernature.com

Author reuse

Please check the Copyright Transfer Statement (CTS) or Licence to Publish (LTP) that you have signed with Springer Nature to find further information about the reuse of your content.

Authors have the right to reuse their article's Version of Record, in whole or in part, in their own thesis. Additionally, they may reproduce and make available their thesis, including Springer Nature content, as required by their awarding academic institution. Authors must properly cite the published article in their thesis according to current citation standards. Material from: 'AUTHOR, TITLE, JOURNAL TITLE, published [YEAR], [publisher - as it appears on our copyright page]'

If you are any doubt about whether your intended re-use is covered, please contact journalpermissions@springernature.com for confirmation.

Self-Archiving

- Journal authors retain the right to self-archive the final accepted version of their manuscript. Please see our self-archiving policy for full details: https://www.springer.com/gp/open-access/authors-rights/self-archiving-policy/2124

- Book authors please refer to the information on this link: https://www.springer.com/gp/open-access/publication-policies/self-archiving-policy

Rights and Permissions

Permissions ←

Obtaining translation and reprint rights

Rights and Permissions at book fairs

Contacts

Report piracy of Springer Nature publications

Springer's text- and data-mining policy

Development of a V5-tag–directed nanobody and its implementation as an intracellular biosensor of GPCR signaling

Received for publication, April 20, 2023, and in revised form, July 19, 2023 Published, Papers in Press, July 28, 2023,
https://doi.org/10.1016/j.jbc.2023.105107

Manel Zeghal[1,‡], Kevin Matte[1,‡], Angelica Venes[1], Shivani Patel[1], Geneviève Laroche[1], Sabina Sarvan[1,2], Monika Joshi[1,2], Jean-Christophe Rain[3], Jean-François Couture[1,2], and Patrick M. Giguère[1,4,*]

From the [1]Department of Biochemistry, Microbiology and Immunology, Faculty of Medicine, and [2]Ottawa Institute of Systems Biology, University of Ottawa, Ottawa, Ontario, Canada; [3]Hybrigenics Services, Évry-Courcouronnes, France; [4]Brain and Mind Research Institute, University of Ottawa, Ottawa, Ontario, Canada

Reviewed by members of the JBC Editorial Board. Edited by Kirill Martemyanov

Protein–protein interactions (PPIs) form the foundation of any cell signaling network. Considering that PPIs are highly dynamic processes, cellular assays are often essential for their study because they closely mimic the biological complexities of cellular environments. However, incongruity may be observed across different PPI assays when investigating a protein partner of interest; these discrepancies can be partially attributed to the fusion of different large functional moieties, such as fluorescent proteins or enzymes, which can yield disparate perturbations to the protein's stability, subcellular localization, and interaction partners depending on the given cellular assay. Owing to their smaller size, epitope tags may exhibit a diminished susceptibility to instigate such perturbations. However, while they have been widely used for detecting or manipulating proteins *in vitro*, epitope tags lack the *in vivo* traceability and functionality needed for intracellular biosensors. Herein, we develop NbV5, an intracellular nanobody binding the V5-tag, which is suitable for use in cellular assays commonly used to study PPIs such as BRET, NanoBiT, and Tango. The NbV5:V5 tag system has been applied to interrogate G protein–coupled receptor signaling, specifically by replacing larger functional moieties attached to the protein interactors, such as fluorescent or luminescent proteins (∼30 kDa), by the significantly smaller V5-tag peptide (1.4 kDa), and for microscopy imaging which is successfully detected by NbV5-based biosensors. Therefore, the NbV5:V5 tag system presents itself as a versatile tool for live-cell imaging and a befitting adaptation to existing cellular assays dedicated to probing PPIs.

Nestled at the heart of the study of molecular biology, protein–protein interaction (PPI) assays stand as heralded experimental techniques used to investigate the interactions between two or more proteins, often informing drug discovery and development, such as for G protein–coupled receptor (GPCR) signaling (1, 2). Cell-based assays also find particular relevance in unraveling PPIs from a physiological context, shedding light on their roles in biological processes, their implications within cellular environments, and the consequences of their dysregulation in disease (3). Considering the varying strengths and limitations inherent to each approach, the selection of an appropriate PPI assay is contingent upon the specific research question being addressed (4). Earlier experimental methodologies, such as pull-down and immunoprecipitation techniques, were commonly employed to detect or isolate protein complexes. However, these approaches exhibit disruptive tendencies towards larger complexes, particularly those involving membrane-spanning proteins (5). A pivotal subset of cell-based assays comes in the form of biosensor-based techniques, which offer indispensable insights into PPIs within the realm of living cells. By utilizing fluorescent/luminescent molecules or functional moieties to label two proteins of interest, the biosensor-based technique enables monitoring their interaction within a cellular milieu. Moreover, these cellular biosensors can measure both high- and low-affinity interactions and transient and stable complexes using endpoint or live assay (6, 7). With respect to GPCR signaling, the most common cellular systems employing such biosensors include the protease-dependent reporter assays such as the Tobacco Etch protease-dependent assay (Tango), bioluminescence resonance energy transfer (BRET), and Nanoluciferase binary technology (NanoBiT) (8). Despite the value of these biosensor-based cellular techniques, the imbroglio of the protein interactome can complicate the execution of its study, and investigations of PPIs at a scaled-up level have been limited thus far. Moreover, PPI assays, such as resonance energy transfer or binary complementation, require cloning of each component in all possible and permissive orientations, specifically at the C terminus or N terminus of the protein, which could translate into over twelve different combinations to be tested (9). Finally, while approaches such as Tango, BRET, and NanoBiT have been designed to provide an understanding of different PPIs, all involve the fusion of large, functionalized tags (tobacco etch virus (TEV), GFP2, Large BiT (LgBiT), respectively) to the proteins of interest (10).

Considering the aforementioned limitations, the adoption of short peptide or epitope tags offers a reasonable possibility to

‡ These authors contributed equally to the work.
* For correspondence: Patrick M. Giguère, patrick.giguere@uottawa.ca.

probe PPIs. Less than 20 residues in length, epitope tags (*e.g.*, HA, Flag, Myc, and V5) are commonplace in protein purification and localization/detection such as microscopy but less so for monitoring dynamic interactions (11). However, although fluorophores (*e.g.*, GFP, mCherry) and other polypeptides (*e.g.*, MBP, GST) are popularly used for probing recombinant proteins in a cellular context, including live cell imaging, reporter assays, and resonance energy transfer, the smaller size of epitope tags could be preferable for these purposes, as the fusion of bulkier fluorophores and polypeptides could interfere with the native behavior and functions of the protein of interest, especially interactions that are particularly proximity- or location-dependent (12). Besides avoiding cross-reactions within the native proteome, epitope tags obviate the need for custom antibody generation for every protein of interest and give rise to the possibility of multiplexing orthogonal peptide tags within the same experiment (11, 13).

Given the indispensability of these peptides, antibodies have continually been developed to recognize existing and newly developed epitope tags. Although conventional antibodies have proven to be robust workhorses in various cell biology research fields, their large size and complex architecture preclude them from functioning within living cells (14, 15). These limitations spurred advances in engineering novel recombinant antibody constructs, termed intracellular antibodies or intrabodies. Although their biophysical properties are unlike the conventional monoclonal antibodies, intrabodies retain the capacities for recognition and/or neutralization with similarly high specificities and affinities, with the added conferred ability to bind specific targets expressed within the same living cell that houses it, typically within the cytoplasm of eukaryotic cells (16). Despite intense efforts, minimal antigen-binding fragments such as single-chain variable fragments or F(ab)-type fragments remain highly unstable in a cellular environment and have limited activity in an intracellular milieu (17–19). The challenges for intrabodies to be expressed in their functional forms are partly due to their aggregation propensity and the reducing environment of the cytoplasm, which prevents intradomain disulfide bond formation (20, 21).

Of greater promise are single-domain antibodies, also referred to as variable domain of heavy-chain antibodies (VHHs) or nanobodies (Nbs), which are the smallest antibody derivatives (12–15 kDa). Although originally derived from members of the Camelidae and *Chondrichthyes* family, human-derived single-domain antibodies have also been engineered from conventional human IgGs (22). Epitope-specific Nbs can be selected by various approaches, including display-based panning or synthetic libraries generated *in vitro* using predesigned scaffolds that undergo complementarity-determining region (CDR) codon randomization (23). Moreover, retrieved Nbs can be affinity-matured to further improve upon the original pharmacological features (24). Structurally, these noncanonical antibodies are more compact, consisting exclusively of shortened heavy chains with three interspersed CDRs that form their antigen-binding domain. Devoid of the hydrophobic interface between heavy and light chains and stabilized by only a single internal disulfide bond, Nbs rival conventional IgGs given their low immunogenicity, enhanced solubility, and stability, all while retaining high binding affinities towards their targets and thereby are more successfully expressed in the cytosol of mammalian cells (25). In terms of binding performance, Nbs have an enhanced ability to target sterically hindered and/or concave epitopes given their slightly convex-shaped paratope (26). As such, the physicochemical and pharmacological properties of Nbs offer a multitude of possibilities for live-cell applications, such as elucidating signaling pathways and PPIs in live cells, targeting proteins or protein complexes formerly inaccessible to biologics, fusing to other functional effectors such as proteases and fluorophores, and visualizing and localizing proteins of interest using conventional and advanced microscopy (27). Moreover, Nbs targeting intracellular targets are plentiful, the majority of which target various cytosolic proteins and more recently, short peptide or epitope tags (28–41). However, Nbs recognizing these small peptide fragments are still scarce, in part due to conformational difficulties of the cleft-like paratope of Nbs for recognizing linear peptides and the needed strength of Nb–peptide tag interaction; based on existing literature, less than 10 peptide-targeted Nbs have been identified, specifically against the EPEA (42), SPOT (43, 44), 6E (45), Moon (46, 47), Myc (48), BC2 (43, 49), and ALFA tags (50, 51). Only two of these antibody-peptide pairs retained binding in cells, the Moon and ALFA tag, allowing for the possibility of multiplexing (52).

Therefore, the paucity of tag-targeted intrabodies is a bottleneck for intracellular interrogations, especially given the pre-existing arrayed or pooled tag-encoded complementary DNA (cDNA) and ORF libraries for overexpression studies. For example, while there are comprehensive human genome-wide and fully annotated V5-tagged libraries developed from the ORFeome project (53) and the *Drosophila* genome-wide V5-tagged library (54), these open resources are mainly limited to phenotypic screenings for living cellular assay or microscopy for *in vitro* assay on fixed tissues. As for the peptide itself, the V5 tag is a universal epitope that has been extensively used since its introduction roughly 30 years ago (55) and has desirable characteristics suitable for intracellular use. More specifically, the V5 tag is of small size (1.42 kDa), possesses an equal number of positively and negatively charged residues exhibiting a pI of 5.85 and no net charge at physiological pH (56, 57), is of prokaryotic origin which circumvents possible background signals when expressed in mammalian and insect cell host, as well as being resistant to cleavage by their endogenous proteases (51). Thus, the development of intracellular Nb recognizing the small peptide V5-tag and its functionalization would be highly amenable to cellular studies of a broader nature using the genome-wide V5-tagged ORF library, as well as more directed investigations of gene function and genetic rescues and protein–protein interactions such as dynamic receptor-protein interfaces, with minimal interference.

To this end, we introduce the NbV5, a novel Nb that interacts with the V5-tag, serving as the foundation of our multipurpose intracellular nanobody-based biosensors. Our

work demonstrates that the NbV5:V5 tag system is suitable for monitoring dynamic PPIs in various adapted cellular assays, specifically in the context of GPCR signaling, and for microscopic imaging techniques.

Results

Generation of a nanobody directed against the V5-tag

The first generation of selective Nbs recognizing the V5-tag was identified using the Hybribody approach, a two-pronged screening strategy involving synthetic VHHs phage display and yeast two-hybrid (Y2H). Peptide phage display was first performed against a purified HaloTag protein harboring a duplicate copy of the V5-tag to select for a synthetic VHH against the V5-tag (sequence in Fig. 1*A*). Following the first round of the phage display screening process, the VHHs demonstrating an interaction for the V5-tag were subsequently cloned into a yeast prey vector to execute the second Y2H (58, 59), yielding 52 distinct VHHs with redundancies ranging from 1 to 37. Among this repertoire of VHHs, the top 20 clones that exhibited the highest degrees of redundancy were selected and subsequently cloned into mammalian expression vector fused at the C terminus with the TEV219. This integrated approach and the utilization of the highly diverse humanized library NaLi-H1 (60) promoted the enrichment of stable and soluble intracellular-targeting Nbs; the overall process is illustrated in Figure 1, *B* and *C*.

To interrogate their binding capabilities and specificities, the potential VHHs were subsequently evaluated using the Tango-based assay, specifically by using the mu-opioid receptor (μ-OR) and angiotensin II receptor type 1 (AT1R) and independently testing each clone using increasing concentrations of the μ-OR agonist DAMGO and AT1R agonist angiotensin II. To maximize the detection of β-arrestin recruitment at these receptors, two variants of tagged-β-arrestin-2 were utilized, either carrying an N- or C-terminal V5-tag (V5-β-arrestin-2 and β-arrestin-2-V5, respectively). The overall schematic of the nanobody-based Tango assay is depicted in Figure 2*A*. Based on these preliminary findings, a particular clone, designated as NbA1, exhibited a robust response with β-arrestin-2-V5 while displaying a barely detectable response with N-terminally tagged V5-β-arrestin-2. Furthermore, codon optimization for human expression enhanced the original nanobody's expression level threefold and thus was selected for further experiments in human cells (Fig. 2, *B* and *C*).

Crystal structure of the NbA1

To address the suboptimal activity of NbA1 toward the N-terminally tagged β-arrestin-2, a computer-aided affinity maturation strategy was opted for. Towards this aim, we initially solved the V5-bound structure of NbA1 at a resolution of 2 Å (Table 1). Structural analysis revealed that NbA1 adopts a typical V-shaped IgG fold connected by a disulfide bond, while the V5 peptide lacks any secondary structures (Fig. 3*A*) (61). The paratope responsible for V5 peptide interaction is primarily mediated by the CDR2 and CDR3 regions, a common feature of Nbs (62). Nbs compensate for their reduced number of CDRs compared to conventional antibodies through distinctive CDR structures and antigen-binding modes; for example, many Nbs possess elongated CDR3 loops to provide a larger antigen interaction surface (43), as observed in NbV5 (Fig. 3*A*). The V5 peptide makes multiple polar and hydrophobic contacts with NbA1 and is oriented at 90 degrees to the central axis of the nanobody. Out of the 14 residues of the tag, 11 directly interact with NbA1 (Fig. 3*B*). The lateral chains of two residues, Lys 2 and Ile 4, point

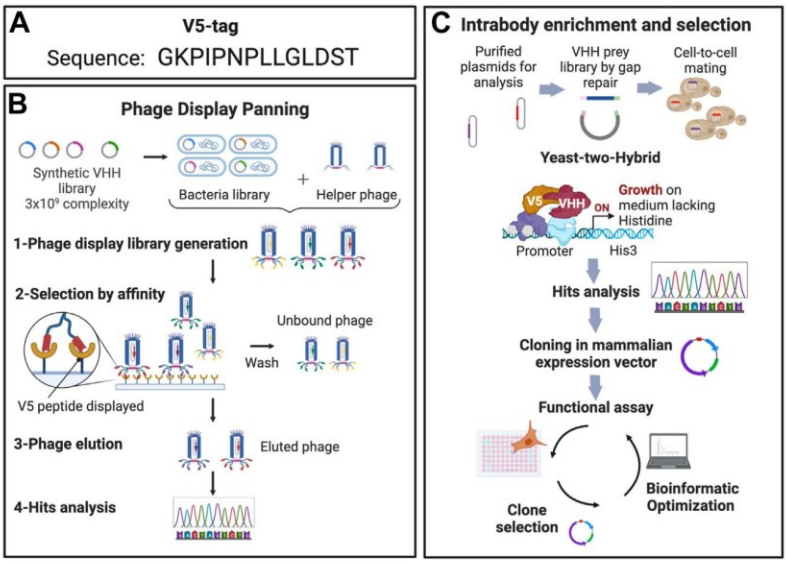

Figure 1. Overview of the selection of a synthetic nanobody interacting with the V5-tag. *A*, sequence of the V5-tag. *B*, schematic of the phage-display panning for the enrichment of nanobodies interacting with the V5-peptide tag. *C*, schematic of the yeast two-hybrid screening (Y2H) for the enrichment of nanobodies interacting with the V5-peptide tag in an intracellular environment (intrabody).

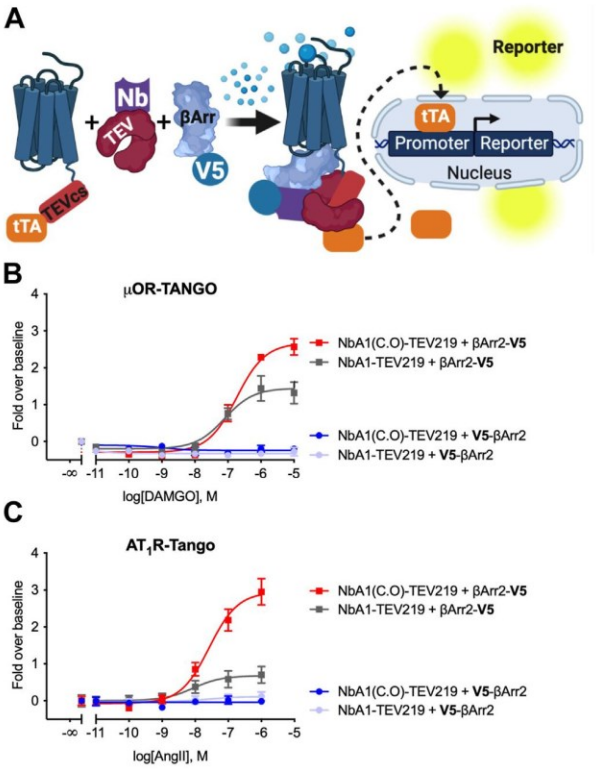

Figure 2. The first generation of the anti-V5 nanobody (NbA1) only recognizes the C-terminal–positioned V5-tag. *A*, schematic of the protease-dependent cell-based assay (TANGO) used to assay the anti-V5 nanobodies. The original NbA1 clone selected from the Y2H screening was fused with the TEV219 protease and cloned into a eukaryotic expression vector. The initial assessment revealed that the nanobody was not well expressed in HEK293 and codon optimization (NbA1(C.O)) increased its expression and consequently its functional activity. The μ-OR-TANGO (*B*) and AT_1R-TANGO (*C*) were cotransfected with β-arrestin2 carrying a C- or N-terminal V5-peptide tag along with either the NbA1-TEV219 or NbA1(C.O)-TEV219 fusion protein the receptor stimulated with dose-response agonists, DAMGO for μ-OR and angiotensin II (AngII) for AT_1R. The original NbA1 clone only recognizes the C-terminally tagged β-arrestin2 (β-arrestin2-V5). Dose-response curves were built using XY analysis for nonlinear regression curve and the 3-parameters dose-response stimulation function from GraphPad Prism. Baseline corrected curves were built using the "Remove baseline and column math" function (Value-Baseline/Baseline). Wells in the absence of ligand were used as the baseline for each condition. All error bars represent SD of three or four technical replicates. Data presented are representative of three biological replicates. μ-OR, mu-opioid receptor; AT1R, angiotensin II receptor type 1; HEK293, human embryonic kidney 293; TEV, tobacco etch virus; Y2H, yeast two-hybrid.

outward but their backbones make water-mediated hydrogen bonds with NbA1. As shown in Figure 3*C*, the interaction is largely mediated by hydrophobic residues, suggesting a strong contribution of entropic forces by the Nb:V5 interfaces (63). Numerous reports have documented the greater paratope diversity of Nbs than the classical Ab VH domain (63), which was exemplified in this study by the distinct recognition mode of NbA1:V5 compared to the NbALFA:ALFA-tag interaction, which involves contacts with all three CDRs and is oriented parallel to the central axis (Fig. S1) of the nanobody. Finally, three residues (Gln57, Gly58, Asp59) within the CDR2 loop are disordered and were unresolved (Figs. 3*A* and S1). The primary coding sequence of NbA1 is shown in Figure 3*D*.

Table 1
Data collection and refinement statistics for NbA1 in complex with the V5 peptide

	NbA1:V5
Data collection	
Space group	P1
Cell dimensions	
a, *b*, *c* (Å)	45.4, 45.4, 70.6
α,β,γ (°)	90.0, 90.0, 97.9
Resolution (Å)	24.59-2.01 (2.08-2.01)[a]
R_{sym} or R_{merge}	0.034 (0.070)
$I/\sigma I$	24.2 (11.6)
Completeness (%)	95.1 (92.1)
Redundancy	2.6 (2.6)
Refinement	
Resolution (Å)	24.59-2.01
No. of reflections	35,510
R_{work}/R_{free}	19.1/23.8
No. of atoms	
Protein (A/B/D/G)	926/936/928/925
V5 (E/C/F/H)	c
Water	288
B-factors (Å^2)	
Protein (E/B/C/D)	30.9/30.8/30.5/30.6
V5	28.0/28.7/29.1/29.0
Water	30.1
R.m.s.ds	
Bond lengths (Å)	0.009
Bond angles (°)	1.136

[a] Values in parentheses are for the highest-resolution shell.

Maturation of the NbA1

A primary objective driving our research was to advance the study of PPIs utilizing a versatile nanobody-based sensor. While NbA1 demonstrates intracellular functionality, it exhibits a marked preference for the C-terminally tagged β-arrestin-2. This partiality can potentially be attributed to the lack of interactions with the last two residues of the V5 tag. To improve the overall affinity, particularly for the N terminus of the V5 tag, *in silico* affinity maturation was performed using the Rosetta modeling software. The generated models were assessed based on their corresponding scores and binding energy metrics, resulting in 10 designed mutants harboring degenerated mutations, which were subsequently synthesized and tested using the Tango assay. Based on the functional evaluation, it was deduced that two mutations (ΔD59 and S60K) resulted in better activity than NbA1, especially for the N-terminal V5-tagged arrestin. Consequently, an optimized nanobody was generated to incorporate only those two mutations, called NbV5. As shown in Figure 3*E*, the maturated NbV5 can recognize both N- or C-terminally tagged β-arrestin-2. In the case of AT1R, no discernible disparity was observed between the two orientations of the tag. However, in the context of μ-OR, a slight reduction in the recognition of β-arrestin-2-V5 was noted; nevertheless, this was compensated by a significant gain of function towards V5-β-arrestin-2 (N-terminal tag) (Fig. 3*E*). Although the precise mode of interaction remains to be elucidated, this optimized NbV5 variant exhibited a notable improvement in its overall behavior within our functional Tango assay, warranting its selection for further development of our nanobody-based biosensors.

Determination of the apparent KD of NbV5 was carried out using yeast surface display in the EBY100 yeast strain. Using the Gap-repair method, NbV5 was cloned in a yeast display

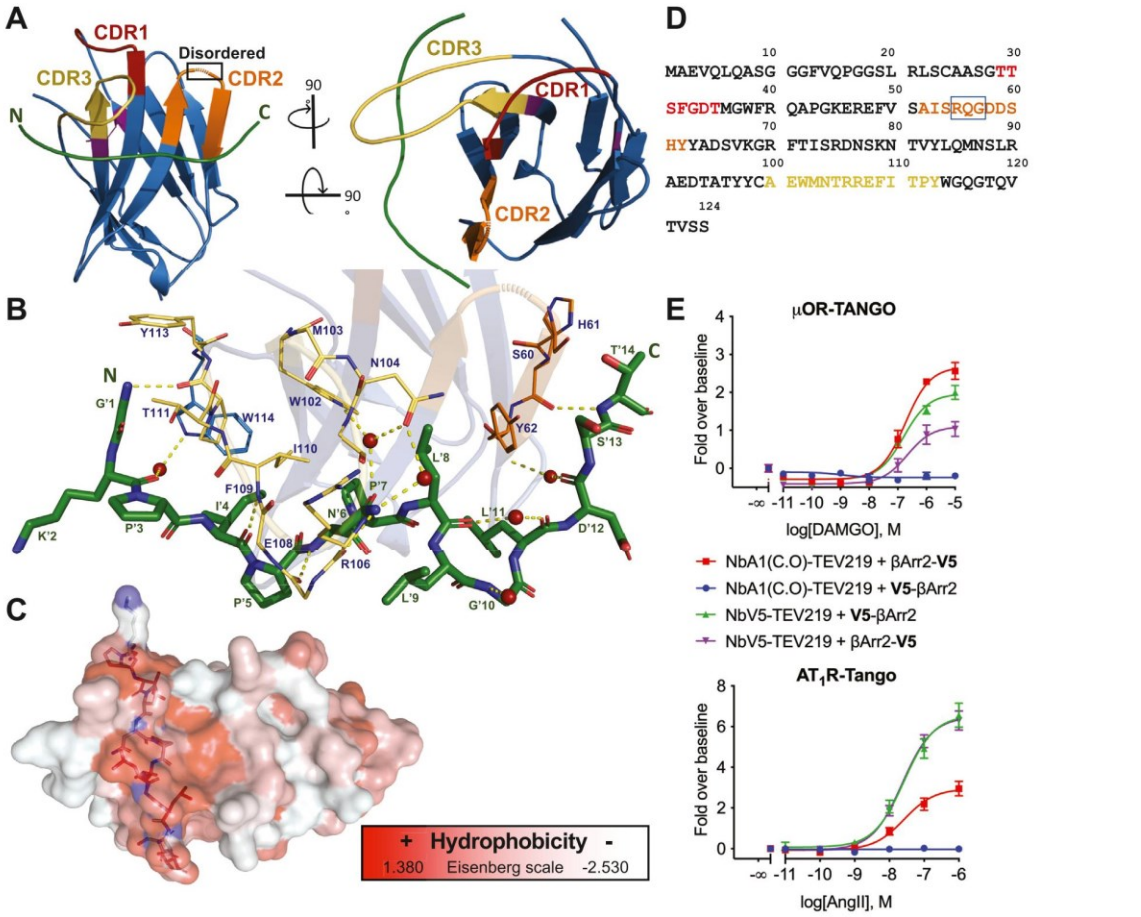

Figure 3. Structure of the NbA1 bound to the V5 peptide. *A*, overview of the NbA1:V5 peptide complex shown as cartoon representation. NbA1 is colored in *blue* with CDRs 1 to 3 colored in *red*, *orange*, and *yellow*, respectively. Three residues from the CDR2 were not resolved in the refined structure. *B*, close-up view of the polar interactions within the complex including water-bridged interaction. The V5-peptide (*green*) is shown as stick representation with the N terminal on the left. Interacting residues from the paratope are labeled in *blue*, while the peptide labels are *green* and marked with a prime symbol. H-bonds are shown as *yellow dashed lines* and water molecules as *red spheres*. *C*, the NbA1:V5 peptide complex shown as surface representation and colored using the color_h script based on the Eisenberg hydrophobicity scale [64]. *D*, sequence of NbA1 with CDRs 1 to 3 colored in *red*, *orange*, and *yellow*, respectively. The square highlights the RQG tripeptide that is disordered in the CDR2 loop. *E*, the μ-OR-TANGO and AT_1R-TANGO were cotransfected with β-arrestin2 carrying a C- or N-terminal V5-peptide tag along with either the NbV5-TEV219 or codon-optimized NbA1(C.O)-TEV219 fusion protein the receptor stimulated with dose-response agonists, DAMGO for μ-OR and angiotensin II (AngII) for AT_1R. The NbV5 recognizes the N- or C-terminally V5-tagged β-arrestin2 with similar logistic parameters (potency and efficacy), while the original NbA1 clone only recognizes the C-terminally tagged β-arrestin2 (β-arrestin2-V5). Dose-response curves were built using XY analysis for nonlinear regression curve and the 3-parameters dose-response stimulation function from GraphPad Prism. Baseline correction was performed using the "Remove baseline and column math" function (Value-Baseline/Baseline). Wells in the absence of ligand were used as the baseline for each condition. All error bars represent SD of three or four technical replicates. Data presented are representative of three biological replicates. μ-OR, mu-opioid receptor; AT1R, angiotensin II receptor type 1; CDR, complementarity-determining region; TEV, tobacco etch virus.

vector (pYD1-Halo) derived from pCTCON2 (64), resulting in the construct NbV5-AGAP2-Halo-myc in N-terminal to C-terminal orientation. Efficient display of the nanobody was verified using flow cytometry (FACS), utilizing Halo-Alexa 488 as the labeling agent (Fig. S2, *A–C*). As for the antigen, we opted for the 1N3R Tau protein isoform (NP_001190180.1) with a V5 insertion between E73 and A74 and labeled with Alexa Fluor 488 succinimidyl ester. This unstructured protein is well-suited for displaying linear epitopes (65), avoiding any bias related to the N-terminal or C-terminal Tag-V5 presentation. Assessment of binding was conducted by FACS, specifically using serial dilutions of labeled Tau-V5 ranging from 500 nM to 0.98 nM. The findings, as presented in Fig. S2*D*, indicated an estimated affinity of 29 nM for NbV5. Nevertheless, it is important to emphasize that *in vitro* affinity measurements may not accurately reflect cellular affinity or activity.

Protein–protein interaction assays

PPIs lie at the core of cellular processes, wherein there is a reciprocal and dynamic interplay between two proteins, often generalized as the "bait" and "prey". In our NbV5:V5 system, the bait represents a membrane receptor from the GPCR

family. Notably, due to the inherent membrane configuration of GPCRs, their fusion is limited to the C-terminal region. Conversely, the prey protein represents any protein of interest tagged with the V5 epitope, which can be positioned at the C terminus, N terminus, or even within the protein sequence itself. As a proof-of-concept, we utilized the well-established GPCR interactors, β-arrestin-1 and β-arrestin-2, as the prey proteins. Within this tripartite system, the NbV5-based biosensor acts as a molecular bridge, reconstituting a functional cell-based assay by orchestrating the interaction between the V5-tagged prey protein and the bait receptor, which carries the complementary functional moiety. Importantly, this setup ensures minimal disruption of the native complex formation and preserves the intrinsic functionality of the prey protein.

The initial characterization of our platform with GPCRs enabled tunable regulation of the interaction dynamics through the utilization of an agonist and, thus, a more precise assessment of biosensor efficiency. Subsequent experiments were conducted using two distinct GPCRs, namely the AT1R and μ-OR, both of which are widely studied receptors in our laboratory and thus would serve well as targets for the characterization of the Nb-V5 biosensors.

NbV5-based protease-dependent reporter assay (Tango)

The first functional assay adapted as a tripartite NbV5:V5 system was the Tango assay. Renowned for its high sensitivity and permissibility, previous efforts have successfully exploited this platform to investigate β-arrestin recruitment at specific GPCRs or to conduct high-throughput screenings of the entire class A GPCR-ome simultaneously (66–68). The Tango assay leverages a modified GPCR, termed Tango-ized GPCR, which carries a transcription factor, tetracycline-controlled transactivator (tTA), fused at its C terminus and preceded by a TEV endopeptidase cleavage site. Upon recruitment of the β-arrestin protein fused with TEV protease (β-arrestin-TEV) to the receptor, the TEV protease cleaves its recognition site, liberating the tTA transcription factor. Subsequently, the translocated tTA engages the nucleus and activates a reporter gene under the control of the tTA-response element. Our study selected an optimized version of the TEV protease, TEV219, which exhibits enhanced efficiency and avoids self-inactivation (69), to improve further the GPCR-TANGO platform's performance (70).

Assessment of the NbV5 biosensors within the Tango assay was conducted using μ-OR and AT1R. Interestingly, a robust dose-response relationship was observed for both β-arrestin-1 and β-arrestin-2, regardless of the position of the V5-tag (Fig. 4, *A* and *B*). It is noteworthy to highlight that the obtained EC50 values were comparable to those obtained from our updated Tango assay featuring a direct fusion of TEV219 at the C terminus of the β-arrestins (Fig. 4*C*). The interassay reproducibility of the Tango assay is presented in Fig. S3*A*, where data from multiple biological replicates were normalized toward the top-performing conditions and pooled. These findings substantiate the suitability and efficacy of our NbV5

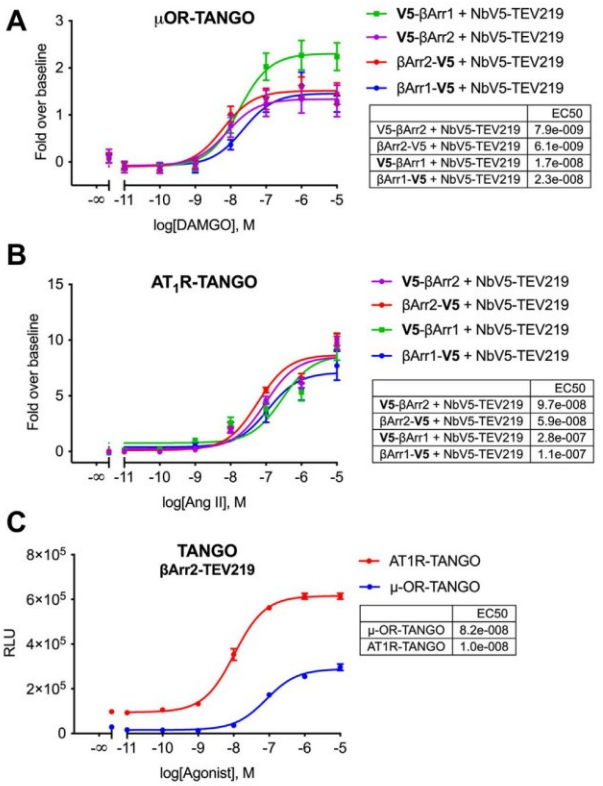

Figure 4. NbV5 as a versatile nanobody-based biosensor: application in protease-dependent cell-based assay (TANGO). The μ-OR-TANGO (*A*) and AT_1R-TANGO (*B*) were cotransfected with β-arrestin1 or β-arrestin2 carrying a C- or N-terminal V5-peptide tag along with the NbV5-TEV219 fusion protein. Dose-response agonist treatments demonstrate the recruitment of β-arrestin in all configurations tested. *C*, the μ-OR-TANGO and AT_1R-TANGO were cotransfected with β-arrestin2-TEV219 and stimulated with agonists showing that EC50 obtained using the original TANGO is similar to the NbV5-adapted TANGO. Dose-response curves were built using XY analysis for nonlinear regression curve and the 3-parameters dose-response stimulation function from GraphPad Prism. Baseline corrected curves were constructed using the "Remove baseline and column math" function (Value-Baseline/Baseline). Wells in the absence of ligand were used as the baseline for each condition. All error bars represent SD of three or four technical replicates. Data presented are representative of three biological replicates. μ-OR, mu-opioid receptor; AT1R, angiotensin II receptor type 1; TEV, tobacco etch virus.

biosensors in conjunction with the TANGO-based assay, further affirming their potential as valuable tools in PPI studies.

NbV5-based BRET

Biophysical techniques involving resonance energy transfer enable monitoring of the formation of dynamic complexes in living cells (71), with their use being well-established and remaining a gold standard in GPCR signaling (8). In the second generation of BRET (BRET2), the receptor is fused at the C terminus with the Renilla Luciferase variant 2 or 8 (RLuc2 or 8) (72), while the nanobody is fused at either N terminus or C terminus with the GFP2 acceptor (Fig. 5*A*) (73, 74). The underlying principle involves the generation of a resonance energy transfer signal when there is sufficient spectral overlap

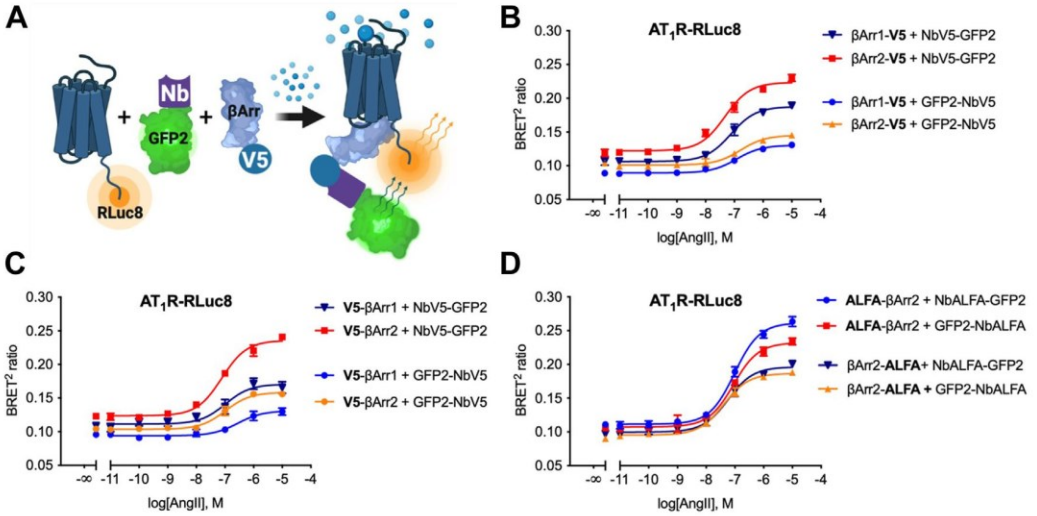

Figure 5. NbV5 as a versatile nanobody-based biosensor: application in *B*ioluminescence *R*esonance *E*nergy *T*ransfer (BRET^2). *A*, schematic of the BRET^2 cell-based assay used to evaluate the NbV5. The recruitment of the β-arrestin–NbV5-GFP2 complex to the receptor fused to RLuc8 allows the energy transfer between the *Renilla reniformis* Luciferase mutant (RLuc8) and the GFP mutant GFP2 in the presence of the RLuc8 substrate Coelenterazine 400a. *B* and *C*, NbV5-based detection of β-arrestin1 and β-arrestin2 recruitment at the AT$_1$R-RLuc8. N- and C-terminally V5-tagged β-arrestins were tested as well as both N- and C-terminally GFP2-tagged NbV5. Dose-response curve treatment with angiotensin II reveals equivalent recruitment of β-arrestin1 and 2 at the AT$_1$R. *D*, similar results were obtained with the nanobody that recognizes the synthetic ALFA-tag (NbALFA). Dose-response curves were built using XY analysis for nonlinear regression curve and the 3-parameters dose-response stimulation function. All error bars represent SD of three biological replicates with two technical replicates (n = 6). AT1R, angiotensin II receptor type 1.

between the acceptor and donor molecules in close proximity, leading to dipole-dipole coupling. Importantly, the extended working distance range afforded by the BRET2 system enables the study of larger protein systems, including GPCR-protein interactor assemblies.

In a manner analogous to the adaptation of the TANGO system, various configurations involving β-arrestin-1 and β-arrestin-2 fused at the N terminus or C terminus with the V5-tag were assessed, alongside the reference ALFA-tag, which served as a benchmark due to the well-characterized performance of the corresponding NbALFA intrabody with different tag placements (N-term, C-term, and internal). As depicted in Figure 5, *B–D*, all configurations exhibited a robust signal; however, it was observed that the C-terminally tagged NbV5 (NbV5-GFP2) yielded a superior BRET2 ratio, while the impact on NbALFA was comparatively less pronounced. One possibility behind this intriguing observation could be explained by the distinct binding orientation of NbALFA, which is oriented at a 90-degree angle relative to NbV5, as illustrated in Fig. S1. Notably, the tag placement within the prey protein did not substantially influence the receptor-β-arrestin coupling under investigation. For the AT1R receptor specifically, both isoforms of β-arrestin were well recruited, with a slight preference observed for β-arrestin-2 within this particular assay. However, it is worth highlighting that we failed to detect a significant β-arrestin BRET signal at the μ-OR receptor, even in the presence of GRK2. While BRET has frequently been employed to quantify β-arrestin2 recruitment at the μ-OR receptor, it is noteworthy that the BRET ratio is always weaker than other GPCRs, including the closely related kappa opioid receptor, which worked in our Nb-V5–adapted BRET assay. The reasons underlying the ineffectiveness of the μ-OR receptor in this assay remain unclear; however, we speculate that the overall conformation of the μ-OR receptor may not be conducive to efficient resonance energy transfer. Notwithstanding this observation, we successfully detected β-arrestin recruitment utilizing the other two assays presented in this study. Consequently, our NbV5-based biosensors demonstrate substantial promise for implementation in BRET assays, but adding a tripartite constituent might not be favorable to efficient resonance energy transfer with specific pairs.

NbV5-based NanoBiT

The NanoBiT assay represents a versatile structural complementation reporter system, harnessing the unique properties of a LgBiT (18 kDa) subunit and its corresponding Small BiT (SmBiT; 11 amino acids) peptide, specifically engineered to exhibit a low affinity for LgBiT. When these two proteins interact, the subunits assemble into an active enzyme which, in the presence of its substrate, furimazine, produces a luminescent signal in living cells, enabling real-time kinetic measurements of protein interaction dynamics (75). In the context of GPCRs, it is conventionally advantageous to fuse the SmBiT peptide to the C terminus of the receptor, likely minimizing perturbations to the receptor's native state or ligand-induced complexes.

As depicted in Figure 6, various configurations of β-arrestin fusions (V5-β-arrestin and β-arrestin-V5) and nanobody fusions (Nbs-LgBiT and LgBiT-Nbs) were compared to evaluate their respective functional performances. In contrast to the

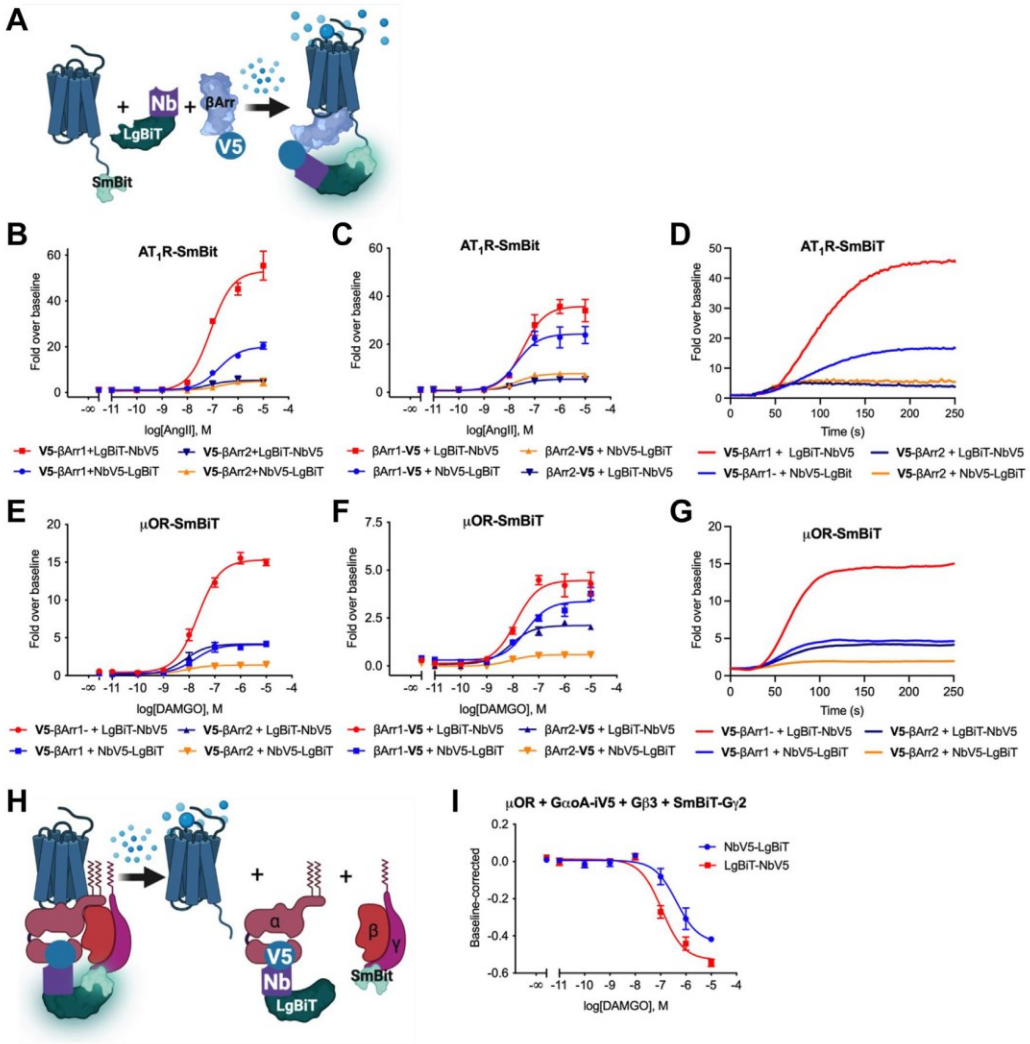

Figure 6. NbV5 as a versatile nanobody-based biosensor: application in *Nano*luciferase *Bi*nary *T*echnology. *A*, schematic of the NanoBiT cell-based assay used to evaluate the NbV5. NbV5-based detection of β-arrestin1 and β-arrestin2 recruitment at the AT_1R-SmBiT (*B–D*) and μ-OR-SmBiT (*E–G*) was assayed. N- and C-terminally V5-tagged β-arrestin was tested as well as both N- and C-terminally LgBiT-tagged NbV5. *D* and *G*, live kinetic trace at 1 μM agonist are shown in (*D*) for the AT1R and (*G*) for the μ-OR. The trace represents the mean of a quadruplicate experiment. *H*, schematic of the NanoBiT cell-based assay used to assess the internal V5-tag. *I*, functional recognition of an internal localized V5-tag was also assayed by NanoBiT by incorporating the V5-tag at position 92 of the GαoA (GαoA-iV5) and measuring the dissociation from the Gβ3 and SmBiT-Gγ2 dimer upon μ-OR activation with DAMGO. *B*, *C*, *E*, *F*, and *I*, dose-response curves were built using XY analysis for nonlinear regression curve and the 3-parameters dose-response stimulation function from GraphPad Prism. Baseline correction was performed using the "Remove baseline and column math" function, calculated as Value-Baseline/Baseline (*B–G*) or Value-Baseline (*I*). Wells in the absence of ligand were used as the baseline for each condition. All error bars represent SD of three or four technical replicates. Data presented are representative of three biological replicates. μ-OR, mu-opioid receptor; AT1R, angiotensin II receptor type 1; LgBiT, Large BiT; NanoBiT, Nanoluciferase Binary Technology; SmBiT, Small BiT.

BRET2 experiment (Fig. 5), LgBiT-NbV5 produced a superior response than NbV5-LgBiT, underscoring the importance of evaluating both orientations to achieve optimal response and sensitivity. Interestingly, the NanoBiT assay revealed a pronounced preference for β-arrestin-1 over β-arrestin-2 at the AT1 receptor, a trend also observed with the ALFA-tag system, thereby confirming that the choice of tag system does not significantly influence the outcomes (Fig. S2*A*). To detect reasonable recruitment at the μ-OR receptor, the co-expression of GPCR kinase 2 (GRK2) is often necessary, particularly considering its absence at endogenous levels in human embryonic kidney 293 (HEK293) cells (76). As shown in Figure 6, *E* and *F*, β-arrestin-1 was favored over β-arrestin-2 at the μ-OR receptor, with the N-terminally V5-tagged β-arrestins and N-terminal LgBiT-NbV5 identified as the optimal orientations for tripartite interaction at this receptor. Fig. S3*B* displays the interassay reproducibility of the NanoBiT assay, wherein data from various biological replicates were normalized relative to the most optimal conditions and then pooled.

The NanoBiT assay offers notable advantages, particularly its suitability and ease for performing live experiments. While it can be employed for endpoint assays on a microplate reader, using an appropriate real-time kinetic reader, such as the Fluorescent Imaging Plate Reader-TETRA, can reveal additional information in live settings. This aspect holds particular relevance for GPCRs, as it is often assumed that all interactions occur under equilibrium conditions, despite it being well-established that the interactions are transitory in nature, especially in the case of heterotrimeric G proteins (77). Thus, to study GPCR signaling under nonequilibrium conditions, kinetic experiments and appropriate models should be favored (78). In light of this, we present a live kinetics experiment in Figure 6, *D* and *G*, wherein the recruitment of V5-tagged β-arrestin at the μ-OR and AT1R receptors is examined at a single concentration of 1 μM selective agonist.

The ability of NbV5 to recognize an internally positioned V5-tag was also evaluated, specifically using the inhibitory G protein GαoA with the V5-tag inserted at position 92. It is well established that inhibitory G proteins tolerate such insertions, commonly employed for the introduction of fluorescent proteins or RLuc8 for BRET experiments. Figure 6*H* illustrates the employed approach, where SmBiT was fused at the N terminus of the Gγ2 subunit and co-expressed with Gβ3, thereby facilitating the assembly of the obligatory Gβγ dimer that interacts with the inactive GDP-bound GαoA. Upon activation by the Gαi/o-coupled μ-OR receptor, G protein activation can be detected through the dissociation of the heterotrimer. As depicted in Figure 6*I*, activation of the μ-OR receptor by its agonist, DAMGO, induces the dissociation of the trimer, which can be monitored using NbV5 fused with LgBiT at the N terminus or C terminus. Hence, our Nb-based sensor enables the measurement of G protein activation through the internal insertion of the V5 sequence, thereby minimizing the potential impact on overall G protein regulation. Furthermore, based on previous experiments conducted in our laboratory, it has been determined that NanoBiT complementary subunits are not well-tolerated when placed internally, further reinforcing the advantage of utilizing the NbV5:V5 tag system.

With regard to epitope tags, these incorporations are highly favorable as they avoid the need to generate custom antibodies for each protein of interest and allow orthogonal peptide tags to be multiplexed within the same experiment (11, 13); thus, the selectivity of the nanobody toward its target peptide tag is of paramount importance. As demonstrated in Fig. S4*B*, NbV5 exhibits remarkable specificity for the V5 epitope while displaying no detectable activity towards the ALFA-tag. This finding underscores the potential for simultaneous utilization of both tags broadening the experimental possibilities of our nanobody-based framework. To illustrate the application for a multiplexing experiment, the C-terminally V5-tagged AT1R was used to bridge the NbV5 carrying the SmBiT to the LgBiT-tagged NbALFA, detecting the recruitment of ALFA-tagged β-arrestin1. All combinations were permissive, but the SmBiT-NbV5 resulted in the best fold-over baseline compared to NbV5-SmBiT. Interestingly, while the fold-over baseline was substantially reduced, a gain into EC50 was observed from ∼10 nM to ∼1 nM (Fig. S4*A* vs. Fig. S4*C*). We do not have a definitive explanation for the observed increase, as the SmBiT-tag (11 aa) is approximatively the same size as the V5-tag (14 aa). However, the higher affinity of both Nbs for their respective tags compared to SmBiT–LgBit interaction could account for this gain or alternatively, it could be attributed to a more favorable spatial orientation of the complex. Together, Fig. S2, *B* and *C* strongly support the selectivity of each tag system and their application for multiplexing configurations.

Nbs as fluorescence trackers for microscopy

To explore the potential application of NbV5 as a genetically encoded tracker, we conducted experiments involving the co-expression of γ-actin tagged with a V5 epitope at its C terminus (γ-actin-V5) along with NbV5 fused with the constitutive fluorescent protein eGFP. As shown in Figure 7, the NbV5-eGFP fusion protein diffuses within the cell when expressed with the control pcDNA3.1 but selectively associates with γ-actin-V5 in its presence. Importantly, discernable actin-related structures like stress fibers and lamellipodia can be observed, indicating that the NbV5-eGFP (green) could efficiently interact with a dynamic protein such as γ-actin without interfering with its natural localization. The selectivity of the interaction is shown by the colocalization (yellow) between γ-actin-V5:NbV5-eGFP staining (green) and direct staining using the phalloidin-568 (red), which is a high-affinity F-actin probe. While the phalloidin selectively stains the actin filaments (F-actin), the γ-actin-V5:NbV5-eGFP also stains the globular actin (G-actin). Therefore, NbV5-based biosensors could be used to track protein remodeling or trafficking in a live cell-based experiment.

Discussion

Existing biotechnological methodologies used for the characterization and validation of putative drug targets and as the elucidation of physiological and pathophysiological cellular processes necessitate a wealth of information pertaining to the abundance, localization, and dynamic interactions of cellular constituents (79). Consequently, the development of intracellular traceable proteins for both endpoint investigations and real-time kinetics diagnostics assumes paramount significance, particularly in light of increasing efforts to acquire a more comprehensive understanding of cellular PPIs and thus extending the applicability of such intracellular tracers to encompass a genome-wide even to an organism (-omics-) scale.

In this study, we contribute to this endeavor by developing and characterizing a V5-tag–targeted nanobody named NbV5 alongside a suite of NbV5-based intracellular biosensors with multipurpose functionalities. The premise of our approach was to avoid the fusion of a large, functionalized tag to a protein while taking advantage the vast repertoire of C-terminally V5-tagged genome-wide open source ORFs. The V5 epitope, an established and widely employed peptide tag for over 3 decades, assumes a pivotal role in our investigation. This 14-mer peptide is devoid of net charge under physiological pH

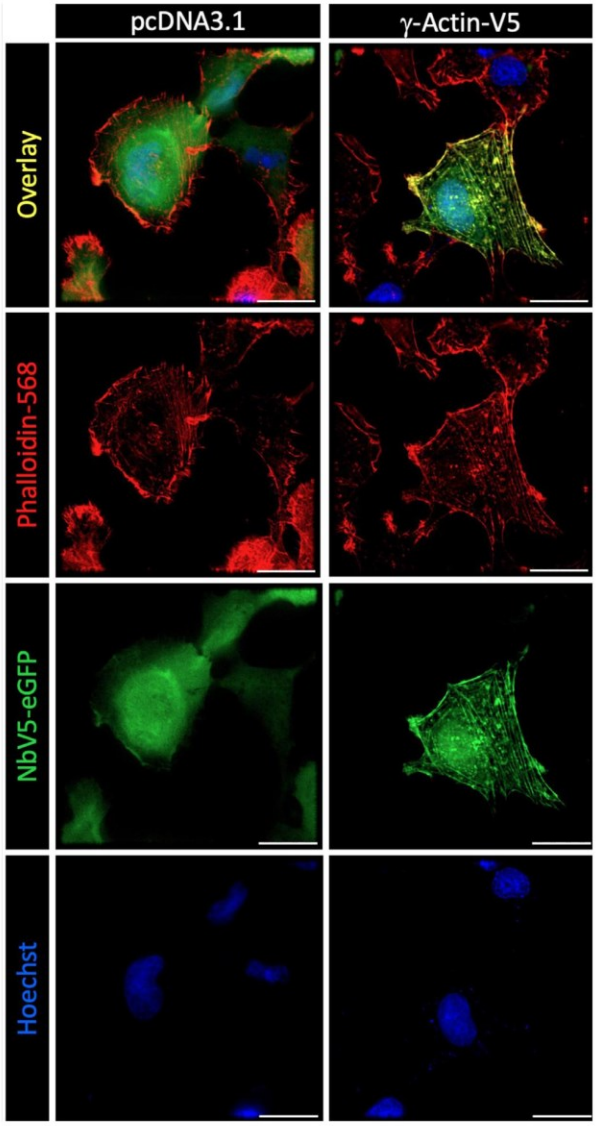

Figure 7. NbV5-based detection of V5-tagged proteins by cell imaging. Fluorescence imaging of HT1080 cells expressing NbV5-eGFP and γ-Actin-V5 or pcDNA3.1+ as a negative control. In the absence of γ-Actin-V5, NbV5-eGFP (*green*) is diffused throughout the cell, while in the presence of γ-Actin-V5, NbV5-eGFP is enriched in actin-rich protrusions and structures. Cells were costained with the F-actin probe Alexa Fluor 568 phalloidin (*red*) and the blue DNA stain Hoechst. The overlay is shown on the *top panel*. Images are representative of 25 cells from three independent experiments. Scale bars represent 25 μm.

conditions and does not have any predicted secondary structures, albeit featuring quite an ordered core owing to the presence of three proline residues. The inherent rigidity is posited to reduce the multidimensional complexity of the conformational landscape, thereby mitigating the impact of environmentally induced secondary structures and conferring stability in solution (80).

Multiple peptide tags have emerged, each bearing its own set of advantages and disadvantages, yet few tags have corresponding functional intrabodies that are thoroughly characterized, as done in this study. While it is worth noting the exceptions of the NbALFA:ALFA-tag (51) and Moon-tag (46, 47), it is crucial to highlight that neither of these were thoroughly characterized for PPI studies as showcased herein with the NbV5; nonetheless, the availability of these tag systems could capitalize on through simultaneous multiplexing implementations in conjunction with the NbV5:V5. Unique to the V5-tag is the associated commercially available V5-tagged genome-wide ORF library, thereby paving the way for the prospect of large-scale PPI investigations. Furthermore, it must be underscored that among the numerous available nanobody structures, only a handful involve those complexed with linear peptide tags, namely ALFA (PDB: 6I2G), BC2 (PDB: 5IVO), and the V5 tag (reported herein). One avenue for future investigation is evaluating whether advanced protein modeling programs, such as Alphafold2, Alphafold Multimer, or IgFold, can provide accurate predictions of nanobody-peptide tag structures (81), which would help inform the development of novel optimize future nanobody scaffolds with an increased propensity for intracellular stability. Recently, Dingus *et al.* have developed a general consensus framework derived from the most highly conserved positional residues across a large group of intracellularly stable Nbs, which would also be a valuable asset for increasing the intracellular stability of Nbs through targeted mutagenesis without compromising target binding (15).

The majority of Nbs available to date have been developed by animal immunization, but the utilization of synthetic *in vitro* platforms, as exemplified in our study, holds immense promise. The Hybribody methodology employed combines peptide phage display and intracellular Y2H techniques, as well as the selection of Nbs wherein the folding of the paratope is independent of disulfide bonds, thus significantly enhancing the enrichment and identification of viable intrabodies (60, 82). This screening approach isolated a cohort of prospective Nbs, among which clone NbA1 emerged as the preeminent candidate as an intrabody. Initial investigations unveiled a low expression level for all Nbs, circumvented through codon optimization tailored for a human expression system. Subsequent characterization in the Tango assay revealed that NbA1 exhibited suboptimal recognition of the N-terminally positioned V5-tag on β-arrestin2. To address this limitation, we sought to resolve its crystal structure, which would provide insight into the binding interface of NbA1:V5 tag. Consequently, NbA1 was purified from the periplasm of SHuffle bacteria, which are best suited for the purification of proteins containing disulfide bonds (83), and the purified NbA1 was then cocrystallized with the V5-tag. The resultant crystal structure served as the foundation for computer-aided maturation, aimed at refining the functionality of the nanobody. The maturation process was confined to the three CDRs, with no discernible mutants predicted to induce significant changes in binding energy. Based on the mutants tested in Tango experiments, it was determined that two specific mutations conferred improved recognition of the V5-tag. The key distinguishing feature of NbV5 vis-à-vis NbA1 lies in its interaction with the N-terminally situated V5-tag, as shown in

Figure 3*E*. Given that these two key mutations, ΔD59 and S60K, are juxtaposed within a disordered loop in CDR2 (Fig. S1), the deletion of a single residue is postulated to confer stability to this region, while Lys60 establishes direct contacts with the CDR2 loop, thereby further stabilizing this region (Fig. S1, *B* and *C*). While it is generally accepted that CDR3 is the most critical region for antigen recognition and binding due to its longer length and higher variability, several reports and as demonstrated herein demonstrate that mutations in CDR1 or CDR2 may optimize affinity or stability, particularly if these regions are directly involved in the paratope interaction (84). Thus, comprehensive optimization strategies should involve exploring mutations in all three CDRs to assess their combined impact on nanobody performance.

Having delineated the general mode of interaction between the nanobody and V5-tag, we proceeded to construct NbV5-based biosensors for versatile applications in the most widely used cellular PPI assays, namely Tango, BRET, and NanoBit assays. As shown herein, our biosensors probed the recruitment of both β-arrestin-1 and β-arrestin-2 at two well-characterized GPCRs, the μ-OR, and the AT1R. The μ-OR serves as the primary target for the most prescribed analgesics such as morphine and fentanyl (85). As for AT1R, this receptor is important for controlling vasocontraction, with AT1R antagonists (ARBs) being prescribed for the treatment of hypertension, congestive heart failure, and diabetic nephropathy (86). Although both receptors are known to engage both β-arrestin isoforms, there exists conflicting data regarding isoform selectivity and, more importantly, the intrinsic drug efficacy. As the measurement of the direct interaction between the receptor and its effector is a key aspect for accurately determining intrinsic drug efficacy (87), the use of smaller tags should mitigate some distortions caused by larger functional tags. With regard to GPCRs, the fusion of a large moiety to its C terminus may introduce artifacts that lead to impaired signaling, altered ligand binding, mislocalization and affect trafficking, and changes to their stability and expression levels, likely due to steric hindrance or altered receptor conformation caused by the GFP fusion (88). Therefore, tag systems such as V5 would enable a more faithful characterization of receptor–effector interactions.

This work's adaptation of common cellular-based PPI assays involved the integration of NbV5-based biosensors, commencing with the TEV-dependent reporter assay (Tango), given its permissibility and sensitivity. Subsequently, our efforts extended to the adaptation of two widely employed PPI assays, namely BRET and NanoBiT. Intriguingly, a discrepancy between BRET and NanoBiT assays surfaced when investigating the selective recruitment of β-arrestin isoforms at the AT1R receptor, with a distinct preference for β-arrestin-1 over β-arrestin-2 observed solely in the NanoBiT assay, while BRET2 and TANGO assays yielded no such disparity. The underlying reasons behind this observation remain unknown. Still, it is plausible to consider that the size and orientation of the tag may exert differential influences contingent upon the assay employed. In essence, these effects could manifest as alterations in the kinetics of PPIs or literal steric hindrance during complex formation. Another layer of complexity emerges from the intrinsic principles governing each assay: BRET, being highly conformationally dependent, necessitates optimal distance and spatial orientation for effective dipole-dipole coupling to facilitate efficient resonance energy transfer (89). One plausible explanation is that the measured BRET2 signal represents an average of recruitment and conformational changes (multistates). Conversely, in binary complementation assays like NanoBiT, the two complementary fragments must assume a favorable spatial arrangement to facilitate complex formation. Moreover, binary complementation assays solely capture newly recruited β-arrestin or a single conformational state of the complex, precluding the monitoring of spatial rearrangements (90). In the case of Tango, the prolonged stimulation and slower kinetics, due to the inherent proteolytic activity of TEV (69), might mitigate any detrimental kinetic effects stemming from tag size or orientation, albeit steric hindrance remains a pertinent consideration. While the implementation of a tag system has the potential to alleviate the impact of steric hindrance or particular arrangements of interacting partners during complex formation, the tag system itself may influence the sensitivity of the assay under specific circumstances. This phenomenon was evidenced within our system, as NbV5 failed to detect arrestin recruitment to the μ-OR in the BRET2 assay while performing well for AT1R. It should also be noted that during the optimization process, diverse sizes of flexible linkers (ranging from 5 to 70 amino acids) were explored to ensure the optimal distance between functional moieties (91); however, varying linker size did not improve the lack of detected at μ-OR. While a modest effect on the observed activity was noted at AT1R, the small (GGGGS)2× fusion linker was ultimately chosen as the optimal peptide for the NbV5-based biosensors.

While the current work primarily focused on utilizing GPCRs as a means to characterize the NbV5-based system, future efforts will be consecrated to expanding the applicability of the NbV5:V5 system to a broad range of PPIs, such as other membrane receptor–protein and protein–protein interactions. Thus, the authors hope that the versatility and adaptability of the NbV5:V5 platform will contribute to probing and unraveling the intricate dynamics of various interaction networks.

Conclusion

Herein, we engineered a novel nanobody that recognizes the V5-tag epitope, a widely employed peptide tag in many expression vectors, including the MISSION TRC3 human genome-wide ORF library. Said nanobody was selected and maturated to optimize its functionality in the intracellular environment, culminating in the development of NbV5. Our NbV5 intrabody offers a broad range of applications, including biosensors in cellular-based PPI assays, such as NanoBiT, Tango, and BRET^2, and for microscopic imaging purposes. Moreover, the potential of NbV5 extends beyond its current scope and can be further expanded to adapt other existing PPI assays. In summary, NbV5 represents a unique tool that offers traceability of intracellular binding proteins with minimal disturbance to the native cellular milieu.

Experimental procedures

Cell culture

HEK293T and HT1080 cells were obtained from the American Type Culture Collection and maintained in Dulbecco's modified Eagle's medium (DMEM) supplemented with 5% fetal bovine serum (FBS) (Thermo Fisher Scientific), 5% bovine calf serum (Thermo Fisher Scientific), and 1× Pen-Strep (100 U/ml penicillin and 100 μg/ml streptomycin) (Thermo Fisher Scientific). HEK293T cells stably expressing μ-OR-SmBiT (μ-OR-SmBiT/HEK293T) were generated by transduction with lentivirus particles, which had been produced in HEK293T cells by transiently cotransfecting the lentiviral packaging plasmid psPAX2 (Addgene #12260), a lentiviral vector encoding μ-OR-SmBiT (pLenti-Blast Addgene #17451), and the envelope plasmid pCMV-VSV-G (gift from Marceline Côté) at a 1:1:1 ratio using PEI transfection reagent. The following day, media was changed, and the supernatant was harvested at 48h posttransfection. Cells were then transduced with lentivirus in standard growth media containing 5 μg/ml polybrene and the next day, selected with blasticidin at 5 μg/ml. All cells were cultured at 37 °C in a humidified atmosphere containing 5% CO_2.

Plasmids and cloning

All plasmid DNA used in this publication were fully sequenced and are available upon request or through Addgene repository (https://www.addgene.org/Patrick_Giguere/). Plasmid encoding ɣ-Actin-V5 was extracted from the MISSION TRC3 Human LentiORF Puromycin library (MilliporeSigma). V5-βArrestin1, V5-βArrestin2, βArrestin1-V5, βArrestin2-V5, βArrestin2-ALFA, ALFA-βArrestin2, βArrestin1-ALFA, and ALFA-βArrestin1 were amplified by PCR, including the V5 tag within the primer, and subsequently cloned into pcDNA3.1$^+$ at the HindIII-XbaI restriction sites. GαoA with internal V5-tag at position 92 was synthesized by IDT (Integrated DNA Technologies) and cloned at HindIII-XbaI sites in pcDNA3.1$^+$. BRET^2 constructs: AT_1R-RLuc8, μ-OR-RLuc8, NbV5-GFP2, GFP2-NbV5, βArrestin2-GFP2, βArrestin2-ALFA-GFP2 were amplified by PCR and cloned in pcDNA3.1$^+$ using NEB HiFi DNA Assembly (New England Biolabs). Gβ3 and Gɣ2-GFP2 were generously gifted by Dr Asuka Inoue (TOHOKU University). NanoBiT constructs: μ-OR-SmBiT and AT_1R-SmBiT were amplified by PCR by including the SmBiT tag within the primer preceded by a $(GGGGS)_{2x}$ linker. NbV5-LgBiT, LgBiT-NbV5, NbALFA-LgBiT, and LgBiT-NbALFA were amplified by PCR and cloned in pcDNA3.1$^+$ using NEB HiFi DNA Assembly (New England Biolabs). Gɣ2-SmBiT was generously gifted by Dr Asuka Inoue (TOHOKU University). TANGO constructs: μ-OR-TANGO and AT_1R-TANGO are from the original PRESTO-TANGO library (29–31). Aforementioned Nbs fused to the TEV219 were cloned by PCR at restriction sites HindIII-BamHI in pcDNA3.1$^+$-X-TEV219 vector. NbV5-eGFP was generated by PCR amplification of NbV5 and cloned into pEGFP-N1 (Clontech) at the HindIII-BamHI sites.

Nanobody development

To identify Nbs that bind to a linear target and that could be expressed from inside the cell (as intrabodies), phage display selection was conducted with the Nali-H1 synthetic library (57), by Hybrigenics Services (Paris, France), using a His-Halo protein fused with three successive V5-tags (Halo-3xV5). The naïve library was first depleted using another antigen fused in the same Halo vector and selected on magnetic streptavidin beads with the biotinylated Halo-3xV5. With the first round presenting a complexity of 3×10^6 colonies, the DNA extracted from the first round were used to construct a Y2H prey library by PCR and Gap repair. The VHH selected after one round of phage display against V5 tag-biotin were cloned into the pP9 yeast prey vector, which is derived from the original pGADGH plasmid; the library had 2.6×10^5 independent clones in yeast. A single V5 tag, as well as two tandem V5 tags, were cloned into pB27 as a C-terminal fusion to LexA (LexA-V5); pB27 is derived from the original pBTM116 plasmid (92). The constructs were verified by sequencing the insert and used as baits to screen the V5-specific VHH library. For the screen, clones were vetted using a mating approach with YHGX13 (Y187 ade2-101:loxP-kanMX-loxP, matα) and L40ΔGal4 (mata) yeast strains as previously described (59). Moreover, the library has been screened at saturation by cell-to-cell mating (59). A total of 264 His+ colonies were selected on a medium lacking tryptophan, leucine, and histidine supplemented with 0.5 mM 3-AT, obtaining 52 different VHH with redundancies from 1 to 37.

Protein purification

The NbA1 was cloned into the expression vector pET26b (+) (Novagen) at NcoI-XhoI restriction sites to generate the pelB leader-NbA1-His_6 construct. The plasmid was transformed in SHuffle T7 Competent *Escherichia coli* (New England BioLabs), and the NbA1 was subsequently purified from the periplasm of SHuffle T7 cells. Bacteria were then grown at 30 °C in Terrific Broth and, after reaching an A600 of ∼0.6 to 0.8, were induced with 1 mM IPTG (Thermo Fisher Scientific) at 25 °C for approximately 16 h. Bacteria were then pelleted and resuspended in a solution of lysis buffer (0.5 M sucrose, 0.2 M Tris pH 8, 0.5 mM EDTA) and water at a ratio of 1:2 to create an osmotic shock. The lysate was then frozen and thawed for more efficient purification. Following, the mixture was stirred for 45 min at 4 °C and brought to a concentration of 150 mM NaCl, 2 mM $MgCl_2$, and 20 mM imidazole and centrifuged at 20,000*g* for 30 min at 4 °C. The supernatant was then filtered through a 0.22 μm filter. After filtration, the supernatant was added to a gravity column containing 4 ml of Ni-NTA (Qiagen). Beads were washed with a high salt buffer (20 mM Hepes pH 7.5, 500 mM NaCl, 20 mM imidazole) and washed three times with low salt buffer (20 mM Hepes pH 7.5, 100 mM NaCl, 20 mM imidazole). The Nbs were then eluted (20 mM Hepes pH 7.5, 100 mM NaCl, 400 mM imidazole) and dialyzed into physiological buffer solution (10 mM Hepes pH 7.4, 140 mM KCl, 10 mM NaCl) and purified using fast protein liquid chromatography (AKTA GE) on an S75 prep size-exclusion column.

Crystallization, data collection, and structure determination

Purified NbA1 (30 mg/ml) was incubated with the V5 peptide in a 1:3 ratio (protein: peptide). The protein complex was crystallized *via* the sitting drop vapor diffusion method at 4 °C with a mother liquor composed of Bis-Tris pH 6.5, 19% (w/v) PEG 3350, and 20% (v/v) ethylene glycol. The crystals were flash-frozen in liquid nitrogen, and a full data set was collected using a Rigaku MicroMax-007HF equipped with a copper anode. Images were collected using an R-Axis IV++ detector (Rigaku) and processed using Structure Studio (Rigaku). The structure was solved by molecular replacement using the structure of NbALFA (PDB 6I2G) as search model and Phaser (50). Following several rounds of NbA1 building and refinement using COOT and Phenix, respectively, V5 was built in the positive Fourier map. The model was completed by adding the molecules and truncating side chains for which no electronic density could be observed. Ramachandran statistics: Nonglycine Ramachandran outliers; 0%, Nonglycine Ramachandran favored; 100%, Molprobity score: 1.65. Statistics of data collection and refinement are summarized in Table1. All structural figures were prepared in PyMOL.

Nanobody maturation

To optimize the NbA1 sequence and potentially increase the affinity of the antibody towards V5, Rosetta single-state design protocol was performed using the Rosetta Software Suite on the crystal structure of the NbA1 complex. The structure of NbA1 was prepared for antibody affinity maturation for Rosetta by manually editing the PDB file in PyMOL. PyMOL command prompts were used to delete the unwanted water molecules and all nonessential ligands and chains. An extra processing step was also performed to remove any protein atoms that are not involved in the antibody-antigen interface; chains were also renamed and reordered to help differentiate the antibody residues from the antigen residues. Next, a resfile (python script) was generated to identify the residues that were within a distance of specified residues that define the NbA1 protein interface. The side chain conformations were optimized using the repacking and relaxing feature in Rosetta protein design, which was performed to minimize backbone phi-phi angles to relieve small clashes between side chains. The relaxed model was then used to generate 10 designed models through RosettaScripts XML file, which contains a design protocol that uses a single round of fixed backbone design. As a control, the same protocol was repeated to generate 10 control models without designing any residues. These control models were generated to compare the scores and the binding energies of the designed models to the native sequence during the analysis stage. The designed sequences were then analyzed by looking at the score, binding energy, and the binding density of the models. The analysis of the metrics was plotted using RosettaScripts which plots the score and the binding energy of the designed models against the control models. Subsequently, specific mutations were identified that resulted in the improvement of the NbA1 complex based on corresponding findings from functional assay experiments (as shown in Fig. 1). Finally, a sequence logo was generated from the designed models in order to determine which mutations were made and their frequencies.

$BRET^2$ assay

HEK293T cells were plated in 6-well plates at 1.2×10^6 cells and subsequently transfected using the PEI precipitation method with $BRET^2$ constructs at a total of 3 μg of DNA per well. Transfected cells were detached and seeded on poly-L-lysine (PLL)-coated white 96-well assay plates (Thermo Fisher Scientific). The following day, spent medium was removed and replaced with 60 μl of 1× Hanks' balanced salt solution (HBSS) buffer, followed by the addition of 10 μl of Coelenterazine 400a (NanoLight Technologies) at 50 μM to each well, for a final concentration of 5 μM. After incubating the plates away from light for 8 min, 30 μl of serial dilutions of agonists at 3× concentration was added. Plates were subsequently read 4 times after 2 min, 10 min, 20 min, and 30 min using the Hidex Sense Beta Plus microplate reader (Gamble Technologies) with 405 nm (RLuc8-Coelenterazine 400a) and 500 nm (GFP2) emission filters, at 1 s/well integration times. Figures shown in the manuscript account for the reads after 20-min incubations with agonist (and correspondingly, approximately 30-min incubations with Coelenterazine 400a). Data were extracted using the integrated software and subjected to nonlinear least-squares regression analysis using the sigmoidal dose-response function provided in GraphPad Prism 9.0 (www.graphpad.com). Data of three independent experiments (N = 3) performed in quadruplicate are presented as $BRET^2$ ratio (acceptor/donor) as indicated in figure legends.

NanoBiT assay

μ-OR-SmBiT/HEK293T and HEK293T cells were plated in 6-well plates at 1.2×10^6 cells and then transfected using the PEI precipitation method with the NanoBiT constructs the next day at a total of 3 μg of DNA per well. Transfected cells were detached and seeded on PLL-coated white 384-well assay plates (Thermo Fisher Scientific) in starvation media (DMEM, 1% FBS, 1× Pen-Strep), The next day, media was removed and replaced with 20 μl of 1× HBSS buffer containing 5 μM furimazine and incubated for a total of 10 min at room temperature before reading on Fluorescent Imaging Plate Reader Tetra system (Molecular Devices). Baseline measurements were initially read before drugs were added into their respective wells (concentration and different drugs in Figure legends). The subsequent changes in relative luminescence signals (relative luminescence unit, RLU) were recorded over time. Data were extracted using the integrated ScreenWorks software (www.moleculardevices.com/products/flipr-penta-high-throughput-cellular-screening-system/screenworks-software) and subjected to nonlinear least-squares regression analysis using the sigmoidal dose-response function provided in GraphPad Prism 9.0. Data of three independent experiments (N = 3) performed in quadruplicate are presented as RLUs or normalized as indicated in figure legends.

Tango assay

HTTL (HEK293T stably expressing a luciferase reporter gene under the tTA-response element-Tight promoter) cells, an in-house developed reporter cell line (70), were seeded in 6-well plates at 1.2 x 10^6 cells and were transfected with Tango-ized constructs using the PEI precipitation method. Twenty hours later, the transfected cells were plated in DMEM supplemented with 1% dialyzed FBS into PLL-coated 384-well white clear bottom cell culture plates at a density of 30,000 cells/well in a total volume of 40 µl for 5 h to ensure proper attachment of cells. Agonist solutions, previously prepared at 3× concentration in sterilized assay buffer (20 mM Hepes, 1× HBSS, pH 7.4), were added to the cells at 20 µl per well. Following overnight incubation, media was removed and 20 µl per well of homemade luciferase detection reagent (108 mM Tris–HCl; 42 mM Tris-Base, 75 mM NaCl, 3 mM $MgCl_2$, 5 mM DTT, 0.2 mM coenzyme A, 0.14 mg/ml D-luciferin, 1.1 mM ATP, 0.25% v/v Triton X-100, 2 mM sodium hydrosulfite) was added to all wells (68). After 10 min of incubation in the dark at room temperature, plates were read using the Hidex Sense Beta Plus microplate reader (Gamble Technologies). Data were subjected to nonlinear least-squares regression analysis using the sigmoidal dose-response function provided in GraphPad Prism 9.0. Data of three independent experiments (N = 3) performed in quadruplicate are presented as RLUs or normalized as indicated in figure legends.

Fluorescence imaging

HT1080 were seeded in an ibiTreat-chambered coverslip (Ibidi) in complete medium to obtain a 50% confluency the following day. The next day, cells were transiently cotransfected using JetPRIME (Polyplus Transfection) with γ-actin-V5/pLX307 or pcDNA3 and NbV5-eGFP/pcDNA3.1+. Twenty-four hours posttransfection, cells were fixed for 10 min in PBS containing 4% (w/v) paraformaldehyde, then washed three times in PBS, and incubated 30 min in PBS containing 0.1% Triton (v/v). The cells were then incubated with Alexa Fluor 568 Phalloidin (Thermo Fisher Scientific) (1:200 dilution) for 45 min and washed three times, followed by an incubation with 2 mM Hoechst 33342 (Thermo Fisher Scientific) for 15 min at room temperature. The coverslips were then washed with PBS, drained, and mounted with permafluor mounting media (Epredia). Cells were imaged on a GE Delta Vision Elite microscope using a 60×, 1.4NA, oil, PlanApo N objective. The images were analyzed using ImageJ software (https://imagej.net/ij/index.html).

Affinity measurement

Yeast Display: pYD1-Halo is derived from the pCTCON2 plasmid while retaining the AGAP2 and Gal4 inducible system. The nanobody is first encoded into the strain EBY100 (64), followed by the Agap2 and the Halo-Tag (pHTC, Promega Corp). Preculture was performed in drop-out media minus tryptophane, with glycerol (1%), lactate (1%), and nonrepressible media with a trace amount of glucose (0.05%) overnight. Subsequently, galactose (2% final concentration) was used to induce the system for 6 h. PBS 1× with 1% bovine serum albumin was utilized for binding and washing, and readings were taken using a Novocyte Flow Cytometer (Agilent Scientific) as per the manufacturer's instructions.

Antigen: The cDNA of the 1N3R Tau protein isoform7 (NP_001190180.1) with a V5-tag inserted between E73 and A74 was cloned in the pET15b vector, and purification was carried out following the protocol described previously (93). Labeling was realized using Alexa Fluor 488 NHS ester (Thermo Fisher Scientific), with a molecular ratio of 2:1 for NHS Alexa:Tau-V5. Binding analysis was performed using FACS, with serial dilutions of labeled Tau-V5 ranging from 500 nM to 0.98 nM. Data were subjected to nonlinear least-squares regression analysis using the sigmoidal dose-response function provided in GraphPad Prism 9.0. Data presented are representative of one biological replicate (n = 1) in triplicate and represents the mean of % fraction bound.

Data availability

Crystal structure is available from Protein Data Bank (https://www.rcsb.org/), PDB # 8SKJ.

The data that support the findings of this study are available from the corresponding authors upon reasonable request.

Supporting information—This article contains supporting information.

Acknowledgments—We would like to acknowledge technical support from the Protein Biophysics Core Facility. We would like to thank Dr Asuka Inoue for his generous gift of different plasmids, as highlighted in the Experimental procedures. Thank you to Hybrigenics (Gard, France) for performing the nanobody selection and Y2H. We would also like to thank the uOttawa CBIA core (RRID: SCR_021845) and core staff, Dr Chloë van Oostende. This work was supported by the Canadian Institutes of Health Research (CIHR grant #MOP142219) and Natural Sciences and Engineering Research Council of Canada (NSERC RGPIN-2017-06151).

Author contributions—P. M. G. supervision; P. M. G. conceptualization; P. M. G. methodology; P. M. G. writing–review and editing; M. Z. writing–original draft; M. Z., K. M., S. P., G. L., S. S., M. J., J.-C. R., and J.-F. C. investigation; M. Z., K. M., A. V., G. L., and J.-C. R. validation; K. M. and G. L. formal analysis; G. L. visualization; S. P., S. S., M. J., and J.-F. C. software; G. L. resources; S. S., M. J., and J.-F. C. data curation.

Funding and additional information—K. M. is supported by a graduate scholarship from the Natural Sciences and Engineering Research Council of Canada. M. Z. is supported by the Alexander Graham Bell Canada Graduate Scholarships-Doctoral Program (CGS-D3) from Natural Sciences and Engineering Research Council of Canada.

Conflict of interests—The authors declare that they have no conflicts of interests with the contents of this article.

Abbreviations—The abbreviations used are: AT1R, angiotensin II receptor type 1; BRET, bioluminescence resonance energy transfer;

cDNA, complementary DNA; CDR, complementarity-determining region; DMEM, Dulbecco's modified Eagle's medium; FBS, fetal bovine serum; GPCR, G protein–coupled receptor; HBSS, Hanks' balanced salt solution; HEK293, human embryonic kidney 293; LgBiT, Large BiT; NanoBiT, Nanoluciferase binary technology; Nbs, nanobodies; PLL, poly-L-lysine; PPI, protein–protein interaction; SmBiT, Small BiT; Tango, Tobacco Etch protease-dependent assay; TEV, tobacco etch virus; tTA, tetracycline-controlled transactivator; VHHs, variable domain of heavy-chain antibodies; Y2H, yeast two-hybrid; μ-OR, mu-opioid receptor.

References

1. Milligan, G., and andWhite, J. H. (2001) Protein-protein interactions at G-protein-coupled receptors. *Trends Pharmacol. Sci.* **22**, 513–518
2. Seychell, B. C., and andBeck, T. (2021) Molecular basis for protein-protein interactions. *Beilstein J. Org. Chem.* **17**, 1–10
3. Kuzmanov, U., and andEmili, A. (2013) Protein-protein interaction networks: probing disease mechanisms using model systems. *Genome Med.* **5**, 37
4. Rao, V. S., Srinivas, K., Sujini, G. N., and andKumar, G. N. (2014) Protein-protein interaction detection: methods and analysis. *Int. J. Proteomics* **2014**, 147648
5. Bell, M. R., Engleka, M. J., Malik, A., and andStrickler, J. E. (2013) To fuse or not to fuse: what is your purpose? *Protein Sci.* **22**, 1466–1477
6. Newman, R. H., Fosbrink, M. D., and andZhang, J. (2011) Genetically encodable fluorescent biosensors for tracking signaling dynamics in living cells. *Chem. Rev.* **111**, 3614–3666
7. Villalobos, V., Naik, S., and andPiwnica-Worms, D. (2007) Current state of imaging protein-protein interactions *in vivo* with genetically encoded reporters. *Annu. Rev. Biomed. Eng.* **9**, 321–349
8. Guo, S., Zhao, T., Yun, Y., and andXie, X. (2022) Recent progress in assays for GPCR drug discovery. *Am. J. Physiol. Cell Physiol.* **323**, C583–C594
9. Sun, Y., Rombola, C., Jyothikumar, V., and andPeriasamy, A. (2013) Forster resonance energy transfer microscopy and spectroscopy for localizing protein-protein interactions in living cells. *Cytometry A* **83**, 780–793
10. Wade, M., Mendez, J., Coussens, N. P., Arkin, M. R., and Glicksman, M. A. (2004) Inhibition of protein-protein interactions: cell-based assays. In: Markossian, S., Grossman, A., Brimacombe, K., Arkin, M., Auld, D., Austin, C., *et al.* eds. *Assay Guidance Manual*, Eli Lilly & Company and the National Center for Advancing Translational Sciences, Bethesda, MD
11. Kimple, M. E., Brill, A. L., and andPasker, R. L. (2013) Overview of affinity tags for protein purification. *Curr. Protoc. Protein Sci.* **73**. https://doi.org/10.1002/0471140864.ps0909s73
12. Kuey, C., Larocque, G., Clarke, N. I., and andRoyle, S. J. (2019) Unintended perturbation of protein function using GFP nanobodies in human cells. *J. Cell Sci.* **132**. https://doi.org/10.1242/jcs.234955
13. Zhao, X., Li, G., and andLiang, S. (2013) Several affinity tags commonly used in chromatographic purification. *J. Anal. Methods Chem.* **2013**, 581093
14. Brilhante-da-Silva, N., de Oliveira Sousa, R. M., Arruda, A., Dos Santos, E. L., Marinho, A. C. M., Stabeli, R. G., *et al.* (2021) Camelid single-domain antibodies for the development of potent diagnosis platforms. *Mol. Diagn. Ther.* **25**, 439–456
15. Dingus, J. G., Tang, J. C. Y., Amamoto, R., Wallick, G. K., and andCepko, C. L. (2022) A general approach for stabilizing nanobodies for intracellular expression. *Elife* **11**. https://doi.org/10.7554/eLife.68253
16. Marschall, A. L., Dubel, S., and andBoldicke, T. (2015) Specific *in vivo* knockdown of protein function by intrabodies. *MAbs* **7**, 1010–1035
17. Bates, A., and andPower, C. A. (2019) David vs. Goliath: the structure, function, and clinical prospects of antibody fragments. *Antibodies (Basel)* **8**. https://doi.org/10.3390/antib8020028
18. Hudson, P. J., and andKortt, A. A. (1999) High avidity scFv multimers; diabodies and triabodies. *J. Immunol. Methods* **231**, 177–189
19. Kabayama, H., Takeuchi, M., Tokushige, N., Muramatsu, S. I., Kabayama, M., Fukuda, M., *et al.* (2020) An ultra-stable cytoplasmic antibody engineered for in vivo applications. *Nat. Commun.* **11**, 336
20. Guglielmi, L., Denis, V., Vezzio-Vie, N., Bec, N., Dariavach, P., Larroque, C., *et al.* (2011) Selection for intrabody solubility in mammalian cells using GFP fusions. *Protein Eng. Des. Sel.* **24**, 873–881
21. Kvam, E., Sierks, M. R., Shoemaker, C. B., and andMesser, A. (2010) Physico-chemical determinants of soluble intrabody expression in mammalian cell cytoplasm. *Protein Eng. Des. Sel.* **23**, 489–498
22. Goldman, E. R., Liu, J. L., Zabetakis, D., and andAnderson, G. P. (2017) Enhancing stability of camelid and shark single domain antibodies: an overview. *Front. Immunol.* **8**, 865
23. Flicker, S., Zettl, I., and andTillib, S. V. (2020) Nanobodies-useful tools for allergy research? *Front. Immunol.* **11**, 576255
24. Muyldermans, S. (2021) A guide to: generation and design of nanobodies. *FEBS J.* **288**, 2084–2102
25. Steeland, S., Vandenbroucke, R. E., and andLibert, C. (2016) Nanobodies as therapeutics: big opportunities for small antibodies. *Drug Discov. Today* **21**, 1076–1113
26. Soetens, E., Ballegeer, M., and andSaelens, X. (2020) An inside job: applications of intracellular single domain antibodies. *Biomolecules* **10**. https://doi.org/10.3390/biom10121663
27. de Beer, M. A., and andGiepmans, B. N. G. (2020) Nanobody-based probes for subcellular protein identification and visualization. *Front. Cell Neurosci.* **14**, 573278
28. Che, T., English, J., Krumm, B. E., Kim, K., Pardon, E., Olsen, R. H. J., *et al.* (2020) Nanobody-enabled monitoring of kappa opioid receptor states. *Nat. Commun.* **11**, 1145
29. Galli, V., Sebastian, R., Moutel, S., Ecard, J., Perez, F., and andRoux, A. (2017) Uncoupling of dynamin polymerization and GTPase activity revealed by the conformation-specific nanobody dynab. *Elife* **6**. https://doi.org/10.7554/eLife.25197
30. Gulati, S., Jin, H., Masuho, I., Orban, T., Cai, Y., Pardon, E., *et al.* (2018) Targeting G protein-coupled receptor signaling at the G protein level with a selective nanobody inhibitor. *Nat. Commun.* **9**, 1996
31. Jullien, D., Vignard, J., Fedor, Y., Bery, N., Olichon, A., Crozatier, M., *et al.* (2016) Chromatibody, a novel non-invasive molecular tool to explore and manipulate chromatin in living cells. *J. Cell Sci.* **129**, 2673–2683
32. Keller, L., Bery, N., Tardy, C., Ligat, L., Favre, G., Rabbitts, T. H., *et al.* (2019) Selection and characterization of a nanobody biosensor of GTP-bound RHO activities. *Antibodies (Basel)* **8**. https://doi.org/10.3390/antib8010008
33. Kruse, A. C., Ring, A. M., Manglik, A., Hu, J., Hu, K., Eitel, K., *et al.* (2013) Activation and allosteric modulation of a muscarinic acetylcholine receptor. *Nature* **504**, 101–106
34. Livingston, K. E., Mahoney, J. P., Manglik, A., Sunahara, R. K., and andTraynor, J. R. (2018) Measuring ligand efficacy at the mu-opioid receptor using a conformational biosensor. *Elife* **7**. https://doi.org/10.7554/eLife.32499
35. Morgenstern, T. J., Park, J., Fan, Q. R., and andColecraft, H. M. (2019) A potent voltage-gated calcium channel inhibitor engineered from a nanobody targeted to auxiliary Ca(V)beta subunits. *Elife* **8**. https://doi.org/10.7554/eLife.49253
36. Schenck, S., Kunz, L., Sahlender, D., Pardon, E., Geertsma, E. R., Savtchouk, I., *et al.* (2017) Generation and characterization of anti-VGLUT nanobodies acting as inhibitors of transport. *Biochemistry* **56**, 3962–3971
37. Singh, S., Murillo, G., Chen, D., Parihar, A. S., and andMehta, R. G. (2018) Suppression of breast cancer cell proliferation by selective single-domain antibody for intracellular STAT3. *Breast Cancer (Auckl)* **12**. https://doi.org/10.1177/1178223417750858
38. Staus, D. P., Wingler, L. M., Strachan, R. T., Rasmussen, S. G., Pardon, E., Ahn, S., *et al.* (2014) Regulation of beta2-adrenergic receptor function by conformationally selective single-domain intrabodies. *Mol. Pharmacol.* **85**, 472–481
39. Truttmann, M. C., Wu, Q., Stiegeler, S., Duarte, J. N., Ingram, J., and andPloegh, H. L. (2015) HypE-specific nanobodies as tools to modulate HypE-mediated target AMPylation. *J. Biol. Chem.* **290**, 9087–9100

40. Van Impe, K., Bethuyne, J., Cool, S., Impens, F., Ruano-Gallego, D., De Wever, O., *et al.* (2013) A nanobody targeting the F-actin capping protein CapG restrains breast cancer metastasis. *Breast Cancer Res.* **15**, R116
41. Wilton, E. E., Opyr, M. P., Kailasam, S., Kothe, R. F., and andWieden, H. J. (2018) sdAb-DB: the single domain antibody database. *ACS Synth. Biol.* **7**, 2480–2484
42. De Genst, E. J., Guilliams, T., Wellens, J., O'Day, E. M., Waudby, C. A., Meehan, S., *et al.* (2010) Structure and properties of a complex of alpha-synuclein and a single-domain camelid antibody. *J. Mol. Biol.* **402**, 326–343
43. Braun, M. B., Traenkle, B., Koch, P. A., Emele, F., Weiss, F., Poetz, O., *et al.* (2016) Peptides in headlock–a novel high-affinity and versatile peptide-binding nanobody for proteomics and microscopy. *Sci. Rep.* **6**, 19211
44. Virant, D., Traenkle, B., Maier, J., Kaiser, P. D., Bodenhofer, M., Schmees, C., *et al.* (2018) A peptide tag-specific nanobody enables high-quality labeling for dSTORM imaging. *Nat. Commun.* **9**, 930
45. Cabalteja, C. C., Sachdev, S., and andCheloha, R. W. (2022) Characterization of a nanobody-epitope tag interaction and its application for receptor engineering. *ACS Chem. Biol.* **17**, 2296–2303
46. Boersma, S., Khuperkar, D., Verhagen, B. M. P., Sonneveld, S., Grimm, J. B., Lavis, L. D., *et al.* (2019) Multi-color single-molecule imaging uncovers extensive heterogeneity in mRNA decoding. *Cell* **178**, 458–472. e419
47. Lutje Hulsik, D., Liu, Y. Y., Strokappe, N. M., Battella, S., El Khattabi, M., McCoy, L. E., *et al.* (2013) A gp41 MPER-specific llama VHH requires a hydrophobic CDR3 for neutralization but not for antigen recognition. *PLoS Pathog.* **9**, e1003202
48. Jin-jing LI, F. X., Yan-wei, J. I., Mei, S. H. U., Zhui, T. U., and Jin-heng, F. U. (2018) Biopanning of anti c-Myc-tag nanobodies and its application for bioimaging China. *Biotechnology* **38**, 61–67
49. Traenkle, B., Emele, F., Anton, R., Poetz, O., Haeussler, R. S., Maier, J., *et al.* (2015) Monitoring interactions and dynamics of endogenous beta-catenin with intracellular nanobodies in living cells. *Mol. Cell Proteomics* **14**, 707–723
50. Cheloha, R. W., Harmand, T. J., Wijne, C., Schwartz, T. U., and and-Ploegh, H. L. (2020) Exploring cellular biochemistry with nanobodies. *J. Biol. Chem.* **295**, 15307–15327
51. Gotzke, H., Kilisch, M., Martinez-Carranza, M., Sograte-Idrissi, S., Rajavel, A., Schlichthaerle, T., *et al.* (2019) The ALFA-tag is a highly versatile tool for nanobody-based bioscience applications. *Nat. Commun.* **10**, 4403
52. Vigano, M. A., Ell, C. M., Kustermann, M. M. M., Aguilar, G., Matsuda, S., Zhao, N., *et al.* (2021) Protein manipulation using single copies of short peptide tags in cultured cells and in Drosophila melanogaster. *Development* **148**. https://doi.org/10.1242/dev.191700
53. Yang, X., Boehm, J. S., Yang, X., Salehi-Ashtiani, K., Hao, T., Shen, Y., *et al.* (2011) A public genome-scale lentiviral expression library of human ORFs. *Nat. Methods* **8**, 659–661
54. Sarov, M., Barz, C., Jambor, H., Hein, M. Y., Schmied, C., Suchold, D., *et al.* (2016) A genome-wide resource for the analysis of protein localisation in Drosophila. *Elife* **5**, e12068
55. Hanke, T., and andRandall, R. E. (1995) Variable domain sequences of mAb with high affinity for a linear oligopeptide. *Immunogenetics* **42**, 442–443
56. Hanke, T., Szawlowski, P., and andRandall, R. E. (1992) Construction of solid matrix-antibody-antigen complexes containing simian immunodeficiency virus p27 using tag-specific monoclonal antibody and tag-linked antigen. *J. Gen. Virol.* **73**, 653–660
57. Randall, R. E., Young, D. F., Goswami, K. K., and andRussell, W. C. (1987) Isolation and characterization of monoclonal antibodies to simian virus 5 and their use in revealing antigenic differences between human, canine and simian isolates. *J. Gen. Virol.* **68**, 2769–2780
58. Bartel, P. L., and andFields, S. (1995) Analyzing protein-protein interactions using two-hybrid system. *Methods Enzymol.* **254**, 241–263
59. Fromont-Racine, M., Rain, J. C., and andLegrain, P. (1997) Toward a functional analysis of the yeast genome through exhaustive two-hybrid screens. *Nat. Genet.* **16**, 277–282
60. Moutel, S., Bery, N., Bernard, V., Keller, L., Lemesre, E., de Marco, A., *et al.* (2016) NaLi-H1: a universal synthetic library of humanized nanobodies providing highly functional antibodies and intrabodies. *Elife* **5**. https://doi.org/10.7554/eLife.16228
61. Padlan, E. A. (1994) Anatomy of the antibody molecule. *Mol. Immunol.* **31**, 169–217
62. Miura, N., Miyamoto, K., Ohtani, Y., Yaginuma, K., Aburaya, S., Kitagawa, Y., *et al.* (2019) Domain swapping of complementarity-determining region in nanobodies produced by Pichia pastoris. *AMB Express* **9**, 107
63. Mitchell, L. S., and andColwell, L. J. (2018) Analysis of nanobody paratopes reveals greater diversity than classical antibodies. *Protein Eng. Des. Sel.* **31**, 267–275
64. Chao, G., Lau, W. L., Hackel, B. J., Sazinsky, S. L., Lippow, S. M., and andWittrup, K. D. (2006) Isolating and engineering human antibodies using yeast surface display. *Nat. Protoc.* **1**, 755–768
65. Danis, C., Dupre, E., Zejneli, O., Caillierez, R., Arrial, A., Begard, S., *et al.* (2022) Inhibition of Tau seeding by targeting Tau nucleation core within neurons with a single domain antibody fragment. *Mol. Ther.* **30**, 1484–1499
66. Kroeze, W. K., Sassano, M. F., Huang, X. P., Lansu, K., McCorvy, J. D., Giguere, P. M., *et al.* (2015) PRESTO-Tango as an open-source resource for interrogation of the druggable human GPCRome. *Nat. Struct. Mol. Biol.* **22**, 362–369
67. Laroche, G., and andGiguere, P. M. (2019) Measurement of beta-arrestin recruitment at GPCRs using the Tango assay. *Methods Mol. Biol.* **1947**, 257–267
68. Zeghal, M., Laroche, G., and andGiguere, P. M. (2020) Parallel interrogation of beta-arrestin2 recruitment for ligand screening on a GPCR-wide scale using PRESTO-tango assay. *J. Vis. Exp.* https://doi.org/10.3791/60823
69. Kim, M. W., Wang, W., Sanchez, M. I., Coukos, R., von Zastrow, M., and andTing, A. Y. (2017) Time-gated detection of protein-protein interactions with transcriptional readout. *Elife* **6**. https://doi.org/10.7554/eLife.30233
70. Zeghal, M., Laroche, G., Freitas, J. D., Wang, R., and andGiguere, P. M. (2023) Profiling of basal and ligand-dependent GPCR activities by means of a polyvalent cell-based high-throughput platform. *Nat. Commun.* **14**, 3684
71. Sun, S., Yang, X., Wang, Y., and andShen, X. (2016) *In Vivo* analysis of protein-protein interactions with bioluminescence resonance energy transfer (BRET): progress and prospects. *Int. J. Mol. Sci.* **17**. https://doi.org/10.3390/ijms17101704
72. Loening, A. M., Fenn, T. D., Wu, A. M., and andGambhir, S. S. (2006) Consensus guided mutagenesis of Renilla luciferase yields enhanced stability and light output. *Protein Eng. Des. Sel.* **19**, 391–400
73. Bertrand, L., Parent, S., Caron, M., Legault, M., Joly, E., Angers, S., *et al.* (2002) The BRET2/arrestin assay in stable recombinant cells: a platform to screen for compounds that interact with G protein-coupled receptors (GPCRS). *J. Recept Signal. Transduct. Res.* **22**, 533–541
74. Jensen, A. A., Hansen, J. L., Sheikh, S. P., and andBrauner-Osborne, H. (2002) Probing intermolecular protein-protein interactions in the calcium-sensing receptor homodimer using bioluminescence resonance energy transfer (BRET). *Eur. J. Biochem.* **269**, 5076–5087
75. Dixon, A. S., Schwinn, M. K., Hall, M. P., Zimmerman, K., Otto, P., Lubben, T. H., *et al.* (2016) NanoLuc complementation reporter optimized for accurate measurement of protein interactions in cells. *ACS Chem. Biol.* **11**, 400–408
76. Nickolls, S. A., Humphreys, S., Clark, M., and andMcMurray, G. (2013) Co-expression of GRK2 reveals a novel conformational state of the micro-opioid receptor. *PLoS One* **8**, e83691
77. Wan, Q., Okashah, N., Inoue, A., Nehme, R., Carpenter, B., Tate, C. G., *et al.* (2018) Mini G protein probes for active G protein-coupled receptors (GPCRs) in live cells. *J. Biol. Chem.* **293**, 7466–7473
78. Culhane, K. J., Gupte, T. M., Madhugiri, I., Gadgil, C. J., and andSivaramakrishnan, S. (2022) Kinetic model of GPCR-G protein interactions reveals allokairic modulation of signaling. *Nat. Commun.* **13**, 1202
79. Wagner, T. R., and andRothbauer, U. (2020) Nanobodies right in the middle: intrabodies as toolbox to visualize and modulate antigens in the living cell. *Biomolecules* **10**. https://doi.org/10.3390/biom10121701

80. Stadler, C., Rexhepaj, E., Singan, V. R., Murphy, R. F., Pepperkok, R., Uhlen, M., *et al.* (2013) Immunofluorescence and fluorescent-protein tagging show high correlation for protein localization in mammalian cells. *Nat. Methods* **10**, 315–323
81. Ruffolo, J. A., Chu, L. S., Mahajan, S. P., and andGray, J. J. (2023) Fast, accurate antibody structure prediction from deep learning on massive set of natural antibodies. *Nat. Commun.* **14**, 2389
82. McMahon, C., Baier, A. S., Pascolutti, R., Wegrecki, M., Zheng, S., Ong, J. X., *et al.* (2018) Yeast surface display platform for rapid discovery of conformationally selective nanobodies. *Nat. Struct. Mol. Biol.* **25**, 289–296
83. Lobstein, J., Emrich, C. A., Jeans, C., Faulkner, M., Riggs, P., and and-Berkmen, M. (2012) SHuffle, a novel Escherichia coli protein expression strain capable of correctly folding disulfide bonded proteins in its cytoplasm. *Microb. Cell Fact* **11**, 56
84. Rabia, L. A., Desai, A. A., Jhajj, H. S., and andTessier, P. M. (2018) Understanding and overcoming trade-offs between antibody affinity, specificity, stability and solubility. *Biochem. Eng. J.* **137**, 365–374
85. Pathan, H., and andWilliams, J. (2012) Basic opioid pharmacology: an update. *Br. J. Pain* **6**, 11–16
86. Dasgupta, C., and andZhang, L. (2011) Angiotensin II receptors and drug discovery in cardiovascular disease. *Drug Discov. Today* **16**, 22–34
87. Salahudeen, M. S., and andNishtala, P. S. (2017) An overview of pharmacodynamic modelling, ligand-binding approach and its application in clinical practice. *Saudi Pharm. J.* **25**, 165–175
88. Milligan, G. (1999) Exploring the dynamics of regulation of G protein-coupled receptors using green fluorescent protein. *Br. J. Pharmacol.* **128**, 501–510
89. El Khamlichi, C., Reverchon-Assadi, F., Hervouet-Coste, N., Blot, L., Reiter, E., and andMorisset-Lopez, S. (2019) Bioluminescence resonance energy transfer as a method to study protein-protein interactions: application to G protein coupled receptor biology. *Molecules* **24**, 537
90. Wouters, E., Vasudevan, L., Crans, R. A. J., Saini, D. K., and andStove, C. P. (2019) Luminescence- and fluorescence-based complementation assays to screen for GPCR oligomerization: current state art. *Int. J. Mol. Sci.* **20**. https://doi.org/10.3390/ijms20122958
91. Chen, X., Zaro, J. L., and andShen, W. C. (2013) Fusion protein linkers: property, design and functionality. *Adv. Drug Deliv. Rev.* **65**, 1357–1369
92. Vojtek, A. B., and andHollenberg, S. M. (1995) Ras-Raf interaction: two-hybrid analysis. *Methods Enzymol.* **255**, 331–342
93. Danis, C., Despres, C., Bessa, L. M., Malki, I., Merzougui, H., Huvent, I., *et al.* (2016) Nuclear magnetic resonance spectroscopy for the identification of multiple phosphorylations of intrinsically disordered proteins. *J. Vis. Exp.* https://doi.org/10.3791/55001

Permissions

As a general rule, permission should be sought from the rights holder to reproduce any substantial part of a copyrighted work. This includes any text, illustrations, charts, tables, photographs, or other material from previously published sources. Obtaining permission to re-use content published by Elsevier is simple. Follow the guide below for a quick and easy route to permission.

Permission guidelines

For further guidelines about obtaining permission, please review our Frequently Asked Questions below:

- When is permission required? +
- When is permission not required? +
- From whom do I need permission? +
- How do I obtain permission to use photographs or illustrations? +
- Do I need to obtain permission to use material posted on a website such as Blogs/Google images/e-commerce websites? +
- What rights does Elsevier require when requesting permission? +
- How do I obtain permission from another publisher? +

What is RightsLink/CCC? +

What should I do if I am not able to locate the copyright owner? +

Can I obtain permission from a Reproduction Rights Organization (RRO)? +

Is Elsevier an STM signatory publisher? +

Do I need to request permission to re-use work from another STM publisher? +

Do I need to request permission to text mine Elsevier content? +

Can I include/use my article in my thesis/dissertation? −

Yes. Authors can include their articles in full or in part in a thesis or dissertation for non-commercial purposes.

For any further clarifications, you can submit your query via our online form ↗

Which uses of a work does Elsevier view as a form of 'prior publication'? +

How do I obtain permission to use Elsevier Journal material such as figures, tables or text excerpts, if the request falls +

Permission guidelines | ScienceDirect content | ClinicalKey content | Tutorial videos | Help and support

How do I obtain permission to use Elsevier Journal material such as figures, tables or text excerpts, if the amount of material I wish to use does not fall within the free limits set out in the STM permissions guidelines? +

How do I obtain permission to use Elsevier Book material such as figures, tables or text excerpts? +

How do I obtain permission to use Elsevier material that is NOT on ScienceDirect or Clinical Key? +

Can I use material from my Elsevier journal article within my thesis/dissertation? +

Can I modify a figure when I have received permission to use it? +

Can I modify Lancet material? +

How do I obtain copies of a book in a format suitable for a person with a disability? +